frontiers | Research Topics

Candida biofilms

Edited by
Juliana Campos Junqueira and Eleftherios Mylonakis

Published in
Frontiers in Microbiology
Frontiers in Cellular and Infection Microbiology

ISSN 1664-8714
ISBN 978-2-83251-356-9
DOI 10.3389/978-2-83251-356-9

About Frontiers

Frontiers is more than just an open access publisher of scholarly articles: it is a pioneering approach to the world of academia, radically improving the way scholarly research is managed. The grand vision of Frontiers is a world where all people have an equal opportunity to seek, share and generate knowledge. Frontiers provides immediate and permanent online open access to all its publications, but this alone is not enough to realize our grand goals.

Frontiers journal series

The Frontiers journal series is a multi-tier and interdisciplinary set of open-access, online journals, promising a paradigm shift from the current review, selection and dissemination processes in academic publishing. All Frontiers journals are driven by researchers for researchers; therefore, they constitute a service to the scholarly community. At the same time, the *Frontiers journal series* operates on a revolutionary invention, the tiered publishing system, initially addressing specific communities of scholars, and gradually climbing up to broader public understanding, thus serving the interests of the lay society, too.

Dedication to quality

Each Frontiers article is a landmark of the highest quality, thanks to genuinely collaborative interactions between authors and review editors, who include some of the world's best academicians. Research must be certified by peers before entering a stream of knowledge that may eventually reach the public - and shape society; therefore, Frontiers only applies the most rigorous and unbiased reviews. Frontiers revolutionizes research publishing by freely delivering the most outstanding research, evaluated with no bias from both the academic and social point of view. By applying the most advanced information technologies, Frontiers is catapulting scholarly publishing into a new generation.

What are Frontiers Research Topics?

Frontiers Research Topics are very popular trademarks of the *Frontiers journals series*: they are collections of at least ten articles, all centered on a particular subject. With their unique mix of varied contributions from Original Research to Review Articles, Frontiers Research Topics unify the most influential researchers, the latest key findings and historical advances in a hot research area.

Find out more on how to host your own Frontiers Research Topic or contribute to one as an author by contacting the Frontiers editorial office: frontiersin.org/about/contact

Candida biofilms

Topic editors

Juliana Campos Junqueira — São Paulo State University, Brazil

Eleftherios Mylonakis — Brown University, United States

Citation

Junqueira, J. C., Mylonakis, E., eds. (2023). *Candida biofilms*. Lausanne: Frontiers Media SA. doi: 10.3389/978-2-83251-356-9

Table of contents

frontiers | Frontiers in Microbiology

TYPE Editorial
PUBLISHED 04 January 2023
DOI 10.3389/fmicb.2022.1128600

OPEN ACCESS

EDITED AND REVIEWED BY
Axel Cloeckaert,
Institut National de recherche pour l'agriculture, l'alimentation et l'environnement (INRAE), France

*CORRESPONDENCE
Juliana Campos Junqueira
✉ juliana.junqueira@unesp.br
Eleftherios Mylonakis
✉ emylonakis@lifespan.org

SPECIALTY SECTION
This article was submitted to Infectious Agents and Disease, a section of the journal Frontiers in Microbiology

RECEIVED 20 December 2022
ACCEPTED 23 December 2022
PUBLISHED 04 January 2023

CITATION
Junqueira JC and Mylonakis E (2023) Editorial: *Candida* biofilms. *Front. Microbiol.* 13:1128600. doi: 10.3389/fmicb.2022.1128600

Editorial: *Candida* biofilms

Juliana Campos Junqueira[1]* and Eleftherios Mylonakis[2]*

[1]Department of Biosciences and Oral Diagnosis, Institute of Science and Technology, São Paulo State University/UNESP, São José dos Campos, Brazil, [2]Division of Infectious Diseases, Rhode Island Hospital, Alpert Medical School of Brown University, Providence, RI, United States

KEYWORDS

biofilms, *Candida* spp., candidiasis, antifungals, fungal-host interactions

Editorial on the Research Topic
Candida biofilms

Biofilm formation is an important factor of *Candida* pathogenesis with several clinical implications. Most *Candida* spp. form biofilms on mucosal and skin surfaces causing different types of superficial candidiasis, as well as on implanted medical devices leading to systemic infections (Horton et al., 2020; Fan et al., 2022). The inherent biofilm resistance to available antifungal drugs results in recurrent infections, chronic persistent infections, and poor clinical outcomes (Ponde et al., 2021). The Research Topic on "*Candida* biofilms" includes a collection of 14 original research articles and three reviews prepared by renowned groups from Brazil, China, Germany, India, Portugal, Spain, United Kingdom, and USA. Taken together the articles in this issue give an overview on the field of *Candida* biofilms and provide insights on their structure and regulatory networks; interactions with the host immune defense; mechanisms involved in antifungal resistance; pathogenicity and clinical relevance; cross-kingdom interactions; and development of novel therapeutic approaches.

In this context, Böttcher et al. present a detailed study about biofilm formation of *C. albicans* with focus on the role of *STP2*, a key transcriptional regulator of extracellular amino acid signaling and metabolism. The results demonstrate that *STP2* mediates the adherence, germ tube formation, metabolic adaptation, and biofilm sustainability, suggesting that regulatory responses to extracellular amino acids are not only involved with nutritional homeostasis, but also coordinate crucial factors for biofilm development. Related to this work, Wang et al. explore the complex mechanism of *C. albicans* to respond to environmental challenges, unveiling that *SPT20* plays an important role to resist hyperosmotic stress through regulating the high osmolarity glycerol 1 mitogen activated protein kinase transduction pathway (Hog1-MAPK). Moving focus to biofilms formed by *Candida glabrata*, Santos et al. demonstrate that Drug:H+ antiporter 1 (DHA1) transporters, involved in the activation of efflux pumps and drug resistance, can also influence the biofilm development by affecting nutrient uptake and cellular adhesion. Taken together, these studies contribute to clarify the intertwined network of pathways involved in biofilms formed by *Candida* spp., making them promising targets for drug development.

Looking into the influence of biofilms on *Candida*-host interactions and the role of biofilm in *Candida* pathogenesis, Eix and Nett bring a comprehensive review on innate immune responses associated with biofilms, highlighting the key mechanisms by which

Candida cells increase their resistance to phagocytosis and alter the mononuclear cell cytokine profile. The authors also examine the insights into host responses to biofilm provided by animal studies, and discuss models that explore biofilms formed on vascular catheters, dental devices, and the mucosal surfaces of rats and mice. Using a mouse model of vaginal candidiasis, Wu et al. demonstrate that *C. albicans* strains can form significant quantities of biotic biofilms on the vaginal epithelium. The formation of these biofilms leads to high resistance to antifungal treatment and promotes the formation of persister cells, providing new experimental evidence that extend the role of biofilms in the pathogenesis of vaginal candidiasis. Notably, the mechanisms employed by *C. albicans* to colonize and to form biofilms on vulvovaginal mucosa are thoroughly discussed in the article performed by Rodríguez-Cerdeira et al., who emphasize the genomic, proteomic and quorum sensing aspects of these biofilms.

In a cohort study, Pentland et al. demonstrate the clinical relevance of biofilms in voice prosthesis of patients that underwent total laryngectomy, and show that biofilms are associated with loss of device performance and its early failure. Interestingly, in most cases of prosthesis failure the investigators found polymicrobial biofilms composed mainly by *Staphylococcus aureus* and *C. albicans*. Indeed, multi-species biofilms formed by *Candida* and bacteria can be formed in various niches of the human body, including the oral cavity, gastrointestinal tract, vulvovaginal region, lungs, and skin (Lohse et al., 2018). The interactions established by *Candida* with different bacterial species have been widely studied (Barbosa et al., 2016; Kong et al., 2016; Kostoulias et al., 2016), however little is known about the possible interactions of *Candida* spp. with other fungi. In pioneering studies, Oliveira et al. and Garcia et al. demonstrate that *C. albicans* can form dual species biofilms with *Paracoccidioides brasiliensis* or *Trichophyton rubrum*, respectively. The results of both studies suggest that *C. albicans* and *P. brasilensis* or *T. rubrum* can coexist in the same environment and establish fungal-fungal interactions on host surfaces.

The cross-kingdom microbial interactions in biofilms have been explored as a potential resource for the identification of new antifungal molecules (Scorzoni et al., 2021). From this perspective, Santos et al. reveal that *Streptococcus mutans,* an important bacterium in dental biofilms, can secrete products capable of inhibiting the oral candidiasis in a murine model. In this work, the authors extracted, fractionated, and identified the fraction of the *S. mutans* UA159 culture (SM-F2) with strong activity against *C. albicans* and high efficacy in the treatment of oral candidiasis. In an innovative study, Rossoni et al. explore the antimicrobial activity of bacterial metabolic products on *Candida auris*, an emerging multidrug-resistant yeast. The results show that crude extract derived from the probiotic bacterium *Lactobacillus paracasei* 28.4 can inhibit the biofilms and persister cells of *C. auris,* and protect the model host *Galleria mellonella* from fungal infection through a direct antifungal activity as well as by modulating the host immune response. Besides to natural compounds from microbial origins, plant extracts have gained much attention with large number of bioactive compounds already isolated and identified (Singla and Dubey, 2019; Scorzoni et al., 2021). This Research Topic highlights two plant-derived natural compounds: the coumarin scopoletin (gelseminic acid) studied by Lemos et al. and the palmitic acid (hexadecenoic acid) studied by Prasath et al. Based on their results, both compounds exhibit an effective inhibition on biofilms formed by *Candida tropicalis*. The mechanism of action of scopoletin involves the alteration on fungal cell and plasma membrane sterols, while the action of palmitic acid seems associated with ROS-mediated mitochondrial dysfunction and regulation of ergosterol biosynthesis. Interestingly, scopoletin also showed activity against the efflux pumps at plasma membrane when combined with fluconazole, suggesting potential synergistic activity against multidrug-resistant *Candida* strains.

Looking at therapeutic strategies targeted to *Candida* biofilms, and based on the evidence that antiretroviral HIV protease inhibitors can influence the secreted aspartyl proteases (Saps) of *Candida* spp. (Cenci et al., 2008; Braga-Silva et al., 2010), Lohse et al. investigate the capacity of 80 protease inhibitors in preventing and treating *Candida* biofilms. Among the 80 protease inhibitors studied, the investigators found that gliotoxin, acivicin, TPCK and nelfinavir show effectiveness against *Candida* biofilms. Moreover, several protease inhibitors exhibit ability to decrease *C. albicans* biofilms when combined with caspofungin or amphotericin B. Reddy and Nancharaiah explore new anti-biofilm approaches using ionic liquids, a novel class of molten salts originates from the combination of cations and anions, with several applications in chemical industry. The prospecting results indicate the imidazolium ionic liquid with hexadecyl group ($[C16MIM]^+[Cl]^-$) as the most effective compound against *C. albicans* biofilms. The antifungal and anti-biofilm activity of imidazolium includes alterations in various cellular process, such as membrane permeability, ergosterol content, and ROS generation. Seeking alternative approaches against *C. auris*, Vazquez-Munoz et al. studied the use of silver nanoparticles (AgNPs) coated with polyvinylpyrrolidone (PVP) and verified strong antimicrobial activity on several *C. auris* strains under planktonic and biofilm growing conditions. Promisingly, this antimicrobial activity against *C. auris* strains is irrespective of their clade, geographical origin, or antifungal-resistant profiles.

Lastly, Vera-González and Shukla discuss the recent advances in antifungal biomaterials for combating *Candida* biofilm infections. This review explores the design of nanoparticles aimed at disrupting existing biofilms and presents innovative technologies that employ polymer-only coatings as well as coatings with conventional or new antifungal agents against biofilm formation. Moreover, the authors outline

future perspectives in the development of biomaterials targeted for *Candida* biofilms, including the use of enzymes to digest the components of extracellular matrix and identification of new drug targets such as extracellular vesicles.

We hope that this Research Topic covers the key points of the development, pathogenesis, and clinical relevance of *Candida* biofilms, and provides an overview about the progress and challenges of new antifungal discovery that will incentivize innovation in the field of *Candida* biofilm pathogenesis and therapeutics.

Author contributions

JJ and EM wrote the manuscript. All authors contributed to the article and approved the submitted version.

Conflict of interest

The authors declare that the research was conducted in the absence of any commercial or financial relationships that could be construed as a potential conflict of interest.

Publisher's note

All claims expressed in this article are solely those of the authors and do not necessarily represent those of their affiliated organizations, or those of the publisher, the editors and the reviewers. Any product that may be evaluated in this article, or claim that may be made by its manufacturer, is not guaranteed or endorsed by the publisher.

References

Barbosa, J. O., Rossoni, R. D., Vilela, S. F., de Alvarenga, J. A., Velloso Mdos, S., Prata, M. C., et al. (2016). *Streptococcus mutans* can modulate biofilm formation and attenuate the virulence of *Candida albicans*. *PLoS ONE* 11, e0150457. doi: 10.1371/journal.pone.0150457

Braga-Silva, L. A., Mogami, S. S., Valle, R. S., Silva-Neto, I. D., and Santos, A. L. (2010). Multiple effects of amprenavir against Candida albicans. *FEMS Yeast Res.* 10, 221–224. doi: 10.1111/j.1567-1364.2009.00595.x

Cenci, E., Francisci, D., Belfiori, B., Pierucci, S., Baldelli, F., Bistoni, F., et al. (2008). Tipranavir exhibits different effects on opportunistic pathogenic fungi. *J. Infect*. 56, 58–64. doi: 10.1016/j.jinf.2007.08.004

Fan, F., Liu, Y., Liu, Y., Lv, R., Sun, W., Ding, W., et al. (2022). Candida albicans biofilms: antifungal resistance, immune evasion, and emerging therapeutic strategies. *Int. J. Antimicrob. Agents*. 60, 106673. doi: 10.1016/j.ijantimicag.2022.106673

Horton, M. V., Johnson, C. J., Kernien, J. F., Patel, T. D., Lam, B. C., Cheong, J. Z. A., et al. (2020). *Candida auris* forms high-burden biofilms in skin niche conditions and on porcine skin. *mSphere*. 5. doi: 10.1128/mSphere.00910-19

Kong, E. F., Tsui, C., Kucharikova, S., Andes, D., Van Dijck, P., and Jabra-Rizk, M. A. (2016). Commensal protection of *Staphylococcus aureus* against antimicrobials by *Candida albicans* biofilm matrix. *mBio*. 7. doi: 10.1128/mBio.01365-16

Kostoulias, X., Murray, G. L., Cerqueira, G. M., Kong, J. B., Bantun, F., Mylonakis, E., et al. (2016). Impact of a cross-kingdom signaling molecule of *Candida albicans* on *Acinetobacter baumannii* physiology. *Antimicrob. Agents Chemother*. 60, 161–167. doi: 10.1128/AAC.01540-15

Lohse, M. B., Gulati, M., Johnson, A. D., and Nobile, C. J. (2018). Development and regulation of single- and multi-species *Candida albicans* biofilms. *Nat. Rev. Microbiol*. 16, 19–31. doi: 10.1038/nrmicro.2017.107

Ponde, N. O., Lortal, L., Ramage, G., Naglik, J. R., and Richardson, J. P. (2021). *Candida albicans* biofilms and polymicrobial interactions. *Crit. Rev. Microbiol*. 47, 91–111. doi: 10.1080/1040841X.2020.1843400

Scorzoni, L., Fuchs, B. B., Junqueira, J. C., and Mylonakis, E. (2021). Current and promising pharmacotherapeutic options for candidiasis. *Exp. Opin. Pharmacother*. 22, 867–887. doi: 10.1080/14656566.2021.1873951

Singla, R. K., and Dubey, A. K. (2019). Molecules and metabolites from natural products as inhibitors of biofilm in candida spp. pathogens. *Curr. Top. Med. Chem*. 19, 2567–2578. doi: 10.2174/1568026619666191025154834

frontiers in Cellular and Infection Microbiology

ORIGINAL RESEARCH
published: 04 February 2020
doi: 10.3389/fcimb.2020.00029

Screening the Drug:H$^+$ Antiporter Family for a Role in Biofilm Formation in *Candida glabrata*

Rui Santos[1,2†‡], *Mafalda Cavalheiro*[1,2†], *Catarina Costa*[1,2], *Azusa Takahashi-Nakaguchi*[3], *Michiyo Okamoto*[3], *Hiroji Chibana*[3] *and Miguel C. Teixeira*[1,2*]

[1] *Department of Bioengineering, Instituto Superior Técnico, Universidade de Lisboa, Lisbon, Portugal,* [2] *Biological Sciences Research Group, Institute for Bioengineering and Biosciences, Instituto Superior Técnico, Lisbon, Portugal,* [3] *Medical Mycology Research Center, Chiba University, Chiba, Japan*

OPEN ACCESS

Edited by:
Juliana Campos Junqueira, São Paulo State University, Brazil

Reviewed by:
Patrícia Pimentel Barros, São Paulo State University, Brazil
Célia F. Rodrigues, University of Porto, Portugal

****Correspondence:***
Miguel C. Teixeira
mnpct@tecnico.ulisboa.pt

† These authors have contributed equally to this work

‡Present address:
Rui Santos, Institute of Parasitology, University of Zurich, Zurich, Switzerland

Specialty section:
This article was submitted to Fungal Pathogenesis, a section of the journal Frontiers in Cellular and Infection Microbiology

Received: *18 November 2019*
Accepted: *15 January 2020*
Published: *04 February 2020*

Citation:
Santos R, Cavalheiro M, Costa C, Takahashi-Nakaguchi A, Okamoto M, Chibana H and Teixeira MC (2020) Screening the Drug:H$^+$ Antiporter Family for a Role in Biofilm Formation in Candida glabrata. Front. Cell. Infect. Microbiol. 10:29. doi: 10.3389/fcimb.2020.00029

Biofilm formation and drug resistance are two key pathogenesis traits exhibited by *Candida glabrata* as a human pathogen. Interestingly, specific pathways appear to be in the crossroad between the two phenomena, making them promising targets for drug development. In this study, the 10 multidrug resistance transporters of the Drug:H$^+$ Antiporter family of *C. glabrata* were screened for a role in biofilm formation. Besides previously identified players in this process, namely CgTpo1_2 and CgQdr2, two others are shown to contribute to biofilm formation: CgDtr1 and CgTpo4. The deletion of each of these genes was found to lead to lower biofilm formation, in both SDB and RPMI media, while their expression was found to increase during biofilm development and to be controlled by the transcription factor CgTec1, a predicted key regulator of biofilm formation. Additionally, the deletion of *CgDTR1, CgTPO4*, or even *CgQDR2* was found to increase plasma membrane potential and lead to decreased expression of adhesin encoding genes, particularly *CgALS1* and *CgEPA1*, during biofilm formation. Although the exact role of these drug transporters in biofilm formation remains elusive, our current model suggests that their control over membrane potential by the transport of charged molecules, may affect the perception of nutrient availability, which in turn may delay the triggering of adhesion and biofilm formation.

Keywords: *Candida glabrata*, drug:H$^+$ antiporters, biofilm formation, CgTpo4, CgDtr1

INTRODUCTION

The human opportunistic pathogen, *Candida glabrata*, is responsible for an estimated death rate of 40–60% after invasive candidiasis (Ghazi et al., 2019). Being the second or third most common cause of this disease (Tscherner et al., 2011; Fuller et al., 2019; Mari et al., 2019), *C. glabrata* successfully infects and prevails in the human host thanks to its ability to adapt, resisting antifungal treatment and the host stressful environment (Pais et al., 2019), often by being able to form biofilms (Cavalheiro and Teixeira, 2018). In order to develop antifungal resistance, *C. glabrata* resorts to the activation of different multidrug efflux pumps of the ATP-binding cassette (ABC) transporter superfamily and the major facilitator superfamily (MFS) (Costa et al., 2014a; Cannon and Holmes, 2015). Although CgCdr1 ABC transporter appears to play a primordial role in azole resistant clinical isolates, the upregulation of some of the MFS drug transporters has also been correlated with at least clotrimazole resistance in clinical isolates (Costa et al., 2016). The activation of several

ABC transporters and MFS transporters is mostly due to the CgPdr1 transcription factor, regulator of multidrug resistance in *C. glabrata* (Costa et al., 2013b; Paul et al., 2014; Pais et al., 2016b; Whaley et al., 2018). This regulator may suffer gain-of-function (GOF) mutations that enhance the activation of such transporters (Moye-Rowley, 2019).

The ABC transporters have two transmembrane domains and two cytoplasmic nucleotide-binding domains, requiring energy from the hydrolysis of ATP, to cross substrates through the membrane. The ones with most dominant role in *C. glabrata* azole resistance are Cdr1, Cdr2, and Snq2 (Sanglard et al., 2009). While the role of ABC transporters has been well-characterized, only more recently MFS transporters have been studied with more detail. The MFS family is divided into two subgroups: Drug:H^+ antiporter 1 (DHA1) and 2 (DHA2) transporter subfamilies, compromising transporters with 12 and 14 transmembrane segments, respectively; both with predicted transporters in the genome of pathogenic fungi: *Candida albicans*, *C. glabrata*, *Cryptococcus neoformans*, and *Aspergillus fumigatus* (Costa et al., 2014a). DHA transporters have important roles in *Saccharomyces cerevisiae* drug resistance (Sá-Correia et al., 2008; Santos et al., 2014) and, as more recently unraveled, in *C. glabrata* (Costa et al., 2014a). In the case of this pathogenic yeast, evidence for a role in antifungal resistance was so far obtained for the DHA transporters: CgAqr1, CgQdr2, CgFlr1_1 and CgFlr1_2, CgTpo1_1, CgTpo1_2, and CgTpo3 (Costa et al., 2013a,b, 2014b; Pais et al., 2016a, 2019). CgAqr1 has been shown to have a role in the resistance to fluconazole and clotrimazole, while being also important in the resistance to acetic acid, which interacts synergistically with these antifungals (Costa et al., 2013a). CgQdr2 transporter confers resistance to miconazole, tioconazole, clotrimazole, and ketoconazole, its expression depending directly on the Pdr1 transcription factor. In addition, CgQdr2 was shown to complement the role of quinidine resistance of its homolog in *Saccharomyces cerevisiae* (Costa et al., 2013b). CgTpo3 is involved in azole resistance but is also important for *C. glabrata* resistance to spermine, complementing its homolog in *S. cerevisiae* (Costa et al., 2014b). Under the control of CgPdr1, but also of CgYap1, transcription factors, are the genes encoding CgFlr1 and CgFlr2, shown to have a role in azole and 5-flucytosine resistance (Pais et al., 2016b). CgTpo1_1 and CgTpo1_2 also contribute to the development of azole resistance (Pais et al., 2016a).

Surprisingly, some of the DHA transporters were additionally found to play important roles in *C. glabrata* virulence. For example, CgTpo1_1 confers resistance to antimicrobial peptides, like histatin-5, thus making *C. glabrata* cells more virulent in a *Galleria mellonella* infection model (Santos et al., 2017). CgTpo1_2 is necessary for the survival of *C. glabrata* upon phagocytosis, and its expression is upregulated upon biofilm formation, while its deletion decreases the expression of adhesin-encoding genes during biofilm formation (Santos et al., 2017). CgDtr1 MFS transporter is not involved in drug resistance, but instead is necessary for *C. glabrata*'s full virulence in the infection model *G. mellonella*. CgDtr1 has a role in the survival upon phagocytosis, being necessary for the resistance to oxidative and acetic acid stress (Romão et al., 2017). More recently, CgQdr2 was also identified as playing a role in biofilm formation, although the underlying mechanisms remained elusive (Widiasih Widiyanto et al., 2019). All the roles described for MFS transporters highlight their promiscuity in transporting many different substrates, which appear to ultimately lead to unexpected roles in processes, such as virulence, immune system evasion, or biofilm formation.

In this work, we screened all the *C. glabrata* DHA1 MFS transporters for a possible role in biofilm formation. Previously characterized CgAqr1, CgQdr2, CgTpo1_1, CgTpo1_2, CgTpo3, CgFlr1_1, CgFlr1_2, and CgDrt1 transporters were studied, as well as two other MFS transporters, CgTpo4 (*CAGL0L10912g*) and CgYhk8 (*CAGL0J00363g*), which had not yet been characterized. The possible involvement of an ortholog of CaTec1 transcription factor in *C. glabrata*, CgTec1 (*CAGL0M01716g*), in the regulation of the MFS transporters during biofilm formation was also assessed. The deletion of those MFS transporters was evaluated in terms of the effect on the expression of given adhesins and on the changes in plasma membrane potential.

RESULTS

Four, Out of the 10, Drug:H^+ Antiporters in *C. glabrata* Are Required for Biofilm Development

Given the previous implication of CgQdr2 and CgTpo1_2 in biofilm formation in *C. glabrata* (Santos et al., 2017; Widiasih Widiyanto et al., 2019), a systematic analysis of the possible involvement of all DHA1 transporters in this pathogenic yeast was carried out. The ability of the KUE100 wild-type strain and derived deletion mutants Δ*cgaqr1,* Δ*cgqdr2,* Δ*cgtpo1_1,* Δ*cgtpo1_2,* Δ*cgtpo3,* Δ*cgtpo4*, Δ*cgflr1_1,* Δ*cgflr1_2,* Δ*cgyhk8*, and Δ*cgdrt1* to form biofilms was assessed in SDB pH 5.6 and RPMI pH 4 media, on polystyrene, by the crystal-violet assay. Following previous studies (KucharíkovA et al., 2011; Gonçalves et al., 2016), RPMI medium was used at pH 4.0, given the acidic nature of some of the niches colonized by *Candida* species, as the vaginal tract (Owen and Katz, 1999; O'Hanlon et al., 2019). The deletion of *CgQDR2* and *CgTPO1_2* was confirmed to significantly decrease biofilm formation comparatively to the wild-type strain, in 30 and 40%, respectively, on both media, CgTpo1_2 playing a more prominent role (**Figures 1**, **2**). Additionally, the deletion of *CgTPO4* and *CgDTR1* was also found to significantly decrease the ability to form biofilms on SDB pH 5.6 medium, in around 30% each, when compared to the wild-type strain (**Figures 1**, **2**). The deletion of *CgFLR1_2*, *CgTPO1_1*, *CgTPO3*, and *CgYHK8* appears to lead to a slight increase in biofilm formation in RPMI medium, but this was not confirmed in SDB medium. Altogether, the obtained results expand current knowledge on the role for MFS transporters in biofilm formation, including two additional players in the process, CgTpo4 and CgDtr1.

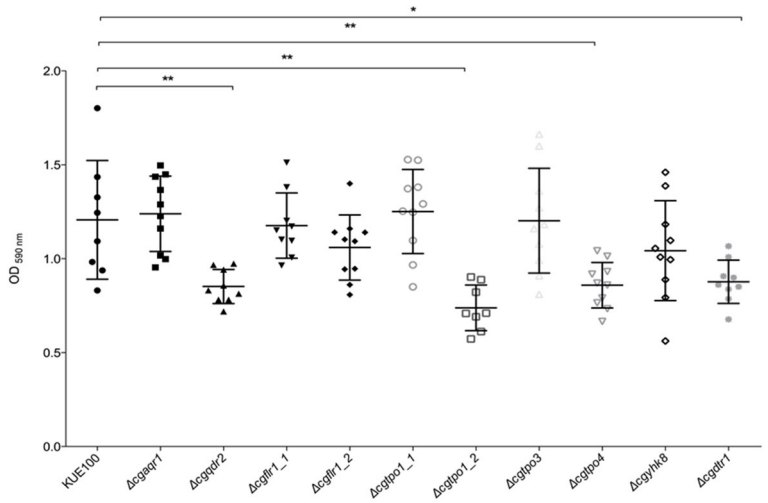

FIGURE 1 | CgQdr2, CgTpo1_2, CgTpo4, and CgDtr1 are necessary for *C. glabrata* biofilm formation on polystyrene, in SDB pH 5.6. Assessment of 24 h biofilm formation was performed by crystal-violet assay in microtiter plates of *C. glabrata* KUE100, Δ*cgaqr1,* Δ*cgqdr2,* Δ*cgflr1_1,* Δ*cgflr1_2,* Δ*cgtpo1_1,* Δ*cgtpo1_2,* Δ*cgtpo3,* Δ*cgtpo4,* Δ*cgyhk8*, and Δ*cgdtr1* strains grown in SDB medium, pH 5.6. The data is displayed in a scatter dot plot, where each dot represents the level of biofilm formed in a sample. Horizontal lines indicate the average levels from at least three independent experiments. Error bars indicate standard deviations. $^{*}P < 0.05$; $^{**}P < 0.01$.

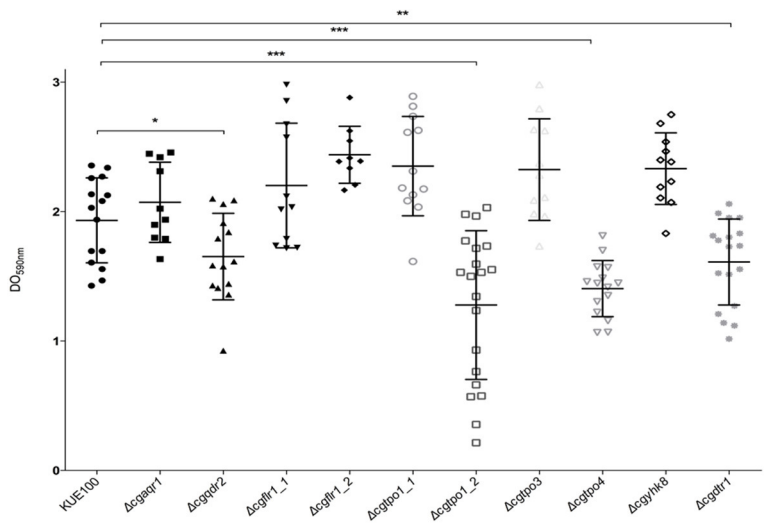

FIGURE 2 | CgQdr2, CgTpo1_2, CgTpo4, and CgDtr1 are necessary for *C. glabrata* biofilm formation on polystyrene, in RPMI pH 4. Assessment of 24 h biofilm formation was performed by crystal-violet assay in microtiter plates of *C. glabrata* KUE100, Δ*cgaqr1,* Δ*cgqdr2,* Δ*cgflr1_1,* Δ*cgflr1_2,* Δ*cgtpo1_1,* Δ*cgtpo1_2,* Δ*cgtpo3,* Δ*cgtpo4,* Δ*cgyhk8*, and Δ*cgdtr1* strains grown in RPMI pH 4. The data is displayed in a scatter dot plot, where each dot represents the level of biofilm formed in a sample. Horizontal lines indicate the average levels from at least three independent experiments. Error bars indicate standard deviations. $^{*}P < 0.05$; $^{**}P < 0.01$; $^{***}P < 0.001$.

CgTec1 Transcription Factor Controls the Expression of *CgQDR2*, *CgTPO4*, and *CgDRT1* Genes in Early Biofilm Formation

Although in *C. glabrata* very little is known about the regulation of biofilm formation, in *C. albicans* one of the major regulators of biofilm formation is CaTec1 transcription factor (Schweizer et al., 2000; Nobile et al., 2012; Daniels et al., 2015; Panariello et al., 2017). The deletion mutant of the predicted ortholog of CaTec1 in *C. glabrata*, encoded by ORF *CAGL0M01716g* and here named CgTec1, was used to assess its possible role controlling the expression of these MFS transporters during early (6 h) and mature (24 h) stages of biofilm formation. Although for the majority of *Candida* spp, 48 h are required to reach mature biofilms, *C. glabrata* biofilms are apparently at an intermediate maturation phase at 24 h of *in vitro* biofilm formation, where a confluent monolayer is already obvious, with the presence

of extracellular matrix (Kucharikova et al., 2014). Upon 24 h of biofilm formation, the expression of *CgQDR2*, *CgTPO1_2*, and *CgTPO4* genes is upregulated in the KUE100 wild-type strain, comparatively to 6 h of biofilm formation (**Figure 3**). Moreover, the deletion of *CgTEC1* gene, leads to a severe decrease in the expression of *CgQDR2*, *CgTPO4*, and *CgDRT1* at 6 h of biofilm formation, but not at 24 h (**Figure 3**). These results indicate that CgTec1 is required for the activation of *CgQDR2*, *CgTPO4*, and *CgDTR1* transcription in the early stages of biofilm formation. This suggests a specific window period in which these transporters act for the benefit of biofilm formation, the early stage of biofilm, under the control of the CgTec1 transcription factor.

The Transcript Levels of Adhesin Encoding Genes Are Repressed in Δ*cgqdr2,* Δ*cgtpo1_2,* Δ*cgtpo4*, and Δ*cgdrt1* Biofilms

Considering the importance of these MFS transporters on biofilm formation, their impact in the expression of a set of 5 adhesin encoding genes, *CgALS1*, *CgEAP1*, *CgEPA1*, *CgEPA6*, and *CgEPA7*, linked to adherence and biofilm formation (de Groot et al., 2013), was assessed. Gene expression was measured at 6 and 24 h of biofilm development in the KUE100 wild-type strain and in the Δ*cgqdr2,* Δ*cgtpo1_2,* Δ*cgtpo4*, and Δ*cgdrt1* deletion mutants (**Figure 4**). The relative expression of the genes in the wild-type strain KUE100 at 6 h of biofilm growth were used as a reference. The results regarding the expression of *CgEPA6* and *CgEPA7* are presented combined given that they share 92% homology and their transcript levels are indistinguishable.

The expression of all selected adhesin encoding genes is upregulated upon 24 h of wild-type strain biofilm formation comparatively to 6 h of biofilm formation. As described previously (Santos et al., 2017), upon the deletion of *CgTPO1_2*, the transcript levels of *CgALS1*, *CgEAP1*, and *CgEPA1* are decrease comparatively to the wild-type strain, in at least one of the time points (**Figures 4A,C,D**). In turn, deletion of *CgQDR2* gene leads to a repression of the expression of all adhesin-encoding genes at 6 h of biofilm formation (**Figures 4A–E**). *CgTPO4* deletion leads to the repression of *CgALS1*, *CgALS3*, and *CgEPA1* genes, at the same time point (**Figures 4A,B**), while the deletion of *CgDTR1* results in a decrease of expression of the *CgALS1*, *CgALS3*, *CgEAP1*, and *CgEPA1* (**Figures 4A,B,D**).

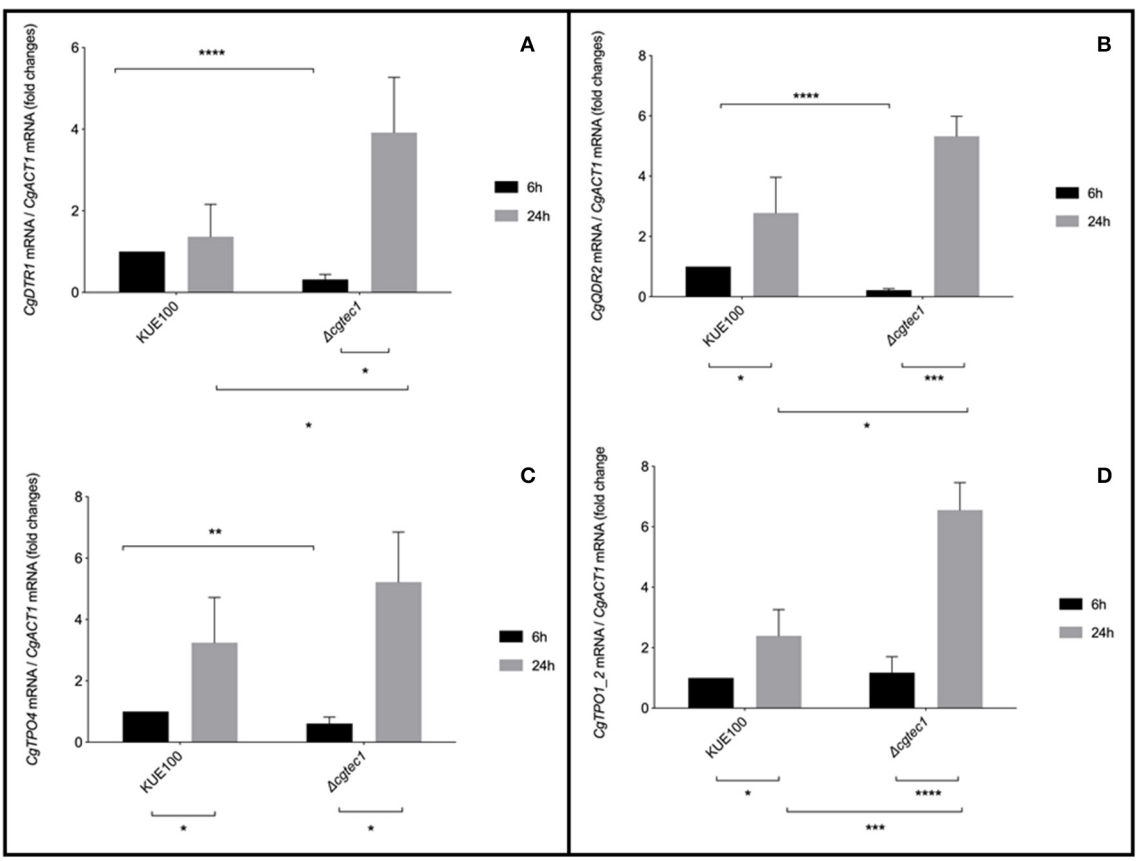

FIGURE 3 | *CgQDR2*, *CgTPO4*, and *CgDTR1* genes are regulated by CgTec1 transcription factor, upon early biofilm formation. Shown are the transcript levels of **(A)** *CgDTR1*, **(B)** *CgQDR2*, **(C)** *CgTPO4*, and **(D)** *CgTpo1_2* in the *C. glabrata* wild-type strain KUE100 and in the derived deletion mutant Δ*cgtec1,* in 6 and 24 h of biofilm formation conditions on polystyrene surface in liquid SDB medium, pH 5.6. Transcript levels were assessed by quantitative RT-PCR, as described in Materials and Methods. Values are averages of results from at least three independent experiments. Error bars represent standard deviations. **P* < 0.05; ***P* < 0.01, ****P* < 0.001; *****P* < 0.0001.

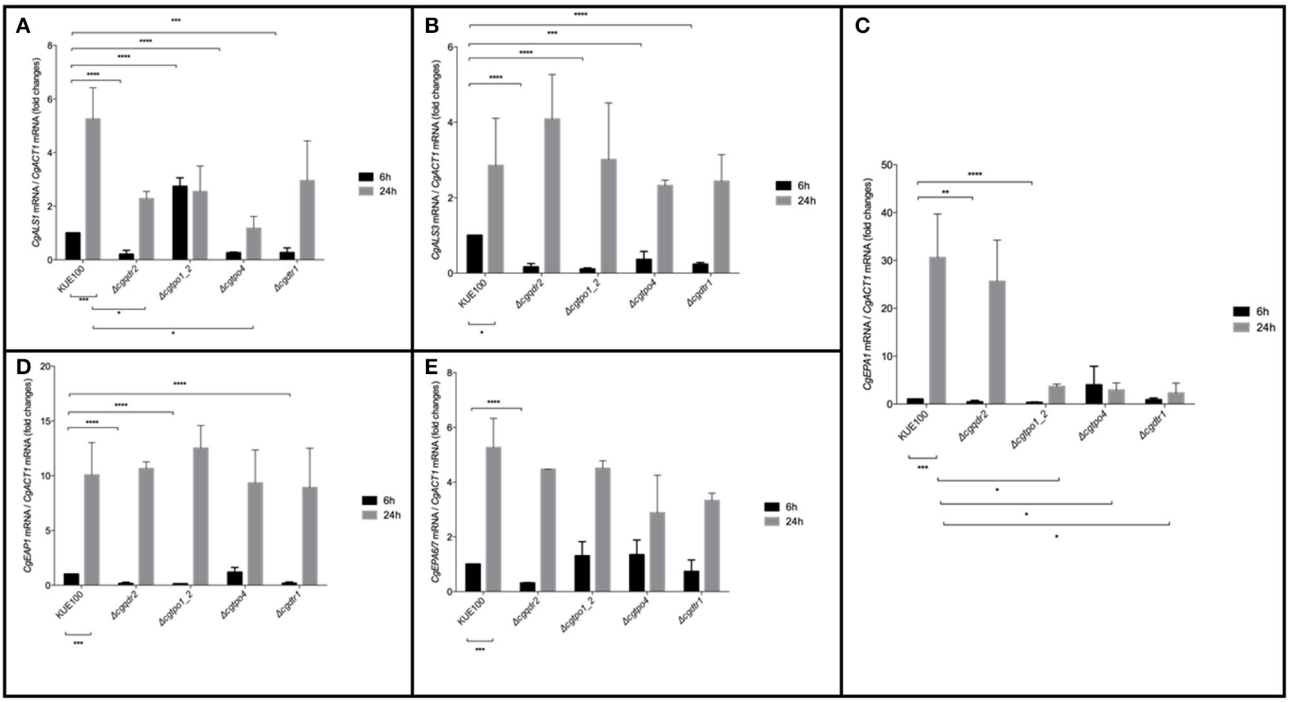

FIGURE 4 | Effect of *CgQDR2, CgTPO1_2, CgTPO4*, and *CgDTR1* gene deletion in the expression of adhesin encoding genes *CgALS1*, *CgEAP1*, *CgEPA1*, and *CgEPA6/7* during biofilm formation. Comparison of the variation of the *CgALS1* **(A)**, *CgALS3* **(B)**, *CgEPA1* **(C)**, *CgEAP1* **(D)**, and *CgEPA6/7* **(E)** transcript levels in KUE100 *C. glabrata* wild-type cells and Δ*cgqdr2,* Δ*cgtpo1_2,* Δ*cgtpo4*, and Δ*cgdrt1* mutant cells, after 6 h (black bars) or 24 h (gray bars) of biofilm development. The presented transcript levels were obtained by quantitative RT-PCR and are normalized to the *CgACT1* mRNA levels, relative to the values registered in wild-type cells after 6 h of biofilm development (6 h). The indicated values are averages of at least three independent experiments. Error bars represent the corresponding standard deviations. *$P < 0.05$; **$P < 0.01$; ***$P < 0.001$; ****$P < 0.0001$.

Such influence on the expression of different adhesin-encoding genes, especially upon 6 h of biofilm formation, indicates once again that CgQdr2, CgTpo1_2, CgTpo4, and CgDrt1 have an important role in the early stage of this process in *C. glabrata* and that they appear to act mostly by indirectly delaying adhesin gene up-regulation.

Membrane Potential Is Increased in the Absence of CgQdr2, CgTpo4, and CgDtr1

Given the clear influence of CgQdr2, CgTpo1_2, CgTpo4, and CgDtr1 in early biofilm formation, we further investigated how these transporters might be contributing for the initiation of this process. It has been described that the environment is a key factor that modulates the adherence and biofilm formation, especially in terms of the deficiency of certain nutrients (Verstrepen and Klis, 2006; Fisher et al., 2011; Riera et al., 2012). The plasma membrane potential directly affects the secondary transporters responsible for nutrient uptake, who have the membrane potential as a driving force. Therefore, changes in membrane potential are likely to affect cell proficiency in the uptake of given nutrients (Goossens et al., 2000), thus influencing the signaling leading to biofilm formation. Having this in mind, we assessed the effect of the absence of each of the genes in study in *C. glabrata* membrane potential. The plasma membrane potential of KUE100 wild-type strain and Δ*cgqdr2*, Δ*cgtpo1_2*, Δ*cgtpo4*, and Δ*cgdrt1* deletion mutant cells was monitored through the accumulation of the fluorescent dye DiOC6(3) (Cabrito et al., 2011). All deletion mutants were found to exhibit increased membrane potential comparatively to the wild-type strain (**Figure 5**), an effect already described for CgTpo1_2 (Santos et al., 2017). These results suggest that CgQdr2, CgTpo1_2, CgTpo4, and CgDtr1 are important for plasma membrane potential homeostasis, which is likely to affect the cellular perception of nutrient availability, a key step in the triggering of biofilm formation.

DISCUSSION

In this study, the previously characterized multidrug transporters CgAqr1, CgQdr2, CgTpo1_1, CgTpo1_2, CgTpo3, CgFlr1_1, CgFlr1_2, and CgDrt1 transporters, as well as two others, CgTpo4 and CgYhk8, all belonging to the DHA1 family, were screened for a possible role in biofilm formation. This systematic screening was driven by the observation that the majority of the MFS transporters characterized so far appear to transport additional substrates beyond drugs (Costa et al., 2013a,b, 2014b; Pais et al., 2016a, 2019), which affect *C. glabrata* pathogenesis and virulence (Romão et al., 2017; Santos et al., 2017).

Besides confirming the previously identified role of CgQdr2 (Widiasih Widiyanto et al., 2019) and CgTpo1_2 (Santos et al., 2017) in biofilm formation, two new DHA transporters were

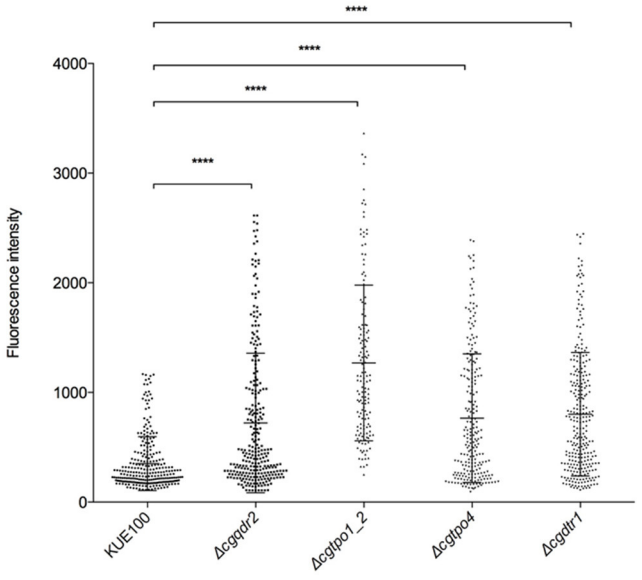

FIGURE 5 | The deletion of *CgQDR2, CgTPO1_2, CgTPO4*, and *CgDTR1* increases plasma membrane potential. *C. glabrata* wild-type KUE100 and derived Δ*cgqdr2,* Δ*cgtpo1_2,* Δ*cgtpo4*, and Δ*cgdrt1* mutant cells were grown to mid-exponential phase of growth in YEPD medium. These cells were incubated with the fluorescent dye DiOC6(3), whose uptake and accumulation depends on the plasma membrane potential, and fluorescence microscopy was used to measure the fluorescence intensity of individual cells. A scatter dot plot representation of the data is shown, where each dot represents the fluorescence intensity of each individual cell. The average level of fluorescence intensity, considering at least three independent experiments, and at least 100 cells per experiment, is indicated by the black line (–), standard deviation being represented by the error bars. ****$P < 0.0001$.

linked to this process: CgTpo4 and CgDtr1. This apparently widespread role of DHA transporters in biofilm formation is consistent with the previously described implication of the DHA transporters CaQdr1, CaQdr2, and CaQdr3 in biofilm formation in *C. albicans*. Deleting all *QDR* genes in *C. albicans* leads to clear defects in the architecture and thickness of the biofilm, which is suggested to be related to the remodeling of lipids *C. albicans* cells suffer upon the loss of such genes (Shah et al., 2014). The role of CgTpo1_2 in biofilm formation was also linked with its effect in ergosterol and fatty acid content, but mostly through its influencing over plasma membrane potential (Santos et al., 2017). Interestingly, CgQdr2, CgTpo4, and CgDtr1 were also found in this study to affect the membrane potential. The alteration of plasma membrane potential by DHA transporters may be related to their role in the transport of small charged molecules, including cations and polycations (Vargas et al., 2007). In *Saccharomyces cerevisiae*, MFS transporters are known to be involved in this type of transport. For instance, ScQdr2 is involved in K^+ import (Vargas et al., 2007) and ScTpo1-4 (Tomitori et al., 2001) and ScQdr3 (Teixeira et al., 2011) are implicated in the export of polyamines. Given that increased plasma membrane potential is implicated in higher secondary transport activity (Eddy and Hopkins, 1998), nutrient uptake capacity may be modified upon the absence of each transporter. This may possibly affect biofilm formation as has been described for bacterial MFS transporters. Indeed, bacterial biofilms are influenced by the nutrients in the environment, given that the uptake of given nutrients acts as a positive or negative signal for the initiation of this process. Therefore, a key role in biofilm formation was identified for bacterial MFS transporters, responsible for nutrient uptake (Pasqua et al., 2019). It is, thus, likely that the same phenomenon may also occur in yeast biofilms.

Given that these transporters have a clear effect on the plasma membrane, we hypothesized if they might influence the presence of given proteins on the plasma membrane and cell wall, involved on biofilm formation. With this in mind, we assessed the expression of adhesin-encoding genes upon the deletion of *CgQDR2, CgTPO1_2, CgTPO4*, and *CgDTR1* genes, in biofilm conditions. *CgALS1* and *CgEPA1* expression was found to be decrease upon the absence of all transporters, for at least one of the time points tested (6 and 24 h). In addition, more adhesins were found to be repressed upon the specific absence of each transporter, highlighting the clear influence MFS transporters have on the presence of adhesins in the cell envelop. It is possible that the absence of these MFS transporters alters the perception of nutrient availability, delaying the activation of adhesin-encoding genes, and ultimately leading to defects on the capacity of *C. glabrata* to adhere and form biofilms.

Interestingly, in *C. albicans*, MFS transporters, CaMdr1 and CaQdr1, have also been linked to biofilm formation and cell dispersion, being up-regulated in both conditions. It is suggested in the work of Uppuluri et al. (2018) that the upregulation of these and other types of transporters is related to the reprogramming of dispersal cells to acquire nutrients and be able to attach and survive in nutrient-starved niches of the host (Uppuluri et al., 2018). It would be interesting to test if CgQdr2, CgTpo1_2, CgTpo4, and CgDtr1 have a role on this last phase of biofilm formation. Nevertheless, our results suggest that their activation is more significant in early stages of biofilm formation than the later.

Although the specific role of these transporters may not yet be clear, *CgQDR2*, *CgTPO4*, and *CgDTR1* genes were found to be activated by the CgTec1 transcription factor in early stages of biofilm formation. CgTec1 has not yet been characterized in *C. glabrata* but it seems to be involved on the regulation of biofilm in this yeast, like its ortholog's role in the regulation of the same process in *C. albicans*. CaTec1 has a minor role in adhesion but is required for the formation of the several layers of cells and hyphal formation, and influences the thickness and integrity of the biofilm (Schweizer et al., 2000; Daniels et al., 2015). CaTec1 is also necessary for the full virulence of *C. albicans* (Yano et al., 2016). It is possible that the CgTec1 transcription factor in *C. glabrata* may have important roles as is ortholog, starting by the control of these transporters at the beginning of biofilm formation.

Based on these results our current model is that the deletion of *CgQDR2, CgTPO1_2, CgTPO4*, and *CgDTR1* genes leads to an increase in plasma membrane potential, which possible affects nutrient uptake, influencing the signaling that triggers cellular adhesion, eventually compromising *C. glabrata* biofilm

formation. Moreover, CgQdr2, CgTpo4, and CgDtr1 expression appears to be controlled by one of the predicted regulators of biofilm formation, CgTec1, highlighting their role in the process. Altogether, DHA transporters appear to be in the crossroad between drug resistance, biofilm formation as well as additional pathogenesis traits (Cavalheiro et al., 2018), highlighting their potential impact in the success of *C. glabrata* infections and in the design of novel antifungal therapeutic approaches.

MATERIALS AND METHODS

Strains, Plasmids, and Growth Medium

Candida glabrata KUE100 (Ueno et al., 2007) strain was used in this study. The *Candida glabrata* Δ*cgtpo1_1*, Δ*cgtpo1_2,* Δ*cgaqr1,* Δ*cgqdr2,* Δ*cgflr1_1,* Δ*flr1_2,* Δ*cgtpo3*, and Δ*cgdrt1* deletion mutants, constructed in previous studies (Costa et al., 2013a,b, 2014b; Pais et al., 2016a; Romão et al., 2017), were also used. Δ*cgtec1*, Δ*cgtpo4*, and Δ*cgyhk8* deletion mutants were constructed as described in the next section.

Candida glabrata cells were cultivated in rich YEPD medium, containing per liter: 20 g D-(+)- glucose (Merk, Darmstadt), 20 g bacterial-peptone (LioChem, Conyers, Georgia) and 10 g of yeast-extract (Difco, Detroit, Michigan). Sabouraud's Dextrose Broth (SDB) pH 5.6, used for *C. glabrata* planktonic and biofilm cultivation, contains 40 g glucose (Merk, Darmstadt) and 10 g peptone (LioChem, Conyers, Georgia) per liter. RPMI 1640 medium pH 4, used for *C. glabrata* planktonic and biofilm cultivation, contains 10,4 g RPMI 1640 (Sigma, Darmstadt), 34,5 g MOPS (Sigma, Darmstadt) and 18 g glucose (Merck, Darmstadt) per liter.

Disruption of the *C. glabrata CgTPO4*, *CgYHK8*, and *CgTEC1* Genes (ORF *CAGL0L10912g CAGL0J00363g* and *CAGL0M01716g*)

The deletion of the *CgTPO4, CgYHK8*, and *CgTEC1* genes was carried out in the parental strain KUE100, using the method described by Ueno et al. (2007). The target genes were replaced by a DNA cassette including the *CgHIS3* gene, through homologous recombination. The DNA cassette was amplified with PCR for which gene disruption primers (**Table 1**) including homologous sequences at 5′ end and as a template the pHIS906 plasmid including CgHIS3 were used. Transformation was performed with the DNA cassette as described previously (Ueno et al., 2007). Recombination locus and gene deletion were verified by PCR using the primers indicated in **Table 1**.

TABLE 1 | List of primers used in this study.

Name	Sequence (5′-3′)
***CgTPO4*, *CgYHK8* gene disruption**	
Δ*CgTPO4_Fw*	GAACTGGTGAAATATAGTATAAGCGTTACAAAGCGAA TAACGAATACATACACCACGGCCGCTGATCACG
Δ*CgTPO4_Rv*	AAGAGCAAAAGTATTCAATTTTTTAAAAATTTAAAGCAA ATCGAAAAAAAGGACTACATCGTGAGGCTGG
Δ*CgYHK8_Fw*	TTGCTCGACTTCTATATCTTACACTATTACACAACCAA AATCAGCAACAATAGAAAGGCCGCTGATCACG
Δ*CgYHK8_Rv*	CTAAAAAAAGATCAAATGGTTCGTGCTGCTGTTATATT CAGGGATAAGGCAGATTACATCGTGAGGCTGG
Δ*CgTEC1_Fw*	AAGAGTACTAATACACATCGTACTCCCCCCCACAAAT AACGCCCTCAATCTATATTGGCCGCTGATCACG
Δ*CgTEC1_Rv*	TCAGCAAAACATTTCTGCAGAAAAAATAAAAATGTAGC ATTCCTACATCTCTCTCACATCGTGAGGCTGG
Gene disruption confirmation	
Δ*CgTPO4_Fw_conf*	CAAGTTGGTGATACTAATAGCA
Δ*CgTPO4_Rv_conf*	CACTTCACTCAAGGGAGC
Δ*CgYHK8_Fw_conf*	GATGAAGGACTCAGATTCG
Δ*CgYHK8_Rv_conf*	CCAGGTTGTCAGGCATTG
Δ*CgTEC1_Fw_conf*	GACAGCTCGGTATCAGATAGGT
Δ*CgTEC1_Rv_conf*	GTGGAGATGATGCTTTCGAAGA
RT-PCR experiments	
CgACT1_Fw	AGAGCCGTCTTCCCTTCCAT
CgACT1_Rv	TTGACCCATACCGACCATGA
CgALS1Fw	GAG CTC AAT GCA GAA GTG TAC TTT G
CgALS1_Rv	GAT CTG ATT GTG GTA TAA AAG TGG TCA T
CgALS3_Fw	GTTGACCCATTTCGTGGAAAA
CgALS3_Rv	GAAGGCCATAATTTCACAGTCAGA
CgEPA1_Fw	TTG ATT GCT GCA GAA GGG ATT
CgEPA1_Rv	ATG GCG TAG GCT TGA TAA TTT CC
CgEAP1_Fw	CAA CAC CAG CCC AAT CAA ATG
CgEAP1_Rv	CGG AAG ACA TCG TTA ATG AAG GA
CgEPA6/7_Fw	TTC CCT TCG CAA CTT ACA CAA CT
CgEPA6/7_Rv	GAA GCA CTC CCA CTG CTA GAG TAA
CgTPO1_2_Fw	AGGACCCGCTCTATCGAAAAA
CgTPO1_2_Rv	GCTGCGACTGCTGACTCAAC
CgTPO4_Fw	TCGTTGGCCCATTTTTGG
CgTPO4_Rv	GCAAACCCGCGATGA
CgDTR1_Fw	GGAGCCAAAATGAGAATGATATGTC
CgDTR1_Rv	ACCACCTTGAAATCGGTGATG
CgQDR2_Fw	TCACTGCATAGTTTCATATCGGACTA
CgQDR2_Rv	CAACTTCAGATAGATCAGGACCATCA

Biofilm Quantification

Candida glabrata strains were tested for their capacity for biofilm formation, recurring to the crystal-violet method (Pathak et al., 2012). For that, the *Candida glabrata* strains were grown in SDB medium and harvested by centrifugation at mid-exponential phase. The cells were inoculated with an initial OD_{600nm} = 0,05 ± 0,005—corresponding to 5 × 10^5 CFU/ml—in 96-well polystyrene microtiter plates (Greiner) in either SDB (pH 5.6) or RPMI (pH 4) media. Cells were cultivated at 30°C during 15 ± 0,5 h with mild orbital shaking (70 rpm), as before (Melo et al., 2006; Pathak et al., 2012; Santos et al., 2017; Cavalheiro et al., 2019). After the incubation time, each well was washed three times with 200 μL of deionized water to remove cells not attached to the biofilm matrix. Then, 200 μL of a 1% crystal-violet (Merck, Darmstadt) alcoholic solution was used to stain the biofilm present in each well. Following 15 min of incubation with the dye, each well was washed with 250 μL of deionized water. The stained biofilm was eluted in 200 μL 96% (v/v) ethanol and the absorbance of each well was read in a microplate

reader at the wavelength of 590 nm (SPECTROstar Nano, BMG Labtech, Ortenberg).

Gene Expression Measurement

The transcript levels of *CgTPO1_2, CgTPO4, CgQDR2*, and *CgDTR1*, and of the adhesin encoding genes *CgALS1*, *CgEAP1*, *CgEPA1*, *CgEPA6*, and *CgEPA7* were determined by quantitative real-time PCR (RT-PCR). Total RNA was extracted from cells grown in biofilm. 40 mL of fresh RPMI 1640 (pH 4) was placed in square polystyrene petri plates (Greiner), and cells were added so that the initial $OD_{600nm} = 0.05 \pm 0{,}005$. The plates were incubated at 30°C and 30 rpm during 6 and 24 h to analyse both young and mature biofilm development for each strain under analysis. A lower agitation speed was used in this case to prevent spilling of part of the culture. It does not compromise aeration, as the surface area of the used petri dishes is much higher than that in microtiter plates. At the end of each period the supernatant was discarded, and the biofilm was removed with a metal spatula. Samples were centrifuged to remove excess water and frozen at −80°C until RNA extraction. Planktonic growing cells, used as control, were cultivated in RPMI 1640 (pH 4) with orbital shaking (250 rpm) at 30°C and harvested by centrifugation at comparable times.

For total RNA extraction, the hot phenol method was applied (Köhrer and Domdey, 1991). Total RNA was converted to cDNA for the real-time Reverse-Transcription PCR (RT-PCR) using the MultiScribe Reverse Transcriptase kit (Applied Biosystems, Foster City, California) and the 7500 RT-PCR thermal cycler block (Applied Biosystems, Foster City, California). The quantity of cDNA for subsequent reactions was kept at ca. 10 ng. The real time PCR step was carried out using adequate primers (**Table 1**) designed by the Primer Express™ Software v3.0.1, SYBR Green® reagents (Applied Biosystems, Foster City, California) and the 7500 RT-PCR thermocycler block (Applied Biosystems, Foster City, California). Default parameters set by the manufacturer were followed, and fluorescence was detected by the instrument and plotted in an amplification graph (7500 Systems SDS Software, Applied Biosystems, Foster City, California). *CgACT1* gene transcript level was used as an internal reference.

Estimation of Plasma Membrane Potential

The estimation of the plasma membrane potential was carried out by measuring the fluorescence intensity of cells exposed to the fluorescent carbocyanine 3,3′-Dihexyloxacarbocyanine Iodide [DiOC6(3)] (Cabrito et al., 2011). Cells were cultivated in SDB media until mid-exponential phase, washed twice in Mes/glucose buffer [10 mM Mes, 0.1 mM $MgCl_2$ and 20 g/l glucose (pH 5,6)] and resuspended in Mes/glucose buffer, supplemented with 250 nM DiOC6(3) (Molecular Probes, Eugene, Oregon), followed by incubation in the dark for 30 min at 30°C with orbital agitation (250 rpm). After centrifugation cells were observed with a Zeiss Axioplan microscope equipped with adequate epifluorescence filters (BP450-490 and LP520). Fluorescence emission was collected with a CCD (charge-coupled device) camera (CoolSNAPFX, Roper Scientific Photometrics, Tucson, Arizona). For the excitation of the fluorescent molecule, radiation with a wavelength of 480 nm was used. The images were analyzed using MetaMorph 3.5. The fluorescence intensity values, obtained pixel-by-pixel in the region of interest, were calculated for a minimum of 100 cells per experiment, considering a minimum of 3 independent experiments, per strain.

Statistical Analysis

Statistical analysis was performed using Graphpad Prism Software version 6.0 and analyzed with Student's *t*-test. *P*-values equal or inferior to 0.05 were considered statistically significant.

DATA AVAILABILITY STATEMENT

All datasets generated for this study are included in the article/supplementary material.

AUTHOR CONTRIBUTIONS

RS, MC, and CC conducted most of the experiments. AT-N and MO played a key role in strain design and construction. MC, RS, and MT wrote the paper. HC and MT conceived and supervised all the work.

FUNDING

This work was supported by FEDER and the Fundação para a Ciência e a Tecnologia (FCT) (contract PTDC/BII-BIO/28216/2017) and by Ph.D. grant to MT (PD/BD/116946/2016). Funding received from FCT (grant UIDB/04565/2020) is acknowledged.

REFERENCES

Cabrito, T. R., Teixeira, M. C., Singh, A., Prasad, R., and Sá-Correia, I. (2011). The yeast ABC transporter Pdr18 (ORF *YNR070w*) controls plasma membrane sterol composition, playing a role in multidrug resistance. *Biochem. J.* 440, 195–202. doi: 10.1042/BJ20110876

Cannon, R. D., and Holmes, A. R. (2015). Learning the ABC of oral fungal drug resistance. *Mol. Oral Microbiol.* 30, 425–437. doi: 10.1111/omi.12109

Cavalheiro, M., Costa, C., Silva-Dias, A., Miranda, I. M., Wang, C., Pais, P., et al. (2019). A transcriptomics approach to unveiling the mechanisms of *in vitro* evolution towards fluconazole resistance of a *Candida glabrata* clinical isolate. *Antimicrob. Agents Chemother.* 63, 1–17. doi: 10.1128/AAC.00995-18

Cavalheiro, M., Pais, P., Galocha, M., and Teixeira, M. C. (2018). Host-pathogen interactions mediated by MDR transporters in fungi: as pleiotropic as it gets! *Genes* 9:332. doi: 10.3390/genes9070332

Cavalheiro, M., and Teixeira, M. C. (2018). *Candida* biofilms: threats, challenges, and promising strategies. *Front. Med.* 5:28. doi: 10.3389/fmed.2018.00028

Costa, C., Dias, P. J., Sá-Correia, I., and Teixeira, M. C. (2014a). MFS multidrug transporters in pathogenic fungi: do they have real clinical impact? *Front. Physiol.* 5:197. doi: 10.3389/fphys.2014.00197

Costa, C., Henriques, A., Pires, C., Nunes, J., Ohno, M., Chibana, H., et al. (2013a). The dual role of *Candida glabrata* drug:H+ antiporter CgAqr1 (ORF CAGL0J09944g) in antifungal drug and acetic acid resistance. *Front. Microbiol.* 4:170. doi: 10.3389/fmicb.2013.00170

Costa, C., Nunes, J., Henriques, A., Mira, N. P., Nakayama, H., Chibana, H., et al. (2014b). *Candida glabrata* drug:H+ antiporter CgTpo3 (ORF CAGL0I10384g): role in azole drug resistance and polyamine homeostasis. *J. Antimicrob. Chemother.* 69, 1767–1776. doi: 10.1093/jac/dku044

Costa, C., Pires, C., Cabrito, T. R., Renaudin, A., Ohno, M., Chibana, H., et al. (2013b). *Candida glabrata* drug: H+ antiporter CgQdr2 confers imidazole drug resistance, being activated by transcription factor CgPdr1. *Antimicrob. Agents Chemother.* 57, 3159–3167. doi: 10.1128/AAC.00811-12

Costa, C., Ribeiro, J., Miranda, I. M., Silva-dias, A. I., Cavalheiro, M., Costa-de-oliveira, S., et al. (2016). Clotrimazole drug resistance in *Candida glabrata* clinical isolates correlates with increased expression of the drug:H+ antiporters CgAqr1, CgTpo1_1, CgTpo3 and CgQdr2. *Front. Microbiol.* 7:526. doi: 10.3389/fmicb.2016.00526

Daniels, K. J., Srikantha, T., Pujol, C., Park, Y. N., and Soll, D. R. (2015). Role of Tec1 in the development, architecture, and integrity of sexual biofilms of *Candida albicans*. *Eukaryotic Cell* 14, 228–240. doi: 10.1128/EC.00224-14

de Groot, P. W. J., Bader, O., de Boer, A. D., Weig, M., and Chauhan, N. (2013). Adhesins in human fungal pathogens: glue with plenty of stick. *Eukaryotic Cell* 12, 470–481. doi: 10.1128/EC.00364-12

Eddy, A. A., and Hopkins, P. (1998). Proton stoichiometry of the overexpressed uracil symport of the yeast *Saccharomyces cerevisiae*. *Biochem. J.* 336, 125–130. doi: 10.1042/bj3360125

Fisher, J. F., Kavanagh, K., Sobel, J. D., Kauffman, C. A., and Newman, C. (2011). Candida urinary tract infection: pathogenesis. *Clin. Infect. Dis.* 52, 437–451. doi: 10.1093/cid/cir110

Fuller, J., Dingle, T. C., Bull, A., Shokoples, S., Laverdière, M., Baxter, M. R., et al. (2019). Species distribution and antifungal susceptibility of invasive *Candida* isolates from Canadian hospitals: results of the CANWARD 2011–16 study. *J. Antimicrob. Chemother.* 74, iv48–iv54. doi: 10.1093/jac/dkz287

Ghazi, S., Rafei, R., Osman, M., El Safadi, D., Mallat, H., Papon, N., et al. (2019). The epidemiology of *Candida* species in the middle east and north Africa. *J. Mycol. Med.* 29, 245–252. doi: 10.1016/j.mycmed.2019.07.006

Gonçalves, B., Ferreira, C., Alves, C. T., Henriques, M., Azeredo, J., and Silva, S. (2016). Vulvovaginal candidiasis: epidemiology, microbiology and risk factors. *Crit. Rev. Microbiol.* 42, 905–927. doi: 10.3109/1040841X.2015.1091805

Goossens, A., de La Fuente, N., Forment, J., Serrano, R., and Portillo, F. (2000). Regulation of yeast H(+)-ATPase by protein kinases belonging to a family dedicated to activation of plasma membrane transporters. *Mol. Cell. Biol.* 20, 7654–7661. doi: 10.1128/MCB.20.20.7654-7661.2000

Köhrer, K., and Domdey, H. (1991). Preparation of high molecular weight RNA. *Meth. Enzymol.* 194, 398–405. doi: 10.1016/0076-6879(91)94030-G

Kucharikova, S., Neirinck, B., Sharma, N., Vleugels, J., Lagrou, K., Van Dijck, P., et al. (2014). *In vivo Candida glabrata* biofilm development on foreign bodies in a rat subcutaneous model. *J. Antimicrob. Chemother.* 70, 846–856. doi: 10.1093/jac/dku447

KucharíkovA, S., Tournu, H., Lagrou, K., van Dijck, P., and Bujdáková, H. (2011). Detailed comparison of *Candida albicans* and *Candida glabrata* biofilms under different conditions and their susceptibility to caspofungin and anidulafungin. *J. Med. Microbiol.* 60, 1261–1269. doi: 10.1099/jmm.0.032037-0

Mari, A.-H., Valkonen, M., Kolho, E., Friberg, N., and Anttila, V.-J. (2019). Clinical and microbiological factors associated with mortality in candidemia in adult patients 2007–2016. *Infect. Dis.* 51, 824_830. doi: 10.1080/23744235.2019.1662941

Melo, A. S. A., Padovan, A. C. B., Serafim, R. C., Puzer, L., Carmona, A. K., Juliano Neto, L., et al. (2006). The *Candida albicans* AAA ATPase homologue of *Saccharomyces cerevisiae* Rix7p (YLL034c) is essential for proper morphology, biofilm formation and activity of secreted aspartyl proteinases. *Genet. Mol. Res.* 5, 664–687.

Moye-Rowley, W. S. (2019). Multiple interfaces control activity of the *Candida glabrata* Pdr1 transcription factor mediating azole drug resistance. *Curr. Genet.* 65, 103–108. doi: 10.1007/s00294-018-0870-4

Nobile, C. J., Fox, E. P., Nett, J. E., Sorrells, T. R., Mitrovich, Q. M., Hernday, A. D., et al. (2012). A recently evolved transcriptional network controls biofilm development in *Candida albicans*. *Cell* 148, 126–138. doi: 10.1016/j.cell.2011.10.048

O'Hanlon, D. E., Come, R. A., and Moench, T. R. (2019). Vaginal pH measured *in vivo*: lactobacilli determine pH and lactic acid concentration. *BMC Microbiol.* 19:8. doi: 10.1186/s12866-019-1388-8

Owen, D. H., and Katz, D. F. (1999). A vaginal fluid simulant. *Contraception* 59, 91–95. doi: 10.1016/S0010-7824(99)00010-4

Pais, P., Costa, C., Pires, C., Shimizu, K., Chibana, H., and Teixeira, M. C. (2016a). Membrane proteome-wide response to the antifungal drug clotrimazole in *Candida glabrata*: role of the transcription factor CgPdr1 and the drug:H+ antiporters CgTpo1_1 and CgTpo1_2. *Mol. Cell. Proteomics* 15, 57–72. doi: 10.1074/mcp.M114.045344

Pais, P., Galocha, M., and Teixeira, M. C. (2019). Genome-wide response to drugs and stress in the pathogenic yeast candida glabrata. *Prog. Mol. Subcell. Biol.* 58, 155–193. doi: 10.1007/978-3-030-13035-0_7

Pais, P., Pires, C., Costa, C., Okamoto, M., Chibana, H., and Teixeira, M. C. (2016b). Membrane proteomics analysis of the *Candida glabrata* response to 5-flucytosine: unveiling the role and regulation of the drug efflux transporters CgFlr1 and CgFlr2. *Front. Microbiol.* 7:2045. doi: 10.3389/fmicb.2016.02045

Panariello, B. H. D., Klein, M. I., Pavarina, A. C., and Duarte, S. (2017). Inactivation of genes *TEC1* and *EFG1* in *Candida albicans* influences extracellular matrix composition and biofilm morphology. *J. Oral Microbiol.* 9, 1–11. doi: 10.1080/20002297.2017.1385372

Pasqua, M., Grossi, M., Zennaro, A., Fanelli, G., Micheli, G., Barras, F., et al. (2019). The varied role of efflux pumps of the MFS family in the interplay of bacteria with animal and plant cells. *Microorganisms* 7, 1–21. doi: 10.3390/microorganisms7090285

Pathak, A. K., Sharma, S., and Shrivastva, P. (2012). Multi-species biofilm of *Candida albicans* and non-*Candida albicans Candida* species on acrylic substrate. *J. Appl. Oral Sci.* 20, 70–75. doi: 10.1590/S1678-77572012000100013

Paul, S., Bair, T. B., and Moye-Rowley, W. S. (2014). Identification of genomic binding sites for *Candida glabrata* Pdr1 transcription factor in wild-type and ρ 0 cells. *Antimicrob. Agents Chemother.* 58, 6904–6912. doi: 10.1128/AAC.03921-14

Riera, M., Mogensen, E., D'Enfert, C., and Janbon, G. (2012). New regulators of biofilm development in Candida glabrata. *Res. Microbiol.* 163, 297–307. doi: 10.1016/j.resmic.2012.02.005

Romão, D., Cavalheiro, M., Mil-Homens, D., Santos, R., Pais, P., Costa, C., et al. (2017). A new determinant of *Candida glabrata* virulence: the acetate exporter CgDtr1. *Front. Cell. Infect. Microbiol.* 7:473. doi: 10.3389/fcimb.2017.00473

Sá-Correia, I., dos Santos, S. C., Teixeira, M. C., Cabrito, T. R., and Mira, N. P. (2008). Drug:H+ antiporters in chemical stress response in yeast. *Trends Microbiol.* 17, 22–31. doi: 10.1016/j.tim.2008.09.007

Sanglard, D., Coste, A., and Ferrari, S. (2009). Antifungal drug resistance mechanisms in fungal pathogens from the perspective of transcriptional gene regulation. *FEMS Yeast Res.* 9, 1029–1050. doi: 10.1111/j.1567-1364.2009.00578.x

Santos, R., Costa, C., Mil-Homens, D., Romão, D., de Carvalho, C. C. C. R., Pais, P., et al. (2017). The multidrug resistance transporters CgTpo1 _ 1 and CgTpo1 _ 2 play a role in virulence and biofilm formation in the human pathogen *Candida glabrata*. *Cell. Microbiol.* 19, 1–13. doi: 10.1111/cmi.12686

Santos, S. C., Teixeira, M. C., Dias, P. J., and Sá-correia, I. (2014). MFS transporters required for multidrug/multixenobiotic (MD/MX) resistance in the model yeast: understanding their physiological function through post-genomic approaches. *Front. Physiol.* 5:180. doi: 10.3389/fphys.2014.00180

Schweizer, A., Rupp, S., Taylor, B. N., Rollinghoff, M., Schroppel, K., Röllinghoff, M., et al. (2000). The TEA/ATTS transcription factor CaTec1p regulates hyphal development and virulence in *Candida albicans*. *Mol. Microbiol.* 38, 2–12. doi: 10.1046/j.1365-2958.2000.02132.x

Shah, A. H., Singh, A., Dhamgaye, S., Chauhan, N., Vandeputte, P., Suneetha, K. J., et al. (2014). Novel role of a family of major facilitator transporters in biofilm development and virulence of *Candida albicans*. *Biochem. J.* 460, 223–235. doi: 10.1042/BJ20140010

Teixeira, M. C., Cabrito, R., Hanif, Z. M., Vargas, R. C., Tenreiro, S., and Sá-Correia, I. (2011). Yeast response and tolerance to polyamine toxicity involving the drug: H+ antiporter Qdr3 and the transcription factors Yap1 and Gcn4. *Microbiology* 157, 945–956. doi: 10.1099/mic.0.043661-0

Tomitori, H., Kashiwagi, K., Asakawa, T., Kakinuma, Y., Michael, A. J., and Igarashi, K. (2001). Multiple polyamine transport systems on the vacuolar membrane in yeast. *Biochem. J.* 353, 681–688. doi: 10.1042/bj3530681

Tscherner, M., Schwarzmüller, T., and Kuchler, K. (2011). Pathogenesis and antifungal drug resistance of the human fungal pathogen *Candida glabrata*. *Pharmaceuticals* 4, 169–186. doi: 10.3390/ph4010169

Ueno, K., Uno, J., Nakayama, H., Sasamoto, K., Mikami, Y., and Chibana, H. (2007). Development of a highly efficient gene targeting system induced by transient repression of YKU80 expression in *Candida glabrata*. *Eukaryotic Cell* 6, 1239–1247. doi: 10.1128/EC.00414-06

Uppuluri, P., Zaldívar, A., Anderson, M. Z., Dunn, M. J., Berman, J., Ribot, J. L. L., et al. (2018). *Candida albicans* dispersed cells are developmentally distinct from biofilm and planktonic cells. *mBio* 9, 1–16. doi: 10.1128/mBio.01338-18

Vargas, R. C., García-Salcedo, R., Tenreiro, S., Teixeira, M. C., Fernandes, A. R., Ramos, J., et al. (2007). Saccharomyces cerevisiae multidrug resistance transporter Qdr2 is implicated in potassium uptake, providing a physiological advantage to quinidine-stressed cells. *Eukaryotic Cell* 6, 134–142. doi: 10.1128/EC.00290-06

Verstrepen, K. J., and Klis, F. M. (2006). Flocculation, adhesion and biofilm formation in yeasts. *Mol. Microbiol*. 60, 5–15. doi: 10.1111/j.1365-2958.2006.05072.x

Whaley, S. G., Zhang, Q., Caudle, K. E., and Rogers, P. D. (2018). Relative contribution of the ABC transporters Cdr1, Pdh1, and Snq2 to azole resistance in *Candida glabrata*. *Antimicrob. Agents Chemother*. 62, e01070– e01118. doi: 10.1128/AAC.01070-18

Widiasih Widiyanto, T., Chen, X., Iwatani, S., Chibana, H., and Kajiwara, S. (2019). Role of major facilitator superfamily transporter Qdr2p in biofilm formation by *Candida glabrata*. *Mycoses* 62, 1154–1163. doi: 10.1111/myc.13005

Yano, J., Yu, A., Fidel, P. L. Jr., and Noverr, M. C. (2016). Transcription factors Efg1 and Bcr1 regulate biofilm formation and virulence during *Candida albicans*-associated denture stomatitis. *PLoS ONE* 11:e0159692. doi: 10.1371/journal.pone.0159692

Conflict of Interest: The authors declare that the research was conducted in the absence of any commercial or financial relationships that could be construed as a potential conflict of interest.

frontiers in Microbiology

ORIGINAL RESEARCH
published: 21 February 2020
doi: 10.3389/fmicb.2020.00213

SPT20 Regulates the Hog1-MAPK Pathway and Is Involved in *Candida albicans* Response to Hyperosmotic Stress

Lianfang Wang[1†], Ruilan Chen[2,3,4†], Qiuting Weng[1], Shaoming Lin[5], Huijun Wang[1], Li Li[6], Beth Burgwyn Fuchs[7], Xiaojiang Tan[1‡] and Eleftherios Mylonakis[7‡]*

[1] Department of Respiratory and Critical Care Medicine, Chronic Airways Diseases Laboratory, Huiqiao Medical Center, Nanfang Hospital, Southern Medical University, Guangzhou, China, [2] The Second Clinical College of Guangzhou University of Chinese Medicine, Guangzhou, China, [3] Department of Intensive Care Unit, Fangcun Branch of Guangdong Provincial Hospital of Chinese Medicine, Guangzhou, China, [4] Guangdong Provincial Academy of Chinese Medical Sciences, Guangzhou, China, [5] Department of Respiratory, Longhua District People's Hospital, Shenzhen, China, [6] Huiqiao Medical Center, Nanfang Hospital, Southern Medical University, Guangzhou, China, [7] Department of Medicine, Division of Infectious Diseases, Rhode Island Hospital, Warren Alpert Medical School of Brown University, Providence, RI, United States

OPEN ACCESS

Edited by:
Dominique Sanglard, Université de Lausanne, Switzerland

Reviewed by:
Adnane Sellam, Laval University, Canada
Jan Quinn, Newcastle University, United Kingdom

***Correspondence:**
Xiaojiang Tan
txjzdk@126.com

[†] These authors have contributed equally to this work

[‡] These authors share senior authorship

Specialty section:
This article was submitted to Infectious Diseases, a section of the journal Frontiers in Microbiology

Received: *25 October 2019*
Accepted: *30 January 2020*
Published: *21 February 2020*

Citation:
Wang L, Chen R, Weng Q, Lin S, Wang H, Li L, Fuchs BB, Tan X and Mylonakis E (2020) SPT20 Regulates the Hog1-MAPK Pathway and Is Involved in Candida albicans Response to Hyperosmotic Stress. Front. Microbiol. 11:213. doi: 10.3389/fmicb.2020.00213

Candida albicans is the most common fungal pathogen and relies on the Hog1-MAPK pathway to resist osmotic stress posed by the environment or during host invasions. Here, we investigated the role of *SPT20* in response to osmotic stress. Testing a *C. albicans spt20*Δ/Δ mutant, we found it was sensitive to osmotic stress. Using sequence alignment, we identified the conserved functional domains between CaSpt20 and ScSpt20. Reconstitution of the Spt20 function in a *spt20*Δ*/CaSPT20* complemented strain found *CaSPT20* can suppress the high sensitivity to hyperosmotic stressors, a cell wall stress agent, and antifungal drugs in the *Saccharomyces cerevisiae spt20*Δ/Δ mutant background. We measured the cellular glycerol accumulation and found it was significantly lower in the *C. albicans spt20*Δ/Δ mutant strain, compared to the wild type strain SC5314 ($P < 0.001$). This result was also supported by quantitative reverse transcription-PCR, which showed the expression levels of gene contributing to glycerol accumulation were reduced in *Caspt20*Δ/Δ compared to wild type (*GPD2* and *TGL1*, $P < 0.001$), while *ADH7* and *AGP2*, whose expression can lead to glycerol decrease, were induced when cells were exposed to high osmolarity (*ADH7*, $P < 0.001$; *AGP2*, $P = 0.002$). In addition, we tested the transcription levels of Hog1-dependent osmotic stress response genes, and found that they were significantly upregulated in wild type cells encountering hyperosmolarity, while the expression of *HGT10*, *SKO1*, *CAT1*, and *SLP3* were not induced when *SPT20* was deleted. Although the transcript of *ORF19.3661* and *ORF19.4370* in *Caspt20*Δ/Δ was induced in the presence of 1 M NaCl, the levels were less than what was observed in the wild type (*ORF19.3661*, $P = 0.007$; *ORF19.4370*, $P = 0.011$). Moreover, the deletion of *CaSPT20* in *C. albicans* reduced phosphorylation levels of Hog1. These findings suggested that *SPT20* is conserved between yeast and *C. albicans* and plays an important role in adapting to osmotic stress through regulating Hog1-MAPK pathway.

Keywords: *Candida albicans*, glycerol, Hog1-MAPK, osmotic stress, *SPT20*

INTRODUCTION

Candida albicans can be isolated from oral-pharyngeal, gastrointestinal, and urogenital tracts (Calderone and Fonzi, 2001), and has emerged as one of the most common causes of nosocomial bloodstream infections (Wisplinghoff et al., 2004). In order to cause colonization and infection, this successful opportunistic pathogen has to overcome environmental challenges, such as host immune defenses, nutrient limitation, competition with resident microbiota, and physiological extremes including: pH, osmotic, and oxidative stresses (Calderone and Fonzi, 2001; Marotta et al., 2013; Dong et al., 2015). *C. albicans* has developed a series of complex mechanisms to respond to these challenges.

The high osmolarity glycerol 1 mitogen activated protein kinase signaling transduction pathway, also known as the Hog1-MAPK pathway, can regulate responses to oxidative, osmotic, and heavy metal stress (Enjalbert et al., 2006). Therefore, the Hog1 signal transduction pathway is crucial for *C. albicans* cells during exposure to stressors encountered during pathogenesis (Alonso-Monge et al., 1999). When cells encounter hyperosmotic conditions, they rapidly trigger the Hog1-MAPK pathway to regulate Hog1-dependent osmotic stress response genes, and the synthesis and accumulation of glycerol. Glycerol is an important compatible cellular solute. When cells encounter osmotic challenge, they can make a comparable change in glycerol content to offset the increasing external osmolarity, thus buffering the osmotic change to maintain normal cell volume and enable survival (Reed et al., 1987).

This important pathway can be influenced by other genes. *SPT20*, an important component of the SAGA complex, helps to maintain the structural integrity of the SAGA complex (Grant et al., 1997; Sterner et al., 1999), controls about 10% of gene expression (Lee et al., 2000), and is highly conserved in eukaryote cells (Sellam et al., 2009). The interaction between Spt20 and Hog1 is essential for osmotic adaption (Zapater et al., 2007). More specifically, when cells were subjected to osmotic stress, Hog1 was activated and bound to osmostress promoters, then recruited SAGA complex components (including Spt20). Further experiment showed Hog1 co-precipitated the Spt20, suggesting that Hog1 associates with Spt20 (Zapater et al., 2007). The activation of human Hog1 did not correlate with an increased recruitment of hSpt20 subunit under endoplasmic reticulum stress (Nagy et al., 2009). However, p38IP, the human ortholog of the yeast Spt20, can directly bind to p38 and is required for the activation of the mammalian ortholog of Hog1 (Zohn et al., 2006). These previous studies indicate that further work is still needed to explore the interaction between Spt20 and Hog1.

In our previous research, we reported that *SPT20* was involved in toleration to high osmotic stress, revealing it was associated with *C. albicans* virulence (Tan et al., 2014). However, the association between *CaSPT20* and Hog1-MAPK signaling pathway in *C. albicans* is still poorly understood. In this study, we perform quantitative reverse transcription-PCR (qRT-PCR) and western blotting to interrogate the relationship between *SPT20* and Hog1-MAPK pathway in *C. albicans*. We describe the conserved role of *SPT20* between *S. cerevisiae* and *C. albicans* and report, for the first time, that *SPT20* takes part in the *C. albicans* response to hyperosmotic stress by regulating the Hog1-MAPK pathway.

MATERIALS AND METHODS

Yeast Strains and Growth Conditions

Wild type *C. albicans* strain SC5314, the *spt20*Δ/Δ null mutant, the *spt20*Δ/*SPT20* reconstituted strain, and *S. cerevisiae* wild type BY4741 were grown in YPD medium (1% yeast extract, 2% peptone, 2% dextrose) at 30°C with shaking. The *Saccharomyces cerevisiae spt20*Δ mutant strain (LCT1) was cultured in YPD medium supplemented with G418 (Sigma-Aldrich, Shanghai, China). Ampicillin-resistant *E. coli* was cultured in LB medium with 100 μg/mL ampicillin at 37°C. Strains with *pYES-CaSPT20-V5* or *pYES2.1/V5-His-TOPO* plasmids were cultured in Sc-Ura3 media. All strains were cultured to logarithmic growth stage.

C. albicans and *S. cerevisiae* strains used in this study are listed in **Table 1**. All *C. albicans* strains were derived from the wild type strain SC5314. All *S. cerevisiae* strains were derived from the wild type BY4741.

Plasmid Construction

All primers and plasmids used in this study are listed in **Tables 2**, **3**, respectively. For the creation of plasmid *pYES-CaSPT20-V5*, SC5314 genomic DNA was used as a template for *CaSPT20ResFwd* and *CaSPT20ResRev* primers, which generated a 2,678 bp DNA fragment containing *Bam*HI and *Bst*EII restriction sites, the promoter, ORF of *CaSPT20* but lacked the stop codon.

The amplified fragment described above and plasmid *pYES2.1/V5-His/lacZ* (Invitrogen, Shanghai, China) were digested with *Bam*HI-*HF* and *Bst*EII-*HF*. The two products were purified, ligated, and the resulting plasmid was transformed to DH5α *E. coli* and colonies were selected on LB plate with 100 μg/mL ampicillin. PCR followed by sequencing were used to validate the correct insertion of *pYES-CaSPT20-V5-His*/lacZ vector (**Supplementary Data**).

Generated Strains

Saccharomyces cerevisiae LCT1 was constructed as previously described (Marotta et al., 2013). The template plasmid pFA6a-5FLAG-KanMX6 was a gift from Eishi Noguchi (Noguchi et al., 2008; Addgene plasmid # 15983; http://n2t.net/addgene:15983; RRID: Addgene 15983). In brief, we used *ScSPT20DelFwd* and *ScSPT20DelRev* as primers and the plasmid *pFA6a-5FLAG-KanMX6* as template to amplify a 1,676 bp DNA fragment containing the kanamycin resistance gene flanked by 20 bp of *ScSPT20* 5′ and 3′ sequences. The PCR product was transferred to *S. cerevisiae* wild type strain BY4741 using a transformation method described previously by Gietz (Gietz, 2014). Transformants with the desired insert were selected on YPD media containing 200 μg/mL G418 and verified by PCR (Marotta et al., 2013). The LCT1 and BY4741 strains were transformed with the *pYES2.1/V5-His-TOPO* vector to generate LCT2 and LCT4 strains,

TABLE 1 | Strains used in this study.

Microbial	Strains	Genotype	Reference or source
E.coli	*DH-5α*	*F-, Δ80dlacZΔM15, Δ(lacZYA-argF)U169, deoR, recA1, endA1, hsdR17 (rk-, mk+), phoA, supE44, λ-, thi-1, gyrA96, relA1*	From Takara
S.cerevisiae	BY4741	*MAT**a** his3Δ1 leu2Δ0 metl5Δ0 ura3Δ0*	From Merck
S.cerevisiae	LCT1	*MAT**a** his3Δ1 leu2Δ0 metl5Δ0 ura3Δ0:spt20:kanMX6*	This study
S.cerevisiae	LCT2	*MAT**a** his3Δ1 leu2Δ0 metl5Δ0 ura3Δ0:spt20:kanMX6 pYES2.1/V5-His-TOPO*	This study
S.cerevisiae	LCT3	*MAT**a** his3Δ1 leu2Δ0 metl5Δ0 ura3Δ0:spt20:kanMX6 pYES- CaSPT20- V5*	This study
S.cerevisiae	LCT4	*MAT**a** his3Δ1 leu2Δ0 metl5Δ0 ura3Δ0 pYES2.1/V5-His-TOPO*	This study
C. albicans	SC5314	Wild type	From Eleftherios Mylonakis
C. albicans	*spt20Δ/Δ*	*spt20Δ:FRT/spt20Δ:FRT*	From Eleftherios Mylonakis
C. albicans	*spt20Δ/SPT20*	*spt20Δ:FRT/SPT20-FRT*	From Eleftherios Mylonakis
C. albicans	*hog1Δ/Δ*	*hog1/hog1*	From Ching-Hsuan Lin
C. albicans	*hog1Δ/HOG1*	*hog1/hog1:HOG1*	From Ching-Hsuan Lin
C. albicans	HOG1-OE	*spt20Δ:FRT/spt20Δ:FRT HOG1/HOG1::pAgTEF1-NAT1-AgTEF1UTR-TDH3-HOG1*	This study
C. albicans	SPT20-OE	*hog1/hog1 SPT20/SPT20::pAgTEF1-NAT1-AgTEF1UTR-TDH3-SPT20*	This study
C. albicans	wt-HOG1-OE	*HOG1/HOG1::pAgTEF1-NAT1-AgTEF1UTR-TDH3-HOG1*	This study

respectively. To create strain LCT3 (*Scspt20Δ/CaSPT20*), the *pYES-CaSPT20-V5* plasmid was transformed to LCT1. All strains were verified by PCR to ensure the correct transformants were used.

The construction of overexpression strains was described previously (Nobile et al., 2008). The *NAT1-TDH3* promoter plasmid *pCJN542* (Nobile et al., 2008) was used for gene overexpression. To construct the *SPT20* overexpression strain (SPT20-OE) in *hog1Δ/Δ* mutant background, the PCR product was amplified using the plasmid *pCJN542* as template and primers *SPT20-OEF* and *SPT20-OER* (**Table 2**) and then transferred to *hog1Δ/Δ* mutant strain. By the same method, the PCR product generated using plasmid *pCJN542* as template for and primers *HOG1-OEF* and *HOG1-OER* (**Table 2**) was transferred to *spt20Δ/Δ* mutant strain to generate *HOG1* overexpression strain (HOG1-OE). Strains that underwent homologous recombination were selected on YPD+ Nourseothricin (Werner BioAgents, Jena, Germany; 400 μg/mL for SPT20-OE strain and 100 μg/mL for HOG1-OE strain) plates and the recombination events were verified by PCR with primers *SPT20-F-2* and *NAT1-R* for SPT20-OE strain, and primers *HOG1-F-2* and *NAT1-OER-det* for HOG1-OE strain, respectively. Function of this overexpression strategy was verified by real-time PCR with primers *HOG1-F* and *HOG1-R* for HOG1-OE strain, and primers *SPT20-F* and *SPT20-R* for SPT20-OE strain, respectively.

Sensitivity Assays

Sensitivity to a range of stresses was evaluated using a solid media assay. All investigational strains were grown to mid-log phase under suitable growth conditions and collected by centrifugation. The pellets were suspended in YPD at 2.5×10^7 cells/mL. Ten-fold serial dilutions from 2.5×10^7 to 2.5×10^3 of all strains were prepared, and 4 μL of each of strain dilutions was spotted onto the agar plates with integrated stimuli. Cells were incubated at 30°C for 48 h and then observed for growth differences.

RNA Isolation and qRT-PCR Analysis

The *C. albicans* strains SC5314, *Caspt20Δ/Δ*, *Caspt20Δ/SPT20* were cultured to logarithmic phase and diluted to OD_{600} = 0.2. The cultures were incubated at 30°C with shaking for 4 h. 5×10^7 cells were counted with a hemocytometer and then collected by centrifugation. After being washed twice with sterile PBS, the pellets were subjected to 1 M NaCl in YPD, while the control group was added to an equal volume of YPD medium. All the cultures were grown at 30°C with shaking for an additional 30 min. After treatment, cells were collected by gentle centrifugation, and total RNA was extracted using an RNeasy Mini Kit (Qiagen, Shanghai, China) according to the manufacturer's protocol. The concentration, purity, and integrity of RNA were checked by Nanodrop spectrophotometer. Generally, RNA samples with an A_{260}/A_{280} ratio between 1.9 and 2.1 were used for further interrogation.

In order to remove potential genomic DNA contamination and synthesize cDNA, we used PrimeScript™ RT reagent Kit with gDNA Eraser (Perfect Real Time; TaKaRa, Dalian, China) following the manufacturer's protocol. Real time reactions were prepared using TB Green™ Premix Ex Taq II™ Kit (Tli RNaseH Plus; TaKaRa, Dalian, China), and quantitative PCR experiments were conducted in a LightCycler480 System (Roche, Switzerland). Transcript levels were normalized against 18S rRNA expression (used as an internal control of gene expression). The gene expression changes were measured in $2^{-\Delta\Delta Ct}$ method. Fold changes of target genes in the *spt20* mutant and reconstituted strains were normalized to the untreated wild type strain.

Intracellular Glycerol Assays

The *C. albicans* production of intracellular glycerol were measured as previously described (Ene et al., 2015). In brief, *C. albicans* strains SC5314, *Caspt20Δ/Δ*, and *Caspt20Δ/SPT20* were grown overnight. An aliquot of 5×10^7 cells were treated with 1 M NaCl in YPD for 30 min. Subsequently, the intracellular glycerol levels were measured using the Free

TABLE 2 | Primers used in this study.

Primers for strains construction		
Name	**Sequence (5′-3′)**	**Usage**
*ScSPT20*DelFwd	ATGAGTGCCAATAGCCCGACAGGAAACGA TCCCCATGTATTTGGTATTCCTGTGAACGCA ACACCATCCAATATGGGTTCGCCAGGCAG TCCAGTTAATGCCGCTAGGGATAACAGGGTA	For the disruption of *ScSPT20*
*ScSPT20*DelRev	AAGTGAGAATTTTTTTTAAATAATGATGT ACTTTAATACAATATATATATATATATATATA TATATATATATATATATATAAGGAATGATAACT CTATTTGAATTCGAGCTCGTTTAAAC	
*ScKan*I deFwd	TGCCTCTTCCGACCATCAAG	For identification of the strain LCT1
*ScKan*I deRev	CCATGAGTGACGACTGAATC	
ScUpI deFwd	TGTTACCCGCTCGTGATACC	
ScUpI deRev	GGGACGAGGCAAGCTAAACA	
ScDownIdeFwd	ATACTAACGCCGCCATCCAG	
ScDownIdeRev	AACCCACTAGAGTGCATGGG	
*ScSPT20*Fwd	TATGCCCTACAACGCCCTTC	
*ScSPT20*Rev	GTGGCAAATACAGGCGCAAA	
*LacZ*Fwd	CAAGCCGTTGCTGATTCGAG	For the construction of LCT2,
*LacZ*Rev	GTGGCCTGATTCATTCCCCA	LCT3, LCT4 strains
Ura3 Fwd	GATAGGGAGCCCTTGCATGA	
Ura3 Rev	CGCTAAAGGCATTATCCGCC	
*CaSPT20*ResFwd	CCCGGATCCATTATATATAGCCCATAAATAAATACTG	
*CaSPT20*ResRev	CCCGGTCACCATTAGCAGGCGCATTTTTCTTCTTCTGAT	
*GAL1*F	AATATACCTCTATACTTTAACGTC	
*CaSPT20*R	GCAACAAGAAGCAAAGATTC	
*CaSPT20*F	CACTTCTGTTCACCCTCCTA	
V5-R	ATCCCTAACCCTCTCCTCGGT	
SPT20-OEF	AACAAAATCAGCAGTCAGTTTTTTCCAAATG GTTTAGATGACTCTTCGATTCTGGAAATGG ACGTTGAATTGAATGACAACTTAATCATAAT AAGAAATCATCAAGCTTGCCTCGTCCCC	For the construction of SPT20-OE strain
SPT20-OER	GTTTTCCACCCTGATTCTGAGTCAGTACTGT TGTACCATTAGATATAGAGTTTCCCACAGTT TTGGATGCAGATCCACTCAAAACTTCAGATTT TATCATATTTGAATTCAATTGTGATG	
HOG1-OEF	GAACACGCAACAATGCTACCGCGACTACAAAT GGTTCAATCTGGAGAGAAACTTCCACC TCAGCTAGTAACACTACTGTTTTTCTATAAACTG TTTTCACATCAAGCTTGCCTCGTCCCC	For the construction of HOG1-OE and wt-HOG1-OE strains
HOG1-OER	ATGCTCCCATTCCCACGGGATTTAGCTCAGTG TATCTATTGGTGATTTCAAAAACAGTC CCAAATATCTGGGTTCTTGTAAATTCTCCATC TGCAGACATATTTGAATTCAATTGTGATG	
HOG1-F-2	GGCATAAAAGTGTTGGTAATGGC	For colony PCR of HOG1-OE and
NAT1-OE-R-det	GCAGTATCATCCAAAGTAGTA	wt-HOG1-OE
SPT20-F-2	CTGCAACTGCACCAAGCTAT	For colony PCR of SPT20-OE
NAT1-R	GAAACAACAACGAAACCAGC	
Primers for qRT-PCR		
Name	**Sequence (5′-3′)**	
18S rRNA-F	CGCAAGGCTGAAACTTAAAGG	
18S rRNA-R	AGCAGACAAATCACTCCACC	
CAT1-F	GGCCAGTGATAAGCCAGTTG	
CAT1-R	TTGGATAGCAGCATCAGCAC	
SKO1-F	AACCACCACCACCACAAAAT	

(Continued)

TABLE 2 | Continued

Primers for qRT-PCR	
Name	**Sequence (5′-3′)**
SKO1-R	CACCACGCAATTCATTCACT
AGP2-F	CAGTCATGGGGTTCCTGTCT
AGP2-R	TACGGTTGGAACCACGATCT
ORF19.3661-F	TTGTGAAGCCACTCCTGTTG
ORF19.3661-R	CCAGTCGGATTAGCTTGGAA
HOG1-F	GACTTGTGGTCTGTGGGTTG
HOG1-R	ACATCAGCAGGAGGTGAGC
TGL1-F	TATGCAAGGTTGTTCCGTCA
TGL1-R	CACTGTTGCTTGCCGATCTA
ADH7-F	TGAAATTGGGTGCTGATGAA
ADH7-R	TGTTCAGTGGCTGGTGGTAA
SPT20-F	ACAAACTACTGCTGACGGGG
SPT20-R	GGAGGGTGAACAGAAGTGGG

TABLE 3 | Plasmids used in this study.

Name	Description	Reference/source
pFA6a-5FLAG-KanMX6	Amp^r, Kan^r	From Eishi Noguchi
pYES2.1/V5-His-TOPO	URA3, Amp^r	From invitrogen
pYES2.1/V5-His/lacZ	URA3, Amp^r, lacZ	From invitrogen
pYES- *CaSPT20*- V5	*CaSPT20* in pYES2.1/V5-His-TOPO	This study
pCJN542	*NAT1-TDH3* promoter	From Aaron P. Mitchell

Glycerol Reagent (Sigma-Aldrich, Shanghai, China) according to the manufacturer's protocol.

Western Blotting

Candida albicans wild type strain SC5314 and null mutant strain *Caspt20*Δ/Δ were grown to mid-exponential phase in YPD at 30°C with shaking. Cells were exposed to hyperosmotic stress for a designated period of time by adding 5 M NaCl stock solution to YPD medium to achieve a final concentration of 2 M NaCl. As a control, equal volume of YPD was added instead of NaCl. Following treatment, *C. albicans* cells were collected and the pellets were washed twice with sterile PBS. To extract protein, pellets were suspended in 200 μL RIPA lysis buffer containing Protease Inhibitor Cocktail (Roche, Shanghai, China), and an equal volume of acid-washed glass beads (Sigma-Aldrich, shanghai, China) was added. The cells were vigorously vortexed for 1 min to mechanically disrupt cell walls then transferred to ice for 1 min, and vortex and chill process repeated six more times. Cell extracts were separated from whole cell debris and glass beads by applying centrifugation at 13,000 rpm at 4°C for 10 min.

The protein concentrations were determined using a Pierce BCA Protein Assay Kit (Thermo Fisher Scientific, Shanghai, China). Equal quantities of protein (40 μg) were loaded onto a 10% gel, analyzed by SDS-PAGE, and then transferred to PVDF membranes. Anti-phospho-P38 antibody (Cell Signaling Technology, Shanghai, China) was used to detect the phosphorylated form of Hog1 (Smith et al., 2004). Total Hog1 level was detected by Hog1 (D-3) antibody (Santa Cruz Biotechnology, Shanghai, China). β-anti-actin antibody (GeneTex, Shenzhen, China) was used as the loading control (Deng and Lin, 2018).

Statistical Analysis

All experiments were performed at least twice as independent replicates. Data were analyzed using SPSS software. Student's *t*-test and the analyses of variance (ANOVA) were used to determine statistical significance. A P-value < 0.05 was considered statistically significant.

RESULTS

Conservation of CaSPT20

We have previously reported that *SPT20* was involved in regulating virulence and stress responses in *C. albicans* (Tan et al., 2014). However, little is known about the underlying molecular mechanisms. The amino acid sequence alignment showed there are conserved functional domains between CaSpt20 and ScSpt20 (**Supplementary Figure 4**). With the hypothesis that *C. albicans SPT20* could be functionally conserved with *Saccharomyces cerevisiae*, we endeavored to determine if *CaSPT20* could restore defects in *ScSPT20* mutant strains. To this end, we constructed *S. cerevisiae* strains LCT1 (*Scspt20*Δ), LCT2 (*pYES2.1/V5-His-TOPO* in the LCT1 background), LCT3 (*pYES2.1/V5-His-TOPO-CaSPT20* in the LCT1 background) and LCT4 (*pYES2.1/V5-His-TOPO* in the background of the wild type strain BY4741), then performed a series of functional complement assays.

The strains were grown on YPD agar plates supplemented with hyperosmotic stressors (NaCl, sorbitol, and glycerol), ethanol stress, cell wall stress agent SDS, or antifungal agents (amphotericin B, fluconazole, and caspofungin), which directly perturb cell membrane component ergosterol synthesis or FKS required for cell wall synthesis. After cultivation for 48 h, cell

growth was observed under the applied stress conditions. The introduction of plasmid *pYES2.1/V5-His-TOPO* had no influence on cell growth, as seen when comparing growth of LCT4 to BY4741, and LCT2 to LCT1. Deletion of *SPT20* impaired normal cell growth of *S. cerevisiae*, which was in agreement with the results reported by Roberts and Winston (Roberts and Winston, 1996), but growth retardation was exacerbated when cells were associated with the tested hyperosmotic stressors and cell membrane targeting antifungal agent fluconazole. Notably, the cell growth of *Scspt20*Δ mutant was rescued with complementation of *CaSPT20*, suggesting that *SPT20* is required for the normal cell growth under extracellular osmolarity and cell membrane stressor exposure. However, the decrease in resistance to the other stresses (such as ethanol, SDS, amphotericin B, and caspofungin) seen in *Scspt20*Δ cells largely matches the decreased growth seen in the BY4741 (**Figure 1**), indicating that the growth defects of *Scspt20*Δ cells in these stresses may not be due to the deletion of *SPT20*. Importantly, complementation of *CaSPT20* restores the growth of *Scspt20*Δ to the wild type levels, supporting that the function of *SPT20* is conserved between *C. albicans* and *S. cerevisiae*.

Hog1 Phosphorylation Is Reduced by Deletion of CaSPT20

The data demonstrates that Spt20 plays a conserved role in protecting cells from osmotic stress. A well-known contributor in protecting fungi from osmotic stress is the Hog1 pathway (Brewster and Gustin, 2014). When *C. albicans* is exposed to high osmolarity, Hog1 is phosphorylated and then induces target gene expression to adapt to osmotic stress (Smith et al., 2004; Day et al., 2017). In other words, phosphorylation of Hog1 is the essential step for *C. albicans* to survive during high osmotic challenge. To test if *CaSPT20* affects Hog1 responses to osmotic stress, we extracted protein from the indicated strains subjected to 2 M NaCl in YPD for various time periods, and then performed western blotting. Specific antibodies were used to detect the levels of total Hog1 and phospho-Hog1, respectively. In this assay, β-actin antibody was used as a loading control.

As reported previously (Alonso-Monge et al., 2003; Smith et al., 2004), Hog1 phosphorylation was induced by osmotic treatment. Hog1 phosphorylation peaked after 10 min under high osmotic stimulation in wild type SC5314, however, *Caspt20*Δ/Δ failed to have the same level of Hog1 phosphorylation after 10 min of osmotic treatment. Indeed, only a very slight increase in phosphorylated Hog1 was observed after 60 min of stimulation (**Figure 2A**). In stark contrast, reconstitution of *SPT20* restored phospho-Hog1 to wild type levels (**Figure 2B**). In addition, the level of total Hog1 transcription in these three strains remained constant, which was in accord with what Enjalbert et al. reported (Enjalbert et al., 2006), indicating that Hog1 phosphorylation occurs independent of total Hog1 expression levels. Thus, it appears that *SPT20* correlated with the phosphorylation of Hog1. We then further explored the effects that deletion of *SPT20* has on Hog1 responses and the *C. albicans* phenotype.

CaSPT20 Affects Expression of Hog1-Dependent Osmotic Stress Response Genes

As shown above, the level of phosphorylated Hog1 in *Caspt20*Δ/Δ was much less than what was seen in the wild type strain, suggesting that *SPT20* affected the level of phosphorylated Hog1, which prompted us to investigate whether the expression levels of Hog1-dependent osmotic stress response genes were affected by the loss of *SPT20*. To this end, we measured the

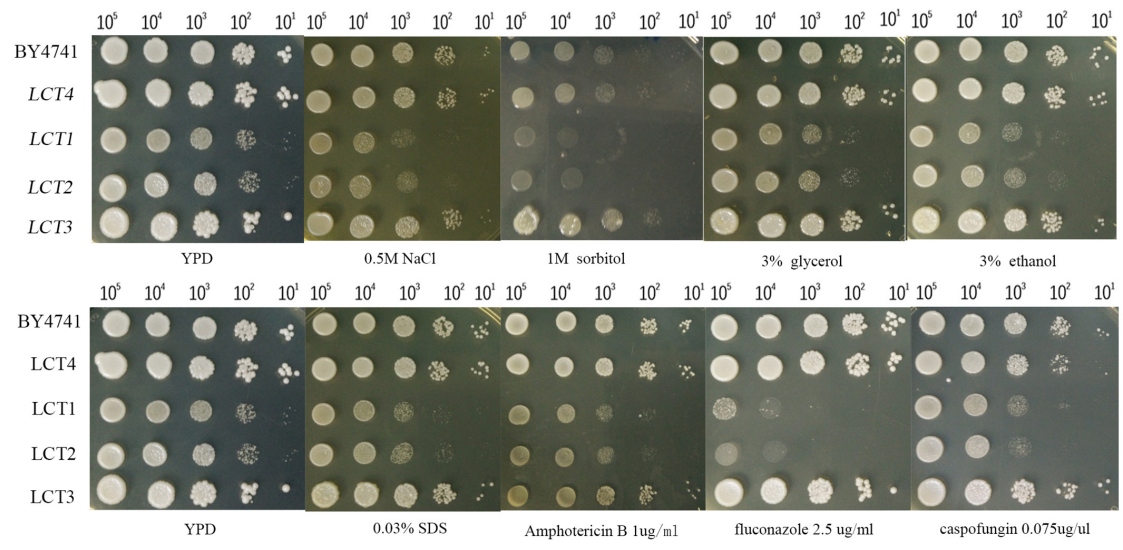

FIGURE 1 | The introduction of *CaSPT20* can restore sensitivity to stresses and antifungal agents caused by the loss of *ScSPT20*. LCT1 (*Scspt20*Δ), LCT2 (*Scspt20*Δ+pYES2.1/V5-His-TOPO), LCT3 (*Scspt20*Δ+*pYES- CaSPT20-V5*), and LCT4(BY4741+pYES2.1/V5-His-TOPO) were constructed in the background of *S. cerevisiae* BY4741 and grown at 30°C for 48 h. The experiment was repeated on 3 independent occasions.

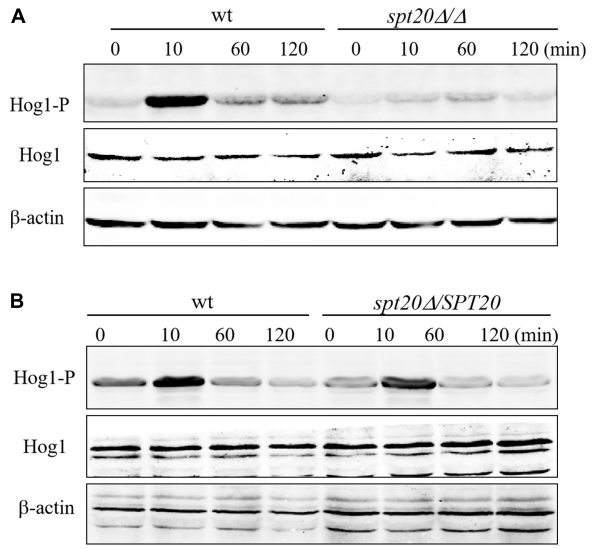

FIGURE 2 | *SPT20* affects the phosphorylation level of Hog1 protein. Cells were exposed to 2 M NaCl for the indicated time. phosphorylated Hog1 (Hog1-P) and total Hog1 (Hog1) levels of wild type, *SPT20* null mutant **(A)**, and *SPT20* reconstitution strain **(B)** were detected by western blotting with specific antibodies. The beta actin antibody was used as the loading control. This experiment was repeated three times independently.

expression of Hog1-dependent osmotic stress response genes. A panel of genes was assembled for interrogation as the previous work did, which reported the expression levels of *HGT10* (encoding a glycerol permease involved in active glycerol uptake), *SKO1* (encoding a transcriptional factor binding to promoters to relieve osmotic stress), *CAT1* (one of core stress genes, encoding a key antioxidant enzyme), *ORF19.4370* (predicted ORF), *ORF19.3661* (encoding a putative deubiquitinating enzyme) and *SLP3* (encoding a putative cation conductance protein) were induced in a Hog1-dependent manner (Enjalbert et al., 2006; Marotta et al., 2013). As showed in **Figure 3**, these Hog1-dependent osmotic stress response genes were significantly upregulated in wild type cells encountering hyperosmolarity, while the expression of *HGT10*, *SKO1*, *CAT1*, and *SLP3* were not induced when *SPT20* was deleted. Although the transcript of *ORF19.3661* and *ORF19.4370* in *Caspt20*Δ/Δ was induced in the presence of 1 M NaCl, it still did not reach the level observed in the wild type (*ORF19.3661*, $P = 0.007$; *ORF19.4370*, $P = 0.011$). Notably, the transcriptional changes caused by the deletion of *SPT20* gene in *C. albicans* were in accordance with that caused by the loss of *HOG1* gene, which also exhibited reduced expression of *HGT10*, *SKO1*, *CAT1*, *ORF19.4370*, *ORF19.3661*, and *SLP3* in the *hog1*Δ/Δ mutant strain during 1 M NaCl stimulation (Marotta et al., 2013). Taken together, we can conclude that *SPT20* plays a role in appropriate expression of Hog1-dependent osmotic stress response genes.

The Cell Growth Defect of Caspt20Δ/Δ Is Rescued by HOG1 Overexpression Under Osmotic Stress

The Hog1-MAPK pathway has been reported to be involved in osmoadaptation, take part in resistance to oxidative stress, and also play a role in morphogenesis changes as well as cell wall biosynthesis (Monge et al., 2006). As we demonstrated

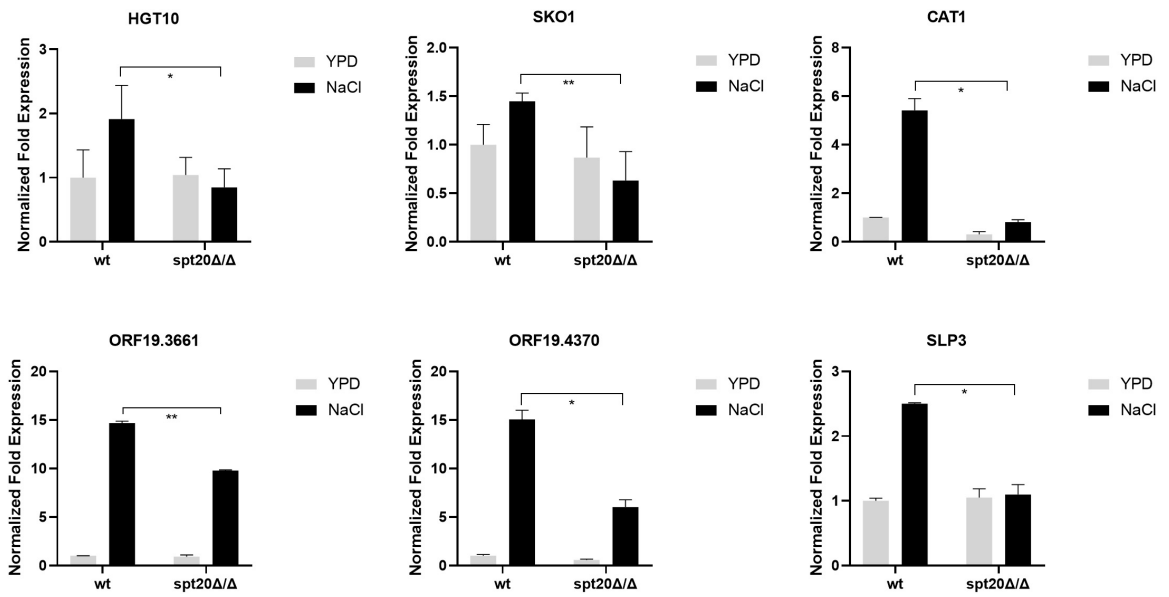

FIGURE 3 | Expression levels of Hog1-dependent osmotic stress response genes changed significantly when *SPT20* was deleted in *C. albicans*. qRT-PCR expression analysis of *C. albicans* Hog1-dependent osmotic stress response genes in the wild type strain, *spt20*Δ/Δ and *spt20*Δ/*SPT20*. Transcript levels were normalized to *C. albicans* 18S rRNA expression and fold changes between strains were normalized to untreated wild type which was adjusted to a value of 1. All genes were analyzed in triplicate. Error bar represents Mean ± SD. *$P < 0.5$, **$P < 0.01$.

earlier, the ability to overcome hyperosmotic stress was impaired in *Caspt20*Δ/Δ, suggesting *CaSPT20* really plays a role in osmostress responses (Tan et al., 2014). To evaluate if *SPT20* responds to osmotic stress in cooperation with the Hog1 pathway, cell growth of strains SC5314, *Caspt20*Δ/Δ, *Caspt20*Δ/*SPT20*, *Cahog1*Δ/Δ and *Cahog1*Δ/*HOG1* were examined during exposure to external hyperosmolarity, comparing growth defects between *Caspt20*Δ/Δ and *Cahog1*Δ/Δ strains. As expected, the knockout of *CaSPT20* or *CaHOG1* both led to impaired cell growth in hyperosmotic conditions imposed by NaCl or sorbitol, and for each, growth was restored to wild type levels when *CaSPT20* and *CaHOG1* were reconstituted, respectively (**Figure 4**). This result, along with the affected phosphorylation level of Hog1 and the expression of Hog1-dependent osmotic stress response genes, suggest a link between *SPT20* and Hog1-MAPK pathway in *C. albicans* osmoadaptation. Thus, we hypothesized that *SPT20* regulated the Hog1-MAPK pathway to respond to external osmotic stress. In order to evaluate this hypothesis, we constructed the *HOG1* overexpression strain in the *Caspt20*Δ/Δ mutant background (HOG1-OE) and in the wild type background (wt-HOG1-OE), and *SPT20* overexpression strain in the *Cahog1*Δ/Δ mutant background (SPT20-OE). The gene overexpression was verified by quantitative reverse transcription-PCR analysis. In addition, the basal levels of phosphorylated Hog1 and total Hog1 in the HOG1 overexpression strains were significantly increased when compared with wild type (**Supplementary Figure 1**). We compared the cell growth of strains SC5314, *Caspt20*Δ/Δ, HOG1-OE, *Cahog1*Δ/Δ, and SPT20-OE, which were treated with NaCl. As illustrated in **Figure 4**, we observed that *HOG1*

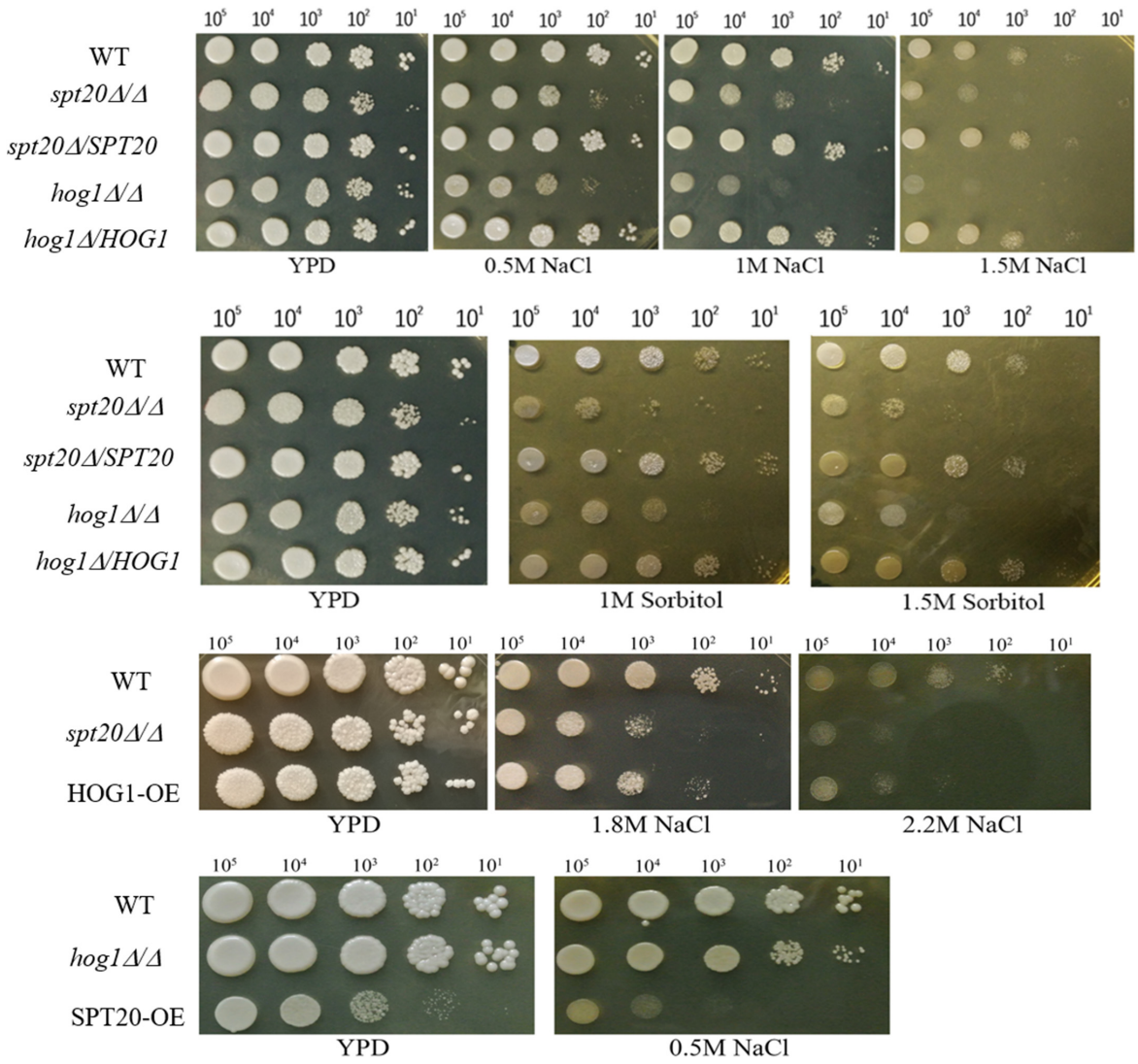

FIGURE 4 | The cell growth defect of *Caspt20*Δ/Δ is similar to that of *Cahog1*Δ/Δ and is rescued by *HOG1* overexpression. Ten-fold serial dilutions of strains were spotted on appropriate plates to evaluate the cell growth defects. Cells were grown at 30°C and then photographed. The experiment was repeated on three independent occasions.

overexpression can partially rescue the growth defect caused by *SPT20* deletion when cells were exposed to a series of high osmotic stress (YPD plate supplements with 1.8 M NaCl, or 2.2 M NaCl), while overexpressing *SPT20* did not confer the ability to resist hyperosmotic stress to the *hog1*Δ/Δ strain. Furthermore, in order to investigate whether there exists a Spt20-independent manner contributing to the increasing resistance of HOG1-OE strain, we observed the cell growth of wt-HOG1-OE strain, and found that overexpressing *HOG1* did not enhance the osmotic tolerance of wild type cells (**Supplementary Figure 2**). These results indicate that *SPT20* influences Hog1 during the *C. albicans* response to osmotic stress.

CaSPT20 Regulates Glycerol Accumulation in *C. albicans*

To investigate the correlation between *CaSPT20* and Hog1-MAPK pathway in hyperosmotic stress response, we measured the intracellular glycerol accumulation of strains SC5314, *Caspt20*Δ/Δ, and *Caspt20*Δ/*SPT20* after exposure to 1 M NaCl for 30 min. Our results showed the basal glycerol contents of these three strains were almost the same, and they all increased strikingly under hyperosmotic condition. However, the ability to accumulate intracellular glycerol was impaired in *Caspt20*Δ/Δ strain ($P < 0.001$) (**Figure 5A**).

Glycerol biosynthesis is catalyzed by glycerol-3-phosphate dehydrogenase (encoded by *GPD1/GPD2*) and glycerol-3-phosphatase (encoded by *RHR2*) (Hohmann, 2002; Fan et al., 2005). Meanwhile, the increased cellular glycerol concentration is also forced by regulated activities of triacylglycerol lipases (encoded by *TGL1/TGL2*) (Wei et al., 2009), alcohol dehydrogenase (encoded by ADH) (Blomberg and Adler, 1989), and amino acid permease (encoded by *AGP2*) (Marotta et al., 2013). To further examine the Spt20 influence on cellular glycerol, we examined expression of these genes involved in glycerol accumulation. *GPD2*, which was reported to increase to a greater extent than *GPD1* and *RHR2* levels in response to osmostress (Smith et al., 2004; Enjalbert et al., 2006; Jacobsen et al., 2018), was suppressed when *CaSPT20* was knocked out. Although *GPD2* was induced in the presence of 1 M NaCl, its expression still did not reach the level observed in the wild type ($P < 0.001$). In contrast, *ADH7* was significantly induced in the *Caspt20*Δ/Δ mutant, both in the absence and presence of osmotic stress (6-fold in the presence of 1 M NaCl compared to wild type; $P < 0.001$). *TGL1* was under-expressed in *Caspt20*Δ/Δ after exposure to osmotic stress (0.31 for the mutant versus 0.76 for wt strain; $P < 0.001$). When compared to wild type, *AGP2*, a gene involved in membrane permeability, experienced reduced expression in the absence of salt exposure in the *Caspt20*Δ/Δ strain, but following osmotic stress treatment, it significantly elevated and was 1.25-fold higher than the expression found in the wild type strain ($P = 0.002$) (**Figure 5B**). The decreased expression of *GPD2* can reduce the accumulation of intercellular glycerol directly. The expression of *ADH7* can reduce the yield of NADH, then lead to the decreasing production of glycerol (Blomberg and Adler, 1989). Meanwhile, the reduced transcript level of *TGL1* blocks the process of transforming triglycerides to glycerol (Jandrositz et al., 2005; Wei et al., 2009), while the upregulation of *AGP2* can cause increasing membrane permeability, so that the intracellular glycerol can spread to extracellular environments. Taken together, these findings suggest that *CaSPT20* participates in the process of glycerol accumulation, since *GPD2*, *ADH7*, *TGL1* and *AGP2* expression were sharply affected when *SPT20* was deleted from *C. albicans*.

DISCUSSION

Osmoregulation by homeostatic mechanisms is crucial in *C. albicans* in order to keep appropriate cell volume, turgor, as well as a suitable intracellular environment for all kinds of biochemical reactions (Hohmann et al., 2007; Fuchs and Mylonakis, 2009). In this paper, we show that CaSpt20 has functional similarity with ScSpt20 and can be used to reconstitute a mutation in the homologous gene. The increased sensitivity of *Caspt20*Δ/Δ to hyperosmolarity is due to its reduced phosphorylation levels of Hog1, thereby causing downregulation of osmotic stress response genes and decrease in glycerol accumulation, suggesting that *SPT20* is involved in resistance to high osmolarity. These findings give us new insight into the role of *SPT20* in *C. albicans* response to osmotic stress, and indicate a new relationship between Spt20 and Hog1.

As an indispensable component of the SAGA complex, *SPT20* has gained enough attention on its function. It was reported that Spt20 was involved in endoplasmic reticulum stress response in human (Nagy et al., 2009), hypoxic response (Hickman et al., 2011) and the functional interaction between other SAGA components and TBP in yeast (Roberts and Winston, 1997), and the calcineurin-mediated Cl^- homeostasis in *Schizosaccharomyces pombe* (Zhou et al., 2013). Furthermore, *SPT20* is required for normal cell growth (Roberts and Winston, 1996) and is essential for yeast survival at high osmolarity (Zapater et al., 2007). Here, we demonstrated that knockout of *ScSPT20* caused significantly further growth defects associated with the tested hyperosmotic stressors (NaCl and sorbitol) compared to a wild type control exposed to the same conditions. Additionally, the ability of *Caspt20*Δ/Δ mutant strain to resist hyperosmolarity was greatly impaired (**Figure 4**). These results suggested that *SPT20* is required for the normal cell growth under osmotic condition, which was in accord with the previous work that reported *SPT20* is essential for yeast survival at high osmolarity (Zapater et al., 2007). The similar phenotypes between *Scspt20*Δ and *Caspt20*Δ/Δ mutant strain, and increasing resistance to osmotic stress due to the complement of *CaSPT20*, supported that the function of *SPT20* was conserved.

The Hog1-MAPK pathway is critical for *C. albicans* to respond to osmotic stress. Hog1, the core component in this pathway, has a strong functional preservation from yeast to mammals (Sheikh-Hamad and Gustin, 2004), and its rapid phosphorylation is an essential step in osmotic toleration (Brewster and Gustin, 2014). Our findings suggest that Spt20 regulates Hog1 activation in *C. albicans* response to hyperosmotic stress. The evidences are the

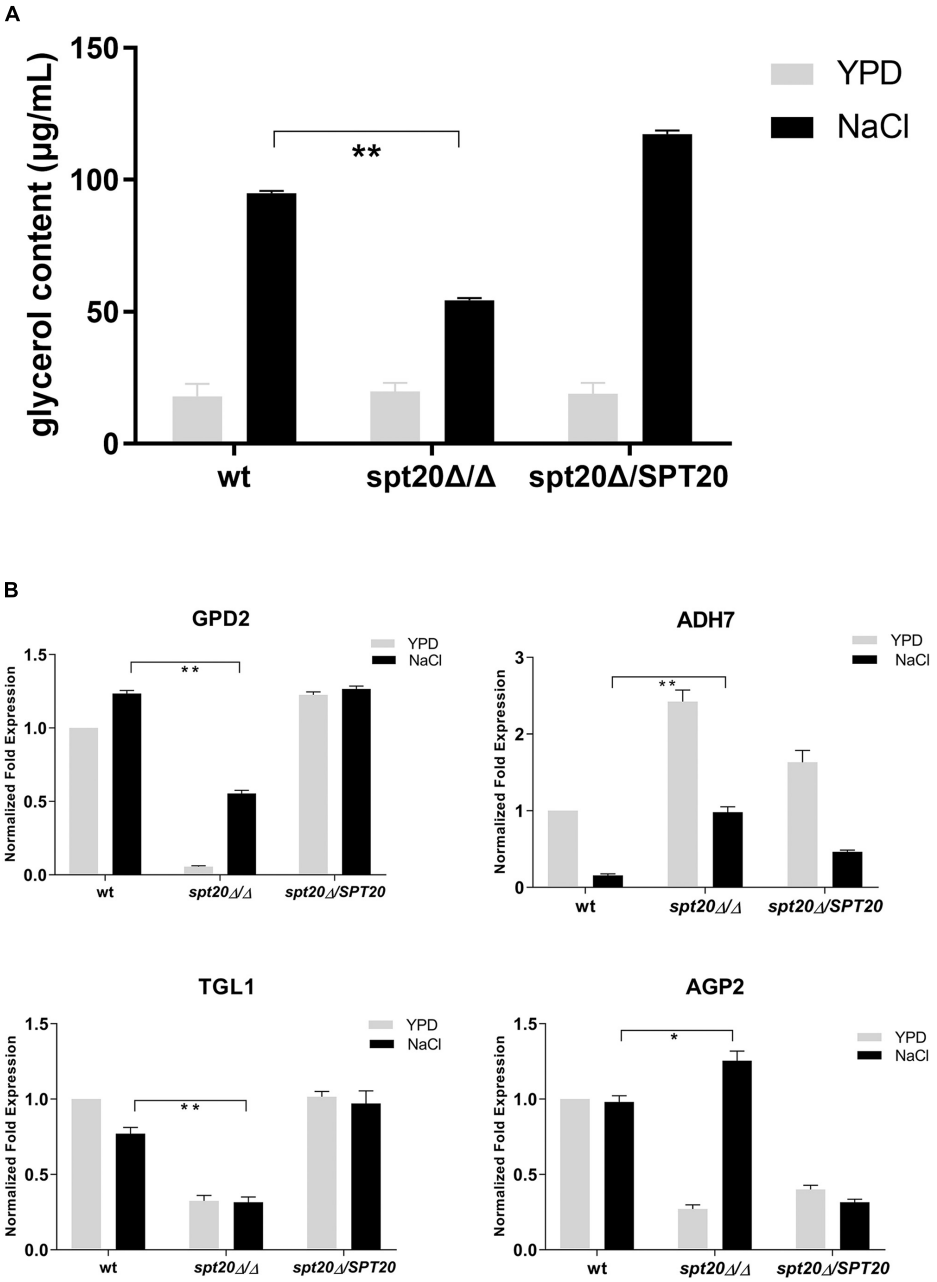

FIGURE 5 | *CaSPT20* regulates intracellular glycerol accumulation under hyperosmotic condition. **(A)** *CaSPT20* has an important effect on intracellular glycerol content under hyperosmotic condition. 5×10^7 cells with or without treatment (1 M NaCl or YPD) were grown at 30°C for an additional 30 min and then used for glycerol measurement. The ability of *spt20*Δ/Δ strain to accumulate cellular glycerol under osmotic stress was impaired. **(B)** *SPT20* affects the expression of genes involved in glycerol accumulation. qRT-PCR analysis was used to measure the expression of genes involved in glycerol accumulation following exposure to 1 M NaCl. The following *C. albicans* strains were evaluated: wild type SC5314, *spt20*Δ/Δ, and *spt20*Δ*/SPT20* and genes were analyzed in triplicate. Expression levels were normalized to 18S rRNA. Fold changes between strains were normalized to untreated wild type, which was adjusted to a value of 1. Three independent biological replicates were conducted. Error bar represents Mean ± SD. *$P < 0.01$, **$P < 0.001$.

following. First, the cell growth defect of *Caspt20*Δ/Δ was similar to that of *Cahog1*Δ/Δ (**Figure 4**). Second, the phosphorylation level of Hog1 was significantly decreased because of the absence of *SPT20* (**Figure 2**). Our western blotting result showed that, as reported previously (Smith et al., 2004), Hog1 was rapidly but transiently phosphorylated during *C. albicans* salt exposure. However, phosphorylation levels were comparably lower in *Caspt20*Δ/Δ, suggesting that *CaSPT20* affected the process of Hog1 phosphorylation. Hog1 phosphorylation is a dynamic event (Alonso-Monge et al., 2003; Smith et al., 2004). The kinetics of

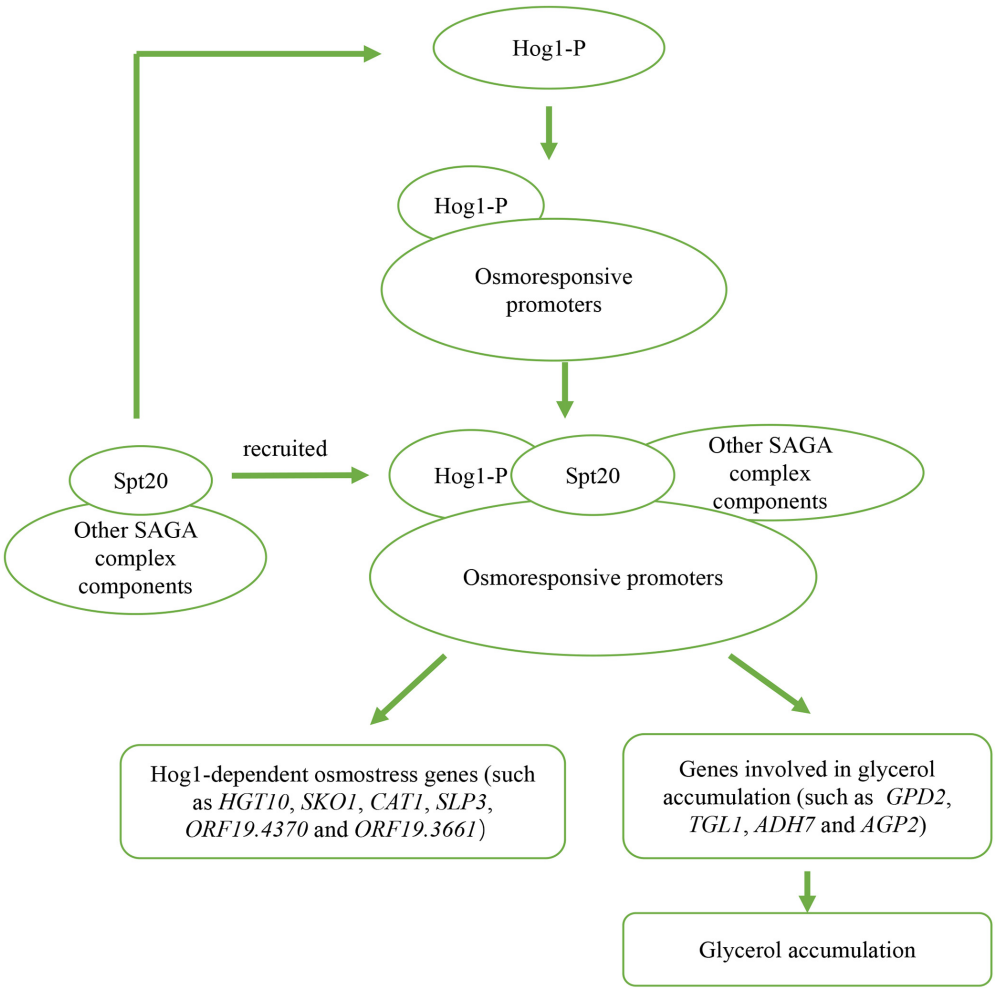

FIGURE 6 | Outline of two potential mechanisms of Spt20 in *C. albicans* response to osmotic stress. Previous work found that when cells are subjected to high osmolarity, Hog1 is activated and bind to osmostress promoters, then recruits SAGA complex components to induce expression of Hog1-dependent osmostress response genes and genes involved in glycerol accumulation. In our study, we found that Spt20 regulates the phosphorylation of Hog1 in response to osmotic stress.

phosphorylation were different in these two strains: wild type strain peaked at about 10 min after exposure to stress, while the mutant strain peaked at about 60 min. However, in both wild type and mutant strains, the peak levels of phospho-Hog1 were diminished over time. Third, overexpressing *HOG1* in the *spt20*Δ/Δ mutant background can partially rescue the growth defect when *spt20*Δ/Δ mutant strain was exposed to osmotic stress, while overexpressing *SPT20* in the *hog1*Δ/Δ mutant background was not able to restore its ability to respond to hyperosmolarity (**Figure 4**). Meanwhile, the HOG1-OE strain demonstrated higher basal level of phosphorylated Hog1 and total Hog1 protein than wild type and *spt20*Δ/Δ mutant strain (**Figure 2** and **Supplementary Figure 1B**), which may contribute to tolerate its osmostress, since *C. albicans* regulates the phosphorylation of Hog1 to respond to hyperosmolarity (Smith et al., 2004). Though the basal phosphorylated Hog1 level of wt-HOG1-OE strain was enhanced as well, overexpression of *HOG1* did not increase the resistance to osmolarity in wild type. Our working hypothesis is that the phospho-Hog1 level in wild type may be similar to that in wt-HOG1-OE strain under osmotic exposure which leads to similar cell growth. Additionally, overexpression *HOG1* did not revert the growth defect of *Caspt20*Δ/Δ mutant strain to a level comparable to the wild type, suggesting that besides the Hog1-MAPK pathway, there may exist another mechanism that accounts for *SPT20* response to osmotic stress. Strikingly, *SPT20* overexpression in the *hog1*Δ/Δ mutant background reduced the cell growth in the YPD plate. This phenotype was not due to the changes in the shape of fungal cells, since the SPT20-OE strain cells grew as unicellular yeast and the shape was similar to that of wild type and *hog1*Δ/Δ mutant strain (**Supplementary Figure 3**). *SPT20* is crucial for the structural integrity of SAGA complex (Grant et al., 1997; Sterner et al., 1999), thus, overexpressing *SPT20* may change the structure of SAGA complex, which would hamper the normal gene expression and then impair normal cell growth.

We noticed that, compared to wild type, the transcript level of genes involved in glycerol accumulation was either reduced or induced in the *Caspt20*Δ/Δ mutant strain (**Figure 5B**). However, the changing patterns of these genes were similar to that of wild type. When *C. albicans* cells were subjected to osmotic stress, the activation of the Hog1-MAPK pathway can regulate the synthesis and accumulation of glycerol (San José et al., 1996; Monge et al., 2006), along with up-regulation of genes contributing to increase the intercellular glycerol levels and down-regulation of genes contributing to reduce the glycerol levels. Although the magnitude of Hog1 activation was significantly decreased in *Caspt20*Δ/Δ mutant strain (**Figure 2A**), the reduced phosphorylated Hog1 can still induce or repress the related gene expression to cope with osmolarity. Strikingly, the fold induction of *GPD2* in *Caspt20*Δ/Δ mutant strain is greater than that in wild type. We hypothesized that the repressed expression of *ADH7* and *TGL1*, together with the up-regulation of *AGP2* contribute to the decrease of intracellular glycerol, which may in turn lead to a greater fold induction of *GPD2* in *Caspt20*Δ/Δ mutant strain response to osmotic stress. Furthermore, in contrast to the induction of *GPD2* expression reported previously (Enjalbert et al., 2006; Marotta et al., 2013), there was no increase in *GPD2* expression in wild type cells when osmotic stress was imposed. However, the transcript level of *GPD2* is dynamic and related to the incubation time upon osmotic stress (Enjalbert et al., 2006) and the *C. albicans* wild type strains used in these studies were different, thus we speculated that the incubation time and the wild type strains were associated with the different *GPD2* expression.

Our study has limitations that need to be taken into account and addressed in the future. First, although the growth defects of *Scspt20*Δ were rescued with complementation of *CaSPT20* (**Figure 1**), *C. albicans SPT20* gene was not codon optimized prior to expression in *S. cerevisiae*, which should be noted as a limitation in our study because it may lead to mistranslation. Also, in future work, we plan to evaluate a *Caspt20*Δ*/hog1*Δ double mutant strain to further assess genetic epistasis between *SPT20* and *HOG1*.

CONCLUSION

In conclusion, we confirm that *SPT20* is functionally conserved between *S. cerevisiae* and *C. albicans*, and report that *SPT20* plays a critical role in *C. albicans* response to hyperosmotic stress through regulating Hog1-MAPK pathway, through both expression and phosphorylation (**Figure 6**). The reduced Hog1 phosphorylation in *Caspt20*Δ/Δ mutant can explain its high sensitivity to osmotic stress, indicating a relationship between Spt20 and Hog1 in the response to altered osmotic conditions.

DATA AVAILABILITY STATEMENT

All datasets generated for this study are included in the article/**Supplementary Material**.

AUTHOR CONTRIBUTIONS

RC, LW, BF, XT, and EM designed the study. LW, RC, SL, and QW performed the experiments. SL, HW, and LL helped to analyze the data. LW, BF, XT, and EM wrote the manuscript. XT contributed to reagents and materials, and supervised the project.

FUNDING

This work was supported by the Science and Technology Planning Project of Guangdong Province, China (Grant 2015A050502026) and National Natural Science Foundation of China (Grant 81570012) to XT. The funders had no role in study design, data collection and analysis, decision to publish, or preparation of the manuscript. All other authors have no financial disclosures.

ACKNOWLEDGMENTS

We thank Ching-Hsuan Lin for providing the *C. albicans hog1*Δ/Δ mutant strain and the hog1Δ/HOG1 strain (Liang et al., 2014), Aaron P. Mitchell for providing plasmid *pCJN542*, and Eishi Noguchi for providing plasmid *pFA6a-5FLAG-KanMX6* (Addgene plasmid # 15983).

SUPPLEMENTARY MATERIAL

The Supplementary Material for this article can be found online at: https://www.frontiersin.org/articles/10.3389/fmicb.2020.00213/full#supplementary-material

REFERENCES

Alonso-Monge, R., Navarro-García, F., Molero, G., Diez-Oreias, R., Gustin, M., Pla, J., et al. (1999). Role of the mitogen-activated protein kinase Hog1p in morphogenesis and virulence of Candida albicans. *J. Bacteriol.* 181, 3058–3068. doi: 10.1128/jb.181.10.3058-3068.1999

Alonso-Monge, R., Navarro-García, F., Román, E., Negredo, A. I., Eisman, B., Nombela, C., et al. (2003). The Hog1 Mitogen-Activated Protein Kinase Is Essential in the Oxidative Stress Response and Chlamydospore Formation in Candida albicans. *Eukaryot. Cell.* 2, 351–361. doi: 10.1128/ec.2.2.351-361.2003

Blomberg, A., and Adler, L. (1989). Roles of glycerol and glycerol-3-phosphate dehydrogenase (n.d.) in acquired osmotolerance of Saccharomyces cerevisiae. *J. Bacteriol.* 171, 1087–1092. doi: 10.1128/jb.171.2.1087-1092.1989

Brewster, J. L., and Gustin, M. C. (2014). Hog1: 20 years of discovery and impact. *Sci. Signal.* 7:re7. doi: 10.1126/scisignal.2005458

Calderone, R. A., and Fonzi, W. A. (2001). Virulence factors of Candida albicans. *Trends. Microbiol.* 9, 327–335. doi: 10.1016/S0966-842X(01)02094-7

Day, A. M., Herrero-de-Dios, C. M., MacCallum, D. M., Brown, A. J. P., and Quinn, J. (2017). Stress-induced nuclear accumulation is dispensable for Hog1-dependent gene expression and virulence in a fungal pathogen. *Scientif. Rep.* 7, 14340–14340. doi: 10.1038/s41598-017-14756-4

Deng, F. S., and Lin, C. H. (2018). Cpp1 phosphatase mediated signaling crosstalk between Hog1 and Cek1 mitogen-activated protein kinases is involved in the phenotypic transition in Candida albicans. *Med. Mycol.* 56, 242–252. doi: 10.1093/mmy/myx027

Dong, Y., Yu, Q., Chen, Y., Xu, N., Zhao, Q., Jia, C., et al. (2015). The Ccz1 mediates the autophagic clearance of damaged mitochondria in response to oxidative stress in Candida albicans. *Int. J. Biochem. Cell. Biol.* 69, 41–51. doi: 10.1016/j.biocel.2015.10.002

Ene, I. V., Walker, L. A., Schiavone, M., Lee, K. K., Martin-Yken, H., Daque, E., et al. (2015). Cell wall remodeling enzymes modulate fungal cell wall elasticity and osmotic stress resistance. *MBio* 6:e00986. doi: 10.1128/mBio.00986-15

Enjalbert, B., Smith, D. A., Cornell, M. J., Alam, I., Nicholls, S., Brown, A. J., et al. (2006). Role of the Hog1 stress-activated protein kinase in the global transcriptional response to stress in the fungal pathogen Candida albicans. *Mol. Biol. Cell.* 17, 1018–1032. doi: 10.1091/mbc.e05-06-0501

Fan, J., Whiteway, M., and Shen, S. H. (2005). Disruption of a gene encoding glycerol 3-phosphatase from *Candida albicans* impairs intracellular glycerol accumulation-mediated salt-tolerance. *FEMS Microbiol. lett.* 245, 107–116. doi: 10.1016/j.femsle.2005.02.031

Fuchs, B. B., and Mylonakis, E. (2009). Our paths might cross: the role of the fungal cell wall integrity pathway in stress response and cross talk with other stress response pathways. *Eukaryot. Cell.* 8, 1616–1625. doi: 10.1128/EC.00193-09

Gietz, R. D. (2014). "Yeast transformation by the LiAc/SS carrier DNA/PEG method," in *The Yeast Genetics,Methods in Molecular Biology*, ed Edn, eds J. Smith, and D. Burke, (New York, NY: Humana Press), 1–12. doi: 10.1007/978-1-4939-1363-3_1

Grant, P. A., Duggan, L., Côté, J., Roberts, S. M., Brownell, J. E., Candau, R., et al. (1997). Yeast Gcn5 functions in two multisubunit complexes to acetylate nucleosomal histones: characterization of an Ada complex and the SAGA (Spt/Ada) complex. *Genes. Dev.* 11, 1640–1650. doi: 10.1101/gad.11.13.1640

Hickman, M. J., Spatt, D., and Winston, F. (2011). The Hog1 mitogen-activated protein kinase mediates a hypoxic response in Saccharomyces cerevisiae. *Genetics* 188, 325–338. doi: 10.1534/genetics.111.128322

Hohmann, S. (2002). Osmotic stress signaling and osmoadaptation in yeasts. *Microbiol. Mol. Biol. Rev.* 66, 300–372. doi: 10.1128/mmbr.66.2.300-372.2002

Hohmann, S., Krantz, M., and Nordlander, B. (2007). Yeast osmoregulation. *Methods Enzymol.* 428, 29–45. doi: 10.1016/S0076-6879(07)28002-4

Jacobsen, M. D., Beynon, R. J., Gethings, L. A., Claydon, A. J., Langridge, J. I., Vissers, J. P. C., et al. (2018). Specificity of the osmotic stress response in Candida albicans highlighted by quantitative proteomics. *Scientif. Rep.* 8, 14492–14492. doi: 10.1038/s41598-018-32792-6

Jandrositz, A., Petschnigg, J., Zimmermann, R., Natter, K., Scholze, H., Hermetter, A., et al. (2005). The lipid droplet enzyme Tgl1p hydrolyzes both steryl esters and triglycerides in the yeast, Saccharomyces cerevisiae. *Biochim. Biophys. Acta* 1735, 50–58. doi: 10.1016/j.bbalip.2005.04.005

Lee, T. I., Causton, H. C., Holstege, F. C., Shen, W. C., Hannett, N., Jennings, E. G., et al. (2000). Redundant roles for the TFIID and SAGA complexes in global transcription. *Nature* 405, 701–704. doi: 10.1038/35015104

Liang, S. H., Cheng, J. H., Deng, F. S., Tsai, P. A., and Lin, C. H. (2014). A novel function for Hog1 stress-activated protein kinase in controlling white-opaque switching and mating in Candida albicans. *Eukaryot. Cell.* 13, 1557–1566. doi: 10.1128/EC.00235-14

Marotta, D. H., Nantel, A., Sukala, L., Teubl, J. R., and Rauceo, J. M. (2013). Genome-wide transcriptional profiling and enrichment mapping reveal divergent and conserved roles of Sko1 in the Candida albicans osmotic stress response. *Genomics* 102, 363–371. doi: 10.1016/j.ygeno.2013.06.002

Monge, R. A., Román, E., Nombela, C., and Pla, J. (2006). The MAP kinase signal transduction network in Candida albicans. *Microbiology* 152, 905–912. doi: 10.1099/mic.0.28616-0

Nagy, Z., Riss, A., Romier, C., le Guezennec, X., Dongre, A. R., Orpinell, M., et al. (2009). The human SPT20-containing SAGA complex plays a direct role in the regulation of endoplasmic reticulum stress-induced genes. *Mol. Cell. Biol.* 29, 1649–1660. doi: 10.1128/MCB.01076-08

Nobile, C. J., Solis, N., Myers, C. L., Fay, A. J., Deneault, J. S., Nantel, A., et al. (2008). Candida albicans transcription factor Rim101 mediates pathogenic interactions through cell wall functions. *Cell. Microbiol.* 10, 2180–2196. doi: 10.1111/j.1462-5822.2008.01198.x

Noguchi, C., Garabedian, M. V., Malik, M., and Noguchi, E. (2008). A vector system for genomic FLAG epitope-tagging in Schizosaccharomyces pombe. *Biotechnol. J.* 3, 1280–1285. doi: 10.1002/biot.200800140

Reed, R. H., Chudek, J. A., Foster, R., and Gadd, G. M. (1987). Osmotic significance of glycerol accumulation in exponentially growing yeasts. *Appl. Environ. Microbiol.* 53, 2119–2123. doi: 10.1128/aem.53.9.2119-2123.1987

Roberts, S. M., and Winston, F. (1996). SPT20/ADA5 encodes a novel protein functionally related to the TATA-binding protein and important for transcription in Saccharomyces cerevisiae. *Mol. Cell. Biol.* 16, 3206–3213. doi: 10.1128/mcb.16.6.3206

Roberts, S. M., and Winston, F. (1997). Essential functional interactions of SAGA, a Saccharomyces cerevisiae complex of Spt, Ada, and Gcn5 proteins, with the Snf/Swi and Srb/mediator complexes. *Genetics* 147, 451–465.

San José, C., Monge, R. A., Pérez-Díaz, R., Pla, J., and Nombela, C. (1996). The mitogen-activated protein kinase homolog HOG1 gene controls glycerol accumulation in the pathogenic fungus Candida albicans. *J. Bacteriol.* 178, 5850–5852. doi: 10.1128/jb.178.19.5850-5852.1996

Sellam, A., Askew, C., Epp, E., Lavoie, H., Whiteway, M., and Nantel, A. (2009). Genome-wide mapping of the co-activator Ada2p yields insight into the functional roles of SAGA/ADA complex in Candida albicans. *Mol. Biol. Cell.* 20, 2389–2400. doi: 10.1091/mbc.e08-11-1093

Sheikh-Hamad, D., and Gustin, M. C. (2004). MAP kinases and the adaptive response to hypertonicity: functional preservation from yeast to mammals. *Am. J. Physiol. Renal Physiol.* 287, F1102–10. doi: 10.1152/ajprenal.00225.2004

Smith, D. A., Nicholls, S., Morgan, B. A., Brown, A. J., and Quinn, J. (2004). A conserved stress-activated protein kinase regulates a core stress response in the human pathogen Candida albicans. *Mol. Biol. Cell.* 15, 4179–4190. doi: 10.1091/mbc.e04-03-0181

Sterner, D. E., Grant, P. A., Roberts, S. M., Duggan, L. J., Belotserkovskaya, R., Pacella, L. A., et al. (1999). Functional organization of the yeast SAGA complex: distinct components involved in structural integrity, nucleosome acetylation, and TATA-binding protein interaction. *Mol. Cell. Biol.* 19, 86–98. doi: 10.1128/MCB.19.1.8610.1091/mbc.e05-06-0501

Tan, X., Fuchs, B. B., Wang, Y., Chen, W., Yuen, G. J., Chen, R. B., et al. (2014). The role of Candida albicans SPT20 in filamentation, biofilm formation and pathogenesis. *PLoS One* 9:e94468. doi: 10.1371/journal.pone.0094468

Wei, M., Fabrizio, P., Madia, F., Hu, J., Ge, H., Li, L. M., et al. (2009). Tor1/Sch9-regulated carbon source substitution is as effective as calorie restriction in life span extension. *PLoS Genet.* 5:e1000467. doi: 10.1371/journal.pgen.1000467

Wisplinghoff, H., Bischoff, T., Tallent, S. M., Seifert, H., Wenzel, R. P., and Edmond, M. B. (2004). Nosocomial bloodstream infections in US hospitals: analysis of 24,179 cases from a prospective nationwide surveillance study. *Clin. Infect. Dis.* 39, 309–317. doi: 10.1086/421946

Zapater, M., Sohrmann, M., Peter, M., Posas, F., and de Nadal, E. (2007). Selective requirement for SAGA in Hog1-mediated gene expression depending on the severity of the external osmostress conditions. *Mol. Cell. Biol.* 27, 3900–3910. doi: 10.1128/MCB.00089-07

Zhou, N., Lei, B. K., Zhou, X., Yu, Y., and Lv, H. (2013). Yi chuan = Hereditas. *SJR* 35, 1135–1142. doi: 10.3724/sp.j.1005.2013.01135

Zohn, I. E., Li, Y., Skolnik, E. Y., Anderson, K. V., Han, J., and Niswander, L. (2006). p38 and a p38-interacting protein are critical for downregulation of E-cadherin during mouse gastrulation. *Cell* 125, 957–969. doi: 10.1016/j.cell.2006.03.048

Conflict of Interest: The authors declare that the research was conducted in the absence of any commercial or financial relationships that could be construed as a potential conflict of interest.

frontiers in Microbiology

ORIGINAL RESEARCH
published: 21 April 2020
doi: 10.3389/fmicb.2020.00730

Alkylimidazolium Ionic Liquids as Antifungal Alternatives: Antibiofilm Activity Against *Candida albicans* and Underlying Mechanism of Action

G. Kiran Kumar Reddy[1,2] *and Y. V. Nancharaiah*[1,2]*

[1] *Biofouling and Biofilm Processes, Water and Steam Chemistry Division, Chemistry Group, Bhabha Atomic Research Centre, Kalpakkam, India,* [2] *Homi Bhabha National Institute, Mumbai, India*

OPEN ACCESS

Edited by:
Juliana Campos Junqueira, São Paulo State University, Brazil

Reviewed by:
Roberta Gaziano, Tor Vergata University of Rome, Italy
Junya Lacorte Singulani, São Paulo State University, Brazil

***Correspondence:**
Y. V. Nancharaiah
yvn@igcar.gov.in;
venkatany@gmail.com

Specialty section:
This article was submitted to Fungi and Their Interactions, a section of the journal Frontiers in Microbiology

Received: *07 October 2019*
Accepted: *27 March 2020*
Published: *21 April 2020*

Citation:
Reddy GKK and Nancharaiah YV (2020) Alkylimidazolium Ionic Liquids as Antifungal Alternatives: Antibiofilm Activity Against Candida albicans and Underlying Mechanism of Action. Front. Microbiol. 11:730. doi: 10.3389/fmicb.2020.00730

Candida albicans is an opportunistic pathogen causes fungal infections that range from common skin infections to persistent infections through biofilm formation on tissues, implants and life threatening systemic infections. New antifungal agents or therapeutic methods are desired due to high incidence of infections and emergence of drug-resistant strains. The present study aimed to evaluate (i) the antifungal and antibiofilm activity of 1-alkyl-3-methyl imidazolium ionic liquids ($[CnMIM]^+[X]^-$, n = 4, 12 and 16) against *Candida albicans* ATCC 10231 and two clinical *C. albicans* strains and (ii) the mechanism of action of promising antifungal ionic liquid on *C. albicans*. Two of the tested compounds were identified as more effective in preventing growth and biofilm formation. These ionic liquid compounds with –dodecyl and –hexadecyl alkyl groups effectively prevented biofilm formation by fluconazole resistant *C. albicans* 10231 and two other clinical *C. albicans* strains. Although both the compounds caused viability loss in mature *C. albicans* biofilms, an ionic liquid with –hexadecyl group ($[C_{16}MIM]^+[Cl]^-$) was more effective in dispersing mature biofilms. This promising ionic liquid compound ($[C_{16}MIM]^+[Cl]^-$) was chosen for determining the underlying mode of action on *C. albicans* cells. Light microscopy showed that ionic liquid treatment led to a significant reduction in cell volume and length. Increased cell membrane permeability in the ionic liquid treated *C. albicans* cells was evident in propidium iodide staining. Leakage of intracellular material was evident in terms of increased absorbance of supernatant and release of potassium and calcium ions into extracellular medium. A decrease in ergosterol content was evident when *C. albicans* cells were cultured in the presence of antifungal ionic liquid. 2′,7′-Dichlorodihydrofluorescein acetate assay revealed reactive oxygen species generation and accumulation in *C. albicans* cells upon treatment with antifungal ionic liquid. The effect of antifungal ionic liquid on mitochondria was evident by decreased membrane potential (measured by Rhodamine 123 assay) and loss of

metabolic activity (measured by MTT assay). This study demonstrated that imidazolium ionic liquid compound exert antifungal and antibiofilm activity by affecting various cellular processes. Thus, imidazolium ionic liquids represent a promising antifungal treatment strategy in lieu of resistance development to common antifungal drugs.

Keywords: imidazolium ionic liquids, antifungal drugs, antibiofilm agents, *Candida albicans* biofilms, ergosterol content, membrane damage, mitochondrial dysfunction, oxidative stress

INTRODUCTION

Fungal pathogens are a major health issue causing over 1.6 million deaths annually (Almeida et al., 2019). Several species of *Candida* are responsible for the fungal infections, collectively called as candidiasis. These are commensal organisms in healthy individuals and reside in gastrointestinal, respiratory, and genitourinary tracts. In immunocompromised or diseased patients, they become opportunistic and cause infections ranging from superficial (oral or vaginal) to life threatening systemic infections[1]. About 50 to 70% of systemic fungal infections are caused by *Candida* spp. (Santos et al., 2018). *Candida albicans* is the most frequently observed organism in candidiasis. Persistent Candida infections are increasingly being reported in medically implanted devices such as catheters, heart valves, pacemakers, vascular bypass grafts, dentures and endotracheal tubes thus leading to high mortalities (Ramage et al., 2006; Sardi et al., 2013; Santos et al., 2018). Biofilm mode of growth by *Candida* spp. further complicates the treatment as the cells reside in biofilms are about 2000 times more resistant to fluconazole and amphotericin B over their planktonic counterparts (Bergamo et al., 2015).

Azoles, polyenes, allylamines, and echinocandins are the current antifungal arsenal available for treating candidiasis (Fuentefria et al., 2018). Fluconazole is most commonly used for treating candidiasis due to its low cost, high bioavailability and possibility of drug administration is various formulations (Martin, 1999). However, well documented resistance of *Candida* spp. to fluconazole makes this drug a less attractive antifungal agent in the current treatment scenario. Besides drug efflux mechanisms, alterations in target sites/gene expression, current challenges in treatment include biofilm formation which directly or indirectly enhances the drug resistance (Fuentefria et al., 2018). Currently applied strategies are ineffective against biofilms warranting prospective new antifungal agents from natural or synthetic origin (Sardi et al., 2013; Gyawali and Ibrahim, 2014; Nobile and Johnson, 2015). A potential antifungal agent should have broad spectrum activity in terms of antifungal and antibiofilm activities with minimal cytotoxicity and side effects to the host.

Ionic liquids are a novel class of molten salts at $\leq$100°C and exclusively made up of combination of cations and anions (Rogers and Seddon, 2003). These salts typically comprises of a large cationic core (often a nitrogen containing group with alkyl substituent) and a small counter anion (Pendleton and Gilmore, 2015). Apart from their applications in chemical industry (Vekariya, 2017), these compounds are promising as components of active pharmaceutical ingredients and antimicrobials (Egorova et al., 2017). The tunable property of ionic liquids by way of changing their constituent ions, allows making large structural diversity of about 10^{18} compounds (Pernak et al., 2007) with altered physical, chemical and biological activities. Some of these ionic liquids have been explored as antimicrobials, antiseptics and antifouling agents (Pernak et al., 2004; Nancharaiah et al., 2012; Egorova et al., 2017). Imidazolium ionic liquids have been reported for effective control of bacterial and phototrophic biofilms (Carson et al., 2009; Busetti et al., 2010; Reddy et al., 2017, 2020). With respect to antifungal activity, –ethyl and –butyl side chain containing imidazolium, pyridinium and cholinium ionic liquids were evaluated against *Penicillium* sp. (Petkovic et al., 2009). Schrekker et al. (2013) reported the efficient antifungal activity of N-alkyl-substituted imidazolium salts with –decane, –tetradecane and –hexadecane side chain containing cations against fungal pathogens with minimum toxicity to leukocytes. Activity of –hexadecyl side chain containing imidazolium ionic liquid against multidrug resistant *Candida tropicalis* and clinical dermatophyte strains showed potential activity against biofilms (Bergamo et al., 2014, 2015; Dalla Lana et al., 2015). Inhibition of conidia germination and mycelial growth was observed in *Fusarium graminearum* (Ribas et al., 2016). Antifungal ionic liquids were incorporated into poly(L-lactide) biomaterials for inhibiting adhesion of *Candida* spp. (Schrekker et al., 2016). Using contaminated acrylic resin strip specimens, 1-n-hexadecyl-3-methylimidazolium chloride was demonstrated as a strong antifungal for mouthwash formulation (Bergamo et al., 2016). Although several studies have reported antifungal activity, effect of imidazolium ionic liquids on preformed fungal biofilms (biofilm eradication potential) is largely unknown (**Table 1**). Evaluation of antifungal ionic liquids on preformed biofilms is of clinical relevance as the biofilm formation often precedes treatment. Cell membrane has been identified as the potential target in the case of imidazolium ionic liquids (Nancharaiah et al., 2012; Benedetto, 2017; Egorova et al., 2017). Other studies indicated that imidazolium ionic liquids can decrease the content of ergosterol, an important component of fungal cell membranes (Schrekker et al., 2013). Ionic liquids are currently seen as promising asset for fighting fungal infections (Hartmann et al., 2016). Due to limited understanding of mechanisms, studies aimed at identifying potential targets and underlying mode of action of antifungal ionic liquids are desired for their prospective use in treating infections.

This study was aimed to determine the antifungal, antibiofilm and biofilm eradication activities of three imidazolium ionic liquids against *C. albicans* strains and to understand the mode of action of potent antifungal imidazolium ionic liquid. Antibiofilm activity was determined as prevention

[1]http://www.cdc.gov/fungal/diseases/candidiasis/

TABLE 1 | Summary of studies on evaluation of ionic liquids against various fungal strains.

Ionic liquid	Fungi	MIC (μmol l^{-1})	MFC (μmol l^{-1})	Effective Antibiofilm concentrations	Biofilm eradication	Reference
$[C_{16}MIM]Cl$	6 isolates of *C. tropicalis*	0.04	ND	0.08–0.65	Killing of biofilm cells.	Bergamo et al., 2014
$[C_nMIM]Cl$ (n = 4, 10, 12, 16, 18);	21 strains of *Microsporum* sp.; 24 strains of *Trichophyton* sp.	Avg MIC_{50} C_4 = 71; C_{10} = 10.16; C_{12} = 6.59; C_{16} = 0.20; C_{18} = 20.03.	C_{16} = 0.6–36 for *Microsporum* sp.; C_{16} = 0.23–36.4 for *Trichophyton* sp.	ND	ND	Dalla Lana et al., 2015
$[C_nMIM]MeS$ (n = 4, 9, 16)	21 strains of *Microsporum* sp.; 24 strains of *Trichophyton* sp.	Avg MIC_{50} C_4 = 53; C_9 = 17.37 C_{16} = 0.12.	C16 = 0.5–31 for *Microsporum* sp.; C16 = 0.5–31 for *Trichophyton* sp.	ND	ND	Dalla Lana et al., 2015
$[C_{16}MIM]Cl$; $[C_{16}MIM]MeS$	*Candida tropicalis*	ND	ND	ND	Killing of biofilm cells	Bergamo et al., 2015
$[C_{16}MIM]Cl$; $[C_{16}MIM]MeS$	4 *Fusarium graminearum* strains	9.1–18.2 and 7.7–15.5	ND	ND	ND	Ribas et al., 2016
$[C_nMIM]Cl$ (n = 4, 12, 16)	Three fluconazole resistant *C. albicans* strains	$C_4 \geq 1000$, C_{12} = 25, C_{16} = 4.68	$C_4 \geq 1000$, C_{12} = 75, C_{16} = 6.25	C_4 = NE, C_{12} = 25, C_{16} = 6.25	C_4 = NE; C_{12} = Biofilm cell killing; C_{16} = Killing and biofilm removal	Current study

$[C_nMIM]Cl$: 1-n-Alkyl-3-methylimidazolium chloride; $[C_nMIM]MeS$: 1-n-Alkyl-3-methylimidazolium methanesulfonate; ND, not determined; NE, no effect.

of biofilm formation in the presence of ionic liquids and antifungal drugs. Biofilm eradication was determined in terms of killing and dispersal activity of ionic liquids on preformed fungal biofilms.

MATERIALS AND METHODS

Organisms, Media and Growth Conditions

This research was conducted using *C. albicans* ATCC 10231 (Microbiologics, United States), a reference strain commonly used for evaluating antifungal and antibiofilm agents. Experiments were conducted with two clinical strains of *C. albicans* [CA i16 (GenBank No. MG757722.1) and CA i21 (GenBank No. MG757724.1)] which were isolated from sputum samples of patients. The clinical strains were obtained from University of Madras, India. These cultures were routinely maintained on potato dextrose agar (PDA) (HiMedia, India). For liquid cultures, a single colony was picked from PDA, transferred to potato dextrose broth (PDB) and incubated for 24 h at 30°C and 120 RPM in a temperature controlled orbital shaker. Cells harvested from PDB were used for growth and biofilm experiments.

Filter sterilized RPMI 1640 medium (L-Glutamine, phenol red, 2 g l^{-1} glucose and 0.165 mol l^{-1} MOPS buffer, pH 7.0) (Part No. AT180, HiMedia, India) was used for biofilm experiments. Cultures were grown in PDB for 24 h, pelleted by centrifugation, re-suspended in RPMI 1640 and adjusted to desired cell density for performing biofilm experiments. For determining the mechanism of action, cells were re-suspended in phosphate buffered saline (PBS).

Imidazolium Ionic Liquids and Antifungal Drugs

1-butyl-3-methylimidazolium chloride ($[C_4MIM][Cl]$), 1-dodecyl-3-methylimidazolium iodide ($[C_{12}MIM][I]$), fluconazole and amphotericin B were purchased from Sigma-Aldrich (United States). 1-hexadecyl-3-methylimidazolium chloride ($[C_{16}MIM][Cl]$) was purchased from Acros (United States). The chemical structures of three ionic liquids used in this study are given in **Supplementary Information** (**Supplementary Figure S1**). Stock solutions (100 mmol l^{-1}) of ionic liquids were prepared in sterile, ultrapure water and stored at room temperature until further use. Stock solutions of fluconazole (32 mmol l^{-1}) and amphotericin B (13 mmol l^{-1}) were prepared, respectively, in ethanol and dimethyl sulfoxide (DMSO). These stock solutions were stored at 4°C until use.

MIC and MFC of Ionic Liquids Against *C. albicans* ATCC 10231

MIC of ionic liquids was determined by microdilution method according to the Clinical and Laboratory Standards Institute (CLSI) guidelines [CLSI (2012)]. Actively growing log phase culture in PDB was pelleted by centrifugation (8000 rpm for 5 min). Cell pellet was re-suspended in RPMI 1640 and cell density was adjusted. MIC and MFC values were determined in RPMI 1640 medium containing initial cell densities of 10^3 or 10^6 cfu ml^{-1}. Initial cell density of 10^3 cfu ml^{-1} is recommended for determining MIC according to CLSI antifungal susceptibility testing [CLSI (2012)]. Initial cell density of 10^6 cfm ml^{-1} often employed in biofilm inhibition studies was also used for determining MIC and MFC values according to Pierce et al. (2008). A two-fold series dilution of ionic liquids

and antifungal drugs (fluconazole and amphotericin B) were prepared in RPMI 1640 containing *C. albicans* cells. Working concentrations in the range of 1000 to 31.25 μmol l^{-1} for [C_4MIM][Cl], 100 to 1.15 μmol l^{-1} for [C_{12}MIM][I] and 50 to 1.15 μmol l^{-1} for [C_{16}MIM][Cl] were prepared in RPMI 1640 and tested. Concentrations of fluconazole and amphotericin B were, respectively, in the range of 3265 to 12.75 μmol l^{-1} and 13 to 0.16 μmol l^{-1}. Subsequently, 200 μl of these dilutions were transferred to the wells of 96-well microtiter plate. Five replicates were set up for each concentration. Control wells received cells in RPMI without the compound. After 24 h of incubation in an orbital shaker at 37°C and 120 RPM, growth was determined by measuring absorbance at 600 nm using a microplate reader (BioTek®, United States). The lowest concentration that prevented *C. albicans* growth (measured as absorbance at 600 nm) was represented as MIC. For MFC estimation, aliquots of suspension from selected microtiter wells were plated onto PDA plates and incubated at 37°C for 48 h. MFC was the lowest concentration at which no colonies of *C. albicans* appeared on PDA plates.

Antibiofilm Activity of Ionic Liquids

For estimating incubation time for maximum biofilm formation, RPMI 1640 containing 10^6 cfu ml^{-1} was aliquoted (200 μl) in 96-well sterile, flat bottom, polystyrene microtiter plates (Tarsons, India). Pierce et al. (2008) recommended 10^6 cfu ml^{-1} as inoculum cell density for developing *C. albicans* biofilms in 96-well plates. Hence, 10^6 cfu ml^{-1} cells were used for all biofilm experiments. Multi-well plates containing cells in RPMI 1640 were incubated at 120 RPM and 37°C for 6, 12, 18, 24 or 48 h. At the end of incubation, biofilm mass and metabolic activity were estimated by crystal violet (CV) and 2,3-Bis-(2-Methoxy-4-Nitro-5-Sulfophenyl)-2H-Tetrazolium-5-Carboxanilide (XTT), respectively. Based on time course experiment on biofilm formation, 24 h incubation time was chosen for quantifying the effect of ionic liquids and antifungal drugs on biofilm formation.

Antibiofilm activity was determined by incubating planktonic and adherent cells separately in the presence of ionic liquids and antifungal drugs. *C. albicans* cell suspensions (200 μl, 10^6 CFU/ml in RPMI 1640) were transferred to each well of a 96-well microtiter plate. Ionic liquids and antifungal drugs were added and serially diluted using two-fold dilution. Final concentrations in the range of 1000 to 125 μmol l^{-1} for [C_4MIM][Cl], 50 to 2.3 μmol l^{-1} for [C_{12}MIM][I] and 25 to 1.1 μmol l^{-1} for [C_{16}MIM][Cl] were tested. Amphotericin B was tested in the range of 13 to 0.168 μmol l^{-1}. Fluconazole concentrations were tested up to 3265 μmol l^{-1}. Effect of anions (Cl^- and I^-) and 1-methylimidazole on growth and biofilm formation of *C. albicans* was determined by incubating with excess concentrations (500–1000 μmol l^{-1}) of NaCl, KI and 1-methylimidazole. For each concentration, five replicate wells were used. The plates were incubated at 37°C in an orbital shaker at 120 rpm to allow biofilm formation. For determining antibiofilm activity using adherent cells, the cell suspensions were transferred to each well of a microtiter plate and incubated for 3 h at 37°C in an orbital shaker at 120 rpm to allow adhesion. Subsequent to adhesion, the non-attached cells were carefully removed from the wells. Then 200 μl of RPMI medium containing different concentration of ionic liquids and antifungal drugs was added to each well. The plates were incubated for 24 h as described above to allow biofilm formation.

The biofilm was quantified using the both CV assay (Nancharaiah et al., 2012) and XTT reduction assay (Henriques et al., 2006). For CV assay, biofilms were stained with 0.1% CV (HiMedia, India) for 10 min. Excess CV was removed by washing the wells with demineralized water (Nancharaiah et al., 2012). Plates were air-dried for overnight and CV bound to the biofilm was eluted with 33% glacial acetic acid. Eluted CV was measured by reading absorbance at 570 nm. Eluted CV was diluted with 33% glacial acetic acid whenever the absorbance exceeded 2. For XTT reduction assay, working solutions of XTT (0.5 mg ml^{-1}) were prepared in sterile PBS, stored as 1.8 ml aliquots at −18°C. As an electron coupler, a stock solution of 0.32 mg ml^{-1} phenazine methosulfate (PMS) was prepared in PBS and stored at −18°C in 0.2 ml aliquots. Prior to the assay, 1.8 ml of XTT was mixed with 0.2 ml PMS and added immediately to each well of the microtiter plate. The plates were incubated at 37°C for 2 h to develop orange colored formazan which was estimated at 492 nm (Nett et al., 2011).

For visualization of biofilms, sterile glass slides were inserted in 50 ml falcon tubes containing 25 ml of RPMI 1640 with 10^6 cfu ml^{-1} cells and different concentrations of ionic liquids. Tubes were incubated at 37°C, 120 RPM for 24 h. Slides were washed with PBS to remove loosely bound cells, stained with BacLight® live/dead stain (Invitrogen, United States) for 15 min and observed under inverted fluorescence microscope (Carl Zeiss, Germany).

Eradication of Preformed Biofilms by Ionic Liquids

For biofilm eradication experiments, 24 h old biofilms were cultivated in RPMI 1640 as described above. After 24 h, spent media was discarded from wells and washed with PBS buffer to remove loosely bound *C. albicans* cells. Different concentrations of ionic liquids were prepared by two-fold dilution in PBS and 200 μl aliquots were transferred to wells. Five wells were used for each concentration. Plates were incubated again for 24 h at 37°C and 120 RPM. After the challenge period, contents in wells were discarded and washed with PBS to remove detached or loosely bound cells. The biofilm remained after exposure to test compounds was quantified with CV assay. Viability and metabolic activity of cells in the challenged biofilms was determined using BacLight® staining and XTT reduction, respectively. For this, working solution of Syto 9 and propidium iodide (PI) mixture was prepared as per manufacturer's recommendations. Challenged biofilms were stained with 200 μl of stain in the dark for 15 min. Syto 9 and PI fluorescence was estimated by multimode reader (BioTek®, United States) using 488 nm excitation. Syto 9 and PI signals were collected at 520 and 620 nm, respectively. The results were represented as the ratio of Syto 9 to PI fluorescence

(Live/Dead ratio). XTT reduction assay was performed as mentioned previously.

Effect of Ionic Liquids on Clinical *C. albicans* Isolates

Biofilm forming clinical isolates (CA i16 and CA i21) were screened for evaluating the efficacy of fluconazole, amphotericin B and ionic liquids. These isolates were cultured overnight in PDB and adjusted to a cell number of 10^6 cfu ml^{-1} in RPMI 1640. Biofilm formation by CA i16 and CA i21 was determined at different time intervals as mentioned above. Then antibiofilm and biofilm eradication experiments were performed in the presence of ionic liquids. Similar experimental procedures, incubation time and estimation assays were used, as mentioned previously.

Mechanism of Action of Antifungal Ionic Liquids

Based on MIC, MFC, antibiofilm and biofilm eradication against *C. albicans* and clinical isolates, the potential ionic liquid [C_{16}MIM][Cl] was selected for identifying possible mode of action. From the previously estimated MIC values, a 10-fold MIC concentration of [C_{16}MIM][Cl] and amphotericin B were prepared in sterile PBS and incubated with 10^6 cfu ml^{-1} for 3 h at 120 RPM. At the end of incubation, cells exposed to the ionic liquid were harvested by centrifugation, washed with PBS and used for various assays (morphological changes, cell membrane permeabilization, leakage of intracellular material, reactive oxygen species and mitochondrial dysfunction) described below. For determining effect on ergosterol content, *C. albicans* 10231 was grown in PDB with sub-MIC concentrations of antifungal ionic liquid.

Morphological Changes Upon Ionic Liquid Exposure

Candida albicans cells exposed to [C_{16}MIM][Cl] were harvested and observed under bright field microscope. The images were analyzed using *ImageJ* 1.37V software for determining the size of cells in terms of overall length. For each treatment, a minimum of 220 cells were analyzed and average cell length was determined.

Effect on Membrane Permeabilization

Alteration in cell membrane permeability was determined by investigating the propidium iodide (PI) uptake by *C. albicans* cells. *C. albicans* cells exposed to ionic liquid were harvested by centrifugation, washed with PBS and stained with 20 μM PI (Invitrogen, United States) for 15 min. Experiment was performed in triplicates. PBS was used as the control. Inverted fluorescence microscope (Carl Zeiss, Germany) was used for visualizing cells exhibiting PI fluorescence. PI uptake by the *C. albicans* cells was measured quantitatively using 485 nm excitation and 630 nm emission settings with multimode reader (BioTek®, United States).

Leakage of Intracellular Material

Leakage of intracellular contents was indirectly measured by the increase in concentrations of metal cations such as potassium and calcium and increase in 260 nm absorbance in cell free supernatants. *C. albicans* cells (10^6 cfu ml^{-1}) in ultra-high pure (UHP) water was exposed to 0.1, 0.25, 0.5, 0.75, and 1 mM of [C_{16}MIM][Cl]. After 3 h incubation at 37°C and 120 RPM, cell suspensions were centrifuged to collect the supernatant. Absorbance of the supernatant was measured at 260 nm using UV-Visible spectrophotometer (Shimadzu). Metal cations were measured in the supernatants by inductively coupled plasma-atomic emission spectrometer (ICP-AES) (Horiba Jovin Yvon, France). Appropriate controls (UHP water, UHP water with 0.1 to 1 mM [C_{16}MIM][Cl]) were used for analyzing absorbance at 260 nm and quantifying metal cations.

Effect on Ergosterol Content

For this, *C. albicans* cells were cultured in 50 mL Erlenmeyer flasks containing 20 ml PDB with sub-MIC concentrations (MIC/2, MIC/4 and MIC/8) of [C_{16}MIM][Cl] and fluconazole (5 and 50 μM). Flasks were incubated for 24 h at 120 RPM and 37°C. Then, cells were harvested, washed with PBS and used for extracting total sterols through saponification (Arthington-Skaggs et al., 2000). Briefly, 3 mL of 25% alcoholic KOH solution (25 g KOH dissolved in 36 ml UHP water with a 100 mL final make up with 100% ethanol) was added to each of the cell pellet in falcon tubes. Each of these suspensions were mixed by vortexing for a minute and incubated for 1 h in 80°C water bath. After incubation, tubes were cooled to room temperature and sterols were extracted by adding a mixture of water (1 mL) and n-hexane (3 mL). These suspensions were vigorously mixed by vortexing for 3 min and left for phase separation. The hexane layer containing sterols was diluted with absolute ethanol and scanned between 200 and 300 nm using UV-Vis spectrophotometer. Ergosterol content was determined and normalized to wet biomass content using established formulae (Arthington-Skaggs et al., 2000).

Effect on Intracellular Reactive Oxygen Species (ROS)

Candida albicans cells exposed to [C_{16}MIM][Cl] were analyzed for intracellular ROS using 2',7'-Dichlorodihydrofluorescein diacetate (DCFH-DA) (Sigma-Aldrich, United States) (Kobayashi et al., 2002). Cell number, treatment with [C_{16}MIM][Cl], incubation and washing procedures were similar to that of membrane permeabilization experiment. Cells exposed to ionic liquid were incubated with 20 μM DCFH-DA at 37°C under dark for 30 min. Experiment was performed in four replicates with appropriate controls. The cells were then observed for 2',7'-dichlorofluorescein (DCF) fluorescence using an inverted fluorescence microscope (Carl Zeiss, Germany). The fluorescence of DCF was quantified with 485 nm excitation and 538 nm emission settings using multimode reader (BioTek®, United States).

Effect on Mitochondrial Membrane Potential and Mitochondrial Activity

Mitochondrial membrane potential ($\Delta\psi_m$) in *C. albicans* after exposure to [C_{16}MIM][Cl] was measured using Rhodamine

123 (Rh123) (Sigma, United States) as per Lopes et al. (2013) with minor modifications. Cells were exposed to [C_{16}MIM][Cl] as detailed in the membrane permeabilization experiment. Experiment was conducted in four replicates. The cells exposed to ionic liquid were stained with 20 μM Rh123 for 30 min in the dark. After incubation, excess stain was removed and washed with PBS. Cells were re-suspended in PBS and observed for Rh123 fluorescence under inverted fluorescence microscope (Carl Zeiss, Germany) through FITC filter. Fluorescence of Rh123 was also quantified with 485 nm excitation and 530 nm emission settings using multimode reader (BioTek®, United States).

MTT assay was used for determining mitochondrial activity of *C. albicans* cells (Lopes et al., 2013). Cells exposed to [C_{16}MIM][Cl] were harvested, re-suspended in PBS containing 0.5 mg ml^{-1} MTT. Cells were incubated at 120 RPM and 37°C for 2 h. End of the incubation, cell suspensions were centrifuged and washed with PBS. Purple formazan product developed from the MTT reduction by mitochondrial dehydrogenases was solubilized in 200 μL DMSO by vigorous vortexing. Suspensions were centrifuged and supernatants were collected for estimating formazan absorbance at 510 nm using UV-Visible spectrophotometer (Shimadzu, Japan). Experiment was performed in duplicates with necessary controls.

Statistical Analysis

Data was processed from replicates and presented as mean ± standard deviation (SD). Student's *t*-test was used for determining the statistical significance. Differences between the control and treatment samples were considered to be significant at *P*-values <0.05, <0.01, and <0.001.

RESULTS

MIC and MFC of Ionic Liquids and Antifungal Drugs

The antifungal activity of three ionic liquids and antifungal drugs was expressed as MIC and MFC against *C. albicans* 10231 (**Table 2**). Growth of *C. albicans* 10231 was not inhibited in the presence of [C_4MIM][Cl] even at the highest concentration (1000 μmol l^{-1}) tested using initial cell densities of 10^3 and 10^6 cfu ml^{-1}. Thus, growth of *C. albicans* 10231 in the presence of [C_4MIM][Cl] was similar to that of control. However, the growth of *C. albicans* 10231 was severely inhibited in the presence of imidazolium ionic liquids containing –dodecyl or –hexadecyl alkyl groups. [C_{12}MIM][I] completely inhibited the growth of 10^3 and 10^6 cfu ml^{-1} cell densities, respectively, at 6.25 and 25 μmol l^{-1}. MFC values at these cell densities was determined to be 37.5 and 75 μmol l^{-1}, respectively. Among the tested compounds, [C_{16}MIM][Cl] showed maximum potency with MIC value of 2.34 and 4.68 μmol l^{-1}, for 10^3 and 10^6 cfu ml^{-1}, respectively. The MFC concentrations for [C_{16}MIM][Cl] were determined to be 4.68 and 6.25 μmol l^{-1}, for 10^3 and 10^6 cfu ml^{-1}, respectively. The MIC values for fluconazole and amphotericin B were determined to >3265 μmol l^{-1} and 1.62 μmol l^{-1} against 10^6 cfu ml^{-1} *C. albicans* 10231, respectively. The MFC values showed that [C_{16}MIM][Cl] was more effective in killing fungal cells than other two ionic liquids and fluconazole. The MFC of [C_{16}MIM][Cl] at 6.25 μmol l^{-1} was slightly greater as compared to 1.62 μmol l^{-1} for amphotericin B.

Antibiofilm Activity of Ionic Liquids

Time course assay of biofilm development by *C. albicans* 10231 revealed highest biofilm mass and metabolic activity at 24 h (**Supplementary Figure S2**). Thus, 24 h incubation time was used for biofilm inhibition experiments. Biofilm formed in presence of different concentrations of imidazolium ionic liquids was quantified by CV and XTT as shown in **Figure 1**. Biofilm inhibition was not evident in the presence of [C_4MIM][Cl] (**Figures 1a,d**). Biofilm formation by *C. albicans* 10231 was severely inhibited in the presence of imidazolium ionic liquids containing –dodecyl and –hexadecyl groups. For example, 50 and 100% inhibition in biofilm formation was achieved, respectively, using 4.6 and 25 μmol l^{-1} [C_{12}MIM][I] (**Figure 1b**). [C_{16}MIM][Cl] was found to be more potent with no biofilm formation beyond 4.68 μmol l^{-1} (**Figure 1c**). Biofilm formation with adhesion step revealed complete inhibition in biofilm formation beyond 25 and 6.25 μmol l^{-1} for [C_{12}MIM][I] and [C_{16}MIM][Cl], respectively (**Supplementary Figure S3**). Complete inhibition in biofilm formation was achieved using 1.62 μmol l^{-1} amphotericin B. However, biofilm formation was not prevented even using 3265 μmol l^{-1} of fluconazole. Inhibition of *C. albicans* 10231 biofilm formation in the presence of imidazolium ionic liquids with –dodecyl or –hexadecyl

TABLE 2 | Antifungal activities of imidazolium ionic liquids and antifungal drugs against *Candida albicans* reference strain (*C. albicans* 10231) and clinical strains (CA i16 and CA i21).

Strain*	Compound (μmol l^{-1})									
	[C_4MIM][Cl]		[C_{12}MIM][I]		[C_{16}MIM][Cl]		Fluconazole		Amphotericin B	
	MIC	MFC	MIC	MFC	MIC	MFC	MIC	MFC	MIC	MFC
C. albicans 10231	>1000	ND	25	75	4.68	6.25	>3265	ND	1.62	1.62
CA i16	>1000	ND	25	50	4.68	6.25	>3265	ND	0.34	0.68
CA i21	>1000	ND	37.5	75	9.38	12.5	>3265	ND	0.67	1.34

**Initial cell density: 10^6 cfu ml^{-1}. ND, not determined.*

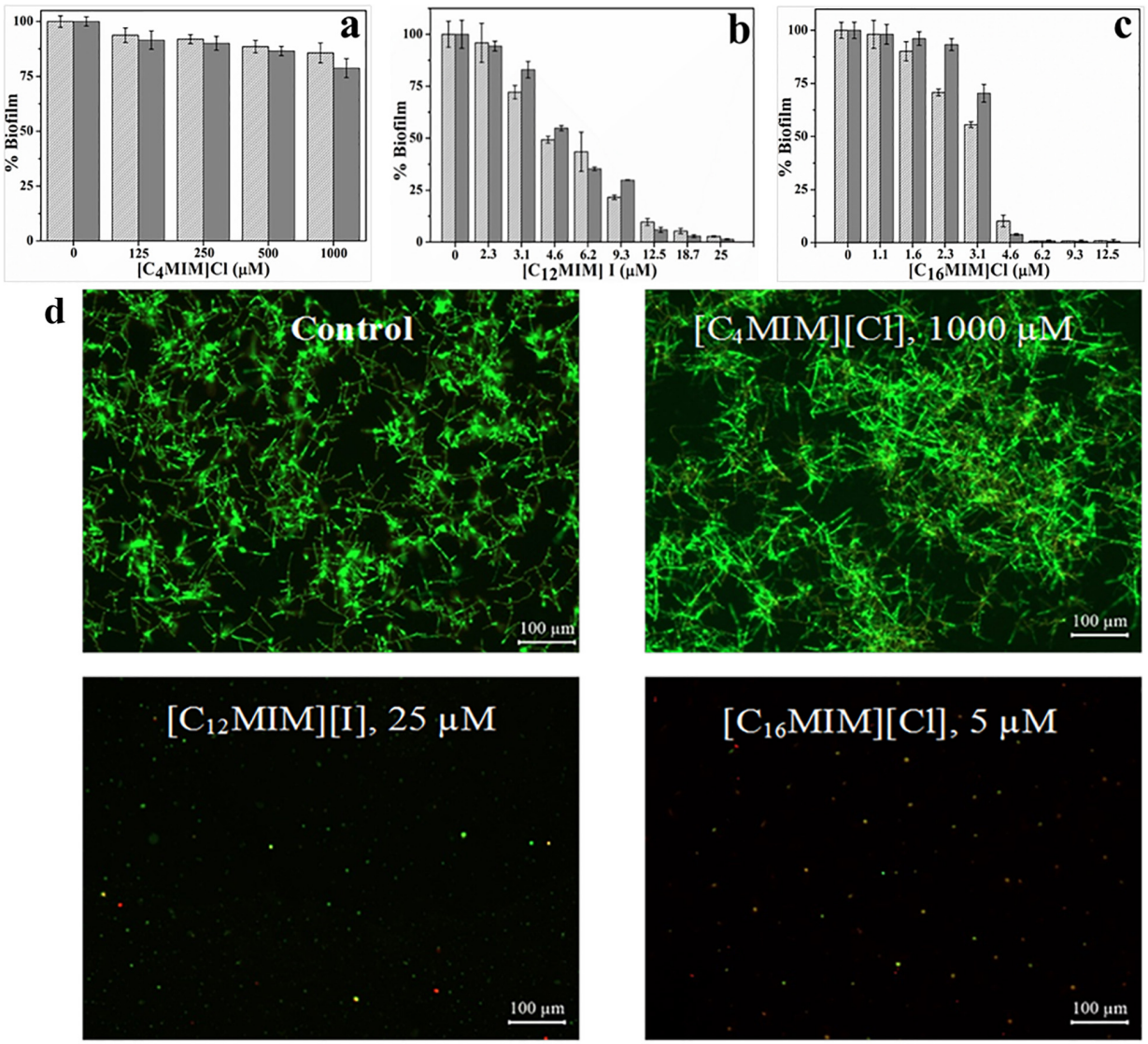

FIGURE 1 | Biofilm formation by *C. albicans* 10231 at different initial concentrations of [C_4MIM][Cl] **(a)**, [C_{12}MIM][I] **(b)**, and [C_{16}MIM][Cl] **(c)**. Biofilm quantified by CV (light gray) and XTT (dark gray) was presented. Fluorescence microscopic images of *C. albicans* biofilms in presence of different concentrations of ionic liquids **(d)**.

groups was clearly evident in the florescence microscopic images (**Figure 1d**). The anion constituents (Cl^- and I^-) and 1-methylimidazole ring did not show any significant effect on the growth and biofilm formation of *C. albicans* 10231 (**Supplementary Figure S4**).

Biofilm Eradication Potential of Ionic Liquids

The biofilm eradication potential of alkylimidazolium ionic liquids was determined in terms of killing of biofilm cells and dislodgement of preformed biofilm. The effect of alkylimidazolium ionic liquids on preformed *C. albicans* 10231 was shown in **Figures 2** and **Supplementary Figure S5**. [C_4MIM][Cl] and [C_{12}MIM][I] did not cause dispersal of 24 h old *C. albicans* 10231 biofilms irrespective of their concentrations (**Figures 2a,b**). A concentration dependent biofilm dispersal was observed in the case of [C_{16}MIM][Cl]. However, biofilm dispersal required much higher concentrations than those required for inhibiting biofilm formation. For example, removal of >90% of biofilm was required 250 μmol l^{-1} [C_{16}MIM][Cl] (**Figure 2c**).

Since [C_4MIM][Cl] and [C_{12}MIM][I] were not causing any biofilm dispersal, their effect was determined in terms of viability and metabolic activity of biofilm cells (**Figure 2d**). There was no change in the Live/Dead (L/D) status or metabolic status of *C. albicans* 10231 biofilms exposed to 1000 μmol l^{-1} [C_4MIM][Cl] for 24 h. However, the L/D status and XTT reduction potential of *C. albicans* 10231 biofilms was drastically decreased upon exposure to 25 to 2500 μmol l^{-1} of [C_{12}MIM][I].

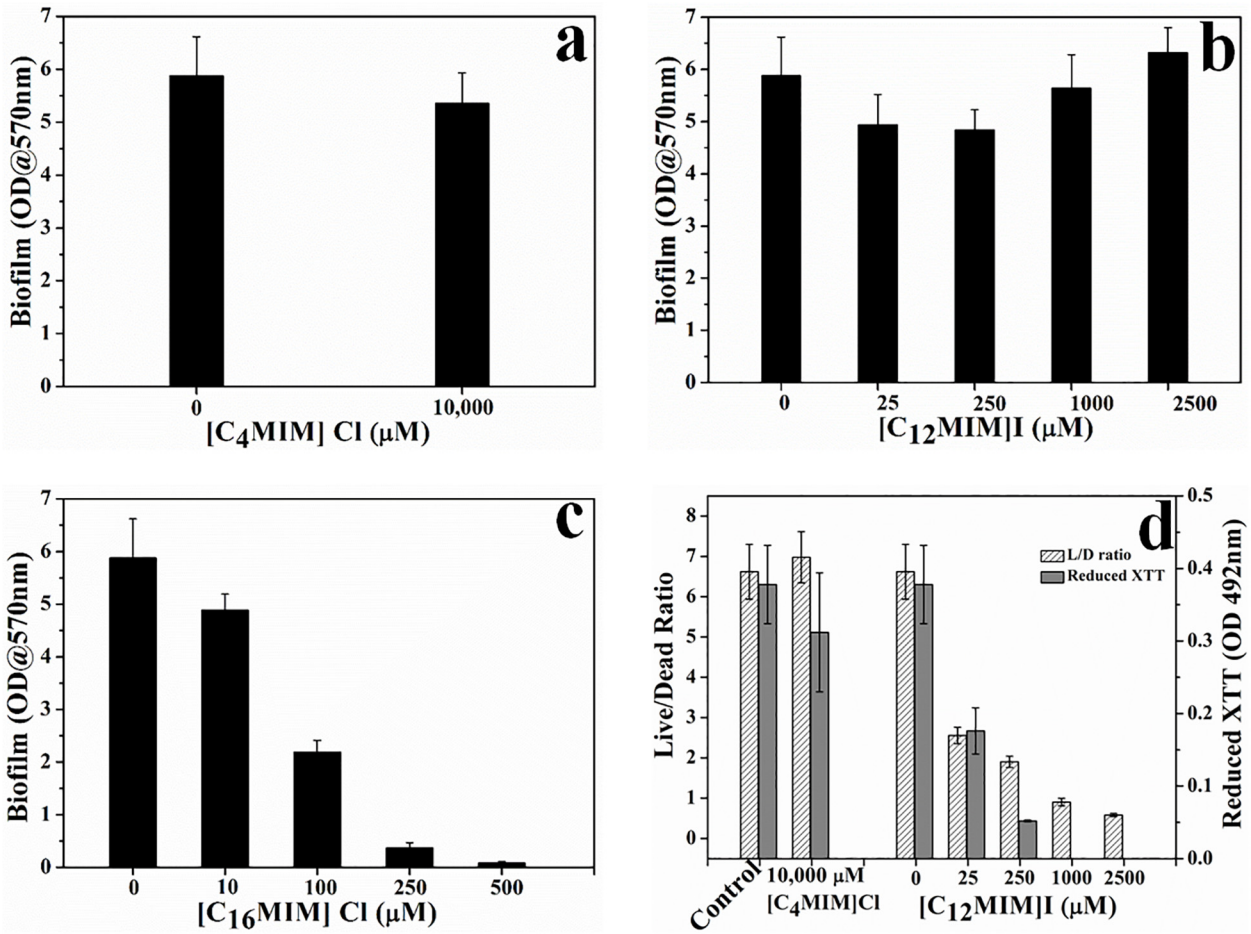

FIGURE 2 | Effect of imidazolium ionic liquids on preformed biofilms. *C. albicans* 10231 biofilms were exposed to imidazolium ionic liquids for 24 h and then residual biofilm was quantified using CV method **(a–c)**. Cell viability in *C. albicans* biofilms upon exposure to ionic liquids that did not exert biofilm dispersal **(d)**.

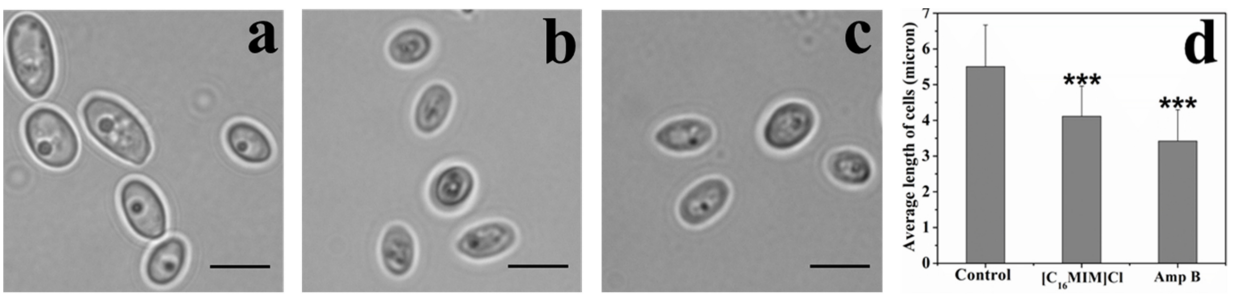

FIGURE 3 | Effect of imidazolium ionic liquids on cell size during short term exposure. Bright field microscopic images of *C. albicans* cells in control **(a)**, [C_{16}MIM][Cl] **(b)** and amphotericin B **(c)** treatments. Scale bar = 5 μm. Graph **(d)** represents the average length of cells in control and treatment. Cells exposed to 10× MIC concentration for 3 h; ***$P < 0.001$, $n = 220$.

Ionic Liquids Against Fluconazole Resistant Clinical *C. albicans* Strains

Clinical strains (CA i16 and CA i21) were selected based on their copious biofilm formation potential and high resistance toward fluconazole. CLSI has fixed MIC breakpoint of ≥64 μg ml^{-1} for fluconazole resistant strains (Manoharan et al., 2017). The clinical strains evaluated in this study were highly resistant to fluconazole and inhibition in growth was not observed up to 1000 μg ml^{-1} fluconazole. MIC and MFC values for ionic liquids and antifungal drugs against clinical *C. albicans* strains were presented in

Table 2. Biofilm formation potential and metabolic activity of both the clinical strains at different time intervals was shown in **Supplementary Figure S6**. Biofilm formation pattern was found to be very similar between the two clinical strains. Incubation time of 24 h was considered optimum based on highest metabolic activity. The tested imidazolium ionic liquids with –dodecyl and –hexadecyl groups were effective in preventing biofilm formation by both the clinical strains. However, there was a marginal difference in the activity toward these two different isolates. Complete inhibition in biofilm formation by clinical isolates required 25 and 6.25 μmol l^{-1}, respectively, for [C_{12}MIM][Cl] and [C_{16}MIM][I] (**Supplementary Figure S7**). Imidazolium ionic liquid with –hexadecyl group was equally effective in dispersing preformed biofilms of clinical strains. Removal of preformed biofilms of clinical strains was about 75 and 100% at 100 and 250 μmol l^{-1}, respectively.

[C_{16}MIM][Cl] Causes Shrinking of *C. albicans* Cells

Initial microscopy observations revealed that potent ionic liquids (containing -dodecyl, -hexadecyl side chain) cause changes in cell size (data not shown). A systematic study with [C_{16}MIM][Cl] exposure to *C. albicans* 10231 cells revealed a significant decrease in the cell size (**Figure 3**). In control population, the cell length was 5.5 $\pm$ 1.1 μm. However, the cell length decreased to 4.1 $\pm$ 0.8 μm upon exposure to [C_{16}MIM][Cl]. In presence of amphotericin B, the average length of cells was further reduced to 3.4 $\pm$ 0.8 μm (**Figure 3d**). The results indicate that, [C_{16}MIM][Cl] decreased the cell volume leading to shrinkage of *C. albicans* 10231 cells.

[C_{16}MIM][Cl] Induces Membrane Permeabilization

Impact of [C_{16}MIM][Cl] on plasma membrane was monitored by PI uptake. Due to high molecular weight, PI can only enter the cells with permeabilized cell membrane. Control cells were not stained by PI (**Figure 4b**). But, ionic liquid and amphotericin B treated cells were stained by the PI (**Figure 4d,f**). Quantitative fluorescence measurement revealed significant uptake of PI by the cells exposed to [C_{16}MIM][Cl] than amphotericin B (**Figure 4g**).

[C_{16}MIM][Cl] Causes Leakage of Intracellular Material

[C_{16}MIM][Cl] induced leakage of intracellular contents was measured from the increase in 260 nm absorbance (nucleic acids) and release of important metal cations (i.e., potassium and calcium). A clear increase in the absorbance at 260 nm was observed in the supernatant upon exposure of cells to potent ionic liquid (**Figure 5a**). ICP-AES data showed efflux of potassium and calcium when *C. albicans* 10231 cells were exposed to [C_{16}MIM][Cl] (**Figure 5b**). Increased absorbance of supernatant and release of metal cations was a clear indication for leakage of intracellular contents during ionic liquid treatment.

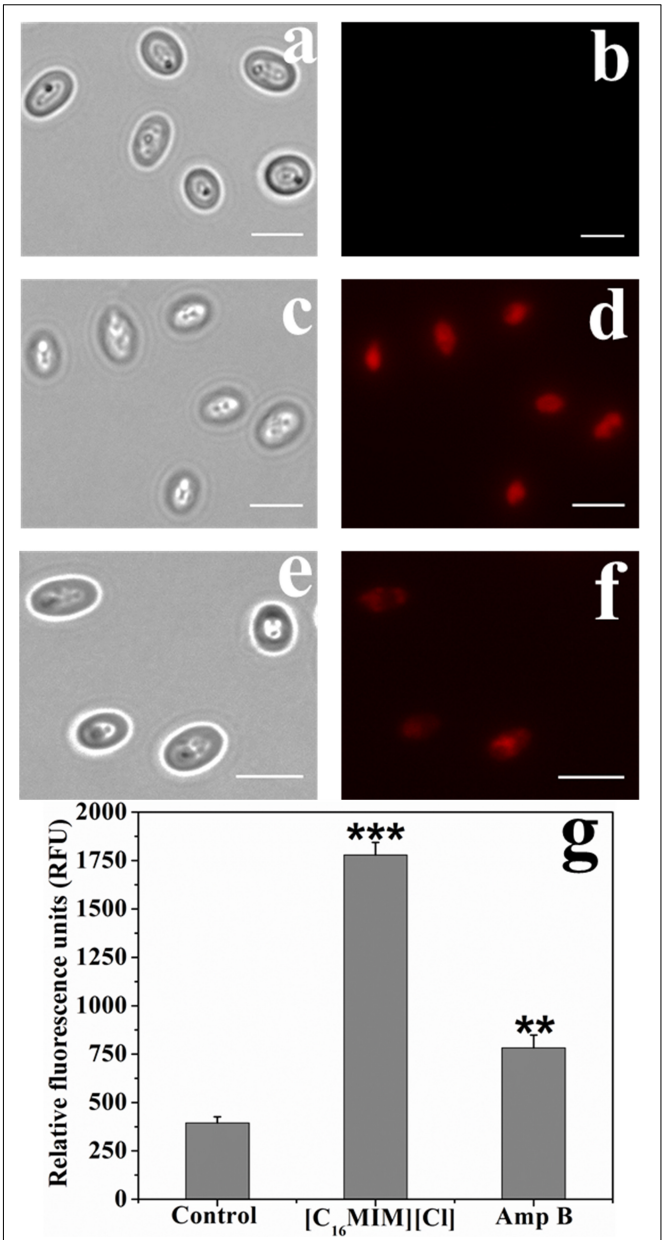

FIGURE 4 | Propidium iodide (PI) uptake by *C. albicans* cells exposed to [C_{16}MIM][Cl]. Bright field and fluorescence microscopy images of control **(a,b)**, ionic liquid treated **(c,d)** and amphotericin B treated **(e,f)** cells. **(g)** PI fluorescence by control, ionic liquid and amphotericin B treated *C. albicans* cells (cells exposed to 10× MIC concentration for 3 h; ***$P < 0.001$, **$P < 0.01$, $n = 3$).

[C_{16}MIM][Cl] Decreases Ergosterol Content

The effect of [C_{16}MIM][Cl] on cell membrane ergosterol content was determined at sub MIC concentrations (MIC/2 to MIC/8). Absorption spectra of extracted sterols were shown in **Figure 6a**. A decrease in the absorbance of the sterols from 250 to 300 nm was evident when *C. albicans* 10231 were grown in the presence of [C_{16}MIM][Cl]. The total sterol content, calculated

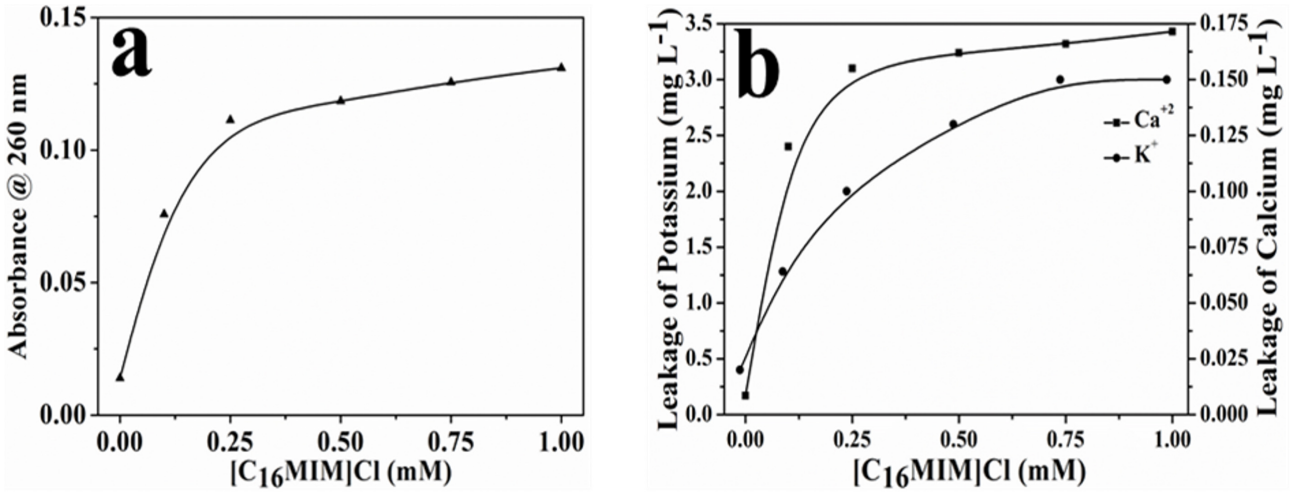

FIGURE 5 | Leakage of intracellular components from *C. albicans* cells upon exposure to [C_{16}MIM][Cl]. **(a)** Absorbance of cell-free supernatant at 260 nm, **(b)** concentration of potassium and calcium in cell-free supernatant.

from absorbance at 282 nm decreased in the cells cultured in the presence of sub MIC concentrations of [C_{16}MIM][Cl]. Normalization to cell weight after ergosterol estimation and comparison with sterol content in control cells indicate the negative effect of ionic liquid on ergosterol content and the effect is concentration dependent (**Figure 6b**).

[C_{16}MIM][Cl] Induces ROS Production

Candida albicans 10231 cells were exposed to [C_{16}MIM][Cl] and amphotericin B and stained with DCFH-DA for determining ROS generation. ROS include superoxide anions, hydroxyl radicals, hydrogen peroxide, and singlet oxygen, which can oxidize DCFH-DA and generate DCF. Accumulation of DCF inside the cells is a direct estimation for ROS generation. Qualitative and quantitative measurement of ROS generation in *C. albicans* 10231 cells was shown in **Figure 7**. Fluorescence microscopic images revealed intense fluorescence from the *C. albicans* 10231 cells treated with [C_{16}MIM][Cl] (**Figure 7d**). Cells treated with amphotericin B were also stained (**Figure 7f**), although to a lesser extent than ionic liquid treated cells. The fluorimetric data indicated significantly higher ROS in the *C. albicans* 10231 cells exposed to ionic liquid (**Figure 7g**). The ROS induced by amphotericin B were found to be significantly lower than that of ionic liquid treatment.

[C_{16}MIM][Cl] Decreases the Mitochondrial Membrane Potential and Inhibits Mitochondrial Activity

$\Delta\psi_m$ is essential for mitochondrial energy metabolism for ATP synthesis (Zorova et al., 2018). Alterations in membrane potential can damage mitochondrial function and could affect the cell survival. Effect of [C_{16}MIM][Cl] on $\Delta\psi_m$ was investigated by Rho123, a dye sequestered by active mitochondria. Hyperpolarization leads to increased accumulation of Rho123. But, depolarization results decreased accumulation of Rho123. Intense Rho123 staining was observed in control cells indicating the active $\Delta\psi_m$ (**Figure 8a**). Ionic liquid exposed *C. albicans* cells indicated faint staining with Rho123, indicating loss of membrane polarization (**Figure 8a**). Quantitative measurement of Rho123 fluorescence showed a significant decrease in ionic liquid exposed cells over control cells (**Figure 8b**). The results suggest that, ionic liquids cause loss of $\Delta\psi_m$ in *C. albicans* 10231 cells.

In addition to $\Delta\psi_m$, mitochondria function was also evaluated by estimating the activity of mitochondrial dehydrogenases. Metabolically active mitochondria can reduce colorless MTT to purple formazan which can be solubilized and measured calorimetrically. Failure of such reduction is an indication for the abnormal mitochondrial activity. MTT reduction to purple formazan was observed in control cells, indicating the normal activity of dehydrogenases. In case of ionic liquid exposed cells, formazan formation was severely impaired due to mitochondrial dysfunction (**Figure 8c**). The formazan development in control *C. albicans* 10231 cells inoculated in microtiter wells can be seen in the inset of **Figure 8c**.

DISCUSSION

The major challenges in developing new antifungal drugs or therapeutic strategies against *Candida albicans* are (i) its opportunistic pathogenicity causing both superficial and systemic fungal infections, (ii) its complex and polymorphic biofilm structure, and (iii) emergence of resistance in *C. albicans* strains against antifungal drugs like fluconazole. These challenges warrant the development of novel antifungal agents for effective treatment therapies. Ionic liquids have attracted attention for medical applications because of huge structural diversity (theoretically, 10^{18} compounds are possible) and tunability of structure which enable attaining desired biological activity and antimicrobial activities (Pendleton and Gilmore, 2015;

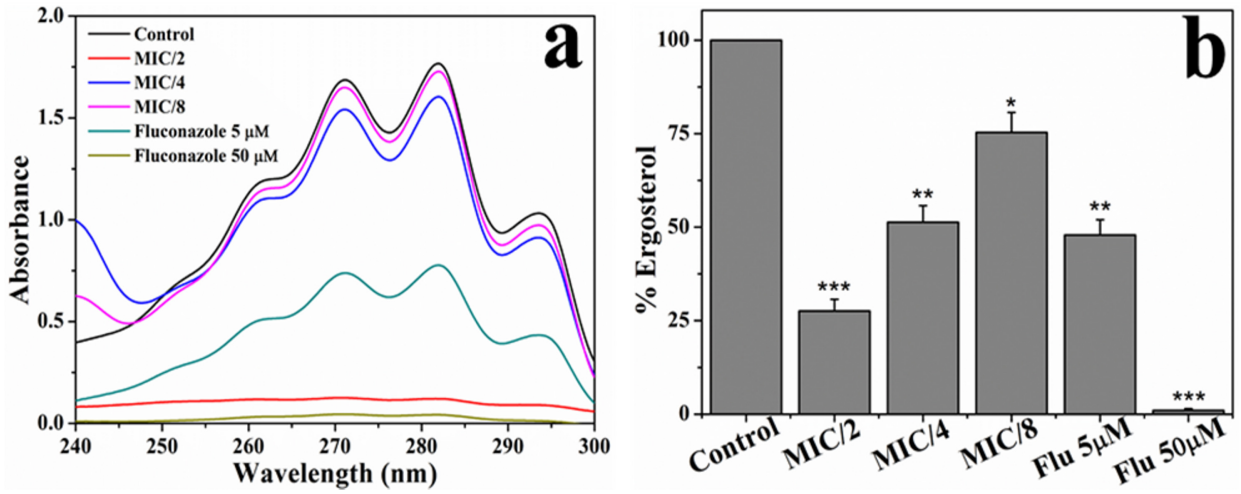

FIGURE 6 | Effect of [C_{16}MIM][Cl] on ergosterol content. **(a)** Absorption spectra of extracted sterols from *C. albicans* cells cultured in the presence of different concentrations of [C_{16}MIM][Cl] and fluconazole. **(b)** Ergosterol content in *C. albicans* cells grown in the presence of [C_{16}MIM][Cl] and fluconazole (*$P < 0.05$, **$P < 0.01$, ***$P < 0.001$, $n = 2$).

Egorova et al., 2017). Among others, imidazolium ionic liquids are well studied for antimicrobial activities (Nancharaiah et al., 2012) and shown to possess antifungal activity (**Table 1**). For antibiofilm agents, it is desirable to have antimicrobial and surfactant activities (Choi et al., 2011). Imidazolium ionic liquids particularly with long-alkyl chains offer both these properties. In this study, we have chosen imidazolium ionic liquids with three different alkyl groups for determining (i) biofilm prevention and biofilm eradication activities on *C. albicans* strains and (ii) mode of action of promising ionic liquid on *C. albicans* cells. Although antifungal and antibiofilm activities of imidazolium ionic liquids have been studied previously (Bergamo et al., 2014, 2015; Dalla Lana et al., 2015; Ribas et al., 2016), their effects on preformed *C. albicans* biofilms and their molecular toxicity mechanisms are largely unknown. This study provided a clear insight into the biofilm eradication potential of alkylimidazolium ionic liquids and mechanism of action of prospective antifungal ionic liquid. Multi-marker approach was adopted for identifying targets and to discern the mode of action of promising antifungal ionic liquid.

Antifungal, Antibiofilm and Biofilm Eradication Activity of Ionic Liquids

The antifungal, antibiofilm and biofilm eradication potential of three ionic liquids was determined *in vitro* against *C. albicans* strains. Alkylimidazolium ionic liquid with -butyl group was not inhibitory to *C. albicans* cells and considered as non-antifungal ionic liquid. Ionic liquids with -dodecyl and - hexadecyl groups were effective in preventing the growth of *C. albicans* and two other clinical strains, hence referred to as antifungal ionic liquids. This study re-confirmed that the antifungal activity of alkylimidazolium ionic liquids was dependent on the carbon chain length of alkyl group. The MIC and MFC values of ionic liquids were dependent on initial cell densities, that is, low concentrations were sufficient to inhibit the growth of 10^3 cfu ml^{-1} than 10^6 cfu ml^{-1}. MIC values of potent antifungal ionic liquids were much lower than fluconazole against *C. albicans* 10231. However, the antifungal activity of two of the tested ionic liquids was comparable or slightly higher than amphotericin B. Biofilm formation by *C. albicans* 10231 and two clinical strains was effectively and completely inhibited in the presence of antifungal ionic liquids. The results of this study in terms of antifungal and antibiofilm activity of alkylimidazolium ionic liquids are in agreement with previous work on *C. albicans* (Schrekker et al., 2013; Bergamo et al., 2014). But, the effect of these antifungal ionic liquids on preformed biofilms is largely unknown (**Table 1**). The effect of antifungal drugs on adherent cells or biofilms is of clinical relevance because (i) biofilm formation often precedes treatment and (ii) biofilms are much more resistant to antifungals. In this context, the biofilm eradication potential of antifungal ionic liquids was determined for the first time in terms of viability loss and dispersal of preformed *C. albicans* biofilms. Antifungal ionic liquid with -hexadecyl group was able to effectively disperse 24 h old *C. albicans* biofilm (**Figure 2c**). Interestingly, antifungal ionic liquid with –dodecyl group was not effective in dispersing the biofilm even at higher concentrations (**Figure 2b** and **Supplementary Figures S5C,D**). But, this antifungal ionic liquid remarkably decreased the viability and metabolic activity of *C. albicans* cells in the preformed biofilm (**Figure 2d**). The biofilm eradication potential results suggest that antifungal ionic liquids are suitable for treating *C. albicans* infections.

Mechanism of Action of Antifungal Ionic Liquids

The microscopic observation revealed that the cells exposed to [C_{16}MIM][Cl] were smaller than the untreated control cells

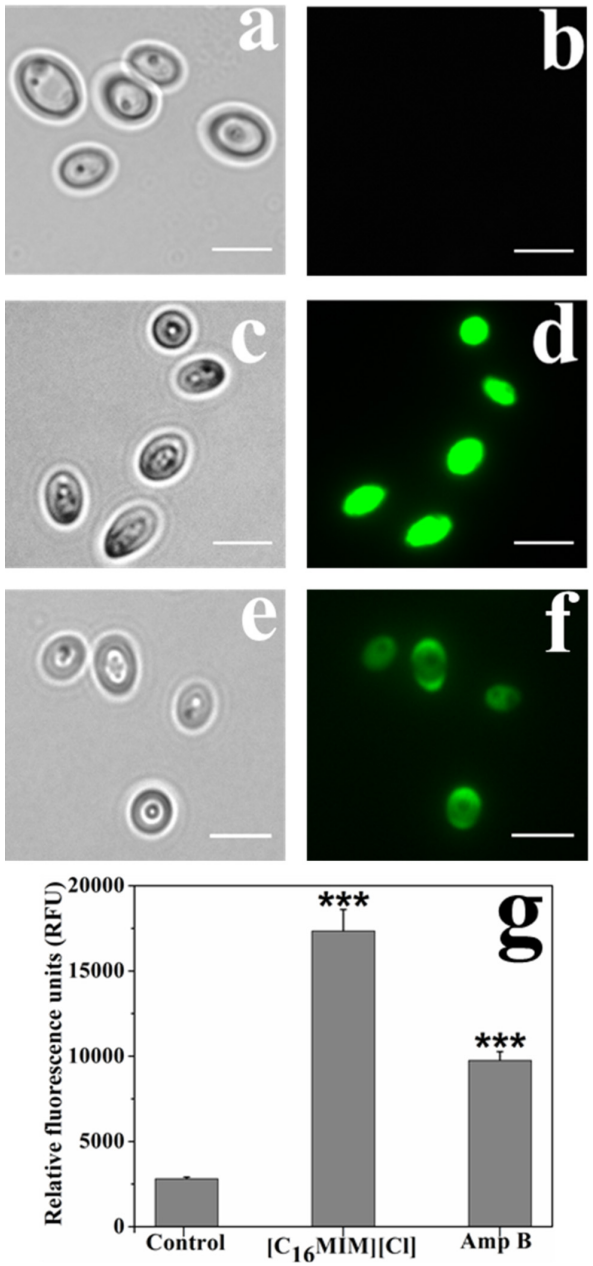

FIGURE 7 | ROS in *C. albicans* cells before and after exposure to $[C_{16}MIM][Cl]$ and amphotericin B. Bright field and fluorescence images of control **(a,b)**, ionic liquid treated **(c,d)** and amphotericin B treated **(e,f)** cells. Scale bar = 5 μm. Quantitative estimation **(g)** of ROS in control, ionic liquid and amphotericin B treated cells. (Cells exposed to 10× MIC concentration for 3 h; $^{***}P < 0.001$, $n = 4$).

(**Figure 3**). A significant reduction in cell volume was noticed in *C. albicans* 10231 cells exposed to antifungal ionic liquid for few hours. Shrinkage of *C. albicans* cells was observed upon exposure to antifungal agents such as apigenin, silver nanoparticles (Li et al., 2013; Lee et al., 2018). The cell shrinkage was often associated with cell membrane permeabilization and leakage of intracellular contents (Lee et al., 2018). Ionic liquid induced cell membrane permeabilization was already reported in bacteria and microalgae (Nancharaiah et al., 2012; Reddy et al., 2017). An increased absorbance (at 260 nm) and metal ions (K^+ and Ca^{2+}) in the water surrounding *C. albicans* 10231 during exposure to antifungal ionic liquid suggested cell membrane permeabilization or damage (**Figure 5**). Membrane permeabilization was indeed confirmed in ionic liquid treated *C. albicans* 10231 cells by the preferential uptake of PI but not by control cells (**Figure 4**). The intracellular concentrations of alkali metal ions (i.e., K^+, Na^+) are important for maintaining cell volume, pH and cell membrane potential in yeasts (Arino et al., 2010). Therefore, leakage of metal cations (K^+ and Ca^{2+}) and other intracellular material (UV absorbing substances) are responsible for reduction in cell volume. Ergosterol, another important constituent of fungal membranes was quantified in *C. albicans* 10231 cells cultured in the presence of $[C_{16}MIM][Cl]$. Ergosterol is a major sterol in the fungal cell membrane and adequate levels are essential for maintaining membrane integrity and other membrane functions (Hu et al., 2017). Hence, ergosterol and its biosynthetic pathways are important targets in the development of antifungal agents (Onyewu et al., 2003). A significant decrease in ergosterol content of *C. albicans* 10231 cells cultured in the presence of antifungal ionic liquid (**Figure 6**) suggests possible inhibition of ergosterol biosynthesis. This was in agreement with the observations of Schrekker et al. (2013) that imidazolium ionic liquids interfere in the ergosterol biosynthesis and cause a reduction in its levels in the cell membrane. It was hypothesized that imidazolium ionic liquids interrupt conversion of lanosterol to ergosterol by inhibiting lanosterol 14α-demethylase (Schrekker et al., 2013). However, this is yet to be validated experimentally.

Generation and accumulation of intracellular ROS was prominent in *C. albicans* 10231 cells treated with $[C_{16}MIM][Cl]$ (**Figure 7**). In yeasts, ROS are majorly produced in the mitochondria (Knorre et al., 2016). High ROS levels are detrimental as they cause oxidative damage to intracellular molecules and cell membrane lipids (Sun et al., 2017). Interestingly, ROS production is one of the mechanisms by which yeast cells senses mitochondrial dysfunction (Knorre et al., 2016). The mitochondrial dysfunction in *C. albicans* 10231 cells was assessed by $\Delta\psi_m$ and dehydrogenases activity. Rho123, a cationic and lipophilic dye used for quantifying $\Delta\psi_m$ because this dye can specifically stain negatively charged mitochondria (Dananjaya et al., 2017). A significant decrease in Rho123 staining by *C. albicans* 10231 upon treatment with antifungal ionic liquid (**Figure 8**) indicated disruption of membrane potential. MTT assay indicated almost complete loss of dehydrogenases activity asserting mitochondrial dysfunction in ionic liquid treated *C. albicans* 10231 cells. Cell volume reduction, intracellular ROS production and mitochondrial dysfunction are often observed in apoptosis (Pereira et al., 2008). Therefore, future experimental work should investigate mode of action of antifungal ionic liquids in this direction.

Clinical Relevance

Fungal infections alone account for approximately 11.5 million life-threatening infections and 1.6 million deaths

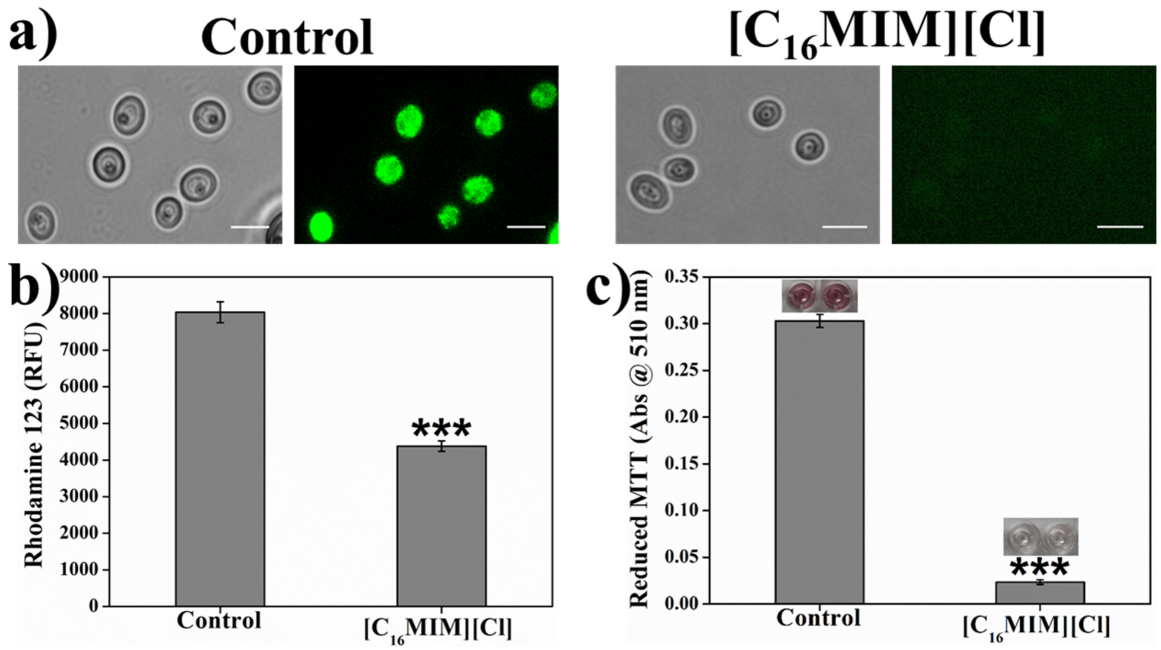

FIGURE 8 | Effect of [C_{16}MIM][Cl] on *C. albicans* mitochondrial membrane potential and mitochondrial activity. Cells exposed with [C_{16}MIM][Cl] were incubated with Rhodamine 123 **(a,b)** and MTT **(c)**. Rhodamine 123 fluorescence from control and treated cells was observed under fluorescence microscope **(a)** and fluorescence was also quantified in multimode reader **(b)**. MTT reduction by control and treated cells is shown in figure **(c)** along with microtiter wells showing reduced MTT in control. Cells exposed to 10× MIC concentration for 3 h; ***$P < 0.001$, $n = 4$ for Rhodamine 123 assay, $n = 2$ for MTT assay.

annually around the globe (Fuentefria et al., 2018; Almeida et al., 2019). Treatment of fungal infections is a challenge in clinical settings because of limited number of antifungal drugs for treating invasive infections, inefficacy in preventing infections, difficulty in administering and combination of all these factors (Desai et al., 2014; Beardsley et al., 2018). This is amplified by emerging antifungal resistance and resistance conferred by fungal biofilms. Ionic liquids, unique class of compounds, are seen as promising assets for treating life-threatening fungal infections due to their structural diversity and tunable physical and chemical properties which contribute to the synthesis of a large number of compounds (Hartmann et al., 2016). Imidazolium ionic liquids are promising because of their strong antifungal and biofilm inhibition activities. The other important attributes of these compounds are (i) broad spectrum activity on bacteria and fungi (Nancharaiah et al., 2012; Dalla Lana et al., 2015; Bergamo et al., 2016) and (ii) multiple cellular targets for exhibiting antifungal activity as demonstrated in this study. Antifungal compounds with multiple pharmaceutical targets are promising for evading resistance development, a menace in antifungal therapy. Antifungal susceptibility testing and other *in vitro* assays can screen a large number of compounds, identify effective compounds and identify cellular targets. Effective ionic liquids are suitable for prospective applications in antifungal creams for topical applications, disinfection of surgical tools and treatment of dental lines in hospital settings. The results of *in vitro* assays are useful for guiding treatment choices (Beardsley et al., 2018) and complementation with *in vivo* studies is necessary for considering potential clinical applications.

Schrekker et al. (2016) evaluated the biocompatibility of imidazolium ionic liquids *in vitro* using L929 fibroblast cells of mice. These tests revealed that cytotoxicity increases with an increase in alkyl chain length from –butyl to –decyl and –hexadecyl group. 1-butyl-3-methylimidazolium chloride was fully biocompatible with no toxicity on fibroblast cells. Whereas, 1-decyl-3-methylimidazolium chloride and 1-hexadecyl-3-methylimidazolium chloride were cytotoxic to fibroblast cells, respectively, at 50 to 500 $\mu g\ ml^{-1}$ and 10 to 500 $\mu g\ ml^{-1}$. Thus, biocompatibility of –hexadecyl containing ionic liquid was reported to be good at $<10\ \mu g\ ml^{-1}$ with minimal toxicity on fibroblast cells suggesting that low concentrations of these compounds are still safe. Cytotoxicity data for 1-dodecyl-3-methylimidazolium iodide is not available, although it can be predicted to possess the toxicity between –decyl and –hexadecyl alkyl group containing imidazolium ionic liquids. The concentrations of 1-hexaydecyl-3-methylimidazolium chloride at $0.84\ \mu g\ ml^{-1}$ and $1.69\ \mu g\ ml^{-1}$ for antifungal and antibiofilm (for complete biofilm prevention) activities, respectively, are below the reported toxicity value of $10\ \mu g\ ml^{-1}$ on fibroblast cells (Schrekker et al., 2016) and seems to be safe. Nevertheless, additional biocompatibility studies of antifungal ionic liquids are warranted for considering these compounds in prospective formulations. Therefore, further research should focus on (i) efficacy, (ii) formulation and co-administration with other compounds, and (iii) cellular toxicity using *in vivo* models.

DATA AVAILABILITY STATEMENT

All datasets generated for this study are included in the article/**Supplementary Material**.

AUTHOR CONTRIBUTIONS

GK and YN conceived and designed the experiments. GK performed the experiments and processed the data. GK and YN interpreted the data. GK and YN wrote the manuscript.

FUNDING

This research was funded by Department of Atomic Energy, Government of India.

SUPPLEMENTARY MATERIAL

The Supplementary Material for this article can be found online at: https://www.frontiersin.org/articles/10.3389/fmicb.2020.00730/full#supplementary-material

REFERENCES

Almeida, F., Rodrigues, M. L., and Coelho, C. (2019). The still underestimated problem of fungal diseases worldwide. *Front. Microbiol.* 10:214. doi: 10.3389/fmicb.2019.00214

Arino, J., Ramos, J., and Sychrova, H. (2010). Alkali metal cation transport and homeostasis in yeasts. *Microbiol. Mol. Biol. Rev.* 74, 95–120. doi: 10.1128/MMBR.00042-09

Arthington-Skaggs, B. A., Warnock, D. W., and Morrison, C. J. (2000). Quantitation of *Candida albicans* ergosterol content improves the correlation between in vitro antifungal susceptibility test results and in vivo outcome after fluconazole treatment in a murine model of invasive candidiasis. *Antimicrob. Agents Chemother.* 44, 2081–2085. doi: 10.1128/aac.44.8.2081-2085.2000

Beardsley, J., Halliday, C. L., Chen, S. C. A., and Sorrell, T. C. (2018). Responding to the emergence of antifungal drug resistance: perspectives from the bench and the bedside. *Future Microbiol.* 13, 1175–1191. doi: 10.2217/fmb-2018-0059

Benedetto, A. (2017). Room-temperature ionic liquids meet biomembranes: the state-of-the-art. *Biophys. Rev.* 9, 309–320. doi: 10.1007/s12551-017-0279-1

Bergamo, V. Z., Balbueno, E. A., Hatwig, C., Pippi, B., Dalla Lana, D. F., Donato, R. K., et al. (2015). 1-n-Hexadecyl-3-methylimidazolium methanesulfonate and chloride salts with effective activities against *Candida tropicalis* biofilms. *Lett. Appl. Microbiol.* 61, 504–510. doi: 10.1111/lam.12488

Bergamo, V. Z., Donato, R. K., Dalla Lana, D. F., Donato, K. J. Z., Ortega, G. G., Schrekker, H. S., et al. (2014). Imidazolium salts as antifungal agents: strong antibiofilm activity against multidrug-resistant *Candida tropicalis* isolates. *Lett. Appl. Microbiol.* 60, 66–71. doi: 10.1111/lam.12338

Bergamo, V. Z., Donato, R. K., Nemitz, M. C., Acasigua, G. A., Selukar, B. S., Lopes, W., et al. (2016). Assessing an imidazolium salt's performance as antifungal agent on a mouthwash formulation. *J. Appl. Microbiol.* 121, 1558–1567. doi: 10.1111/jam.13283

Busetti, A., Crawford, D. E., Earle, M. J., Gilea, M. A., Gilmore, B. F., Gorman, S. P., et al. (2010). Antimicrobial and antibiofilm activities of 1-alkylquinolinium bromide ionic liquids. *Green Chem.* 12, 420–425.

Carson, L., Chau, P. K. W., Earle, M. J., Gilea, M. A., Gilmore, B. F., Gorman, S. P., et al. (2009). Antibiofilm activities of 1-alkyl-3-methylimidazolium chloride ionic liquids. *Green Chem.* 11, 492–497.

Choi, S. Y., Rodriguez, H., Mirjafari, A., Gilpin, D. F., McGrath, S., Malcolm, K. R., et al. (2011). Dual functional ionic liquids as plasticisers and antimicrobial agents for medical polymers. *Green Chem.* 13, 1527–1535.

CLSI (2012). *Reference Method for Broth Dilution Antifungal Susceptibility Testing of Yeasts, Approved Standard*, 3rd Edn. Wayne, PA: CLSI.

Dalla Lana, D. F., Donato, R. K., Bundchen, C., Guez, C. M., Bergamo, V. Z., Oliveira, L. F. S., et al. (2015). Imidazolium salts with antifungal potential against multidrug-resistant dermatophytes. *J. Appl. Microbiol.* 119, 377–388. doi: 10.1111/jam.12862

Dananjaya, S. H. S., Udayangani, R. M. C., Oh, C., Nikapitiya, C., Lee, J., and De Zoysa, M. (2017). Green synthesis, physio-chemical characterization and anti-candidal function of biocompatible chitosan gold nanocomposite as a promising antifungal therapeutic agent. *RSC Adv.* 7, 9182–9193. doi: 10.1039/c6ra26915j

Desai, J. V., Mitchell, A. P., and Andes, D. R. (2014). Fungal biofilms, drug resistance, and recurrent infection. *Cold Spring Harb. Perspect. Med.* 4:a019729. doi: 10.1101/cshperspect.a019729

Egorova, K. S., Gordeev, E. G., and Ananikov, V. P. (2017). Biological activity of ionic liquids and their application in pharmaceutics and medicine. *Chem. Rev.* 117, 7132–7189. doi: 10.1021/acs.chemrev.6b00562

Fuentefria, A. M., Pippi, B., Dalla Lana, D. F., Donato, K. K., and de Andrade, S. F. (2018). Antifungals discovery: an insight into new strategies to combat antifungal resistance. *Lett. Appl. Microbiol.* 66, 2–13. doi: 10.1111/lam.12820

Gyawali, R., and Ibrahim, S. A. (2014). Natural products as antimicrobial agents. *Food Control* 46, 412–429.

Hartmann, D. O., Petkovic, M., and Pereira, C. S. (2016). Ionic liquids as unforeseen assets to fight life-threatening mycotic diseases. *Front. Microbiol.* 7:111. doi: 10.3389/fmicb.2016.00111

Henriques, M., Azeredo, J., and Oliveira, R. (2006). *Candida albicans* and *Candida dubliniensis*: comparison of biofilm formation in terms of biomass and activity. *Br. J. Biomed. Sci.* 63, 5–11. doi: 10.1080/09674845.2006.11732712

Hu, Z., He, B., Ma, L., Sun, Y., Niu, Y., and Zeng, B. (2017). Recent advances in ergosterol biosynthesis and regulation mechanisms in Saccharomyces cerevisiae. *Indian J. Microbiol.* 57, 270–277. doi: 10.1007/s12088-017-0657-1

Knorre, D. A., Sokolov, S. S., Zyrina, A. N., and Severin, F. F. (2016). How do yeast sense mitochondrial dysfunction? *Microb. Cell* 3, 532–539. doi: 10.15698/mic2016.11.537

Kobayashi, D., Kondo, K., Uehara, N., Otokozawa, S., Tsuji, N., Yagihashi, A., et al. (2002). Endogenous reactive oxygen species is an important mediator of miconazole antifungal effect. *Antimicrob. Agents Chemother.* 46, 3113–3117. doi: 10.1128/aac.46.10.3113-3117.2002

Lee, H., Woo, E. R., and Lee, D. G. (2018). Apigenin induces cell shrinkage in *Candida albicans* by membrane perturbation. *FEMS Yeast Res.* 18, foy003.. doi: 10.1093/femsyr/foy003

Li, C., Wang, X., Chen, F., Zhang, C., Zhi, X., Wang, K., et al. (2013). The antifungal activity of graphene oxide-silver nanocomposites. *Biomaterials* 34, 3882–3890. doi: 10.1016/j.biomaterials.2013.02.001

Lopes, G., Pinto, E., Andrade, P. B., and Valenta, P. (2013). Antifungal activity of phlorotannins against dermatophytes and yeasts: approaches to the mechanism of action and influence on *Candida albicans* virulence factor. *PloS One* 8:e72203. doi: 10.1371/journal.pone.0072203

Manoharan, R. K., Lee, J. H., and Lee, J. (2017). Antibiofilm and antihyphal activities of cedar leaf essential oil, camphor, and fenchone derivatives against *Candida albicans*. *Front. Microbiol.* 8:1476. doi: 10.3389/fmicb.2017.01476

Martin, M. V. (1999). The use of fluconazole and itraconazole in the treatment of *Candida albicans* infections: a review. *J. Antimicrob. Chemother.* 44, 429–437. doi: 10.1093/jac/44.4.429

Nancharaiah, Y. V., Reddy, G. K. K., Lalithamanasa, P., and Venugopalan, V. P. (2012). The ionic liquid 1-alkyl-3-methylimidazolium demonstrates comparable antimicrobial and antibiofilm behaviour to a cationic surfactant. *Biofouling* 28, 1141–1149. doi: 10.1080/08927014.2012.736966

Nett, J. E., Cain, M. T., Crawford, K., and Andes, D. R. (2011). Optimizing a *Candida* biofilm microtiter plate model for measurement of antifungal susceptibility by tetrazolium salt assay. *J. Clin. Microbiol.* 49, 1426–1433. doi: 10.1128/JCM.02273-10

Nobile, C. J., and Johnson, A. J. (2015). *Candida albicans* biofilms and human disease. *Annu. Rev. Microbiol.* 69, 71–92.

Onyewu, C., Blankenship, J. R., Poeta, M. D., and Heitman, J. (2003). Ergosterol biosynthesis inhibitors become fungicidal when combined with calcineurin inhibitors against *Candida albicans*, *Candida glabrata*, and *Candida krusei*.

Antimicrob. Agents Chemother. 47, 956–964. doi: 10.1128/aac.47.3.956-964.2003

Pendleton, J. N., and Gilmore, B. F. (2015). The antimicrobial potential of ionic liquids: a source of chemical diversity for infection and biofilm control. *Inter. J. Antimicrob. Agents* 46, 131–139. doi: 10.1016/j.ijantimicag.2015.02.016

Pereira, C., Silva, R. D., Saraiva, L., Johansson, B., Sousa, M. J., and Côrte-Real, M. (2008). Mitochondria-dependent apoptosis in yeast. *Biochim. Biophys. Acta* 1783, 1286–1302. doi: 10.1016/j.bbamcr.2008.03.010

Pernak, J., Goc, I., and Mirska, I. (2004). Anti-microbial activities of protic ionic liquids with lactate anion. *Green Chem.* 6, 323–329.

Pernak, J., Syguda, A., Mirska, I., Pernak, A., Newrot, J., Pradzyñska, A., et al. (2007). Choline-derivative-based ionic liquids. *Chemistry* 13, 6817–6827. doi: 10.1002/chem.200700285

Petkovic, M., Ferguson, J., Bohn, A., Trindade, J., Martins, I., Carvalho, M. B., et al. (2009). Exploring fungal activity in the presence of ionic liquids. *Green Chem.* 11, 889–894. doi: 10.1186/s13068-017-0822-0

Pierce, C. G., Uppuluri, P., Tristan, A. R., Wormley, FL Jr, Mowat, E., Ramage, G., et al. (2008). A simple and reproducible 96-well plate-based method for the formation of fungal biofilms and its application to antifungal susceptibility testing. *Nat. Protoc.* 3, 1494–1500. doi: 10.1038/nport.2008.141

Ramage, G., Martinez, J. P., and Lopez-Ribot, J. L. (2006). *Candida* biofilms on implanted biomaterials: a clinically significant problem. *FEMS Yeast Res.* 6, 979–986. doi: 10.1111/j.1567-1364.2006.00117.x

Reddy, G. K. K., Nancharaiah, Y. V., and Venugopalan, V. P. (2017). Long alkyl-chain imidazolium ionic liquids: antibiofilm activity against phototrophic biofilms. *Colloids Surf. B Biointerfaces* 155, 487–496. doi: 10.1016/j.colsurfb.2017.04.040

Reddy, G. K. K., Rajitha, K., and Nancharaiah, Y. V. (2020). Antibiofouling potential of 1-alkyl-3-methylimidazolium ionic liquids: studies against biofouling barnacle larvae. *J. Mol. Liq.* 302:112497. doi: 10.1016/j.molliq.2020.112497

Ribas, A. D., Ponte, E. M., Dalbem, A. M., Dalla-Lana, D., Bundchen, C., Donato, R. K., et al. (2016). Imidazolium salts with antifungal potential for the control of head blight of wheat caused by Fusarium graminearum. *J. Appl. Microbiol.* 121, 445–452. doi: 10.1111/jam.13125

Rogers, R. D., and Seddon, K. R. (2003). Ionic liquids–solvents of the future? *Science* 302, 792–793. doi: 10.1126/science.1090313

Santos, G. C., Vasconcelos, C. C., Lopes, A. J. O., Cartagenes, M. D. S. D. S., Filho, A. K. D. B., do Nascimento, F. R. F., et al. (2018). *Candida* infections and therapeutic strategies: mechanisms of action for traditional and alternative agents. *Front. Microbiol.* 9:1351. doi: 10.3389/fmicb.2018.01351

Sardi, J. C. O., Scorzoni, L., Bernardi, T., Fusco-Almeida, A. M., and Mendes Giannini, M. J. S. (2013). *Candida* species: current epidemiology, pathogenicity, biofilm formation, natural antifungal products and new therapeutic options. *J. Med. Microbiol.* 62, 10–24. doi: 10.1099/jmm.0.045054-0

Schrekker, C. M. L., Sokolovicz, Y. C. A., Raucci, M. G., Selukar, B. S., Klitzke, J. S., Lopes, W., et al. (2016). Multitask imidazolium salt additives for innovative poly(L-Lactide) biomaterials: morphology control, *Candida* Spp. biofilm inhibition, human mesenchymal stem cell biocompatibility, and skin tolerance. *ACS Appl. Mater. Interfaces* 8, 21163–21176. doi: 10.1021/acsami.6b06005

Schrekker, H. S., Donato, R. K., Fuentefria, A. M., Bergamo, V., Oliveira, L. F., and Machado, M. M. (2013). Imidazolium salts as antifungal agents: activity against emerging yeast pathogens, without human leukocyte toxicity. *MedChemComm.* 4, 1457–1460.

Sun, L., Liao, K., Hang, C., and Wang, D. (2017). Honokiol induces reactive oxygen species-mediated apoptosis in *Candida albicans* through mitochondrial dysfunction. *PLoS One* 12:e172228. doi: 10.1371/journal.pone.0172228

Vekariya, R. L. (2017). A review of ionic liquids: applications towards catalytic organic transformations. *J. Mol. Liq.* 227, 44–60. doi: 10.1007/s12551-017-0389-9

Zorova, L. D., Popkov, V. A., Plotnikov, E. Y., Silachev, D. N., Pevzner, I. B., Jankauskas, S. S., et al. (2018). Mitochondrial membrane potential. *Anal. Biochem.* 552, 50–59. doi: 10.1016/j.ab.2017.07.009

Conflict of Interest: The authors declare that the research was conducted in the absence of any commercial or financial relationships that could be construed as a potential conflict of interest.

frontiers in Microbiology

ORIGINAL RESEARCH
published: 30 April 2020
doi: 10.3389/fmicb.2020.00794

The Transcription Factor Stp2 Is Important for *Candida albicans* Biofilm Establishment and Sustainability

*Bettina Böttcher[1], Bianca Hoffmann[2], Enrico Garbe[1], Tobias Weise[3], Zoltán Cseresnyés[2], Philipp Brandt[1], Stefanie Dietrich[2], Dominik Driesch[3], Marc Thilo Figge[2,4] and Slavena Vylkova[1]**

[1] Septomics Research Center, Friedrich Schiller University and Leibniz Institute for Natural Product Research and Infection Biology – Hans Knöll Institute, Jena, Germany, [2] Applied Systems Biology, Leibniz Institute for Natural Product Research and Infection Biology – Hans Knöll Institute, Jena, Germany, [3] BioControl Jena, Jena, Germany, [4] Institute of Microbiology, Faculty of Biological Sciences, Friedrich Schiller University Jena, Germany

OPEN ACCESS

Edited by:
Juliana Campos Junqueira, São Paulo State University, Brazil

Reviewed by:
Clarissa J. Nobile, University of California, Merced, United States
Ian A. Cleary, Grand Valley State University, United States

***Correspondence:**
Slavena Vylkova
Slavena.Vylkova@leibniz-hki.de

Specialty section:
This article was submitted to Infectious Diseases, a section of the journal Frontiers in Microbiology

Received: *07 February 2020*
Accepted: *03 April 2020*
Published: *30 April 2020*

Citation:
Böttcher B, Hoffmann B, Garbe E, Weise T, Cseresnyés Z, Brandt P, Dietrich S, Driesch D, Figge MT and Vylkova S (2020) The Transcription Factor Stp2 Is Important for Candida albicans Biofilm Establishment and Sustainability. Front. Microbiol. 11:794. doi: 10.3389/fmicb.2020.00794

The fungal pathogen *Candida albicans* forms polymorphic biofilms where hyphal morphogenesis and metabolic adaptation are tightly coordinated by a complex intertwined network of transcription factors. The sensing and metabolism of amino acids play important roles during various phases of biofilm development – from adhesion to maturation. Stp2 is a transcription factor that activates the expression of amino acid permease genes and is required for environmental alkalinization and hyphal growth *in vitro* and during macrophage phagocytosis. While it is well established that Stp2 is activated in response to external amino acids, its role in biofilm formation remains unknown. In addition to widely used techniques, we applied newly developed approaches for automated image analysis to quantify Stp2-regulated filamentation and biofilm growth. Our results show that in the *stp2*Δ deletion mutant adherence to abiotic surfaces and initial germ tube formation were strongly impaired, but formed mature biofilms with cell density and morphological structures comparable to the control strains. Stp2-dependent nutrient adaptation appeared to play an important role in biofilm development: *stp2*Δ biofilms formed under continuous nutrient flow displayed an overall reduction in biofilm formation, whereas under steady conditions the mutant strain formed biofilms with lower metabolic activity, resulting in increased cell survival and biofilm longevity. A deletion of *STP2* led to increased rapamycin susceptibility and transcriptional activation of *GCN4*, the transcriptional regulator of the general amino acid control pathway, demonstrating a connection of Stp2 to other nutrient-responsive pathways. In summary, the transcription factor Stp2 is important for *C. albicans* biofilm formation, where it contributes to adherence and induction of morphogenesis, and mediates nutrient adaption and cell longevity in mature biofilms.

Keywords: Biofilms, filamentation, *Candida albicans*, amino acids, metabolism, Stp2, automated image analysis

INTRODUCTION

Candida albicans is the fungal species most frequently associated with the healthy human gastrointestinal, vaginal and skin microbiome. Under certain circumstances, such as immune suppression or disruptions of the associated microbiota, it can become pathogenic and infect virtually any part of the human body. Particularly problematic is its ability to adhere to catheters and indwelling medical devices, such as artificial heart valves and joint replacements, and proliferate to form biofilms (Nobile and Johnson, 2015). These highly antibiotic-resistant, complex cell communities can serve as a reservoir of infection, since detached biofilm cells can disseminate to multiple body sites (Uppuluri et al., 2018), resulting in life-threatening diseases like sepsis. In most cases, the removal of infected biomedical devices with auxiliary antibiotic administration remains the only effective treatment (Cornely et al., 2012). Even so, *Candida* spp. are consistently the third leading cause of device-associated bloodstream infections with mortality rate of up to 50% (Kojic and Darouiche, 2004).

The ability of *C. albicans* to undergo a morphogenetic transition from yeast to hyphae is critical for proper biofilm formation (Richard et al., 2005). Hyphae-associated factors, like the Als family of adhesins promote anchoring to a substratum, cell-cell adhesion, and are important for biofilm establishment particularly under fluid flow and mechanical shear force conditions (Nobile et al., 2008; Grubb et al., 2009; Finkel et al., 2012). Further, the elongated filaments serve as a scaffold in the mature biofilm, which is composed of a dense network of yeasts, hyphae, and pseudohyphae embedded into extracellular matrix. Biofilm-associated hyphal growth is regulated by seven key transcription factors, which, together with two regulators of glycolysis and carbon metabolism, comprise a tightly controlled intertwined network (Bonhomme et al., 2011; Cleary et al., 2012; Fox et al., 2015). Thus, both filamentation and fungal metabolism play a critical role in *C. albicans* biofilm formation. Indeed, increased biomass limits the diffusion of nutrients, oxygen and water, leading to constant metabolic adaptations. Previous reports describe dynamic transcriptional and proteomic rearrangements in glucose and amino acid metabolism, the tricarboxylic acid (TCA) cycle, and the respiratory chain (García-Sánchez et al., 2004; Lattif et al., 2008; Fox et al., 2015). High glucose levels support biofilm development by activating the yeast-to-hypha transition via the Ras/cAMP/PKA pathway (Sabina and Brown, 2009; Santana et al., 2013). *C. albicans* strains capable of producing robust biofilms are signified by specific upregulation of genes in different amino acid metabolic pathways, a process coordinated by the aspartate aminotransferase Aat1 (Rajendran et al., 2016).

In *C. albicans* two distinct, but partially interconnected regulatory systems control the sensing and uptake of amino acids. Environmental oligopeptides and amino acids are sensed via the SPS (Ssy1−Ptr3−Ssy5) signaling pathway, where the Ssy5 endoproteinase cleaves the N-terminal cytoplasm-retaining domain of the transcription factors Stp1 and Stp2, inducing the expression of oligopeptide transporter and amino acid permease-encoding genes, respectively (Martínez and Ljungdahl, 2005; Miramón and Lorenz, 2016). Sensing of intracellular amino acids is coordinated by the TOR-pathway, and nutrient starvation or a direct inhibition of the TOR complex by rapamycin blocks the signaling cascade and leads to de-repression of nitrogen catabolism (Lee et al., 2018).

The TOR pathway has broad functions in *C. albicans* where it influences virulence features including flocculation, filamentation, chlamydosporulation, and biofilm formation (Bastidas et al., 2009; Böttcher et al., 2016; Flanagan et al., 2017). Additional regulators also control both nitrogen metabolism and biofilm formation. Arg81, a transcription factor required for utilization of ornithine as a nitrogen source, is important for adherence under flow conditions (Finkel et al., 2012), whereas Gcn4, the key regulator of the general amino acid control (GAAC) pathway, is required for normal biofilm growth (García-Sánchez et al., 2004). While these reports demonstrate the extensive role for factors responding to intracellular amino acid levels in biofilm development, the importance of the SPS pathway in biofilm formation remain poorly characterized.

Here, we investigated the role of Stp2, the key transcriptional regulator of extracellular amino acid signaling and metabolism, in biofilm development. The results indicate that Stp2 regulates adherence and germ tube formation, which are essential for biofilm initiation. At later time points, *stp2*Δ strains formed robust biofilms with morphology and density comparable to the control strains. However, Stp2-defective mature biofilms displayed significantly reduced metabolic activity and prolonged survival. Therefore, Stp2-mediated metabolic adaptation supports the fundamental steps of *C. albicans* biofilm development and coordinates biofilm lifespan.

RESULTS

Stp2 Is Required for Adherence to Abiotic Surfaces

Nutrient sensing and utilization is important for *C. albicans* filamentation and biofilm formation, and mature biofilms are linked to activation of the TCA cycle and amino acid metabolism. Since the transcription factor Stp2 controls utilization of extracellular amino acids, we investigated its role for biofilm establishment and maturation. Biofilms are initiated by adherence of individual cells to solid biotic or abiotic surfaces, so we tested the role of Stp2 in attachment to polystyrene culture plates. Cells lacking *STP2* had a significantly decreased ability to adhere to surfaces as compared to the wild type SC5314, *stp2*Δ + *STP2* and the $STP2^{OE}$ strains (**Figures 1A,B**). *C. albicans* adherence is closely coupled to germ tube formation, and we noted that in addition to the impaired adherence *stp2*Δ cells had defect in filamentation (**Figure 1B**), which further contributed to the reduction in optical density. The overexpression of *STP2* did not promote cell adherence to the abiotic surface beyond the wild-type level. No growth defects were observed for the *stp2*Δ and $STP2^{OE}$ strains compared to wild type and complemented strains in liquid RPMI medium (**Supplementary Figure S1**).

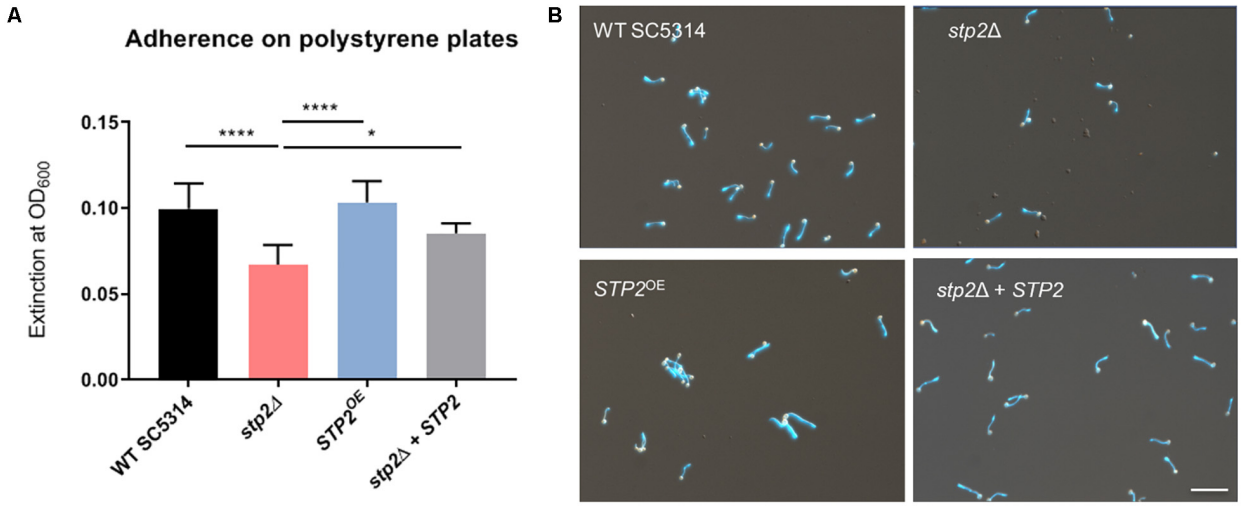

FIGURE 1 | *C. albicans* Stp2 mediates adherence to polystyrene surfaces. *C. albicans* strains were incubated on 24 well polystyrene plates for 90 min in RPMI and non-adherent cells were washed off. **(A)** The density of the remaining cells was measured optically by $OD_{600\ nm}$. Statistical comparison revealed a significantly lower cell density for the *STP2* deletion strain to all the other strains ($n = 3$, One-way ANOVA with Tukey's multiple comparisons test, $p < 0.0001$), indicating the importance of Stp2 in the process of adherence to abiotic surfaces. **(B)** Imaging of adherent cells after dual staining with rhodamine and calcofluor white. Microscopic analyses of *stp2*Δ showed a reduced cell number and shorten hyphae length. Scale bar: 50 μm.

Reduced Expression of Early Hyphae Aassociated Genes Correlates With Stp2 Processing

To gain further insight into the effect of Stp2 on hyphal morphogenesis, we established an automated method to quantify yeast-to-hyphae transition in shaking culture. For this purpose, the surface of mother yeast cells was stained with rhodamine, followed by incubation in RPMI medium at 37°C under shaking conditions to induce hyphal growth. After 90 min all cells, including budding yeasts and hyphal elements, were counterstained with calcofluor white and visualized by fluorescence microscopy. By automated image analysis, the hyphal filaments were segmented and separated from their mother yeast cells. Sample sizes of 83 to 100 elements per strain were examined for the number of germ tubes per yeast cell and the hyphal length.

This novel approach revealed that the *stp2*Δ mutant formed significantly shorter filaments than the strains with a functional Stp2, with an average hyphae length of 19.05 μm, compared to 30.27 μm in wild type cells and 29.2 μm in the heterozygous *STP2* revertant (**Figure 2A**). Notably, *STP2* overexpression led to a significant increase in hyphae length compared to the wild type (32.96 μm; 8% longer). In addition, the number of hyphal filaments per mother cell was calculated and an average *stp2*Δ cell formed 1.12 germ tubes, resulting in a higher tendency to form multiple filaments per yeast cell, whereas the mean number of germ tubes was close to one for all other strains (**Figure 2B**).

To test if the filamentation delay can be detected on transcriptional level, we analyzed the expression of early hyphae associated-genes *ECE1*, *ALS3* and *HWP1* by qRT-PCR. Their expression was significantly downregulated in the *stp2*Δ mutant compared to the SC5314 strain (**Figure 3**), showing that the altered filamentation is also reflected on gene expression level. Importantly, similar effects were also observed when cells were grown under strong Stp2-stimulating conditions, since *stp2*Δ cells had reduced expression of hyphae-associated genes (*ECE1*, *ALS3*, and *HWP1*) with a significant effect for *HWP1* (**Supplementary Figure S2**). *C. albicans stp2*Δ + *STP2* cells grown in RPMI medium restored the transcript level of early hyphal genes to an intermediate degree, and the *STP2* overexpression brought gene expression to the wild type level, except for expression of *ALS3*, which was significantly lower.

Genes for amino acid permeases (AAPs) are known targets of Stp2 and their enhanced transcription suggests active Stp2 processing. As expected, the impact of this transcription factor on AAP gene expression was apparent in casamino acid-rich (CAA) conditions, since we noted that the *stp2*Δ cells had significantly reduced expression of *CAN2*, *HIP1,* and most of the *GAP* genes (**Supplementary Figure S2**). In contrast, *GAP4* was upregulated suggesting that either additional transcriptional activator regulates the expression of this gene or that Stp2 acts as a repressor. We also tested AAPs gene expression in RPMI medium, condition that resulted in downregulation of *GAP1* and *HIP1* in cells lacking *STP2* compared to the wild type (**Figure 3**). However, the expression of these genes was still higher than for the hyphae-associated genes, further suggesting regulation by alternative or redundant transcription factors. Indeed, the expression of *GCN4*, a key regulator of nitrogen starvation responses, was enhanced in the *stp2*Δ mutant compared to the wild type. Counter-intuitively, the basic amino acid permease gene *CAN2* was not differentially regulated, and thus its gene expression was independent of Stp2 in the tested condition.

The activation of Stp2 is initiated by post-translational N-terminal cleavage, and removal of the cytoplasmic retention

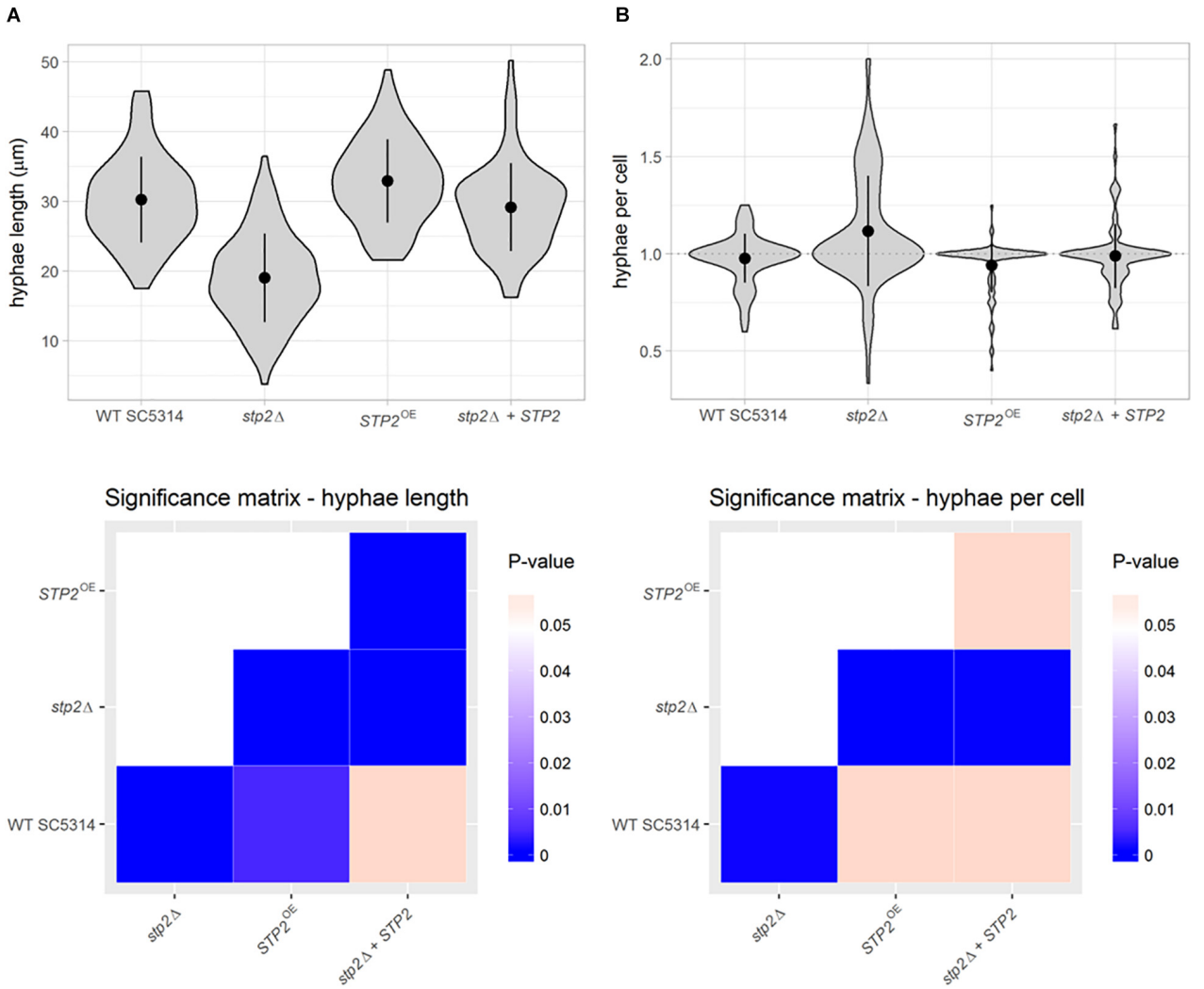

FIGURE 2 | Stp2 contributes to filamentation in liquid RPMI medium. Filamentation of *C. albicans* strains was initiated in liquid medium for 90 min. Dual staining facilitated the differentiation of yeast and hyphae parts of the germinating cells. **(A)** Hyphal length in RPMI was determined using automated object identification and segmentation. The *stp2*Δ mutant and the *STP2* overexpression strain showed significantly shorter or longer hyphae, respectively, compared to the SC5314 and the stp2Δ + *STP2* strains. **(B)** The number of hyphae per mother cell was significantly higher for the *stp2*Δ mutant compared to the wild type, complemented and overexpression strains. P-values were obtained by pairwise Wilcoxon rank sum tests and corrected for multiple testing by the Benjamini-Hochberg procedure.

signal allows migration to the nucleus (Martínez and Ljungdahl, 2005). Since we noted Stp2-dependent expression of hyphal and AAPs genes in RPMI medium, we questioned whether these conditions stimulate Stp2 activation. Thus, processing of the Stp2 protein was analyzed after incubation in RPMI medium and compared to the conditions that stimulate Stp2 processing (CAA medium) or not (SD medium). As expected, Western Blot analyses of Stp2 processing revealed no cleavage of Stp2 in SD medium and nearly full processing in CAA. Partial processing of Stp2 was observed upon growth in RPMI medium (**Figure 4**). Thus, the amino acids available in this medium are sufficient to activate Stp2, leading to reduced expression of early hyphae-associated and AAP genes, and contributing to the notable filamentation defect in the *stp2*Δ mutant.

Deletion of *STP2* Enhances the Starvation-Induced Hyphal Morphogenesis

Hyphae formation in planktonic liquid cultures and on solid agar surfaces can differ in their manifestation, since they rely on different genetic programs (Azadmanesh et al., 2017). Therefore, a range of solid media and conditions were tested for hyphae formation and radial filamentation, regardless of inner colony wrinkling, was scored (**Supplementary Figure S3**). The nitrogen-limiting SLAD agar promotes filamentation in *C. albicans* in line with the starvation response. Stp2-defective strain growth on SLAD agar formed longer filaments under all temperatures and pH conditions tested, with a more pronounced effect at pH 4.2 (**Figure 5A**).This phenotype was exclusively observed

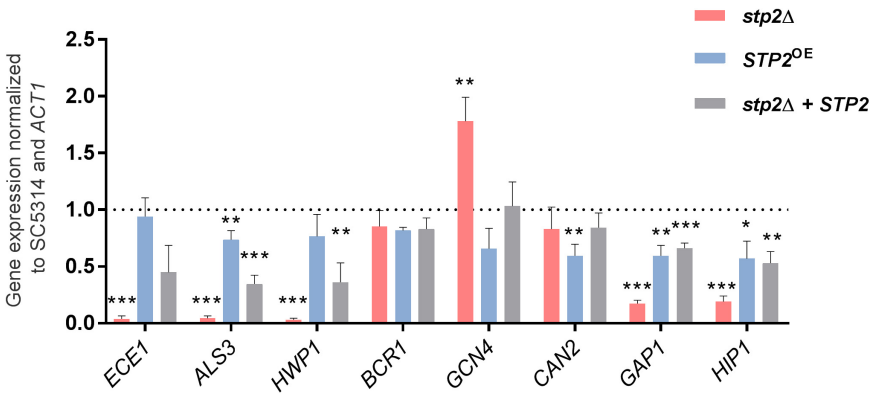

FIGURE 3 | STP2-defective *C. albicans* strain has lower relative gene expression of hyphae-associated and amino acid permeases genes in RPMI medium. Early transcriptional response of cells grown in shaking, planktonic RPMI cultures after 60 min was analyzed using quantitative real time PCR. Two groups of genes were analyzed: the key morphology-associated genes *ECE1*, *ALS3, HWP1*, and *BCR1*; and amino acid and nitrogen metabolism genes *GCN4*, *CAN2*, *GAP1*, and *HIP1*. Depicted bars represent the relative fold expression change normalized to the housekeeping gene *ACT1* and the wild type SC5314 gene expression using the $2^{-\Delta\Delta CT}$ method (Pfaffl, 2001). Shown are means and standard deviations from three biological and three technical replicates and the dashed line represents the wild-type expression level. Statistical analyses compared each sample to the SC5314 wild type level (Multiple unpaired *t*-test, ***p < 0.001; **p < 0.005, and *p < 0.01; for samples that passed the False Discovery Rate approach by the Benjamini–Hochberg procedure with 1% threshold, $n = 3$). The *stp2*Δ mutant strain showed significantly reduced expression levels compared to the wild type SC5314 for all genes tested, but *CAN2*.

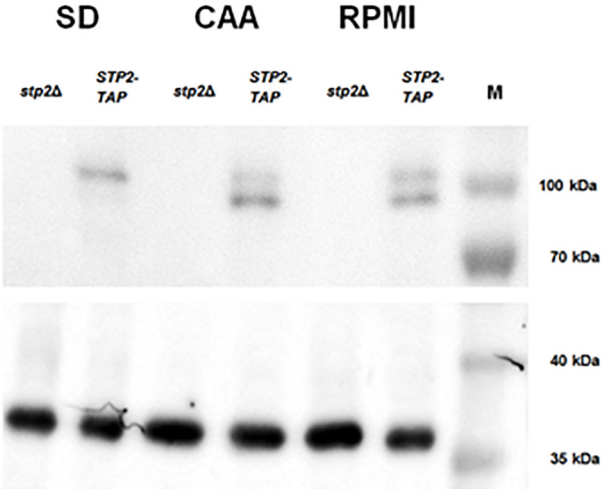

FIGURE 4 | Growth in RPMI induces partial Stp2 processing. *STP2-TAP* and the parental *stp2*Δ strain were cultivated in liquid SD (4 h), CAA (4 h) or RPMI (90 min) media and protein processing was analyzed by Western blot. As expected, growth in the amino acid-free SD medium did not activate Stp2 processing, since only the full-length protein was detected. The amino acid-containing media CAA and RPMI induced N-terminal cleavage, as both the shorter and full-length Stp2 protein forms were detected. Tdh3 was used as a loading control and the PageRuler™ protein ladder (10–180 kDa).

on SLAD agar, but not in liquid conditions (**Supplementary Figure S4**). Incubation on Spider agar induced colony wrinkling in all strains tested. However, while radial filaments were barely seen in the wild type strain, the *STP2*-defective mutant formed a prominent hyphal fringe at the edge of the colony. Interestingly, this effect was rather mild at 37°C, but striking at an incubation temperature of 30°C (**Figure 5B**). The incubation in liquid Spider medium for 90 min at 37°C revealed more robust filamentation for the wild type compared to the *stp2*Δ mutant (**Supplementary Figure S4**), pointing toward differential responses to liquid and solid conditions. In contrast, filamentation on solid RPMI medium was reduced in the *stp2*Δ deletion strain regardless of the incubation temperature (**Figure 5C**). Growth on another typical mammalian cell culture medium, medium M199, brought out a similar phenotype (**Supplementary Figure S3**). Therefore, Stp2 controls filamentation in a nutrient-dependent manner.

*Stp2*Δ Mutant Forms Thinner Biofilms Under Flow Conditions

Maturation from attached monolayers of germ tubes to a dense, matrix-embedded population of cells is the third step of the biofilm development. Thus, we evaluated the effect of Stp2 on biofilm maturation. After the initial adherence phase, the medium was renewed and mature biofilms were allowed to form at 37°C with gentle shaking. Calculation of biofilm formation after 24 h of growth revealed no significant differences for all strains tested, showing that although the *stp2*Δ cells had defects in the early stages of biofilm formation, they were able to reach the density of the Stp2-containing biofilm formers (**Figure 6A**).

Flow conditions promote *C. albicans* biofilm formation due to the increased availability of nutrients and imposed shear stress (Mukherjee et al., 2009; Uppuluri et al., 2009). Therefore, we applied a microfluidic technology to grow biofilms under flow conditions. After cells were allowed to adhere to the fluidic chamber under static conditions for 90 min the non-adherent cells were rinsed. At this stage the morphology and cell density the *stp2*Δ mutant strain appeared comparable to those obtained from the static cultures, since fewer cells attached to the surface, and those that remained showed a reduced germ tube length (**Supplementary Material M1**). Next,

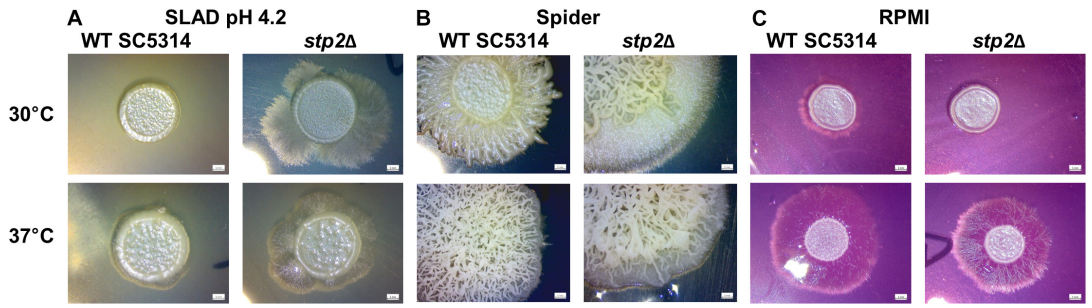

FIGURE 5 | Stp2 controls filamentation on solid media depending on the available nutrient sources. 5 μl of *C. albicans* SC3514 or *stp2*Δ suspensions were dropped onto different nutritional agar media and incubated for 5 days at 30 or 37°C, respectively. The *stp2*Δ mutant formed an extended hyphal fringe on nitrogen starvation medium (SLAD) **(A)** or mannitol-containing Spider agar **(B)**. In contrast, hyphae formation was reduced on RPMI medium **(C)**.

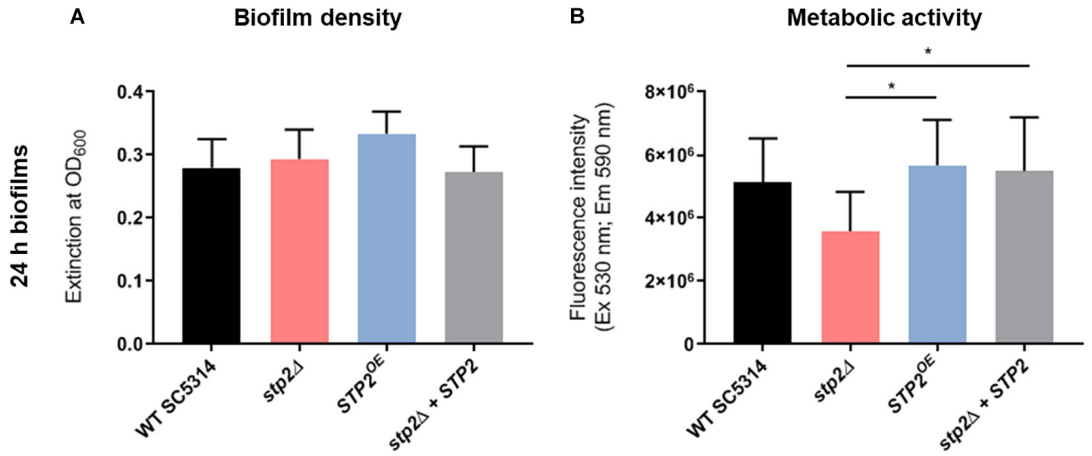

FIGURE 6 | Characterization the role of Stp2 in cell density and respiration of mature *C. albicans* biofilms. *C. albicans* biofilms were grown for 24 h in RPMI on polystyrene plates, then analyzed for cell density by measuring the optical density **(A)** and for respiration of metabolically active cells using resazurin reduction assay **(B)**. *stp2*Δ biofilms were significantly less metabolically active compared to the *STP2* overexpression and gene revertant strains (One-way ANOVA, $p = 0.0188$, $n = 3$).

shear flow of RPMI medium was applied at 0.2 dyne/cm^2. Biofilm formation was recorded by imaging of the microfluidic chambers every 20 min for 24 h (**Supplementary Material M1**). The progress of biofilm formation was monitored using an automated computational approach, which analyzed the gray-scale values of the microscopic images (Weise et al., 2020). Based on this, the specific rates of biofilm development were calculated. Interestingly, biofilm maturation differed from static experiments in that the strain lacking *STP2* had an overall slower growth rate, resulting in lower maximal biomass (**Figures 7A,B**). Moreover, the growth and plateau phase were delayed, and never reached the wild type biofilm confluency as notable differences in biofilm density were detected (**Figure 7A**). However, hyphae appeared indistinguishable between the two strains at later stages of biofilm development. Biofilm formation by the *STP2* overexpression strain was similar to the wild type under static growth (**Figure 6A**), and slightly increased under shear flow conditions and (**Figure 7**). Although some variance within the technical replicates was observed (**Figure 7C**), the comparative analyses of related measurements revealed a consistent pattern of retarded growth rates for the *stp2*Δ mutant (**Figure 7C**). The applied analysis not only provided high temporal and spatial resolution of the growing flow-induced *C. albicans* biofilms, but also allowed for the calculation of maximal growth rates and investigation of experimental reproducibility.

Mature *STP2*-Defective Biofilms Differ in Metabolic Activity and Longevity

Although the *STP2* deficient strain was able to reach the density of wild type mature biofilm under static conditions, its metabolic activity was markedly reduced after 24 h of growth (**Figure 6B**). This phenotype was fully restored in the revertant and overexpression strains. Differences in the total metabolic activity could result from variations in total biomass, energy flux, or the number of live cells. Thus, the viability of cells in wild type and *stp2*Δ biofilms was investigated. At early time points (8 h), nearly all adherent germ tubes or young biofilm cells of the wild type and *stp2*Δ mutant were alive (**Figure 8**). After biofilm maturation at 24 and 30 h, the wild

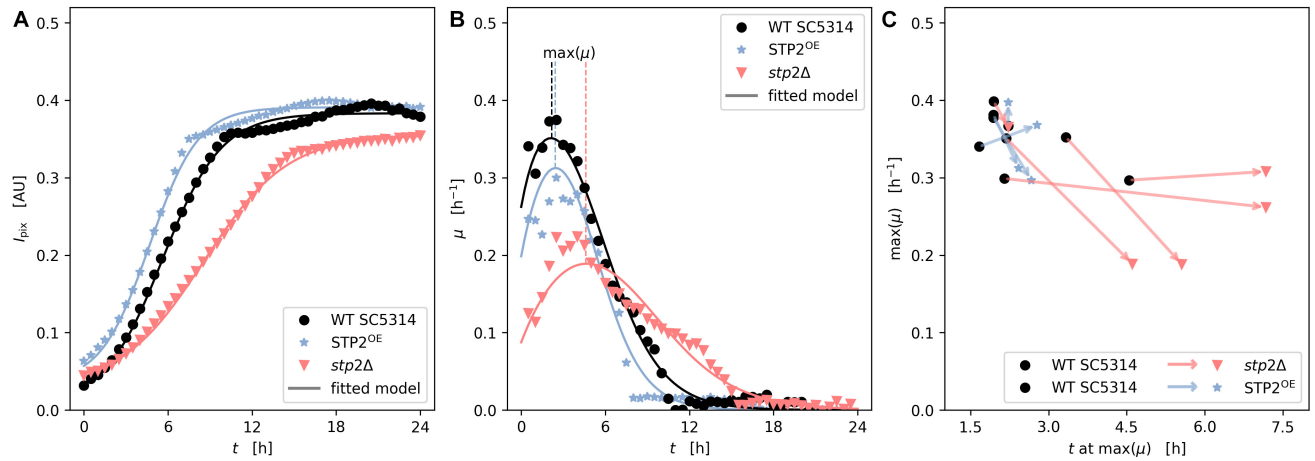

FIGURE 7 | Stp2 plays a crucial role during biofilm formation under flow conditions. Yeast cells were inoculated into a channel system of microfluidic plates and adherence took place for 90 min in RPMI medium without any medium flow. Non-adherent cells were rinsed by a short, but impulsive flush with medium and biofilms were allowed to form under constant slow medium flow. Biofilm architecture and biomass accumulation was monitored microscopically every 20 min over 24 h. **(A)** Time series of measured and modeled cell density (expressed as mean pixel intensity) showing growth over time. **(B)** Time series of measured and modeled specific growth rate representing the relative growth velocity. **(C)** Scatter subplot of height and time of maximal observed growth rate from independent replicates (n = 5 for *stp2*Δ vs wild type and n = 4 for *STP2*^{OE} vs wild type). The arrows link the maximal growth of *STP2* deletion and overexpression strains (arrow head) to their respective wild types (arrow tail) during one technical approach.

type biofilms had a large proportion (26 and 31%, respectively) of dead cells (**Figure 8**). In stark contrast, *stp2*Δ biofilms had enhanced longevity since only a limited number of dead cells were detectable at the same time point. After 2 days the *stp2*Δ biofilms contained about 22% of dead cells, whereas about the half of all wild type biofilm cells were PI-positive. This indicates that absence of the *STP2* results in a notable delay in death of cells within a biofilm. Taken together, although *stp2*Δ mutant formed comparable to the wild type strain static 24 h biofilms, they contained more live cells but with lower metabolic activity.

Deletion of *STP2* Increases Cellular Sensitivity to the Tor1 Inhibitor Rapamycin

The TOR pathway, active under high levels of intracellular carbon and nitrogen sources, can impact filamentation and adhesion in *C. albicans* (Bastidas et al., 2009). In *S. cerevisiae* TOR controls components of the SPS pathway among others (Shin et al., 2009). Therefore, we investigated whether similar link exists in *C. albicans*. As expected, addition of 7.5 nM rapamycin resulted in a flattened slope of the growth curve in the wild type SC5314 compared to growth in pure YPD medium (**Figures 9A,B**). The *stp2*Δ mutant exhibited an increased sensitivity to rapamycin during the first 36 h of growth, but eventually reached the cell density of the control strains at the stationary phase. An overexpression of *STP2* increased the growth rate during the early time points, indicating an increased rapamycin resistance. Growth of *stp2*Δ and *STP2*^{OE} strains in pure YPD medium was comparable to the wild type and the complemented strains. Therefore, there was a notable *STP2* gene dosage effect in sensitivity to rapamycin.

DISCUSSION

The *C. albicans* three component sensor SPS (Ssy1-Ptr3-Ssy5) coordinates the proteolytic cleavage and activation of the transcription factors Stp1 and Stp2 in response to increased levels of exogenous oligopeptides and amino acids, respectively (Martínez and Ljungdahl, 2005; Ljungdahl, 2009; Tumusiime et al., 2011). The proper uptake of amino acids, in particular, is critical for fungal pathogenicity, since the SPS pathway is essential for damage and escape from the macrophages, and for full virulence (Vylkova and Lorenz, 2014; Miramón and Lorenz, 2016; Silao et al., 2019). Sensing and metabolism of certain amino acids, such as arginine, proline and methionine, trigger morphological transition from yeast to hyphae, a well-defined virulence factor. Biofilms represent a microenvironment where morphogenesis and nutrient adaptation are tightly connected. In this study, we investigated how Stp2 drives different stages of biofilm growth. We developed novel approaches for quantitative image analysis and used them to obtain precise measurements of hyphae initiation, biofilm growth rates, and density. Our results show that at the early stage of biofilm formation the *stp2*Δ mutant had impaired adherence to abiotic surfaces and delayed germination, but ultimately formed mature biofilms with density and morphology comparable to control strains. However, *STP2*-deficient biofilms had significantly lower metabolic activity, leading to increased biofilm longevity and sustainability. Taken together, this study demonstrates that

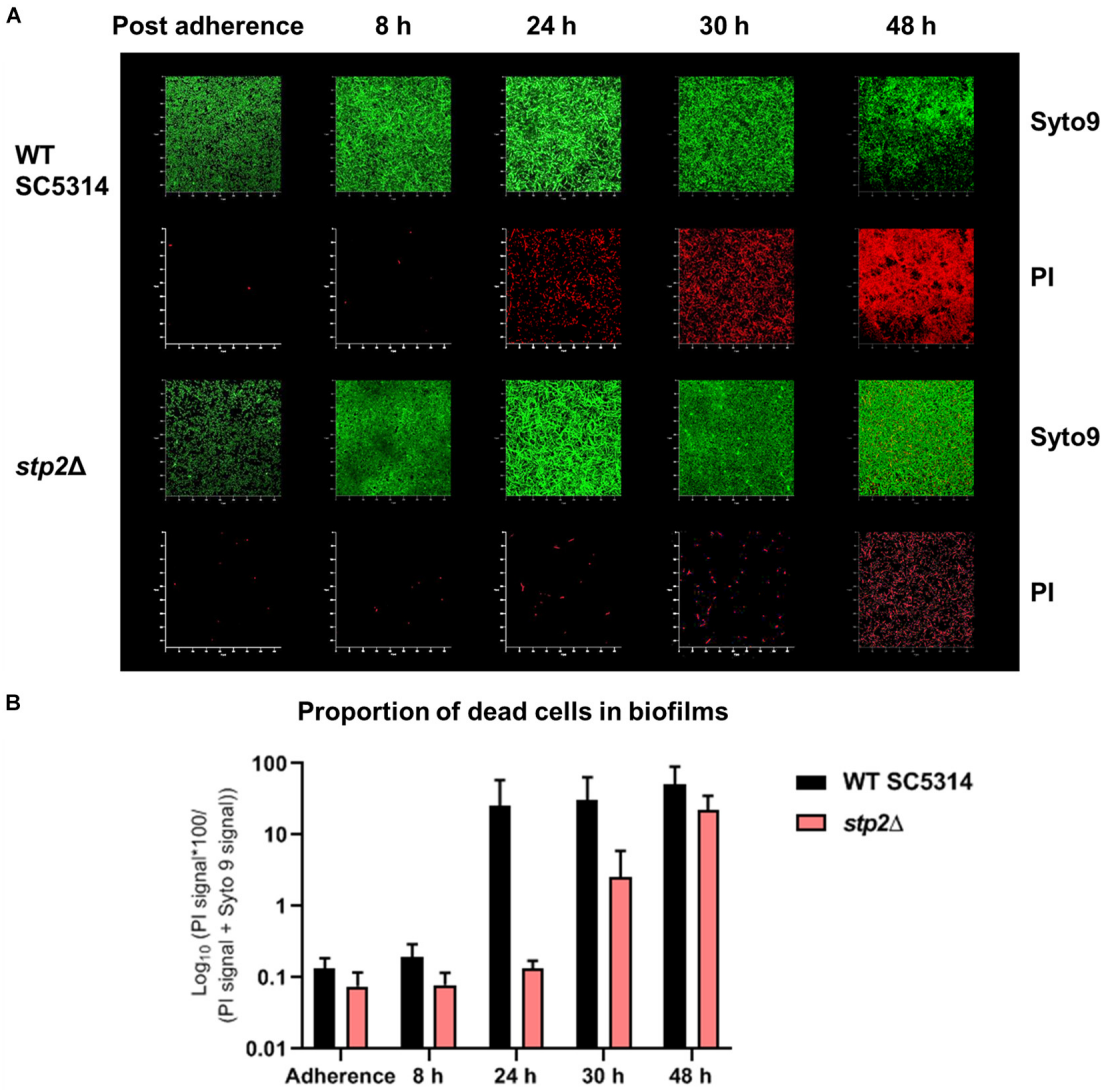

FIGURE 8 | Loss of *STP2* enhances longevity of *C. albicans* biofilms. Biofilms of the *stp2*Δ mutant and wild type were grown on polymer imaging dishes in RPMI medium for up to 48 h. To evaluate cell viability, live-dead staining (Syto9 and PI staining) was applied to single dishes at different time points. Partial cell death of the wild type occurred already after 24 h, whereas cells of the *stp2*Δ mutant biofilm started to die with a large temporal delay at 48 h. **(A)** Exemplary render images of *C. albicans* wild type SC5314 and *stp2*Δ biofilms in time series with live-dead staining in split Syto9 and PI channels. **(B)** The ratio of the red PI signal over the entire cell population (PI + Syto9) was calculated over the z-stack and the median of biological triplicates with SD was plotted in percentage on a $\log_{10}$ scale. (n = 3).

C. albicans Stp2-coordinated processes are critical for biofilm formation and longevity.

Adherence to surfaces is the initial step of biofilm formation. In *C. albicans* this is mediated by GPI-modified cell wall proteins named adhesins. The induced expression of hyphae-associated adhesins, such as Hwp1 and Als3, during the yeast-to-hyphae switch promotes adhesion to epithelial and endothelia host cells and mature biofilm structure on silicone surfaces (Zhao et al., 2004, 2006; Wächtler et al., 2011). In this study, Stp2 regulated the adherence to abiotic surfaces, as fewer *stp2*Δ mutant cells attached to the bottom of the polystyrene well or the microfluidic channels. Stp2-dependent expression of *HWP1* and *ALS3* was also notable in planktonic cultures, which strengthens the link between amino acids metabolism and adherence. In this regard, a screening of transcription factor library for adherence in YPD under flow condition revealed a number of adhesion-defective mutants that are regulators of amino acid and general nitrogen metabolism (Finkel et al., 2012). These include controllers of branched-chain or sulfur-containing amino acid biosynthesis genes (Leu3, Met4), utilization of ornithine (Arg81), and putative arginine biosynthesis (Dal81) (Finkel et al., 2012), highlighting the importance of amino acid metabolism for adhesion.

Aside from the observed reduction in the number of adherent cells, we noted a marked decrease in germ tube formation

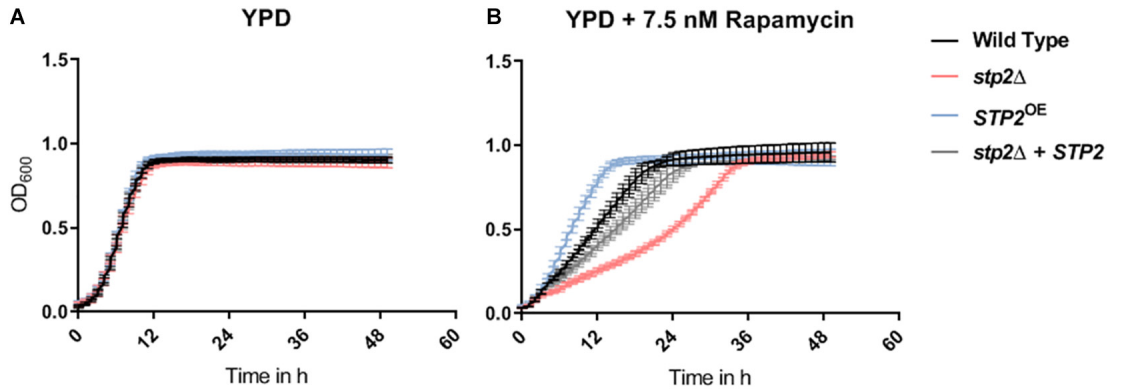

FIGURE 9 | STP2-defective mutants are unrestricted in growth but are suppressed by an antagonist of the TOR pathway. All strains (Wild type SC5314, *stp2*Δ, *STP2*^{OE} and *stp2*Δ + *STP2*) were set to a defined $OD_{600\ nm}$ of 0.01 in 200 µl pure and rapamycin-supplemented YPD **(A, B)** media. Incubation was carried out at 30°C and increase of cell density was monitored every 30 min over 2 days ($n = 3$). Although no Stp2-specific effects occurred in standard YPD, the addition of rapamycin to the medium decreased the growth rate of the *STP2* deletion mutant, while increased the growth for the overexpression strain as compared to wild type and revertant strains.

in the *stp2*Δ mutant. The recognition and uptake of certain extracellular amino acids induces morphological changes (Lee et al., 1975; Dabrowa et al., 1976; Kraidlova et al., 2011). For instance, Silao et al. (2019) recently discovered that metabolism of proline results in Ras1/cAMP/PKA-mediated hyphae formation. Defects in filamentation were also described for mutants in key components of the SPS pathway, which senses increase in the extracellular level of some amino acids, but not proline. The Ssy1 sensor is important for filamentation on solid Lee's plates or serum-containing medium (Brega et al., 2004), while Stp2 is required for yeast-to-hyphae switch on ornithine agar (Silao et al., 2019). A reduced ability of the Stp2-deficient strain to initiate hyphal morphogenesis was also observed here - in the context of biofilms, in liquid RPMI, and on solid media. Interestingly, the filamentation defect in liquid medium corresponded to the degree of Stp2 processing – *stp2*Δ fails to filament in amino-acid rich medium (Vylkova and Lorenz, 2014), a strong Stp2-stimulating condition (Miramón and Lorenz, 2016), whereas partial processing in RPMI only caused a germination delay. We hypothesize that the observed lag in hyphal growth in the latter condition is achieved by activation of alternative pathways that react to changes in the intracellular nutritional state, and that such compensatory mechanisms fail in cells with gross growth defects (such as *stp2*Δ cells in CAA). In *C. albicans* the former effects might be driven by the Gcn4-controlled general amino acid control (GAAC) or the TOR pathways, which are linked to the SPS pathway and to each other by mutual control hubs (Garbe and Vylkova, 2019). Indeed, we show that loss of Stp2 results in enhanced expression of *GCN4,* which is regulated mostly at the transcriptional level in *C. albicans* (Tournu et al., 2005), and an increased sensitivity to the Tor1-inhibitor rapamycin, supporting the idea of compensatory nutrient responses by these pathways. A correlation between the Stp1/2 transcription factors and TOR signaling was already described in *S. cerevisiae*, where *stp1*Δ cells were hypersensitive to rapamycin and Stp1 protein degradation was controlled by ScTORC1 (Shin et al., 2009). Since the components of the TOR-complex differ fundamentally between *S. cerevisiae* and *C. albicans* (Tatebe and Shiozaki, 2017), the connections between TOR and members of the SPS pathway could have been rewired.

Several studies revealed a transcriptional upregulation of amino acid uptake and biosynthesis genes in mature biofilms. The basic amino acid permease gene *CAN2* is one of the common core target genes of the master biofilm regulators, and shared a transcriptional response with the hyphae-associated core target genes *ALS1*, *HYR1*, and *HWP1* (Nobile et al., 2012). Rajendran and colleagues compared high and low *C. albicans* biofilm forming isolates in the context of amino acid biosynthesis, and showed that the aspartate aminotransferase Aat1 is a key factor for biofilm heterogeneity (Rajendran et al., 2016). Further, the transcription factor of sulfur amino acid biosynthesis Met4 is required for adherence (Finkel et al., 2012), and its target genes for methionine biosynthesis strongly upregulated in mature biofilms (García-Sánchez et al., 2004). The role of amino acid biosynthesis was further shown by metabolomic analysis, where amino acids were intracellularly enriched during the whole process of *C. albicans* biofilm formation (Zhu et al., 2013). A high number of amino acid biosynthesis genes are regulated by Gcn4, and this transcription factor is required for biofilm formation (García-Sánchez et al., 2004). Interestingly, *gcn4*Δ mutant biofilms have the same proportion of hyphae compared to the wild type (García-Sánchez et al., 2004), in line with our observations of *stp2*Δ mature biofilms. Based on these reports and data presented here, we propose that Stp2-mediated amino acid sensing and uptake is particularly important during the early phase of biofilm formation, whereas the GAAC activation in the maturing biofilm leads to increased amino acid biosynthesis. Consistent with this, constant supply of fresh nutrients under flow, a condition that presumably does not require induction of amino acid biosynthesis, leads to prolonged filamentation defect in the *stp2*Δ mutant. A main question that remains to be

answered is why *C. albicans* biofilm growth requires such tight control of amino acid homeostasis.

Many longevity pathways are highly conserved in eukaryotes, including mitochondrial function, TOR and PKA signaling, and metabolic pathways such as NAD^+ biosynthesis (Lin and Austriaco, 2014). Although the exact mechanisms for how these factors coordinate longevity are yet to be discovered, it is now well established that nutritional restriction enhances lifespan in many eukaryotes. In *S. cerevisiae,* for example, the process is mediated through the Tor1-Sch9 and Ras2-cAMP-PKA pathways (Longo, 2003; Deprez et al., 2018), whereas in *C. albicans* low glucose levels were able to extend the lifespan of *goa1*Δ mutant, which has impaired mitochondrial function (Chen et al., 2012). Cells lacking *STP2* formed mature biofilms with reduced metabolic activity compared to the control strains. Thus, failure to take up amino acids likely leads to intracellular nutrient deficiency, which could result in lowered nutrient consumption rates. In this study, we observed a plethora of dead wild type cells after 24 h of biofilm formation, whereas the cell death was notable first in 30 h *stp2*Δ biofilms, indicating increased survival rate. Although calorie reduction is often investigated in form of glucose depletion, a role of amino acid limitation was demonstrated in *S. cerevisiae*: high Gcn4 activation was sufficient to repress protein synthesis, which further increased yeast lifespan and longevity (Steffen et al., 2008). Rapamycin enhanced the Gcn4-associated lifespan extension and intracellular proline accumulation extended the replicative lifespan, suggesting that cellular amino acid homeostasis is critical for yeast aging (Mittal et al., 2017; Mukai et al., 2019). Indeed, failure to properly sense and uptake extracellular amino acids, such as in the *S. cerevisiae* SPS signaling cascade deletion mutants, resulted in enhanced longevity and replicative lifespan under both rich and calorie restricted growth conditions (Tsang et al., 2015), a phenotype that is similar to the longevity effect of *stp2*Δ biofilms described here. Further studies are required to characterize the regulators of lifespan in *C. albicans* and the contribution of this process to adaption and survival in different body niches and fungal pathogenicity.

Overall, our data describe a novel role for *C. albicans* transcription factor Stp2 in adherence, germ tube initiation, and biofilm sustainability, showing that the SPS-mediated responses to extracellular amino acids are critical for biofilm development. In this setting, amino acids not only represent an important alternative nutrient source, but also coordinate hyphal growth, fitness, and biofilm lifespan. The connection between Stp2-regulated processes to pathways that control intracellular nutritional homeostasis points toward a larger regulatory network that remains to be investigated further.

MATERIALS AND METHODS

Strains and Culture Conditions

C. albicans strains were routinely passaged on YPD agar (2% peptone, 1% yeast extract, 2% glucose, 1.5% agar) at 30°C and stored as frozen stocks in YPD medium using Roti®-Store yeast cryovials (Carl Roth GmbH + Co. KG). RPMI with stable glutamine (Merck–Biochrom) was used as induction media for *in vitro* biofilm and planktonic cultures assays. Liquid CAA medium (0.17% YNB, 0.5% ammonium sulfate and 1% casamino acids; pH 4.5) was used to trigger Stp2 activation, while SD medium (0.17% YNB, 0.5% ammonium sulfate and 2% glucose; pH 4.5) was used as synthetic minimal medium that does not stimulate the SPS-pathway. *C. albicans* strains used in this work are listed in **Table 1**.

Growth Assays

General proliferation was evaluated via growth curve assays. Strains were pre-cultured overnight in YPD at 30°C and diluted to $OD_{600\ nm}$ of 0.01 in different growth media (YPD, YPD with 7.5 nm rapamycin, RPMI, RPMI with 0.5% ammonium sulfate). Cultures were incubated at 30°C in a Magellan TECAN plate reader and $OD_{600\ nm}$ determined prior 30 s shaking every 30 min over 48 h. Changes in cell density ($OD_{600\ nm}$) were plotted in biological triplicates against the incubation time.

Strain Construction

Plasmid Construction

For the ectopic overexpression of *STP2,* the previously described pADH1-GFP (Hünniger et al., 2014) was used. *STP2* was amplified with the primer pair 5'STP2-XhoI and 3'STP2-EcoRV and cloned via *Xho*I/*Eco*RV into the plasmid, thereby replacing *GFP*. The created plasmid was named pSTP2OE_w/o_TAG.

Tagging of *STP2* was done using the Gateway™ cloning approach (Legrand et al., 2018). The *STP2* gene was amplified from genomic DNA with the primer pair STP2_Gateway_fwd and STP2_Gateway_rev and subsequently cloned into pDONR221™ (Thermo Fischer) via BP Clonase™ reaction. The resulting *STP2* donor vector was added to a LR Clonase™ reaction with the expression vector pDEST2303 (Legrand et al., 2018) to generate an expression plasmid carrying *STP2* with a C-terminal TAP-tag under control of the *TDH3* promoter and a *SAT1* selection marker. The created plasmid was named pDEST2303_(STP2).

C. albicans Transformation

For the integration of *STP2* in the Ca*ADH1* locus, a transformation cassette was created via *Nar*I/*Sac*I-restriction

TABLE 1 | *C. albicans* strains in this study.

Name	Genotype	References
Wild type SC5314	wild type	Fonzi and Irwin, 1993
*stp2*Δ	*stp2*Δ::*FRT/stp2*Δ::*FRT/stp2*Δ::*FRT*	Vylkova and Lorenz, 2014
*stp2*Δ+*STP2*	*stp2*Δ::*FRT/stp2*Δ::*FRT/stp2*Δ::*FRT-STP2*	Vylkova and Lorenz, 2014
$STP2^{OE}$	*ADH1/adh1::STP2-SAT1*	this study
STP2-TAP	*stp2*Δ::*FRT/stp2*Δ::*FRT/stp2*Δ::*FRT RPS1/rps1::TDH3p-STP2-TAP-SAT1*	this study

of pSTP2OE_w/o_TAG, while pDEST2303_ (STP2) was digested with *Stu*I for integration in the Ca*RPS1* locus. The resulting transformation cassettes were purified via gel extraction (QIAquick Gel Extraction Kit, Qiagen) and used for *C. albicans* transformation using the previously described lithium-acetate-method (Walther and Wendland, 2003). After the heat shock, the cells were incubated for 4 h in YPD at 37°C prior to plating on YPD agar plates containing 200 μg/ml nourseothricin (Werner BioAgents). Transformants were validated via colony PCR. The validation primers are listed in **Supplementary Table S1**.

Morphological and Biofilm Tests

Germ Tube Assay

For hyphae induction in liquid medium, *Candida* strains were pre-cultured in liquid YPD overnight (30°C, 180 rpm), washed with PBS, and stained for 30 min with 1% rhodamine and 0.05% Tween 80 in the dark. The cells were washed twice with PBS and a final cell density of $OD_{600\ nm}$ of 0.4 (8×10^6 cells) was transferred into 500 μl RPMI induction medium for 90 min cultivation at 37°C. After germ tube induction, the cells were counterstained with 2% calcofluor white for 5 min and the morphology of the washed samples was analyzed microscopically (Axiovert, Carl Zeiss, AG). The experiment was performed in biological quadruplicates.

Filamentation Assay

Candida cells from YPD overnight cultures were washed and 5 μl cell suspensions ($OD_{600\ nm}$ of 0.5) were spotted on the following agar plates (2% Kobe I agar, Carl Roth GmbH + Co., KG): YPD; Spider (1% nutrient broth, 1% mannitol, 0.2% K_2HPO_4); SLAD (synthetic low ammonium dextrose: 0.17% YNB w/o amino acids and w/o ammonium sulfate, 2% glucose, pH 4.2 and pH 7); M199 (without phenol red, pH 4 and pH 7, from Sigma-Aldrich Chemie GmbH); YNB + 2% Glucose; YNB + 2% Glucose + 10% fetal bovine serum (ZellBio GmbH); YNB + 2% N-acetylglucosamine (Sigma-Aldrich Chemie GmbH) or RPMI (Merck–Biochrom, liquid medium supplemented with water agar). Colony filamentation was investigated after incubation at 30°C or at 37°C in either atmospheric or 5% CO_2-enriched air after 5 days incubation using a binocular (Stemi 305, Carl Zeiss AG). Radial filamentation was scored from 0 (yeast) to 4 (elongated hyphae). Filamentation assays in liquid media were performed in Spider, M199 (pH 4 and pH 7) and SLAD (pH 4.5 and pH 7) media. The composition of the liquid media was equivalent to the solid media, except the agar and the addition of 50 μM ammonium sulfate to the SLAD media. *Candida* cells from YPD overnight cultures were washed, transferred into 500 μl induction media (OD_{600} nm of 0.1) and incubated for 90 min at 37 °C under constant shaking (180 rpm). The morphology was investigated microscopically scored from 0 (yeasts only) to 4 (true hyphae only).

Adherence Assay

Assays for *C. albicans* adherence and biofilm formation were adapted from established protocols [summarized in Gulati et al. (2018)]. Briefly, *C. albicans* cells were pre-grown in YPD overnight and PBS washed cells were set to $OD_{600\ nm}$ of 0.5 in 1 ml RPMI medium in 24 well plates (Costar®, Corning®). For microscopic analyses, cells were set to a lower density ($OD_{600\ nm}$ of 0.05) and seeded in microscopy-optimized 24 well plates (μ-Plate 24 Well Black, IBIDI). Cells were allowed to adhere for 90 min at 37 °C under constant shaking (100 rpm). Non-adherent cell were washed three times with cold PBS and the density of the remaining cells was measured by extinction at $OD_{600\ nm}$. Cell morphology was assessed microscopically.

Biofilm Assay

The first steps of biofilm assay are identical to the adherence protocol starting with $OD_{600\ nm}$ of 0.5 cultures, with the cell staining steps omitted. Following cell adherence, 1 ml of pre-warmed RPMI medium (or the indicated medium) was added and biofilms were formed for 24 h at 37°C and 100 rpm. Next, supernatants were discarded, and biofilms were washed once with PBS. Biofilms were quantified for cell density ($OD_{600\ nm}$) and metabolic activity with the help of resazurin reduction assays. For this, biofilms were resuspended in 500 μl PBS plus 50 μl of resazurin (0.15 mg/mL) and incubated at 37°C for 1hr in the dark. Fluorescent intensity (excitation 530 nm and emission 590 nm) of the reduced product resorufin was measured in a TECAN plate reader.

Biofilm Assay Under Flow Condition

Biofilm formation under shear flow conditions was monitored using the Bioflux1000 device (Fluxion Biosciences, Inc.) following established protocols (Gulati et al., 2017). In short, *C. albicans* overnight cultures were washed and set to $OD_{600\ nm}$ of 0.5 in pre-warmed RPMI medium. Cells were seeded with 2 dyne/cm^2 (0.2 Pa) for 2–5 s from the outlet well into the channels of Bioflux1000 48 well plates, which were primed before with warm medium. The cells were allowed to adhere to the channels for 90 min without any flow (0 dyne/cm^2), followed by removal of non-adherent cells by flowing fresh, pre-warmed RPMI medium with 2 dyne/cm^2 for 5 s. Shear flow was set to 0.2 dyne/cm^2 for time series experiments over 24 h biofilm formation and images were captured every 20 min. Two channels were investigated in parallel having a 10 × magnification to allow a direct comparison between a mutant and a reference strain. Image capturing and stacks to movies was performed using the MetaMorph® software (Molecular Devices).

Three-Dimensional Analysis of the Biofilm Morphology and Vitality

The general biofilm protocol was adapted for high resolution imaging as follows: cells were seeded with $OD_{600\ nm}$ of 0.5 in 2 ml colorless RPMI in imaging dishes (μ-Dish 35 mm, high and uncoated, IBIDI) and adherent cells and maturing biofilms were stained for alive and dead cells using the Filmtracer kit (Filmtracer™ LIVE/DEAD™ Biofilm Viability Kit, Invitrogen™). Syto9 and propidium iodide were applied at a 1:2000 dilution. Z-stack were collected with confocal laser scanning microscopy (CLSM, LSM 780, Carl Zeiss AG) at

1.0 μm intervals and the images were compiled to generate three-dimensional renderings. All confocal parameters were used as standard settings for comparison to the wild type and mutant biofilms produced at different time points. CLSM z-stack processing was performed using the ZEISS ZEN black edition.

Gene Expression Analyses

Candida overnight cultures were set to $OD_{600\ nm}$ of 0.3 in 10 ml fresh YPD and were incubated at 37°C, 180 rpm until they reached $OD_{600\ nm}$ of 1. Logarithmic cultures were harvested and washed in RPMI prior to the transfer in 50 ml RPMI ($OD_{600\ nm}$ of 0.3) and incubation for 60 min (37°C, 180 rpm). Sampling from CAA medium was done similarly except the differences in culture volumes (50 ml YPD medium for logarithmic cultures and 30 ml of a CAA culture). Shock frozen cell pellets were used for RNA isolation by a phenol-chloroform method previously described by Martin et al. (2011). A BioAnalyzer instrument (Agilent) was used to measure RNA quality and RNA concentration was determined via NanoDrop (Thermo Fisher Scientific). Finally, a total amount of 100 ng RNA was used for each qRT-PCR reaction that included SYBRGreen® as fluorescent dye (Brilliant II SYBR Green qPCR Master Mix, Agilent). The experiments were performed in a thermal cycler (Stratagene MxPro-mx3005P, Agilent) and run in biological and technical triplicates. The indicated expression rates are relative to the expression values of the housekeeping gene *ACT1* following the mathematical model from Pfaffl (2001). All primers are listed in **Supplementary Table S1**.

Protein Extraction and Western Blot Analysis

To visualize *STP2* processing, *stp2*Δ and *STP2-TAP* were incubated overnight in YPD at 37°C, washed twice with sterile H_2O, and then set to $OD_{600\ nm}$ of 0.3 in 10 ml of SD, CAA or RPMI medium. The samples for RPMI were collected after 90 min, and for SD and CAA after 240 min. The cell pellets were immediately frozen in liquid nitrogen. For extraction of total protein the cell pellets were dissolved in 500 μl of protein extraction buffer (50 mM Tris-HCl, 150 mM NaCl, 0.1% Triton X-100, 1mM DTT, 10% Glycerol) with proteinase inhibitor (Halt Proteinase Inhibitor, 100 μl per 10 ml buffer, Life Technologies) and an equivalent amount of ice-cold glass beads. The cells were then disrupted via vortexing for 10 × 1 min with 1 min recovery breaks on ice in between. Subsequently, the supernatant was transferred into a fresh tube after 10 min centrifugation and the protein concentration measured via BCA assay (Thermo Fischer). A total amount of 7 mg protein was then loaded onto a SDS-gel (Novex™ 10% Tris-Glycine Mini Gels, Thermo Fischer) and run for 1 h with 100 V. The proteins were then transferred onto a PVDF membrane via western blot for 1 h with 100 V, the membrane blocked in 5% milk and cut. Tdh3 was detected as a loading control using the Tdh3-antibody GT239 (also Anti-GAPDH, GeneTex) with Donkey Anti-Mouse DyLight549 (Jackson Immuno Research) as the secondary antibody. *STP2-TAP* was detected with the *TAP* tag polyclonal Antibody CAB1001 (Invitrogen) and Goat Anti-Rabbit HRP (Invitrogen) as the secondary antibody.

Automated Image Analyses

Automated Determination of Hyphal Length in RPMI Medium

Multichannel z-stacks of differentially stained *Candida* cells were first pre-processed with the software Fiji v1.51n (Schindelin et al., 2012). For both channels, stained either with rhodamine (cell bodies) or calcofluor white (cell bodies and hyphae), edge detection was applied and the variance of pixel intensity values of each slice in the z-stack was measured to find the slice with best focus, which is expected to have the highest variance. The rhodamine channel was shifted in x-direction by 1 pixel and in y-direction by two pixels to compensate for an offset between the two channels and resulting black image borders were removed by image cropping. The *Despeckle* function was applied to reduce noise and background subtraction with a rolling ball radius of 250 pixels was performed to homogenize illumination. The rhodamine channel was then exported for segmentation of yeast cell bodies.

Yeast cell detection and splitting of cell clumps was implemented in Python v3.7 using the computer vision library OpenCV (Bradski and Kaehler, 2000). Pixel values of pre-processed rhodamine images were first scaled to a range from 0 to 255. Adaptive thresholding with a Gaussian window and block size of 21 pixels was performed to binarize images. Foreground objects with an area less than 30 pixels were removed to omit small objects that are not expected to be yeast cells. Cell regions missed by adaptive thresholding were filled by applying a global threshold set at 1.3 times the threshold value obtained by Otsu's method and adding the result to the previous segmentation result. Objects with solidity less than 0.6 were removed and holes of remaining objects were filled. Hyphal structures were then removed by morphological opening with a circle of 7 pixels diameter. Splitting of cell clumps was performed as described by Brandes et al. (2017) with parameters set to $n = 5$, $m = 3$, $min_{dst} = 3$, $min_{area} = 60$, $l_{min} = n$, $w_{min} = m$, $l_{max} = 5n$, $w_{max} = 5n$, and $shift = 3$. In brief, contours of foreground objects containing at least min_{area} pixels were scanned in intervals of *shift* pixels for concavity points using chords of length n. Only concavities with a depth of at least min_{dst} pixels were taken into account. A dynamic window with minimum length l_{min} and width w_{min} and maximum length l_{max} and width w_{max} was used to find split lines between identified concavity points. Resulting split lines were then refined in a post-processing step and small objects with an area less than 5 pixels, created during cell clump splitting, as well as objects larger than 2000 pixels were removed. Additionally, only objects with a mean intensity value of at least 20 were kept to remove remaining artifacts with intensities lower than yeast cells. The final binary objects were used as a mask for hyphal length quantification.

Hyphal lengths were measured in Fiji. First, the calcofluor white channel was smoothed by convolution with the edge-preserving Kuwahara filter with a sampling window width of 3 pixels. A global threshold value was obtained by multiplying the value of Li's autothreshold with factor 1.5 and used to binarize the image. Small artifacts were removed by applying the *Remove Outliers* function with *radius* = 2 and *threshold* = 50. All remaining foreground objects were detected using the *Analyze Particles* function excluding objects that touch the image border and images with more than 500 objects were skipped to avoid length measurement inaccuracies due to crossing hyphae. For the remaining images, the number of yeast cells present in each foreground object was counted based on the yeast cell mask image and only objects containing one cell were taken into account to avoid crossing hyphae in cell clumps. The mask image was dilated two times and subtracted from the skeletonized objects image to obtain an image containing only hyphae with one pixel thickness. The function *Analyze Skeleton (2D/3D)* was then used to find the largest branch for each skeleton, omitting smaller artifacts that are unwanted concomitants of object skeletonization. All remaining skeletons with a length smaller than 2 μm were removed to exclude remaining artifacts that are probably no hyphae. The average hyphal length and distribution of hyphae per cell were exported for each image stack.

Images Analyses to Determine Biofilm Growth Under Flow Condition

Computations regarding image pre-processing, image analysis and modeling were performed using the programming language python Python v3.6.9. Source material provided as AVI files was converted into single TIFF images as well as data frames containing meta data annotations. The individual image contains two growth chambers (wild type and mutant) separated by four edge lines. Images were rotated automatically to vertical alignment in order to carry out an automated chamber detection and analysis. The mean pixel intensity (i.e., gray scale value; reflecting cell density) of the individual chamber was calculated and added into the respective data frame. An ODE model reflecting logistic growth as well as a lag phase was fitted to the individual experiments. Fitting was carried out by minimizing a cost function (unweighted least-squares-based) using the *Nelder-Mead*-algorithm (Nelder and Mead, 1965). Growth rate time series generated from the fitted model were used to compare wild type and mutant regarding the maximum observed growth rates as at their respective time points.

Detailed protocols regarding the above analyses can be found under: (Weise et al., 2020)

Quantification of Proportion of Dead Cells of Filmtracer-Stained Biofilms

The original 4D (X,Y,Z, color) confocal images were saved and provided for analysis in the native CZI (Carl Zeiss Image) format. The LIVE/DEAD staining technique provided two color channels for each z-stack: one for red (PI staining of dead cells) and one for green (Syto9 staining of live cells) labeling. The death ratio analysis was carried out on by a custom-written Fiji macro, using ImageJ version 1.52 s (Schindelin et al., 2012; Rueden et al., 2017). The preprocessing and analysis parameters were adjustable via an easy-to-use graphical user interface (GUI), also written in the Fiji macro language. The workflow of the death ratio calculation was as follows:

(i) Each channel was assigned its color (red or green) via the GUI;
(ii) Optionally the top and bottom of the z-stack was trimmed to avoid having very low signal to noise ratio (SNR) images to interfere with the reliability of the results. The number of Z layers to be cut off from the top or the bottom was controlled via the GUI;
(iii) The channels were lightly smoothed by a Gaussian filter, using a 2-pixel wide window;
(iv) Outliers were removed from the smoothed images on a per-channel basis, the size limit was adjusted via the GUI. This step served the purpose of removing salt-and-pepper type noise from the images, to further increase SNR. The size limit was adjustable for each channel independently, but in practice the same values (two pixels) were used in the entire analysis.
(v) The red and green channels were thresholded using the Otsu algorithm (Otsu, 1979) as provided by Fiji.
(vi) The foreground pixels were counted for both the red and green channels and the ratio of red/(red + green) was calculated to characterize the share of dead cells in the entire cell population.

All calculations in steps (i) to (vi) were carried out on a per-layer basis in the z-stacks for both channels. The results of the ratio calculations were saved in text files using the CSV format and provided for further analysis. Images from biological triplicates were analyzed and the median values were used to calculate the ratio of dead cell over a z-stack.

DATA AVAILABILITY STATEMENT

All datasets generated for this study are included in the article/**Supplementary Material**.

AUTHOR CONTRIBUTIONS

BB, EG, and PB designed and performed the wet lab experiments and analyzed the data. BH, TW, ZC, and SD analyzed the image data and derived the models. BB, BH, TW, and EG designed the figures. MF, DD and SV discussed the results and supervised the project. BB, and SV wrote the manuscript in consultation with BH, EG, PB, TW, SD, DD, and MF.

FUNDING

This work was supported by the German Ministry for Education and Science in the program Unternehmen Region (BMBF

03Z2JN11) and by the Deutsche Forschungsgemeinschaft [TRR 124 FungiNet, project C2 (to SV) and project B4 (to MF)], SFB 1278 PolyTarget 316213987 - project Z01 (to MF).

ACKNOWLEDGMENTS

We are grateful to D. Rosenberger for the provided technical assistance. We are further thankful to Amelia Barber for critical proof-reading and all the members of the SV lab for the insightful discussions.

SUPPLEMENTARY MATERIAL

The Supplementary Material for this article can be found online at: https://www.frontiersin.org/articles/10.3389/fmicb.2020.00794/full#supplementary-material

REFERENCES

Azadmanesh, J., Gowen, A. M., Creger, P. E., Schafer, N. D., and Blankenship, J. R. (2017). Filamentation involves two overlapping, but distinct, programs of filamentation in the pathogenic fungus *Candida albicans*. *G3* 7, 3797–3808. doi: 10.1534/g3.117.300224

Bastidas, R. J., Heitman, J., and Cardenas, M. E. (2009). The protein kinase Tor1 regulates adhesin gene expression in *Candida albicans*. *PLoS Pathog.* 5:e1000294. doi: 10.1371/journal.ppat.1000294

Bonhomme, J., Chauvel, M., Goyard, S., Roux, P., Rossignol, T., and d'Enfert, C. (2011). Contribution of the glycolytic flux and hypoxia adaptation to efficient biofilm formation by *Candida albicans*. *Mol. Microbiol.* 80, 995–1013. doi: 10.1111/j.1365-2958.2011.07626.x

Böttcher, B., Pöllath, C., Staib, P., Hube, B., and Brunke, S. (2016). *Candida* species rewired hyphae developmental programs for chlamydospore formation. *Front. Microbiol.* 7:1697. doi: 10.3389/fmicb.2016.01697

Bradski, G., and Kaehler, A. (2000). OpenCV. *Dobbs J. Softw. Tools* 120, 122–125.

Brandes, S., Dietrich, S., Hünniger, K., Kurzai, O., and Figge, M. T. (2017). Migration and interaction tracking for quantitative analysis of phagocyte–pathogen confrontation assays. *Med. Image Anal.* 36, 172–183. doi: 10.1016/j.media.2016.11.007

Brega, E., Zufferey, R., and Mamoun, C. B. (2004). *Candida albicans* Csy1p is a nutrient sensor important for activation of amino acid uptake and hyphal morphogenesis. *Eukaryot. Cell* 3, 135–143. doi: 10.1128/EC.3.1.135-143.2004

Chen, H., Calderone, R., Sun, N., Wang, Y., and Li, D. (2012). Caloric restriction restores the chronological life span of the goa1 null mutant of *Candida albicans* in spite of high cell levels of ROS. *Fungal Genet. Biol.* 49, 1023–1032. doi: 10.1016/j.fgb.2012.09.007

Cleary, I. A., Lazzell, A. L., Monteagudo, C., Thomas, D. P., and Saville, S. P. (2012). BRG1 and NRG1 form a novel feedback circuit regulating *Candida albicans* hypha formation and virulence. *Mol. Microbiol.* 85, 557–573. doi: 10.1111/j.1365-2958.2012.08127.x

Cornely, O., Bassetti, M., Calandra, T., Garbino, J., Kullberg, B., Lortholary, O., et al. (2012). ESCMID* guideline for the diagnosis and management of *Candida* diseases 2012: non-neutropenic adult patients. *Clin. Microbiol. Infect* 18, 19–37. doi: 10.1111/1469-0691.12039

Dabrowa, N., Taxer, S. S., and Howard, D. H. (1976). Germination of *Candida albicans* induced by proline. *Infect. Immun.* 13, 830–835. doi: 10.1128/iai.13.3.830-835.1976

Deprez, M.-A., Eskes, E., Winderickx, J., and Wilms, T. (2018). The TORC1-Sch9 pathway as a crucial mediator of chronological lifespan in the yeast *Saccharomyces cerevisiae*. *FEMS Yeast Res.* 18:foy048. doi: 10.1093/femsyr/foy048

Finkel, J. S., Xu, W., Huang, D., Hill, E. M., Desai, J. V., Woolford, C. A., et al. (2012). Portrait of *Candida albicans* adherence regulators. *PLoS Pathog.* 8:e1002525. doi: 10.1371/journal.ppat.1002525

Flanagan, P. R., Liu, N.-N., Fitzpatrick, D. J., Hokamp, K., Köhler, J. R., and Moran, G. P. (2017). The *Candida albicans* TOR-activating GTPases Gtr1 and Rhb1 coregulate starvation responses and biofilm formation. *mSphere* 2:e00477-17.

Fonzi, W. A., and Irwin, M. Y. (1993). Isogenic strain construction and gene mapping in *Candida albicans*. *Genetics* 134, 717–728.

Fox, E. P., Bui, C. K., Nett, J. E., Hartooni, N., Mui, M. C., Andes, D. R., et al. (2015). An expanded regulatory network temporally controls *Candida albicans* biofilm formation. *Mol. Microbiol.* 96, 1226–1239. doi: 10.1111/mmi.13002

Garbe, E., and Vylkova, S. (2019). Role of amino acid metabolism in the virulence of human pathogenic fungi. *Curr. Clin. Microbiol. Rep.* 6, 108–119. doi: 10.1007/s40588-019-00124-5

García-Sánchez, S., Aubert, S., Iraqui, I., Janbon, G., Ghigo, J.-M., and d'Enfert, C. (2004). *Candida albicans* biofilms: a developmental state associated with specific and stable gene expression patterns. *Eukaryot. Cell* 3, 536–545. doi: 10.1128/ec.3.2.536-545.2004

Grubb, S. E. W., Murdoch, C., Sudbery, P. E., Saville, S. P., Lopez-Ribot, J. L., and Thornhill, M. H. (2009). Adhesion of *Candida albicans* to endothelial cells under physiological conditions of flow. *Infect. Immun.* 77, 3872–3878. doi: 10.1128/IAI.00518-09

Gulati, M., Ennis, C. L., Rodriguez, D. L., and Nobile, C. J. (2017). Visualization of biofilm formation in *Candida albicans* using an automated microfluidic device. *JoVE J.o Vis. Exp.* 130:e56743. doi: 10.3791/56743

Gulati, M., Lohse, M. B., Ennis, C. L., Gonzalez, R. E., Perry, A. M., Bapat, P., et al. (2018). *In vitro* culturing and screening of *Candida albicans* biofilms. *Curr. Protoc. Microbiol.* 50:e60. doi: 10.1002/cpmc.60

Hünniger, K., Lehnert, T., Bieber, K., Martin, R., Figge, M. T., and Kurzai, O. (2014). A virtual infection model quantifies innate effector mechanisms and *Candida albicans* immune escape in human blood. *PLoS Comput. Biol.* 10:e1003479. doi: 10.1371/journal.pcbi.1003479

Kojic, E. M., and Darouiche, R. O. (2004). *Candida* infections of medical devices. *Clin. Microbiol. Rev.* 17, 255–267. doi: 10.1128/cmr.17.2.255-267.2004

Kraidlova, L., Van Zeebroeck, G., Van Dijck, P., and Sychrová, H. (2011). The *Candida albicans* GAP gene family encodes permeases involved in general and specific amino acid uptake and sensing. *Eukaryot. Cell* 10, 1219–1229. doi: 10.1128/EC.05026-11

Lattif, A., Chandra, J., Chang, J., Liu, S., Zhou, G. R., Chance, M., et al. (2008). Proteomics and pathway mapping analyses reveal phase-dependent over-expression of proteins associated with carbohydrate metabolic pathways in *Candida albicans* biofilms. *Open Proteomics J.* 1, 5–26. doi: 10.2174/1875039700801010005

Lee, K., Buckley, H. R., and Campbell, C. C. (1975). An amino acid liquid synthetic medium for the development of mycellal and yeast forms of *Candida albicans*. *Sabouraudia J. Med. Vet. Mycol.* 13, 148–153. doi: 10.1080/00362177585190271

Lee, Y.-T., Fang, Y.-Y., Sun, Y. W., Hsu, H.-C., Weng, S.-M., Tseng, T.-L., et al. (2018). THR1 mediates GCN4 and CDC4 to link morphogenesis with nutrient sensing and the stress response in *Candida albicans*. *Int. J. Mol. Med.* 42, 3193–3208. doi: 10.3892/ijmm.2018.3930

Legrand, M., Bachellier-Bassi, S., Lee, K. K., Chaudhari, Y., Tournu, H., Arbogast, L., et al. (2018). Generating genomic platforms to study *Candida albicans* pathogenesis. *Nucleic Acids Res.* 46, 6935–6949. doi: 10.1093/nar/gky594

Lin, S.-J., and Austriaco, N. (2014). Aging and cell death in the other yeasts, Schizosaccharomyces pombe and *Candida albicans*. *FEMS Yeast Res.* 14, 119–135. doi: 10.1111/1567-1364.12113

Ljungdahl, P. O. (2009). Amino-acid-induced signalling via the SPS-sensing pathway in yeast. *Biochem. Soc. Trans.* 37, 242–247. doi: 10.1042/bst0370242

Longo, V. D. (2003). The Ras and Sch9 pathways regulate stress resistance and longevity. *Exp. Gerontol.* 38, 807–811. doi: 10.1016/S0531-5565(03)00113-X

Martin, R., Moran, G. P., Jacobsen, I. D., Heyken, A., Domey, J., Sullivan, D. J., et al. (2011). The *Candida albicans*-specific gene EED1 encodes a key regulator of hyphal extension. *PLoS One* 6:e18394. doi: 10.1371/journal.pone.0018394

Martínez, P., and Ljungdahl, P. O. (2005). Divergence of Stp1 and Stp2 transcription factors in *Candida albicans* places virulence factors required for

proper nutrient acquisition under amino acid control. *Mol. Cell. Biol.* 25, 9435–9446. doi: 10.1128/MCB.25.21.9435-9446.2005

Miramón, P., and Lorenz, M. C. (2016). The SPS amino acid sensor mediates nutrient acquisition and immune evasion in *Candida albicans*. *Cell Microbiol.* 18, 1611–1624. doi: 10.1111/cmi.12600

Mittal, N., Guimaraes, J. C., Gross, T., Schmidt, A., Vina-Vilaseca, A., Nedialkova, D. D., et al. (2017). The Gcn4 transcription factor reduces protein synthesis capacity and extends yeast lifespan. *Nat. Commun.* 8:457. doi: 10.1038/s41467-017-00539-y

Mukai, Y., Kamei, Y., Liu, X., Jiang, S., Sugimoto, Y., Mat Nanyan, N. S. B., et al. (2019). Proline metabolism regulates replicative lifespan in the yeast Saccharomyces cerevisiae. *Microb. Cell* 6, 482–490. doi: 10.15698/mic2019.10.694

Mukherjee, P. K., Chand, D. V., Chandra, J., Anderson, J. M., and Ghannoum, M. A. (2009). Shear stress modulates the thickness and architecture of *Candida albicans* biofilms in a phase-dependent manner. *Mycoses* 52, 440–446. doi: 10.1111/j.1439-0507.2008.01632.x

Nelder, J. A., and Mead, R. (1965). A simplex method for function minimization. *Comput. J.* 7, 308–313. doi: 10.1093/comjnl/7.4.308

Nobile, C. J., Fox, E. P., Nett, J. E., Sorrells, T. R., Mitrovich, Q. M., Hernday, A. D., et al. (2012). A recently evolved transcriptional network controls biofilm development in *Candida albicans*. *Cell* 148, 126–138. doi: 10.1016/j.cell.2011.10.048

Nobile, C. J., and Johnson, A. D. (2015). *Candida albicans* biofilms and human disease. *Annu. Rev. Microbiol.* 69, 71–92. doi: 10.1146/annurev-micro-091014-104330

Nobile, C. J., Schneider, H. A., Nett, J. E., Sheppard, D. C., Filler, S. G., Andes, D. R., et al. (2008). Complementary adhesin function in *C. albicans* biofilm formation. *Curr. Biol.* 18, 1017–1024. doi: 10.1016/j.cub.2008.06.034

Otsu, N. (1979). A threshold selection method from gray-level histograms. *IEEE Trans. Syst. Man Cybernet.* 9, 62–66. doi: 10.1109/tsmc.1979.4310076

Pfaffl, M. W. (2001). A new mathematical model for relative quantification in real-time RT–PCR. *Nucleic Acids Res.* 29:e45. doi: 10.1093/nar/29.9.e45

Rajendran, R., May, A., Sherry, L., Kean, R., Williams, C., Jones, B. L., et al. (2016). Integrating *Candida albicans* metabolism with biofilm heterogeneity by transcriptome mapping. *Sci. Rep.* 6, 35436–35436. doi: 10.1038/srep35436

Richard, M. L., Nobile, C. J., Bruno, V. M., and Mitchell, A. P. (2005). *Candida albicans* biofilm-defective mutants. *Eukaryot. Cell* 4, 1493–1502. doi: 10.1128/EC.4.8.1493-1502.2005

Rueden, C. T., Schindelin, J., Hiner, M. C., DeZonia, B. E., Walter, A. E., Arena, E. T., et al. (2017). ImageJ2: imageJ for the next generation of scientific image data. *BMC Bioinformatics* 18:529. doi: 10.1186/s12859-017-1934-z

Sabina, J., and Brown, V. (2009). Glucose sensing network in *Candida albicans*: a sweet spot for fungal morphogenesis. *Eukaryot. Cell* 8, 1314–1320. doi: 10.1128/ec.00138-09

Santana, I. L., Gonçalves, L. M., Vasconcellos, A. A. D., Cury, J. A., and Cury, A. A. D. B. (2013). Dietary carbohydrates modulate *Candida albicans* biofilm development on the denture surface. *PLoS One* 8:e64645. doi: 10.1371/journal.pone.0064645

Schindelin, J., Arganda-Carreras, I., Frise, E., Kaynig, V., Longair, M., Pietzsch, T., et al. (2012). Fiji: an open-source platform for biological-image analysis. *Nat. Methods* 9, 676–682. doi: 10.1038/nmeth.2019

Shin, C.-S., Kim, S. Y., and Huh, W.-K. (2009). TORC1 controls degradation of the transcription factor Stp1, a key effector of the SPS amino-acid-sensing pathway in *Saccharomyces cerevisiae*. *J. Cell Sci.* 122, 2089–2099. doi: 10.1242/jcs.047191

Silao, F. G. S., Ward, M., Ryman, K., Wallström, A., Brindefalk, B., Udekwu, K., et al. (2019). Mitochondrial proline catabolism activates Ras1/cAMP/PKA-induced filamentation in *Candida albicans*. *PLoS Genet.* 15:e1007976. doi: 10.1371/journal.pgen.1007976

Steffen, K. K., MacKay, V. L., Kerr, E. O., Tsuchiya, M., Hu, D., Fox, L. A., et al. (2008). Yeast life span extension by depletion of 60s ribosomal subunits is mediated by Gcn4. *Cell* 133, 292–302. doi: 10.1016/j.cell.2008.02.037

Tatebe, H., and Shiozaki, K. (2017). Evolutionary conservation of the components in the TOR signaling pathways. *Biomolecules* 7:77. doi: 10.3390/biom7040077

Tournu, H., Tripathi, G., Bertram, G., Macaskill, S., Mavor, A., Walker, L., et al. (2005). Global role of the protein kinase Gcn2 in the human pathogen *Candida albicans*. *Eukaryot. Cell* 4, 1687–1696. doi: 10.1128/EC.4.10.1687-1696.2005

Tsang, F., James, C., Kato, M., Myers, V., Ilyas, I., Tsang, M., et al. (2015). Reduced Ssy1-Ptr3-Ssy5 (SPS) signaling extends replicative life span by enhancing NAD+ homeostasis in *Saccharomyces cerevisiae*. *J. Biol. Chem.* 290, 12753–12764. doi: 10.1074/jbc.M115.644534

Tumusiime, S., Zhang, C., Overstreet, M. S., and Liu, Z. (2011). Differential regulation of transcription factors Stp1 and Stp2 in the Ssy1-Ptr3-Ssy5 amino acid sensing pathway. *J. Biol. Chem.* 286, 4620–4631. doi: 10.1074/jbc.M110.195313

Uppuluri, P., Acosta Zaldívar, M., Anderson, M. Z., Dunn, M. J., Berman, J., Lopez Ribot, J. L., et al. (2018). *Candida albicans* dispersed cells are developmentally distinct from biofilm and planktonic cells. *mBio* 9:e01338-18. doi: 10.1128/mBio.01338-18

Uppuluri, P., Chaturvedi, A. K., and Lopez-Ribot, J. L. (2009). Design of a simple model of *Candida albicans* biofilms formed under conditions of flow: development, architecture, and drug resistance. *Mycopathologia* 168, 101–109. doi: 10.1007/s11046-009-9205-9

Vylkova, S., and Lorenz, M. C. (2014). Modulation of Phagosomal pH by *Candida albicans* promotes hyphal morphogenesis and requires Stp2p, a regulator of amino acid transport. *PLoS Pathog.* 10:e1003995. doi: 10.1371/journal.ppat.1003995

Wächtler, B., Wilson, D., Haedicke, K., Dalle, F., and Hube, B. (2011). From attachment to damage: defined genes of *Candida albicans* mediate adhesion, invasion and damage during interaction with oral epithelial cells. *PLoS One* 6:e17046. doi: 10.1371/journal.pone.0017046

Walther, A., and Wendland, J. (2003). An improved transformation protocol for the human fungal pathogen *Candida albicans*. *Curr. Genet.* 42, 339–343. doi: 10.1007/s00294-002-0349-0

Weise, T., Böttcher, B., and Vylkova, S. (2020). Bioflux Analyses. doi: 10.17504/protocols.io.bb7qirmw

Zhao, X., Daniels, K. J., Oh, S.-H., Green, C. B., Yeater, K. M., Soll, D. R., et al. (2006). *Candida albicans* Als3p is required for wild-type biofilm formation on silicone elastomer surfaces. *Microbiology* 152(Pt 8), 2287–2299. doi: 10.1099/mic.0.28959-0

Zhao, X., Oh, S.-H., Cheng, G., Green, C. B., Nuessen, J. A., Yeater, K., et al. (2004). ALS3 and ALS8 represent a single locus that encodes a *Candida albicans* adhesin; functional comparisons between Als3p and Als1p. *Microbiology* 150, 2415–2428. doi: 10.1099/mic.0.26943-0

Zhu, Z., Wang, H., Shang, Q., Jiang, Y., Cao, Y., and Chai, Y. (2013). Time course analysis of *Candida albicans* metabolites during biofilm development. *J. Proteome Res.* 12, 2375–2385. doi: 10.1021/pr300447k

Conflict of Interest: TW and DD were employed by BioControl Jena.

The remaining authors declare that the research was conducted in the absence of any commercial or financial relationships that could be construed as a potential conflict of interest.

frontiers in Microbiology

ORIGINAL RESEARCH
published: 08 May 2020
doi: 10.3389/fmicb.2020.00864

Palmitic Acid Inhibits the Virulence Factors of *Candida tropicalis*: Biofilms, Cell Surface Hydrophobicity, Ergosterol Biosynthesis, and Enzymatic Activity

*Krishnan Ganesh Prasath, Hariharan Tharani, Mourya Suraj Kumar and Shunmugiah Karutha Pandian**

Department of Biotechnology, Alagappa University, Karaikudi, India

Biofilm is the fortitude of *Candida* species infections which eventually causes candidiasis in human. *C. tropicalis* is one of the predominant *Candida* species commonly found in systemic infections, next to *C. albicans*. In *Candida* species, biofilm maturity initiates irreversible surface attachment of cells and barricades the penetration of conventional antifungals. Hence, the current study investigated the antifungal and antivirulence potency of palmitic acid (PA) against *C. tropicalis* mature biofilm and its associated virulence factors. *In vitro* results revealed an effective inhibition of biofilm in PA-treated *C. tropicalis*, compared to *C. albicans* and *C. glabrata*. Also, PA reduced *C. tropicalis* mature biofilm at various time points. Further, PA treatment triggered apoptosis in *C. tropicalis* through ROS mediated mitochondrial dysfunction as demonstrated by confocal microscopic observation of PI, DAPI and DCFDA staining. PA regulated other virulence factors such as cell surface hydrophobicity, ergosterol biosynthesis, protease and lipase after 48 h of treatment. Downregulation of *ERG11* (Lanosterol 14-alpha demethylase) was contributed to the reduction of ergosterol in PA-treated *C. tropicalis*. However, enhanced hyphal growth was observed in PA-treated *C. tropicalis* through upregulation *HWP1* (Hyphal wall protein) and *EFG1* (Enhanced filamentous growth). This study highlighted the antibiofilm and antivirulence potency of PA against *C. tropicalis*. Hence, PA could be applied synergistically with other antifungal agents to increase the efficacy for regulating NCAC infections.

Keywords: *Candida tropicalis*, mature biofilm, palmitic acid, ROS, virulence factors

OPEN ACCESS

Edited by:
Juliana Campos Junqueira, São Paulo State University, Brazil

Reviewed by:
Rodnei Dennis Rossoni, São Paulo State University, Brazil
Melyssa Negri, State University of Maringá, Brazil

****Correspondence:***
Shunmugiah Karutha Pandian
sk_pandian@rediffmail.com

Specialty section:
This article was submitted to Infectious Diseases, a section of the journal Frontiers in Microbiology

Received: *04 February 2020*
Accepted: *14 April 2020*
Published: *08 May 2020*

Citation:
Prasath KG, Tharani H, Kumar MS and Pandian SK (2020) Palmitic Acid Inhibits the Virulence Factors of Candida tropicalis: Biofilms, Cell Surface Hydrophobicity, Ergosterol Biosynthesis, and Enzymatic Activity. Front. Microbiol. 11:864. doi: 10.3389/fmicb.2020.00864

INTRODUCTION

Clinically, non-C. albicans Candida (NCAC) species are increasingly reported as both colonizers and pathogenic in bloodstream infections. A multicenter study on candidemia epidemiology reported that the prevalence of *C. albicans* infection is higher in European nations (Poikonen et al., 2010; Asmundsdottir et al., 2012; Hesstvedt et al., 2015) but in case of United States (Cleveland et al., 2012), countries in Latin America (Nucci et al., 2013) and India (Chakrabarti et al., 2015), the occurrence of NCAC infections are higher than *C. albicans* infections. Among NCACs, *C. tropicalis*

is the most commonly distributed compared to other species such as *C. glabrata*, *C. parapsilosis*, *C. krusei,* and *C. kefyr* (Kumari et al., 2014; Pahwa et al., 2014). A study at Indian rural tertiary hospital reported that the occurrence of *C. tropicalis* is phenomenal in urine, blood and oral scrapings from candidemia patients compared to *C. albicans* (Kaur et al., 2016). Also, *C. tropicalis* infection is found in surgical related infection such as osteomyelitis (Miller and Mejicano, 2001).

In our previous study, myristic acid from Nutmeg extract was shown to inhibit biofilm and hyphal formation by *C. albicans* by regulating proteins involved in sterol, sphingolipid and Multi-drug resistance pathways (Prasath et al., 2019). In addition, hexadecanoic acid was identified as a second major component through GC-MS analysis of nutmeg extract (Prasath et al., 2019). Hexadecanoic acid or Palmitic acid (PA), a saturated fatty acid is richly abundant in oil palms, meat, dairy products and many plants. PA possesses antimicrobial activity against numerous pathogens such as *Streptococcus mutants, Streptococcus gordonii, Streptococcus sanguis, C. albicans, Aggregatibacter actinomycetemcomitans* (Huang et al., 2011) but fails in *Propionibacterium acnes* (Yang et al., 2009).

Palmitic acid is one of the major components in cellular fatty acids of *Candida* species such as *C. parapsilosis, C. albicans, C. tropicalis*, and *C. famata* (Missoni et al., 2005). Also, PA is a product of Fatty acid Synthase (FAS) complex and is crucial for subsequent desaturation of fatty acid in *C. albicans* (Nguyen et al., 2009). PA at 2.5 mg mL^{-1} increases the cellular toxicity in *C. parapsilosis* and the rate of cell death is even higher in *ole1* (gene responsible for fatty acid desaturation) mutants by inducing Reactive oxygen species (ROS) (Nguyen and Nosanchuk, 2011). ROS are the aerobic by-product in both prokaryotes and eukaryotes during mitochondrial electron transport and metal catalyzed oxidation. The building up of ROS causes severe damage in cellular DNA, RNA and protein levels (Ray et al., 2012). Also, generation of ROS plays a vital role in altering virulence processes of the cell and most of the antifungal drugs induce ROS in both planktonic and biofilm cells (Delattin et al., 2014).

Similar to *C. albicans*, *C. tropicalis* is a dimorphic pathogen expressing a wide range of virulence factors such as biofilm, yeast-hyphal transition, hydrolytic enzymes and sterol synthesis. The expression level of these virulence factors are predominant during log growth phase. Also, the log-phase yeast cell resists external toxicity such as glucotoxicity by lipid storage mechanisms (Nguyen and Nosanchuk, 2011). The biofilm strengthens on excessive production of extracellular polymeric substance during late- log phase and forms mature biofilm (Montanaro et al., 2011). In *Candida* spp., the mature biofilm forms a complex structure and releases more daughter cells that disseminates to different niches to develop into new biofilms (Cavalheiro and Teixeira, 2018). During dual-biofilm formation, *C. albicans* suppresses the filamentation of *C. tropicalis* but the latter overpowers in biofilm formation during its association with *C. albicans* (Pathirana et al., 2019). Some conventional antibiotics holds potent antibiofilm activity on early-biofilm formation but fails to inhibit mature biofilm (Reiter et al., 2012). The antibiofilm activity of triazole drugs are not consistent and especially, fluconazole does not influence on the thickness of *C. albicans* biofilm (Chandra and Ghannoum, 2018). In this backdrop, the present study unveils the anti-infective potential of PA on mature biofilm and its associated virulence factors of *C. tropicalis* at different concentrations and time points.

MATERIALS AND METHODS

Candida spp. Culture Conditions and Compound Concentration in This Study

1.2×10^5 CFU mL^{-1} of *C. tropicalis* (MTCC 186), *C. albicans* (ATCC 90028), and *C. glabrata* (MTCC 3019) were cultured in YEPD medium (1% yeast extract, 2% peptone, 2% dextrose, Himedia Laboratories, Mumbai, India) by incubating at 37°C for 12 h at 160 rpm. Biofilm and dimorphism were analyzed by culturing 1.5×10^7 CFU mL^{-1} of *Candida* spp. yeast cells in spider medium (1% mannitol, 0.25% K_2HPO_4, and 1% nutrient broth, Himedia Laboratories, Mumbai, India) and incubated for 48 h at 37°C. Palmitic acid (TCI chemicals, Japan) was dissolved in methanol as vehicle control with stock concentration of 10 mg mL^{-1}.

Determination of MIC of Palmitic Acid

The MIC of PA against *C. tropicalis* was determined using a macro broth dilution assay as per CLSI guidelines. Briefly, 3.2×10^7 cells of *C. tropicalis* were allowed to grow in YEPD medium containing PA in a range of concentrations such as 2, 1, 0.5, 0.25, 0.125, 0.0625, 0.03125, and 0 mg mL^{-1} with 10 μg mL^{-1} of amphotericin B as positive control. The cells were incubated at 37°C for 10 h with agitation of 160 rpm. After incubation, cells were centrifuged and washed thrice with 1× PBS. The antifungal activity of PA was evaluated by measuring the absorbance of the cells at 600 nm (CLSI, 2017). In addition, the overnight grown *C. tropicalis* cells in the absence and presence of PA were serially diluted in PBS. Then, 3.1×10^5 CFU mL^{-1} cells were spotted on YEPD agar medium followed by incubation at 37°C for 10 h. After incubation, the plates were documented in XR^+ Bio-Rad gel doc system, United States.

Effect of PA on *C. tropicalis* Biofilm Formation

The antibiofilm activity of PA was examined against the *C. tropicalis* at different concentrations such as 100, 200, 300, 400, 500, and 600 μg mL^{-1} in 24 well MTP. Briefly, 3.2×10^7 cells were allowed to form biofilm in 24 well MTP in spider medium without and with PA and the plate was incubated at 37°C for 48 h. The biofilm cells were stained by 0.1% crystal violet (Sigma Aldrich, United States) followed by destaining with 10% glacial acetic acid. The absorbance of the solution was measured at 570 nm using Spectra Max 3 (Molecular Devices, United States). The percentage of biofilm inhibition was calculated using the formula,% Biofilm Inhibition = [(Absorbance of Control-Absorbance of Treated)/(Absorbance of Control)] × 100. In addition, antibiofilm activity of PA was also evaluated on *C. albicans* and *C. glabrata* biofilm formation.

Determination of Biofilm Inhibitory Concentration of PA

In this experiment, PA at different concentrations (0, 25, 50, 75, 100, 125, 150, 175, 200, 225, and 250 μg mL^{-1}) were added in spider medium in 24 well MTP. To that, 3.2 × 107 CFU mL^{-1} of *C. tropicalis* cells were inoculated and incubated at 37°C for 48 h. After incubation, the plate was stained with 0.1% crystal violet followed by destaining the plate with 10% glacial acetic acid. The absorbance of the destained solution was measured at 570 nm. The percentage of biofilm inhibition was calculated using the formula as mentioned above. The concentration of PA at which maximum percentage inhibition of *C. tropicalis* biofilm occurs, would be the BIC of PA. For growth assessment, the cells were harvested by centrifugation followed by washing twice with 1× PBS. The effect of PA on the growth of *C. tropicalis* was examined by spectrometric measurement of cell growth at 600 nm.

Alamar Blue Assay

The effect of PA on the metabolism of *C. tropicalis* was determined by Resazurin, an oxidation-reduction indicator of cell viability. Briefly, Cells were allowed to grow in YEPD medium in the absence and presence of the PA at various concentrations as mentioned above in 96 well MTP for 12 h at 37°C. After incubation, 10 μg mL^{-1} of resazurin (Sigma Aldrich, United States) was added and incubated at 37°C for 4 h. The reduction of dye to pink color indicated the viability of cells and the reduction was measured in an excitation and emission wavelength of 560 nm and 590 nm, respectively (Selvaraj et al., 2019).

Growth Kinetics of *C. tropicalis*

The effect of PA on *C. tropicalis* growth was analyzed by growth kinetics at different time points. Briefly, 3.2 × 10^7 CFU mL^{-1} cells were used to inoculate in the presence and absence of PA at different concentrations such as 100, 200, 400, and 800 μg mL^{-1} at 37°C for 20 h. Also, 10 μg mL^{-1} of amphotericin B was used as a positive control. The absorbance of *C. tropicalis* in the absence and presence of PA was measured at 600 nm for every 2 h.

Efficacy of the Compound on *C. tropicalis* Mature Biofilm

For mature biofilm study, 1.8 × 10^5 CFU mL^{-1} *C. tropicalis* was used to inoculate in spider medium in 24 well MTP and incubated at various time points such as 1, 2, 4 and 7 days at 37°C. After the growth of *C. tropicalis* at the prescribed time points, the medium were removed and fresh spider medium along with PA (0, 100, 200, and 400 μg mL^{-1}) were added. The plates were incubated on different time points such as 12, 24, and 48 h. After incubation, the planktonic cells were removed and the plates were stained with 0.1% crystal violet stain. Then, the stain was removed and washed with d.H_2O. The plates were destained with 10% glacial acetic acid and the solution was quantified spectrophotometrically at 570 nm. The percentage biofilm inhibition of PA-treated cells was calculated by a formula as mentioned above.

Light Microscopic Analysis of *C. tropicalis* Mature Biofilm

The effect of the compound on biofilm and hyphae formed by *C. tropicalis* was also observed using light microscopic analysis. Briefly, *C. tropicalis* was allowed to form biofilm in 1 × 1 cm sterile glass slides in spider medium in 24-well MTP and incubated at 37°C for 7 days. After incubation, PA at different concentrations such as 0, 100, 200, and 400 μg mL^{-1} were added and incubated at 37°C for 24 and 48 h. After incubation, the slides were washed with d.H_2O to remove unbound cells and stained with crystal violet. *C. tropicalis* dimorphism and biofilm were visualized at 400× magnification by using binocular optical microscope and documented by Nikon Eclipse, Ti 100 digital camera.

Evaluation of 3-D Biofilm Architecture by Confocal Microscopic Analysis

The inoculation of *C. tropicalis* and the treatment of PA were followed as stated above in 1 × 1 cm sterile glass slides in spider medium in 24 well MTP. Then, the slides were washed and stained with 0.1% of acridine orange (Sigma Aldrich, United States). After that, the biofilm construction was visualized using confocal laser scanning microscopy (CLSM) (Zeiss LSM 710, Carl Zeiss, Gottingen, Germany) by using argon laser with an excitation and emission filter of 488 nm and 500–640 nm, respectively (Gowrishankar et al., 2016). The thickness and 3-dimension visualization of biofilm construction were observed by image acquisition software (Zen 2009, Carl Zeiss).

Colony Forming Unit Assay for Growth

The fungicidal effect of PA at different concentrations such as 0, 100, 200, and 400 μg mL^{-1} on *C. tropicalis* was examined in YEPD medium at 37°C for 24 and 48 h. After incubation, cells were washed thrice with 1× PBS. Then, the cells were subjected to serial dilutions followed by spreading on Sabouraud Dextrose Agar (SDA) and incubated at 37°C for 16 h. The colonies were counted in logarithmic scale and the plates were documented in Bio-Rad Gel Doc XR + System (United States).

Scanning Electron Microscopy Analysis of Colony Morphology

The impact of PA on morphology of *C. tropicalis* was visualized in scanning electron microscope (SEM). *C. tropicalis* was allowed to grow in 1 × 1 cm glass slides in the absence and presence of PA for 48 h as mentioned above. The slides were washed and fixed with 2.5% glutaraldehyde for 2 h. Then, the slides were dehydrated with increasing concentration gradient of absolute ethanol from 50 to 100%. The dehydrated slides were visualized in SEM (Quanta FEG 250, United States) with the magnification of 2500×, 5000×, and 10000× (Prasath et al., 2019).

Live and Dead Cell Analysis

The viability of *C. tropicalis* was also counter checked by live-dead cell analysis by using acridine orange (AO) and ethidium bromide (EtBr) stains. After treatment with PA at different concentrations (0, 100, 200, and 400 μg mL^{-1}) for 24 and 48 h,

the cells were stained with 1 mg mL^{-1} of AO and EtBr. The live and dead cells were visualized using CLSM with excitation and emission wavelength of 502 and 528 nm, respectively for AO and 470 and 600 nm for EtBr (Liu et al., 2015).

Quantification of Apoptosis

The programmed cell death was quantified by Propidium Iodide (PI- Sigma Aldrich, United States) staining solution which is permeable only in the dead cells. Briefly, the treated and untreated cells were collected at different time points such as 4 h, 8 h, 12 h, 24 h and 48 h. Then, the cells were washed with 1× PBS, stained with 50 μg mL^{-1} of PI solution and incubated in dark for 15 min. The apoptosis in untreated and treated cells was quantified by measuring the fluorescence intensity of PI with the excitation and emission wavelength of 535 and 617 nm, respectively (Crowley et al., 2016).

Evaluation of DNA Damage

The DNA damage in *C. tropicalis* upon PA treatment was evaluated by 4', 6-diamidino-2-phenylindole (DAPI - Sigma Aldrich, United States) staining. Briefly, *C. tropicalis* was treated in the absence and presence of PA at two different time points (24 and 48 h). After incubation, cells were harvested, stained with 2 μg mL^{-1} of DAPI and incubated in dark for 10 min. After the incubation, cells were washed with ice-cold PBS and the fluorescence intensity was visualized using CLSM with the excitation and emission wavelength of 358 and 461 nm, respectively (Rajavel et al., 2018).

Detection of Reactive Oxygen Species

The apoptosis mediated by cellular reactive oxygen species (ROS) was studied using 2',7'-dichlorodihydrofluorescein diacetate (DCFDA-Sigma Aldrich, United States) stain. ROS oxidize DCFDA to a fluorescence emitting DCF and the extent of fluorescence generated is directly proportional to the rate of ROS generated inside the cells. Briefly, untreated and PA-treated *C. tropicalis* cells at 24 and 48 h were stained with 15 μM DCFDA and incubated in dark for 1 h. After incubation, the cell suspension was centrifuged and excess staining solution was aspirated. Then, 500 μL of 1× PBS was added and the cell pellet was dispersed well in the solution. The difference in level ROS produced by untreated and treated cells at different time points were visualized in CLSM and quantified by florescence spectrophotometer with the excitation and emission wavelength of 488 and 530 nm, respectively (Shanmuganathan et al., 2019).

Assessment of Mitochondrial Damage

The ROS mediated mitochondrial damage was assessed by measuring mitochondrial membrane potential ($\Delta\Psi$ m) using Rhodamine 123 (Sigma Aldrich, United States) stain. Briefly, *C. tropicalis* cells were treated with PA at different concentrations (0, 100, 200, and 400 μg mL^{-1}) and time points (24 and 48 h). After the incubation time, cells were fixed in 4% paraformaldehyde and stained with 10 μg mL^{-1} of Rhodamine 123. After incubation, fluorescence intensity was observed using CLSM and the images were documented (Wang and Youle, 2009).

H_2O_2 Sensitivity Assay

Candida tropicalis cells grown for 24 and 48 h in the absence and presence of PA were adjusted to 0.3 of absorbance at 600 nm. Then, the cells were swabbed in YEPD agar plates and 10 mm filter paper discs (Himedia Laboratories, Mumbai, India) was mounted. Then the discs were loaded with 50 mM H_2O_2 and incubated at 37°C for 16 h. After incubation, the zone of clearance around the disc was measured and the plates were documented in Gel-doc system (Hassett et al., 1998).

Evaluation of Superoxide Dismutase and Catalase by Native PAGE

The intracellular proteins of untreated and PA-treated *C. tropicalis* for 24 and 48 h were extracted by sonication. The extracted crude protein was separated in 8 and 10% native PAGE for catalase and SOD analysis, respectively. The gels were subjected to pre-run using running buffer (187.5 mM Tris and 1 mM EDTA) at 50 V for 20 min to eliminate excessive ammonium per sulfate. Then, the proteins were resolved in 50 mM Tris, 300 mM glycine and 1.8 mM EDTA running buffer at 60 V and 20°C. For catalase, gel was washed with 50 mM Potassium Phosphate buffer (pH 7) and incubated in 4 mM H_2O_2 for 10 min. After incubation, gel was stained with 1% potassium ferricyanide and 1% ferric chloride. The appearance of clear bands in the gel against dark green background indicated the presence of catalase activity of *C. tropicalis* (Sethupathy et al., 2016). For SOD, gel was stained in the 50 mM KPi (pH 7.8) buffer solution containing 0.1 mM EDTA, 2 mg riboflavin and 16 mg nitro blue tetrazolium (NBT). The reaction was initiated by adding 400 μL of Tetramethylethylenediamine (TEMED) to reduce NBT and incubated in dark for 1 h. After incubation, the gel was suspended in 50 mM KPi (pH 7.8) buffer solution followed by exposing the gels in bright light. The appearance of achromatic bands indicated the SOD activity of *C. tropicalis* (Prasath et al., 2019).

Microbial Adhesion to Hydrocarbon Assay

The cell surface hydrophobicity (CSH) is the ability of cells that adhere to any hydrophobic substratum. The cells with greater hydrophobicity is directly correlated with the biofilm formation. CSH in *C. tropicalis* was determined through MATH assay as described by Sivasankar et al. (2015). Briefly, the treated and untreated cells were collected by centrifugation at 12000 rpm for 15 min. The cells were washed with 1× PBS thrice and the absorbance of cell suspension was measured at 600 nm. After that, 1 mL of toluene was added to the cell suspension and vortexed vigorously for 10 min. Then the solution was allowed to stand for phase separation. The organic phase was removed and the optical density (OD) of cell suspension in aqueous phase was measured spectrophotometrically at 600 nm. CSH was measured as hydrophobicity index using the following formula:

$$\text{Hydrophobicity index} = [1 - (OD_{600 \text{ fter vortexing}}/OD_{600 \text{ before vortexing}})] \times 100$$

Lipase Assay

The effect of PA on *C. tropicalis* lipase was evaluated by both qualitative and quantitative method. For qualitative analysis, 3.5×10^5 CFU mL^{-1} of untreated and treated *C. tropicalis* were spotted on the spider medium containing 0.1% of tributyrin as lipase substrate and incubated at 37°C for 5 days. After incubation, the zone of clearance around the cell growth indicates lipase activity of *C. tropicalis* (Muthamil et al., 2018). In addition, the lipase activity was measured quantitatively by mixing culture supernatant and 4-Nitro Phenyl palmitate (substrate) in the ratio 1:4. Then the solution was incubated in dark for 2 h and the absorbance of the solution was measured at 410 nm (Ramnath et al., 2017). The percentage of lipase inhibition was calculated using the following formula:

$$\%\text{of Lipase Inhibition} = [(\text{Control OD}_{410\ \text{nm}} - \text{TreatedOD}_{410\ \text{nm}})/(\text{ControlOD}_{410\ \text{nm}})] \times 100$$

Proteinase Assay

The extracellular proteinase produced by *C. tropicalis* was detected on Bovine Serum Albumin (BSA) agar medium containing dextrose – 2%, KH_2PO_4– 0.1%, $MgSO_4$ – 0.05%, agar 2% and BSA 1% (Himedia Laboratories, Mumbai, India). Briefly, 3.5×10^5 CFU mL^{-1} of untreated and PA-treated *C. tropicalis* was swabbed on BSA agar medium and incubated at 37°C for 7 days. The extracellular proteinase cleaves BSA and the zone of precipitation was observed around the *C. tropicalis* cells (Staib, 1965).

Ergosterol Biosynthesis Assay

The untreated and PA-treated *C. tropicalis* cells for 24 and 48 h were harvested by centrifugation at 8000 rpm for 10 min and the cells were washed with 2 mL of 1× PBS thrice. Two mL of 20% alcoholic KOH was added to the cell pellet followed by incubation at 85°C for 1 h. Then, 1 mL of n-Heptane was added to the cell suspension and vortexed vigorously. After phase separation, the organic layer was transferred to a fresh tube and incubated at −20°C overnight. Absolute ethanol was added to the organic layer in the ratio 5:1 and the ergosterol content was measured spectrophotometrically in the range of 200–300 nm (Arthington-Skaggs et al., 1999).

Filamentation Assay

The untreated and PA-treated *C. tropicalis* cells as mentioned above were adjusted to 0.3 of absorbance at 600 nm. Then, 3.5×10^5 CFU mL^{-1} was spotted in spider agar medium and incubated at 37°C for 5 days. After incubation, the growth of hyphae on untreated and PA-treated (100, 200, and 400 μg mL^{-1}) *C. tropicalis* was observed and the plates were documented in Bio-Rad Gel Doc XR + System (Liu et al., 1994).

RNA Isolation and cDNA Conversion

Based on the virulence assays, the anti-infective potential of PA on virulence factors of *C. tropicalis* was validated by quantitative PCR (qPCR). RNA was isolated from untreated and PA-treated at 200 μg mL^{-1} for 48 h *C. tropicalis* cells by hot phenol method (Schmitt et al., 1990). The resulted RNA was observed by agarose gel electrophoresis and quantified by Nano spectrophotometer (Shimadzu, Japan) and 1 mg of total RNA was used for cDNA construction by Superscript III kit (Invitrogen Inc., United States).

Virulence Gene Expression by Quantitative PCR

The cDNA and primers were added in the ratio 1:5 in a solution containing Quantinova SYBR Green PCR kit (Qiagen, Germany). The primers (**Table 1**) were designed by using Primer3 (Version: 0.4.0) software (Koressaar and Remm, 2007; Untergasser et al., 2012) and qPCR was performed in 7500 Sequence Detection System (Applied Biosystems Inc., Foster, CA, United States). The differential expression of virulence genes were normalized with β-actin of *C. tropicalis* and the relative fold change of gene expression levels were calculated using $2\text{-}^{\Delta\Delta CT}$ formula ($2^{-\Delta\Delta CT} > 1$- Upregulation and $2^{-\Delta\Delta CT} < 1$- Downregulation of gene expression) (Prasath et al., 2019).

Statistical Analysis

Power and sample sizes were calculated using G*Power (UCLA, Los Angels, United States) (Faul et al., 2007). At 0.05 level of significance, the application of the one-way analysis of variance (ANOVA) *F*-test would have a power of 80.72% with sample size of 24 ($n = 6$ per group) and medium effect size value (difference of the means between the lowest and the highest value) of 0.75.

All the experiments were performed in three biological replicates with experimental triplicates. The data were presented as mean ± standard deviation. The mean differences between control and treated samples were analyzed statistically by one-way ANOVA and Duncan's *post hoc* test was performed with the significant *p*-value of < 0.05, < 0.01, and < 0.001 using SPSS statistical software, version 17.0, United States. The symbols "✻", "✯"and "✦" denoted statistical significance with $p < 0.05$, < 0.01, and < 0.001, respectively.

RESULTS

Antifungal Activity of PA Against *C. tropicalis*

Plants are the known source of novel bioactives with different functional groups such as phenolic, quinones, flavonoids and saponins, which possess antifungal activity (Arif et al., 2009). In this experiment, the effect of PA (2–0.03125 mg mL^{-1}) on the growth of *C. tropicalis* was evaluated by broth dilution and spot assays. At lower concentrations, PA (at concentration range of 0.03125–0.25 mg mL^{-1}) did not affect the growth of *C. tropicalis*. Beyond that, PA reduced the growth at 0.5 mg mL^{-1} with $p < 0.05$. Further, PA at 1 and 2 mg mL^{-1} prevented the visible growth of *C. tropicalis* significantly with $p < 0.001$ (**Figure 1A**). The antifungal activity of PA was corroborated with the amphotericin B ($p < 0.001$) as positive control. Contemporarily, the antifungal activity of PA was

TABLE 1 | List of virulent genes, functions and primer sequences used in qPCR study.

S. NO	GENE	PROTEIN	FUNCTION	PRIMER
1.	*ACT1*	Actin	Conserved protein involved in cell motility	F 5′- TTGCTCTCCGGCAACTTATT -3′ R 5′- TCGATCTTAATCGGGAGGTG3′
2.	*ERG11*	Lanosterol 14-alpha demethylase	Crucial step in ergosterol biosynthesis	F 5′- GAAAGAGAACCATTACCAGG -3′ R 5′- AGGAATCGACGGATCAC -3′
3.	*HWP1*	Hyphal wall protein	Hyphal cell wall protein plays role in hyphal developement	F 5′- CCCAGAAAGTTCTGTCCCAGT- 3′ R 5′- CCAGCAGGAATTGTTTCCAT -3′
4.	*TUP1*	Negative regulator of transcription	Represses *HWP1* for initiating filamentous growth	F 5′ -TTGCACCAGTTTCTGCAGTC-3′ R 5′- TTCAGCACCAGTAGCCAAGA -3′
5.	*NRG1*	Negative regulator of transcription	Regulation of chlamydospore formation, hyphal growth	F 5′- CCAAGTACCTCCACCAGCAT-3′ R 5′- GGGAGTTGGCCAGTAAATCA-3′
6.	*UME6*	Positive regulator of transcription	Promotes hyphal elongation	F 5′- ACCACCACTACCACCACCAC -3′ R 5′- TATCCCCATTTCCAAGTCCA - 3′
7.	*EFG1*	Enhanced filamentous growth protein 1	Important for filamentous growth	F 5′- GCCTCGAGCACTTCCACTGT R 5′- TTTTTTCATCTTCCCACATGGTAGT-3′

counterchecked with spot assay (**Figure 1B**), which reflected the same as in broth dilution method. Both studies revealed that PA at 1 mg mL^{-1} was found to be MIC against *C. tropicalis*.

Effect of PA on *Candida* Species Biofilm Formation

The broth dilution assay revealed that PA was antifungal in the range of 500 $\mu g\ mL^{-1}$. Hence, the antibiofilm activity of PA at different concentrations ranges from 100 to 600 $\mu g\ mL^{-1}$ were tested against various *Candida* species such as *C. albicans, C. tropicalis* and *C. glabrata*. In *C. albicans* and *C. glabrata,* biofilm inhibition was observed PA-treated cells at 500 $\mu g\ mL^{-1}$ with percentage inhibition of 54.22% ($p < 0.01$) and 59.37%, respectively. But PA effectively inhibited 52.98% of biofilm formed by *C. tropicalis* at 100 $\mu g\ mL^{-1}$ (**Figures 1C,D**). Also, significant reduction of biofilm was observed in PA-treated *C. tropicalis* at 200, 500, and 600 $\mu g\ mL^{-1}$ with percentage inhibition of 80.02% ($p < 0.001$), 85.64% ($p < 0.001$), and 84.03% ($p < 0.001$). From this study, it is apparent that the antibiofilm activity of PA was higher in *C. tropicalis* than other *Candida* species.

Effect of PA on *C. tropicalis* Biofilm in Dose-Dependent Concentrations

The effect of PA was evaluated on *C. tropicalis* biofilm at dose-dependent concentrations such as 25, 50, 75, 100, 125, 150, 175, 200, 225, 250 $\mu g\ mL^{-1}$. *C. tropicalis* biofilm was inhibited with an increasing concentration of PA as shown in **Figure 1E**. Besides that, the biofilm inhibition of *C. tropicalis* was higher at 150 $\mu g\ mL^{-1}$ (66.91%) with $p < 0.01$ and maximum inhibition was observed at 200 $\mu g\ mL^{-1}$ (79.62%) with $p < 0.01$. Also, the cell accumulation on the medium surface was increased with increasing concentration of PA (**Figure 1F**). This proved that PA possessed the ability to disrupt the *C. tropicalis* biofilm with minimum biofilm inhibitory concentration (mBIC) at 200 $\mu g\ mL^{-1}$.

PA Impacted on *C. tropicalis* Growth

The effect of PA on the growth of *C. tropicalis* was evaluated by spectrophotometric method and the concentrations (W/V) of PA were compared with the corresponding concentrations (V/V) of vehicle control (methanol). Compared to control cells, the growth was intact in PA-treated *C. tropicalis* at 25, 50, 100, and 200 $\mu g\ mL^{-1}$. The growth was reduced significantly at 400 and 800 $\mu g\ mL^{-1}$ PA-treated *C. tropicalis*. However, vehicle control did not have any substantial effect even at higher concentrations (**Figure 1G**). Hence, PA with increasing concentrations regulated biofilm and growth of *C. tropicalis* without any influence of vehicle control.

Assessment of Metabolic Activity of *C. tropicalis* Using Alamar Blue

In healthy cells, reduction of resazurin to pink colored resorufin by mitochondrial dehydrogenase, signifies the viability of cellular metabolism. The absorbance of the reduced substrate in untreated and PA-treated *C. tropicalis* was measured at 570 nm. Compared to control, metabolic activity of cells was not reduced until 0.5× BIC of PA. The metabolic activity was reduced significantly in PA-treated *C. tropicalis* at 400 ($p < 0.05$) and 800 $\mu g\ mL^{-1}$ ($p < 0.05$) (**Figure 1G**).

Effect of PA on *C. tropicalis* Growth Kinetics

Spectrometric analysis and metabolic assay demonstrated that BIC of PA reduced the growth of *C. tropicalis* and were counter examined by growth curve analysis. The cell growth was stable in both control and 100 $\mu g\ mL^{-1}$ PA-treated cells with slight deterioration at 200 $\mu g\ mL^{-1}$ PA-treated cells. At 400 and 800 $\mu g\ mL^{-1}$, the growth of *C. tropicalis* was fungistatic and the antifungal activity was compared with the 10 $\mu g\ mL^{-1}$ of amphotericin B (**Figure 1H**). Our previous experiments showed that PA was effective on *C. tropicalis* biofilm with impact on the cell growth. Moreover, the antibiofilm activity of PA at 400 and 800 $\mu g\ mL^{-1}$ treatment was found to be analogous. Hence, the

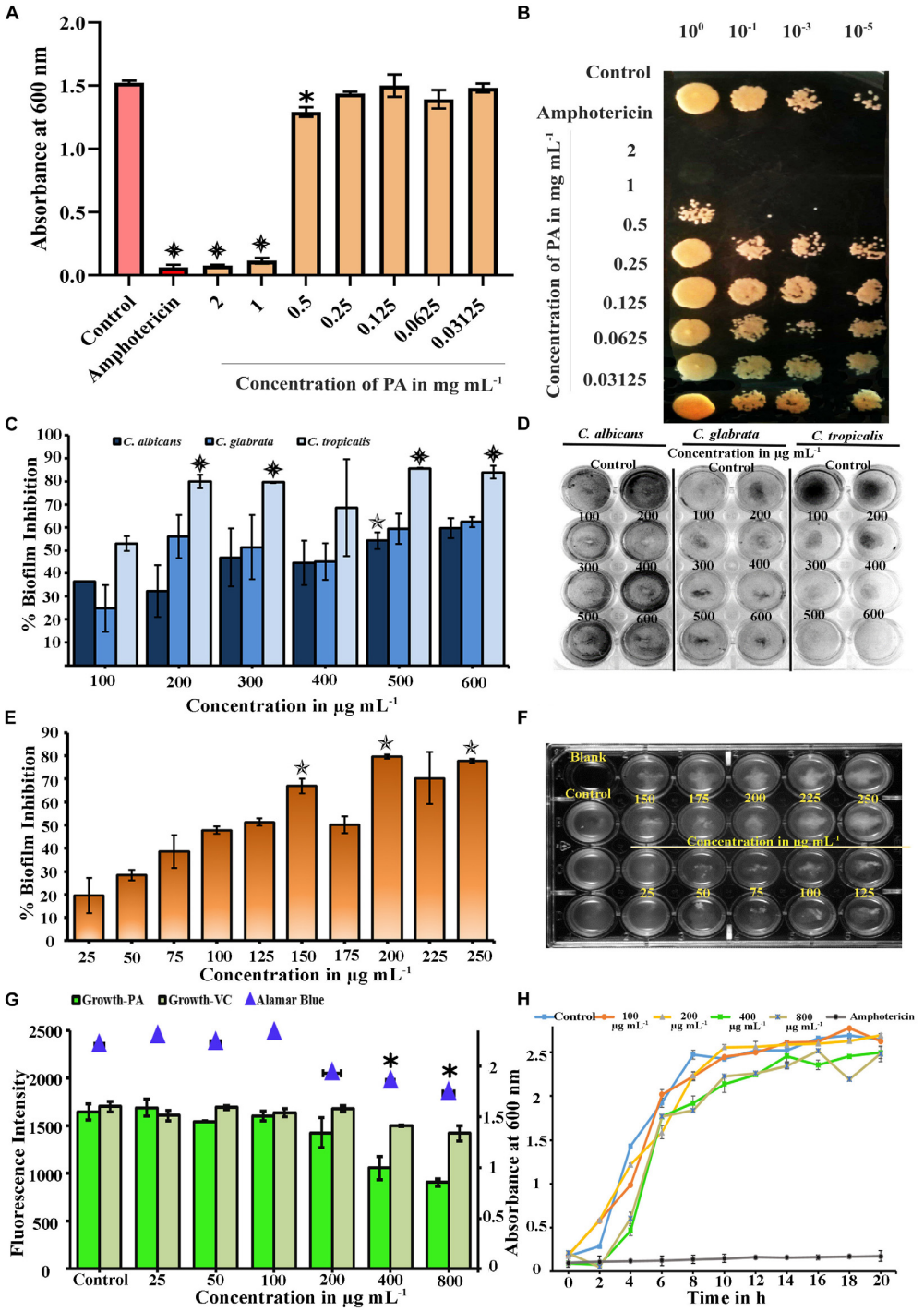

FIGURE 1 | (A) Microbial Inhibitory Concentration (MIC) of PA against *C. tropicalis* was determined by Broth Dilution assay. PA reduced visible growth of *C. tropicalis* at 2 ($p < 0.001$) and 1 mg mL^{-1} ($p < 0.001$) and antifungal effect was compared with 10 µg mL^{-1} of amphotericin ($p < 0.001$). **(B)** Effect of PA on growth of Control and PA-treated *C. tropicalis* after serial dilution and spotting in YEPD agar medium with amphotericin B as positive control **(C)** Effect of palmitic acid (PA) on *Candida* species biofilm grown in spider medium. PA decreased the biofilm at 200, 300, 500, and 600 µg mL^{-1} ($p < 0.001$) in *C. tropicalis* and did not inhibit significantly in *C. albicans* and *C. glabrata*. **(D)** Influence of PA on *Candida* species biofilm stained with CV, a representative image. **(E)** Inhibitory effect of PA on *C. tropicalis* biofilm and maximum inhibition was at 200 µg mL^{-1} ($p < 0.01$). **(F)** Representative MTP plate showing biofilm disruption ability of PA. **(G)** Difference between the impact of PA and its vehicle control on *C. tropicalis* growth and metabolic activity at different concentrations (25–800 µg mL^{-1}). **(H)** Growth curve analysis of *C. tropicalis* with absence and presence of PA (100, 200, 400, and 800 µg mL^{-1}) and 10 µg mL^{-1} of amphotericin B as positive control. The values are expressed as means and error bars depict standard deviation ($n = 6$). Significant values were determined by one-way ANOVA in terms of *p*-value ("✻", "★", and "✸" denote $p < 0.05$, $p < 0.01$, and $p < 0.001$, respectively) followed by Duncan *post hoc* test.

concentrations of PA was narrowed down to 400 μg mL^{-1} for further experiments.

Time Killing Assay for *C. tropicalis* Mature Biofilm

Some antibiofilm agents are effective on reducing early biofilm but not good enough against the mature biofilm. Farnesol, a quorum sensing molecule of *C. albicans,* inhibits germination of blastospores and biofilm but fails on mature biofilm (Blankenship and Mitchell, 2006). In our study, the effect of PA at different concentrations such as 100, 200, and 400 μg mL^{-1} were evaluated on 1, 2, 4 and 7 days matured biofilm with treatment time of PA on 12, 24 and 48 h (**Figure 2A**). On 1 day matured biofilm, PA at 200 μg mL^{-1} disrupted 30.84% with $p < 0.05$ after 24 h of treatment. Further, the efficacy of PA at 200 and 400 μg mL^{-1} was increased with 44.85% ($p < 0.01$) and 53.84% ($p < 0.01$), respectively after 48 h of treatment. Similar effect of PA was observed in 2 days matured *C. tropicalis* biofilm with 43.40% ($p < 0.01$) and 50.10% ($p < 0.01$) of inhibition upon 48 h of PA-treatment at 200 and 400 μg mL^{-1}, respectively. On 4 and 7 days matured biofilm, the effect of PA (100, 200, and 400 μg mL^{-1}) was moderated upon 12 and 24 h of treatment. But in case of 48 h treatment, PA at 200 μg mL^{-1} inhibited 31.38% and 34.20% of 4 and 7 days matured biofilm, respectively. At 400 μg mL^{-1} of PA, 4 and 7 days matured biofilm was reduced further with 40.71% ($p < 0.05$) and 36.25%.

Light Microscopic Analysis of Mature Biofilm

The effect of PA on *C. tropicalis* 7 days matured biofilm was examined in optical microscope with 200 x magnification. Results showed that the mature biofilm formation was disturbed in a concentration-dependent manner. Upon 24 h of treatment, significant inhibition of biofilm was found in PA-treated *C. tropicalis* at 200 μg mL^{-1}. On the other hand, a notable disruption in biofilm was observed beyond 100 μg mL^{-1} and the disruption was increased at 200 and 400 μg mL^{-1} of PA after 48 h treatment (**Figure 2B**).

PA Reduced Biofilm Thickness and Density

The biofilm thickness and density formed by *C. tropicalis* was assessed by Z-stack of CLSM. The untreated *C. tropicalis* cells were enhanced with both hyphal and yeast cells (**Figure 2C**). Both biofilm thickness and density were reduced in the presence of PA with increasing concentrations on both 24 and 48 h treatment. But hyphal cells were observed even at higher concentration of PA upon treatment on both the time points.

Time-Dependent Assessment of *C. tropicalis* Growth on PA Treatment

Biofilm and the associated virulence factors proliferate on late-log phase of *C. tropicalis.* The effect of PA upon 24 and 48 h treatment on 10 h grown *C. tropicalis* was examined by CFU method. After treatment with PA, the cells were serially diluted and spread on SDA agar medium. On 24 h treatment of PA, *C. tropicalis* colonies got reduced at 400 μg mL^{-1} compared to control. But after 48 h treatment, the colony reduction was seen even at 100 μg mL^{-1} and reduced further with increasing concentration of PA (**Figure 3A (i)**). The logarithmic conversion of untreated and PA-treated *C. tropicalis* CFU is shown in **Figure 3A (ii)**.

Testing Viability of *C. tropicalis* by Live – Dead Staining

Acridine orange (AO) is a cell-membrane permissible dye, whereas ethidium bromide (EtBr) cannot penetrate the live cells. Post treatment of PA at different time points on viability of *C. tropicalis* were assessed by staining the cells with AO and EtBr. Compared to control, dead cells were not seen in 100 μg mL^{-1}, whereas countable dead cells were present at 200 and 400 μg mL^{-1} PA-treated cells upon 24 h. Further on 48 h of treatment, PA (200 and 400 μg mL^{-1}) increased the membrane permeability of *C. tropicalis* with increasing concentrations that reflects higher number of dead cells (**Figure 3B**).

SEM Analysis of *C. tropicalis* Cellular Morphology

As shown in CFU assay and Live-Dead staining, PA reduced the cellular growth of *C. tropicalis* after 48 h of treatment. Hence SEM was used to analyze the colony morphology of 48 h PA-treated *C. tropicalis* (**Figure 3C**). The untreated *C. tropicalis* composed of intact hyphae and yeast cells. PA at 100 μg ml^{-1} began to impose stress on cellular surface. At higher concentrations (200 and 400 μg mL^{-1}) of PA, stress was surged and damage cells were observed. Here, SEM analysis proved that PA is fungistatic by mediating stress condition on *C. tropicalis* at higher concentrations upon 48 h of treatment.

Quantification of Programmed Cell Death by PA in *C. tropicalis*

When a compound inhibits the growth of the cells, it would induce apoptosis mediated cell death. The apoptosis in the cells was quantified using PI which is impermeable in live cells. The apoptosis in PA-treated cells at different time points (4, 8, 12, 24, and 48 h) was quantified by measuring the fluorescence intensity of PI. The absorbance level is proportional to the number of dead cells in the cell suspension. Compared to control, the absorbance was not increased in 4 and 8 h PA-treated cells (**Figure 4A**). But in 24 and 48 h treated cells, the absorbance of PI was greater and significantly increased in 200 ($p < 0.05$ and $p < 0.05$, respectively) and 400 μg mL^{-1} ($p < 0.05$ and $p < 0.01$, respectively). Thus, the number of dead cells increased with the increasing concentration gradient of PA (**Figure 4A**).

Assessment of DNA Damage by DAPI

Scanning electron microscope analysis confirmed morphological variation in *C. tropicalis* caused by PA and hence the PA induced DNA damage was evaluated by DAPI staining. The elevated fluorescence level was observed in 48 h and 24 h PA-treated *C. tropicalis* at 200 and 400 μg mL^{-1}. This showed that PA induced apoptosis by mediating DNA fragmentation and condensed chromatin in *C. tropicalis*. Besides, the intense

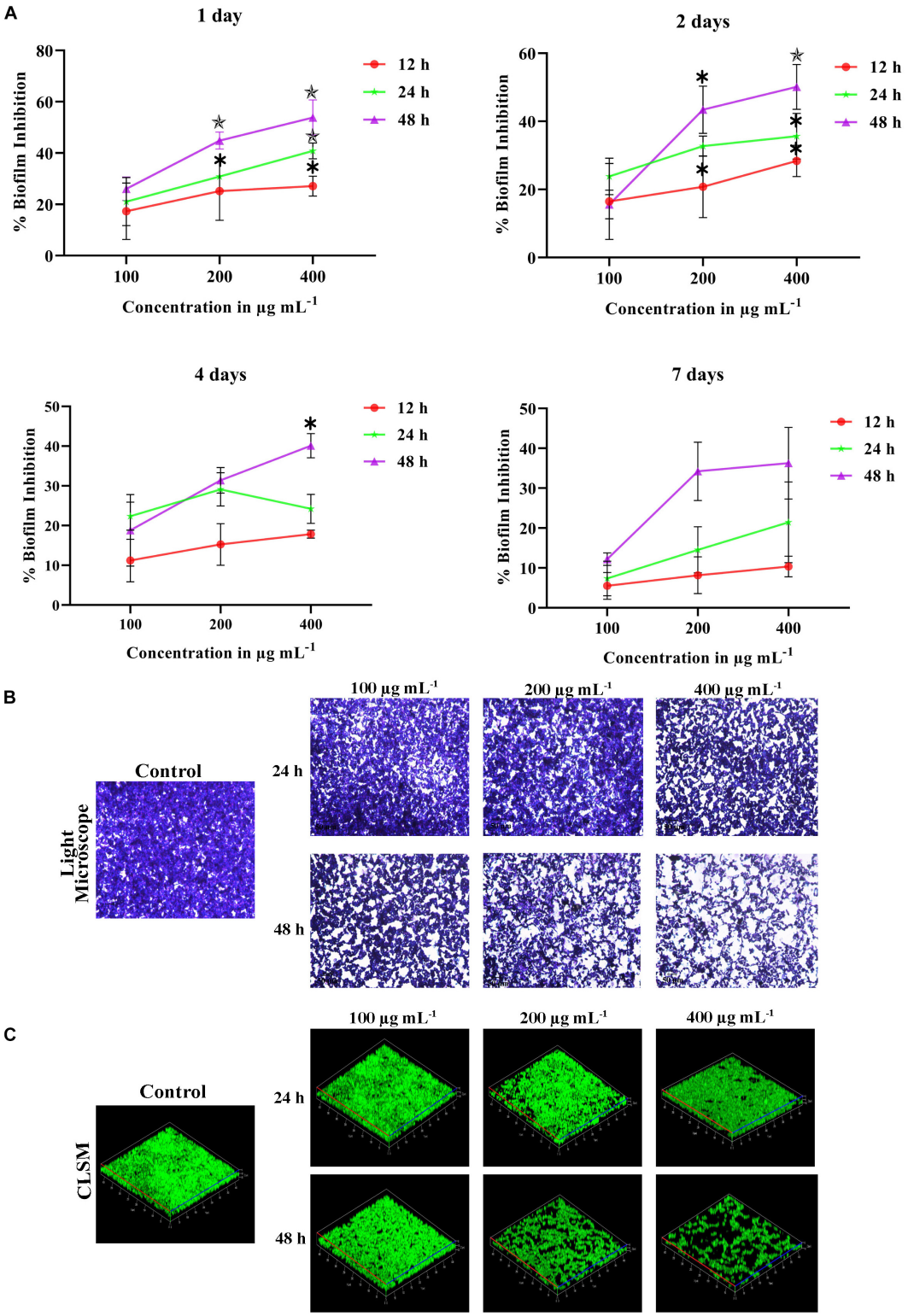

FIGURE 2 | (A) Time killing of 1, 2, 4 and 7 days matured biofilm formed by *C. tropicalis* by PA at different time points (12, 24, and 48 h) and concentrations (100, 200, and 400 µg mL^{-1}. The values are expressed as means and error bars indicate standard deviation of triplicates ($n = 6$). Control and PA-treated for 24 h and 48 h *C. tropicalis* biofilm (7 days matured) formed on 10 × 10 mm glass surfaces, as observed under **(B)** optical (Magnification – 400×, Scale bar – 50 µm) and **(C)** Confocal Microscope. *$p < 0.05$, *$p < 0.01$, and ✦$p < 0.001$, significantly different when compared with control.

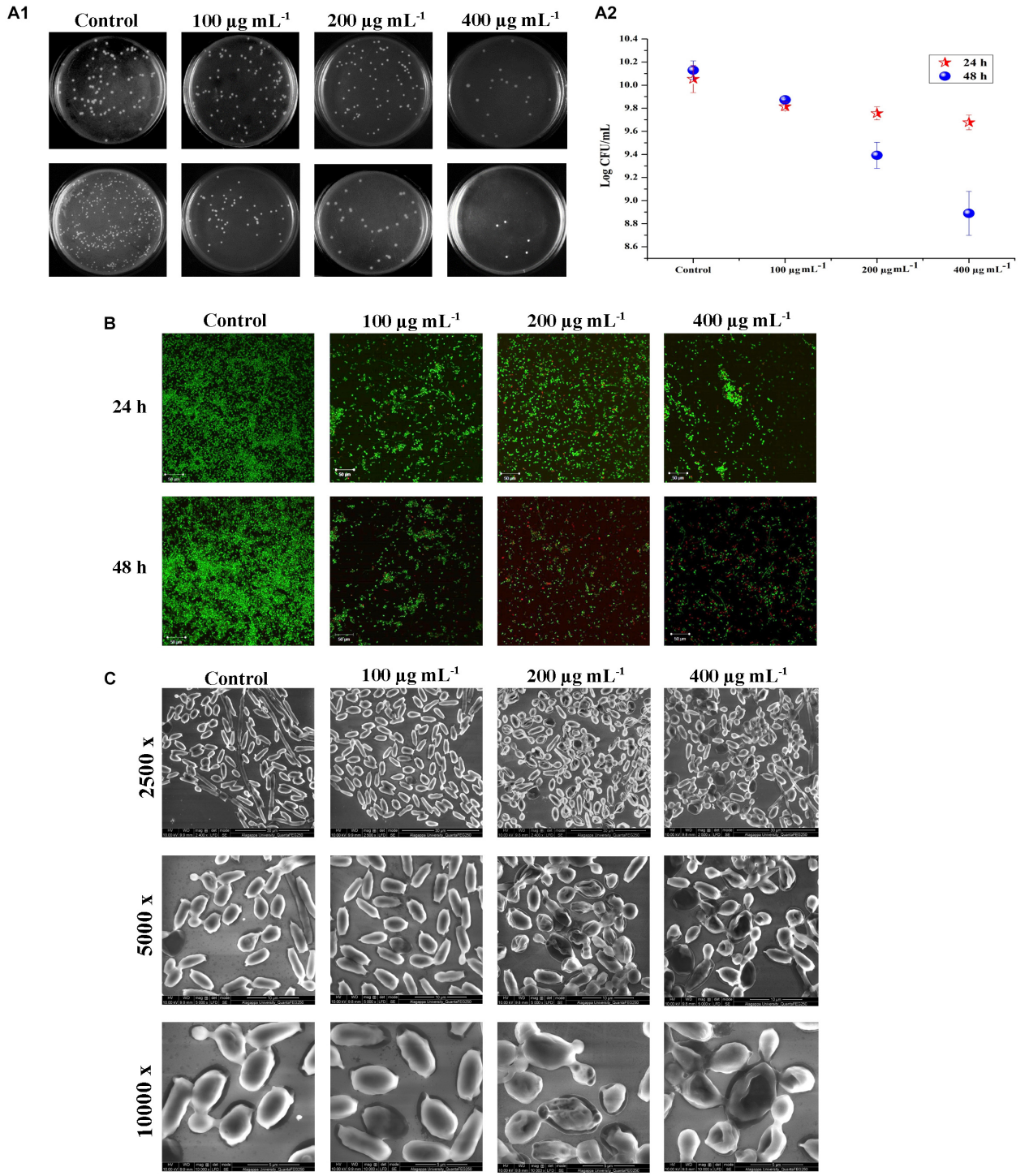

FIGURE 3 | Effect of PA (0, 100, 200, and 400 µg mL^{-1}) on *C. tropicalis* survival after 24 and 48 h of treatment. **[A (i)]** Image displaying the effect of PA on *C. tropicalis* survival, grown on SDA agar medium. **[A (ii)]** CFU of *C. tropicalis* in the absence and presence of PA determined in logarithmic scale. **(B)** Confocal microscopic examination of *C. tropicalis* revealing the efficacy of inducing cell death which was assessed using AO/EtBr staining. **(C)** SEM analysis of *C. tropicalis* colony morphology in the absence and presence of PA (100, 200, and 400 µg mL^{-1}) after 24 and 48 h of treatment.

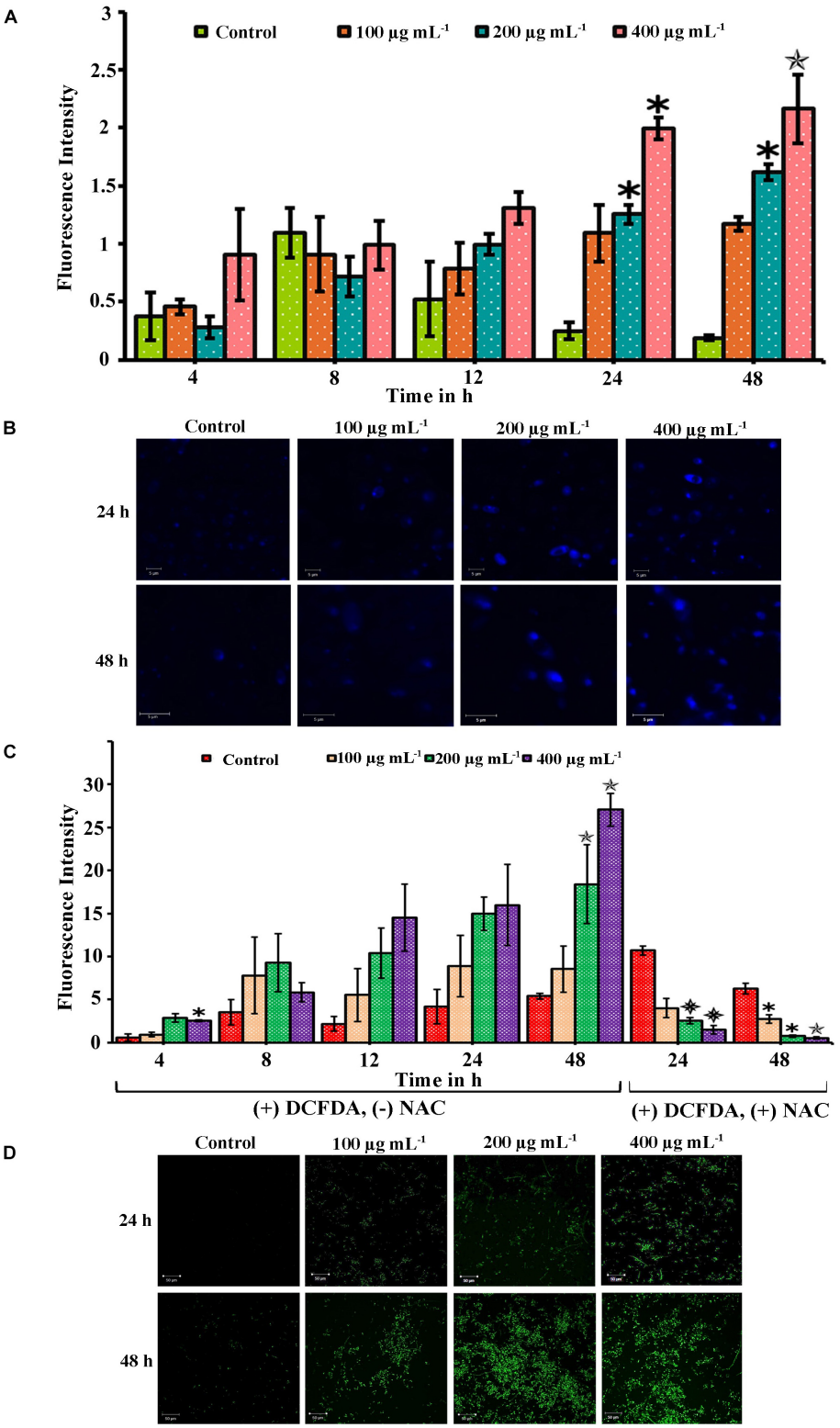

FIGURE 4 | Palmitic acid induced apoptosis and ROS associated with DNA damage in *C. tropicalis*. **(A)** Efficacy of PA inducing apoptosis in *C. tropicalis* at different concentrations (0, 100, 200, and 400 µg mL^{-1}) and time points (4–48 h) which was quantified using propidium iodide. **(B)** DNA damage induced by PA at different concentrations were assessed by DAPI staining and visualized in CLSM. **(C)** Extent of ROS produced by PA in *C. tropicalis* after 24 and 48 h treatment was quantified by DCFDA and addition of 10 mM NAC reversed the ROS production in *C. tropicalis*. **(D)** Also, the induction of ROS PA in *C. tropicalis* was visualized in CLSM by DCFDA stain. The values are expressed as means and error bars indicate standard deviation of triplicates ($n = 6$). ✻$p < 0.05$, ⋆$p < 0.01$, and ✱$p < 0.001$, significantly different when compared with control.

fluorescence was not inferred in control cells on both time points (**Figure 4B**).

PA Triggers ROS Generation in *C. tropicalis*

The extrinsic induction of ROS plays a significant role in apoptosis mediated cell death. This study assessed the qualitative and quantitative analysis of ROS generation in PA-treated *C. tropicalis* by DCF-DA stain. Initially we determined the ROS levels in PA-treated *C. tropicalis* cells at different time points (24 and 48 h) using the ROS specific fluorescent stain DCF-DA. CLSM images revealed the generation of DCF fluorescence initiated at 24 h of PA treatment and it remarkably spiked-up at 48 h time point, with greater generation of ROS at 200 and 400 $\mu g\ mL^{-1}$ of PA (**Figure 4D**). ROS produced by the cells was directly proportional to the extent DCFDA to DCF conversion. Also, the effect of PA in induction of ROS was quantitatively measured at different time points (4, 8, 12, 24, and 48 h). Upon 48 h treatment, PA significantly induced ROS at 200 ($p < 0.01$) and 400 $\mu g\ mL^{-1}$ ($p < 0.01$). However, the presence of NAC (ROS scavenger) along with PA significantly revoked the PA induced DNA damage and ROS production in *C. tropicalis* on both 24 h ($p < 0.001$ at 200 and 400 $\mu g\ mL^{-1}$) and 48 h ($p < 0.05$ at 100 and 200 $\mu g\ mL^{-1}$; $p < 0.01$ at 400 $\mu g\ mL^{-1}$) treatment (**Figure 4C**).

PA Induced Mitochondrial Dysfunction Mediated Apoptosis

Mitochondrial membrane potential ($\Delta\Psi$ m) is important for normal cellular functions such as protein and ATP synthesis (Ott et al., 2007). The intrinsic apoptotic cell death happens during loss of $\Delta\Psi$ m (Henry-Mowatt et al., 2004). Hence, this study investigated the PA-induced apoptosis mediated by mitochondrial damage using mitochondrial specific probe Rhodamine 123. The stain binds to the active mitochondria and the fluorescence rate was higher in untreated *C. tropicalis* on both 24 and 48 h time points. The fluorescence intensity was decreased with increasing concentrations of PA-treated *C. tropicalis* (**Figure 5A**). These results clearly indicated that loss of $\Delta\Psi$ m was associated with PA induced apoptosis thereby activating cell death in *C. tropicalis*.

Effect of PA on H_2O_2 Sensitivity, Catalase, and Superoxide Dismutase *C. tropicalis*

Eukaryotic cell contains antioxidant enzymes such as superoxide dismutase (SOD), catalases and peroxidases that regulates intrinsic ROS-damaging effects. The elevated expression of these antioxidant enzymes would increase the antifungal resistance in *C. albicans* (Seneviratne et al., 2008). We investigated the effect of PA on 24 and 48 h treated *C. tropicalis* catalase and SOD. Briefly, the intracellular proteins of untreated and 24 and 48 h PA-treated *C. tropicalis* at different concentrations were isolated and resolved in native PAGE. PA with increasing concentrations did not affect the *C. tropicalis* catalase on both the time points (**Figure 5D**). Similarly, PA did not show any impact on *C. tropicalis* SOD1 and SOD2 on 24 h treatment. But upon 48 h of PA treatment, the expression levels of both SODs were reduced with increasing concentrations of PA (**Figure 5C**). The repression of SOD sensitizes the cells to the oxidative stress and the effect was examined by H_2O_2 sensitivity assay. The zone of clearance around the disc signifies the H_2O_2 induced oxidative stress in *C. tropicalis*. In 24 h PA-treated *C. tropicalis*, the zone of clearance was similar to control cells (**Figure 5B**). As expected, the zone was greater in 200 and 400 $\mu g\ mL^{-1}$ PA-treated *C. tropicalis* upon 48 h of treatment.

PA Reduced Cell Surface Hydrophobicity of *C. tropicalis*

Cell surface hydrophobicity (CSH) is a putative virulence attribute in *Candida* spp. on biofilm formation and the effect of PA on CSH of *C. tropicalis* was evaluated by MATH assay. The hydrophobic cells possesses greater affinity toward non-polar solvents. After incubation, the PA-treated and untreated cells were vortexed with toluene and hydrophobicity index was calculated. Results showed that, the affinity of cells to toluene was higher in untreated *C. tropicalis* and the affinity was reduced in 24 h PA-treated cells with increasing concentrations (**Figure 6A**). But upon 48 h PA treatment, cell affinity toward the solvent was reduced to 40.2% in 400 $\mu g\ mL^{-1}$ of PA compared to control (82.95%) (**Figure 6A**).

Effect of PA on *C. tropicalis* Extracellular Lipase Production

The lipase activity of untreated and PA-treated *C. tropicalis* was measured quantitatively by using P-Nitro Phenol Palmitate as a substrate. Upon 24 h treatment, PA inhibited lipase at 100 and 200 $\mu g\ mL^{-1}$ and significantly got reduced at 400 $\mu g\ mL^{-1}$ ($p < 0.05$) (**Figure 6B (ii)**). Similarly after 48 h treatment, lipase production was found to be decreased in a concentration dependent manner and reduced at 200 and 400 $\mu g\ mL^{-1}$ with percentage inhibition of 53.83 and 72.55% ($p < 0.05$), respectively. In addition, the lipase activity was qualitatively measured by tributyrin substrate in solid spider agar medium, resulting in zone of clearance around the growth as shown in **Figure 6B (i)**. The lipase activity in 24 h PA-treated *C. tropicalis* was as similar to control and slight inhibition was observed at 400 $\mu g\ mL^{-1}$. But in case of 48 h treated cells, the phospholipase activity was inhibited with increasing in the concentration of PA and significant reduction was observed at 200 and 400 $\mu g\ mL^{-1}$.

Qualitative Analysis of *C. tropicalis* Protease

The effect of PA on *C. tropicalis* protease was examined in BSA solid medium. In this, protease cleaves BSA (substrate) thereby forming zone of precipitation around the cells. In untreated 24 and 48 h cells, a thick zone of precipitation was observed. Upon 24 h PA treatment, the precipitation zone decreased with increasing concentrations and in case of 48 h treatment, the zone was completely inhibited at 200 and 400 $\mu g\ mL^{-1}$ PA-treated *C. tropicalis* (**Figure 6C**).

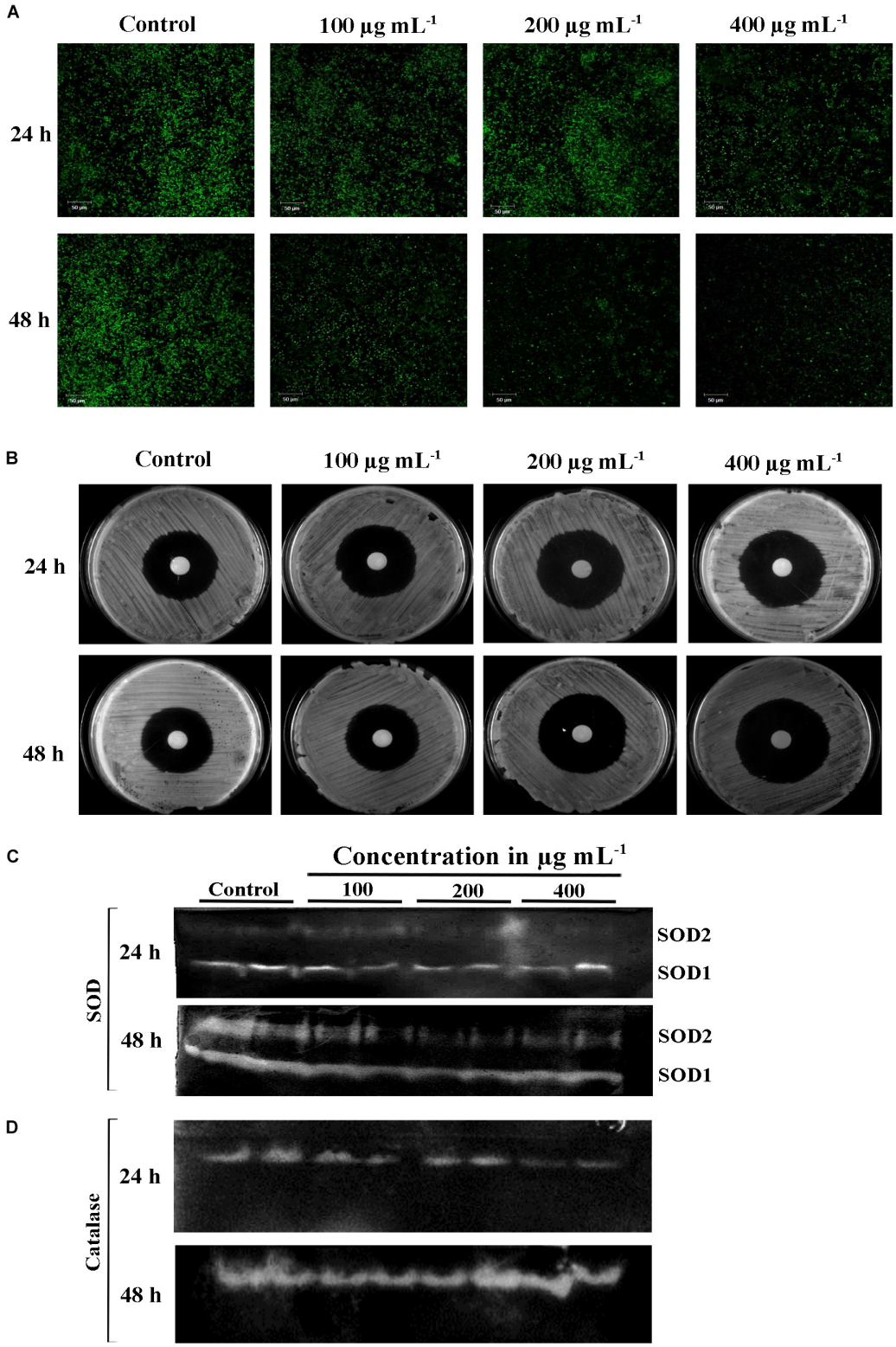

FIGURE 5 | (A) Loss of mitochondrial membrane potential ($\Delta\Psi m$) in *C. tropicalis* at different time points (24 and 48 h) and concentrations (100, 200, and 400 µg mL^{-1}) of PA as imaged in CLSM by Rhodamine 123 staining. Presence of PA mediated loss of mitochondrial membrane permeability and induced apoptosis in *C. tropicalis*. **(B)** Representative SDA agar plates depicting the effect of PA on the sensitivity of *C. tropicalis* to H_2O_2. Native PAGE revealing expression of superoxide dismutase (SOD) **(C)** and catalase **(D)** in PA (0, 100, 200, and 400 µg mL^{-1}) treated *C. tropicalis* after 24 and 48 h.

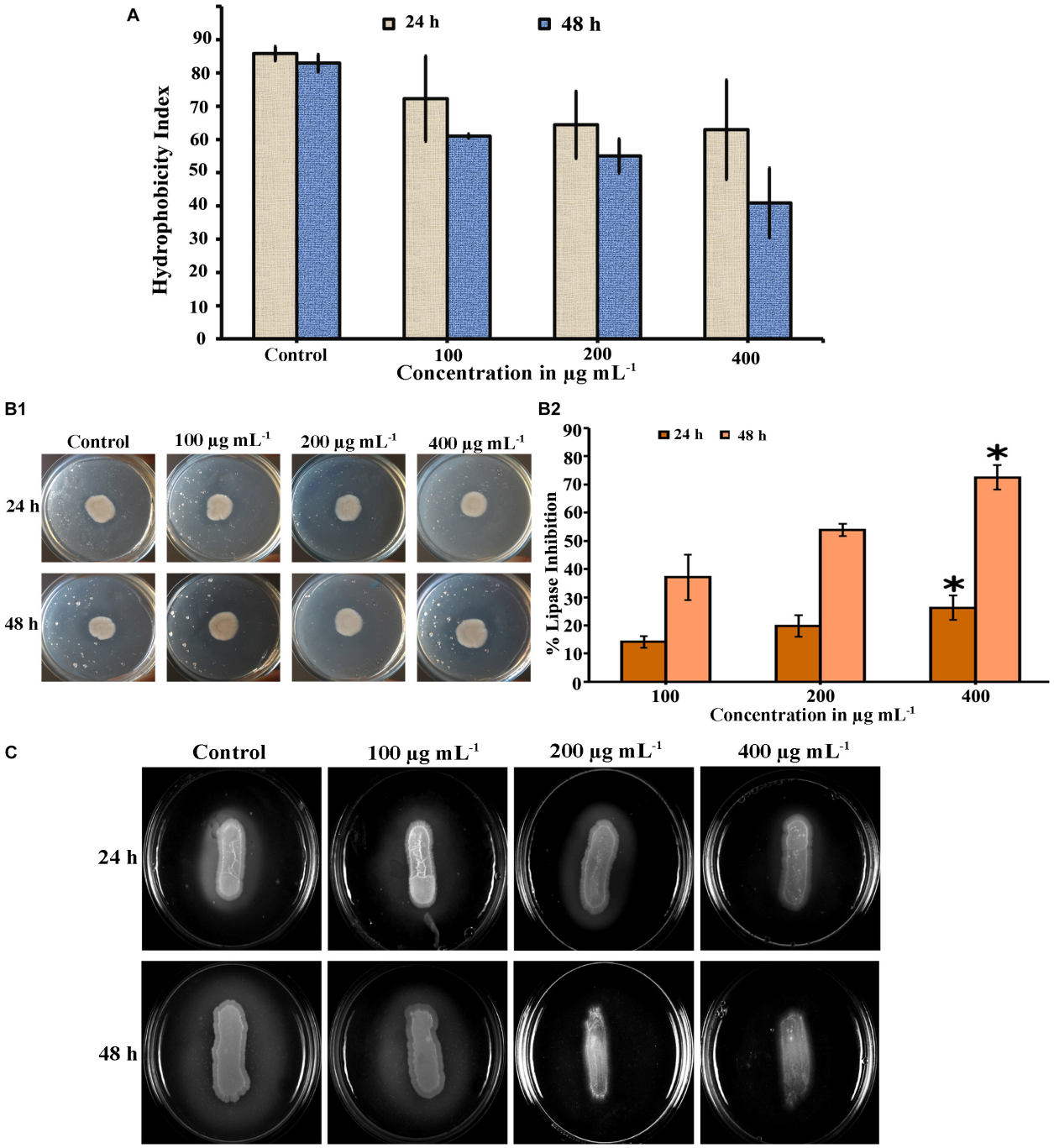

FIGURE 6 | Inhibitory effect of PA on virulence factors of *C. tropicalis*. **(A)** Bar graph showing the reduction of cell surface hydrophobicity in PA-treated (100, 200, and 400 µg mL^{-1}) *C. tropicalis* after 24 h and 48 h treatment. **(B)** Effect of PA at different concentrations (100–400 µg mL^{-1}) on *C. tropicalis* lipase measured **(i)** quantitatively and **(ii)** qualitatively after 24 and 48 h of treatment. **(C)** Effect of PA on the extracellular protease production of *C. tropicalis* on BSA agar medium. The values are expressed as means and error bars indicate standard deviation of triplicates ($n = 6$). ✻$p < 0.05$, ⋆$p < 0.01$ and ✦$p < 0.001$, significantly different when compared with control.

Ergosterol Biosynthesis of PA-Treated *C. tropicalis*

The efficacy of PA was investigated on *C. tropicalis* ergosterol biosynthesis at different time points and concentrations. Total ergosterol was isolated from untreated and PA-treated cells by alcoholic KOH followed by extraction with n-heptane. The ergosterol content was measured by UV-spectrophotometer through a unique spectral peak between 240 and 300 nm.

PA at 100 and 200 μg mL^{-1} reduced ergosterol production significantly in both the time points when compared to control (**Figures 7A,B**). Interestingly, ergosterol level of 24 h PA-treated *C. tropicalis* at 400 μg mL^{-1} was similar to 200 μg mL^{-1} (**Figure 7A**). However, in 48 h treated *C. tropicalis* the ergosterol level in 400 μg mL^{-1} of PA was reduced further to the previous concentration (**Figure 7B**).

PA Induces *C. tropicalis* Hyphal Formation

Hyphal formation is one of the virulence factors along with lipase, protease, ergosterol and biofilm in *Candida* spp. The effect of PA was investigated in selective spider medium for hyphal formation in *C. tropicalis*. After treatment with PA on 12 h grown *C. tropicalis* at different concentrations in two different time points such as 24 h and 48 h, the cells were spotted on spider agar medium. Interestingly, PA did not inhibit the *C. tropicalis* hyphae and the level of hyphal formation was similar to control upon 24 h PA treatment. On the contrary, PA at increasing concentrations induced the hyphae in *C. tropicalis* upon 48 h of treatment (**Figure 7C**). Hence it is obvious that PA did not impact the redevelopment of hyphae but induce the dimorphism with increasing concentrations.

Validation of Anti-virulence Aspects of *C. tropicalis* by qPCR

Our previous experiments substantiated that PA at 200 μg mL^{-1} upon 48 h effectively reduced mature biofilm, proteases, ergosterol and lipases but failed to inhibit *C. tropicalis* hyphae. Hence, the effect of PA at the above-mentioned concentration and time point was evaluated on *C. tropicalis* virulence genes such as *ERG11, NRG1, TUP1, UME6, HWP1 and EFG* by qPCR. Result showed that PA downregulated the *ERG11* (gene encodes for Lanosterol 14-alpha demethylase) of *C. tropicalis.* Besides, *HWP1* and *EFG1* (gene encodes for Hyphal formation) were overexpressed in PA-treated cells. Interestingly, negative transcription regulators of hyphae such as *NRG1* and *TUP1* were negatively regulated and *UME6,* positive transcription regulator of hyphae was upregulated.

DISCUSSION

Candidiasis is an infection caused by *Candida* spp. in clinically associated and system specific infections. The occurrence of candida infection on blood stream is known as candidemia. Globally, *Candida* species are the fourth most common pathogen causing Candidemia with the mortality of 38% - 61% (Gudlaugsson et al., 2003) with *C. albicans* at the top. The prevalence of NCAC in candidemia is greater than *C. albicans* with higher mortality in clinically infected immunocompetent patients (Dimopoulos et al., 2008). Mainly in India, the morbidity rate of *C. tropicalis* infection is more prevalent in blood stream infections with 35.3% followed by *C. albicans* (21.5%), *C. parapsilosis* (20%), *C. glabrata* (17.5%), *C. Krusei* (3.3%), *C. haemulonii* (1.5%) and *C. guilliermondii* (1%) (Xess et al., 2007; Chakrabarti et al., 2015). Clinically, the pathogenicity of *C. tropicalis* is more severe than *C. albicans* in oncology patients and neonatal infections (Kothavade et al., 2010). Several virulence factors of *C. tropicalis* such as biofilm and hyphal formation, sterol synthesis, production of hydrolytic enzymes are responsible for invasive infections in immunocompromised patients.

Biofilms are formed by well-structured communication of cells that possess the capacity to penetrate human tissues and thereby causing infections at various sites of the human body (Costerton et al., 1999). The extensive biofilm and hydrolytic enzyme productions in clinically isolated *Candida* spp. makes them more virulent and the longer colonization increases probability of hematogenous infections (Gokce et al., 2007). Also, the adhesion and biofilm in *C. albicans* are the important factors for surface attachment in dental implants (Noumi et al., 2010). In *C. albicans,* hydrolytic enzymes are important for the host-cell membrane damage that promotes invasion and colonization (Monroy-Pérez et al., 2016). The dense biofilm matrices resists the passage of conventional antifungal drugs thereby becoming ineffective (Taff et al., 2013). The compounds derived from natural sources could be a suitable alternative for overcoming antifungal limitations (Rates, 2001), and these compounds are known to have the anti-inflammatory and antimicrobial properties (Ahmad et al., 2014). The broth dilution study and spot assay revealed that PA inhibited 15.23% of growth at 500 μg mL^{-1}. The growth was reduced further at 1 mg mL^{-1} with 92.00% of inhibition and reduces the visibile growth of *C. tropicalis*. This study unveiled the MIC of PA against *C. tropicalis* was 1 mg mL^{-1}.

Further, the study investigated the antibiofilm activity of Palmitic acid against *C. tropicalis* and other candida spp. such as *C. albicans* and *C. glabrata*. PA inhibited 50% of *C. tropicalis* biofilm even at 100 μg mL^{-1} but failed in case of *C. albicans* and *C. glabrata* biofilm. The dose dependent examination of PA against *C. tropicalis* biofilm revealed the maximum inhibition at 200 μg mL^{-1} and was taken as BIC of PA. Furthermore, the effect of PA on *C. tropicalis* growth was tested using metabolic activity, growth curve and cell viability assays which showed that the PA at BIC showed up a negative regulation of growth and the inhibition was higher at 2× and 4× BIC of PA. *Candida* species produces quorum sensing molecules such as farnesol, tyrosol and farnesoic acid for the maintenance of cellular aggregation for forming biofilms. The extrinsic addition of farnesol inhibits growth mediated biofilm formation of *C. albicans* yeast cells (Uppuluri et al., 2007).

The communication of yeast cells through quorum sensing molecules leads to the cell pile-up thereby forming mature biofilm (Ramage et al., 2002). Hence, the effect of PA on *C. tropicalis* 1, 2, 4, and 7 days matured biofilm was examined at different time points (12, 24, and 48 h). PA at 200 and 400 μg mL^{-1} inhibited more than 50% of 1 and 2 days matured biofilm upon 48 h of treatment and in case of 4 and 7 days matured biofilm, PA was found to inhibit 35.49% of biofilm (**Figure 2A**). The optical and confocal micrographs of the time killing assay reveals that PA could effectively reduce the biofilm density and thickness upon 48 h of treatment at 200 and 400 μg mL^{-1}

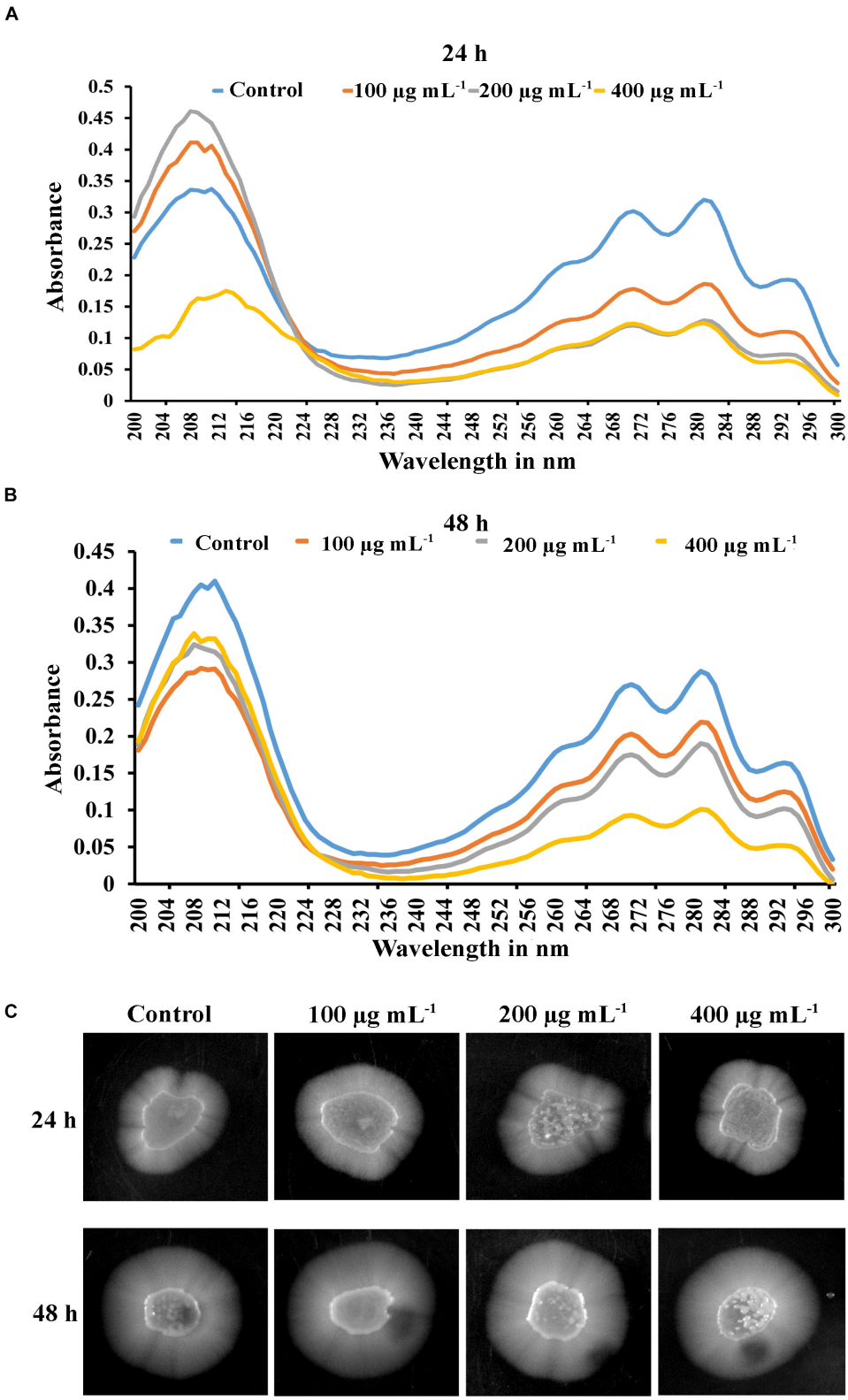

FIGURE 7 | Inhibitory effect of PA (100, 200, and 400 µg mL^{-1}) on ergosterol biosynthesis of *C. tropicalis* after 24 h **(A)** and 48 h **(B)** treatment. Ergosterol was extracted by n-heptane and unique sterol spectral profiles of *C. albicans* was measured in the range between 240 and 300 nm. **(C)** PA induced *C. tropicalis* hyphae on spider agar medium with increasing concentrations on both the time points.

(**Figures 2B,C**). The heterogeneous matrix of mature biofilm retards the penetration of conventional antifungals (Al-Fattani and Douglas, 2004). The potency of PA on *C. tropicalis* mature biofilm formation was higher with increasing concentrations and treatment times. The microbial biofilms are more resistant to antibiotics than early biofilm due to the excessive EPS production (Bowler et al., 2012). However, PA was effective against both early and mature *C. tropicalis* biofilm.

Colony forming unit and Live-dead staining assay showed that the number of dead cells were higher in PA-treated *C. tropicalis* with increasing concentrations and time points. Also, SEM analysis revealed a shrinkage in morphology of 48 h PA-treated *C. tropicalis* at 200 and 400 $\mu g\ mL^{-1}$. Hence, it is construed that the ability of PA on *C. tropicalis* mature biofilm disruption could be due to the compound intervention on cellular growth (**Figures 3A–C**). PA > 1 $mg\ mL^{-1}$ increases DNA fragmentation in rat pancreatic cells and the subsequent induction of apoptosis creates a damaging effect on β cell mass (Maedler et al., 2001). In this study, the rate of apoptosis was quantified in PA-treated *C. tropicalis* by propidium iodide and the dead cells were higher in 200 and 400 $\mu g\ mL^{-1}$ upon 48 h treatment (**Figure 4A**). Similarly, PA generated DNA damage in *C. tropicalis* to a greater extent at the above-mentioned concentrations and time point.

Ceramide is a part of sphingolipid pathway and acts as an activator of apoptosis cascade due to the cellular stress (Haimovitz-Friedman et al., 1997). But PA generates oxidative stress mediated apoptosis through non-ceramide pathway in Chinese Hamster Ovary (CHO) cells (Listenberger et al., 2001). In *C. tropicalis,* the level of ROS was higher even in 200 and 400 $\mu g\ mL^{-1}$ PA-treated cells and the presence of NAC scavenged the ROS generation in PA-treated cells. The excessive generation of ROS creates abnormal mitochondrial permeability. Hence, rhodamine 123 was used to measure the mitochondrial membrane potential ($\Delta\Psi$ m) and the membrane potential of *C. tropicalis* was reduced with increasing concentrations of PA after 48 h treatment (**Figure 5A**). Collectively, these results confirmed that the excessive accumulation of ROS and DNA fragmentation in PA-treated cells could contribute to the loss of mitochondrial membrane potential ($\Delta\Psi$ m) in *C. tropicalis*.

In normal cellular metabolism, balancing of redox homeostasis ensures the survival of cells under oxidative stress conditions. The regulation of antioxidant enzymes, such as superoxide dismutases (SODs), catalases, catalase-peroxidases and peroxiredoxins would result in elevated levels of ROS (Aguirre et al., 2005). SODs are crucial for *Candida* spp. to shield itself from the oxidative mediated cell death (Gleason et al., 2014). Native PAGE revealed that PA regulated SOD2 on both the time points and the reduction of SOD2 sensitized *C. tropicalis* to H_2O_2 stress. Surprisingly, PA did not inhibit the catalase activity even at 400 $\mu g\ mL^{-1}$.

Clinically, the surface chemistry of medical implants which are more hydrophobic, would increase the bioavailability of devices (Tang et al., 2008). But the hydrophobic nature of cell membrane in pathogens prompts to interact with implants surface and forms biofilm. The treatment of PA reduced the cell surface hydrophobicity of *C. tropicalis* at both the time points (24 and 48 h) and concentrations (100, 200, and 400 $\mu g\ mL^{-1}$). Also, lipases and proteases are considered as major virulence factors of *C. tropicalis*. These hydrolytic enzymes contribute to the tissue invasion, colonization and morphological switching in *Candida* species (Park et al., 2013). Previously, myristic acid from *Myristica fragrans* was shown to inhibit lipase and protease by regulating the putative lipase (ATG15) and Candidapepsin (SAP6), respectively (Prasath et al., 2019). In this study, PA at 200 $\mu g\ mL^{-1}$ significantly reduced both lipase and protease after 48 h of treatment but the reduction was not detected in 24 h treatment.

Ergosterol is one of the predominant virulence factors found in eukaryotic fungi. The sterol is an essential component for structural organization and function of the plasma membrane in *Candida* species (Lv et al., 2016). In the present study, PA at both the time points reduced the ergosterol content of *C. tropicalis* and significantly inhibited at 200 $\mu g\ mL^{-1}$. Most of the antifungals such as azole drugs, nystatin and amphotericin BB targets ergosterol biosynthesis pathway. The prolonged exposure of azole drugs induces expression of Lanosterol α14 - Demethylase (*ERG11*) in *C. albicans* and contributes to the development of resistance against azole drugs (Henry et al., 2000; Song et al., 2004). Hence, the differential expression of *ERG11* in control and 48 h PA-treated *C. tropicalis* at 200 $\mu g\ mL^{-1}$ was evaluated by qPCR. The result showed that the expression of *ERG11* was downregulated in PA-treated *C. tropicalis*. Azoles interrupt the ergosterol pathway by interacting with heme group on the active site of lanosterol demethylase (Ji et al., 2000). Mutations in ERG11 plays a major role in development of resistance against antifungals (Xiang et al., 2013). PA effectively downregulated the *ERG11* thereby dwindling the resistance development in *C. tropicalis*.

Yeast – hyphal transition occurs in dimorphic fungus based on the host- pathogen interactions and tissue invasion (Li and Nielsen, 2017). Besides, the filamentation assay revealed that PA induced the hyphal elongation in *C. tropicalis* with increasing concentration after 24 and 48 h treatment (**Figure 7C**). Hyphal wall protein *(HWP1)* is highly expressive in yeast – hyphal transition in dimorphic *Candida* species (Nobile et al., 2008). TUP1 is the transcriptional repressor of filamentous growth and the deletion of the TUP1 gene causes overexpression of hyphae in *C. albicans* (Braun and Johnson, 1997). Also, *NRG1* regulates the hyphal formation and acts as a transcriptional repressor along with *TUP1* and *RFG1* (Braun et al., 2001). The result of filamentation assay was reflected in qPCR with upregulation of *HWP1* and downregulation of *TUP1* and *NRG1* in PA-treated *C. tropicalis* (**Figure 8A**). However, *UME6,* a positive regulator of hyphal elongation and specific gene for germ tube formation was upregulated. In *C. albicans*, *HWP1* mutant influences on host-pathogen interactions and pathogen morphology with the extent of biofilm production remains unaffected (Orsi et al., 2014). This proved that *Candida* species biofilm and hyphal formation works on different mechanisms and the efficacy of the bioactive(s) on pathogens' virulence would differ from one factor to another.

Enhanced filamentous growth (EFG1) permits hyphal morphogenesis in *C. albicans* and independent of *TUP1* regulatory mechanism for filamentation (Braun and Johnson, 2000). Similar to *HWP1,* the expression of *EFG1* was also

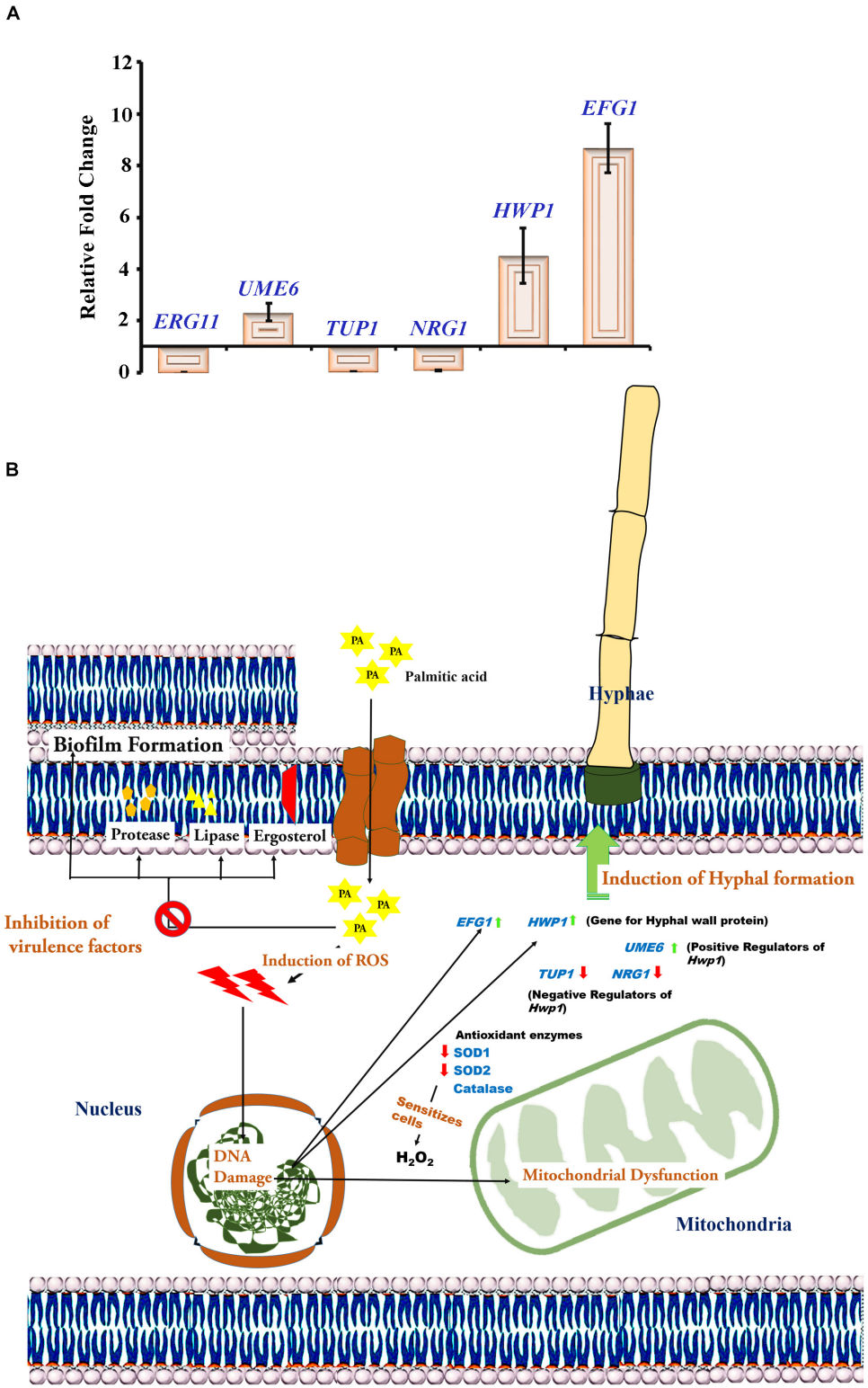

FIGURE 8 | (A) Gene expression analysis untreated and PA-treated of *C. tropicalis* at 200 μg mL^{-1} after 48 h. Effect of PA on the differential expression of *ERG11*, *TUP1, NRG1, HWP1, UME6* and *EFG1* using qPCR. The values are expressed as means and error bars indicate standard deviation. **(B)** Molecular Mechanisms of PA at 200 μg mL^{-1} after 48 h inhibiting specific virulence factors of *C. albicans* such as mature biofilm, ergosterol, lipase, protease and cell surface hydrophobicity but induced hyphal formation.

upregulated in PA-treated *C. tropicalis* (**Figure 8A**). Secreted aspartyl proteases (SAP4-6) are abundant in hyphal cells of *Candida* species. But *SAP4-6* mutants exhibit the filamentation with less invasiveness and the expression of *SAP4-6* is drastically increased in *EFG1* mutants (Felk et al., 2002). Similarly, significant reduction of protease at 200 μg mL^{-1} PA-treated *C. tropicalis* after 48 h of treatment was noticed in the present study (**Figure 6C**). In *C. albicans*, the extent of hyphal formation is associated with increasing ROS generation in germinating cells (Schroter et al., 2000). Many antifungal agents cause apoptosis through ROS generation in cell death mechanisms against *Candida* infections (Peralta et al., 2015). Curcumin, a well-known potential bioactive exhibits ROS mediated inhibition of biofilm in *C. albicans* but reduces hyphae through *TUP1* repressor pathway (Sharma et al., 2010). Thus, it is predicted that PA reduces virulence factors of *C. tropicalis* through ROS mediated apoptosis but induced hyphal formation. The molecular mechanisms of 48 h PA-treated at 200 μg mL^{-1} targeting specific virulence aspects of *C. tropicalis* is presented in **Figure 8B**.

CONCLUSION

The aggregation of *C. tropicalis* biofilm cells enhances their capacity to evade the host defense and to resist conventional antibiotics. The cell-aggregation of biofilm community in close proximity displays similar transcriptomic pattern especially in genes coding for antibiotic resistance (Bjarnsholt et al., 2013). This kind of community is well established in mature biofilm by means of robust exopolymers. Also, the failure of conventional antifungal arises due to the restricted penetration in mature biofilm. The current study explicated that PA at 200 μg mL^{-1} induced ROS and apoptosis in *C. tropicalis* thereby reducing various virulence factors such as mature biofilm, cell surface hydrophobicity, ergosterol, lipases and proteases after 48 h of treatment. Besides, PA induced hyphal formation in *C. tropicalis* with increasing concentrations. In addition, gene expression analysis revealed that PA downregulated *ERG11* and reduced the probability of developing antifungal resistance. Further, PA upregulated genes responsible for hyphal formation, i.e., *EFG1* and *HWP1* that correlates the filamentation assay. Thus, the efficacy of PA targeting biofilm associated virulence, could be used in the synergistic strategy that provides improved therapeutic effects against NCAC infections.

DATA AVAILABILITY STATEMENT

All datasets generated for this study are included in the article/supplementary material.

AUTHOR CONTRIBUTIONS

SP conceived and supervised all the experiments and KP designed the work flow. KP, HT, and MK performed the experiments and data analyses. KP wrote the main manuscript text and prepared all the figures. All authors reviewed the manuscript.

ACKNOWLEDGMENTS

The authors sincerely acknowledge the computational and bioinformatics facility provided by the Bioinformatics Infrastructure Facility (funded by DBT, GOI; File No. BT/BI/25/012/2012, BIF) and University Science Instrumentation Centre (USIC), Alagappa University for CLSM, SEM, and qPCR. The authors also thankfully acknowledge DST-FIST [Grant No. SR/FST/LSI-639/2015(C)], UGC-SAP [Grant No. F.5-1/2018/DRS-II (SAP-II)] and DST-PURSE [Grant No. SR/PURSE Phase 2/38 (G)] for providing instrumentation facilities. KP thanks UGC for financial assistance in the form of a Basic Scientific Research Fellowship [Sanction No. 25-1/2014-15(BSR)/7-326/2011(BSR)]. SP is thankful to UGC for Mid-Career Award [F.19-225/2018(BSR)] and RUSA 2.0 [F.24-51/2014-U, Policy (TN Multi-Gen), Dept. of Edn, GoI].

REFERENCES

Aguirre, J., Ríos-Momberg, M., Hewitt, D., and Hansberg, W. (2005). Reactive oxygen species and development in microbial eukaryotes. *Trends Microbiol.* 13, 111–118. doi: 10.1016/j.tim.2005.01.007

Ahmad, S., Ahmad, S., Bibi, A., Ishaq, M. S., Afridi, M. S., Kanwal, F., et al. (2014). Phytochemical analysis, antioxidant activity, fatty acids composition, and functional group analysis of *Heliotropium bacciferum*. *Sci. World J.* 2014:829076. doi: 10.1155/2014/829076

Al-Fattani, M. A., and Douglas, L. J. (2004). Penetration of *Candida* biofilms by antifungal agents. *Antimicrob. Agents Chemother.* 48, 3291–3297. doi: 10.1128/AAC.48.9.3291-3297.2004

Arif, T., Bhosale, J. D., Kumar, N., Mandal, T. K., Bendre, R. S., Lavekar, G. S., et al. (2009). Natural products–antifungal agents derived from plants. *J. Asian Nat. Prod. Res.* 11, 621–638. doi: 10.1080/10286020902942350

Arthington-Skaggs, B. A., Jradi, H., Desai, T., and Morrison, C. J. (1999). Quantitation of ergosterol content: novel method for determination of fluconazole susceptibility of *Candida albicans*. *J. Clin. Microbiol.* 37, 3332–3337.

Asmundsdottir, L. R., Erlendsdottir, H., and Gottfredsson, M. (2012). Nationwide study of candidemia, antifungal use and antifungal drug resistance in Iceland, 2000-2011. *J. Clin. Biol.* 51, 841–848. doi: 10.1128/JCM.02566-12

Bjarnsholt, T., Ciofu, O., Molin, S., Givskov, M., and Hoiby, N. (2013). Applying insights from biofilm biology to drug development—can a new approach be developed? *Nat. Rev. Drug Discov.* 12, 791–808. doi: 10.1038/nrd4000

Blankenship, J. R., and Mitchell, A. P. (2006). How to build a biofilm: a fungal perspective. *Curr. Opin. Microbiol.* 9, 588–594. doi: 10.1016/j.mib.2006.10.003

Bowler, L. L., Zhanel, G. G., Ball, T. B., and Saward, L. L. (2012). Mature *Pseudomonas aeruginosa* biofilms prevail compared to young biofilms in the presence of ceftazidime. *Antimicrob. Agents Chemother.* 56, 4976–4979. doi: 10.1128/AAC.00650-12

Braun, B. R., and Johnson, A. D. (1997). Control of filament formation in *Candida albicans* by the transcriptional repressor TUP1. *Science* 277, 105–109. doi: 10.1126/science.277.5322.105

Braun, B. R., and Johnson, A. D. (2000). TUP1, CPH1 and EFG1 make independent contributions to filamentation in *Candida albicans*. *Genetics* 155, 57–67.

Braun, B. R., Kadosh, D., and Johnson, A. D. (2001). NRG1, a repressor of filamentous growth in *C. albicans*, is down-regulated during filament induction. *EMBO J.* 20, 4753–4761. doi: 10.1093/emboj/20.17.4753

Cavalheiro, M., and Teixeira, M. C. (2018). *Candida* biofilms: threats, challenges, and promising strategies. *Front. Med.* 5:28. doi: 10.3389/fmed.2018.00028

Chakrabarti, A., Sood, P., Rudramurthy, S. M., Chen, S., Kaur, H., Capoor, M., et al. (2015). Incidence, characteristics and outcome of ICU-acquired candidemia in India. *Intensive Care Med.* 41, 285–295. doi: 10.1007/s00134-014-3603-2

Chandra, J., and Ghannoum, M. A. (2018). CD101, a novel echinocandin, possesses potent antibiofilm activity against early and mature *Candida albicans* biofilms. *Antimicrob. Agents Chemother.* 62:e01750-17. doi: 10.1128/AAC.01750-17

Cleveland, A. A., Farley, M. M., Harrison, L. H., Stein, B., Hollick, R., Lockhart, S. R., et al. (2012). Changes in incidence and antifungal drug resistance in candidemia: results from population-based laboratory surveillance in Atlanta and Baltimore, 2008–2011. *Clin. Infect. Dis.* 55, 1352–1361. doi: 10.1093/cid/cis697

CLSI (2017). *Reference Method for Broth Dilution Antifungal Susceptibility Testing of Yeasts— Fourth Edition: M27*. Wayne, PA: Clinical and Laboratory Standards Institute. doi: 10.1093/cid/cis697

Costerton, J. W., Stewart, P. S., and Greenberg, E. P. (1999). Bacterial biofilms: a common cause of persistent infections. *Science* 284, 1318–1322. doi: 10.1126/science.284.5418.1318

Crowley, L. C., Marfell, B. J., Scott, A. P., and Waterhouse, N. J. (2016). Quantitation of apoptosis and necrosis by annexin V binding, propidium iodide uptake, and flow cytometry. *Cold Spring Harb. Protoc.* 2016:pdb prot087288. doi: 10.1101/pdb.prot087288

Delattin, N., Cammue, B. P., and Thevissen, K. (2014). Reactive oxygen species-inducing antifungal agents and their activity against fungal biofilms. *Future Med. Chem.* 6, 77–90. doi: 10.4155/fmc.13.189

Dimopoulos, G., Ntziora, F., Rachiotis, G., Armaganidis, A., and Falagas, M. E. (2008). *Candida albicans* versus non-albicans intensive care unit-acquired bloodstream infections: differences in risk factors and outcome. *Anesth. Analg.* 106, 523–529. doi: 10.1213/ane.0b013e3181607262

Faul, F., Erdfelder, E., Lang, A.-G., and Buchner, A. (2007). G*Power 3: a flexible statistical power analysis program for the social, behavioral, and biomedical sciences. *Behav. Res. Methods* 39, 175–191. doi: 10.3758/bf03193146

Felk, A., Kretschmar, M., Albrecht, A., Schaller, M., Beinhauer, S., Nichterlein, T., et al. (2002). *Candida albicans* hyphal formation and the expression of the Efg1-regulated proteinases Sap4 to Sap6 are required for the invasion of parenchymal organs. *Infect. Immun.* 70, 3689–3700. doi: 10.1128/iai.70.7.3689-3700.2002

Gleason, J. E., Li, C. X., Odeh, H. M., and Culotta, V. C. (2014). Species-specific activation of cu/Zn SOD by its CCS copper chaperone in the pathogenic yeast *Candida albicans*. *J. Biol. Inorg. Chem.* 19, 595–603. doi: 10.1007/s00775-013-1045-x

Gokce, G., Cerikcioglu, N., and Yagci, A. (2007). Acid proteinase, phospholipase, and biofilm production of *Candida* species isolated from blood cultures. *Mycopathologia* 164, 265–269. doi: 10.1007/s11046-007-9053-4

Gowrishankar, S., Kamaladevi, A., Balamurugan, K., and Pandian, S. K. (2016). *In vitro and in vivo* biofilm characterization of methicillin-resistant *Staphylococcus aureus* from patients associated with pharyngitis infection. *Biomed. Res. Int.* 2016:1289157. doi: 10.1155/2016/1289157

Gudlaugsson, O., Gillespie, S., Lee, K., Berg, J. V., Hu, J., Messer, S., et al. (2003). Attributable mortality of nosocomial candidemia, revisited. *Clin. Infect. Dis.* 37, 1172–1177. doi: 10.1086/378745

Haimovitz-Friedman, A., Kolesnick, R. N., and Fuks, Z. (1997). Ceramide signaling in apoptosis. *Br. Med. Bull.* 53, 539–553. doi: 10.1093/oxfordjournals.bmb.a011629

Hassett, D. J., Elkins, J. G., Ma, J. F., and McDermott, T. R. (1998). *Pseudomonas aeruginosa* biofilm sensitivity to biocides: use of hydrogen peroxide as model antimicrobial agent for examining resistance mechanisms. *Methods Enzymol.* 310, 599–608. doi: 10.1016/s0076-6879(99)10046-6

Henry, K. W., Nickels, J. T., and Edlind, T. D. (2000). Upregulation of ERG genes in *Candida* species by azoles and other sterol biosynthesis inhibitors. *Antimicrob Agents Chemother.* 44, 2693–2700. doi: 10.1128/aac.44.10.2693-2700.2000

Henry-Mowatt, J., Dive, C., Martinou, J. C., and James, D. (2004). Role of mitochondrial membrane permeabilization in apoptosis and cancer. *Oncogene* 23, 2850–2860. doi: 10.1038/sj.onc.1207534

Hesstvedt, L., Gaustad, P., Andersen, C. T., Haarr, E., Hannula, R., Haukland, H. H., et al. (2015). Twenty-two years of candidaemia surveillance: results from a Norwegian national study. *Clin. Microbiol. Infect.* 21, 938–945. doi: 10.1016/j.cmi.2015.06.008

Huang, C. B., Alimova, Y., Myers, T. M., and Ebersole, J. L. (2011). Short-and medium-chain fatty acids exhibit antimicrobial activity for oral microorganisms. *Arch. Oral Biol.* 56, 650–654. doi: 10.1016/j.archoralbio.2011.01.011

Ji, H., Zhang, W., Zhou, Y., Zhang, M., Zhu, J., Song, Y., et al. (2000). A three-dimensional model of lanosterol 14α-demethylase of *Candida albicans* and its interaction with azole antifungals. *J. Med. Chem.* 43, 2493–2505. doi: 10.1021/jm990589g

Kaur, R., Dhakad, M. S., Goyal, R., and Kumar, R. (2016). Emergence of non-albicans *Candida* species and antifungal resistance in intensive care unit patients. *Asian Pac. J. Trop. Biomed.* 6, 455–460.

Koressaar, T., and Remm, M. (2007). Enhancements and modifications of primer design program Primer3. *Bioinformatics* 23, 1289–1291. doi: 10.1093/bioinformatics/btm091

Kothavade, R. J., Kura, M. M., Valand, A. G., and Panthaki, M. H. (2010). *Candida tropicalis*: its prevalence, pathogenicity and increasing resistance to fluconazole. *J. Med. Microbiol.* 59, 873–880. doi: 10.1099/jmm.0.013227-0

Kumari, K. S., Raghunath, P., Harshavardhan, B., and Chaudhury, A. (2014). Distribution of *Candida albicans* and the non-albicans *Candida* species in different clinical specimens from South India. *Int. J. Microbiol. Res.* 5, 1–5. doi: 10.5829/idosi.ijmr.2014.5.1.8232

Li, Z., and Nielsen, K. (2017). Morphology changes in human fungal pathogens upon interaction with the host. *J. Fungi (Basel)* 3:66. doi: 10.3390/jof3040066

Listenberger, L. L., Ory, D. S., and Schaffer, J. E. (2001). Palmitate-induced apoptosis can occur through a ceramide-independent pathway. *J. Biol. Chem.* 276, 14890–14895. doi: 10.1074/jbc.M010286200

Liu, H., Kohler, J., and Fink, G. R. (1994). Suppression of hyphal formation in *Candida albicans* by mutation of a STE12 homolog. *Science* 266, 1723–1726. doi: 10.1126/science.7992058

Liu, K., Liu, P. C., Liu, R., and Wu, X. (2015). Dual AO/EB staining to detect apoptosis in osteosarcoma cells compared with flow cytometry. *Med. Sci. Monit. Basic Res.* 21, 15–20. doi: 10.12659/MSMBR.893327

Lv, Q. Z., Yan, L., and Jiang, Y. Y. (2016). The synthesis, regulation, and functions of sterols in *Candida albicans*: well-known but still lots to learn. *Virulence* 7, 649–659. doi: 10.1080/21505594.2016.1188236

Maedler, K., Spinas, G. A., Dyntar, D., Moritz, W., Kaiser, N., and Donath, M. Y. (2001). Distinct effects of saturated and monounsaturated fatty acids on -cell turnover and function. *Diabetes* 50, 69–76. doi: 10.2337/diabetes.50.1.69

Miller, D. J., and Mejicano, G. C. (2001). Vertebral osteomyelitis due to *Candida* species: case report and literature review. *Clin. Infect. Dis.* 33, 523–530. doi: 10.1086/322634

Missoni, E. M., Rade, D., Nederal, S., Kalenic, S., Kern, J., and Babic, V. V. (2005). Differentiation between *Candida* species isolated from diabetic foot by fatty acid methyl ester analysis using gas chromatography. *J. Chromatogr. B. Analyt. Technol. Biomed. Life Sci.* 822, 118–123. doi: 10.1016/j.jchromb.2005.06.002

Monroy-Pérez, E., Paniagua-Contreras, G. L., Rodríguez-Purata, P., Vaca-Paniagua, F., Vázquez-Villaseñor, M., Díaz-Velásquez, C., et al. (2016). High virulence and antifungal resistance in clinical strains of *Candida albicans*. *Can. J. Infect. Dis. Med. Microbiol.* 2016:5930489. doi: 10.1155/2016/5930489

Montanaro, L., Poggi, A., Visai, L., Ravaioli, S., Campoccia, D., Speziale, P., et al. (2011). Extracellular DNA in biofilms. *Int. J. Artif. Organ.* 34, 824–831. doi: 10.5301/ijao.5000051

Muthamil, S., Balasubramaniam, B., Balamurugan, K., and Pandian, S. K. (2018). Synergistic effect of quinic acid derived from *Syzygium cumini* and undecanoic acid against *Candida* spp. biofilm and virulence. *Front. Microbiol.* 9:2835. doi: 10.3389/fmicb.2018.02835

Nguyen, L. N., and Nosanchuk, J. D. (2011). Lipid droplet formation protects against gluco/lipotoxicity in *Candida parapsilosis*: an essential role of fatty acid desaturase Ole1. *Cell Cycle* 10, 3159–3167. doi: 10.4161/cc.10.18.16932

Nguyen, L. N., Trofa, D., and Nosanchuk, J. D. (2009). Fatty acid synthase impacts the pathobiology of *Candida parapsilosis* in vitro and during mammalian infection. *PLoS One* 4:e8421. doi: 10.1371/journal.pone.0008421

Nobile, C. J., Schneider, H. A., Nett, J. E., Sheppard, D. C., Filler, S. G., Andes, D. R., et al. (2008). Complementary adhesin function in *C. albicans* biofilm formation. *Curr. Biol.* 18, 1017–1024. doi: 10.1016/j.cub.2008.06.034

Noumi, E., Snoussi, M., Hentati, H., Mahdouani, K., Del Castillo, L., Valentin, E., et al. (2010). Adhesive properties and hydrolytic enzymes of oral *Candida albicans* strains. *Mycopathologia* 169, 269–278. doi: 10.1007/s11046-009-9259-8

Nucci, M., Queiroz-Telles, F., Alvarado-Matute, T., Tiraboschi, I. N., Cortes, J., Zurita, J., et al. (2013). Epidemiology of candidemia in Latin America: a laboratory-based survey. *PLoS One* 8:e59373. doi: 10.1371/journal.pone.0059373

Orsi, C. F., Borghi, E., Colombari, B., Neglia, R. G., Quaglino, D., Ardizzoni, A., et al. (2014). Impact of *Candida albicans* hyphal wall protein 1 (HWP1) genotype on biofilm production and fungal susceptibility to microglial cells. *Microb. Pathog.* 69, 20–27. doi: 10.1016/j.micpath.2014.03.003

Ott, M., Gogvadze, V., Orrenius, S., and Zhivotovsky, B. (2007). Mitochondria, oxidative stress and cell death. *Apoptosis* 12, 913–922. doi: 10.1007/s10495-007-0756-2

Pahwa, N., Kumar, R., Nirkhiwale, S., and Bandi, A. (2014). Species distribution and drug susceptibility of *Candida* in clinical isolates from a tertiary care centre at Indore. *Indian J. Med. Microbiol.* 32, 44–48. doi: 10.4103/0255-0857.124300

Park, M., Do, E., and Jung, W. H. (2013). Lipolytic enzymes involved in the virulence of human pathogenic fungi. *Mycobiology* 41, 67–72. doi: 10.5941/MYCO.2013.41.2.67

Pathirana, R. U., McCall, A. D., Norris, H. L., and Edgerton, M. (2019). Filamentous non-albicans *Candida* species adhere to *Candida albicans* and benefit from dual biofilm growth. *Front. Microbiol.* 10:1188. doi: 10.3389/fmicb.2019.01188

Peralta, M. A., da Silva, M. A., Ortega, M. G., Cabrera, J. L., and Paraje, M. G. (2015). Antifungal activity of a prenylated flavonoid from Dalea elegans against *Candida albicans* biofilms. *Phytomedicine* 22, 975–980. doi: 10.1016/j.phymed.2015.07.003

Poikonen, E., Lyytikainen, O., Anttila, V. J., Koivula, I., Lumio, J., Kotilainen, P., et al. (2010). Secular trend in candidemia and the use of fluconazole in Finland, 2004-2007. *BMC Infect. Dis.* 10:312. doi: 10.1186/1471-2334-10-312

Prasath, K. G., Sethupathy, S., and Pandian, S. K. (2019). Proteomic analysis uncovers the modulation of ergosterol, sphingolipid and oxidative stress pathway by myristic acid impeding biofilm and virulence in *Candida albicans*. *J. Proteomics* 208:103503. doi: 10.1016/j.jprot.2019.103503

Rajavel, T., Packiyaraj, P., Suryanarayanan, V., Singh, S. K., Ruckmani, K., and Devi, K. P. (2018). β-Sitosterol targets Trx/Trx1 reductase to induce apoptosis in A549 cells via ROS mediated mitochondrial dysregulation and p53 activation. *Sci. Rep.* 8:2071. doi: 10.1038/s41598-018-20311-6

Ramage, G., Saville, S. P., Wickes, B. L., and Lopez−Ribot, J. L. (2002). Inhibition of *Candida albicans* biofilm formation by farnesol, a quorum−sensing molecule. *Appl. Environ. Microbiol.* 68, 5459–5463. doi: 10.1128/aem.68.11.5459-5463.2002

Ramnath, L., Sithole, B., and Govinden, R. (2017). Identification of lipolytic enzymes isolated from bacteria indigenous to Eucalyptus wood species for application in the pulping industry. *Biotechnol. Rep.* 15, 114–124. doi: 10.1016/j.btre.2017.07.004

Rates, S. M. (2001). Plants as source of drugs. *Toxicon* 39, 603–613. doi: 10.1016/S0041-0101(00)00154-9

Ray, P. D., Huang, B. W., and Tsuji, Y. (2012). Reactive oxygen species (ROS) homeostasis and redox regulation in cellular signaling. *Cell. Signal.* 24, 981–990. doi: 10.1016/j.cellsig.2012.01.008

Reiter, K. C., Sambrano, G. E., Villa, B., Paim, T. G., Oliveira, C. F., and d'Azevedo, P. A. (2012). Rifampicin fails to eradicate mature biofilm formed by methicillin-resistant *Staphylococcus aureus*. *Rev. Soc. Bras. Med. Trop.* 45, 471–474. doi: 10.1590/s0037-86822012000400011

Schmitt, M. E., Brown, T. A., and Trumpower, B. L. (1990). A rapid and simple method for preparation of RNA from *Saccharomyces cerevisiae*. *Nucleic Acids Res.* 18, 3091–3092. doi: 10.1093/nar/18.10.3091

Schroter, C., Hipler, U. C., Wilmer, A., Kunkel, W., and Wollina, U. (2000). Generation of reactive oxygen species by *Candida albicans* in relation to morphogenesis. *Arch. Dermatol. Res.* 292, 260–264. doi: 10.1007/s004030050484

Selvaraj, A., Jayasree, T., Valliammai, A., and Pandian, S. K. (2019). Myrtenol attenuates MRSA biofilm and virulence by suppressing sarA expression dynamism. *Front. Microbiol.* 10:2027. doi: 10.3389/fmicb.2019.02027

Seneviratne, C. J., Wang, Y., Jin, L., Abiko, Y., and Samaranayake, L. P. (2008). *Candida albicans* biofilm formation is associated with increased anti−oxidative capacities. *Proteomics* 8, 2936–2947. doi: 10.1002/pmic.200701097

Sethupathy, S., Prasath, K. G., Ananthi, S., Mahalingam, S., Balan, S. Y., and Pandian, S. K. (2016). Proteomic analysis reveals modulation of iron homeostasis and oxidative stress response in *Pseudomonas aeruginosa* PAO1 by curcumin inhibiting quorum sensing regulated virulence factors and biofilm production. *J. Proteome* 145, 112–126. doi: 10.1016/j.jprot.2016.04.019

Shanmuganathan, B., Sathya, S., Balasubramaniam, B., Balamurugan, K., and Devi, K. P. (2019). Amyloid-β induced neuropathological actions are suppressed by *Padina gymnospora* (Phaeophyceae) and its active constituent α-bisabolol in Neuro2a cells and transgenic *Caenorhabditis elegans* Alzheimer's model. *Nitric Oxide* 91, 52–66. doi: 10.1016/j.niox.2019.07.009

Sharma, M., Manoharlal, R., Puri, N., and Prasad, R. (2010). Antifungal curcumin induces reactive oxygen species and triggers an early apoptosis but prevents hyphae development by targeting the global repressor TUP1 in *Candida albicans*. *Biosci. Rep.* 30, 391–404. doi: 10.1042/BSR20090151

Sivasankar, C., Ponmalar, A., Bhaskar, J. P., and Pandian, S. K. (2015). Glutathione as a promising anti−hydrophobicity agent against *Malassezia* spp. *Mycoses* 58, 620–631. doi: 10.1111/myc.12370

Song, J. L., Harry, J. B., Eastman, R. T., Oliver, B. G., and White, T. C. (2004). *Candida albicans* lanosterol 14-alpha-demethylase (ERG11) gene promoter is maximally induced after prolonged growth with antifungal drugs. *Antimicrob. Agents Chemother.* 48, 1136–1144. doi: 10.1128/aac.48.4.1136-1144.2004

Staib, F. (1965). Serum-proteins as nitrogen source for yeastlike fungi. *Sabouraudia* 4, 187–193. doi: 10.1080/00362176685190421

Taff, H. T., Mitchell, K. F., Edward, J. A., and Andes, D. R. (2013). Mechanisms of *Candida* biofilm drug resistance. *Fut. Microbiol.* 8, 1325–1337. doi: 10.2217/fmb.13.101

Tang, L., Thevenot, P., and Hu, W. (2008). Surface chemistry influences implant biocompatibility. *Curr. Top. Med. Chem.* 8, 270–280. doi: 10.2174/156802608783790901

Untergasser, A., Cutcutache, I., Koressaar, T., Ye, J., Faircloth, B. C., Remm, M., et al. (2012). Primer3 - new capabilities and interfaces. *Nucleic Acids Res.* 40:e115. doi: 10.1093/nar/gks596

Uppuluri, P., Mekala, S., and Chaffin, W. L. (2007). Farnesol−mediated inhibition of *Candida albicans* yeast growth and rescue by a diacylglycerol analogue. *Yeast* 24, 681–693. doi: 10.1002/yea.1501

Wang, C., and Youle, R. J. (2009). The role of mitochondria in apoptosis. *Annu. Rev. Genet.* 43, 95–118. doi: 10.1146/annurev-genet-102108-134850

Xess, I., Jain, N., Hasan, F., Mandal, P., and Banerjee, U. (2007). Epidemiology of candidemia in a tertiary care centre of north India: 5-year study. *Infection* 35, 256–259. doi: 10.1007/s15010-007-6144-6

Xiang, M. J., Liu, J. Y., Ni, P. H., Wang, S., Shi, C., Wei, B., et al. (2013). Erg11 mutations associated with azole resistance in clinical isolates of *Candida albicans*. *FEMS Yeast Res.* 13, 386–393. doi: 10.1111/1567-1364.12042

Yang, D., Pornpattananangkul, D., Nakatsuji, T., Chan, M., Carson, D., Huang, C. M., et al. (2009). The antimicrobial activity of liposomal lauric acids against *Propionibacterium acnes*. *Biomaterials* 30, 6035–6040. doi: 10.1016/j.biomaterials.2009.07.033

Conflict of Interest: The authors declare that the research was conducted in the absence of any commercial or financial relationships that could be construed as a potential conflict of interest.

frontiers in Microbiology

ORIGINAL RESEARCH
published: 20 May 2020
doi: 10.3389/fmicb.2020.00975

Precision Antifungal Treatment Significantly Extends Voice Prosthesis Lifespan in Patients Following Total Laryngectomy

*Daniel R. Pentland[1], Sarah Stevens[2], Leila Williams[2], Mark Baker[2], Carolyn McCall[2], Viktorija Makarovaite[1], Alistair Balfour[2], Friedrich A. Mühlschlegel[3] and Campbell W. Gourlay[1]**

[1] Kent Fungal Group, School of Biosciences, University of Kent, Kent, United Kingdom, [2] East Kent Hospitals, University NHS Foundation Trust, Kent, United Kingdom, [3] Laboratoire National de Santé, Dudelange, Luxembourg

Indwelling silicone valves called voice prostheses (VPs) are the gold standard for speech rehabilitation in patients with laryngeal cancer following total laryngectomy. Reported VP lifespans amongst these patients are highly variable but when devices fail patients experience loss of voice and an increase risk of chest infection. Early failure of VP is a current clinical concern that is associated with regular hospital visits, reduced quality of life and associated medical cost. Poly-microbial biofilms comprised of both bacterial and fungal microorganisms readily colonize VPs and are linked to loss of device performance and its early failure in addition to providing a reservoir for potential infection. Our detailed analysis of poly-microbial biofilm composition on 159 early failing VPs from 48 total laryngectomy patients confirmed *Candida albicans* as the predominant fungal species and *Staphylococcus aureus* as the most common bacterial colonizer within our patient cohort. Using a combination of microbiological analysis, patient data and a high-throughput antifungal test assay mimicking *in vivo* conditions we established an evidence based precision antifungal treatment approach to VP management. Our approach has allowed us to implement a personalized VP management pathway, which increases device *in situ* lifespan by an average of 270%. Our study represents a significant step forward in both our understanding of the cause of VP failure and a new effective treatment pathway that offers tangible benefit to patients.

Keywords: *Candida*, voice prosthesis, laryngectomy, speech therapy, microbiology, antifungal

OPEN ACCESS

Edited by:
Juliana Campos Junqueira, São Paulo State University, Brazil

Reviewed by:
Renátó Kovács, University of Debrecen, Hungary
Patrícia Pimentel Barros, São Paulo State University, Brazil

****Correspondence:***
Campbell W. Gourlay
C.W.Gourlay@kent.ac.uk

Specialty section:
This article was submitted to Fungi and Their Interactions, a section of the journal Frontiers in Microbiology

Received: *17 December 2019*
Accepted: *22 April 2020*
Published: *20 May 2020*

Citation:
Pentland DR, Stevens S, Williams L, Baker M, McCall C, Makarovaite V, Balfour A, Mühlschlegel FA and Gourlay CW (2020) Precision Antifungal Treatment Significantly Extends Voice Prosthesis Lifespan in Patients Following Total Laryngectomy. Front. Microbiol. 11:975. doi: 10.3389/fmicb.2020.00975

INTRODUCTION

Head and neck cancer is the sixth most common cancer worldwide and the eighth most common cancer in the United Kingdom with 650,000 new cases (12,000 in the United Kingdom) and 350,000 deaths (4,000 in the United Kingdom) attributed to it each year worldwide (Leonhard and Schneider-Stickler, 2015; Cancer Research UK, 2018). Laryngeal malignancy is the most frequent head and neck cancer, making up 26.2% of newly diagnosed male cases and 13.1% of female cases in the United Kingdom (Cancer Research UK, 2018). Laryngeal malignancy is treated with radiotherapy if it is diagnosed at an early stage, however, at later stages treatment involves surgery often in conjunction with radiotherapy (Brook, 2013). The majority of head and neck cancers are diagnosed at an advanced stage; for example 62% of new diagnoses in Northern Ireland are reported to be at Stage III or Stage IV (Stage IV alone accounts for 45%) (Cancer Research UK, 2018). Late diagnosis means that many cases of

laryngeal cancer have to undergo a partial or total laryngectomy. It has been estimated that there are currently 50,000–60,000 laryngectomees living in the United States (Brook, 2013).

Following a laryngectomy, the patient will no longer be able to form speech on their own. The gold standard for speech rehabilitation is tracheesophageal speech which requires the use of a small silicone valve known as a voice prosthesis (VP) (Bunting, 2004). Voice prostheses are susceptible to colonization by microbial biofilms (Busscher et al., 1997a). Such contamination may be enhanced by the environment of the esophagus, e.g., foods, liquids (including saliva), humidity and constant temperature (Holmes et al., 2014; Talpaert et al., 2015), and device failure has been attributed to such microbial growth as it can prevent valve closure (Leunisse et al., 2001; Oosterhof et al., 2005) and leakage of esophageal contents into the trachea. A loss of valve functionality leads to poor speech and requires replacement of the device (Ticac et al., 2010; Leonhard and Schneider-Stickler, 2015). Moreover, the microbial colonization may act as a reservoir of potential pathogens which, subsequent to aspiration, may lead to life-threatening infections such as pneumonia (Delank and Scheuermann, 2008). The mean VP lifespan is highly variable across different studies and has historically been reported as being between 120 and 200 days (Schafer et al., 2001; Sayed et al., 2012). However, a recent large-scale study which analyzed the lifespan of 3648 VPs reported an average of 86 days (Lewin et al., 2017). A number of strategies have been proposed to increase VP lifespan, such as the use of magnets to support the closing of the valve (Hilgers et al., 2003) and the incorporation of compounds, for example silver oxide, within the VP material to prevent microbial colonization (Hilgers et al., 2009). VPs containing magnets such as the Provox ActiValve have been shown to have longer *in situ* lifespans than other models (Kress et al., 2014; Lewin et al., 2017). However, overall, the levels of success with these approaches has been variable and importantly the average VP device lifespan has not significantly increased over the last 10 years (Lewin et al., 2017).

Co-colonization of VPs by bacterial and fungal species within poly-microbial biofilms is commonly reported. However, it is not clear to what extent yeast and bacterial biofilm colonization contributes to early VP failure, nor how effective their prevention may be in extending device lifespan. Medically, biofilms are of particular importance because it is thought that a significant percentage of human microbial infections include biofilm formation (Costerton et al., 1999; Donlan, 2001a,b). Furthermore, cells within biofilms can be up to 1000x more resistant to antimicrobial treatment than their planktonic counterparts (Chandra et al., 2001; Donlan and Costerton, 2002). The exact microbial composition on any particular VPs is influenced by several factors including patient diet, lifestyle and the voice prosthesis management regime to which they subscribe (Talpaert et al., 2015).

Streptococcal species such as *Streptococcus mitis* and *Streptococcus sobrinus*, *Staphylococcal* species such as *Staphylococcus aureus* (Neu et al., 1994), and *Pseudomonas aeruginosa* (Sayed et al., 2012) are among the major bacterial microorganisms frequently isolated from VPs biofilms. *Candida albicans* is reported as the most prevalent fungal colonizer of a VP surface (Bauters et al., 2002; Buijssen et al., 2012), it is a commensal yeast that is found on the mucosal surfaces of the oral cavity, gastrointestinal tract and genitourinary tract of most healthy individuals (Berman and Sudbery, 2002; Ganguly and Mitchell, 2011). *C. albicans* is a dimorphic fungus and biofilm formation of this organism involves a switch from growing in the typical budding yeast form to a filamentous hyphal form.

Here we characterize the microflora found on early failing voice prosthesis from 48 patients within Kent (South East United Kingdom) over a 5-year period (2011–2016). We observed that multi-species biofilms form in most cases, with *C. albicans* and *S. aureus* being the most prevalent. We demonstrate that the high CO_2 environment experienced in the airway promotes *C. albicans* biofilm formation on VPs, providing an explanation for its prevalence on these devices. To determine whether yeast colonization acts as a driver for early VP failure we devised an evidence based strategy to manage contamination using a newly developed high-throughput assay that mimics *in situ* conditions in combination with drug sensitivity data. We report results from a 20 patient study that applies our principles of precision antimicrobial assessment that verifies antifungal treatment as a highly effective approach to VP lifespan extension. The study documented voice prosthesis lifespan pre- and post-management pathway implementation and statistical analyses confirmed a significant increase in VP lifespan within the patient cohort. Our guidelines represent a significant advance in both our understanding of the underlying cause of VP failure and a new effective method to increase VP lifespan by an average of 2.7-fold.

MATERIALS AND METHODS

Patient Cohort and Voice Prostheses

Biofilms from a total of 159 early failing VPs from 48 patients (41 males and 7 females; mean age = 69.5 years, range 35–90 years) were analyzed for microorganism composition over a 5-year period (2011–2016). All prostheses were removed from patients attending one of the three main acute hospital sites within East Kent, United Kingdom: William Harvey Hospital, Ashford; Canterbury Hospital, Canterbury; Queen Elizabeth the Queen Mother Hospital, Margate. 38 of these patients had multiple voice prosthesis failures and were followed as part of a *Candida* management guideline impact study, which documented the voice prosthesis lifespans before and after implementation of a set of treatment guidelines designed to limit fungal growth. Treatment guidelines for the treatment of VPs with anti-fungal drugs were approved by the East Kent Hospital University Foundation Trust (EKHUFT) Voice Prosthesis Infection Management Multi-disciplinary team (MDT), EKHUFT Antimicrobial Stewardship Group, EKHUFT Drugs and Therapeutics Committee, EKHUFT ENT Audit Group, EKHUFT Adult Speech and Language Therapy Service, East Kent Prescribing Group. This study was approved by the EKHUFT Research and Innovation Department (2018/GAP/20) in accordance with the Department of Health's Research Governance Framework for Health and Social Care and

EKHUFT Research and Innovation policy. All patient data was anonymised prior to use in this study.

Please contact the corresponding authors for information if you wish to start using the *Candida* Management clinical guidelines for voice prosthesis management used in this study.

Microorganism Isolation and Identification

To determine which microorganisms were present, a failed voice prosthesis was removed from the patient and sealed in a sterile bag. Upon receipt at the microbiology laboratory, the voice prosthesis was added to 2 ml saline solution along with glass beads and vortexed at 2500 rpm for 30 s. The resulting suspension was plated on chromogenic agar to facilitate identification of bacterial species. 50 μl of the suspension was also plated on Sabouraud Dextrose Agar (SDA) plates (Oxoid, CM0041) containing 100 μg/ml chloramphenicol (Oxoid, SR0078) to promote the growth of fungal species while inhibiting bacterial growth. Chromogenic agar and SDA plates were incubated for 48 h at 37°C. Bacterial colonies were then picked from the chromogenic plates and fungal colonies were picked from the SDA plates, species were identified using matrix assisted laser desorption ionization time-of-flight mass spectrometry (MALDI-ToF).

MALDI-ToF Mass Spectrometry Identification of Microorganisms

MALDI-ToF mass spectrometry was used to identify species isolated from failed VPs within this study. Fungal and bacterial colonies were picked and applied to a steel MALDI target plate before being overlaid with an α-cyano-4-hydroxycinnamic acid (4-HCCA) matrix (Sigma-Aldrich, 70990) (Gobom et al., 2001). MALDI-ToF mass spectrometry was performed using a Bruker MALDI Biotyper (Bruker) as per the manufacturer's instructions. The resulting mass spectra were compared to a reference database for identification using the MBT Compass and MBT Explorer Software along with the MBT Compass Library which comprises approximately 2750 species from 471 microorganism genera.

Antifungal Sensitivity Testing

Antifungal sensitivity testing was performed using the Fungitest^{TM} commercial testing kit (BioRad, 60780) as per the manufacturer's instructions. Isolates were assigned sensitive, intermediate, or resistant based upon the European Committee on Antimicrobial Sensitivity Testing (EUCAST) breakpoint recommendations for each antifungal and/or species (European Committee on Antimicrobial Susceptibility Testing, 2018).

Antibacterial Sensitivity Testing

Antibacterial sensitivity testing was carried out to determine the minimum inhibitory concentrations (MICs) of clinically commonly used antibiotics. Isolates were assigned sensitive, intermediate, or resistant based upon the EUCAST breakpoint recommendations for each antibiotic and/or species (European Committee on Antimicrobial Susceptibility Testing, 2019).

Scanning Electron Microscopy (SEM) of Voices Prosthesis Surfaces

Segments were taken from the valve and flange of a Provox Vega voice prosthesis and mounted onto 12.5 mm aluminum SEM specimen stubs (Agar Scientific, AGG301) with superglue. The surfaces were imaged at ambient temperature with a Hitachi S-3400N scanning electron microscope, using the variable pressure scanning electron microscopy (VP-SEM) mode with a chamber pressure of 30 Pa and accelerating voltage of 10 kV. The backscattered electron (BSE) detector in conjunction with the energy dispersive X-ray spectroscopy (EDS) detector was used throughout with a working distance of 10 mm. The acquisition software was Oxford Instruments INCA and images were exported directly from this.

Atomic Force Microscopy (AFM) of Voice Prosthesis Surfaces

Segments were taken from the valve and flange of a Provox Vega voice prosthesis and mounted onto 15 mm AFM specimen disks (Agar Scientific, F7003) with superglue. These surfaces were imaged at ambient temperature using a Bruker Multimode 8 scanning probe microscope with a Nanoscope V controller, using the ScanAsyst peak-force tapping mode with a 50 μm × 50 μm scan area and a 700 nm scan height. SCANASYST-AIR (Bruker) silicon nitride cantilevers (tip height of 2.5–8.0 μm, nominal tip radius of 2 nm) with a nominal spring constant of 0.4 N/m and a resonance frequency of 70 kHz were used throughout. The image acquisition software was Nanoscope 8.15 R3sr5 and the processing software was Nanoscope Analysis.

Candida Strains and Growth Media

Candida strains (**Supplementary Table S3**) were routinely grown at 30°C in yeast peptone dextrose (YPD) media (2% peptone (BD Bacto), 2% D-glucose (Fisher Scientific), 1% yeast extract (BD Bacto). For the biofilm growth assays, *Candida* biofilms were grown at 37°C in RPMI-1640 media (Sigma-Aldrich, R8755) supplemented with 80 μg/ml uridine (Sigma-Aldrich, U3750). *Candida* strains were maintained in YPD + 20% glycerol at −80°C for long-term storage and revived at 30°C on YPD + 2% Technical Agar (Oxoid) plates.

In vitro Biofilm Growth Assays

To investigate fungal biofilm formation and its treatment on VPs a high-throughput assay was developed. *C. albicans* biofilms were grown on a PDMS silicone elastomer (Provincial Rubber, S1). The silicone was cut into 1 cm^2 squares and placed in clips in a modified 24-well plate lid (Academic Centre for Dentistry Amsterdam, AAA-model) so they could be suspended in media within a sterile 24-well plate (Greiner Bio-one, CELLSTAR, 662160). Silicone squares were incubated in 1 ml 50% donor bovine serum (DBS) (Gibco, 16030074) for 30 min at 30°C, then washed twice with 1 ml Phosphate-Buffered Saline (PBS – 137 mM NaCl, 2.7 mM KCl, 10 mM Na_2HPO_4, 1.8 mM KH_2PO_4, pH 7.4) to remove excess DBS. *Candida* strains were inoculated into a test tube containing 5 ml YPD media and placed in a 30°C orbital shaking incubator with constant shaking at 180 rpm for

18 h. OD_{600} measurements were taken and a volume of overnight culture corresponding to OD_{600} = 1.0 (3×10^7 CFU/ml) was removed. These cells were pelleted by centrifugation at 4000 rpm for 5 min at which point the supernatant was discarded. The resultant pellet was re-suspended in 5 ml PBS to wash and centrifuged again at 4000 rpm for 5 min. The PBS supernatant was discarded and the pellet re-suspended in fresh PBS (at an OD_{600} of 1.0). The OD_{600} 1.0 standard cell suspension was added to wells (1 ml per well) in a pre-sterilized 24-well plate and the lid with the silicone squares attached was placed on top so the silicone squares protruded into the cell suspension. These plates were then incubated at 37°C (in either 0.03% CO_2 or 5% CO_2) without shaking for 90 min to allow cell attachment to the silicone. After the attachment phase, the silicone squares were washed twice with 1 ml PBS to remove any unattached cells and transferred to 1 ml RPMI-1640 media (Sigma-Aldrich, R8755). They were then incubated at 37°C (in either 0.03% CO_2 or 5% CO_2) without shaking for up to 48 h to allow biofilm maturation. Growth of biofilms on the surface of a sterile VP was conducted using the same protocol.

Biofilm Quantification via XTT Assay

Biofilm growth was quantified using an XTT assay (Kuhn et al., 2002). Biofilms were washed twice with 1 ml PBS to remove any planktonic cells before proceeding to quantification. After washing, the biofilms were transferred to a new pre-sterilized 24-well plate (Greiner Bio-one, CELLSTAR, 662160) containing 30 μg/ml XTT labeling reagent (Roche, 11465015001) and incubated at 37°C for 4 h. After incubation, the biofilms were removed from the 24-well plate and the absorbance of the remaining XTT labeling reagent was measured at 492 nm using a BMG LABTECH FLUOstar Omega plate reader machine.

Antifungal Treatment of Biofilms

Biofilms were seeded on silicone elastomer sections as described above and grown in RPMI-1640 for 24 h at 37°C. The biofilms were then transferred to fresh RPMI-1640 media containing an antifungal, either; Fluconazole, Miconazole, or Nystatin at indicated concentrations. Fluconazole (Santa Cruz Biotechnology, sc-205698) was made as a 50 mg/ml stock solution in ethanol and diluted in RPMI-1640 final concentrations of 128 and 32 μg/ml. Miconazole (Santa Cruz Biotechnology, sc-205753) was made as a 50 mg/ml stock solution in DMSO and also diluted in RPMI-1640 to final concentrations of 32 and 128 μg/ml. Nystatin (Santa Cruz Biotechnology, sc-212431) was made as a 5 mg/ml stock solution in DMSO and diluted in RPMI-1640 to final concentrations of 2 and 8 μg/ml. Drug vehicle controls (0.25% ethanol for Fluconazole, 0.25% DMSO for Miconazole, and 0.15% DMSO for Nystatin) were used to ensure the solvents were not affecting biofilm growth. The biofilms matured in the RPMI-1640 media containing the select antifungal for a further 24 h at 37°C in both 0.03 and 5% CO_2 before proceeding to quantification via the XTT assay. Experiments were performed in biological and technical triplicate.

Mixed Species Biofilm Competition Assays

Biofilms were set up as described previously, except that for mixed biofilms *C. albicans* and *C. parapsilosis* clinical isolate overnight cultures were each counted and adjusted to 1.5×10^7 CFU/ml to give a 3×10^7 CFU/ml overall inoculum (equivalent to OD_{600} of 1.0) for the 90 min attachment phase. After attachment, the silicone squares were washed twice with 1 ml PBS to remove any unattached cells and transferred to 1 ml RPMI-1640 media (Sigma-Aldrich, R8755). They were then incubated at 37°C in both 0.03% CO_2 or 5% CO_2 without shaking for 48 h to allow biofilm maturation before proceeding to quantification via the XTT assay. Experiment was performed in biological and technical triplicate.

Biofilm Composition Analysis via Chromogenic Agar

Silicone squares with biofilms on them were dropped into 2 ml PBS and vortexed for 10 s at 2500 rpm to release the biofilm cells from the surface. The resulting biofilm cell suspension was plated on Candida Ident Agar (Fluka Analytical, 94382) in triplicate (200 μl per plate). The chromogenic agar plates were incubated at 30°C for 48 h, at which point photographs of the plates were taken. *C. albicans* colonies appeared green and *C. parapsilosis* colonies stayed white on the Candida Ident Agar plates.

Analysis of Voice Prosthesis Lifespans

Voice prosthesis lifespans at the Speech and Language Therapy Centre at the Kent and Canterbury Hospital were investigated over the course of 8 years (2010–2018). In total, 38 patients had their voice prosthesis lifespan documented. However, 18 patients were removed from further analysis due to a lack of adherence to the guidelines, moving out of the hospital catchment area resulting in incomplete data entries, or simply not enough VPs failures/changes in the time period. The voice prosthesis lifespans of the remaining 20 patients, before and after the implementation of our treatment pathway, were analyzed using the Online Application for Survival Analysis 2 (OASIS 2) platform (Kim et al., 2016). In total, 143 VPs before and 176 after implementation of the pathway were included in this study. Kaplan–Meier survival curves were plotted and log-rank tests performed to statistically compare device lifespans before and after the treatment pathway. Wilcoxon Signed-Rank tests were also carried out to determine if the pathway effect was significant when taking into account the inherent differences in device lifespan from patient to patient. For all analyses, the significance level (α) was 0.05.

RESULTS

Analysis of Microorganisms Found on Early Failing Voice Prostheses

*Staphylococcus aureus w*as the most frequently isolated bacterial species (**Figure 1B**), being found on multiple early failing VP (**Figures 1B,C**). This finding is in line with previous

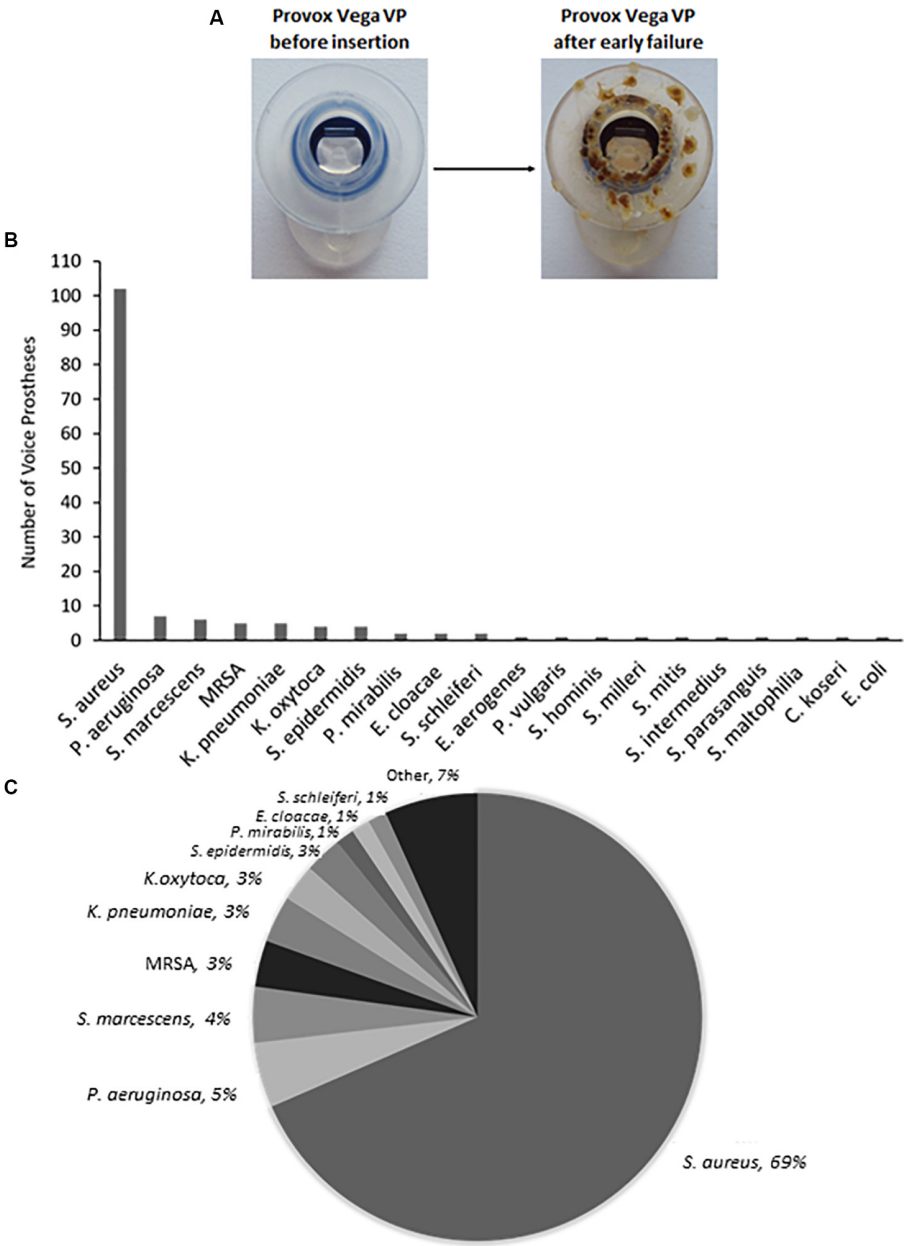

FIGURE 1 | The range and distribution of bacterial species found on voice prostheses within this study. **(A)** An example of a failed voice prosthesis removed from a patient. Note the ring of colonization on the prosthesis hood around the valve mechanism. **(B)** Bar graph representation of absolute numbers of times each bacterial species was isolated from 159 early failing VPs. **(C)** Pie chart representation of percentage of total bacteria isolated from 159 early failing VPs.

studies that also identified *S. aureus* as the prevalent bacterial organism found within VP biofilms (Neu et al., 1994; van Weissenbruch et al., 1997). However, *S. aureus* was one of several *Staphylococcal* species identified, the others being identified at lower frequencies included *Staphylococcus epidermidis* and *Staphylococcus schleiferi* (**Figures 1B,C**). We also identified the *S. aureus* strain methicillin-resistant *S. aureus* (MRSA) on 5 VPs and counted these separately from the rest of the *S. aureus* isolates (**Figures 1B,C**). *P. aeruginosa* was the second most frequent bacterial species found on early failing VPs (**Figures 1B,C**). Previous studies have also identified *P. aeruginosa* as a prevalent bacterial species found within VP biofilms (Sayed et al., 2012). Several *Streptococcus* species were also identified, but at a low frequency, including *Streptococcus milleri*, *Streptococcus mitis,* and *Streptococcus intermedius* (**Supplementary Table S1**).

Yeast species were isolated from the vast majority of the 159 early failing VPs; 107 (67.3%) were colonized by a single yeast species, 37 (23.3%) were colonized by multiple yeast species, and just 15 (9.4%) showed no yeast species presence. In total, 178 yeast isolates were identified and 168 (94.4%) of these

were *Candida* species, the remaining 10 fungal isolates were made up of *Saccharomyces cerevisiae* (8) and *Pichia manshurica* (2). *S. cerevisiae* and *P. manshurica* isolates were normally found alongside *Candida* species (62.5 and 100% respectively). The most frequently isolated yeast species was *C. albicans* (**Figures 2A,B**). This is in line with previous studies which identified *C. albicans* as the yeast species most commonly found on VPs (Everaert et al., 1997; Bauters et al., 2002; Buijssen et al., 2012). The non-*albicans Candida* isolates constituted 44.4% of all fungal isolates, with *Candida glabrata* being the most common of these (**Supplementary Table S2**).

The same bacterial and fungal species were frequently isolated from sequential VPs removed from the same patient implicating a common pattern of biofilm establishment. In total, 38 of the 48 patients had more than one voice prosthesis failure during the course of the study. 30 of these (78.9%) had the same bacterial species present on at least 2 VPs while 29 (76.3%) had the same fungal species on at least 2 VPs. 25 of the 29 patients which had reoccurring fungal species also had the same bacterial species on at least 2 VPs. The most commonly reoccurring fungal species was *C. albicans*, being found on multiple VPs within 18 patients.

It is worth noting that fungal and bacterial species were often found together on early failing VPs, 134 (84.3%) had at least one species of each present. The two most numerous species in this study, *S. aureus* and *C. albicans*, were the most commonly co-isolated species, being found together on 60 (37.7%) VPs. It was very rare for only fungal species to be present; only 10 (6.3%) VPs harbored solely fungal species and intriguingly all of these were either the first or second VP failure of their respective patients. The significance of this, if any, is yet to be determined. The two most commonly co-isolated fungal species were *C. albicans* and *C. glabrata* which were found together on 17 (10.7%) VPs.

It is of importance to highlight that the most prevalent voice prosthesis colonizing organisms within our patient cohort

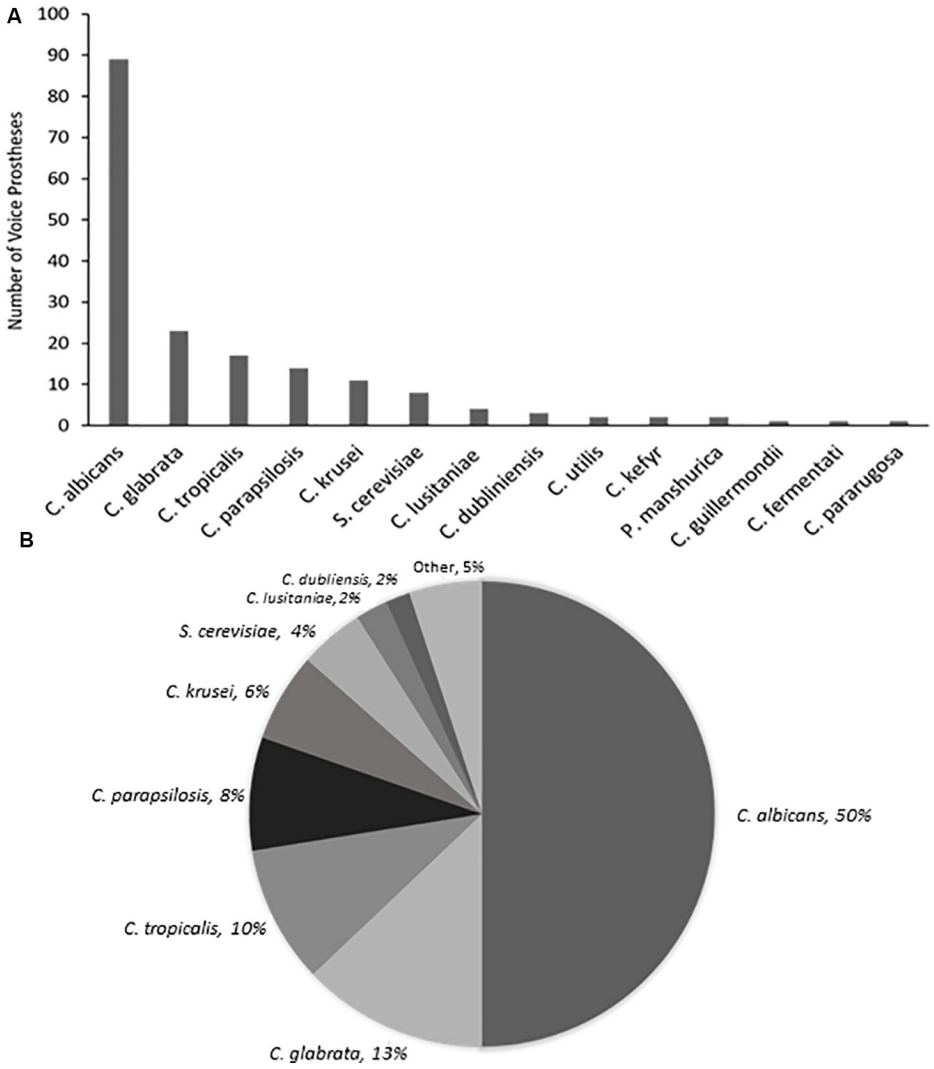

FIGURE 2 | The range and distribution of fungal species found on early failing VP. **(A)** Bar graph representation of absolute numbers of times each yeast species was isolated from 159 early failing VPs. **(B)** Pie chart representation of percentage of total yeast isolated from 159 early failing VPs.

correlate with previous findings. This suggests that an effective treatment plan designed to tackle biofilm formation on VP in our cohort may have wide-reaching applicability.

Factors Promoting Microbial Colonization of Voice Prostheses

Our routine examination of early failing VPs often suggested concentration of microbial growth on certain regions of the device surface (**Figure 1A**). We investigated surface topography using atomic force and scanning electron microscopy as roughness has been shown to be an important driver of colonization (Radford et al., 1998; Nevzatoğlu et al., 2007). The flange (**Figure 3A**) of the device exhibited a significantly rougher topography than the valve which appeared smooth using these high resolution techniques (**Figures 3B,C**). The roughness of the flange was particularly evident in the AFM 3D plot of its surface (**Figure 3D**). In line with previous studies, this may suggest

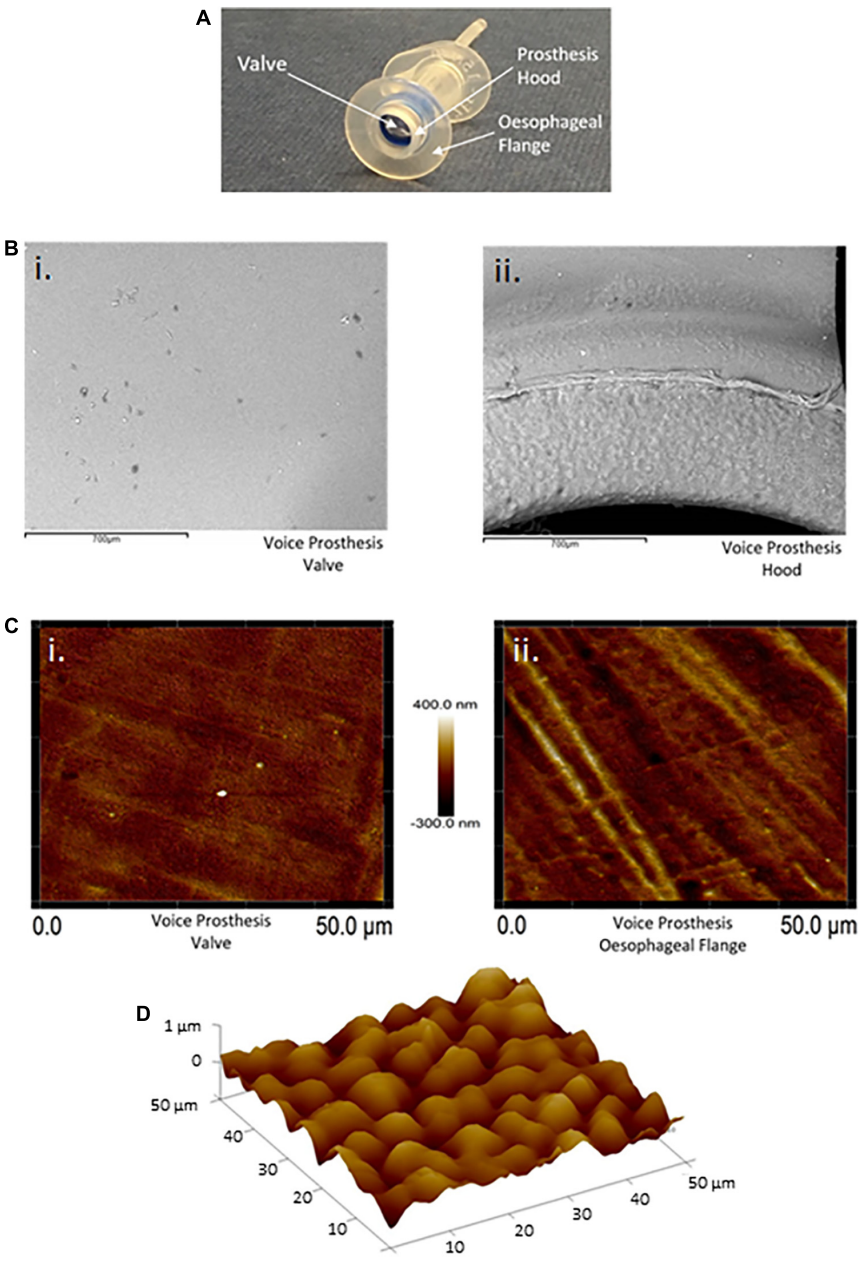

FIGURE 3 | Atomic force and scanning electron microscopy surface topography of the valve and esophageal flange of the Provox Vega voice prosthesis. **(A)** The Provox Vega voice prosthesis. **(B)** SEM images of the valve and inner-side of the prosthesis hood were taken at x120 magnification. The scale bars represent 700 µm. **(C)** AFM images of the valve and esophageal flange were taken of 50 µm × 50 µm surface areas with a scan height of 700 nm. **(D)** AFM 3D plot of a 50 µm × 50 µm area of the esophageal flange. Z-axis is 0–1 µm. Several images were taken and representative examples are presented.

that the flange, specifically the valve-flange interface, provides a more likely site for initial attachment (Leunisse et al., 2001). This proposition is also consistent with our observations that failed VPs often exhibit heavy colonization on the flange, particularly at the rougher inner edge where the flange interfaces with the valve (**Figures 1A**, **3Bii**).

Due to the high CO_2 levels (∼5%) experienced in the airway as a result of exhaled breath (Tsoukias et al., 1998), we contemplated whether CO_2 could be exerting an effect on *C. albicans* biofilm formation in the voice prosthesis scenario. Indeed, when seeded onto a voice prosthetic surface, *C. albicans* has increased biofilm growth in 5% CO_2 after 24 h than in atmospheric air (**Figure 4**). Constant exposure of the valve mechanism and parts of the esophageal flange to exhaled air may therefore contribute to the prevalence of *C. albicans* colonization upon VPs.

C. parapsilosis Does Not Have a Competitive Advantage Over *C. albicans* in Biofilm Establishment

We observed that *Candida parapsilosis* was rarely co-isolated with another *Candida* species. Of the 14 VPs which harbored *C. parapsilosis*, only 1 also had another *Candida* species present. This is a stark contrast to other *Candida* species, such as *C. glabrata* which was found on 23 VPs, 19 of which also had additional *Candida* species. This led us to investigate whether *C. parapsilosis* exhibited a competitive advantage over *C. albicans* with regards to biofilm growth. A *C. parapsilosis* clinical isolate found as the sole yeast species on a failed VP was selected for this investigation. Biofilms were seeded using equal cell numbers of the *C. albicans* and *C. parapsilosis* clinical isolates either alone or in combination and incubated for 48 h to mature. Overall biofilm growth was analyzed by measuring the metabolic activity of the biofilms using the XTT colorimetric assay (Kuhn et al., 2002) (**Figure 5**). The proportions of *C. albicans* and *C. parapsilosis* cells were then analyzed by removing biofilms from the silicone surface and plating the resulting cell suspension on chromogenic agar (**Supplementary Figure S1**). Strikingly, while the *C. albicans* G-3065 clinical isolate was able to form a robust biofilm on the silicone surface, the *C. parapsilosis* G10402 clinical isolate was not (**Figure 5**). Moreover, when these two clinical isolates were seeded together, the resultant biofilm was composed primarily of *C. albicans* cells (**Supplementary Figure S1**). In addition, while *C. albicans* biofilms were significantly increased when grown in the presence of increased CO_2 this was not observed for *C. parapsilosis*. These data suggest that the identification of *C. parapsilosis* in isolation on failed VPs is unlikely to arise from a competitive advantage over *C. albicans*.

Antimicrobial Sensitivity of Clinical Isolates

The sensitivities of the five most common bacterial species found on early failing VP to an example antibiotic from the five major antibiotic classes (Coates et al., 2011) are reported (**Table 1**). Only 10 (8.5%) of the most common bacterial isolates tested for sensitivity against the β-lactam antibiotic amoxicillin were judged to be sensitive, and these were all *S. aureus* isolates. All of the

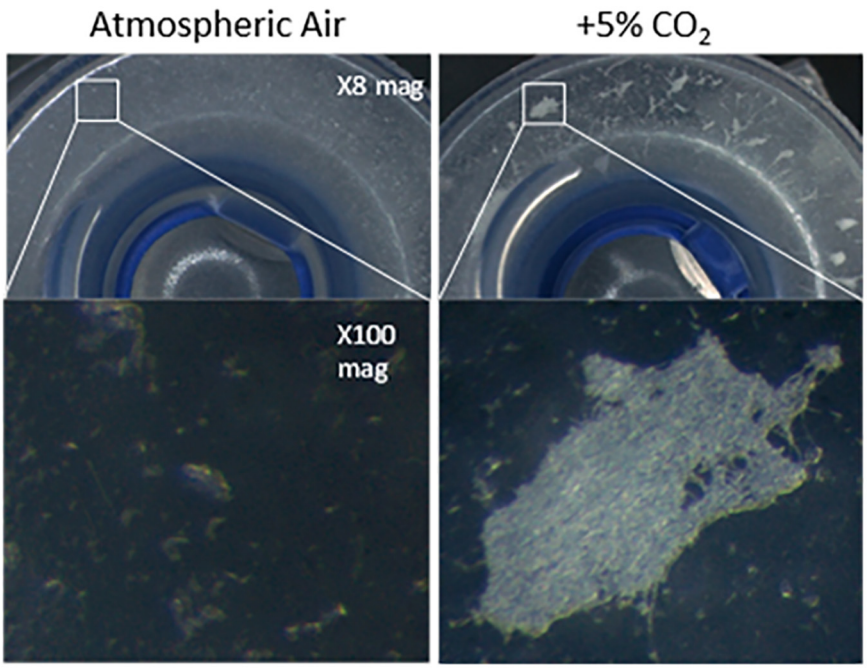

FIGURE 4 | *Candida albicans* biofilm forming on the flange of a voice prosthesis *in vitro* in both atmospheric air and elevated CO_2 conditions. *C. albicans* biofilm formation was assessed on a Provox Vega VP at 37°C under atmospheric air and elevated CO_2 conditions that mimic exhaled breath. Images were collected after 24 h at x8 and x100 magnification. The experiment was repeated three times and representative images are presented.

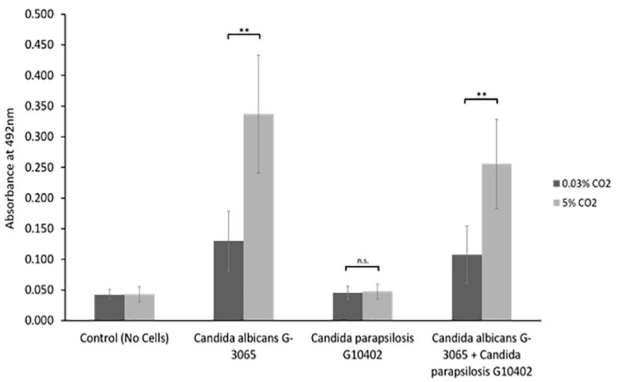

FIGURE 5 | *In vitro* biofilm assay using *C. albicans* and *C. parapsilosis* early failing VP clinical isolates. Biofilms were seeded and grown for 48 h to mature, the resulting biofilms were quantified using the XTT assay which produces a red product that can be measured spectrophotometrically at 492 nm (higher cell number = higher absorbance). The *C. albicans* G-3065 clinical isolate makes bigger biofilms than the *C. parapsilosis* G10402 clinical isolate, and this biofilm formation is influenced by CO_2 concentration. The graph represents three independent experiments each containing triplicates, error bars denote Standard Deviation. Paired two-tail *t*-tests were carried out: $*p < 0.05$, $**p < 0.01$, $***p < 0.001$, n.s. = not significant.

P. aeruginosa, *S. marcescens*, MRSA, and *K. pneumoniae* isolates tested for amoxicillin sensitivity were resistant. 76 (74.5%) were deemed to be sensitive to the macrolide erythromycin, with a significant number of *S. aureus* isolates being found to be resistant. The majority of the common bacterial isolates were sensitive to the fluoroquinolone Ciprofloxacin with 111 (93.3%) being judged as sensitive, however, all of the MRSA isolates tested were resistant to Ciprofloxacin. Likewise, a high number of isolates were sensitive to Tetracycline (104–87.4%), but this antibiotic did not exhibit good activity against the *P. aeruginosa* and *S. marcescens* isolates with 5 (83.3%) of both species being resistant. Finally, 115 (96.6%) of the common bacterial isolates tested were sensitive to the aminoglycoside Gentamicin, this was in fact the most effective antibiotic tested in this study (**Table 1**).

The sensitivities of the five most frequently isolated fungal species in this study to Fluconazole, Miconazole and Nystatin, three commonly used antifungals in the clinical setting, are reported (**Table 2**). Of the 168 *Candida* isolates, 155 were tested for Fluconazole sensitivity and 139 of these were found to be sensitive (89.7%). Moreover, 123 of the *Candida* isolates were tested for Miconazole sensitivity and 107 were sensitive (87.0%). Finally, 129 of the *Candida* isolates were tested for Nystatin sensitivity and 126 of these were found to be sensitive (97.7%). Nystatin therefore appeared to be the most effective antifungal with regards to inhibition of growth of *Candida* species obtained from early failing VPs in this patient cohort.

Antifungal Sensitivity of *C. albicans* Clinical Isolates Within Biofilms

The antifungal drugs Nystatin, Miconazole, and Fluconazole are commonly used as agents to treat fungal colonization of the ear, nose, and throat. We therefore tested their efficacy against *C. albicans* biofilms grown from isolates recovered from early failing VPs. The clinical isolates displayed higher resistances to Fluconazole and Miconazole compared to Nystatin when growing as biofilms (**Table 3**). Moreover, this azole resistance was significantly increased in biofilms grown in high CO_2 environments (**Supplementary Figure S2**). For instance, G-8424 biofilms grown in 0.03% CO_2 had an average decrease in XTT activity of 59% relative to the untreated control upon treatment with 32 μg/ml Fluconazole ($p < 0.001$), whereas there was no significant decrease in relative XTT activity in the 5% CO_2 G-8424 biofilms (**Table 3** and **Supplementary Figure S2**). This was also true for the 128 μg/ml Miconazole treatments in all three isolates (**Table 3** and **Supplementary Figure S3**). Furthermore, despite the fact that 0.03 and 5% CO_2 G-1625 biofilms both displayed significant decreases in relative XTT activity upon Fluconazole treatment, the relative XTT activity was still significantly higher in the biofilms grown in 5% CO_2 (**Supplementary Figure S2**). Nystatin sensitivities were generally independent of CO_2 concentration (**Figure 6**). The G-3065 and G-8424 clinical isolate biofilms were more resistant to Fluconazole and Miconazole than the G-1625 isolate, however, all isolate biofilms exhibited good sensitivity to Nystatin (**Table 3**). Based on these data, we conclude that Nystatin is the most potent against *C. albicans* biofilms on silicone surfaces and also offers the greatest protection against the CO_2 biofilm activation. However, Fluconazole and Miconazole are still both efficacious against some isolates. This approach, which extended current drug susceptibility testing practice to better represent *in vivo* biofilm growth conditions, was crucial in our decision to make use of Nystatin as the lead compound in the development of antifungal treatment guidelines.

Development and Clinical Testing of Antifungal Treatment Guidelines (ATG) to Extend VP Lifespan

Although VP biofilms are likely to be formed from several species we hypothesized that an antifungal approach to reduce colonization may effective in extending device lifespan. The rationale behind this was based on three observations. First, yeast contamination contributes significant biomass which in turn is more likely to impair valve function. Second, the elevated physiological CO_2 environment in which a VP sits promotes biofilm growth of the most commonly isolated yeast, *C. albicans*. Third, since other commonly isolated bacteria, such as *S. aureus* and *P. aeruginosa* have been reported to use *Candida* hyphae as a scaffold to attach to during biofilm formation (Harriott and Noverr, 2009), it may be the case that antifungal treatment also attenuates the bacterial colonization.

The antifungal drugs selected for treatment were chosen based upon the fungal sensitivity data with Nystatin being demonstrated to be the most effective as it had the lowest levels of resistance (**Table 2**). Previous studies have also identified that most non-*albicans Candida* species have higher azole MICs (Ribeiro et al., 2001; Singh et al., 2002), whereas all *Candida* species have low *in vitro* Nystatin MICs (Nenoff et al., 2016). Moreover, *C. albicans* sensitivity to Nystatin when in a biofilm

TABLE 1 | Antibiotic sensitivity of the five most common bacterial species isolated from early failing VPs.

Species	Total number of isolates tested	Number of isolates in each category (%)		
		Sensitive	Intermediate	Resistant
Amoxicillin				
Staphylococcus aureus	96	10 (10.4)	0	76 (79.2)
Pseudomonas aeruginosa	6	0	0	6 (100)
Serratia marcescens	6	0	0	6 (100)
MRSA	5	0	0	5 (100)
Klebsiella pneumoniae	5	0	0	5 (100)
Total	**118**	**10 (8.5)**	**0**	**98 (83.1)**
Erythromycin				
Staphylococcus aureus	97	71 (73.2)	1 (1.0)	25 (25.8)
Pseudomonas aeruginosa	0	–	–	–
Serratia marcescens	0	–	–	–
MRSA	5	5 (100)	0	0
Klebsiella pneumoniae	0	–	–	–
Total	**102**	**76 (74.5)**	**1 (1.0)**	**25 (24.5)**
Ciprofloxacin				
Staphylococcus aureus	97	95 (97.9)	0	1 (1.0)
Pseudomonas aeruginosa	6	5 (83.3)	0	1 (16.7)
Serratia marcescens	6	6 (100)	0	0
MRSA	5	0	0	5 (100)
Klebsiella pneumoniae	5	5 (100)	0	0
Total	**119**	**111 (93.3)**	**0**	**7 (5.9)**
Tetracycline				
Staphylococcus aureus	97	95 (97.9)	0	2 (2.1)
Pseudomonas aeruginosa	6	0	0	5 (83.3)
Serratia marcescens	6	0	1 (16.7)	5 (83.3)
MRSA	5	5 (100)	0	0
Klebsiella pneumoniae	5	4 (80)	0	1 (20)
Total	**119**	**104 (87.4)**	**1 (0.8)**	**13 (10.9)**
Gentamicin				
Staphylococcus aureus	97	93 (95.9)	0	4 (4.1)
Pseudomonas aeruginosa	6	6 (100)	0	0
Serratia marcescens	6	6 (100)	0	0
MRSA	5	5 (100)	0	0
Klebsiella pneumoniae	5	5 (100)	0	0
Total	**119**	**115 (96.6)**	**0**	**4 (3.4)**

The number of sensitive, intermediate, and resistant isolates based upon EUCAST breakpoint recommendations are given for the five most commonly isolated bacterial species.

appears to be unaffected by CO_2 level (**Figure 6**). Our antifungal voice prosthesis management guidelines involve determining the identity and antimicrobial sensitivities of microorganisms present on a failed VP. Based on the antifungal sensitivities of the colonizing fungal species, a course of antifungals (most commonly Nystatin) is suggested and prescribed for topical application directly on the VP.

To test the effectiveness of our antifungal approach to managing VP data from 38 patients was assessed. VP lifespan data from the patient cohort before and after their placement on the ATG was assessed. Over the course of the study, 18 patients were removed from further analysis because of either; concerns over a lack of adherence to the ATG, moving out of the hospital catchment area resulting in incomplete data entries, or insufficient VP replacement data. This left 20 patients with complete VP lifespan data entries before and after guideline implementation on which to conduct statistical analyses.

TABLE 2 | Antifungal sensitivity of the five most common *Candida* species isolated from early failing VPs.

Species	Total number of isolates tested	Number of isolates in each category *(%)*		
		Sensitive	**Intermediate**	**Resistant**
		Fluconazole		
Candida albicans	83	81 (97.6)	2 (2.4)	0
Candida glabrata	23	21 (91.3)	2 (8.7)	0
Candida tropicalis	15	15 (100)	0	0
Candida parapsilosis	14	12 (85.8)	0	2 (14.3)
Candida krusei	9	1 (11.1)	2 (22.2)	6 (66.7)
Total	**144**	**130 (90.3)**	**6 (4.2)**	**8 (5.5)**
		Miconazole		
Candida albicans	62	59 (95.1)	3 (4.9)	0
Candida glabrata	19	19 (100)	0	0
Candida tropicalis	13	7 (53.9)	6 (46.1)	0
Candida parapsilosis	9	4 (44.4)	4 (44.4)	1 (11.1)
Candida krusei	9	8 (88.9)	1 (11.1)	0
Total	**112**	**97 (86.6)**	**14 (12.5)**	**1 (0.9)**
		Nystatin		
Candida albicans	65	64 (98.5)	0	1 (1.6)
Candida glabrata	20	18 (90.0)	1 (5.0)	1 (5.0)
Candida tropicalis	15	15 (100)	0	0
Candida parapsilosis	9	9 (100)	0	0
Candida krusei	9	9 (100)	0	0
Total	**118**	**115 (97.4)**	**1 (0.9)**	**2 (1.7)**

The number of sensitive, intermediate, and resistant isolates based upon EUCAST breakpoint recommendations are given for the five most commonly isolated yeast species.

TABLE 3 | Antifungal sensitivity of biofilms of three *C. albicans* clinical isolates from early failing VPs.

Antifungal	***C. albicans* G-3065**		***C. albicans* G-8424**		***C. albicans* G-1625**	
	0.03% CO_2	**5% CO_2**	**0.03% CO_2**	**5% CO_2**	**0.03% CO_2**	**5% CO_2**
Fluconazole						
32 μg/ml	+	+	++	−	+++	++
128 μg/ml	+	+	+++	−	+++	++
Miconazole						
32 μg/ml	−	−	−	−	−	+
128 μg/ml	++	−	+++	−	+++	+
Nystatin						
2 μg/ml	+++	+++	−	+	+	+
8 μg/ml	+++	+++	++	+++	+++	+++

Action of antifungals was measured via the XTT assay activity relative to untreated in both 0.03 and 5% CO_2: − >80%, + 60–80%, ++ 40–60%, +++ <40%.

Throughout the 8 year course of the study, the lifespan of 319 VPs (143 before and 176 after guidelines) across the 20 patient cohort were analyzed. These 319 VPs represented all the changes for the 20 patients when the removed VP was replaced by the same model of the same size. This ensured there were no external factors such as VP surface/surface area influencing the results. We also included all changes and not just those specifically attributed to the presence of *Candida* growth to remove bias.

Overall, implementation of the ATG resulted in a significant ($p < 0.001$) increase in VP lifespan within our patient cohort (**Figure 7A**). Importantly, this lifespan increase was not dependent on VP manufacturer/model as both the Blom-Singer Classic and the Provox Vega (the two most common VPs in this study) exhibited similar increases in lifespan (**Figure 7B**). It is also important to highlight that the lifespans of these two models were not significantly different before or after the pathway implementation (**Figure 7B**).

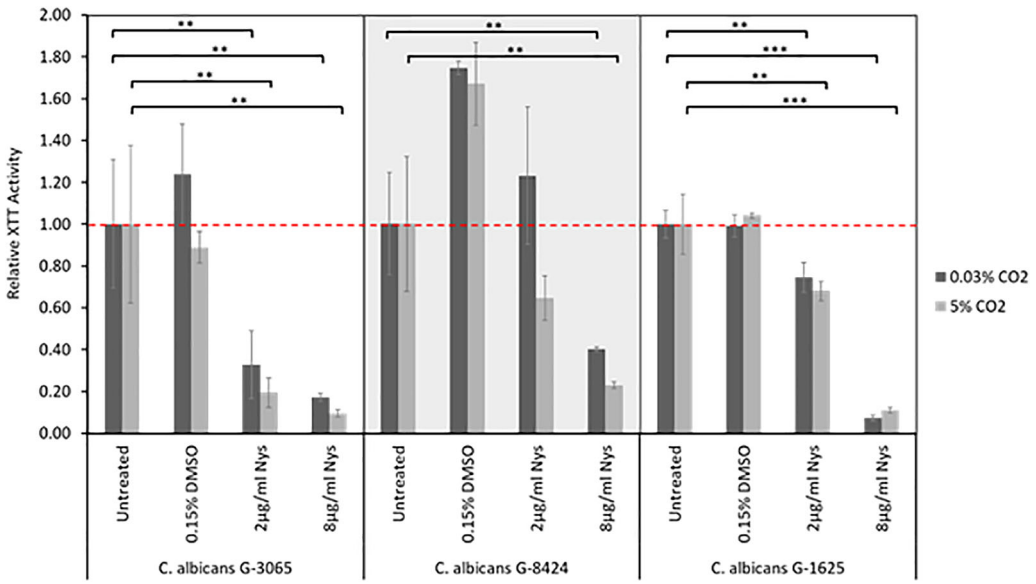

FIGURE 6 | Nystatin sensitivities of *C. albicans* clinical isolate biofilms. Biofilms were seeded and grown for 24 h before addition of Nystatin, they were then grown for a further 24 h before quantification using the XTT assay. The relative XTT activity is presented with the 0.03% CO_2 biofilms being normalized to the 0.03% CO_2 untreated control and the 5% CO_2 biofilms being normalized to the 5% CO_2 untreated control. This prevents the general higher growth of 5% CO_2 biofilms impacting the analysis. Graphs represent three independent experiments each containing triplicates, error bars denote Standard Deviation. Two-way ANOVAs followed by a Tukey test for multiple comparisons were carried out: $^{*}p < 0.05$, $^{**}p < 0.01$, $^{***}p < 0.001$. Stars directly above the bars indicate a significant difference to untreated in the same CO_2 environment.

Although there was variation in average post-pathway VP lifespan increase between patients, the majority of the patients in our cohort enjoyed an overall increase in device lifespan (**Figure 8A**). Two patients did not exhibit an increase in VP lifespan, instead having a slight decrease of −2.4 and −45.5 days respectively (**Figure 8A**). However, these two patients had long-lived VPs on average (97.1 and 193.3 days respectively) in comparison with the rest of the cohort prior to the introduction of the new antifungal clinical guidelines. This was particularly evident for patient 16 whose VPs were already lasting longer than the post-pathway mean lifespan across all patients. Thus, the treatment guidelines may be of most benefit to patients who are experiencing early failing VP. The mean VPs lifespan before guideline implementation was 71.9 days and this increased to 192.0 days after implementation of the antifungal management pathway representing an average 2.7-fold increase in lifespan (**Figure 8B**).

We did not identify any cases of increased drug resistance to antifungal application within the study. However, our guidelines recommend a 6 months (180 days) limit before VP change. This length of time was chosen primarily to ensure that the VP remains structurally sound. Before ATG use only 8 VPs (5.6%) reached this target across all 20 patients, while post-ATG 63 VPs (35.8%) lasted at least 180 days (**Figure 7A**). It is worth noting that after the treatment guidelines were implemented, several VPs were being routinely changed because they had been *in situ* for >6 months and not because they had actually failed. The full set of guidelines can be obtained by contacting the authors and are briefly summarized in **Figure 8C**.

DISCUSSION

The colonization of VP by mixed biofilms has been reported as a potential cause for their early failure. However, a mechanistic understanding as to such biofilms may drive early failure and to what extend bacterial or fungal presence underlies failure is not well-understood. In this study we sought to investigate whether an antifungal treatment regime would provide an effective option for prevention early VP failure. Using a dedicated extraction protocol combined with high-powered microbiology identification we confirmed *Candida albicans* as the most prevalent fungal microorganism found on early failing VP. Our findings are in-line with previous studies where *C. albicans* was the most common fungal species isolated from VP (Buijssen et al., 2012). It is however likely that differences in the identification methods used, different patient demographics or lifestyles and different lifestyles or dietary habits will impact upon the microbial colonization of VP. For instance, Chaturvedi et al. (2014) found that *C. tropicalis* was the most prevalent fungal species colonizing VP within an Indian patient cohort. The high consumption of dairy products such as yogurt and buttermilk in India has been proposed to influence biofilm growth on VPs. For example, the presence of *Streptococcus thermophilus* and *Lactobacillus* in yogurt may reduce biofilm formation (Havenaar and Huis In't Veld, 1992; Busscher et al., 1997b), while the high lactoferrin content (also found in saliva) in buttermilk has antibacterial and antifungal properties against organisms such as *C. albicans* and *Streptococcus mutans* (Soukka et al., 1991, 1992; Nikawa et al., 1993).

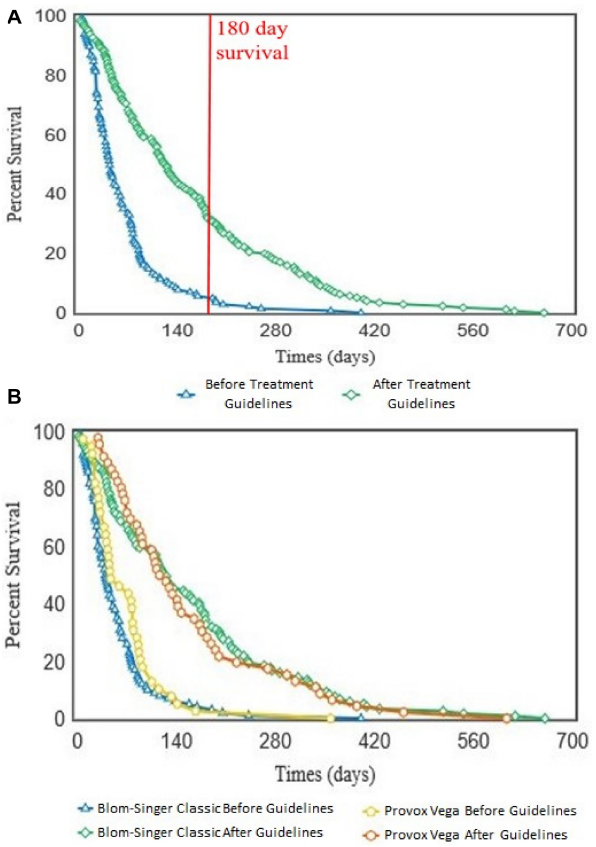

FIGURE 7 | Kaplan–Meier survival curves showing the voice prosthesis *in situ* lifespans before and after implementation of our antifungal treatment pathway. **(A)** Device lifespans were documented before and after implementation of the ATG. Kaplan–Meier survival curves were plotted using the OASIS2 online platform and a log-rank test was used to compare the survival curves: $p < 0.001$. Red line is at 180 days lifespan which we targeted as the ideal lifespan to achieve. **(B)** After lifespan analysis across all devices was performed, the lifespans were categorized into groups depending on which VP model a patient was using. Kaplan–Meier survival curves were again plotted using the OASIS2 online platform and log-rank tests were used to compare them: Blom-Singer Classic, Before vs. After; $p < 0.001$. Provox Vega, Before vs. After; $p < 0.001$.

Our study found *S. aureus* as the most prevalent bacterial species on failed VPs, present on 64.2% of VPs, and was frequently found in combination with one or more *Candida* species. This may be expected as *S. aureus* is a member of the normal oral and perioral microbiota (McCormack et al., 2015). Moreover, it is the third most commonly isolated organism with *C. albicans* in poly-microbial infections (a significant proportion of which are nosocomial infections) (Klotz et al., 2007). Synergistic relationships between *S. aureus* and *C. albicans* have previously been documented. *S. aureus* is poor at forming biofilms on its own, however, it has been suggested that the hyphal *C. albicans* cells provide a scaffold on which the bacteria can attach within a poly-microbial biofilm (Harriott and Noverr, 2009). *S. aureus* has been proposed attach to *C. albicans* hyphae as they penetrate epithelial layers and this has been proposed as relevant for the invasion of human tissues during infection (Schlecht et al., 2015). Within a mixed biofilm, *S. aureus* cells have also been shown to become coated in *C. albicans* matrix material, enhancing its antibiotic resistance (Kong et al., 2016). Furthermore, *S. aureus* and *C. albicans* mixed biofilms can withstand higher shear stresses than pure *C. albicans* biofilms (Lin et al., 2013). Given the high frequency with which these two microorganisms are found together, along with the synergy they have been previously shown to exhibit, their inter-species relationship in with respect to biofilm formation on medical implant devices requires further investigation. However, it is quite plausible that by treating fungal contamination we may also decrease the burden of important bacterial pathogens, such as *S. aureus* on medical devices such as VPs. The potential impact of this relationship is highlighted by the fact co-infection results in increased mortality in mouse models than either microorganism alone (Carlson, 1982, 1983).

We have demonstrated that the lifespan of VP can be significantly increased by applying a highly effective personalized antimicrobial treatment regime focusing on *Candida* colonization, without directly treating the bacterial colonization. Initially we hypothesized that as VP failure occurs as a result of valve blockage then tackling the more significant biomass caused by yeast contamination then we may see better results than attempting to treat bacterial growth. However, our data also suggest that the rougher silicone surfaces of the VP and more significantly the high CO_2 environment within exhaled breath can promote *Candida* biofilm establishment. Another important reason for tackling yeast contamination is that *C. albicans* has been shown to be able to degrading silicone rubber (Buijssen et al., 2012) which may contribute further to device failure. An antifungal approach may also be advantageous because bacteria such as *S. aureus* and *P. aeruginosa* have been reported to attach to *Candida* hyphae during biofilm formation (Harriott and Noverr, 2009), meaning antifungal treatment may also attenuate the bacterial colonization.

Prior to implementation of our VPs management pathway, the average *in situ* lifespan of VPs within our patient cohort was 71.9 days. This is similar to a recent large-scale study of voice prosthesis lifespans in the U.S. by Lewin et al. (2017) which found an average lifespan of 86 days . While being slightly less than a study by Kress et al. (2014) which found an average lifespan of 108 days. The average device lifespan within our patient cohort increased to 192 days after clinicians started following the management guidelines – a 270% increase. Importantly, the increase in lifespan was not affected by the make or model of VP within the study group, suggesting that this treatment regime may be applicable to a broad range of patients. The actual lifespan of VPs post-pathway may be higher than the 192 days reported here, as we recommended the clinicians at the Kent and Canterbury Hospital Speech and Language Therapy Centre change VPs prophylactically after 6 months (180 days) *in situ*. This ensures there is no biofilm formation around the TEP as well as no structural deterioration of the device due to mechanical stress and the constant application of antifungals. It should be noted that two of our patients did not experience

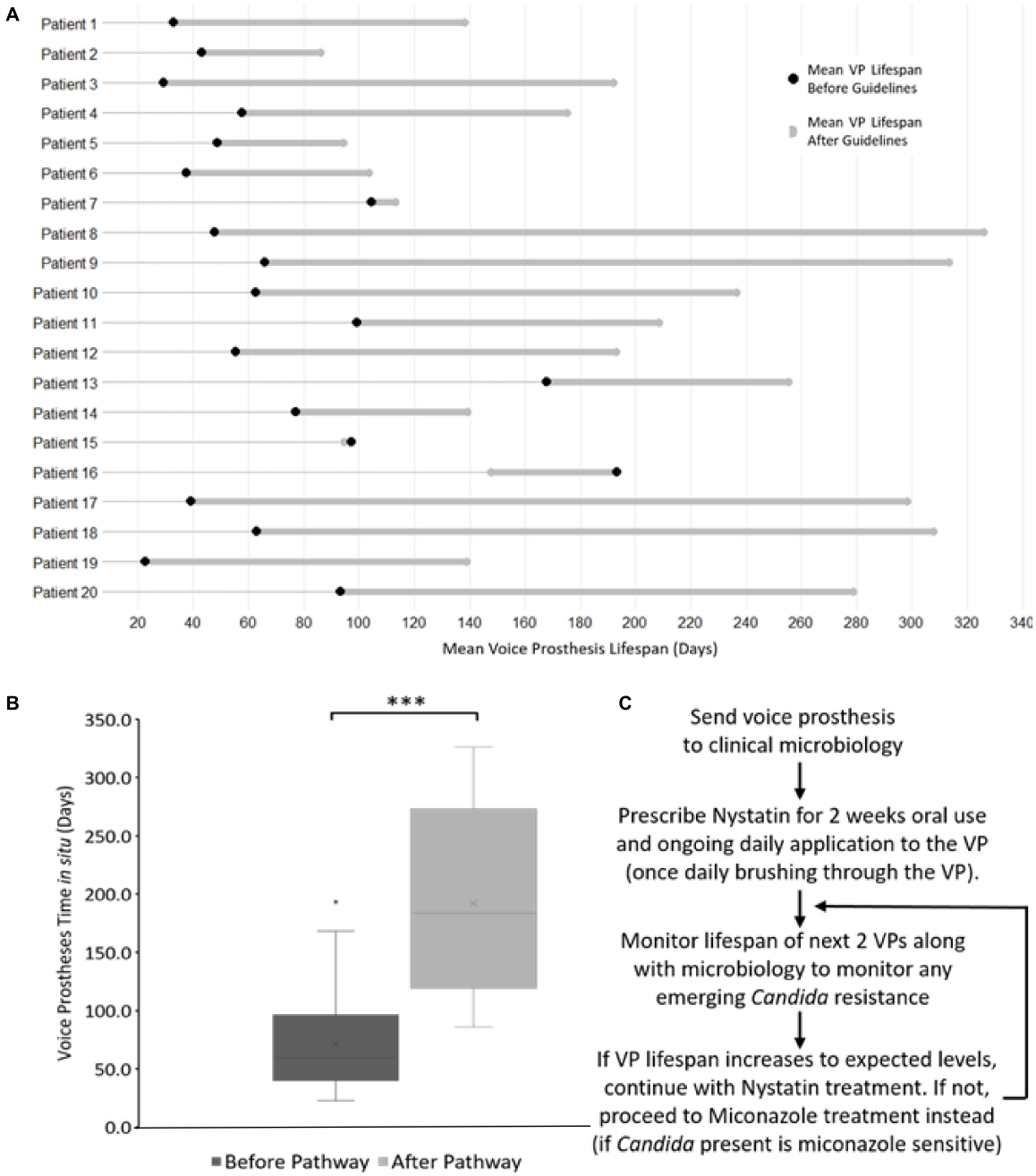

FIGURE 8 | The antifungal treatment guidelines along with its effects on voice prosthesis lifespan within each patient. **(A)** Dumbbell chart representation of the mean VP lifespan difference after guideline implementation for each of the 20 patients. **(B)** Box plot representation of VP *in situ* lifespans before and after guideline implementation, Wilcoxon Signed-Rank test: ***$p < 0.001$. **(C)** Summary of the treatment pathway. As of January 2019, this management pathway has been distributed to 34 different speech and language therapy centers (32 in the United Kingdom, 2 internationally) upon request.

an increase in VP lifespan while using the antifungal treatment guidelines; such a result may be expected within such a multi-factorial clinical scenario. In both cases the patients exhibited relatively long lived VPs before treatment began, and these serve to highlight the importance of patient monitoring and that fungal colonization may not be the cause of early VP failure in every case.

CONCLUSION

Candida albicans was the most prevalent fungal species found on failed VPs within our patient group and we have demonstrated that the topical application of antifungals significantly extends voice prosthesis lifespan in the majority of patients. Our anti-fungal treatment guidelines have been fully ratified by the

relevant EKHUFT NHS committees and have distributed widely throughout the United Kingdom. Given that several studies have identified similar microorganisms as predominant colonizers of VP it is possible that our ATG protocol may be widely applied and at time of submission it has been distributed to 34 speech and language therapy centers (32 in the United Kingdom and 2 internationally). Given the success of this approach it will be imperative to investigate the use of precision antifungal methodologies to tackle biofilm formation on a wider range of medical devices and tubing as a means to reducing infection, morbidity and mortality associated with their use.

DATA AVAILABILITY STATEMENT

All datasets generated for this study are included in the article/**Supplementary Material**.

ETHICS STATEMENT

The studies involving human participants were reviewed and approved by East Kent Hospital University Foundation Trust (EKHUFT), EKHUFT Antimicrobial Stewardship Group, EKHUFT Drugs and Therapeutics Committee, EKHUFT ENT Audit Group, EKHUFT Adult Speech and Language Therapy Service, East Kent Prescribing Group. Written informed consent for participation was not required for this study in accordance with the national legislation and the institutional requirements.

AUTHOR CONTRIBUTIONS

This work was made possible through the collaborative efforts of the members of the *Candida* management multi-disciplinary team, all of whom played important roles and are placed as authors of this manuscript. DP performed data analysis, experimental procedures and was the primary author of this manuscript. CG, FM, AB, VM, and SS were responsible for conception of the study, experimental design, and editing of the manuscript. SS, LW, and CM were responsible for patient data collection. Microorganism identification from early failing VPs and initial antimicrobial sensitivity testing was carried out by MB.

ACKNOWLEDGMENTS

We acknowledge the contributions of East Kent Hospital University Foundation Trust committees for their role in ratifying the Candida management voice prosthesis pathway guidelines. We are also grateful for the support and positive comments of patients within the study and to other NHS trusts who have implemented the pathway and reported upon its effectiveness. Our gratitude is extended to the Kent Cancer Trust who provided funds to support Mr. DP through his Ph.D. and to SS and LW while patient data was collated.

SUPPLEMENTARY MATERIAL

The Supplementary Material for this article can be found online at: https://www.frontiersin.org/articles/10.3389/fmicb.2020.00975/full#supplementary-material

REFERENCES

Bauters, T. G. M., Moerman, M., Vermeersch, H., and Nelis, H. J. (2002). Colonization of voice prostheses by albicans and non-albicans *Candida* species. *Laryngoscope* 112, 708–712. doi: 10.1097/00005537-200204000-00021

Berman, J., and Sudbery, P. E. (2002). *Candida albicans*: a molecular revolution built on lessons from budding yeast. *Nat. Rev. Genet.* 3, 918–930. doi: 10.1038/nrg948

Brook, I. (2013). *The Laryngectomee Guide*. Scotts Valley, CA: Createspace Independent Publication.

Buijssen, K. J. D. A., van der Laan, B. F. A. M., van der Mei, H. C., Atema-Smit, J., van den Huijssen, P., Busscher, H. J., et al. (2012). Composition and architecture of biofilms on used voice prostheses. *Head Neck* 34, 863–871. doi: 10.1002/hed.21833

Bunting, G. W. (2004). Voice following laryngeal cancer surgery: troubleshooting common problems after tracheoesophageal voice restoration. *Otolaryngol. Clin. North Am.* 37, 597–612. doi: 10.1016/j.otc.2004.01.007

Busscher, H. J., Geertsema-Doornbusch, G. I., and van der Mei, H. C. (1997a). Adhesion to silicone rubber of yeasts and bacteria isolated from voice prostheses: influence of salivary conditioning films. *J. Biomed. Mater. Res.* 34, 201–209. doi: 10.1002/(sici)1097-4636(199702)34:2<201::aid-jbm9>3.0.co;2-u

Busscher, H. J., van Hoogmoed, C. G., Geertsema-Doornbusch, G. I., van der Kuijl-Booij, M., and van der Mei, H. C. (1997b). *Streptococcus thermophilus* and its biosurfactants inhibit adhesion by *Candida* spp. on silicone rubber. *Appl. Environ. Microbiol.* 63, 3810–3817.

Cancer Research UK (2018). *Head and Neck Cancers Incidence Statistics*. Available online at: https://www.cancerresearchuk.org/health-professional/cancer-statistics/statistics-by-cancer-type/head-and-neck-cancers/incidence. (accessed October, 31 2018).

Carlson, E. (1982). Synergistic effect of *Candida albicans* and *Staphylococcus aureus* on mouse mortality. *Infect. Immun.* 38, 921–924.

Carlson, E. (1983). Effect of strain of *Staphylococcus aureus* on synergism with *Candida albicans* resulting in mouse mortality and morbidity. *Infect. Immun.* 42, 285–292.

Chandra, J., Kuhn, D., Mukherjee, P. K., Hoyer, L. L., Mccormick, T., and Ghannoum, M. A. (2001). Biofilm formation by the fungal pathogen *Candida albicans*: development, architecture, and drug resistance. *J. Bacteriol.* 183, 5385–5394. doi: 10.1128/jb.183.18.5385-5394.2001

Chaturvedi, P., Sayed, S., Pawar, P., Kelkar, R., Biswas, S., Datta, S., et al. (2014). Microbial colonization of Provox voice prosthesis in the Indian scenario. *Indian J. Cancer* 51:184. doi: 10.4103/0019-509X.138303

Coates, A. R., Halls, G., and Hu, Y. (2011). Novel classes of antibiotics or more of the same? *Br. J. Pharmacol.* 163, 184–194. doi: 10.1111/j.1476-5381.2011.01250.x

Costerton, J. W., Stewart, P. S., and Greenberg, E. P. (1999). Bacterial biofilms: a common cause of persistent infections. *Science* 284, 1318–1322. doi: 10.1126/science.284.5418.1318

Delank, K., and Scheuermann, K. (2008). Practical aspects of voice prosthesis use after laryngectomy. *Laryngorhinootologie* 87, 160–166. doi: 10.1055/s-2007-995370

Donlan, R. M. (2001a). Biofilms and device-associated infections. *Emerg. Infect. Dis.* 7, 277–281. doi: 10.3201/eid0702.010226

Donlan, R. M. (2001b). Biofilm formation: a clinically relevant microbiological process. *Clin. Infect. Dis.* 33, 1387–1392. doi: 10.1086/322972

Donlan, R. M., and Costerton, J. W. (2002). Biofilms: survival mechanisms of clinically relevant microorganisms. *Clin. Microbiol. Rev.* 15, 167–193. doi: 10.1128/cmr.15.2.167-193.2002

European Committee on Antimicrobial Susceptibility Testing (2018). *Clinical Breakpoints for Antifungals*. Available online at: http://www.eucast.org/astoffungi/clinicalbreakpointsforantifungals/. (Accessed January 16, 2019).

European Committee on Antimicrobial Susceptibility Testing (2019). *Clinical Breakpoints for Bacteria*. Available online at: http://www.eucast.org/clinical_breakpoints/. (Accessed January 16, 2019).

Everaert, E., Mahieu, H. F., Wong Chung, R. P., Verkerke, G. J., van der Mei, H. C., and Busscher, H. J. (1997). A new method for in vivo evaluation of biofilms on surface-modified silicone rubber voice prostheses. *Eur. Arch. Otorhinolaryngol.* 254, 261–263. doi: 10.1007/bf02905983

Ganguly, S., and Mitchell, A. P. (2011). Mucosal biofilms of *Candida albicans*. *Curr. Opin. Microbiol.* 14, 380–385.

Gobom, J., Schuerenberg, M., Mueller, M., Theiss, D., Lehrach, H., and Nordhoff, E. (2001). α-Cyano-4-hydroxycinnamic acid affinity sample preparation. A protocol for MALDI-MS peptide analysis in proteomics. *Anal. Chem.* 73, 434–438. doi: 10.1021/ac001241s

Harriott, M. M., and Noverr, M. C. (2009). *Candida albicans* and *Staphylococcus aureus* form polymicrobial biofilms: effects on antimicrobial resistance. *Antimicrob. Agents Chemother.* 53, 3914–3922. doi: 10.1128/AAC.00657-09

Havenaar, R., Huis In't, and Veld, J. H. J. (1992). Probiotics: a general view. *Lactic Acid Bacteria* 1, 151–170. doi: 10.1007/978-1-4615-3522-5_6

Hilgers, F. J. M., Ackerstaff, A. H., Balm, A., van den Brekel, M. W. M., Tan, I. B., and Persson, J.-O. (2003). A new problem-solving indwelling voice prosthesis, eliminating the need for frequent *Candida*- and 'underpressure'-related replacements: provox activalve. *Acta Otolaryngol.* 123, 972–979. doi: 10.1080/00016480310015371

Hilgers, F. J. M., Ackerstaff, A. H., Jacobi, I., Balm, A., Tan, I. B., and van den Brekel, M. W. M. (2009). Prospective clinical phase II study of two new indwelling voice prostheses (provox vega 22.5 and 20 Fr) and a novel anterograde insertion device (provox smart inserter). *Laryngoscope* 120, 1135–1143. doi: 10.1002/lary.20925

Holmes, A. R., Rodrigues, E., van der Wielen, P., Lyons, K. M., Haigh, B. J., Wheeler, T. T., et al. (2014). Adherence of *Candida albicans* to silicone is promoted by the human salivary protein SPLUNC2/PSP/BPIFA2. *Mol. Oral Microbiol.* 29, 90–98. doi: 10.1111/omi.12048

Kim, S., Lee, D., Lee, H., Kim, D., Son, H. G., Yang, J.-S., et al. (2016). OASIS 2: online application for survival analysis 2 with features for the analysis of maximal lifespan and healthspan in aging research. *Oncotarget* 7, 56147–56152. doi: 10.18632/oncotarget.11269

Klotz, S. A., Chasin, B. S., Powell, B., Gaur, N. K., and Lipke, P. N. (2007). Polymicrobial bloodstream infections involving *Candida* species: analysis of patients and review of the literature. *Diagn. Microbiol. Infect. Dis.* 59, 401–406. doi: 10.1016/j.diagmicrobio.2007.07.001

Kong, E. F., Tsui, C., Kucharíková, S., and Andes, D. (2016). Commensal protection of *Staphylococcus aureus* against antimicrobials by *Candida albicans* biofilm matrix. *mBio* 7:e01365-16. doi: 10.1128/mBio.01365-16

Kress, P., Schäfer, P., Schwerdtfeger, F. P., and Rösler, S. (2014). Are modern voice prostheses better? A lifetime comparison of 749 voice prostheses. *Eur. Arch. Oto Rhino Laryngol.* 271, 133–140. doi: 10.1007/s00405-013-2611-0

Kuhn, D. M., Chandra, J., Mukherjee, P. K., and Ghannoum, M. A. (2002). Comparison of biofilms formed by *Candida albicans* and *Candida* parapsilosis on bioprosthetic surfaces. *Infect. Immun.* 70, 878–888. doi: 10.1128/iai.70.2.878-888.2002

Leonhard, M., and Schneider-Stickler, B. (2015). Voice prostheses, microbial colonization and biofilm formation. *Adv. Exp. Med. Biol.* 830, 123–136. doi: 10.1007/978-3-319-11038-7_8

Leunisse, C., Weissenbruch, R., Busscher, H. J., van der Mei, H. C., Dijk, F., and Albers, F. W. J. (2001). Biofilm formation and design features of indwelling silicone rubber tracheoesophageal voice prostheses–an electron microscopical study. *J. Biomed. Mater. Res.* 58, 556–563. doi: 10.1002/jbm.1054

Lewin, J. S., Baumgart, L. M., Barrow, M. P., and Hutcheson, K. A. (2017). Device life of the tracheoesophageal voice prosthesis revisited. *JAMA Otolaryngol. Head Neck Surg.* 143, 65–71. doi: 10.1001/jamaoto.2016.2771

Lin, Y. J., Alsad, L., Vogel, F., Koppar, S., Nevarez, L., Auguste, F., et al. (2013). Interactions between *Candida albicans* and *Staphylococcus aureus* within mixed species biofilms. *Bios* 84, 30–39.

McCormack, M. G., Smith, A. J., Akram, A. N., Jackson, M., Robertson, D., Edwards, G., et al. (2015). Staphylococcus aureus and the oral cavity: an overlooked source of carriage and infection? *Am. J. Infect. Control* 43, 35–37. doi: 10.1016/j.ajic.2014.09.015

Nenoff, P., Krüger, C., Neumeister, C., Schwantes, U., and Koch, D. (2016). In vitro susceptibility testing of yeasts to nystatin – low minimum inhibitory concentrations suggest no indication of *in vitro* resistance of *Candida albicans*, *Candida* species or non-*Candida* yeast species to nystatin. *Clin. Med. Investig.* 1, 71–76.

Neu, T., Verkerke, G. V., Herrmann, I. F., Schutte, H. K., Vander Mei, H. C., and Busscher, H. J. (1994). Microflora on explanted silicone rubber voice prostheses: taxonomy, hydrophobicity and electrophoretic mobility. *J. Appl. Bacteriol.* 76, 521–528. doi: 10.1111/j.1365-2672.1994.tb01111.x

Nevzatoğlu, E. U., Özcan, M., Kulak-Ozkan, Y., and Kadir, T. (2007). Adherence of *Candida albicans* to denture base acrylics and silicone-based resilient liner materials with different surface finishes. *Clin. Oral Investig.* 11, 231–236. doi: 10.1007/s00784-007-0106-3

Nikawa, H., Samaranayake, L. P., Tenovuo, J., Pang, K. M., and Hamada, T. (1993). The fungicidal effect of human lactoferrin on *Candida albicans* and *Candida krusei*. *Arch. Oral Biol.* 38, 1057–1063.

Oosterhof, J. J. H., van der Mei, H. C., Busscher, H. J., Free, R. H., Kaper, H. J., van Weissenbruch, R., et al. (2005). In vitro leakage susceptibility of tracheoesophageal shunt prostheses in the absence and presence of a biofilm. *J. Biomed. Mater. Res. B Appl. Biomater.* 73, 23–28. doi: 10.1002/jbm.b.30422

Radford, D. R., Sweet, S. P., Challacombe, S. J., and Walter, J. D. (1998). Adherence of *Candida albicans* to denture-base materials with different surface finishes. *J. Dent.* 26, 577–583. doi: 10.1016/s0300-5712(97)00034-1

Ribeiro, M. A., Dietze, R., Paula, C. R., Da Matta, D. A., and Colombo, A. L. (2001). Susceptibility profile of vaginal yeast isolates from Brazil. *Mycopathologia* 151, 5–10. doi: 10.1023/a:1010909504071

Sayed, S., Kazi, R., Sengupta, S., Chowdhari, A., and Jagade, M. (2012). Microbial colonization of Blom-Singer indwelling voice prostheses in laryngectomized patients: a perspective from India. *Ear Nose Throat J.* 91, E19–E22. doi: 10.1177/014556131209100418

Schafer, P., Klutzke, N., and Schwerdtfeger, F. P. (2001). Voice restoration with voice prosthesis after total laryngectomy. Assessment of survival time of 378 Provox-1, Provox-2 and Blom Singer voice prosthesis. *Laryngorhinootologie* 80, 677–681. doi: 10.1055/s-2001-18276

Schlecht, L. M., Peters, B., Krom, B. P., Freiberg, J. A., Hänsch, G. M., Filler, S. G., et al. (2015). Systemic Staphylococcus aureus infection mediated by *Candida albicans* hyphal invasion of mucosal tissue. *Microbiology* 161, 168–181. doi: 10.1099/mic.0.083485-0

Singh, S., Bhargava, P., Sobel, J. D., Boikov, D., and Vazquez, J. A. (2002). Vaginitis due to *Candida krusei*: epidemiology, clinical aspects, and therapy. *Clin. Infect. Dis.* 35, 1066–1070. doi: 10.1086/343826

Soukka, T., Lumikari, M., and Tenovuo, J. (1991). Combined inhibitory effect of lactoferrin and lactoperoxidase system on the viability of *Streptococcus mutans*, serotype c. *Scand. J. Dent. Res.* 99, 390–396. doi: 10.1111/j.1600-0722.1991.tb01046.x

Soukka, T., Tenovuo, J., Lenander-Lumikari, M., and Fungicidal. (1992). effect of human lactoferrin against *Candida albicans*. *FEMS Microbiol. Lett.* 69, 223–228.

Talpaert, M. J., Balfour, A., Stevens, S., Baker, M., Muhlschlegel, F. A., and Gourlay, C. W. (2015). *Candida* biofilm formation on voice prostheses. *J. Med. Microbiol.* 64, 199–208.

Ticac, B., Tiæac, R., Rukavina, T., Kesovija, P. G., Pedisiæ, D., Maljevac, B., et al. (2010). Microbial colonization of tracheoesophageal voice prostheses (Provox2) following total laryngectomy. *Eur. Arch. Otorhinolaryngol.* 267, 1579–1586. doi: 10.1007/s00405-010-1253-8

Tsoukias, N. M., Tannous, Z., Wilson, A. F., and George, S. C. (1998). Single-exhalation profiles of NO and CO2 in humans: effect of dynamically changing flow rate. *J. Appl. Physiol.* 85, 642–652. doi: 10.1152/jappl.1998.85.2.642

van Weissenbruch, R., Albers, F. W. J., Bouckaert, S., Neils, H. J., Criel, G., Remon, J. P., et al. (1997). Deterioration of the Provox silicone tracheoesophageal voice prosthesis: microbial aspects and structural changes. *Acta Otolaryngol.* 117, 452–458. doi: 10.3109/00016489709113420

Conflict of Interest: The authors declare that the research was conducted in the absence of any commercial or financial relationships that could be construed as a potential conflict of interest.

frontiers in Microbiology

ORIGINAL RESEARCH
published: 25 May 2020
doi: 10.3389/fmicb.2020.01027

Combination of Antifungal Drugs and Protease Inhibitors Prevent *Candida albicans* Biofilm Formation and Disrupt Mature Biofilms

Matthew B. Lohse[1,2], Megha Gulati[3†], Charles S. Craik[4], Alexander D. Johnson[1] and Clarissa J. Nobile[3]**

[1] Department of Microbiology and Immunology, University of California, San Francisco, San Francisco, CA, United States, [2] Department of Biology, BioSynesis, Inc., San Francisco, CA, United States, [3] Department of Molecular and Cell Biology, University of California, Merced, Merced, CA, United States, [4] Department of Pharmaceutical Chemistry, University of California, San Francisco, San Francisco, CA, United States

OPEN ACCESS

Edited by:
Juliana Campos Junqueira, São Paulo State University, Brazil

Reviewed by:
Rohitashw Kumar, University at Buffalo, United States
Isabel M. Miranda, University of Porto, Portugal

***Correspondence:**
Alexander D. Johnson
ajohnson@cgl.ucsf.edu
Clarissa J. Nobile
cnobile@ucmerced.edu

†Present address:
Megha Gulati, Molecular Cell – Cell Press, Cambridge, MA, United States

Specialty section:
This article was submitted to Infectious Diseases, a section of the journal Frontiers in Microbiology

Received: *11 March 2020*
Accepted: *27 April 2020*
Published: *25 May 2020*

Citation:
Lohse MB, Gulati M, Craik CS, Johnson AD and Nobile CJ (2020) Combination of Antifungal Drugs and Protease Inhibitors Prevent Candida albicans Biofilm Formation and Disrupt Mature Biofilms. Front. Microbiol. 11:1027. doi: 10.3389/fmicb.2020.01027

Biofilms formed by the fungal pathogen *Candida albicans* are resistant to many of the antifungal agents commonly used in the clinic. Previous reports suggest that protease inhibitors, specifically inhibitors of aspartyl proteases, could be effective antibiofilm agents. We screened three protease inhibitor libraries, containing a total of 80 compounds for the abilities to prevent *C. albicans* biofilm formation and to disrupt mature biofilms. The compounds were screened individually and in the presence of subinhibitory concentrations of the most commonly prescribed antifungal agents for *Candida* infections: fluconazole, amphotericin B, or caspofungin. Although few of the compounds affected biofilms on their own, seven aspartyl protease inhibitors inhibited biofilm formation when combined with amphotericin B or caspofungin. Furthermore, nine aspartyl protease inhibitors disrupted mature biofilms when combined with caspofungin. These results suggest that the combination of standard antifungal agents together with specific protease inhibitors may be useful in the prevention and treatment of *C. albicans* biofilm infections.

Keywords: *Candida albicans*, biofilms, antimicrobial resistance, therapeutics, protease inhibitors, aspartyl protease inhibitors

INTRODUCTION

Candida albicans is a member of the human microbiota which asymptomatically colonizes the skin, mouth, and gastrointestinal tract of healthy humans (Douglas, 2003; Nobile and Johnson, 2015; Gulati and Nobile, 2016; Lohse et al., 2018). This fungal species is also one of the most common pathogens of humans, typically causing superficial dermal and mucosal infections (Kennedy and Volz, 1985; Kullberg and Oude Lashof, 2002; Kumamoto, 2002, 2011; Douglas, 2003; Achkar and Fries, 2010; Ganguly and Mitchell, 2011; Kim and Sudbery, 2011). When a host's immune system is compromised (e.g., in patients undergoing chemotherapy or with AIDS), *C. albicans* can also cause disseminated bloodstream infections with mortality rates exceeding 40% (Wenzel, 1995; Calderone and Fonzi, 2001; Douglas, 2003; Pappas et al., 2004; López-Ribot, 2005).

An important virulence trait of *C. albicans* is its ability to form biofilms, structured communities of cells several hundred microns thick, that can form on both biotic and abiotic surfaces (Chandra et al., 2001; Douglas, 2002, 2003; Kumamoto, 2002; Ramage et al., 2009; Fox and Nobile, 2012;

Lohse et al., 2018). When mature, these biofilms contain a mixture of yeast, pseudohyphal, and hyphal cells surrounded by an extracellular matrix (Chandra et al., 2001; Douglas, 2003; Ramage et al., 2009; Fox and Nobile, 2012; Gulati and Nobile, 2016). *C. albicans* forms biofilms on mucosal surfaces, epithelial cell linings, and on implanted medical devices, such as catheters, dentures, and heart valves (Kojic and Darouiche, 2004; Ramage et al., 2006). Mature *C. albicans* biofilms also release yeast cells, which can seed new infections elsewhere in the host (Uppuluri et al., 2010, 2018).

Candida albicans biofilms are typically resistant to antifungal drugs at the concentrations that are normally effective against planktonic (free-floating) cells, thus requiring higher drug concentrations, which can lead to host side effects, such as liver and kidney damage (Donlan, 2001; Kojic and Darouiche, 2004; Ramage et al., 2006; Tumbarello et al., 2007, 2012; Lebeaux et al., 2014). Furthermore, *C. albicans* can also form polymicrobial biofilms with several companion bacterial species (Bamford et al., 2009, 2015; Jarosz et al., 2009; Peleg et al., 2010; Peters and Noverr, 2013; Lindsay and Hogan, 2014; Pammi et al., 2014; Jack et al., 2015), further complicating treatment strategies. These polymicrobial biofilms can, for example, protect their bacterial inhabitants from environmental hazards (e.g., oxygen in the case of anaerobic bacteria) (Fox et al., 2014) and antibiotic treatments (e.g., protecting *Staphylococcus aureus* from vancomycin) (Harriott and Noverr, 2009, 2010; Kong et al., 2016). The drug-resistant nature of both single species and polymicrobial biofilms frequently makes removal of biofilm-infected medical devices the only treatment. However, this recourse is problematic when patients are critically ill or when device removal involves complicated surgical procedures (e.g., heart valve replacement) (Kojic and Darouiche, 2004; Andes et al., 2012; Fox et al., 2015b).

Currently, the three major classes of antifungal drugs used to treat *C. albicans* infections are the polyenes, azoles, and echinocandins (Fox et al., 2015b; Prasad et al., 2016). The polyenes (e.g., amphotericin B) target ergosterol in the fungal cell membrane and are fungicidal against *C. albicans*. The azoles (e.g., fluconazole) inhibit the demethylase enzyme Erg11 from the ergosterol biosynthesis pathway and are fungistatic against *C. albicans*. Echinocandins (e.g., caspofungin), the most recently developed class of antifungal drugs, inhibit synthesis of the cell wall crosslinking component β-1,3-glucan and are fungicidal against *C. albicans*. Although novel derivatives within these classes have been introduced over the years, new classes of drugs have not been introduced. The limited size of the existing antifungals, both in terms of the distinct classes and in the number of drugs within several of these classes, creates several problems. As noted above, these classes of drugs typically have reduced effectiveness against biofilms relative to planktonic cells (Donlan, 2001; Kojic and Darouiche, 2004; Ramage et al., 2006; Tumbarello et al., 2007, 2012; Lebeaux et al., 2014). Furthermore, long term exposure to these drugs, especially to members of the azole class, can give rise to antifungal resistance. Although the development of new antifungal agents is clearly called for, several recent *in vitro* studies have shown that combinations of antifungals with other extant drugs can be effective against *C. albicans* biofilms (Delattin et al., 2014; De Cremer et al., 2015).

Recently, we demonstrated the importance of several secreted proteases (Saps) for *C. albicans* biofilm formation (Nobile et al., 2012; Winter et al., 2016). Deletion of Sap5 and Sap6, both of whose expression is upregulated in biofilms (Nobile et al., 2012), reduced biofilm formation *in vitro* and *in vivo* (Winter et al., 2016). Previous reports showed that treatment with aspartyl protease inhibitors, a class of drug commonly used to treat HIV patients, reduced the occurrence of oral candidiasis in immunocompromised patients independent of effects of the drug on the immune system through HIV remediation (Cauda et al., 1999; Diz Dios et al., 1999; Cassone et al., 2002). Further work showed that several of the commonly used antiretroviral HIV aspartyl protease inhibitors could inhibit the Saps (Cassone et al., 1999; Gruber et al., 1999b,a; Korting et al., 1999; Pichová et al., 2001; Skrbec and Romeo, 2002; Cenci et al., 2008; Braga-Silva et al., 2010). Exposure to these protease inhibitors also reduced *C. albicans* adherence to materials commonly used in medical devices and to layers of host cells (Borg-von Zepelin et al., 1999; Bektic et al., 2001; Tsang and Hong, 2009), although the magnitude of the latter effect differs greatly between distinct cell types (Falkensammer et al., 2007). Aspartyl protease inhibitors have also been observed to reduce *C. albicans*-induced tissue damage, proliferation, and virulence *in vivo* in a rat vaginal model (Cassone et al., 1999; de Bernardis et al., 1999). Finally, one study suggested that aspartyl protease inhibitors and the antifungal agents fluconazole or amphotericin B act synergistically against *C. albicans* in the planktonic form (Casolari et al., 2004). To date, the studies of aspartyl protease inhibitors with regards to *C. albicans* emphasized their effects on planktonic cells. The one exception found that exposure to amprenavir, a common HIV antiretroviral protease inhibitor, could reduce *C. albicans* biofilm formation *in vitro* (Braga-Silva et al., 2010).

Given the number of protease inhibitors already approved for use in humans, including inhibitors of aspartyl proteases or other classes of proteases, we sought to evaluate the ability of a wide range of protease inhibitors to prevent (either alone or in combination with other antifungals) the formation of *C. albicans* biofilms or to act against mature biofilms. To evaluate the efficacy of these compounds in this regard, we screened three libraries containing 80 protease inhibitors in both biofilm inhibition and disruption assays. Each protease inhibitor was screened for biofilm efficacy individually and in combination with fluconazole, amphotericin B, or caspofungin. Although few of the protease inhibitors were effective against biofilms on their own, several, especially members of the aspartyl protease inhibitor class, were effective against biofilms when combined with either caspofungin or amphotericin B.

MATERIALS AND METHODS

Strains and Media

All assays were performed using SNY425, a SC5314-derived prototrophic a/α strain (Noble et al., 2010); the sensitivity of this strain to amphotericin B, caspofungin, and fluconazole in

our assays are reported in **Supplementary Table S1** "SN425 Sensitivity". *C. albicans* cells were cultured as previously described; in brief, cells were recovered from glycerol stocks for two days at 30°C on yeast extract peptone dextrose (YEPD) plates (2% Bacto^{TM} peptone, 2% dextrose, 1% yeast extract, 2% agar). Overnight cultures were grown approximately 16 h at 30°C in YEPD media (2% Bacto^{TM} peptone, 2% dextrose, 1% yeast extract). Biofilm assays were performed in RPMI-1640 media (containing L-glutamine and lacking sodium biocarbonate, MP Biomedicals #0910601) supplemented with 34.5 g/L MOPS (Sigma, M3183), adjusted to pH 7.0 with sodium hydroxide, and sterilized with a 0.22 μm filter (Lohse et al., 2017; Gulati et al., 2018).

Compound Libraries

The 53 member SCREEN-WELL® Protease Inhibitor Library[1] was purchased from Enzo Life Sciences. The two aspartyl protease inhibitor libraries (from which we focused on nine FDA-approved HIV-1 protease inhibitors, the ten macrocycles, and eight linear peptidomimetics) have been previously reported (Clarke et al., 2016). Due to limited quantities of several aspartyl protease inhibitors, a minority of compounds were only screened in one biofilm assay. In these cases, we prioritized the Disruption Biofilm Assay over the Sustained Inhibition Biofilm Assay. Four other compounds from these libraries [one FDA-approved HIV-1 protease inhibitor and three linear peptidomimetics (API7-9)] were not used in any assay. A list of compounds tested can be found in **Supplementary Table S1**.

Biofilm Assays

The Sustained Inhibition and Disruption Standard Optical Density Biofilm Assays followed previously reported protocols for the 384-well format of biofilm screening assays (Nobile et al., 2014; Fox et al., 2015a; Lohse et al., 2017; Gulati et al., 2018). Compounds and antifungal agents were added during the 90-min adherence and 24-h growth steps of the Sustained Inhibition Biofilm Assay or for the second 24-h growth step of the Disruption Biofilm Assay. In brief, 1 μl of overnight culture was added to 90 μl media (or media with drug) in a well (final OD_{600} = 0.15, roughly 2×10^6 cells/ml). Plates were then sealed with Breathe-Easy® sealing membranes (Diversified Biotech BEM-1) and shaken at 37°C for 90 min at 350 rpm in an ELMI (DTS-4) incubator. Media was removed, wells were washed with PBS, and fresh media (or media with drug) was added back to wells. Plates were then resealed and shaken for a further 24 h. For the Sustained Inhibition Biofilm Assay, media was removed at this point and the absorbance (OD_{600}) was determined on a Tecan Infinite M1000 Pro or a Tecan M200. For the Disruption Biofilm Assays, media was instead removed in groups of 6–12 wells and fresh media containing the compound of interest was carefully added back to the wells. Plates were then resealed and shaken for an additional 24 h before removing media and recording absorbance as described above.

[1]http://www.enzolifesciences.com/BML-2833/screen-well-protease-inhibitor-library/

Standalone Assays

Compounds were tested at 40 μM in both the Sustained Inhibition and Disruption Standard Optical Density Biofilm Assays (Lohse et al., 2017; Gulati et al., 2018). Individual repeats of candidate compounds and DMSO solvent controls were performed. Each plate had groups of control wells spread throughout the plate to minimize position effects. For the SCREEN-WELL® Protease Inhibitor Library, the 53 compounds were screened once in both the Sustained Inhibition Biofilm Assay and the Disruption Biofilm Assay. Promising compounds from these initial screens were then tested a second time in the relevant assay(s). For the two aspartyl protease inhibitor libraries, we initially screened 21 compounds in the Sustained Inhibition Biofilm Assay and 25 compounds in the Disruption Biofilm Assay. Promising compounds from these initial screens were then tested two more times in the relevant assay(s). An additional three repeats were performed for four compounds (atazanavir, indinavir, nelfinavir, tipranavir) in the Disruption Biofilm Assay. For each experimental set of eight wells, significance was evaluated versus all of the control wells from the same plate by performing Welch's *t*-test (two-tailed, assuming unequal variance). In order to correct for the multiple comparisons performed, we then applied the Bonferroni Correction with $\alpha = 0.05$. All of the comparisons for a given type of assay were pooled for this multiple comparisons correction step, giving a number of hypotheses, m, of 104 for the Sustained Inhibition Biofilm Assay and of 125 for the Disruption Biofilm Assay (final thresholds 4.81×10^{-4} and 4.00×10^{-4}, respectively). We then determined whether each experimental repeat had an average absorbance of less than the average of the control wells and was significant after the multiple comparisons correction. To be considered a validated hit, a compound had to satisfy both these criteria. Data and statistics for the Standalone Sustained Inhibition and Disruption Optical Density Biofilm Assays are compiled in **Supplementary Table S1** "Standalone Inhibition" and "Standalone Disruption". A summary of hits from these assays are included in **Supplementary Table S1** "Hit Listing By Type."

BIC Assays

We determined the biofilm inhibitory concentration (BIC) of nelfinavir, tipranavir, and TPCK using the 384-well format Sustained Inhibition Standard Optical Density Biofilm Assay (Lohse et al., 2017; Gulati et al., 2018). Both nelfinavir and tipranavir were serially diluted two-fold from a maximum concentration of 200 μM to a minimum concentration of 0.1 μM. TPCK was serially diluted two-fold from a maximum concentration of 512 μM to a minimum concentration of 0.06 μM. Equivalent volumes of DMSO were used as loading controls for the compounds. Statistical testing was performed as described above with the following changes. Significance was evaluated for a given concentration of compound (e.g., 50 μM nelfinavir) compared to the equivalent DMSO loading control (e.g., the 50 μM loading control). All BIC comparisons were then pooled for multiple comparisons correction, giving a number of hypotheses, m, of 38 ($\alpha = 0.05$, final threshold

1.32×10^{-3}). We then determined whether each concentration of a drug had an average absorbance of less than the average of the relevant control wells and was significant after the multiple comparisons correction. The BIC of a compound was defined as the lowest concentration that met both of these requirements for which all higher concentrations of the same compound also met these requirements. If no concentration met these requirements, the BIC is indicated as greater than the highest concentration tested for that compound. Data and statistics for the BIC Sustained Inhibition Optical Density Biofilm Assay are compiled in **Supplementary Table S1** "Inhibition BIC."

Combination Assays

The combination (candidate compound plus known antifungal agent) Sustained Inhibition and Disruption Biofilm Assays followed the protocols described above with the following modifications. The candidate compounds were included at 12.5 μM in both assays except for TPCK, Dec-RVKR-CMK, AEBSF·HCl, N-Ethylmaleimide, and acivicin, which were included at 4 μM, and gliotoxin, which was included at 1 μM. The Sustained Inhibition Biofilm Assays used 1 μg/mL amphotericin B, 0.125 μg/mL caspofungin, or 256 μg/mL fluconazole. The Disruption Biofilm Assays used 2 μg/mL amphotericin B, 0.5 μg/mL caspofungin, or 256 μg/mL fluconazole. The sensitivity of the strain used in this study to amphotericin B, caspofungin, and fluconazole are reported in **Supplementary Table S1** "SN425 Sensitivity."

Compounds and two sets of controls were included for all candidate compounds and antifungal agents tested on a given plate. The first set of controls contained the candidate compound, but no antifungal agent, while the second set of controls contained the antifungal agent, but no candidate compound. The concentration of candidate compound or antifungal agent in these control wells was the same as the experimental wells. In general, one set of wells was included for each experimental or control condition on a given plate. Statistical analysis was performed using Welch's *t*-test and the Bonferroni Correction as described above with the following modifications. Each experimental condition was compared to both the relevant antifungal agent and candidate controls (e.g., a nelfinavir plus caspofungin experiment was compared to the nelfinavir-only control and the caspofungin-only control from the same plate). All of the same comparisons for a given assay were pooled for the multiple comparisons correction, giving a number of hypotheses, m, of 213 for both the antifungal agent and candidate comparisons in the Sustained Inhibition Biofilm Assay ($\alpha = 0.05$, final threshold 2.35×10^{-4}). The number of hypotheses, m, was 240 for both the antifungal agent and candidate comparisons in the Disruption Biofilm Assay ($\alpha = 0.05$, final threshold 2.08×10^{-4}). To be considered a hit, any given experimental condition must have an average absorbance of less than the averages of both sets of relevant control wells and remain significant for both sets of comparisons after the multiple comparisons correction. Data, statistics, and concentrations used for the combination Sustained Inhibition and Disruption Optical Density Biofilm Assays are compiled in **Supplementary Table S1** "Combination Inhibition" and "Combination Disruption." A summary of hits from these assays are included in **Supplementary Table S1** "Hit Listing By Type."

RESULTS

Protease Inhibitor Libraries

We selected three libraries of protease inhibitors to screen for compounds with the abilities to inhibit and/or disrupt *C. albicans* biofilm formation *in vitro*. The first library, the SCREEN-WELL® Protease Inhibitor Library (Enzo Life Sciences), contains 53 protease inhibitors effective against several classes of proteases (**Supplementary Table S1**). The remaining two libraries contain 31 compounds known or predicted to specifically inhibit aspartyl proteases (Clarke et al., 2016), of which we tested 27 in at least one assay. We focused on nine FDA-approved aspartyl protease inhibitors, developed to inhibit HIV-1 protease, ten macrocycles (API12-21), and eight linear peptidomimetics (API1-6, 10, and 11) that were originally synthesized with the goal of identifying new aspartyl protease inhibitors (Clarke et al., 2016).

Standalone Screens

We screened the three libraries for their abilities to inhibit biofilm formation or to disrupt mature biofilms using the Sustained Inhibition Biofilm Assay and Disruption Biofilm Assay (Lohse et al., 2017; Gulati et al., 2018), respectively. In the Sustained Inhibition Biofilm Assay, compounds were included in media during the 90-m adherence and 24-h growth steps of the biofilm assay; the compounds were evaluated for their ability to reduce or prevent biofilm formation (**Figure 1A**). In the Disruption Biofilm Assay, a biofilm was grown for 24 h before the compound of interest was added. The biofilm was then incubated for an additional 24 h before determining whether the compound affected the mature biofilm (**Figure 1A**). In both assays, compounds were tested at a concentration of 40 μM.

Three of the 53 compounds in the SCREEN-WELL® Protease Inhibitor library, acivicin, gliotoxin, and TPCK, inhibited biofilm formation on their own (**Figure 1B**, **Supplementary Table S1** "Standalone Inhibition"). One of these compounds, gliotoxin, also disrupted mature biofilms on its own (**Figure 1C**, **Supplementary Table S1** "Standalone Disruption"). TPCK irreversibly inhibits chymotrypsin (a serine peptidase) and can also inhibit some cysteine peptidases while gliotoxin inhibits the chymotrypsin-like activity of the 20S proteasome. Acivicin, on the other hand, is an inhibitor of gamma-glutamyl transpeptidase, an enzyme that transfers gamma-glutamyl groups from peptide donors to peptide acceptors as well as acting as a hydrolase to remove gamma-glutamyl groups from peptides. None of the 25 aspartyl protease inhibitors tested were able to disrupt mature *C. albicans* biofilms on their own, and only one of the 22 aspartyl protease inhibitors tested, the HIV-1 protease

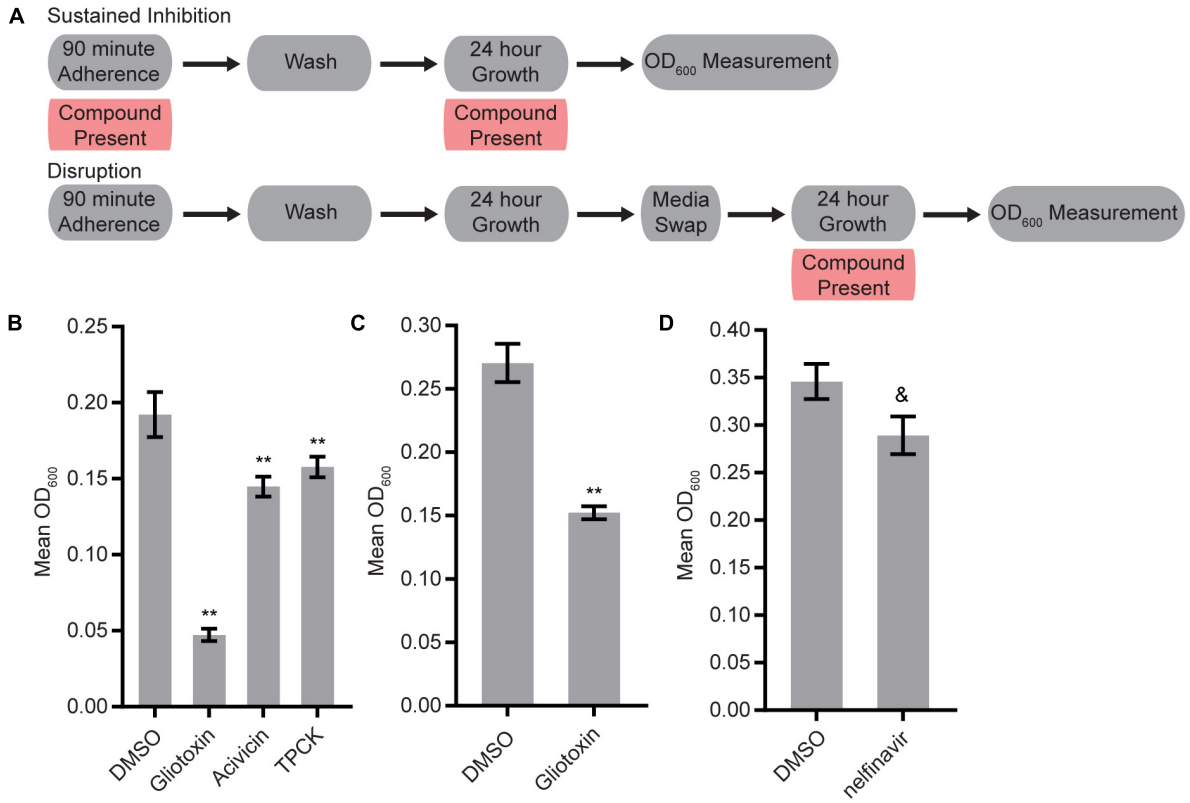

FIGURE 1 | Four protease inhibitors either inhibited biofilm formation or disrupted mature biofilms on their own. **(A)** Overview of the experimental setups for the Sustained Inhibition and Disruption Biofilm Assays used for these experiments. For the Sustained Inhibition Biofilm Assay, compounds were included during both the 90-min adherence step and the 24-h growth step of a standard biofilm assay. For the Disruption Biofilm Assay, compounds were included during a second 24-h growth step. **(B,C)** Statistically significant hits from the standalone **(B)** Sustained Inhibition and **(C)** Disruption assays with the SCREEN-WELL® Protease Inhibitor Library. Mean OD_{600} readings with standard deviations are shown; significant differences from the DMSO solvent control as determined by Welch's *t*-test (two-tailed, assuming unequal variance) with the Bonferroni Correction are indicated for $\alpha = 0.05$ (*) and $\alpha = 0.01$ (**). Although a single repeat is shown, the indicated threshold was met by all of the repeats of each compound shown. **(D)** Statistically significant hit from the standalone Sustained Inhibition assays with the two aspartyl protease inhibitor libraries. Mean OD_{600} readings with standard deviations are shown; significant differences from the DMSO solvent control as determined by Welch's *t*-test (two-tailed, assuming unequal variance) with the Bonferroni Correction are indicated. A single repeat is shown; the indicated significance threshold was met by two of the three repeats at $\alpha = 0.01$ while the third repeat did not pass at $\alpha = 0.05$. The "&" symbol indicates this mixed result.

inhibitor nelfinavir, was able to inhibit biofilm formation on its own (BIC 50 μM) (**Figure 1D**, **Supplementary Table S1** "Standalone Disruption" and "Standalone Inhibition").

Combination Screens

We tested whether any compounds from the three protease inhibitor libraries could inhibit biofilm formation and/or disrupt mature biofilms in the presence of sub-inhibitory concentrations of amphotericin B, caspofungin, or fluconazole (see methods for concentrations). Five compounds from the SCREEN-WELL® Protease Inhibitor library inhibited biofilm formation in the Sustained Inhibition Biofilm Assay when combined with fluconazole (**Figure 2A**, **Supplementary Table S1** "Combination Inhibition"). We did not observe any synergies with amphotericin B or caspofungin in this assay. Two of these five compounds, gliotoxin and TPCK, were also "hits" in the standalone Sustained Inhibition Biofilm Assay described above. The remaining three compounds, lisinopril, Z-Prolyl-prolinal, and NNGH, were unique to the Sustained Inhibition Biofilm assay for synergies with fluconazole. Lisinopril inhibits the metalloprotease angiotensin-converting enzyme (ACE), NNGH inhibits matrix metalloproteinase 3 (MMP-3), and Z-Prolyl-prolinal inhibits prolyl endopeptidase (a serine protease). Two compounds from the SCREEN-WELL® Protease Inhibitor library, gliotoxin and Dec-RVKR-CMK, disrupted mature biofilms when combined with an antifungal agent (**Figures 2B-C**, **Supplementary Table S1** "Combination Disruption"). Gliotoxin disrupted mature biofilms when combined with fluconazole (**Figure 2C**, **Supplementary Table S1** "Combination Disruption") while Dec-RVKR-CMK disrupted mature biofilms when combined with caspofungin (**Figure 2B**, **Supplementary Table S1** "Combination Disruption"). Dec-RVKR-CMK, also known as furin convertase inhibitor, inhibits the subtilisin (Kex2p-like) proprotein convertase (a type of serine protease).

We next evaluated 17 aspartyl protease inhibitors in the Sustained Inhibition Biofilm Assay and 26 aspartyl protease inhibitors in the Disruption Biofilm Assay in combination with the same three antifungal agents. Seven

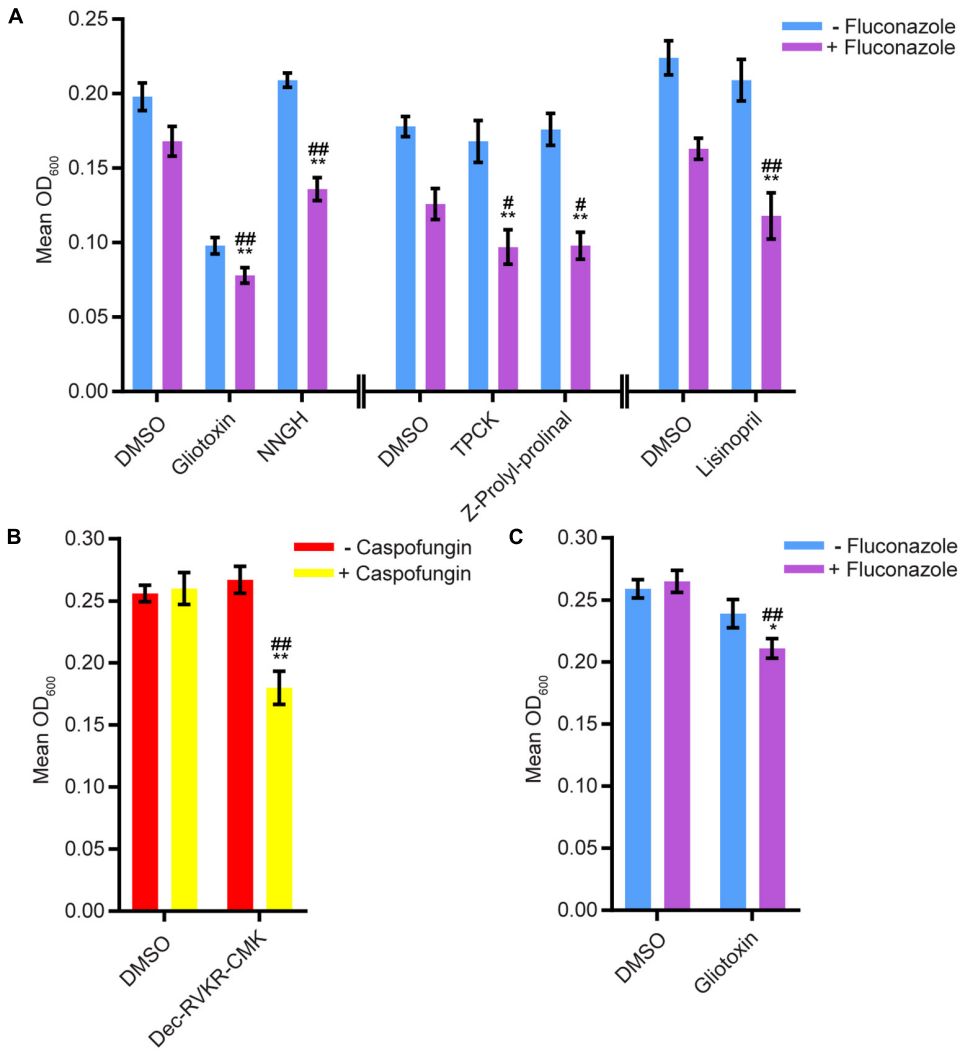

FIGURE 2 | Six compounds from the SCREEN-WELL® Protease Inhibitor Library either inhibited biofilm formation or disrupted mature biofilms in combination with one or more antifungal agents. **(A)** Statistically significant hits from the combination Sustained Inhibition Biofilm Assays with fluconazole. For each compound, the wells with fluconazole (+fluconazole) are indicated in purple and the wells without fluconazole (–fluconazole) are indicated in blue. **(B)** Statistically significant hits from the combination Disruption Biofilm Assays with caspofungin. For each compound, the wells with caspofungin (+caspofungin) are indicated in yellow and the wells without caspofungin (–caspofungin) are indicated in red. **(C)** Statistically significant hits from the combination Disruption Biofilm Assays with fluconazole. For each compound, the wells with fluconazole (+fluconazole) are indicated in purple and the wells without fluconazole (–fluconazole) are indicated in blue. For panels a–c, mean OD_{600} readings with standard deviations are shown; significant differences from the compound without antifungal agent control (e.g., gliotoxin, – fluconazole), as determined by Welch's *t*-test (two-tailed, assuming unequal variance) with the Bonferroni Correction, are indicated for $\alpha = 0.05$ (*) and $\alpha = 0.01$ (**). Significant differences from the antifungal agent without compound control (e.g., DMSO, +fluconazole), as determined by Welch's *t*-test (two-tailed, assuming unequal variance) with the Bonferroni Correction, are indicated for $\alpha = 0.05$ (#) and $\alpha = 0.01$ (##). Data from separate plates are separated by two vertical lines on the *x*-axis; the DMSO solvent control is shown for each plate.

aspartyl protease inhibitors (four HIV-1 protease inhibitors and three macrocycles) inhibited biofilm formation when combined with one or more of the antifungal agents (six with caspofungin, five with amphotericin B, and one with fluconazole) (**Figure 3**, **Supplementary Table S1** "Combination Inhibition"). Specifically, lopinavir and API13 inhibited biofilm formation in combination with caspofungin while API19 inhibited biofilm formation in combination with amphotericin B. Ritonavir, saquinavir, and API15 inhibited biofilm formation in combination with caspofungin and amphotericin B while nelfinavir inhibited biofilm formation in combination with all three antifungal agents tested (**Figure 3**, **Supplementary Table S1** "Combination Inhibition"). Nine aspartyl protease inhibitors (the HIV-1 protease inhibitors atazanavir, indinavir, lopinavir, nelfinavir, ritonavir, saquinavir; and the macrocycles API15, API16, API19) disrupted mature biofilms in combination with caspofungin (**Figure 4**, **Supplementary Table S1**, "Combination Disruption"). None of the 26 aspartyl protease inhibitors tested disrupted biofilms in the presence of amphotericin B or fluconazole. We were surprised to find compounds that

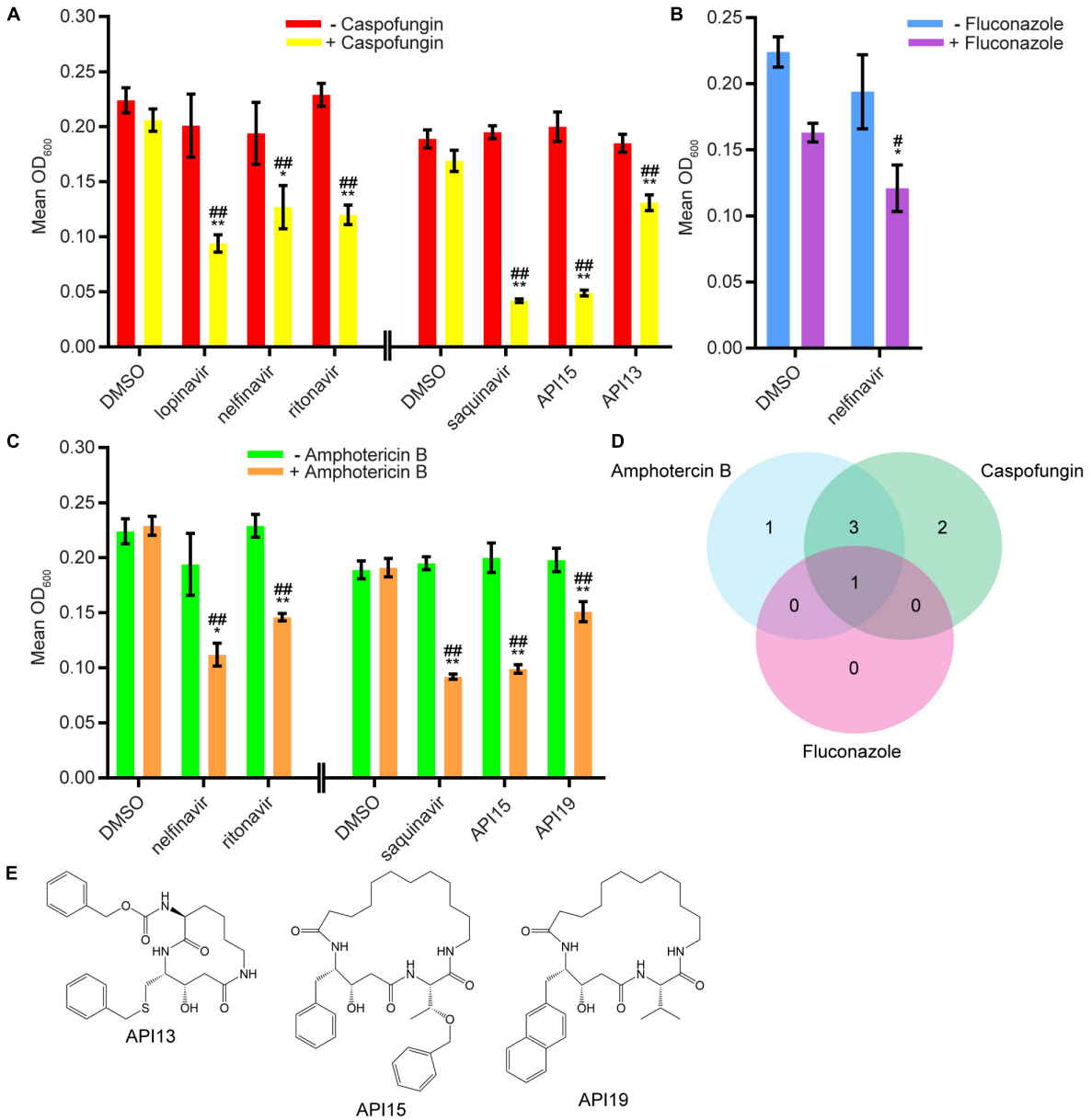

FIGURE 3 | Seven aspartyl protease inhibitors were capable of inhibiting biofilm formation in combination with one or more of the three antifungal agents tested. **(A)** Statistically significant hits from the combination Sustained Inhibition Biofilm Assays with caspofungin. For each compound, the wells with caspofungin (+caspofungin) are indicated in yellow and the wells without caspofungin (–caspofungin) are indicated in red. **(B)** Statistically significant hit from the combination Sustained Inhibition Biofilm Assays with fluconazole. For each compound, the wells with fluconazole (+fluconazole) are indicated in purple and the wells without fluconazole (–fluconazole) are indicated in blue. **(C)** Statistically significant hits from the combination Sustained Inhibition Biofilm Assays with amphotericin B. For each compound, the wells with amphotericin B (+amphotericin B) are indicated in orange and the wells without amphotericin B (–amphotericin B) are indicated in green. For panels a–c, mean OD_{600} readings with standard deviations are shown; significant differences from the compound without antifungal agent control (e.g., lopinavir, – caspofungin), as determined by Welch's *t*-test (two-tailed, assuming unequal variance) with the Bonferroni Correction, are indicated for $\alpha = 0.05$ (*) and $\alpha = 0.01$ (**). Significant differences from the antifungal agent without compound control (e.g., DMSO, +caspofungin), as determined by Welch's *t*-test (two-tailed, assuming unequal variance) with the Bonferroni Correction, are indicated for $\alpha = 0.05$ (#) and $\alpha = 0.01$ (##). Data from separate plates are separated by two vertical lines on the *x*-axis; the DMSO solvent control is shown for each plate. **(D)** Venn diagram illustrating the degree of overlap between the combination aspartyl protease inhibitor Sustained Inhibition Biofilm Assay screens with amphotericin B, caspofungin, or fluconazole. **(E)** Structure of the aspartyl protease inhibitors API13, API15, and API19.

were effective at disrupting mature biofilms, but were not effective at inhibiting biofilm formation, namely atazanavir, indinavir, and API16. We also note that the macrocycle API19 had a synergistic effect with amphotericin B in the Sustained Inhibition Biofilm Assay but with caspofungin in the Disruption Biofilm Assay.

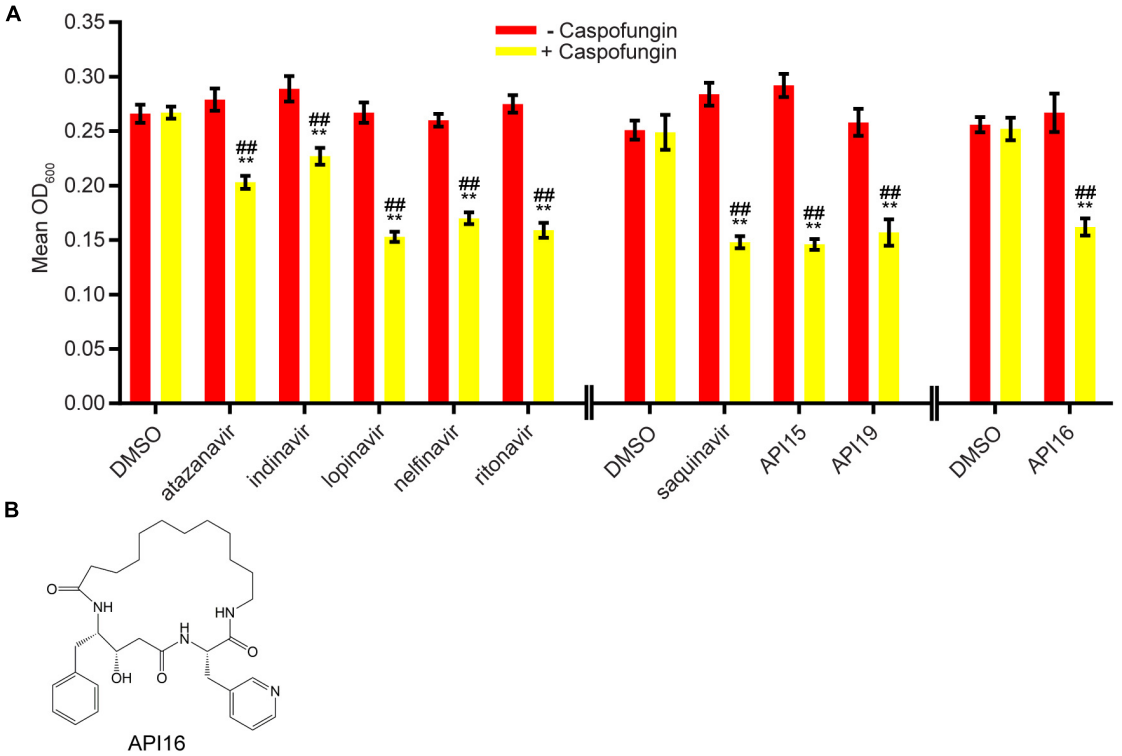

FIGURE 4 | Nine aspartyl protease inhibitors disrupted mature biofilms in combination with the antifungal agent caspofungin. **(A)** Statistically significant hits from the combination Disruption Biofilm Assays with caspofungin. For each compound, the wells with caspofungin (+caspofungin) are indicated in yellow and the wells without caspofungin (–caspofungin) are indicated in red. Mean OD_{600} readings with standard deviations are shown; significant differences from the compound without the caspofungin control (e.g., atazanavir, – caspofungin), as determined by Welch's *t*-test (two-tailed, assuming unequal variance) with the Bonferroni Correction, are indicated for $\alpha = 0.05$ (*) and $\alpha = 0.01$ (**). Significant differences from the caspofungin without compound control (e.g., DMSO, +caspofungin), as determined by Welch's *t*-test (two-tailed, assuming unequal variance) with the Bonferroni Correction, are indicated for $\alpha = 0.05$ (#) and $\alpha = 0.01$ (##). Data from separate plates are separated by two vertical lines on the *x*-axis; the DMSO solvent control is shown for each plate. **(B)** Structure of the aspartyl protease inhibitor API16.

DISCUSSION

The ability of *C. albicans* to form biofilms on biotic and abiotic surfaces presents a serious treatment challenge in the clinic as biofilms are typically resistant to all classes of antifungal drugs used to treat planktonic infections. Our results suggest that proteolysis is important for the maintenance of the *C. albicans* biofilm structure since anti-proteolytic agents contribute to the prevention and disruption of these biofilms. Proteases may play several different roles in *C. albicans* biofilm formation, an idea supported by the fact that proteases are dynamically expressed throughout the course of *C. albicans* biofilm formation (Nailis et al., 2010; Fox et al., 2015a). For example, Sap5 and Sap6, two secreted aspartyl proteases that are highly upregulated at certain stages of biofilm formation, are known to mediate adhesion of *C. albicans* cells to surfaces and possibly of *C. albicans* cells to one another (Kumar et al., 2015; Winter et al., 2016). Proteases may also contribute to the breakdown and acquisition of nutrients, the processing of molecules important for biofilm formation (e.g., adhesion molecules), quorum sensing, and/or extracellular matrix production throughout biofilm formation and maintenance. Although the involvement of secreted proteases in biofilm formation is a relatively new concept, there is some precedent for this idea in bacterial biofilms, where extracellular proteases were found to be involved in the processing of adhesion molecules during biofilm formation of *Staphylococcus* species (Koziel and Potempa, 2013; Paharik et al., 2017; Martínez-García et al., 2018).

In this study, we identify several protease inhibitors from different classes that are effective at preventing biofilm formation and/or at disrupting established biofilms when combined with caspofungin, fluconazole, or amphotericin B, members of the three major antifungal classes used to treat fungal infections in the clinic. Aspartyl protease inhibitors, in particular those that inhibit HIV-1 protease, were the most effective compounds tested when combined with traditional antifungal agents. Combined with the known dependence on Sap5 and Sap6 for biofilm formation (Winter et al., 2016) and previous reports that aspartyl protease inhibitors affect *C. albicans in vitro* and *in vivo* (Borg-von Zepelin et al., 1999; Cassone et al., 1999, 2002; Cauda et al., 1999; de Bernardis et al., 1999; Diz Dios et al., 1999; Gruber et al., 1999b,a; Korting et al., 1999; Bektic et al., 2001; Pichová et al., 2001; Skrbec and Romeo, 2002; Cenci et al., 2008; Tsang and Hong, 2009; Braga-Silva et al., 2010), aspartyl protease inhibitors are potentially promising combination treatments for *C. albicans* biofilm infections which are recalcitrant to single drug

treatments. We note, however, that we screened fewer inhibitors of other classes of proteases than we did for aspartyl proteases. Despite this bias, we succeeded in identifying several inhibitors of two additional classes of proteases, serine and metalloproteases. It may prove rewarding to conduct additional screens of FDA-approved drugs whose mechanisms rely on the inhibition of other classes of proteases with the goal of repurposing these drugs as novel antifungals.

Perhaps the most unexpected result from this study was the identification of compounds capable of disrupting mature biofilms that were unable to prevent biofilm formation (**Figure 5**). Unlike the opposite case, where a compound that could prevent biofilm formation might be unable to penetrate a mature biofilm to have an effect, it is not readily apparent how the capacity to disrupt an established biofilm would not also inhibit the formation of a biofilm. Although we do not understand the basis for this result, it demonstrates that compounds that disrupt biofilms are not simply a subset of those that inhibit formation (**Figure 5**). This observation underscores the importance of screening compounds for their antibiofilm capabilities in both types of assays.

Although we focused on one type of compound, protease inhibitors, this study raises several points to consider when screening for antibiofilm agents. First, consistent with previous reports (Delattin et al., 2014; De Cremer et al., 2015), our results highlight the importance of screening for synergistic interactions, as we detected more hits and hits with stronger effects against biofilms when existing antifungal agents were present along with the compound of interest (**Figure 5**). Second, our results highlight the importance of screening using biofilms as opposed to planktonic cultures. For example, in our biofilm assays with saquinavir, amphotericin B showed more synergy than fluconazole whereas the opposite relationship was reported for planktonic cultures (Casolari et al., 2004). We also note that we identified compounds that had effects on their own but not in combination with existing antifungal agents, as well as the reverse. As such, pursuing multiple assays (e.g., planktonic versus biofilm, standalone compounds versus combinations) maximizes the chance of identifying useful compounds.

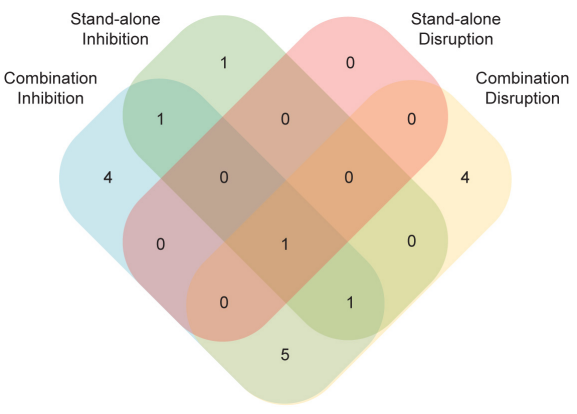

FIGURE 5 | A number of compounds had effects in just a subset of the four biofilm assays. Compounds with an effect in either the standalone or the combination versions of the Sustained Inhibition or Disruption Biofilm Assays are indicated. In total, 17 compounds had an effect in at least one of the four assays.

Finally, we note that this study was largely inspired by the discovery of the biofilm defects of the *sap5* and *sap6* single and double mutant strains (Winter et al., 2016). Thus, future compound library screening could be informed by other sets of gene knockouts with biofilm defects; likewise, results from chemical screens could identify genes (and their protein products) required for biofilm formation if the mechanism of action of the chemical compound is known. To further develop the idea of exploiting existing compounds, it should be possible to screen existing *C. albicans* mutant strain libraries for biofilm defects that arise in the presence of subinhibitory concentrations of traditional antifungal agents. Should biofilm formation by specific classes of mutant strains prove particularly sensitive to traditional antifungal agents, a subsequent combination screen between the traditional antifungal agents and compounds that affect that particular pathway of genes might prove informative.

DATA AVAILABILITY STATEMENT

All datasets generated for this study are included in the article/**Supplementary Material**.

AUTHOR CONTRIBUTIONS

ML, MG, CN, and AJ conceptualized the study. ML and MG worked on the methodology and carried out the investigation. ML contributed to validation, formal analysis, the data curation, and writing the original draft. ML and MG worked on the methodology and carried out the investigation. CC, CN, and AJ helped with the resources. ML, CC, MG, CN, and AJ reviewed and edited the manuscript. ML and CN helped with the visualization. ML, CN, and AJ were responsible for the supervision and project administration. ML, CC, CN, and AJ acquired the funding.

FUNDING

This work was supported by the National Institutes of Health (NIH) grants R43AI131710 (to ML), P50AI150476 (to CC), R01AI083311 (to AJ), and R35GM124594, and R41AI112038 (to CN). This work was also supported by the Kamangar family in the form of an endowed chair (to CN). The content is the sole responsibility of the authors and does not represent the views of the funders. The funders had no role in the design of the study; in the collection, analyses, or interpretation of data; in the writing of the manuscript; and in the decision to publish the results.

ACKNOWLEDGMENTS

We thank Drs. Michael Winter and Starlynn Clarke for advice. This manuscript has been released as a pre-print at bioRxiv (Lohse et al., 2020).

SUPPLEMENTARY MATERIAL

The Supplementary Material for this article can be found online at: https://www.frontiersin.org/articles/10.3389/fmicb.2020.01027/full#supplementary-material

TABLE S1 | Compiled data and statistics from the standalone and combination Sustained Inhibition and Disruption Optical Density Biofilm Assays as well as the BIC Sustained Inhibition Optical Density Biofilm Assay. For each compound, the concentration used, average OD_{600}, average OD_{600} of relevant control(s), and value(s) for Welch's *t*-test versus the relevant control(s) are provided. Whether the average OD_{600} was below the average OD_{600} of the relevant control(s) and whether the difference from the relevant control(s) remains significant following the Bonferroni Correction ($\alpha = 0.05$) are also indicated. The sensitivity of SNY425 to amphotericin B, caspofungin, and fluconazole in planktonic and biofilms assays are also indicated. A list of the 80 compounds from the three protease inhibitor libraries tested in this study and a summary of the hits from the standalone and combination Sustained Inhibition and Disruption Optical Density Biofilm Assays are also included.

REFERENCES

Achkar, J. M., and Fries, B. C. (2010). *Candida* infections of the genitourinary tract. *Clin. Microbiol. Rev.* 23, 253–273. doi: 10.1128/cmr.00076-09

Andes, D. R., Safdar, N., Baddley, J. W., Playford, G., Reboli, A. C., Rex, J. H., et al. (2012). Impact of treatment strategy on outcomes in patients with candidemia and other forms of invasive candidiasis: a patient-level quantitative review of randomized trials. *Clin. Infect. Dis.* 54, 1110–1122. doi: 10.1093/cid/cis021

Bamford, C. V., D'Mello, A., Nobbs, A. H., Dutton, L. C., Vickerman, M. M., and Jenkinson, H. F. (2009). *Streptococcus gordonii* modulates *Candida albicans* biofilm formation through intergeneric communication. *Infect. Immun.* 77, 3696–3704. doi: 10.1128/IAI.00438-09

Bamford, C. V., Nobbs, A. H., Barbour, M. E., Lamont, R. J., and Jenkinson, H. F. (2015). Functional regions of *Candida albicans* hyphal cell wall protein Als3 that determine interaction with the oral bacterium *Streptococcus gordonii*. *Microbiology* 161, 18–29. doi: 10.1099/mic.0.083378-0

Bektic, J., Lell, C. P., Fuchs, A., Stoiber, H., Speth, C., Lass-Flörl, C., et al. (2001). HIV protease inhibitors attenuate adherence of *Candida albicans* to epithelial cells *in vitro*. *FEMS Immunol. Med. Microbiol.* 31, 65–71. doi: 10.1111/j.1574-695x.2001.tb01588.x

Borg-von Zepelin, M., Meyer, I., Thomssen, R., Würzner, R., Sanglard, D., Telenti, A., et al. (1999). HIV-protease inhibitors reduce cell adherence of *Candida albicans* strains by inhibition of yeast secreted aspartic proteases. *J. Invest. Dermatol.* 113, 747–751. doi: 10.1046/j.1523-1747.1999.00747.x

Braga-Silva, L. A., Mogami, S. S. V., Valle, R. S., Silva-Neto, I. D., and Santos, A. L. S. (2010). Multiple effects of amprenavir against *Candida albicans*. *FEMS Yeast Res.* 10, 221–224. doi: 10.1111/j.1567-1364.2009.00595.x

Calderone, R. A., and Fonzi, W. A. (2001). Virulence factors of *Candida albicans*. *Trends Microbiol.* 9, 327–335.

Casolari, C., Rossi, T., Baggio, G., Coppi, A., Zandomeneghi, G., Ruberto, A., et al. (2004). Interaction between saquinavir and antimycotic drugs on *C. albicans* and *C. neoformans* strains. *Pharmacol. Res.* 50, 605–610. doi: 10.1016/j.phrs.2004.06.008

Cassone, A., De Bernardis, F., Torosantucci, A., Tacconelli, E., Tumbarello, M., and Cauda, R. (1999). *In vitro* and *in vivo* anticandidal activity of human immunodeficiency virus protease inhibitors. *J. Infect. Dis.* 180, 448–453. doi: 10.1086/314871

Cassone, A., Tacconelli, E., De Bernardis, F., Tumbarello, M., Torosantucci, A., Chiani, P., et al. (2002). Antiretroviral therapy with protease inhibitors has an early, immune reconstitution–independent beneficial effect on *Candida* virulence and oral candidiasis in human immunodeficiency virus–infected subjects. *J. Infect. Dis.* 185, 188–195. doi: 10.1086/338445

Cauda, R., Tacconelli, E., Tumbarello, M., Morace, G., De Bernardis, F., Torosantucci, A., et al. (1999). Role of protease inhibitors in preventing recurrent oral candidosis in patients with HIV infection: a prospective case-control study. *J. Acquir. Immune Defic. Syndr.* 21, 20–25. doi: 10.1097/00126334-199905010-00003

Cenci, E., Francisci, D., Belfiori, B., Pierucci, S., Baldelli, F., Bistoni, F., et al. (2008). Tipranavir exhibits different effects on opportunistic pathogenic fungi. *J. Infect.* 56, 58–64. doi: 10.1016/j.jinf.2007.08.004

Chandra, J., Kuhn, D. M., Mukherjee, P. K., Hoyer, L. L., McCormick, T., and Ghannoum, M. A. (2001). Biofilm formation by the fungal pathogen *Candida albicans*: development, architecture, and drug resistance. *J. Bacteriol.* 183, 5385–5394.

Clarke, S. C., Dumesic, P. A., Homer, C. M., O'Donoghue, A. J., La Greca, F., Pallova, L., et al. (2016). Integrated activity and genetic profiling of secreted peptidases in *Cryptococcus neoformans* reveals an aspartyl peptidase required for low pH survival and virulence. *PLoS Pathog.* 12:e1006051. doi: 10.1371/journal.ppat.1006051

de Bernardis, F., Mondello, F., Scaravelli, G., Pachì, A., Girolamo, A., Agatensi, L., et al. (1999). High aspartyl proteinase production and vaginitis in human immunodeficiency virus-infected women. *J. Clin. Microbiol.* 37, 1376–1380. doi: 10.1128/jcm.37.5.1376-1380.1999

De Cremer, K., Lanckacker, E., Cools, T. L., Bax, M., De Brucker, K., Cos, P., et al. (2015). Artemisinins, new miconazole potentiators resulting in increased activity against *Candida albicans* biofilms. *Antimicrob. Agents Chemother.* 59, 421–426. doi: 10.1128/AAC.04229-14

Delattin, N., De Brucker, K., Vandamme, K., Meert, E., Marchand, A., Chaltin, P., et al. (2014). Repurposing as a means to increase the activity of amphotericin B and caspofungin against *Candida albicans* biofilms. *J. Antimicrob. Chemother.* 69, 1035–1044. doi: 10.1093/jac/dkt449

Diz Dios, P., Ocampo, A., Miralles, C., Otero, I., Iglesias, I., and Rayo, N. (1999). Frequency of oropharyngeal candidiasis in HIV-infected patients on protease inhibitor therapy. *Oral Surg Oral Med. Oral Pathol. Oral Radiol. Endod.* 87, 437–441. doi: 10.1016/s1079-2104(99)70242-8

Donlan, R. M. (2001). Biofilm formation: a clinically relevant microbiological process. *Clin. Infect. Dis.* 33, 1387–1392. doi: 10.1086/322972

Douglas, L. J. (2002). Medical importance of biofilms in *Candida* infections. *Rev. Iberoam. Micol.* 19, 139–143.

Douglas, L. J. (2003). *Candida* biofilms and their role in infection. *Trends Microbiol.* 11, 30–36. doi: 10.1016/s0966-842x(02)00002-1

Falkensammer, B., Pilz, G., Bektiæ, J., Imwidthaya, P., Jöhrer, K., Speth, C., et al. (2007). Absent reduction by HIV protease inhibitors of *Candida albicans* adhesion to endothelial cells. *Mycoses* 50, 172–177. doi: 10.1111/j.1439-0507.2006.01353.x

Fox, E. P., Bui, C. K., Nett, J. E., Hartooni, N., Mui, M. C., Andes, D. R., et al. (2015a). An expanded regulatory network temporally controls *Candida albicans* biofilm formation. *Mol. Microbiol.* 96, 1226–1239. doi: 10.1111/mmi.13002

Fox, E. P., Singh-Babak, S. D., Hartooni, N., and Nobile, C. J. (2015b). "Biofilms and antifungal resistance," in *Antifungals: From Genomics to Resistance and the Development of Novel Agents*, eds A. T. Coste and P. Vandeputte (Norfolk: Caister Academic Press), 71–90. doi: 10.21775/9781910190012.04

Fox, E. P., Cowley, E. S., Nobile, C. J., Hartooni, N., Newman, D. K., and Johnson, A. D. (2014). Anaerobic bacteria grow within *Candida albicans* biofilms and induce biofilm formation in suspension cultures. *Curr. Biol.* 24, 2411–2416. doi: 10.1016/j.cub.2014.08.057

Fox, E. P., and Nobile, C. J. (2012). A sticky situation: untangling the transcriptional network controlling biofilm development in *Candida albicans*. *Transcription* 3, 315–322. doi: 10.4161/trns.22281

Ganguly, S., and Mitchell, A. P. (2011). Mucosal biofilms of *Candida albicans*. *Curr. Opin. Microbiol.* 14, 380–385. doi: 10.1016/j.mib.2011.06.001

Gruber, A., Berlit, J., Speth, C., Lass-Flörl, C., Kofler, G., Nagl, M., et al. (1999a). Dissimilar attenuation of *Candida albicans* virulence properties by human immunodeficiency virus type 1 protease inhibitors. *Immunobiology* 201, 133–144. doi: 10.1016/s0171-2985(99)80052-7

Gruber, A., Speth, C., Lukasser-Vogl, E., Zangerle, R., Borg-von Zepelin, M., Dierich, M. P., et al. (1999b). Human immunodeficiency virus type 1 protease inhibitor attenuates *Candida albicans* virulence properties *in vitro*. *Immunopharmacology* 41, 227–234. doi: 10.1016/s0162-3109(99)00035-1

Gulati, M., Lohse, M. B., Ennis, C. L., Gonzalez, R. E., Perry, A. M., Bapat, P., et al. (2018). *In vitro* culturing and screening of *Candida albicans* biofilms. *Curr. Protoc. Microbiol.* 50:e60. doi: 10.1002/cpmc.60

Gulati, M., and Nobile, C. J. (2016). *Candida albicans* biofilms: development, regulation, and molecular mechanisms. *Microbes Infect.* 18, 310–321. doi: 10.1016/j.micinf.2016.01.002

Harriott, M. M., and Noverr, M. C. (2009). *Candida albicans* and *Staphylococcus aureus* form polymicrobial biofilms: effects on antimicrobial resistance. *Antimicrob. Agents Chemother.* 53, 3914–3922. doi: 10.1128/AAC.00657-09

Harriott, M. M., and Noverr, M. C. (2010). Ability of *Candida albicans* mutants to induce *Staphylococcus aureus* vancomycin resistance during polymicrobial biofilm formation. *Antimicrob. Agents Chemother.* 54, 3746–3755. doi: 10.1128/AAC.00573-10

Jack, A. A., Daniels, D. E., Jepson, M. A., Vickerman, M., Lamont, R. J., Jenkinson, H. F., et al. (2015). *Streptococcus gordonii* comCDE (competence) operon modulates biofilm formation with *Candida albicans*. Microbiology 161, 411–421. doi: 10.1099/mic.0.000010

Jarosz, L. M., Deng, D. M., van der Mei, H. C., Crielaard, W., and Krom, B. P. (2009). *Streptococcus mutans* competence-stimulating peptide inhibits *Candida albicans* hypha formation. *Eukaryot. Cell* 8, 1658–1664. doi: 10.1128/EC.00070-09

Kennedy, M. J., and Volz, P. A. (1985). Ecology of *Candida albicans* gut colonization: inhibition of *Candida* adhesion, colonization, and dissemination from the gastrointestinal tract by bacterial antagonism. *Infect. Immun.* 49, 654–663. doi: 10.1128/iai.49.3.654-663.1985

Kim, J., and Sudbery, P. (2011). *Candida albicans*, a major human fungal pathogen. *J. Microbiol.* 49, 171–177. doi: 10.1007/s12275-011-1064-7

Kojic, E. M., and Darouiche, R. O. (2004). *Candida* infections of medical devices. *Clin. Microbiol. Rev.* 17, 255–267. doi: 10.1128/cmr.17.2.255-267.2004

Kong, E. F., Tsui, C., Kucharíková, S., Andes, D., Van Dijck, P., and Jabra-Rizk, M. A. (2016). Commensal protection of *Staphylococcus aureus* against antimicrobials by *Candida albicans* biofilm matrix. *mBio* 7:e01365-16.

Korting, H. C., Schaller, M., Eder, G., Hamm, G., Böhmer, U., and Hube, B. (1999). Effects of the human immunodeficiency virus (HIV) proteinase inhibitors saquinavir and indinavir on *in vitro* activities of secreted aspartyl proteinases of *Candida albicans* isolates from HIV-infected patients. *Antimicrob. Agents Chemother.* 43, 2038–2042. doi: 10.1128/aac.43.8.2038

Koziel, J., and Potempa, J. (2013). Protease-armed bacteria in the skin. *Cell Tissue Res.* 351, 325–337. doi: 10.1007/s00441-012-1355-2

Kullberg, B. J., and Oude Lashof, A. M. L. (2002). Epidemiology of opportunistic invasive mycoses. *Eur. J. Med. Res.* 7, 183–191.

Kumamoto, C. A. (2002). *Candida* biofilms. *Curr. Opin. Microbiol.* 5, 608–611.

Kumamoto, C. A. (2011). Inflammation and gastrointestinal *Candida* colonization. *Curr. Opin. Microbiol.* 14, 386–391. doi: 10.1016/j.mib.2011.07.015

Kumar, R., Saraswat, D., Tati, S., and Edgerton, M. (2015). Novel aggregation properties of *Candida albicans* secreted aspartyl proteinase Sap6 mediate virulence in oral candidiasis. *Infect. Immun.* 83, 2614–2626. doi: 10.1128/iai.00282-15

Lebeaux, D., Ghigo, J. M., and Beloin, C. (2014). Biofilm-related infections: bridging the gap between clinical management and fundamental aspects of recalcitrance toward antibiotics. *Microbiol. Mol. Biol. Rev.* 78, 510–543. doi: 10.1128/mmbr.00013-14

Lindsay, A. K., and Hogan, D. A. (2014). *Candida albicans*: molecular interactions with *Pseudomonas aeruginosa* and *Staphylococcus aureus*. Fungal Biol. Rev. 28, 85–96. doi: 10.1016/j.fbr.2014.10.002

Lohse, M. B., Gulati, M., Arevalo, A. V., Fishburn, A., Johnson, A. D., and Nobile, C. J. (2017). Assessment and optimizations of *Candida albicans in vitro* biofilm assays. *Antimicrob. Agents Chemother.* 61:e02749-16.

Lohse, M. B., Gulati, M., Craik, C. S., Johnson, A. D., and Nobile, C. J. (2020). Combination of antifungal drugs and protease inhibitors prevent *Candida albicans* biofilm formation and disrupt mature biofilms. *bioRxiv [Preprint]*

Lohse, M. B., Gulati, M., Johnson, A. D., and Nobile, C. J. (2018). Development and regulation of single- and multi-species *Candida albicans* biofilms. *Nat. Rev. Microbiol.* 16, 19–31. doi: 10.1038/nrmicro.2017.107

López-Ribot, J. L. (2005). *Candida albicans* biofilms: more than filamentation. *Curr. Biol.* 15, R453–R455. doi: 10.1016/j.cub.2005.06.020

Martínez-García, S., Rodríguez-Martínez, S., Cancino-Diaz, M. E., and Cancino-Diaz, J. C. (2018). Extracellular proteases of *Staphylococcus epidermidis*: roles as virulence factors and their participation in biofilm. *APMIS* 126, 177–185. doi: 10.1111/apm.12805

Nailis, H., Kucharíková, S., Ricicová, M., Van Dijck, P., Deforce, D., Nelis, H., et al. (2010). Real-time PCR expression profiling of genes encoding potential virulence factors in *Candida albicans* biofilms: identification of model-dependent and -independent gene expression. *BMC Microbiol.* 10:114. doi: 10.1186/1471-2180-10-114

Nobile, C. J., Fox, E. P., Hartooni, N., Mitchell, K. F., Hnisz, D., Andes, D. R., et al. (2014). A histone deacetylase complex mediates biofilm dispersal and drug resistance in *Candida albicans*. *mBio* 5:e01201-14. doi: 10.1128/mBio.01201-14

Nobile, C. J., Fox, E. P., Nett, J. E., Sorrells, T. R., Mitrovich, Q. M., Hernday, A. D., et al. (2012). A recently evolved transcriptional network controls biofilm development in *Candida albicans*. *Cell* 148, 126–138. doi: 10.1016/j.cell.2011.10.048

Nobile, C. J., and Johnson, A. D. (2015). *Candida albicans* biofilms and human disease. *Annu. Rev. Microbiol.* 69, 71–92.

Noble, S. M., French, S., Kohn, L. A., Chen, V., and Johnson, A. D. (2010). Systematic screens of a *Candida albicans* homozygous deletion library decouple morphogenetic switching and pathogenicity. *Nat. Genet.* 42, 590–598. doi: 10.1038/ng.605

Paharik, A. E., Kotasinska, M., Both, A., Hoang, T.-M. N., Büttner, H., Roy, P., et al. (2017). The metalloprotease SepA governs processing of accumulation-associated protein and shapes intercellular adhesive surface properties in *Staphylococcus epidermidis*. *Mol. Microbiol.* 103, 860–874. doi: 10.1111/mmi.13594

Pammi, M., Zhong, D., Johnson, Y., Revell, P., and Versalovic, J. (2014). Polymicrobial bloodstream infections in the neonatal intensive care unit are associated with increased mortality: a case-control study. *BMC Infect. Dis.* 14:390. doi: 10.1186/1471-2334-14-390

Pappas, P. G., Rex, J. H., Sobel, J. D., Filler, S. G., Dismukes, W. E., Walsh, T. J., et al. (2004). Guidelines for treatment of candidiasis. *Clin. Infect. Dis.* 38, 161–189. doi: 10.1086/380796

Peleg, A. Y., Hogan, D. A., and Mylonakis, E. (2010). Medically important bacterial-fungal interactions. *Nat. Rev. Microbiol.* 8, 340–349. doi: 10.1038/nrmicro2313

Peters, B. M., and Noverr, M. C. (2013). *Candida albicans-Staphylococcus aureus* polymicrobial peritonitis modulates host innate immunity. *Infect. Immun.* 81, 2178–2189. doi: 10.1128/IAI.00265-13

Pichová, I., Pavlícková, L., Dostál, J., Dolejsí, E., Hrusková-Heidingsfeldová, O., Weber, J., et al. (2001). Secreted aspartic proteases of *Candida albicans*, *Candida tropicalis*, *Candida parapsilosis* and *Candida lusitaniae*. Inhibition with peptidomimetic inhibitors. *Eur. J. Biochem.* 268, 2669–2677. doi: 10.1046/j.1432-1327.2001.02152.x

Prasad, R., Shah, A. H., and Rawal, M. K. (2016). Antifungals: mechanism of action and drug resistance. *Adv. Exp. Med. Biol.* 892, 327–349. doi: 10.1007/978-3-319-25304-6_14

Ramage, G., Martínez, J. P., and López-Ribot, J. L. (2006). *Candida* biofilms on implanted biomaterials: a clinically significant problem. *FEMS Yeast Res.* 6, 979–986. doi: 10.1111/j.1567-1364.2006.00117.x

Ramage, G., Mowat, E., Jones, B., Williams, C., and Lopez-Ribot, J. (2009). Our current understanding of fungal biofilms. *Crit. Rev. Microbiol.* 35, 340–355.

Skrbec, D., and Romeo, D. (2002). Inhibition of *Candida albicans* secreted aspartic protease by a novel series of peptidomimetics, also active on the HIV-1 protease. *Biochem. Biophys. Res. Commun.* 297, 1350–1353. doi: 10.1016/s0006-291x(02)02372-0

Tsang, C. S. P., and Hong, I. (2009). HIV protease inhibitors differentially inhibit adhesion of *Candida albicans* to acrylic surfaces. *Mycoses* 53, 488–494. doi: 10.1111/j.1439-0507.2009.01743.x

Tumbarello, M., Fiori, B., Trecarichi, E. M., Posteraro, P., Losito, A. R., De Luca, A., et al. (2012). Risk factors and outcomes of candidemia caused by biofilm-forming isolates in a tertiary care hospital. *PLoS One* 7:e33705. doi: 10.1371/journal.pone.0033705

Tumbarello, M., Posteraro, B., Trecarichi, E. M., Fiori, B., Rossi, M., Porta, R., et al. (2007). Biofilm production by *Candida* species and inadequate antifungal therapy as predictors of mortality for patients with candidemia. *J. Clin. Microbiol.* 45, 1843–1850. doi: 10.1128/jcm.00131-07

Uppuluri, P., Acosta Zaldívar, M., Anderson, M. Z., Dunn, M. J., Berman, J., Lopez Ribot, J. L., et al. (2018). *Candida albicans* dispersed cells are developmentally distinct from biofilm and planktonic cells. *mBio* 9:e01338-18. doi: 10.1128/mBio.01338-18

Uppuluri, P., Chaturvedi, A. K., Srinivasan, A., Banerjee, M., Ramasubramaniam, A. K., Köhler, J. R., et al. (2010). Dispersion as an important step in the *Candida albicans* biofilm developmental cycle. *PLoS Pathog.* 6:e1000828. doi: 10.1371/journal.ppat.1000828

Wenzel, R. P. (1995). Nosocomial candidemia: risk factors and attributable mortality. *Clin. Infect. Dis.* 20, 1531–1534. doi: 10.1093/clinids/20.6.1531

Winter, M. B., Salcedo, E. C., Lohse, M. B., Hartooni, N., Gulati, M., Sanchez, H., et al. (2016). Global identification of biofilm-specific proteolysis in *Candida albicans*. *mBio* 7:e01514-16. doi: 10.1128/mBio.01514-16

Conflict of Interest: CN and AJ are cofounders of BioSynesis, Inc., a company developing inhibitors and diagnostics of *C. albicans* biofilms. ML was formerly an employee and currently is a consultant for BioSynesis, Inc. MG was formerly a consultant for BioSynesis, Inc.

The remaining author declares that the research was conducted in the absence of any commercial or financial relationships that could be construed as a potential conflict of interest.

frontiers in Microbiology

ORIGINAL RESEARCH
published: 05 June 2020
doi: 10.3389/fmicb.2020.01117

Biofilm Formation of *Candida albicans* Facilitates Fungal Infiltration and Persister Cell Formation in Vaginal Candidiasis

Xueqing Wu[1,2†], Sisi Zhang[1†], Haiying Li[2], Laien Shen[1], Chenle Dong[1], Yao Sun[3], Huale Chen[3], Boyun Xu[1], Wenyi Zhuang[2], Margaret Deighton[4] and Yue Qu[3,5]*

[1] Department of Obstetrics and Gynecology, The First Affiliated Hospital of Wenzhou Medical University, Wenzhou, China, [2] Department of Obstetrics and Gynecology, Shenzhen University General Hospital, Shenzhen, China, [3] Department of Laboratory Medicine, The First Affiliated Hospital of Wenzhou Medical University, Wenzhou, China, [4] School of Applied Sciences, RMIT University, Bundoora, VIC, Australia, [5] Wenzhou Medical University-Monash BDI Alliance in Clinical and Experimental Biomedicine, Monash University, Clayton, VIC, Australia

OPEN ACCESS

Edited by:
Juliana Campos Junqueira,
São Paulo State University, Brazil

Reviewed by:
Carmen Rodriguez-Cerdeira,
University Hospital Complex of Vigo, Spain
Haroldo Oliveira,
Instituto Carlos Chagas (ICC), Brazil

***Correspondence:**
Yue Qu
yue.qu@monash.edu

[†] These authors have contributed equally to this work

Specialty section:
This article was submitted to Infectious Diseases, a section of the journal Frontiers in Microbiology

Received: 01 February 2020
Accepted: 05 May 2020
Published: 05 June 2020

Citation:
Wu X, Zhang S, Li H, Shen L, Dong C, Sun Y, Chen H, Xu B, Zhuang W, Deighton M and Qu Y (2020) Biofilm Formation of Candida albicans Facilitates Fungal Infiltration and Persister Cell Formation in Vaginal Candidiasis. Front. Microbiol. 11:1117. doi: 10.3389/fmicb.2020.01117

Background: Vaginal candidiasis is an important medical condition awaiting more effective treatment. How *Candida albicans* causes this disease and survives antifungal treatment is not yet fully understood. This study aimed to establish a comprehensive understanding of biofilm-related defensive strategies that *C. albicans* uses to establish vaginal candidiasis and to survive antifungal treatment.

Methods: A mouse model of vaginal candidiasis was adopted to examine the formation of biotic biofilms on the vaginal epithelium and fungal infiltration by laboratory and clinical strains of *C. albicans*. Histopathological changes and local inflammation in the vaginal epithelium caused by *C. albicans* of different biofilm phenotypes were compared. Antifungal susceptibility testing was carried out for *C. albicans* grown as planktonic cells, microplate-based abiotic biofilms, and epithelium-based biotic biofilms. Formation of persister cells by *C. albicans* in different growth modes was also quantified and compared.

Results: *C. albicans* wild-type reference strains and clinical isolates, but not the biofilm-defective mutants, formed a significant number of biotic biofilms on the vaginal epithelium of mice and infiltrated the epithelium. Biofilm formation and epithelial invasion induced local inflammatory responses and histopathological changes in the vaginal epithelium including neutrophil infiltration and subcorneal microabscesses. Biofilm growth on the vaginal epithelium also led to high resistance to antifungal treatments and promoted the formation of antifungal-tolerant persister cells.

Conclusion: This study comprehensively assessed biofilm-related microbial strategies that *C. albicans* uses in vaginal candidiasis and provided experimental evidence to support the important role of biofilm formation in the histopathogenesis of vaginal candidiasis and the recalcitrance of the infection to antifungal treatment.

Keywords: vaginal candidiasis, recurrent vaginal candidiasis, biofilm formation, fungal infiltration, persister cells, antifungal tolerance, mouse model

INTRODUCTION

Vaginal candidiasis is one of the commonest medical conditions affecting otherwise healthy women of reproductive age. It was estimated that 23–49% of women of reproductive age suffer from vaginal candidiasis, with the majority having uncomplicated infections (less than 3–4 episodes within a 12-month period) and a considerable number (6–9% of the patients) presenting with recurrent infections (at least 3–4 episodes in 1 year); the latter is a stubborn condition characterized by complex pathogenicity and tolerance to antifungal treatment (Ilkit and Guzel, 2011; Sobel, 2016; Blostein et al., 2017). Although vaginal candidiasis is believed to be an immunopathological condition of the human vagina with "neutrophy anergy" as the underlying mechanism, invading microorganisms might still play an important role in its pathogenicity (Yano et al., 2018). *Candida albicans* is the leading agent causing both uncomplicated and recurrent vaginal candidiasis (Liu et al., 2014; Goncalves et al., 2016). Proposed virulence determinants of *C. albicans* involved in the pathogenesis of vaginal candidiasis include fungal morphogenesis, adhesion to vaginal epithelial cells, the production of phospholipases and proteinase such as secreted aspartyl proteases (Saps), and the presence of candidalysin, a well-identified secreted cytolytic peptide toxin encoded by *ece1* (Kalkanci et al., 2013; Richardson et al., 2017).

While much has been done to define host- and pathogen-related factors contributing to the establishment of vaginal candidiasis (Ilkit and Guzel, 2011; Bruno et al., 2015; Yano et al., 2018), little effort has been placed on microbial mechanisms driving vaginal candidiasis to resist antifungal treatment and further develop into a more troublesome recurrent infection. Despite the fact that most *C. albicans* isolates from patients with uncomplicated or recurrent vaginal candidiasis showed sensitivities to many first-line antifungals, clinical ineffectiveness of these drugs in eradicating *Candida* or curing recurrent vaginal candidiasis has been constantly reported (Richter et al., 2005; Gamarra et al., 2014; Nagashima et al., 2016; Ying et al., 2016; Adjapong et al., 2017). This suggests that in addition to the host-related factors such as different host sensitivity to pathological responses, microbial strategies other than intrinsic resistance might be involved in the pathogenesis and persistence of vaginal candidiasis (Peters et al., 2014; Sobel, 2016).

Candida albicans and its related species are known to be able to adopt a major pathogenicity strategy, biofilm formation, to initiate and maintain infections, in particular on patients with breached immune defense (Hagerty et al., 2003; Kojic and Darouiche, 2004). Indeed, the role of epithelium-associated *C. albicans* biofilm in the development of vaginal candidiasis has been proposed (Harriott et al., 2010; Rodriguez-Cerdeira et al., 2019), though a recent study by Swidsinski et al. (2019) did not detect evident biofilms from the vaginal biopsies from patients with confirmed vaginal candidiasis. Two different types of biofilms might be involved in vaginal candidiasis: abiotic biofilms that require a plastic or metal substratum, such as intrauterine devices (IUDs; Auler et al., 2010; Cakiroglu et al., 2015), and biotic biofilms that use the vaginal epithelium as the supporting base (Harriott et al., 2010; Muzny and Schwebke, 2015). Epithelium-associated biotic biofilms were considered to be more important in the pathogenesis of recurrent vaginal candidiasis, as many patients suffer from recurrent infections without any IUDs implanted or after the removal of IUDs (Cakiroglu et al., 2015). Using a mouse vaginal candidiasis model, Harriott et al. (2010) successfully established *C. albicans* biofilms on the vaginal epithelium and raised the hypothesis that formation of epithelium-associated biofilms may be an initiating event for the infection (Harriott et al., 2010). A direct link between the formation of epithelium-associated biofilms and histopathological change of the vaginal epithelium, however, is still missing. Although antifungal resistance of *Candida* biofilms formed by clinical isolates from patients with vaginal candidiasis has been reported, the tests were mostly done on abiotic biofilms prepared in 96-well microplates (Gao et al., 2016; Sherry et al., 2017). Epithelium-associated biotic biofilms grown in a dynamic vaginal environment might differ from *in vitro* abiotic biofilms in many different ways, including their susceptibility to conventional antifungals (Bjarnsholt et al., 2013).

The typical dynamics of recurrent vaginal candidiasis coincides with the relapsing biofilm infection model proposed by Lewis (2010), suggesting possible involvement of persister cells (Lewis, 2010). Many studies, including our own, have found that persister cells are responsible for antimicrobial tolerance of many biofilm-related bacterial infections (Qu et al., 2010; Yang et al., 2015). Lafleur et al. (2006) first isolated *Candida* persister cells and linked their formation to the adherence growth mode of *C. albicans*. It is thus reasonable to hypothesize that biotic biofilms grown on the vaginal epithelium also harbor a small number of persister cells. Treatment of persister cells is known to be troublesome. Conventional antimicrobial agents, unless used at very high dose for an extended period, will not eradicate persister cells residing in biofilms (Yang et al., 2015; Wu et al., 2019). Our study aimed to establish a comprehensive understanding of the importance of *C. albicans* biofilm formation in the pathogenesis of vaginal candidiasis, in order to identify specific microbial targets for more efficient antifungal therapies.

MATERIALS AND METHODS

Ethics Statement

This study was approved by the Ethics Committee of Wenzhou Medical University, China (Ethics approval number: Wydw2016-0214). All experiments were performed in accordance with the National Institutes of Health guide for the care and use of laboratory animals.

Strains and Identification

Two biofilm-producing *C. albicans* laboratory reference strains, *C. albicans* DAY185 and *C. albicans* DAY286, and their biofilm-defective mutant strains, *med31*ΔΔ and *bcr1*ΔΔ, were used in this study (Lafleur et al., 2006; Uwamahoro et al., 2012).

Two *C. albicans* clinical isolates designated as VVC2 and VVC4 were also included. These two isolates were from patients with clinically diagnosed vaginal candidiasis (two and four episodes within a 12-month period, respectively) at The First Affiliated Hospital of Wenzhou Medical University. The clinical isolates were identified to a species level using the following tests: CHROMagar *Candida* medium (CHROMagar, Paris, France) and the Vitek matrix-assisted laser desorption/ionization-time of flight mass spectrometry (MALDI-TOF MS, bioMérieux, Craponne, France).

Mouse Vaginal Epithelial Biofilm Assay

An *in vivo* model of vaginal epithelium-associated biofilms was used essentially as previously described (Harriott et al., 2010). Firstly, BABL/C female mice of 6–8 weeks old were administered 0.1 mg of estrogen (17β-estradiol; Sigma) dissolved in 0.1 ml of sesame oil subcutaneously for three consecutive days prior to inoculation with *C. albicans*. *C. albicans* cells were grown in yeast peptone dextrose broth (YPD, 200 rpm, 30°C) for 20 h. One hundred microliters of fungal suspensions containing 7×10^5 colony-forming units (CFU) of *C. albicans* cells was used to infect mice via an intravaginal pathway. Mice were maintained in an animal facility and euthanized after 72 h before the vagina was removed. Fungal growth on the vaginal epithelium and underlying tissue was assessed qualitatively using scanning electronic microscopy (SEM, see below) and quantitatively with the CFU-based viable count method.

Scanning Electronic Microscopy

For SEM, dissected mouse vaginal tissues were fixed with glutaraldehyde for 2 h (2.5%, v/v, in 0.1 M cacodylate buffer, pH 7.0) at room temperature, and dehydrated with gradually increased ethanol levels (50, 75, 85, 95, 100, and absolute 100%) (Gargani et al., 1989). Samples were coated with gold using a Balzers SCD005 sputter coater and viewed under a scanning electron microscope (SEM; Hitachi, H-7500, Japan).

CFU-Based Viable Counts

For CFU-based viable counts, dissected mouse vaginal tissues were weighted, homogenized in PBS using a tissue homogenizer, followed by vortexing vigorously for 30 s four times and sonication at 42 kHz for 10 min. The suspensions were serially diluted with PBS and plated on YPD for 72 h for enumeration of CFUs.

Histopathology

For histopathological study of the infected vagina, tissues were fixed in 4% paraformaldehyde and selected tissue blocks were processed using a routine overnight cycle in a tissue processor. The tissue blocks were then embedded in wax, serially sliced into 5-μm sections. The transverse sections were stained with Periodic acid–Schiff (PAS) staining for the presence of *C. albicans* yeast/hyphae cells or Hematoxylin–Eosin (H&E) staining for tissue damage, and then imaged under a light microscope (Nikon ECLPSE 80i, Tokyo, Japan).

Enzyme-Linked Immunosorbent Assay

Concentrations of two representative inflammatory effectors in mouse vaginal lavage fluids, innate cytokine IL-1β and an alarmin S100A8, were analyzed using commercially available enzyme-linked immunosorbent assay (ELISA) kits (Boyun Biotech Co., Ltd, Shanghai, China) per the instructions from the manufacturer (Peters et al., 2014). Enzyme immunoassay/radioimmunoassay (EIA/RIA) plates were incubated with dilutions of lavage fluid (at 1:10 for IL-1β and 1:100 for S100A8) and serially diluted protein standards for 2 h. After washing, the plates were treated with biotinylated polyclonal goat anti-mouse IL-1β or S100A8 antibodies for 2 h, followed by incubation with streptavidin horseradish peroxidase (HRP) for 20 min. A tetramethylbenzidine-H_2O_2 substrate solution was added to the plates and the reactions were measured with a microplate reader at 450 nm.

In vitro Biofilm Formation on IUDs

Candida albicans biofilms were grown on two copper IUDs for qualitative analysis. Intrauterine devices were pretreated with fetal bovine serum (Sigma, North Ryde, Australia) overnight at 37°C with gentle shaking (75 rpm), washed twice with PBS, and transferred to a 24-well plate containing 1 ml of freshly prepared fungal suspensions (3×10^7 cells/ml in RPMI-1640 at pH 4.0). The plate was incubated for 1.5 h at 37°C with gentle shaking (75 rpm) to allow the yeast cells to adhere to the surfaces. The IDUs were then gently washed with PBS and transferred to a new 24-well plate with RPMI-1640 media (pH 4.0), followed by incubation at 37°C with shaking (75 rpm) for 48 h. The established biofilms were examined with SEM. Two IUDs were used in this study; an indomethacin releasing round copper IUD (Medsuture, Shanghai, China), and a yuan-gong type copper IUD (Yantai Jishengyaoxie Co., Ltd., Shangdong, China).

Antifungal Susceptibility Tests for Planktonic Cells and Abiotic Biofilms

Minimum inhibitory concentrations (MICs) were determined using the broth microdilution method according to CLSI guidelines M27-A3. Drug concentrations ranged from 0.125 to 64 μg/ml for clotrimazole and nystatin and 0.025–128 μg/ml for amphotericin B. The MIC was defined as the concentration resulting in complete growth inhibition for amphotericin B and an inhibition of at least 50% of fungal growth for other drugs, corresponding to a score of 2 in the NCCLS M27-A3 protocol. Abiotic biofilm MICs were determined by challenging *C. albicans* biofilms pre-grown in 96-well microplates with antifungal agents prepared in RPMI-1640 for 24 h (Qu et al., 2016). 3-Bis-(2-methoxy-4-nitro-5-sulfophenyl)-2H-tetrazolium-5-carboxanilide (XXT, Sigma-Aldrich, Australia) was used to assess the inhibitory efficacy of antifungal agents on the established abiotic biofilms. Biofilm MIC_{80} was determined as the lowest concentration that inhibited ≥80% of fungal biofilm growth. RPMI-1640 of pH 7.2 and pH 4.0 were used as growth medium, respectively, to examine the effect of different environmental acidity on antifungal efficacy as local pH has been found to impact on the

antifungal-mediated killing of *C. albicans* (Ilkit and Guzel, 2011; Kasper et al., 2015).

Ex vivo Antifungal Susceptibility Tests for Biotic Biofilms

For *ex vivo* antifungal susceptibility testing, epithelium-associated *C. albicans* biofilms were grown for 72 h before removal from the euthanized animals. Concentrations of selected antifungals ranged from 2 to 32 μg/ml for nystatin, 0.5–1280 μg/ml for clotrimazole, and 1–16 μg/ml for amphotericin B. Infected vaginal tissues were sectioned into small blocks of 3 mm × 5 mm × 5 mm and exposed to antifungal agents prepared at selected concentrations in RPMI-1640 (pH 4.0 and pH 7.2, respectively) for 24 h. The treated vaginal tissue blocks were washed with PBS, homogenized with tissue homogenizer. Colony-forming units counting was carried out by plating an aliquot onto YPD plates followed by an incubation at 37°C for 48 h. Vaginal tissue treated with RPMI-1640 served as untreated control.

Quantification of Persister Cells From Planktonic Cultures, Abiotic Biofilms, and Biotic Biofilms

To isolate persister cells from planktonic cultures, suspensions of single cells from cultures at mid-log phase were adjusted to densities of ∼3 × 10^7 CFU/ml and exposed to amphotericin B at 100 mg/ml for 24 h (Lafleur et al., 2006). To isolate the persister cell population from abiotic biofilms, *in vitro* biofilms of *C. albicans* were grown in 6-well microplates and collected using a cell scraper. Collected biofilms were then re-suspended into suspensions of single cells at densities of ∼3 × 10^7 CFU/ml (LaFleur et al., 2010). Biofilm cells were statically exposed to amphotericin B at 100 mg/ml for 24 h. To isolate the persister cell population in epithelium-associated biotic biofilms, vagina tissues were removed from the euthanized animals and then sectioned into small blocks of 3 mm × 5 mm × 5 mm and homogenized with tissue homogenizer. Obtained suspensions were adjusted to densities of ∼3 × 10^7 CFU/ml and statically challenged with amphotericin B at 100 mg/ml for 24 h. To avoid antifungal carryover and accurately quantify the number of persister cells, the antifungal treated suspensions were centrifuged at 3000 *g* for 5 min, washed twice with PBS, and re-suspended to the same volume with YPD broth. Colony-forming units counting was done by plating serially diluted aliquots onto YPD plates followed by incubation at 35°C for 72 h to maximize recovery of persister cells. The percentage of persister cells in different populations was calculated as follows: (fungal density after antifungal treatment)/(fungal density before antifungal treatment) × 100%, as described before (Wu et al., 2019).

Data Analysis and Statistical Methods

One-way ANOVA or a non-parametric test was carried out to compare two means, depending on the data distribution. Statistical significance was assumed at a p value of less than 0.05. Data analysis was performed using Minitab 16 software (Minitab, State College PA, United States).

RESULTS

C. albicans Forms Epithelium-Associated Biofilms in the Mouse Vagina Accompanied by Fungal Infiltration of the Epithelial Layer

We examined *C. albicans* laboratory strains and clinical isolates for *in vivo* biofilm formation on the mouse vaginal epithelium at 72 h post-inoculation. This time point was chosen because our preliminary experiment using *C. albicans* DAY185 suggested that fungal invasion and mouse immune response were both evident at this stage of the infection. Qualitative SEM showed that both DAY185 and DAY286 were able to irreversibly attach to the mouse vaginal epithelium, forming monolayer biofilms, with both yeast cells and hyphal elements distributed on the epithelium and apparently internalized by epithelial cells (**Figure 1A**). Two transcription factor mutant strains that are defective in biofilm formation *in vitro*, *med31*ΔΔ and *bcr1*ΔΔ, also formed monolayer biofilms on the vaginal epithelium, but to a lower extent (**Figure 1A**). Parallel quantitative viable counts also suggested biofilm formation of *C. albicans* on the vaginal epithelium, with *med31*ΔΔ and *bcr1*ΔΔ showing densities approximately 1 log CFU/g of infected tissue less than that of the wild-type strains (**Figure 1B**). Periodic acid–Schiff staining clearly showed *Candida* hyphal infiltration of the vaginal epithelial layers. This phenotype, however, was only found for wild-type DAY185 and DAY286, not the mutant strains (**Figure 2**). Two clinical isolates from patients with vaginal candidiasis also formed significant biofilms on the mouse vaginal epithelium and presented epithelial infiltration, as suggested by SEM imaging, viable counts, and histopathological examination (**Figures 1A,B**, **2**). We also assessed biofilm formation of *C. albicans* clinical isolates on IUDs, using an *in vitro* model of biofilm cultivation. At a vaginal physiological pH of 4.0, *C. albicans* clinical isolates VVC2 and VVC4 formed three-dimensional multilayer biofilms on the surface of IUD wire and in the gaps between neighboring wires (**Figure 3**). The intricate three-dimensional structure of the IUDs, particularly the inter-wire space, appeared to support robust biofilm formation of *C. albicans* (**Figure 3**).

Histopathological Changes of the Vaginal Epithelium Responsive to the Formation of Biotic *C. albicans* Biofilms and Fungal Infiltration

One of the key research questions, and also the focus of this study was whether the presence of epithelium-associated biofilms is directly related to the pathological changes within vaginal tissues. We assessed the histopathological changes of the vaginal epithelium and associated alarmin/cytokine responses. Hematoxylin–Eosin staining showed evident neutrophil infiltration and subcorneal microabscesses, two changes of vaginal mucosae typically related to fungal infections in the epithelial layer (**Figure 4A**). Little change was found when mutant strains (*med31*ΔΔ and *bcr1*ΔΔ) were used to infect

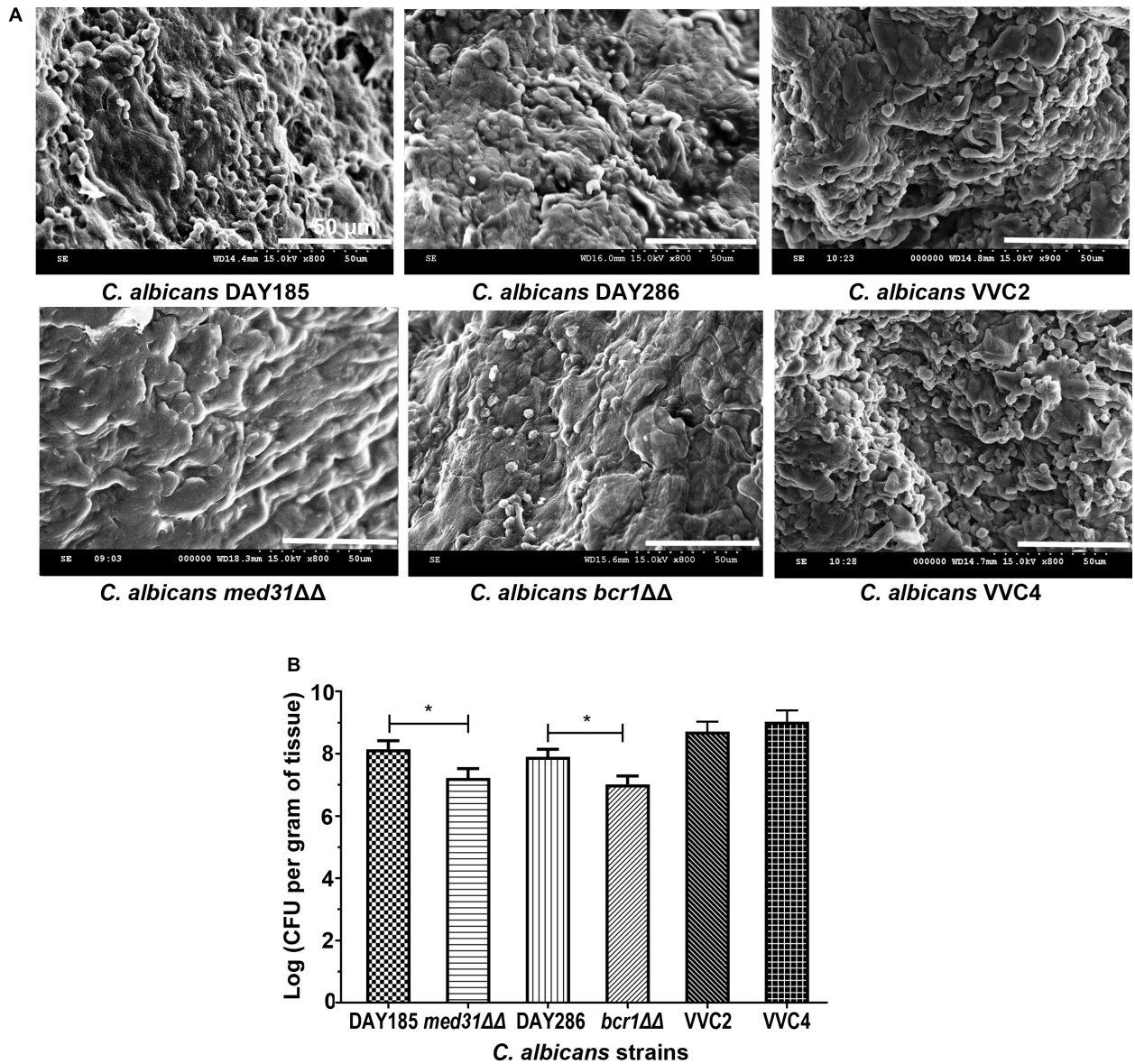

FIGURE 1 | *Candida albicans* forms biotic biofilms on mouse vaginal mucosae. **(A)** Scanning electron microscopy of epithelium-associated biotic biofilms formed by *C. albicans* DAY185 and its *med31*ΔΔ mutant strain, *C. albicans* DAY286 and its *bcr1*ΔΔ mutant strain, and two clinical isolates from patients with vaginal candidiasis. The experiments were repeated on three different occasions. Scale bar = 50 μm. **(B)** Quantitative analysis of vaginal epithelium-associated biofilms formed by *C. albicans* DAY185 and its *med31*ΔΔ mutant strain, *C. albicans* DAY286 and its *bcr1*ΔΔ mutant strain, and two clinical isolates from patients with vaginal candidiasis. CFU-based viable counts were performed. The experiments were repeated three times in triplicate. Means and standard errors were presented. One-way ANOVA was used for two-set comparisons. $^*p < 0.05$.

the mice (**Figure 4A**). Enzyme-linked immunosorbent assay targeting cytoplasmic protein S100A8 and cytokine IL-1β demonstrated a raised level of both agents in mice infected with any of the *C. albicans* strains and indicated an inflammatory condition (**Figure 4B**). *C. albicans* DAY185 and DAY286 had readings of S100A8 and IL-1β significantly higher than the mutant strains (*med31*ΔΔ and *bcr1*ΔΔ), suggesting a possible linkage between the formation of biotic biofilms by *C. albicans*, fungal infiltration, and the harmful immune responses to infected vaginal tissues. Significant histopathological changes and induction of inflammatory responses were also observed when two clinical isolates were introduced to the mouse vagina (**Figure 4B**).

Formation of Epithelium-Associated Biofilms by *C. albicans* in the Vagina Leads to Higher Antifungal Resistance

We further tested antifungal susceptibilities of DAY185 and two clinical isolates grown in different modes, including planktonic

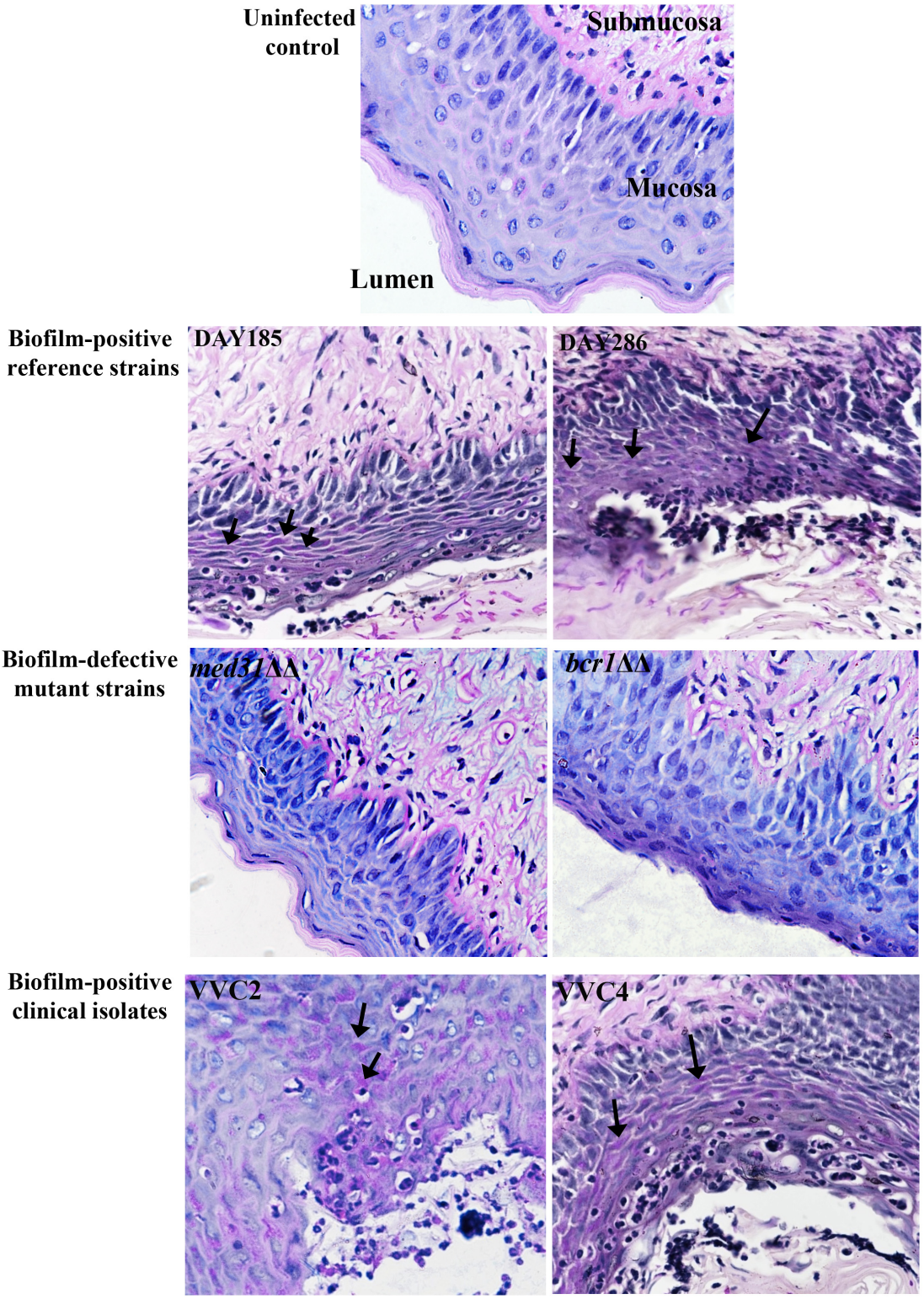

FIGURE 2 | Histology of the vagina of mice infected by *C. albicans* shows fungal infiltration within the vaginal epithelium. Vaginal histopathological examination (PAS staining, 400×) showed that *C. albicans* penetrated the cornified epithelium and formed fungal infiltrations in the mucosal layer. The lumen, mucosa, and submucosa in the uninfected control are denoted for orientation. Evident endocytosed hyphae or fungal infiltrations (black arrows) in the mucosa were observed when *C. albicans* biofilm-positive reference strains (DAY185 and DAY286) and clinical isolates (VVC2 and VVC4), but not biofilm-negative mutants (*med31*ΔΔ and *bcr1*ΔΔ), were used to infect mice. The experiments were repeated on three different occasions.

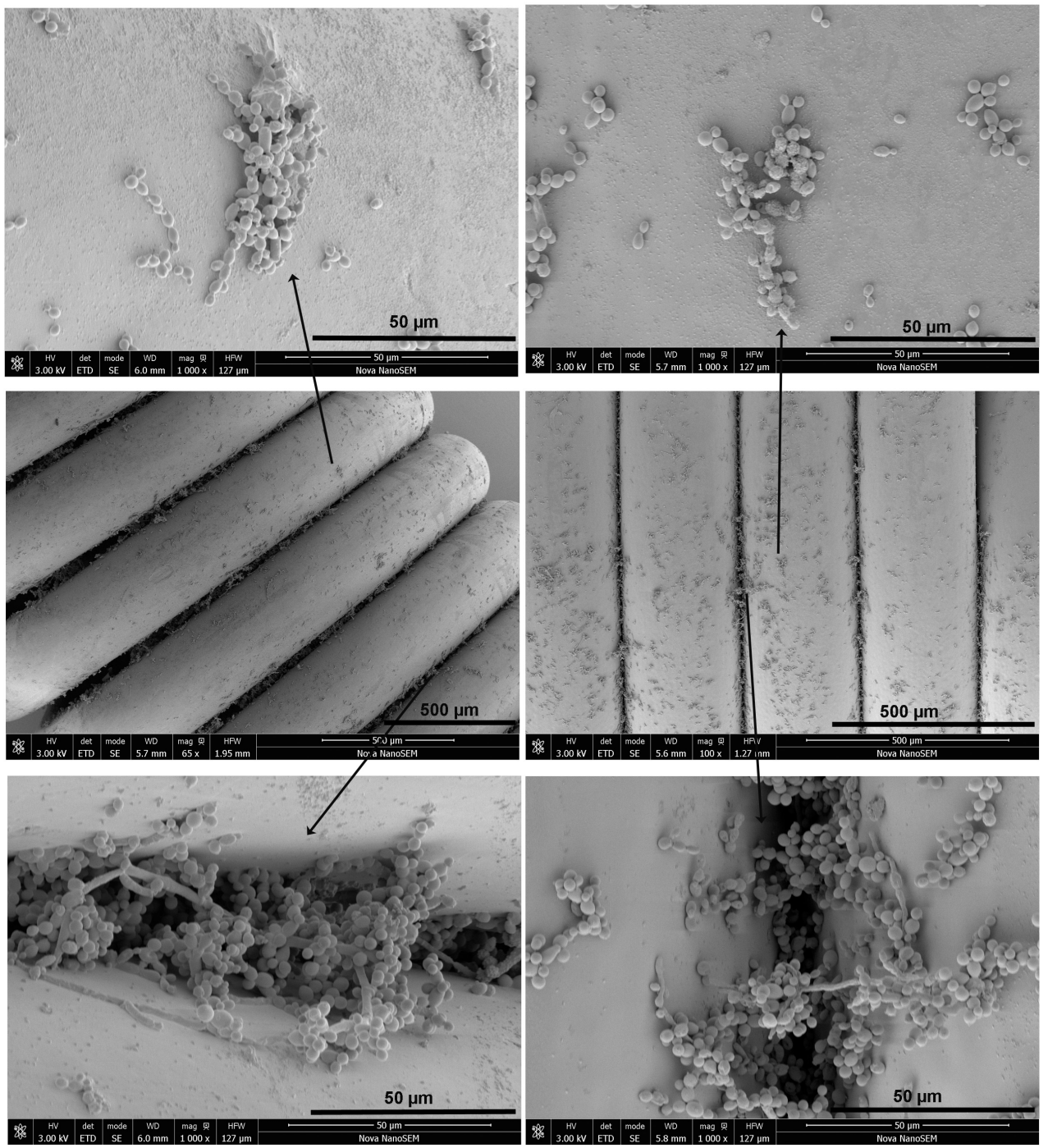

FIGURE 3 | Biofilm formation on IUDs. Qualitative assessment of biofilm formation by *C. albicans* clinical isolates on IUDs. *C. albicans* biofilms were grown on two different IUDs for 48 h. Growth medium RPMI-1640 pre-adjusted to a pH of 4.0 was used for biofilm growth (as described in section "Materials and Methods"). SEM was employed for qualitative examination of biofilm formation. It was noticed that *C. albicans* formed three-dimensional biofilms on the IUD wire surface and in the inter-wire space of IUDs; the latter harbors more biofilm cells. The experiments were repeated on three different occasions.

cells, microplate-based abiotic biofilms, and epithelium-associated biotic biofilms, to three conventional agents under neutral and acidic conditions, respectively (**Table 1**). At pH 7.2, planktonic cultures of DAY185 and both clinical isolates remained sensitive to all three agents used in this study. Acidic condition of the vagina significantly impacted on the

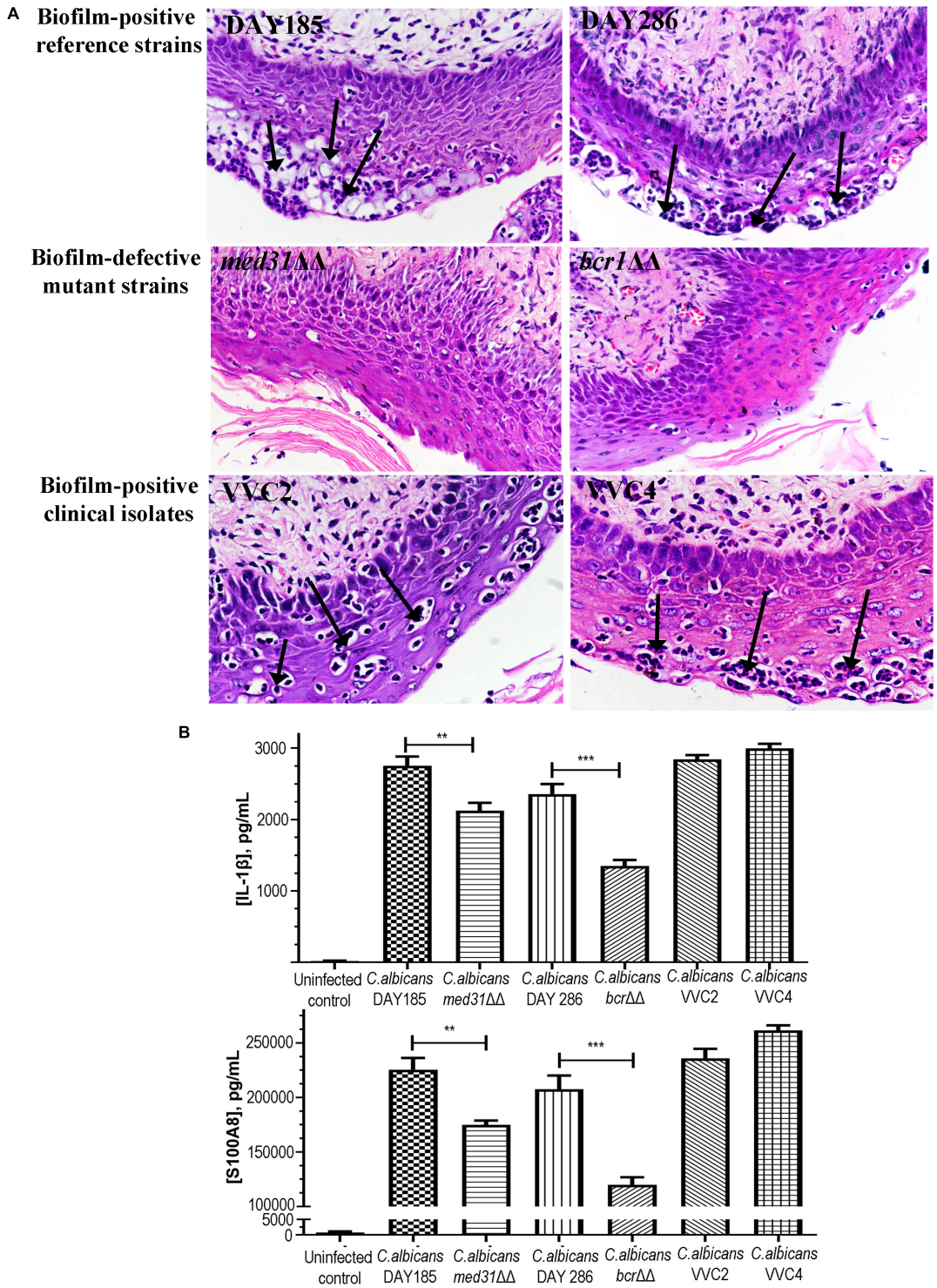

FIGURE 4 | Histopathological and inflammatory changes of the vaginal epithelium after exposure to *C. albicans* of different biofilm phenotypes. **(A)** Vaginal histopathological examination (H&E staining, 400×) showed the formation of numerous microabscesses and neutrophil infiltration (black arrows) in the cornified epithelium after mice were infected with biofilm-positive *C. albicans* reference strains (DAY185 and DAY286) and clinical isolates (VVC2 and VVC4). Minimal neutrophil infiltration and microabscesses were seen when biofilm-defective mutant strains (*med31*ΔΔ and *bcr1*ΔΔ) were used to infect the mice. The experiments were repeated on three different occasions. **(B)** Local inflammatory responses to *C. albicans* infections in the mouse vagina. *C. albicans* DAY185 and its *med31*ΔΔ mutant strain, *C. albicans* DAY286 and its *bcr1*ΔΔ mutant strain, and two clinical isolates from patients with vaginal candidiasis were tested respectively. Cytoplasmic protein S100A8 and cytokine IL-1β were selected as the representative inflammatory effectors. The experiments were repeated three times in duplicate. Means and standard errors were shown. One-way ANOVA or a non-parametric test was used for two-set comparisons. $^{**}p < 0.01$, $^{***}p < 0.001$.

TABLE 1 | Antifungal susceptibility of *C. albicans*: planktonic cells, microplate-based abiotic biofilms, and vaginal epithelium-associated biotic biofilms.

Antifungals	Planktonic MIC (mg/l)			Abiotic biofilm MIC80 (mg/l)			Biotic biofilm MIC80 (mg/l)		
	C. albicans strains			*C. albicans* strains			*C. albicans* strains		
	DAY185	VVC2	VVC4	DAY185	VVC2	VVC4	DAY185	VVC2	VVC4
pH 7.2									
Nystatin	4	2	4	32	64	64	32	>32	>32
Clotrimazole	0.5	2	1	>1280	>1280	>1280	1280	1280	>1280
Amphotericin B	1	2	1	1	4	4	2	16	16
pH 4.0									
Nystatin	16	32	32	16	64	128	32	32	>32
Clotrimazole	8	8	16	1280	>1280	>1280	>1280	>1280	>1280
Amphotericin B	2	2	4	2	4	16	2	>16	>16

Experiments for antifungal susceptibility testing were repeated on three different occasions in triplicate. Geometric means of planktonic MICs and biofilm MIC80s were calculated and presented in the table. Definitions and detailed methods for planktonic MIC and biofilm MIC80 can be found in the main text.

susceptibility of nystatin and clotrimazole but not amphotericin B, increasing MICs of nystatin and clotrimazole by 4–16 times. When grown as abiotic biofilms, *C. albicans* strains generally gained higher resistance to clotrimazole (ratio biofilm MIC80/planktonic MIC: >160-fold) and nystatin (1- to 16-fold) and remained relatively sensitive to amphotericin B (1- to 4-fold). Epithelium-associated biotic biofilms demonstrated highly elevated resistance to antifungal agents, with two clinical isolates showing biofilm MIC80 even higher than that of microplate-based abiotic biofilms (**Table 1**).

Formation of Epithelium-Associated Biotic Biofilms by *C. albicans* Prompts the Formation of Persister Cells

Persister cells residing in planktonic cultures, microplate-based abiotic biofilms, and epithelium-associated biotic biofilms were quantified. When grown as planktonic cultures at a mid-log phase, *C. albicans* DAY185 and two clinical isolates produced only very few persister cells (0.0001–0.0008%; **Figure 5**). Formation of abiotic biofilms by *C. albicans* on biomaterials significantly increased the number of persister cells in the population; the percentage seemed to be strain-dependent with DAY185 reaching 0.05%, VVC2 reaching 0.1%, and VVC4 reaching 1%. Growth of biotic biofilms on the vaginal epithelium further promoted persister cells of VVC2 to 0.6%, and VVC4 to 3.3%, significantly higher than that for abiotic biofilms or planktonic cultures (**Figure 5**).

DISCUSSION

Biofilm formation has been proposed as one of the most important virulence factors of *C. albicans* causing vaginal candidiasis, contributing to the establishment and recurrence of the infection (Muzny and Schwebke, 2015). Although biofilm formation of *C. albicans* has been extensively studied with clinical isolates from vaginal candidiasis patients, most studies used *in vitro* systems for biofilm cultivation that might only represent biofilms formed on IUDs (Cakiroglu et al., 2015; Gao et al., 2016; Sherry et al., 2017). Only a few studies have been carried out on biofilms grown on the vaginal epithelium (Harriott et al., 2010; Peters et al., 2014). Harriott et al. (2010) characterized *in vivo* biofilm formation of *C. albicans* on the vaginal epithelium; Peters et al. (2014) discovered a link between fungal morphogenesis of *C. albicans* and the immunopathology of vaginal candidiasis (Peters et al., 2014). Using the mouse model developed by Harriott et al. (2010), we further dissected the role of *C. albicans* biofilms in the histopathogenesis and persistence of vaginal candidiasis. Key findings of our study include the following: *C. albicans* infects the vagina by establishing epithelium-associated biofilms and fungal infiltration; histopathological changes of the vaginal epithelium and local inflammation are in relation to the formation of epithelium-associated biofilms; biofilm formation by *C. albicans* on the vaginal epithelium leads to high antifungal resistance; formation of biotic biofilms on the vaginal epithelium promotes the formation of persister cells.

By comparing biofilm-positive *C. albicans* reference strains and their biofilm-defective mutant strains, we established a link between biofilm formation and the disease state of vaginal candidiasis. *C. albicans* wild-type reference strain DAY286 and its *bcr1*ΔΔ mutant have been previously studied for *in vivo* biofilm formation on the mouse vaginal epithelium (Nobile et al., 2006; Harriott et al., 2010). Bcr1 is a transcription factor regulating many important biological processes in *C. albicans*; its mutant demonstrates normal filamentation but a reduction in biofilm formation on abiotic substrate and host organs (Nobile et al., 2006). Another wild-type reference strain *C. albicans* DAY185 experimentally causes systematic infection in mice; its *med31* deletion mutant showed a reduction in both filamentation and biofilm formation (Uwamahoro et al., 2012). Our study found that biofilm-positive wild-type reference strains, not the biofilm-defective mutants, induced evident histopathological damages and local inflammation, supporting an important role of biofilm formation in the histopathogenesis of vaginal candidiasis. One hurdle in attributing biofilm formation of *C. albicans* to its pathogenesis is to exclude other co-existing virulence strategies that might also be involved in *C. albicans* pathogenicity (Sudbery,

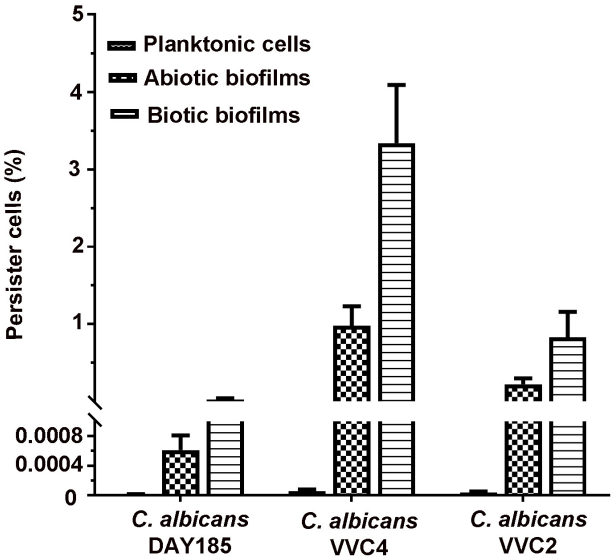

FIGURE 5 | Quantitative assessment of persister cells formed by *C. albicans* in three different growth modes. *C. albicans* cells were grown as planktonic cells, abiotic biofilms on tissue culture-treated polystyrene surfaces, and biotic biofilms on the mouse vaginal epithelium, respectively. Biofilm cells and planktonic cells were re-suspended to a density of ~3×10^7 CFU/ml in RPMI-1640, followed by exposure to amphotericin B at 100 mg/l overnight. Survivors were recovered after 72 h incubation on YPD plates and counted as the percentage of the initial population. The experiments were repeated three times in triplicate. Means and standard errors were presented.

2011). Most transcription factors or their encoding genes often synchronously regulate biofilm formation of *C. albicans* and other important programs such as yeast-hyphae morphogenesis (Nobile et al., 2006; Sudbery, 2011; Uwamahoro et al., 2012). The pathogenesis of vaginal candidiasis has been essentially linked to the hyphal invasive form of *C. albicans* that is required to penetrate the intact epithelial layer and induce immunopathology (Sudbery, 2011). Fortunately, the *bcr1*ΔΔ mutant, which has a defect in biofilm formation but not morphogenesis (Peters et al., 2014), demonstrated a reduced capacity to elicit an immune response or histopathological damage, as found in this study. We also noticed a relation between biofilm formation and candida infiltration of the vaginal epithelium, with biofilm-defective mutant strains presenting less fungal infiltration. Recent work by Swidsinski et al. (2019) found endocytosed hyphae or pseudohyphae in the vaginal epithelium in patients with confirmed vaginal candidiasis, although no typical multi-layer biofilm structure was detected in the human vagina (Swidsinski et al., 2019). We propose that the biofilm-related fungal infiltration might resemble microcolony biofilms that are more frequently found *in vivo*, and share some important traits with *in vivo* biofilms, such as harboring antifungal-tolerant persister cells (Bjarnsholt et al., 2013; Xu et al., 2019). It is now known that dense microbial growth in a confined space promotes the formation of persister cells (Qu et al., 2010).

We also presented experimental evidence to explain the tolerance of vaginal candidiasis to antifungal treatment. Similar to microplate-based abiotic biofilms, epithelium-associated biotic biofilms are highly resistant to first-line antifungals. More importantly, epithelium-associated biofilms act as a conducive environment that facilitates the formation of persister cells. Using a regimen that kills the bulk of fungal cells with normal susceptibilities, our recent study has successfully isolated persister cells from the vaginal epithelium of mice infected with *C. albicans* (Wu et al., 2019). These persister cells could not be eradicated by conventional antifungal drugs at very high concentrations and might be the main culprit responsible for the recalcitrance of infections to antifungal treatment (Wu et al., 2019). The current study further established a connection between biofilm growth by *C. albicans* in the vaginal epithelium and the formation of persister cells, supporting a role of *Candida* biofilm formation in the recurrence of vaginal candidiasis.

One of the possible limitations of this study was that the mouse model of vaginal candidiasis still differs from human vaginal candidiasis in several physical aspects, including a lack of *C. albicans* as part of the vaginal microbiota, neutral vaginal pH, and dependence on exogenous estrogen to initiate fungal colonization (Harriott et al., 2010; Cassone and Sobel, 2016). Differences in responses to *Candida* infection between human and mice or other rodents cannot be neglected (Sobel, 2015; Vecchiarelli et al., 2015; Cassone and Sobel, 2016). This small animal model, however, remains a valuable research tool to study vaginal candidiasis as it closely parallels the chronic nature of the diseases in women and is cost-effective (Vecchiarelli et al., 2015; Yano et al., 2018). Another limitation is the small number of clinical isolates used in this study. The conclusion drawn from this study might not fully represent vaginal candidiasis caused by other *C. albicans* clinical isolates or other *Candida* spp. The cost, labor, and requirements from the ethics aspect have limited the use of a greater number of *C. albicans* strains in our study.

CONCLUSION

In summary, our study provides a comprehensive understanding of biofilm-related factors involved in the pathogenicity and persistence of vaginal candidiasis caused by *C. albicans*.

DATA AVAILABILITY STATEMENT

The datasets generated for this study are available on request to the corresponding author.

ETHICS STATEMENT

The animal study was reviewed and approved by Ethics Committee of Wenzhou Medical University, China.

AUTHOR CONTRIBUTIONS

YQ and XW conceived and designed the study. SZ, HL, CD, LS, YS, HC, BX, WZ, and YQ carried out the experiments. YQ, SZ,

XW, and MD performed data analysis. YQ wrote the manuscript. YQ, MD, and XW edited the manuscript. All authors reviewed the manuscript and provided critical comments.

FUNDING

This work was supported by the National Natural Science Foundation of China (grant number 81772241 to YQ), the National Natural Science Foundation of China (grant number 81873822 to XW), and the Shenzhen Science and Technology Innovation Projects (grant numbers JCY20170818100355169 and JCY201908083000479 to XW).

ACKNOWLEDGMENTS

The authors wish to acknowledge Prof. Ana Traven from Monash University for kindly donating *C. albicans* strains including DAY286, DAY185, *med31*ΔΔ, and *bcr1*ΔΔ.

REFERENCES

Adjapong, G., Hale, M., and Garrill, A. (2017). A comparative investigation of azole susceptibility in Candida isolates from vulvovaginal candidiasis and recurrent vulvovaginal candidiasis patients in Ghana. *Med. Mycol.* 55, 686–689.

Auler, M. E., Morreira, D., Rodrigues, F. F., Abr Ao, M. S., Margarido, P. F., Matsumoto, F. E., et al. (2010). Biofilm formation on intrauterine devices in patients with recurrent vulvovaginal candidiasis. *Med. Mycol.* 48, 211–216. doi: 10.3109/13693780902856626

Bjarnsholt, T., Alhede, M., Alhede, M., Eickhardt-Sorensen, S. R., Moser, C., Kuhl, M., et al. (2013). The in vivo biofilm. *Trends Microbiol* 21, 466–474.

Blostein, F., Levin-Sparenberg, E., Wagner, J., and Foxman, B. (2017). Recurrent vulvovaginal candidiasis. *Ann. Epidemiol.* 27, 575.e–582.e.

Bruno, V. M., Shetty, A. C., Yano, J., Fidel, P. L. Jr., Noverr, M. C., et al. (2015). Transcriptomic analysis of vulvovaginal candidiasis identifies a role for the NLRP3 inflammasome. *mBio* 6:e0182-15.

Cakiroglu, Y., Caliskan, S., Doger, E., Ozcan, S., and Caliskan, E. (2015). Does removal of CU-IUD in patients with biofilm forming candida really maintain regression of clinical symptoms? *J. Obstet. Gynaecol.* 35, 600–603. doi: 10.3109/01443615.2014.986442

Cassone, A., and Sobel, J. D. (2016). Experimental models of vaginal candidiasis and their relevance to human candidiasis. *Infect. Immun.* 84, 1255–1261. doi: 10.1128/iai.01544-15

Gamarra, S., Morano, S., Dudiuk, C., Mancilla, E., Nardin, M. E., De Los Angeles Mendez, E., et al. (2014). Epidemiology and antifungal susceptibilities of yeasts causing vulvovaginitis in a teaching hospital. *Mycopathologia* 178, 251–258. doi: 10.1007/s11046-014-9780-2

Gao, M., Wang, H., and Zhu, L. (2016). Quercetin assists fluconazole to inhibit biofilm formations of fluconazole-resistant *Candida albicans* in in vitro and in vivo antifungal managements of vulvovaginal candidiasis. *Cell Physiol. Biochem.* 40, 727–742. doi: 10.1159/000453134

Gargani, G., Zecchi Orlandi, S., Campisi, E., Pini, G., and Orlandini, G. E. (1989). Scanning electron microscopic pattern of recurrent vaginitis by *Candida albicans* in the mouse. *Mycoses* 32, 644–651. doi: 10.1111/j.1439-0507.1989.tb02197.x

Goncalves, B., Ferreira, C., Alves, C. T., Henriques, M., Azeredo, J., and Silva, S. (2016). Vulvovaginal candidiasis: epidemiology, microbiology and risk factors. *Crit. Rev. Microbiol.* 42, 905–927. doi: 10.3109/1040841x.2015.1091805

Hagerty, J. A., Ortiz, J., Reich, D., and Manzarbeitia, C. (2003). Fungal infections in solid organ transplant patients. *Surg. Infect.* 4, 263–271. doi: 10.1089/109629603322419607

Harriott, M. M., Lilly, E. A., Rodriguez, T. E., Fidel, P. L. Jr., and Noverr, M. C. (2010). *Candida albicans* forms biofilms on the vaginal mucosa. *Microbiology* 156, 3635–3644. doi: 10.1099/mic.0.039354-0

Ilkit, M., and Guzel, A. B. (2011). The epidemiology, pathogenesis, and diagnosis of vulvovaginal candidosis: a mycological perspective. *Crit. Rev. Microbiol* 37, 250–261. doi: 10.3109/1040841x.2011.576332

Kalkanci, A., Guzel, A. B., Jabban, I., Aydin, M., Ilkit, M., and Kustimur, S. (2013). Candida vaginitis in non-pregnant patients: a study of antifungal susceptibility testing and virulence factors. *J. Obstet. Gynaecol.* 33, 378–383. doi: 10.3109/01443615.2013.767323

Kasper, L., Miramon, P., Jablonowski, N., Wisgott, S., Wilson, D., Brunke, S., et al. (2015). Antifungal activity of clotrimazole against *Candida albicans* depends on carbon sources, growth phase and morphology. *J. Med. Microbiol.* 64, 714–723. doi: 10.1099/jmm.0.000082

Kojic, E. M., and Darouiche, R. O. (2004). Candida infections of medical devices. *Clin. Microbiol. Rev.* 17, 255–267. doi: 10.1128/cmr.17.2.255-267.2004

Lafleur, M. D., Kumamoto, C. A., and Lewis, K. (2006). *Candida albicans* biofilms produce antifungal-tolerant persister cells. *Antimicrob. Agents Chemother.* 50, 3839–3846. doi: 10.1128/aac.00684-06

LaFleur, M. D., Qi, Q., and Lewis, K. (2010). Patients with long-term oral carriage harbor high-persister mutants of *Candida albicans*. *Antimicrob. Agents Chemother.* 54, 39–44. doi: 10.1128/aac.00860-09

Lewis, K. (2010). Persister cells. *Annu. Rev. Microbiol.* 64, 357–372.

Liu, X. P., Fan, S. R., Peng, Y. T., and Zhang, H. P. (2014). Species distribution and susceptibility of Candida isolates from patient with vulvovaginal candidiasis in Southern China from 2003 to 2012. *J. Mycol. Med.* 24, 106–111. doi: 10.1016/j.mycmed.2014.01.060

Muzny, C. A., and Schwebke, J. R. (2015). Biofilms: an underappreciated mechanism of treatment failure and recurrence in vaginal infections. *Clin. Infect. Dis.* 61, 601–606. doi: 10.1093/cid/civ353

Nagashima, M., Yamagishi, Y., and Mikamo, H. (2016). Antifungal susceptibilities of *Candida* species isolated from the patients with vaginal candidiasis. *J. Infect. Chemother.* 22, 124–126. doi: 10.1016/j.jiac.2015.08.008

Nobile, C. J., Andes, D. R., Nett, J. E., Smith, F. J., Yue, F., Phan, Q. T., et al. (2006). Critical role of Bcr1-dependent adhesins in *C. albicans* biofilm formation in vitro and in vivo. *PLoS Pathog.* 2:e63. doi: 10.1371/journal.ppat.0020063

Peters, B. M., Palmer, G. E., Nash, A. K., Lilly, E. A., Fidel, P. L. Jr., et al. (2014). Fungal morphogenetic pathways are required for the hallmark inflammatory response during *Candida albicans* vaginitis. *Infect. Immun.* 82, 532–543. doi: 10.1128/iai.01417-13

Qu, Y., Daley, A. J., Istivan, T. S., Rouch, D. A., and Deighton, M. A. (2010). Densely adherent growth mode, rather than extracellular polymer substance matrix build-up ability, contributes to high resistance of *Staphylococcus epidermidis* biofilms to antibiotics. *J. Antimicrob. Chemother.* 65, 1405–1411. doi: 10.1093/jac/dkq119

Qu, Y., Locock, K., Verma-Gaur, J., Hay, I. D., Meagher, L., and Traven, A. (2016). Searching for new strategies against polymicrobial biofilm infections: guanylated polymethacrylates kill mixed fungal/bacterial biofilms. *J. Antimicrob. Chemother.* 71, 413–421. doi: 10.1093/jac/dkv334

Richardson, J. P., Willems, H. M. E., Moyes, D. L., Shoaie, S., Barker, K. S., Tan, S. L., et al. (2017). Candidalysin drives epithelial signaling, neutrophil recruitment, and immunopathology at the vaginal mucosa. *Infect. Immun.* 86, e645–e617.

Richter, S. S., Galask, R. P., Messer, S. A., Hollis, R. J., Diekema, D. J., and Pfaller, M. A. (2005). Antifungal susceptibilities of Candida species causing vulvovaginitis and epidemiology of recurrent cases. *J. Clin. Microbiol.* 43, 2155–2162. doi: 10.1128/jcm.43.5.2155-2162.2005

Rodriguez-Cerdeira, C., Gregorio, M. C., Molares-Vila, A., Lopez-Barcenas, A., Fabbrocini, G., Bardhi, B., et al. (2019). Biofilms and vulvovaginal candidiasis. *Colloids Surf. B Biointerfaces* 174, 110–125.

Sherry, L., Kean, R., Mckloud, E., O'donnell, L. E., Metcalfe, R., Jones, B. L., et al. (2017). Biofilms formed by isolates from recurrent vulvovaginal candidiasis patients are heterogeneous and insensitive to fluconazole. *Antimicrob. Agents Chemother.* 61:e01065-17.

Sobel, J. D. (2015). Editorial commentary: Vaginal biofilm: much ado about nothing, or a new therapeutic challenge? *Clin. Infect. Dis.* 61, 607–608. doi: 10.1093/cid/civ358

Sobel, J. D. (2016). Recurrent vulvovaginal candidiasis. *Am. J. Obstet. Gynecol.* 214, 15–21.

Sudbery, P. E. (2011). Growth of *Candida albicans* hyphae. *Nat. Rev. Microbiol.* 9, 737–748. doi: 10.1038/nrmicro2636

Swidsinski, A., Guschin, A., Tang, Q., Dorffel, Y., Verstraelen, H., Tertychnyy, A., et al. (2019). Vulvovaginal candidiasis: histologic lesions are primarily polymicrobial and invasive and do not contain biofilms. *Am. J. Obstet. Gynecol.* 220:e91.

Uwamahoro, N., Qu, Y., Jelicic, B., Lo, T. L., Beaurepaire, C., Bantun, F., et al. (2012). The functions of Mediator in *Candida albicans* support a role in shaping species-specific gene expression. *PLoS Genet.* 8:e1002613. doi: 10.1371/journal.pgen.1002613

Vecchiarelli, A., Gabrielli, E., and Pericolini, E. (2015). Experimental models of vaginal candidiasis and inflammation. *Future Microbiol.* 10, 1265–1268. doi: 10.2217/fmb.15.52

Wu, X., Zhang, S., Xu, X., Shen, L., Xu, B., Qu, W., et al. (2019). RAFT-derived polymethacrylates as a superior treatment for recurrent vulvovaginal candidiasis by targeting biotic biofilms and persister cells. *Front. Microbiol.* 10:2592. doi: 10.3389/fmicb.2019.02592

Xu, B., Deighton, M., and Qu, Y. (2019). Should we absolutely reject the hypothesis that epithelium-based *Candida* biofilms contribute to the pathogenesis of human vulvovaginal candidiasis?. *Am. J. Obst. Gynecol.* 221, 372–373. doi: 10.1016/j.ajog.2019.07.007

Yang, S., Hay, I. D., Cameron, D. R., Speir, M., Cui, B., Su, F., et al. (2015). Antibiotic regimen based on population analysis of residing persister cells eradicates *Staphylococcus epidermidis* biofilms. *Sci. Rep.* 5:18578.

Yano, J., Peters, B. M., Noverr, M. C., and Fidel, P. L. Jr. (2018). Novel mechanism behind the immunopathogenesis of vulvovaginal candidiasis: "neutrophil anergy". *Infect. Immun.* 86:e00684-17.

Ying, C., Zhang, H., Tang, Z., Chen, H., Gao, J., and Yue, C. (2016). Antifungal susceptibility and molecular typing of 115 *Candida albicans* isolates obtained from vulvovaginal candidiasis patients in 3 Shanghai maternity hospitals. *Med. Mycol.* 54, 394–399. doi: 10.1093/mmy/myv082

Conflict of Interest: The authors declare that the research was conducted in the absence of any commercial or financial relationships that could be construed as a potential conflict of interest.

frontiers in Microbiology

MINI REVIEW
published: 25 June 2020
doi: 10.3389/fmicb.2020.01437

How Biofilm Growth Affects *Candida*-Host Interactions

*Emily F. Eix and Jeniel E. Nett**

Departments of Medicine and Medical Microbiology and Immunology, University of Wisconsin-Madison, Madison, WI, United States

Candida spp. proliferate as surface-associated biofilms in a variety of clinical niches. These biofilms can be extremely difficult to eradicate in healthcare settings. Cells within biofilm communities grow as aggregates and produce a protective extracellular matrix, properties that impact the ability of the host to respond to infection. Cells that disperse from biofilms display a phenotype of enhanced pathogenicity. In this review, we highlight host-biofilm interactions for *Candida*, focusing on how biofilm formation influences innate immune responses.

Keywords: *Candida*, biofilm, host, neutrophil, macrophage, matrix, immunity, dispersion

OPEN ACCESS

Edited by:
Juliana Campos Junqueira, São Paulo State University, Brazil

Reviewed by:
Cheshta Sharma, The University of Texas Health Science Center at San Antonio, United States
Renátó Kovács, University of Debrecen, Hungary

***Correspondence:**
Jeniel E. Nett
jenett@medicine.wisc.edu

Specialty section:
This article was submitted to Fungi and Their Interactions, a section of the journal Frontiers in Microbiology

Received: *12 March 2020*
Accepted: *03 June 2020*
Published: *25 June 2020*

Citation:
Eix EF and Nett JE (2020) How Biofilm Growth Affects Candida-Host Interactions. Front. Microbiol. 11:1437. doi: 10.3389/fmicb.2020.01437

INTRODUCTION

Candida spp. are the primary cause of nosocomial fungal infections and recently rose to the leading pathogen group causing nosocomial bloodstream infections (Magill et al., 2014). *Candida* spp. exhibit the propensity to proliferate as adherent biofilms (Magill et al., 2014; Nobile and Johnson, 2015). These aggregated communities exhibit resistance to antifungals as well as host immune responses, making them extremely difficult to eradicate (Chandra et al., 2001a; Donlan, 2001b; Douglas, 2003). In the hospital setting, *Candida* spp. form biofilms on artificial medical devices, such as vascular catheters, which can lead to bloodstream infection and disseminated disease with associated mortality of approximately 30% (Donlan, 2001a; Kojic and Darouiche, 2004; Wisplinghoff et al., 2004; Kumamoto and Vinces, 2005; Pfaller and Diekema, 2007; Tumbarello et al., 2007). It is estimated that nearly 80% of patients with invasive candidiasis have implanted medical devices (Andes et al., 2012). The ability of *Candida* spp. to persist as a biofilm on these devices poses a serious issue for treatment of *Candida* infections, as device removal is often the only option (Pfaller and Diekema, 2007; Andes et al., 2012). However, even with catheter removal, mortality rates remain high in the setting of invasive candidiasis (Andes et al., 2012). The observation that removal of catheters decreases the risk of persistent candidemia and rate of mortality suggests that biofilm formation plays a major role in the pathogenesis of invasive candidiasis (Andes et al., 2012; Ala-Houhala and Anttila, 2020).

Candida albicans, the most prevalent *Candida* spp., has served as a model organism for study of biofilm formation (Hawser and Douglas, 1994; Chandra et al., 2001b; Ramage et al., 2001; Uppuluri et al., 2010). However, biofilm formation is not unique to *C. albicans,* as many other clinically relevant *Candida* spp., including *C. glabrata, C. tropicalis, C. parapsilosis,* and the emerging pathogen *C. auris,* also form biofilms (Kuhn et al., 2002; Lewis et al., 2002; Jain et al., 2007; Bizerra et al., 2008; Sherry et al., 2017). While biofilms formed by different *Candida* spp. may vary in morphology and density, the structures uniformly contain a polymeric extracellular matrix that encases and protects the fungal cells. The components of the extracellular matrix differ from those found in the *Candida* cell wall, and these moieties are proposed to modulate host recognition by concealing the cell wall components that typically interact with the immune system

(Johnson et al., 2016; Zawrotniak et al., 2017; Hoyer et al., 2018). In addition, cells dispersed from biofilms exhibit characteristics distinct from cells growing under non-biofilm conditions (Sellam et al., 2009; Uppuluri et al., 2010). In this review, we highlight key host interactions with *Candida* biofilms, describing how the host responds differently to *Candida* during biofilm and non-biofilm growth (**Figure 1**).

IMPACT OF BIOFILM FORMATION ON NEUTROPHIL RESPONSES

Neutrophils serve as primary innate immune responders to *Candida* and are critical for controlling invasive infection (FidelJr., 2002). The susceptibility of neutropenic patients to severe fungal infections, including candidiasis, highlights the importance of these leukocytes (EdwardsJr., Lehrer et al., 1978; Erwig and Gow, 2016). However, when growing as a biofilm, *Candida* resists damage and killing by neutrophils (Katragkou et al., 2010, 2011a,b; Xie et al., 2012; Johnson et al., 2016; Kernien et al., 2017). Compared to the neutrophil response to planktonic *C. albicans*, neutrophils exhibit an up to 5-fold lower activity against biofilms formed by *C. albicans* (Katragkou et al., 2010, 2011b; Xie et al., 2012; Johnson et al., 2016). This process appears to involve induction of an inhibitory pathway, as neutrophils exposed to *C. albicans* resist activation by potent stimuli, such as phorbol ester. Additionally, priming of neutrophils with pro-inflammatory cytokines, including interferon-γ and granulocyte colony-stimulating factor, does not restore neutrophil killing of biofilms (Katragkou et al., 2011b). This inhibitory process appears independent of filamentation, as *C. albicans* biofilms of various architectures, including those comprised primarily of yeast morphotypes, similarly impair neutrophil function. Consistent with this, biofilms formed by *C. glabrata* and *C. parapsilosis*, which lack true hyphae, also resist neutrophil attack (Katragkou et al., 2011a; Johnson et al., 2017).

Neutrophils respond to pathogens via a variety of effector mechanisms, including phagocytosis, production of reactive oxygen species (ROS), and the formation of neutrophil extracellular traps (NETs), which are web-like structures containing DNA, histones, and antimicrobial proteins (Brinkmann et al., 2004). While neutrophils are capable of phagocytosing *Candida* yeast cells, the elongated hyphal cells cannot be completely engulfed. Instead, in response to *C. albicans* hyphae and other large or aggregated pathogens, neutrophils release NETs (Urban et al., 2006; Branzk et al., 2014). This process of NET formation would arguably be an effective neutrophil response against biofilm, considering their large size and the inability of the structures to be completely phagocytosed. However, NETs are not produced in response to *C. albicans* biofilms (Johnson et al., 2016; Kernien et al., 2017). *C. albicans* biofilms do not trigger neutrophils to generate ROS, a signaling pathway that governs many forms of NET formation (Brinkmann et al., 2004; Xie et al., 2012; Johnson et al., 2016). These impaired responses have been attributed, in part, to the presence of an extracellular matrix encasing the cells (Johnson et al., 2016).

MONOCYTE AND MACROPHAGE RESPONSES TO BIOFILM

The formation of biofilm influences a variety of mononuclear innate immune cell responses, including migration, phagocytosis, and cytokine production (Chandra et al., 2007; Katragkou et al., 2010; Alonso et al., 2017; Simitsopoulou et al., 2018; Arce Miranda et al., 2019). In addition, the presence of these and other cells can impact biofilm formation by *Candida*. For example, when incubated with *C. albicans* biofilm, peripheral blood mononuclear cells fail to engage in phagocytosis (Chandra et al., 2007). However, the presence of these cells promotes the formation of a thicker, hyphal-rich biofilm, which has been linked to a biofilm-enhancing soluble factor produced by the mononuclear cells during co-culture with biofilm (Chandra et al., 2007).

In addition to avoiding phagocytosis, mononuclear cells exposed to biofilms also display an altered cytokine profile, when compared to those interacting with planktonic *C. albicans* (Chandra et al., 2007). Observed differences for biofilm exposure include increases in both pro-inflammatory cytokines (IL-1β and MCP-1), as well as the anti-inflammatory cytokine, IL-10 (Chandra et al., 2007). Additional studies utilizing a human monocytic cell line (THP-1) have also shown differing cytokine responses to biofilm and planktonic *C. albicans,* including lower TNF-α production upon biofilm exposure (Katragkou et al., 2010). Modulation of cytokine production by biofilm likely influences immunity, but little is known about this process. However, it appears that cytokine responses to *Candida* biofilm may vary among species (Simitsopoulou et al., 2018).

Investigations using murine macrophage cell lines are beginning to shed light on the impact of *Candida* biofilm formation on macrophage interactions (Alonso et al., 2017; Arce Miranda et al., 2019). During the initiation of biofilm formation, macrophages are capable of phagocytosing *C. albicans* (Arce Miranda et al., 2019). However, as biofilms mature, macrophages do not exhibit activity against them, and may even enhance biofilm production (Arce Miranda et al., 2019). This pattern of impaired activity against mature biofilms is similar to that observed for both human mononuclear cells and neutrophils (Chandra et al., 2007; Katragkou et al., 2010, 2011a,b; Xie et al., 2012; Johnson et al., 2016; Kernien et al., 2017). Like the neutrophil response to *C. albicans* biofilms, macrophage-biofilm interactions also involve diminished ROS production (Xie et al., 2012; Johnson et al., 2016; Arce Miranda et al., 2019). Another response impaired by *C. albicans* biofilms is macrophage migration. Murine macrophages move at rates approximately 2-fold lower in response to biofilm when compared to incubation with planktonic *C. albicans* (Alonso et al., 2017).

ROLE OF *Candida* BIOFILM MATRIX IN IMMUNITY

The development of *Candida* biofilm begins with adherence to a substrate, which is followed by proliferation and the assembly of an extracellular matrix, a hallmark characteristic of mature

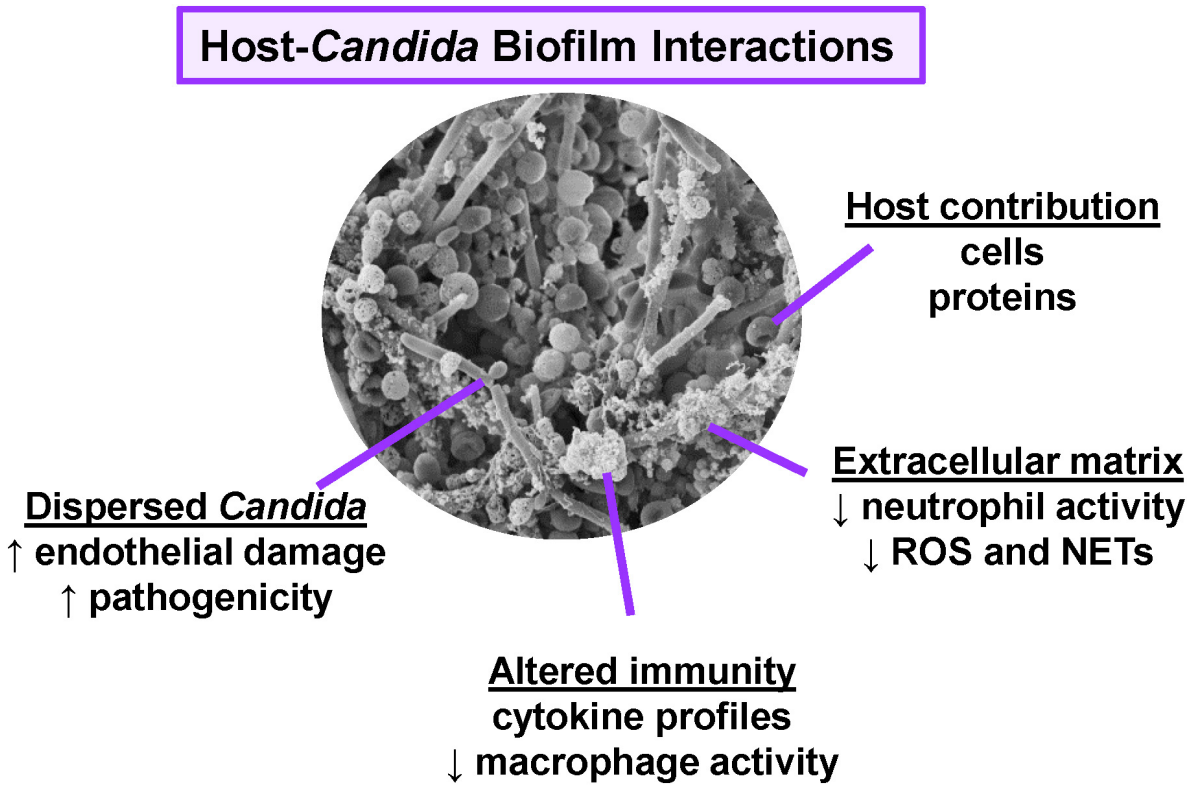

FIGURE 1 | Overview of host interactions with *Candida* biofilms. Scanning electron micrograph reveals *C. albicans* (SC5314) growing as a biofilm on the luminal surface of a rat vascular catheter. Biofilm formation influences host interactions, immunity, and pathogenesis.

biofilm formation (Chandra et al., 2001a; Uppuluri et al., 2010; Wall et al., 2019). This extracellular matrix encases the cells and presents unique structures which conceal the cell wall components that are typically encountered by innate immune cells (Chaffin et al., 1998; Hawser et al., 1998). Many studies have demonstrated altered immune cell interactions with *Candida* biofilms (Chandra et al., 2007; Katragkou et al., 2011a; Kernien et al., 2017; Xie et al., 2012; Johnson et al., 2016, 2017; Alonso et al., 2017; Arce Miranda et al., 2019). For neutrophils, this phenotype appears to require an intact extracellular matrix, as disruption of biofilm matrix can restore neutrophil activity, including their ability to produce NETs and damage biofilms (Katragkou et al., 2010; Johnson et al., 2016). It is likely that extracellular matrix contributes to other aspects of immune modulation by biofilms as well.

Analysis of *C. albicans* biofilms demonstrates that extracellular matrix contains a mixture of biopolymers, including proteins (55%), carbohydrates (25%), lipids (15%), and nucleic acids (5%) (Zarnowski et al., 2014). Many of these components differ from those found in the cell wall. For example, the biofilm extracellular matrix of *C. albicans* contains an abundant high molecular weight α-1,2-branched α-1,6 mannan, which assembles with linear β-1,6 glucan to form a mannan-glucan complex that is not found in the cell wall (Chaffin et al., 1998; Zarnowski et al., 2014; Mitchell et al., 2015). This complex has been linked to the capacity of *C. albicans* biofilms to inhibit neutrophil function, as *C. albicans* biofilms with genetic disruption of this pathway activate neutrophils (Johnson et al., 2016). Neutrophils then generate ROS and produce NETs in response to these mutants lacking extracellular matrix, ultimately resulting in fungal damage (Johnson et al., 2016). The fungal components involved in triggering this response are not certain. The finding that neutrophils are also activated by biofilms following treatment with echinocandin drugs, which unmask β-1,3 glucan, suggests a role for this polysaccharide (Katragkou et al., 2010; Hoyer et al., 2018; Simitsopoulou et al., 2018).

The production of matrix mannan-glucan complex is conserved across *Candida* species, including *C. albicans, C. tropicalis, C. parapsilosis, C. glabrata*, and *C. auris* (Dominguez et al., 2018, 2019). It is anticipated that similar mechanisms of neutrophil evasion may occur upon encounter with biofilms formed by these species as well. However, species-specific immune responses have been observed (Simitsopoulou et al., 2018). Additional study is needed to delineate the neutrophil-biofilm interactions for these and other emerging species.

HOST RESPONSE TO DISPERSED BIOFILMS

Throughout biofilm development, cells detach from biofilms, allowing *Candida* to disseminate to the bloodstream and cause

invasive disease (Uppuluri et al., 2010). Various environmental responses, including carbon source and pH, trigger this regulated process for *C. albicans* (Sellam et al., 2009; Uppuluri et al., 2010). During dispersion, yeast-like cells bud from the upper biofilm layer of hyphae and are release as elongated cells (Uppuluri et al., 2010). Although the cells resemble yeast, the newly dispersed cells display enhanced pathogenicity traits, including heightened capacities for filamentation, adhesion, and biofilm formation (Uppuluri et al., 2010). Even more striking, the dispersed cells exhibit enhanced virulence in a murine model of invasive candidiasis and exert more damage to endothelial cells (Uppuluri et al., 2010). The transcriptional profile of dispersed cells broadly differs from both biofilm and planktonic *C. albicans*, consistent with their unique phenotype (Sellam et al., 2009; Uppuluri et al., 2018). These cells likely play a major role in the pathogenesis of vascular catheter and other device-associated infections that result in disseminated disease. In this setting, environmental cues can trigger the detachment of yeast-form cells with a heightened propensity to disseminate though the bloodstream, adhere to endothelial cells, and damage tissues (Uppuluri et al., 2010).

INSIGHT INTO HOST RESPONSES TO BIOFILM THROUGH ANIMAL MODELS

Candida spp. interact extensively with the host during infection, and animal models are ideal for examining this interface *in vivo*. Invasive candidiasis frequently involves biofilm proliferation on indwelling vascular catheters, which can lead to catheter-associated bloodstream infection and disseminated disease (Kojic and Darouiche, 2004; Andes et al., 2012). Models in mice, rats, and rabbits mimicking vascular catheter-associated infection have shed light on biofilm-host interactions (Andes et al., 2004; Schinabeck et al., 2004; Lazzell et al., 2009). These models reveal differences between *in vitro* and *in vivo* biofilms, including the formation of a thicker biofilm matrix *in vivo*. Interestingly, *in vivo* biofilm models reveal that a striking number (>95%) of host-derived proteins incorporate into the extracellular matrix, indicating a major host contribution to *C. albicans* biofilms (Nett et al., 2015). Host proteins depositing in the biofilm matrix include matricellular proteins, and proteins indicating the presence of erythrocytes and leukocytes. Imaging of catheters similarly shows the incorporation of many host cells, including erythrocytes and neutrophils (Andes et al., 2004). These findings suggest that neutrophils recruit to *C. albicans* biofilms *in vivo*, but lack significant anti-biofilm activity.

Urinary catheter biofilm models have been developed in mice and rats, allowing the study of catheter-associated candiduria (Wang and Fries, 2011; Nett et al., 2014; Capote-Bonato et al., 2018). As seen with the vascular catheter models, on urinary catheters, *C. albicans* also forms thick biofilms with dense extracellular matrix (Wang and Fries, 2011; Nett et al., 2015). Biofilms in this environment also incorporate numerous host cells and proteins, which contribute to the extracellular matrix (Nett et al., 2015). *C. tropicalis* similarly forms biofilms on urinary catheter segments in mice (Capote-Bonato et al., 2018). It appears that host response to both *C. albicans* and *C. tropicalis* biofilms involves a degree of neutrophilic infiltration (Nett et al., 2015; Capote-Bonato et al., 2018). However, the biofilms persist despite this response.

In addition to the vascular and urinary placement of catheters, models have employed subcutaneous implantation of catheters or other devices in mice and rats to elucidate host interactions with *Candida* biofilms (Ricicova et al., 2010; Nieminen et al., 2014; Kucharikova et al., 2015). These models primarily involve the insertion of preformed biofilms that continue to propagate *in vivo*. Both *C. albicans* and *C. glabrata* proliferate as biofilms in this setting (Ricicova et al., 2010; Nieminen et al., 2014; Kucharikova et al., 2015). The subcutaneous *C. albicans* biofilms induce an infiltration of inflammatory cells consisting predominantly of neutrophils and macrophages (Nieminen et al., 2014). Consistent with this, tissue sections adjacent to subcutaneous biofilms show an inflammatory profile with an increased abundance of inflammatory mediators, including matrix metalloproteinases and myeloperoxidase (Nieminen et al., 2014). Similar to other models of *C. albicans* biofilm formation, the biofilms withstand this defense.

Oral biofilms represent one of the most common niches for *Candida* biofilm formation (Douglas, 2002). Rats have predominantly been utilized to study host-biofilm interactions, particularly for the analysis of dental devices and the associated denture stomatitis (Nett et al., 2010; Lee et al., 2011; Johnson et al., 2012; Tobouti et al., 2016; Sultan et al., 2019; Yano et al., 2019). In these models, *Candida* spp. adhere to the artificial devices, proliferating as a biofilm (Nett et al., 2010; Chen et al., 2011; Johnson et al., 2012; Tobouti et al., 2016; Sultan et al., 2019). Similar to other sites of infection, host materials become intertwined in the extracellular matrix of these *C. albicans* biofilms, with integration of salivary proteins and immune cells into the matrix (Nett et al., 2015). The mucosal response involves the recruitment of inflammatory cells to the palate mucosa and epithelial changes consistent with the histopathology of dental stomatitis seen clinically (Nett et al., 2010; Johnson et al., 2012; Tobouti et al., 2016; Sultan et al., 2019).

While the clinical relevance of *Candida* biofilm in the pathogenesis of vulvovaginal candidiasis is not well-understood, murine vaginitis models reveal that *C. albicans* forms biofilm on the vaginal mucosa (Harriott et al., 2010). These mucosal biofilms are characterized by the presence of an extracellular matrix surrounding yeast and hyphal cells, typical of *in vitro C. albicans* biofilms and biofilms formed at other sites of infection (Harriott et al., 2010). Clinically, vulvovaginal candidiasis is associated with a robust neutrophil response leading to acute inflammation. A similar acute inflammatory response is recapitulated in a murine model of *C. albicans* infection, which appears to be mediated by the release of S100 alarmins from epithelial cells (Yano et al., 2010, 2012). Interestingly, this likely represents a species-specific host interaction, as *C. glabrata* does not form biofilm or elicit a strong inflammatory response in this model (Nash et al., 2016). Further studies are required to fully elucidate the complex host response to *Candida* biofilms during vaginal infection.

HOST RESPONSES TO *Candida* IN MIXED-SPECIES BIOFILMS

Many studies have focused on the proliferation of *Candida* in a single-species biofilm, but *Candida* spp. also form polymicrobial biofilms in a variety of niches, including the oropharynx and skin. In these mixed-species biofilms, the immune response to one species may influence immunity to another organism. For example, *Staphylococcus aureus* has been shown to preferentially adhere to *C. albicans* hyphae and form mixed-species biofilms (Peters et al., 2010; Zago et al., 2015; de Carvalho Dias et al., 2017). In this setting *C. albicans* promotes the phagocytosis of *Staphylococcus aureus,* which can be carried by phagocytes from the oral cavity to the lymphatic system and cause invasive, disseminated disease in murine model of candidiasis (Allison et al., 2019). In addition, formation of a mixed biofilm triggers differential production of soluble factors and proteins that are anticipated to modulate immunity and enhance the virulence of both species (Peters et al., 2010; de Carvalho Dias et al., 2017).

Chronic wounds frequently become colonized by polymicrobial biofilms, and *Candida* spp. are increasingly recognized as major contributors to these infections (Kalan et al., 2016; Kalan and Grice, 2018). Not only are *Candida* spp. among the most frequently isolated fungal pathogens from diabetic foot ulcers, the presence of fungi in these wounds correlates with longer healing times (Kalan et al., 2016). *In vitro* wound biofilm models recapitulate the chronic wound environment and shed light on interactions among common colonizers, including *C. albicans*, *Pseudomonas aeruginosa*, and *Staphylococcus aureus* in this context (Townsend et al., 2016, 2017). In a three-dimensional wound biofilm model, combined antibiotic and antifungal treatments are most effective in eliminating polymicrobial biofilms, emphasizing the importance of considering fungal presence in chronic wounds (Townsend et al., 2017). While much of the host response to these chronic wound biofilms has not yet been elucidated, this represents an important topic for future studies.

In addition to forming polymicrobial biofilms with bacteria, *C.albicans* also establishes mixed-species biofilms with other *Candida* (Pathirana et al., 2019; Tati et al., 2016; Vipulanandan et al., 2018). One common clinical example of this is oropharyngeal candidiasis, which often involves multiple *Candida* species (Redding, 2001). In a mouse model of oropharyngeal candidiasis, colonization by *C. glabrata* requires the presence of *C. albicans* (Tati et al., 2016). Co-culture of the organisms lead to upregulation of *C. glabrata* cell surface proteins that allow for adhesion to *C. albicans* hyphae (Tati et al., 2016). Additional examples of species involved in mixed-species biofilms include *C. dubliniensis* and *C. tropicalis,* both of which appear to adhere to *C. albicans* and exhibit a growth benefit (Pathirana et al., 2019). When co-cultured together, these species form biofilms that achieve higher surface coverage. The influence of these altered biofilm structures on host responses remains unclear. However, the host interface for mixed biofilms may be quite distinct from that observed for either species alone.

CONCLUSIONS AND FUTURE DIRECTIONS

Candidiasis frequently involves the formation of surface-associated biofilms. These structures have a multifaceted interaction with the host. Compared to cells grown in free-floating conditions, *Candida* biofilms exhibit resistance to phagocytosis by neutrophils, monocytes, and macrophages. In addition, biofilm formation alters mononuclear cell cytokine profiles, broadly influencing immunity. Biofilms modulate immunity throughout various developmental stages. During mature biofilm formation, extracellular matrix contributes to resistance to host defenses. As fungal cells disperse, a more virulent phenotype results in enhanced pathogenesis.

Further understanding of the impact of biofilm formation on host immunity will be of interest. Many biofilm studies have explored immune cell interactions *ex vivo*. However, biofilm composition is highly impacted by *in vivo* conditions, and little is known about how the host contribution to biofilm may alter immune recognition. In addition, studies are just beginning to shed light on the complexity of immunity to mixed biofilms. Furthermore, it will fascinating to see how biofilm formation by emerging species, such as *C. auris*, influences host responses, as *C. albicans* has primarily been utilized as a model organism.

AUTHOR CONTRIBUTIONS

EE and JN wrote the manuscript. Both authors contributed to the article and approved the submitted version.

FUNDING

JN was supported by the National Institutes of Health (R01 AI145939), the Burroughs Welcome Fund (1012299), and the Doris Duke Charitable Foundation (112580130). EE was supported by the University of Wisconsin Graduate School, part of the Office of Vice Chancellor for Research and Graduate Education, with funding from the Wisconsin Alumni Research Foundation.

REFERENCES

Ala-Houhala, M., and Anttila, V. J. (2020). Persistent versus non-persistent candidaemia in adult patients in 2007-2016: a retrospective cohort study. *Mycoses* 63, 617–624. doi: 10.1111/myc.13085

Allison, D. L., Scheres, N., Willems, H. M. E., Bode, C. S., Krom, B. P., and Shirtliff, M. E. (2019). The host immune system facilitates disseminated *Staphylococcus aureus* disease due to phagocytic attraction to *Candida albicans* during coinfection: a case of bait and switch. *Infect. Immun.* 87:e00137-19.

Alonso, M. F., Gow, N. A. R., Erwig, L. P., and Bain, J. M. (2017). Macrophage migration is impaired within *Candida albicans* biofilms. *J. Fungi (Basel)* 3:31. doi: 10.3390/jof3030031

Andes, D., Nett, J., Oschel, P., Albrecht, R., Marchillo, K., and Pitula, A. (2004). Development and characterization of an in vivo central venous catheter *Candida albicans* biofilm model. *Infect. Immun.* 72, 6023–6031. doi: 10.1128/iai.72.10.6023-6031.2004

Andes, D. R., Safdar, N., Baddley, J. W., Playford, G., Reboli, A. C., Rex, J. H., et al. (2012). Impact of treatment strategy on outcomes in patients with candidemia and other forms of invasive candidiasis: a patient-level quantitative review of randomized trials. *Clin. Infect. Dis.* 54, 1110–1122. doi: 10.1093/cid/cis021

Arce Miranda, J. E., Baronetti, J. L., Sotomayor, C. E., and Paraje, M. G. (2019). Oxidative and nitrosative stress responses during macrophage-*Candida albicans* biofilm interaction. *Med. Mycol.* 57, 101–113. doi: 10.1093/mmy/myx143

Bizerra, F. C., Nakamura, C. V., de Poersch, C., Estivalet Svidzinski, T. I., Borsato Quesada, R. M., Goldenberg, S., et al. (2008). Characteristics of biofilm formation by *Candida tropicalis* and antifungal resistance. *FEMS Yeast Res.* 8, 442–450. doi: 10.1111/j.1567-1364.2007.00347.x

Branzk, N., Lubojemska, A., Hardison, S. E., Wang, Q., Gutierrez, M. G., Brown, G. D., et al. (2014). Neutrophils sense microbe size and selectively release neutrophil extracellular traps in response to large pathogens. *Nat. Immunol.* 15, 1017–1025. doi: 10.1038/ni.2987

Brinkmann, V., Reichard, U., Goosmann, C., Fauler, B., Uhlemann, Y., Weiss, D. S., et al. (2004). Neutrophil extracellular traps kill bacteria. *Science* 303, 1532–1535. doi: 10.1126/science.1092385

Capote-Bonato, F., Bonato, D. V., Ayer, I. M., Magalhaes, L. F., and Magalhaes, G. M. (2018). Pereira da Camara Barros FF, et al. Murine model for the evaluation of candiduria caused by *Candida tropicalis* from biofilm. *Microb. Pathog.* 117, 170–174. doi: 10.1016/j.micpath.2018.02.036

Chaffin, W. L., Lopez-Ribot, J. L., Casanova, M., Gozalbo, D., and Martinez, J. P. (1998). Cell wall and secreted proteins of *Candida albicans*: identification, function, and expression. *Microbiol. Mol. Biol. Rev.* 62, 130–180. doi: 10.1128/mmbr.62.1.130-180.1998

Chandra, J., Kuhn, D. M., Mukherjee, P. K., Hoyer, L. L., McCormick, T., and Ghannoum, M. A. (2001a). Biofilm formation by the fungal pathogen *Candida albicans*: development, architecture, and drug resistance. *J. Bacteriol.* 183, 5385–5394.

Chandra, J., McCormick, T. S., Imamura, Y., Mukherjee, P. K., and Ghannoum, M. A. (2007). Interaction of *Candida albicans* with adherent human peripheral blood mononuclear cells increases *C. albicans* biofilm formation and results in differential expression of pro- and anti-inflammatory cytokines. *Infect. Immun.* 75, 2612–2620. doi: 10.1128/iai.01841-06

Chandra, J., Mukherjee, P. K., Leidich, S. D., Faddoul, F. F., Hoyer, L. L., Douglas, L. J., et al. (2001b). Antifungal resistance of candidal biofilms formed on denture acrylic in vitro. *J. Dent. Res.* 80, 903–908. doi: 10.1177/00220345010800031101

Chen, Y. L., Brand, A., Morrison, E. L., Silao, F. G., Bigol, U. G., Malbas, F. F. Jr., et al. (2011). Calcineurin controls drug tolerance, hyphal growth, and virulence in *Candida dubliniensis*. *Eukaryot. Cell* 10, 803–819. doi: 10.1128/ec.00310-10

de Carvalho Dias, K., Barbugli, P. A., de Patto, F., Lordello, V. B., de Aquino Penteado, L., Medeiros, A. I., et al. (2017). Soluble factors from biofilm of *Candida albicans* and *Staphylococcus aureus* promote cell death and inflammatory response. *BMC Microbiol.* 17:146. doi: 10.1186/s12866-017-1031-5

Dominguez, E., Zarnowski, R., Sanchez, H., Covelli, A. S., Westler, W. M., Azadi, P., et al. (2018). Conservation and divergence in the *Candida* species biofilm matrix mannan-glucan complex structure, function, and genetic control. *mBio* 9:e00451-18.

Dominguez, E. G., Zarnowski, R., Choy, H. L., Zhao, M., Sanchez, H., Nett, J. E., et al. (2019). Conserved role for biofilm matrix polysaccharides in *Candida auris* drug resistance. *mSphere* 4:e00680-18.

Donlan, R. M. (2001a). Biofilms and device-associated infections. *Emerg. Infect. Dis.* 7, 277–281. doi: 10.3201/eid0702.010226

Donlan, R. M. (2001b). Biofilm formation: a clinically relevant microbiological process. *Clin. Infect. Dis.* 33, 1387–1392. doi: 10.1086/322972

Douglas, L. J. (2002). Medical importance of biofilms in *Candida infections*. *Rev. Iberoam. Micol.* 19, 139–143.

Douglas, L. J. (2003). *Candida* biofilms and their role in infection. *Trends Microbiol.* 11, 30–36. doi: 10.1016/s0966-842x(02)00002-1

Edwards, J. E. Jr., Lehrer, R. I., Stiehm, E. R., Fischer, T. J., and Young, L. S. (1978). Severe candidal infections: clinical perspective, immune defense mechanisms, and current concepts of therapy. *Ann. Intern. Med.* 89, 91–106.

Erwig, L. P., and Gow, N. A. (2016). Interactions of fungal pathogens with phagocytes. *Nat. Rev. Microbiol.* 14, 163–176. doi: 10.1038/nrmicro.2015.21

Fidel, P. L. Jr. (2002). Immunity to *Candida*. *Oral Dis.* 8(Suppl. 2), 69–75.

Harriott, M. M., Lilly, E. A., Rodriguez, T. E., Fidel, P. L., and Noverr, M. C. (2010). *Candida albicans* forms biofilms on the vaginal mucosa. *Microbiology* 156(Pt 12), 3635–3644. doi: 10.1099/mic.0.039354-0

Hawser, S. P., Baillie, G. S., and Douglas, L. J. (1998). Production of extracellular matrix by *Candida albicans* biofilms. *J. Med. Microbiol.* 47, 253–256. doi: 10.1099/00222615-47-3-253

Hawser, S. P., and Douglas, L. J. (1994). Biofilm formation by *Candida* species on the surface of catheter materials in vitro. *Infect. Immun.* 62, 915–921. doi: 10.1128/iai.62.3.915-921.1994

Hoyer, A. R., Johnson, C. J., Hoyer, M. R., Kernien, J. F., and Nett, J. E. (2018). Echinocandin treatment of *Candida albicans* biofilms enhances neutrophil extracellular trap formation. *Antimicrob. Agents Chemother.* 62:e00797-18.

Jain, N., Kohli, R., Cook, E., Gialanella, P., Chang, T., and Fries, B. C. (2007). Biofilm formation by and antifungal susceptibility of *Candida* isolates from urine. *Appl. Environ. Microbiol.* 73, 1697–1703. doi: 10.1128/aem.02439-06

Johnson, C. C., Yu, A., Lee, H., Fidel, P. L. Jr., and Noverr, M. C. (2012). Development of a contemporary animal model of *Candida albicans*-associated denture stomatitis using a novel intraoral denture system. *Infect. Immun.* 80, 1736–1743. doi: 10.1128/iai.00019-12

Johnson, C. J., Cabezas-Olcoz, J., Kernien, J. F., Wang, S. X., Beebe, D. J., Huttenlocher, A., et al. (2016). The extracellular matrix of *Candida albicans* biofilms impairs formation of neutrophil extracellular traps. *PLoS Pathog.* 12:e1005884. doi: 10.1371/journal.ppat.1005884

Johnson, C. J., Kernien, J. F., Hoyer, A. R., and Nett, J. E. (2017). Mechanisms involved in the triggering of neutrophil extracellular traps (NETs) by *Candida glabrata* during planktonic and biofilm growth. *Sci. Rep.* 7:13065.

Kalan, L., and Grice, E. A. (2018). Fungi in the wound microbiome. *Adv. Wound Care (New Rochelle)* 7, 247–255. doi: 10.1089/wound.2017.0756

Kalan, L., Loesche, M., Hodkinson, B. P., Heilmann, K., Ruthel, G., Gardner, S. E., et al. (2016). Redefining the chronic-wound microbiome: fungal communities are prevalent, dynamic, and associated with delayed healing. *mBio* 7:e01058-16.

Katragkou, A., Chatzimoschou, A., Simitsopoulou, M., Georgiadou, E., and Roilides, E. (2011a). Additive antifungal activity of anidulafungin and human neutrophils against *Candida parapsilosis* biofilms. *J. Antimicrob. Chemother.* 66, 588–591. doi: 10.1093/jac/dkq466

Katragkou, A., Kruhlak, M. J., Simitsopoulou, M., Chatzimoschou, A., Taparkou, A., Cotten, C. J., et al. (2010). Interactions between human phagocytes and *Candida albicans* biofilms alone and in combination with antifungal agents. *J. Infect. Dis.* 201, 1941–1949.

Katragkou, A., Simitsopoulou, M., Chatzimoschou, A., Georgiadou, E., Walsh, T. J., and Roilides, E. (2011b). Effects of interferon-gamma and granulocyte colony-stimulating factor on antifungal activity of human polymorphonuclear neutrophils against *Candida albicans* grown as biofilms or planktonic cells. *Cytokine* 55, 330–334. doi: 10.1016/j.cyto.2011.05.007

Kernien, J. F., Johnson, C. J., and Nett, J. E. (2017). Conserved Inhibition of neutrophil extracellular trap release by clinical *Candida albicans* biofilms. *J. Fungi* 3:49. doi: 10.3390/jof3030049

Kojic, E. M., and Darouiche, R. O. (2004). *Candida* infections of medical devices. *Clin. Microbiol. Rev.* 17, 255–267. doi: 10.1128/cmr.17.2.255-267.2004

Kucharikova, S., Neirinck, B., Sharma, N., Vleugels, J., Lagrou, K., and Van Dijck, P. (2015). In vivo *Candida glabrata* biofilm development on foreign bodies in a rat subcutaneous model. *J. Antimicrob. Chemother.* 70, 846–856. doi: 10.1093/jac/dku447

Kuhn, D. M., Chandra, J., Mukherjee, P. K., and Ghannoum, M. A. (2002). Comparison of biofilms formed by *Candida albicans* and *Candida parapsilosis* on bioprosthetic surfaces. *Infect. Immun.* 70, 878–888.

Kumamoto, C. A., and Vinces, M. D. (2005). Alternative *Candida albicans* lifestyles: growth on surfaces. *Annu. Rev. Microbiol.* 59, 113–133.

Lazzell, A. L., Chaturvedi, A. K., Pierce, C. G., Prasad, D., Uppuluri, P., and Lopez-Ribot, J. L. (2009). Treatment and prevention of *Candida albicans* biofilms with caspofungin in a novel central venous catheter murine model of candidiasis. *J. Antimicrob. Chemother.* 64, 567–570. doi: 10.1093/jac/dkp242

Lee, H., Yu, A., Johnson, C. C., Lilly, E. A., Noverr, M. C., and Fidel, P. L. Jr. (2011). Fabrication of a multi-applicable removable intraoral denture system for rodent research. *J. Oral Rehabil.* 38, 686–690. doi: 10.1111/j.1365-2842.2011.02206.x

Lewis, R. E., Kontoyiannis, D. P., Darouiche, R. O., Raad, I. I., and Prince, R. A. (2002). Antifungal activity of amphotericin B, fluconazole, and voriconazole in an in vitro model of *Candida* catheter-related bloodstream infection. *Antimicrob. Agents Chemother.* 46, 3499–3505. doi: 10.1128/aac.46.11.3499-3505.2002

Magill, S. S., Edwards, J. R., Bamberg, W., Beldavs, Z. G., Dumyati, G., Kainer, M. A., et al. (2014). Multistate point-prevalence survey of health care-associated infections. *N. Engl. J. Med.* 370, 1198–1208. doi: 10.1056/nejmoa1306801

Mitchell, K. F., Zarnowski, R., Sanchez, H., Edward, J. A., Reinicke, E. L., Nett, J. E., et al. (2015). Community participation in biofilm matrix assembly and function. *Proc. Natl. Acad. Sci. U.S.A.* 112, 4092–4097. doi: 10.1073/pnas.1421437112

Nash, E. E., Peters, B. M., Lilly, E. A., Noverr, M. C., and Fidel, P. L. Jr. (2016). A murine model of *Candida glabrata* vaginitis shows no evidence of an inflammatory immunopathogenic response. *PLoS One* 11:e0147969. doi: 10.1371/journal.pone.0147969

Nett, J. E., Brooks, E. G., Cabezas-Olcoz, J., Sanchez, H., Zarnowski, R., Marchillo, K., et al. (2014). Rat indwelling urinary catheter model of *Candida albicans* biofilm infection. *Infect. Immun.* 82, 4931–4940. doi: 10.1128/iai.02284-14

Nett, J. E., Marchillo, K., Spiegel, C. A., and Andes, D. R. (2010). Development and validation of an in vivo *Candida albicans* biofilm denture model. *Infect. Immun.* 78, 3650–3659. doi: 10.1128/iai.00480-10

Nett, J. E., Zarnowski, R., Cabezas-Olcoz, J., Brooks, E. G., Bernhardt, J., Marchillo, K., et al. (2015). Host contributions to construction of three device-associated *Candida albicans* biofilms. *Infect. Immun.* 83, 4630–4638. doi: 10.1128/iai.00931-15

Nieminen, M. T., Hernandez, M., Novak-Frazer, L., Kuula, H., Ramage, G., Bowyer, P., et al. (2014). DL-2-hydroxyisocaproic acid attenuates inflammatory responses in a murine *Candida albicans* biofilm model. *Clin. Vaccine Immunol.* 21, 1240–1245. doi: 10.1128/cvi.00339-14

Nobile, C. J., and Johnson, A. D. (2015). *Candida albicans* biofilms and human disease. *Annu. Rev. Microbiol.* 69, 71–92.

Pathirana, R. U., McCall, A. D., Norris, H. L., and Edgerton, M. (2019). Filamentous non-*albicans Candida* species adhere to *Candida albicans* and benefit from dual biofilm growth. *Front. Microbiol.* 10:1188. doi: 10.3389/fmicb.2019.01188

Peters, B. M., Jabra-Rizk, M. A., Scheper, M. A., Leid, J. G., Costerton, J. W., and Shirtliff, M. E. (2010). Microbial interactions and differential protein expression in *Staphylococcus aureus -Candida albicans* dual-species biofilms. *FEMS Immunol. Med. Microbiol.* 59, 493–503. doi: 10.1111/j.1574-695x.2010.00710.x

Pfaller, M. A., and Diekema, D. J. (2007). Epidemiology of invasive candidiasis: a persistent public health problem. *Clin. Microbiol. Rev.* 20, 133–163. doi: 10.1128/cmr.00029-06

Ramage, G., Vandewalle, K., Wickes, B. L., and Lopez-Ribot, J. L. (2001). Characteristics of biofilm formation by *Candida albicans*. *Rev. Iberoam. Micol.* 18, 163–170.

Redding, S. W. (2001). The role of yeasts other than *Candida albicans* in oropharyngeal candidiasis. *Curr. Opin. Infect. Dis.* 14, 673–677. doi: 10.1097/00001432-200112000-00002

Ricicova, M., Kucharikova, S., Tournu, H., Hendrix, J., Bujdakova, H., Van Eldere, J., et al. (2010). *Candida albicans* biofilm formation in a new in vivo rat model. *Microbiology* 156(Pt 3), 909–919. doi: 10.1099/mic.0.033530-0

Schinabeck, M. K., Long, L. A., Hossain, M. A., Chandra, J., Mukherjee, P. K., Mohamed, S., et al. (2004). Rabbit model of *Candida albicans* biofilm infection: liposomal amphotericin B antifungal lock therapy. *Antimicrob. Agents Chemother.* 48, 1727–1732. doi: 10.1128/aac.48.5.1727-1732.2004

Sellam, A., Al-Niemi, T., McInnerney, K., Brumfield, S., Nantel, A., and Suci, P. A. (2009). A *Candida albicans* early stage biofilm detachment event in rich medium. *BMC Microbiol.* 9:25. doi: 10.1186/1471-2180-9-25

Sherry, L., Ramage, G., Kean, R., Borman, A., Johnson, E. M., Richardson, M. D., et al. (2017). Biofilm-forming capability of highly virulent, multidrug-resistant *Candida auris*. *Emerg. Infect. Dis.* 23, 328–331. doi: 10.3201/eid2302.161320

Simitsopoulou, M., Chlichlia, K., Kyrpitzi, D., Walsh, T. J., and Roilides, E. (2018). Pharmacodynamic and immunomodulatory effects of micafungin on host responses against biofilms of *Candida parapsilosis* in comparison to those of *Candida albicans*. *Antimicrob. Agents Chemother.* 62:e00478-18.

Sultan, A. S., Rizk, A. M., Vila, T., Ji, Y., Masri, R., and Jabra-Rizk, M. A. (2019). Digital design of a universal rat intraoral device for therapeutic evaluation of a topical formulation against *Candida*-associated denture stomatitis. *Infect. Immun.* 87:e00617-19.

Tati, S., Davidow, P., McCall, A., Hwang-Wong, E., Rojas, I. G., Cormack, B., et al. (2016). *Candida glabrata* binding to *Candida albicans* hyphae enables its development in oropharyngeal candidiasis. *PLoS Pathog.* 12:e1005522. doi: 10.1371/journal.ppat.1005522

Tobouti, P. L., Casaroto, A. R., de Almeida, R. S., de Paula Ramos, S., Dionisio, T. J., Porto, V. C., et al. (2016). Expression of secreted aspartyl proteinases in an experimental model of *Candida albicans*-associated denture stomatitis. *J. Prosthodont.* 25, 127–134. doi: 10.1111/jopr.12285

Townsend, E. M., Sherry, L., Kean, R., Hansom, D., Mackay, W. G., Williams, C., et al. (2017). Implications of antimicrobial combinations in complex wound biofilms containing fungi. *Antimicrob. Agents Chemother.* 61:e00672-17.

Townsend, E. M., Sherry, L., Rajendran, R., Hansom, D., Butcher, J., Mackay, W. G., et al. (2016). Development and characterisation of a novel three-dimensional inter-kingdom wound biofilm model. *Biofouling* 32, 1259–1270. doi: 10.1080/08927014.2016.1252337

Tumbarello, M., Posteraro, B., Trecarichi, E. M., Fiori, B., Rossi, M., Porta, R., et al. (2007). Biofilm production by *Candida* species and inadequate antifungal therapy as predictors of mortality for patients with candidemia. *J. Clin. Microbiol.* 45, 1843–1850. doi: 10.1128/jcm.00131-07

Uppuluri, P., Acosta Zaldivar, M., Anderson, M. Z., Dunn, M. J., Berman, J., Lopez Ribot, J. L., et al. (2018). *Candida albicans* dispersed cells are developmentally distinct from biofilm and planktonic cells. *mBio* 9:e01338-18.

Uppuluri, P., Chaturvedi, A. K., Srinivasan, A., Banerjee, M., Ramasubramaniam, A. K., Kohler, J. R., et al. (2010). Dispersion as an important step in the *Candida albicans* biofilm developmental cycle. *PLoS Pathog.* 6:e1000828. doi: 10.1371/journal.ppat.1000828

Urban, C. F., Reichard, U., Brinkmann, V., and Zychlinsky, A. (2006). Neutrophil extracellular traps capture and kill *Candida albicans* yeast and hyphal forms. *Cell Microbiol.* 8, 668–676. doi: 10.1111/j.1462-5822.2005.00659.x

Vipulanandan, G., Herrera, M., Wiederhold, N. P., Li, X., Mintz, J., Wickes, B. L., et al. (2018). Dynamics of mixed- *Candida* species biofilms in response to antifungals. *J. Dent. Res.* 97, 91–98. doi: 10.1177/0022034517729351

Wall, G., Montelongo-Jauregui, D., Vidal Bonifacio, B., Lopez-Ribot, J. L., and Uppuluri, P. (2019). *Candida albicans* biofilm growth and dispersal: contributions to pathogenesis. *Curr. Opin. Microbiol.* 52, 1–6. doi: 10.1016/j.mib.2019.04.001

Wang, X., and Fries, B. C. (2011). A murine. *J. Med. Microbiol.* 60(Pt 10), 1523–1529.

Wisplinghoff, H., Bischoff, T., Tallent, S. M., Seifert, H., Wenzel, R. P., and Edmond, M. B. (2004). Nosocomial bloodstream infections in US hospitals: analysis of 24,179 cases from a prospective nationwide surveillance study. *Clin. Infect. Dis.* 39, 309–317. doi: 10.1086/421946

Xie, Z., Thompson, A., Sobue, T., Kashleva, H., Xu, H., Vasilakos, J., et al. (2012). *Candida albicans* biofilms do not trigger reactive oxygen species and evade neutrophil killing. *J. Infect. Dis.* 206, 1936–1945. doi: 10.1093/infdis/jis607

Yano, J., Lilly, E., Barousse, M., and Fidel, P. L. Jr. (2010). Epithelial cell-derived S100 calcium-binding proteins as key mediators in the hallmark acute neutrophil response during *Candida* vaginitis. *Infect. Immun.* 78, 5126–5137. doi: 10.1128/iai.00388-10

Yano, J., Noverr, M. C., and Fidel, P. L. (2012). Cytokines in the host response to *Candida* vaginitis: identifying a role for non-classical immune mediators, S100 alarmins. *Cytokine* 58, 118–128. doi: 10.1016/j.cyto.2011.11.021

Yano, J., Yu, A., Fidel, P. L. Jr., and Noverr, M. C. (2019). *Candida glabrata* has no enhancing role in the pathogenesis of *Candida*-associated denture stomatitis in a rat model. *mSphere* 4:e00191-19.

Zago, C. E., Silva, S., Sanita, P. V., Barbugli, P. A., Dias, C. M., Lordello, V. B., et al. (2015). Dynamics of biofilm formation and the interaction between *Candida albicans* and methicillin-susceptible (MSSA) and -resistant *Staphylococcus aureus* (MRSA). *PLoS One* 10:e0123206. doi: 10.1371/journal.pone.0123206

Zarnowski, R., Westler, W. M., Lacmbouh, G. A., Marita, J. M., Bothe, J. R., Bernhardt, J., et al. (2014). Novel entries in a fungal biofilm matrix encyclopedia. *mBio* 5:e01333-14.

Zawrotniak, M., Bochenska, O., Karkowska-Kuleta, J., Seweryn-Ozog, K., Aoki, W., Ueda, M., et al. (2017). Aspartic proteases and major cell wall components in *Candida albicans* trigger the release of neutrophil extracellular traps. *Front. Cell. Infect. Microbiol.* 7:414. doi: 10.3389/fcimb.2017.00414

Conflict of Interest: The authors declare that the research was conducted in the absence of any commercial or financial relationships that could be construed as a potential conflict of interest.

frontiers in Microbiology

ORIGINAL RESEARCH
published: 07 July 2020
doi: 10.3389/fmicb.2020.01525

Antifungal Activity of the Natural Coumarin Scopoletin Against Planktonic Cells and Biofilms From a Multidrug-Resistant *Candida tropicalis* Strain

Ari S. O. Lemos[1], Jônatas R. Florêncio[1], Nícolas C. C. Pinto[1], Lara M. Campos[1], Thiago P. Silva[2], Richard M. Grazul[3], Priscila F. Pinto[4], Guilherme D. Tavares[5], Elita Scio[1], Ana Carolina M. Apolônio[6], Rossana C. N. Melo[2] and Rodrigo L. Fabri[1]†*

[1] Bioactive Natural Products Laboratory, Department of Biochemistry, Institute of Biological Sciences, Federal University of Juiz de Fora, Juiz de Fora, Brazil, [2] Laboratory of Cellular Biology, Department of Biology, Institute of Biological Sciences, Federal University of Juiz de Fora, Juiz de Fora, Brazil, [3] Department of Chemistry, Institute of Exact Sciences, Federal University of Juiz de Fora, Juiz de Fora, Brazil, [4] Protein Structure and Function Study Laboratory, Department of Biochemistry, Institute of Biological Sciences, Federal University of Juiz de Fora, Juiz de Fora, Brazil, [5] Laboratory of Nanostructured Systems Development, Department of Pharmacy, Federal University of Juiz de Fora, Juiz de Fora, Brazil, [6] Department of Parasitology, Microbiology, and Imunology, Institute of Biological Sciences, Federal University of Juiz de Fora, Juiz de Fora, Brazil

OPEN ACCESS

Edited by:
Juliana Campos Junqueira, São Paulo State University, Brazil

Reviewed by:
Taissa Vila, University of Maryland, Baltimore, United States
Jonatas Rafael De Oliveira, Anhembi Morumbi University, Brazil

***Correspondence:**
Rodrigo L. Fabri
rodrigo.fabri@ufjf.edu.br

†**ORCID:**
Rodrigo L. Fabri
orcid.org/0000-0002-0167-2277

Specialty section:
This article was submitted to Infectious Diseases, a section of the journal Frontiers in Microbiology

Received: *10 February 2020*
Accepted: *12 June 2020*
Published: *07 July 2020*

Citation:
Lemos ASO, Florêncio JR, Pinto NCC, Campos LM, Silva TP, Grazul RM, Pinto PF, Tavares GD, Scio E, Apolônio ACM, Melo RCN and Fabri RL (2020) Antifungal Activity of the Natural Coumarin Scopoletin Against Planktonic Cells and Biofilms From a Multidrug-Resistant Candida tropicalis Strain. Front. Microbiol. 11:1525. doi: 10.3389/fmicb.2020.01525

Candida tropicalis is one the most relevant biofilm-forming fungal species increasingly associated with invasive mucosal candidiasis worldwide. The amplified antifungal resistance supports the necessity for more effective and less toxic treatment, including the use of plant-derived natural products. Scopoletin, a natural coumarin, has shown antifungal properties against plant yeast pathogens. However, the antifungal activity of this coumarin against clinically relevant fungal species such as *C. tropicalis* remains to be established. Here, we investigated the potential antifungal properties and mechanisms of action of scopoletin against a multidrug-resistant *C. tropicalis* strain (ATCC 28707). First, scopoletin was isolated by high-performance liquid chromatography from *Mitracarpus frigidus*, a plant species (family *Rubiaceae*) distributed throughout South America. Next, scopoletin was tested on *C. tropicalis* cultivated for 48h in both planktonic and biofilm forms. Fungal planktonic growth inhibition was analyzed by evaluating minimal inhibitory concentration (MIC), time-kill kinetics and cell density whereas the mechanisms of action were investigated with nucleotide leakage, efflux pumps and sorbitol and ergosterol bioassays. Finally, the scopoletin ability to affect *C. tropicalis* biofilms was evaluated through spectrophotometric and whole slide imaging approaches. In all procedures, fluconazole was used as a positive control. MIC values for scopoletin and fluconazole were 50 and 250 μg/L respectively, thus demonstrating a fungistatic activity for scopoletin. Scopoletin induced a significant decrease of *C. tropicalis* growth curves and cell density (91.7% reduction) compared to the growth control. Its action was related to the fungal cell wall, affecting plasma membrane sterols. When associated with fluconazole, scopoletin led to inhibition of efflux pumps at the plasma membrane. Moreover, scopoletin not only inhibited the growth rate of preformed biofilms (68.2% inhibition at MIC value) but also significantly decreased the extent of biofilms growing on the surface of coverslips, preventing the formation of elongated

fungal forms. Our data demonstrate, for the first time, that scopoletin act as an effective antifungal phytocompound against a multidrug-resistant strain of *C. tropicalis* with properties that affect both planktonic and biofilm forms of this pathogen. Thus, the present findings support additional studies for antifungal drug development based on plant isolated-scopoletin to treat candidiasis caused by *C. tropicalis.*

Keywords: *Candida tropicalis*, scopoletin, *Candida spp.*, antifungal agents, fungal biofilms

INTRODUCTION

Invasive fungal infections produced by *Candida* spp. persist as the primary hospital-acquired bloodstream infections and are associated with high morbidity and mortality, especially in intensive care units (Kauffman, 2015; McCarthy and Walsh, 2017; Butts et al., 2019). While *Candida albicans* remains as the most frequent fungal species isolated from candidemic patients, other *Candida* species are often identified in clinical isolates (Reviewed in Guinea, 2014).

Currently, *Candida tropicalis* is one the most relevant non-albicans *Candida species* [reviewed in Silva et al. (2012), Cavalheiro and Teixeira (2018)]. This pathogen has been frequently detected in patients from intensive care units, mainly those under prolonged catheterization and treatment with broad-spectrum antibiotics (Silva et al., 2012). *C. tropicalis* is also implicated in infections of cancer patients (Chai et al., 2010; Silva et al., 2012). *C. tropicalis* is highly prevalent in tropical countries and responsible for elevated mortality rate due to candidiasis (Godoy et al., 2003; Chai et al., 2010; Chander et al., 2013). Globally, the frequency of *C. tropicalis* is also expanding (Guinea, 2014).

Biofilms of *Candida* species can cause challenging superficial and systemic diseases and represent structures with high tolerance to antifungal agents (Cavalheiro and Teixeira, 2018). *C. tropicalis* biofilm formation has been increasingly linked to the development of resistance to antifungal drugs such as fluconazole and amphotericin B (Fernandes et al., 2015; Cavalheiro and Teixeira, 2018).

The growing use of antifungal agents has been correlated with emergence of multidrug-resistant strains of *Candida* species to commonly used antifungal drugs such as azoles and echinocandins (Perlin et al., 2015), thus requiring intensive search for new drug therapies, including phytocompounds originated from natural sources. Coumarins represent a diverse group of natural polyphenols found in a variety of plants and known by their varied pharmacological properties (Reviewed in Kostova et al., 2011; Pinto and Silva, 2017; Tomasz Kubrak et al., 2017). Scopoletin is one type of coumarin with promising biological activities including antioxidant (Jamuna et al., 2015; Zhang et al., 2017), anti-inflammatory (Jamuna et al., 2015; Leema and Tamizhselvi, 2018), anti-aging (Jamuna et al., 2015) and anti-tumoral (Pinto and Silva, 2017; Gupta et al., 2018) effects.

Scopoletin has natural and *in vitro* antifungal properties against pathogenic yeast species of plants (Goy et al., 1993; Valle et al., 1997; Prats et al., 2006; Sun et al., 2014; Ramírez-Pelayo et al., 2019). However, the antifungal activity of this coumarin against clinically relevant fungal species is poorly understood. Previous works have demonstrated a moderate anti-*C. albicans* effect for plant-isolated scopoletin (Navarro-Garcia et al., 2011; Lu et al., 2017), but if this phytocompound is effective against *C. tropicalis* remains to be established.

In the present work, we isolated scopoletin, for the first time, from the aerial parts of *Mitracarpus frigidus* (Willd. ex Roem.& Schult.) K. Shum, a species from the family Rubiaceae distributed throughout South America (Pereira et al., 2006). *M. frigidus*-originated scopoletin was then investigated and showed significant antifungal activity against a multidrug-resistant strain of *C. tropicalis*, affecting both planktonic and biofilm forms of this pathogen.

MATERIALS AND METHODS

Plant Material

The aerial parts of *Mitracarpus frigidus* (Willd. Ex Roem. & Schult.) K. Shum (Rubiaceae) were collected in Juiz de Fora, Minas Gerais State, Brazil, in May 2011 (Latitude: 21°45′51″S and Longitude: 43°20′59″W of Greenwich). A voucher specimen (CESJ 46076) was deposited at the Leopoldo Krieger Herbarium at UFJF, Brazil.

Extraction and Fractionation

A crude dichloromethane (CH_2Cl_2) extract was prepared from aerial parts of *M. frigidus* as previously described (Fabri et al., 2009). The purification of this extract was carried out as follows: The CH_2Cl_2 extract (1.3 g) was chromatographed on a 74 × 4 cm column of silica gel (70–230 mesh) with a gradient of increasing polarity (Hexane, Hexane-CH_2Cl_2, CH_2Cl_2-MeOH, MeOH) to obtain a total of six fractions. Fractions were analyzed by thin layer chromatography on silica gel 60 F_{254} (Merck) using CH_2Cl_2: MeOH, 97:3, *v/v* and CH_2Cl_2: MeOH, 95:5 *v/v* as the mobile phase for fractions F_1 to F_3 and fractions F_4 to F_6, respectively. Detection was performed with a UV lamp (254 and 365 nm) and by spraying with vanillin:sulfuric acid followed by heating. The fractions were pooled and concentrated on a rotary evaporator under reduced pressure.

High-Performance Liquid Chromatography (HPLC) Analysis

The analyses were performed with an Agilent Technologies 1200 series purification system (Agilent Technologies, Waldbronn, Germany) equipped with a Zorbax SB-18 column (250 × 10 mm, 5 μm particle size), a PDA detector and an automatic injector.

A linear gradient of a binary solvent system, A:B, which varied from 0 to 100% B ran at a flow rate of 1 mL/min over 30 min where A consisted of acetonitrile: H_2O, 5:95, pH adjusted to 4.0 with H_3PO_4 and B of acetonitrile: H_2O, 90:10, pH adjusted to 4.0 with H_3PO_4. The mobile phase was returned to its original composition over the course of 30 min, and an additional 10 min were allowed for the column to re-equilibrate before injection of the next sample. The sample volume was 10 μL at a concentration of 1 g/L. Detection was performed simultaneously at 210, 230, 254 and 280 nm.

Isolation of Scopoletin by Semi-Preparative HPLC

Scopoletin was isolated from fraction 2 (300 mg) by semi-preparative HPLC (Agilent Technologies) as above. Flow-rate and sample volume were 3.5 and 1.0 mL/min, respectively (25 g/L). The eluate from the outlet of the column was monitored at 254 nm and the peak fractions were collected according to the chromatogram.

Structural Elucidation of Scopoletin

^{1}H-NMR (500 MHz) and ^{13}C-NMR (125 MHz) spectra were recorded on a Bruker DRX spectrometer (Bruker Biospin, Rheinstetten, Germany) using the residual solvent peak ($CDCl_3$) as reference. Infrared spectra were recorded on a Bomem 102 FT-IR spectrometer with KBr pellets. The UV spectrum was acquired in MeOH and MeOH + NaOH on a Shimadzu UV160 spectrophotometer (Tokyo, Japan). The EI mass spectrum was obtained on a Hewlett-Packard 5973 MSD spectrometer (Agilent, Palo Alto, CA, United States) by direct insertion in the positive ion mode (70 eV).

Fungal Strain

Scopoletin was evaluated against *C. tropicalis* ATCC® 28707, a yeast strain resistant to fluconazole, itraconazole and amphotericin B, which was originally isolated from human pyelonephritis (Woods et al., 1974; Ishida et al., 2011). The strains were cultured (35°C, 48 h) in Sabouraud dextrose agar (SDA) and subcultured in Sabouraud dextrose broth (SDB; 35°C, overnight) before the subsequent experiments.

Determination of the Minimal Inhibitory Concentration (MIC)

The minimal inhibitory concentration (MIC) of scopoletin for *C. tropicalis* ATCC® 28707 was determined by a microdilution method using two different media: RPMI 1640 buffered with MOPS, pH 7-7.2 (CSLI, 2017) and the Brain Heart Infusion (BHI) medium (Khan et al., 2006). The stock solution of scopoletin was diluted in dimethylsulfoxide (DMSO - final concentration of 1%) with concentrations ranging from 200 to 12.5 μg/mL. Growth controls and positive controls were established with scopoletin vehicle (DMSO 1%) or fluconazole (1000 to 7.81 μg/mL), respectively. Sterility controls were performed with RPMI or BHI broth and scopoletin vehicle. All tests were performed in a volume of 200 μL, with final inoculum ranging from 0.5×10^3 to 2.5×10^3 CFU/mL (calculated from stock inoculum obtained according to 0.5 McFarland turbidity standards), and plates were incubated at 35°C for 48 h. The MIC values were calculated as the highest dilution showing complete inhibition of tested strain. All analyses were performed in duplicate. Of note, subsequent experiments were performed using only BHI medium.

Minimum Fungicidal Concentration (MFC)

Samples (10 μL) from each well that showed no visible growth in the MIC assay were inoculated on freshly prepared SDA plates and incubated at 35°C for 48 h. The MFC was reordered as the concentration of the scopoletin inhibiting the visible growth on a new set of agar plates (Campos et al., 2018).

Fungal Killing Assay

Fungal killing assay was performed as before (Campos et al., 2018) with some modifications. To determine the time-kill kinetics for *C. tropicalis* strain, freshly grown yeasts in BHI (35°C, overnight) were standardized to 10^6 cells/mL in sterile water and inoculated in test tubes with BHI broth and different concentrations of scopoletin or fluconazole (MIC, MIC/2 and MIC/4 values). Scopoletin vehicle served as fungal growth control. Optical density (OD) at 530 nm was recorded at 4, 8, 24, 28, 32 and 48 h of incubation at 35°C. Graphs of turbidity versus incubation time were plotted and a time-death curve established. The experiment was carried out in triplicate.

Fungal Cell Density

Cell enumeration was performed in cytocentrifuged cell preparations, which use carefully controlled centrifugation to separate and deposit a thin layer of cells on slides while maintaining cellular integrity (Silva et al., 2014). *C. tropicalis* was inoculated in tubes of BHI broth containing scopoletin (MIC value) and incubated (35°C, 48 h). Vehicle or fluconazole (MIC value) inoculation served as negative or positive controls, respectively. Samples were diluted 10 times (1 mL) in saline, fixed with free-particle formaldehyde (final concentration 4%) and stained for 10 min with DAPI (4′, 6-Diamidino-2-Phenylindole, final concentration 0.1 μg/mL, Vector Laboratories, Burlingame, CA, United States) for DNA labeling. Samples were prepared in a cytocentrifuge (Shandon Cytospin 4, Thermo, United Kingdom), at 254 *g* for 10 min. Analyses were performed on a fluorescence microscope (BX-60, Olympus, Melville, NY, United States) using U-MWU2 filter (330–385 nm). Fungal cell numbers were determined by counting 20 random fields at 1,000× magnification using an ocular grid. The final count was determined by multiplying by the dilution factor (10×).

Nucleotide Leakage

Nucleotide release was evaluated as before (Khan et al., 2013; Campos et al., 2018). After 48 h incubation in BHI broth, yeast cells were washed, resuspended in 10 mM PBS (pH 7.4, $\sim 10^6$ cells/mL) and incubated with scopoletin (MIC value). Cultures incubated only with PBS (10 mM, pH 7.4) or fluconazole

(MIC value) served as growth controls and positive controls, respectively. Following incubation, cell suspensions in different time points (0, 1, 2, 3, 4 and 5 h) were centrifuged at 10,000 × *g* for 10 min and the supernatants diluted for OD evaluation at 260 nm (specific wavelength for reading nucleotides) in a spectrophotometer (Multiskan Go, Thermo Scientific, Waltham, MA, United States) at room temperature. Experiments were carried out in triplicate.

Sorbitol Protection Assay

To evaluate potential mechanisms involved in the antifungal activity of the scopoletin on the yeast cell wall, we used the sorbitol assay (Frost et al., 1995; Khan et al., 2013), which was applied after determination of the MIC values for scopoletin. Serial microdilution was performed on a 96-well sterile microplate using doubly concentrated BHI broth enriched in 0.8 M sorbitol. The stock solution of scopoletin was diluted in dimethylsulfoxide (DMSO - final concentration of 1%) thus obtaining concentrations ranging from 200 to 12.5 μg/mL. Growth controls and positive controls were established with scopoletin vehicle (DMSO 1%) or fluconazole (1000 to 62.5 μg/mL), respectively. All the wells were inoculated with 100 μL of cell suspension (0.5 McFarland). After 48 h of incubation at 35°C, the MIC values with sorbitol were read as the lowest concentration in which there was no detectable visible growth.

Ergosterol Binding Assay

This assay evaluates the ability of the tested compound to bind to membrane sterols by MIC value determination in presence of exogenous ergosterol (Khan et al., 2013; Leite et al., 2014). The scopoletin (MIC value) against *C. tropicalis* was determined on a 96-well sterile microplate by serial microdilution in doubly concentrated BHI broth plus ergosterol (400 μg/mL) as before (Ana et al., 2017). The stock solution of scopoletin was diluted in concentrations ranging from 200 to 12.5 μg/mL. Plates were read after 48 h of incubation at 35°C and MIC was determined as the lowest concentration of tested agent inhibiting the visible growth. Nystatin (100 to 6.25 μg/mL), whose interaction with membrane ergosterol is well known (Leite et al., 2014), was used as positive control.

Efflux Pump Inhibition Assay

Overexpression of drug efflux pumps located at the plasma membrane is considered a mechanism for fungal escape from the action of antifungal drugs (Hans et al., 2019). To evaluate the effect of scopoletin on the efflux pump inhibition we performed a phenotypic susceptibility assay (Hans et al., 2019) using promethazine, an inhibitor of plasma membrane efflux pumps. First, the MIC value of promethazine (12.5 a 0.01 μg/mL) for *C. tropicalis* was tested by broth microdilution method. Second, a new MIC assay for fluconazole (250 to 3.9 μg/mL) was performed including sub-inhibitory concentrations of promethazine (MIC/4 = 0.78 μg/mL) or scopoletin (MIC/4 = 12.5 μg/mL) to the final fungal inoculum.

Effect on the Growth Rate of Preformed Biofilms

Candida tropicalis (1×10^6 cells/mL) was grown as biofilms using BHI broth with 1% glucose in 96 well polystyrene microtiter plates for 48 h at 35°C. After this incubation, the wells were gently washed three times with sterile water for removal of planktonic-phase cells. At this step, biofilm formation on wells was verified. Having confirmed the presence of grown biofilms, next, the wells were filled with 200 μL of BHI with scopoletin or fluconazole at MIC, MIC/2 and MIC/4 (0 h) and incubated for 48 h at 35°C. Vehicle alone (same used for the scopoletin group) served as a control for biofilm growth. OD at 530 nm was measured at 0 and 48 h after incubation. The proportion of the inhibition of biofilm proliferation was based on the reduction between the OD at 48 h and the OD at 0 h, as following: [(ODr control) – (ODr treated)/(ODr control)], where ODr = [OD at 48 h–OD at 0 h] (Gupta et al., 2018). The experiments were performed in triplicate.

Effect on Biofilm Formation and Adhesion

Evaluation of biofilm formation and adhesion was performed using high-resolution Whole Slide Imaging (WSI). This technology allows scanning and imaging of the entire slide surface and translate it into a digital format for morphometric evaluations (Amaral et al., 2017). For this, *C. tropicalis* strain (1×10^6 cells/mL) was seeded in SDA (Sabouraud Agar media), incubated (48 h, 35°C), and inoculated into a tube with 5 mL of BHI broth and 1% glucose. Then, 500 μL of the inoculated broth were added in plates (24 wells) containing round glass coverslips (13 mm, Glasscyto®). Treatment (n = 3) was performed by adding 500 μL of scopoletin (final concentration per well = 4xMIC). For negative (n = 3) and positive (n = 3) controls, 500 μL of sterile water or fluconazole (4xMIC) were added, respectively. Accumulated biofilms on glass coverslips were fixed in formaldehyde 3.7% and stained with 10 μL of DAPI (0.01 μg/mL) for 10 min. Next, each coverslip (side opposite to biofilm) was attached on the surface of a regular glass slide using a double-sided tape. Slides were digitally scanned using a 3D Scan Pannoramic Histech scanner (3D HistechKft, Budapest, Hungary) connected to a computer (Fujitsu Technology Solutions GmbH, Munich, Germany). High-resolution images were obtained using Pannoramic Viewer 1.15.2 SP2 RTM software (3D Histechkft Budapest, Hungary) and the total area occupied by the biofilms was measured using Image J software (National Institutes of Health, United States). All experiments and analyses were performed in triplicate.

Statistical Analysis

Results were expressed as mean values with the standard error. The statistical analyses were performed using ANOVA test followed by Bonferroni to compare controls and treated groups at a significance level of 5%.

RESULTS

Isolation and Identification of Scopoletin

Scopoletin eluted as a narrow peak at 9.58 min and had a chromatographic purity of 96%. Then, the chemical structure of scopoletin was elucidated (**Figure 1**).

Scopoletin (1): amorphous pale yellow powder; chromatographic purity >96 Area% by GC; UV λ_{max} nm (MeOH) 227, 297, 339; (MeOH + NaOH) 210, 390; ^{1}H NMR ($CDCl_3$, 500 MHz), calibrated from residual $CHCl_3$ solvent peak,δ 7.62 (1H, d, J = 9.5), 6.94 (1H, s), 6.87 (1H, s), 6.29 (1H, d, J = 9.5), 3.98 (3H, s); ^{13}C NMR ($CDCl_3$, 125 MHz); δ 161.4, 150.3, 149.7, 144.0, 143.3, 113.5, 111.5, 107.5, 103.2, 56.4; EI-MS 70eV, m/z (relative intensity,%) 193.05 (12.68) [M + H$^+$], 192.05 (100.0) [M$^+$], 177.05 (53.5), 164.10 (19.44), 149.05 (37.2) [M-HCO_2H], 121.05 (14.9), 149 (16.3).

Minimal Inhibitory Concentration (MIC) and Minimum Fungicidal Concentration (MFC)

First, we confirmed the resistance of the *C. tropicalis* strain to fluconazole. As expected, the MIC value found (250 μg/mL, **Table 1**) was much higher than the upper limit of the reported resistance range (0.12– ≥64 μg/mL) (Rex, 2008). In contrast, the MIC value of scopoletin for the multidrug-resistant *C. tropicalis* strain was 50 μg/mL (**Table 1**), indicating an antifungal activity (fungistatic effect) of this coumarin against *C. tropicalis*. Parallel MIC analyses of two additional species of *Candida* (*C. albicans* ATCC®18804 and *C. glabrata* ATCC®2001ATCC) also indicated a fungistatic property for scopoletin (**Supplementary Table S1**).

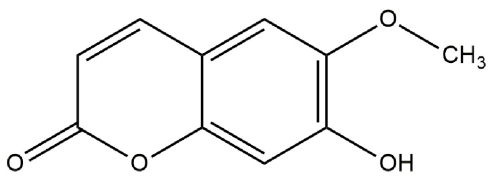

FIGURE 1 | Structure of scopoletin.

TABLE 1 | Minimal Inhibitory Concentration (MIC) values for scopoletin, fluconazole, nystatin, and promethazine against *C. tropicalis* ATCC® 28707 in the presence or absence of sorbitol or ergosterol.

Tested compounds	MIC (μg/mL)				
	BHI	BHI + Sorbitol	BHI + Ergosterol	BHI + Scopoletin	BHI + Promethazole
Scopoletin	50	>200	>200	–	–
Fluconazole	250	250	–	62.5*	31.25
Nystatin	25	–	>100	–	–
Promethazine	3.12	–	–	–	–

*The MIC for fluconazole (MIC/4) * in the presence of scopoletin or promethazole is also shown. MIC assay was performed by microtiter broth dilution method. MIC range: 100 to 0.1 μg/mL. BHI: Brain Heart Infusion.*

Of note, the MIC values did not vary with the culture medium (**Supplementary Table S1**) as previously demonstrated (Khan et al., 2006). The MFC value of scopoletin for the strains evaluated was not found for the doses tested.

Fungal Killing Assay

Next, the growth inhibitory action of scopoletin on the *C. tropicalis* strain was tested by time-kill kinetics along 48 h. Our analysis showed a significant decrease in growth cycle curves of *C. tropicalis* treated with scopoletin or fluconazole (MIC, MIC/2, and MIC/4) after 4h compared with the growth control (vehicle treatment) ($P < 0.0001$; **Figure 2**). Thus, scopoletin, mainly at MIC value, leads to fungal growth inhibition compared to fluconazole.

Fungal Cell Density

The analysis of cell density enables microscopic assessment of microorganisms in cell suspensions at single-cell level (Silva et al., 2014; Gamalier et al., 2017). The cell density of *C. tropicalis* in cultures was investigated at MIC treatments after 48 h. Our quantitative analyses using fluorescence microscopy showed that fungal cell density significantly decreased with both scopoletin ($P < 0.001$) and fluconazole treatments ($P < 0.0008$), compared with growth control (growth control = $7.13 \pm 1.12 \times 10^5$ cells/mL; scopoletin = $0.58 \pm 0.15 \times 10^5$ cells/mL; fluconazole $1.12 \pm 0.19 \times 10^5$ cells/mL). Thus, scopoletin induced an effective reduction of fungal cells (91.7%) similar to fluconazole (84.3%) after 48 h of treatment ($P > 0.99$) (**Figure 3**).

Nucleotide Leakage

Our analysis showed a significant increase in OD (260 nm) of scopoletin-treated cultures compared to the negative control (at 1 h: $P < 0.03$, at 2–5 h: $P < 0.0001$). The positive control with fluconazole also increased the OD ($P < 0.0001$) similar to scopoletin treatment (**Figure 4**).

Effect of Scopoletin on the Fungal Cell Wall and Membrane

To evaluate the effect of scopoletin on the fungal cell wall and plasma membrane, we used sorbitol protection and ergosterol binding assays, respectively (**Table 1**). Our data showed an increase in the scopoletin MIC value with sorbitol (>200 μg/mL) compared to the scopoletin MIC without sorbitol (50 μg/mL). Likewise, we found MIC increase for scopoletin when in presence of ergosterol (>200 μg/mL). Our results indicate a potential scopoletin action on both fungal cell wall and plasma membrane sterols.

Additionally, we evaluated the ability of scopoletin to modulate plasma membrane efflux pumps from *C. tropicalis* treated with fluconazole performing a phenotypic susceptibility assay (Hans et al., 2019). This test revealed (**Table 1**) a MIC reduction of fluconazole (62.5 and 31.25 μg/mL) when tested with sub-inhibitory (MIC/4) concentrations of scopoletin and promethazine, respectively. Considering that the resistance of *C. tropicalis* ATCC® 28707 to fluconazole is mostly based on efflux pumps activity, these data implicate scopoletin in the

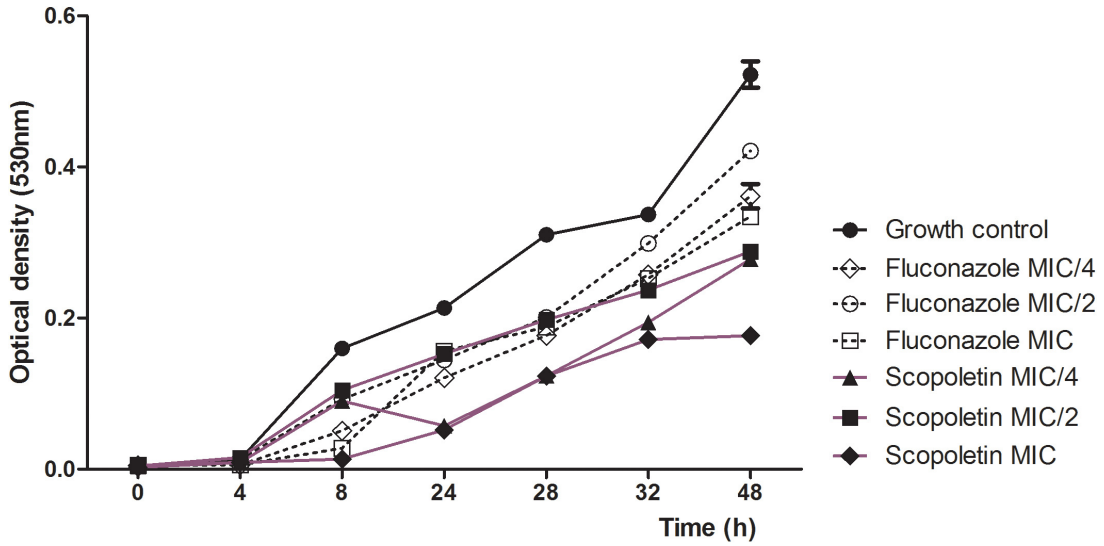

FIGURE 2 | Time-kill curve for *C. tropicalis* ATCC® 28707 treated with different concentrations of scopoletin or fluconazole. Yeasts strain in BHI broth with scopoletin or fluconazole in different concentrations (MIC, MIC/2 and MIC/4) were evaluated by OD (530 nm) at 0, 2, 4, 6, 8, and 24 h of incubation at 35°C. Yeasts cultures with scopoletin vehicle served as growth control. The experiments were carried out in triplicate. Graphs were plotted as turbidity versus incubation time, and data represent the mean ± SEM.

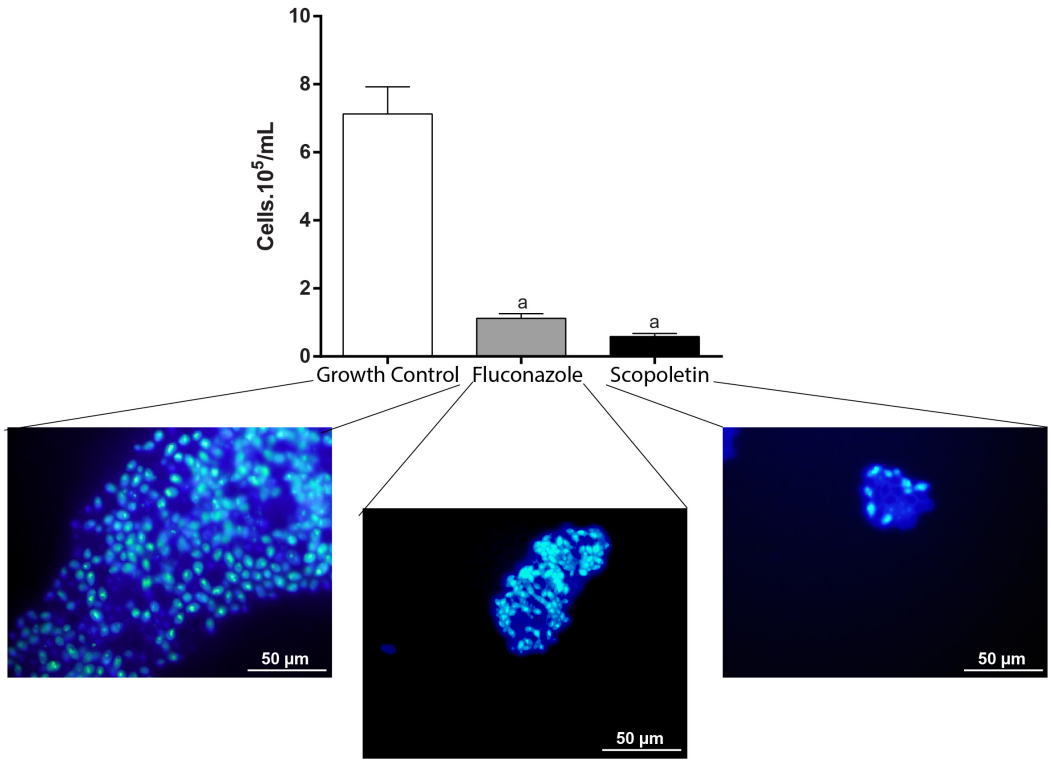

FIGURE 3 | Effect of scopoletin treatment on cell density of *C. tropicalis* ATCC® 28707. Compared with negative control (vehicle treatment), treatment with scopoletin induced a decrease in cell density similar to fluconozole treatment (positive control). Yeasts cells were stained with DAPI and counted under fluorescence microscopy. Representative images from DAPI-stained *C. tropicalis* are shown for each experimental group. Experiments were done in triplicate and data represent the mean ± SEM of yeast counted from 10 randomly selected fields/slide (n = 9 slides/time point). Letter (a) indicates statistically differences (ANOVA followed by Bonferroni, $P < 0.05$).

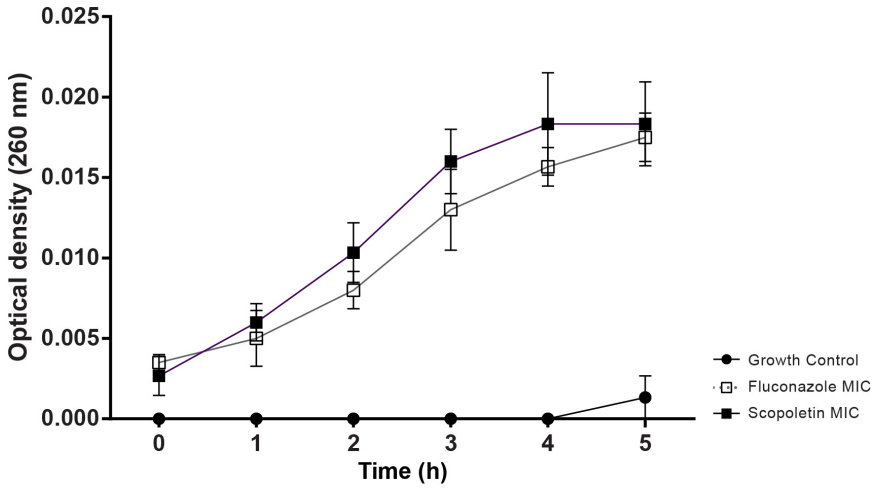

FIGURE 4 | Scopoletin treatment induces nucleotide released from *C. tropicalis* ATCC® 28707. Cultures treated with scopoletin (SCO) or fluconazole (FLU, positive control) were evaluated by nucleotide leakage test. Negative controls (GC) did not receive any treatment. Experiments were carried out in triplicate and data represent the mean ± SD.

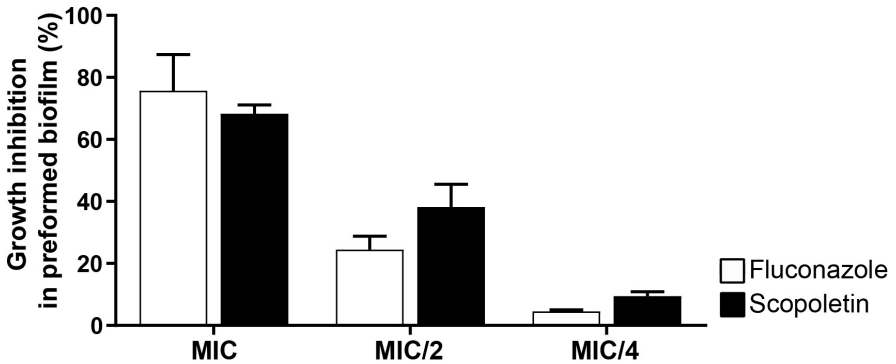

FIGURE 5 | Effect of scopoletin on preformed biofilms of *C. tropicalis* ATCC® 28707. Scopoletin treatment similar to fluconazole at the same concentrations. In each point, data represent mean ± SEM from at least two independent experiments performed in triplicate. The mean proportions of biofilm inhibition were compared between scopoletin *versus* fluconazole treatments at the same concentration (MIC: $P > 0.999$, MIC/2: $P > 0.40$, MIC/4: $P > 0.999$; ANOVA followed by Bonferroni, $P < 0.05$).

inhibition of efflux pumps at plasma membrane when associated with fluconazole.

Effect on Preformed Biofilms

The ability of the scopoletin to affect the growth rate of preformed biofilms of *C. tropicalis* ATCC® 28707 was tested at the MIC, MIC/2, and MIC/4 values. In response to scopoletin, preformed *Candida* biofilms showed a 68.2% ± 2.87 (mean ± SEM) reduction of their growth after 48 h of treatment (**Figure 5**). There was no significant difference in the proportion of the growth rate inhibition of preformed biofilms when scopoletin and fluconazole treatments were compared at the same concentrations (MIC: $P > 0.999$, MIC/2: $P > 0.40$, MIC/4: $P > 0.999$; **Figure 5**). Thus, scopoletin as well as fluconazole treatments were able to reduce the growth rate of preformed *C. tropicalis* biofilms (**Figure 5**).

Biofilm Formation

Biofilm formation was investigated through WSI analyses of the biofilm grown on coverslips. The use of a slide scanner provided a fast and reliable view of the total area covered by the biofilm (**Figures 6A–C**). Remarkably, the use of high-resolution WSI enabled the observation of cellular morphological features (**Figures 6Ai–Cii**) and revealed the occurrence of hyphae forms only in the controls (**Figures 6Ai, Aii, arrows**). Quantitative computational analyses showed a reduction of the area occupied by biofilms on the surface of coverslips treated with scopoletin compared to controls ($P < 0.01$) (**Figure 6D**).

DISCUSSION

The secondary metabolites of plants represent a large but still unexplored amount of compounds that are important sources

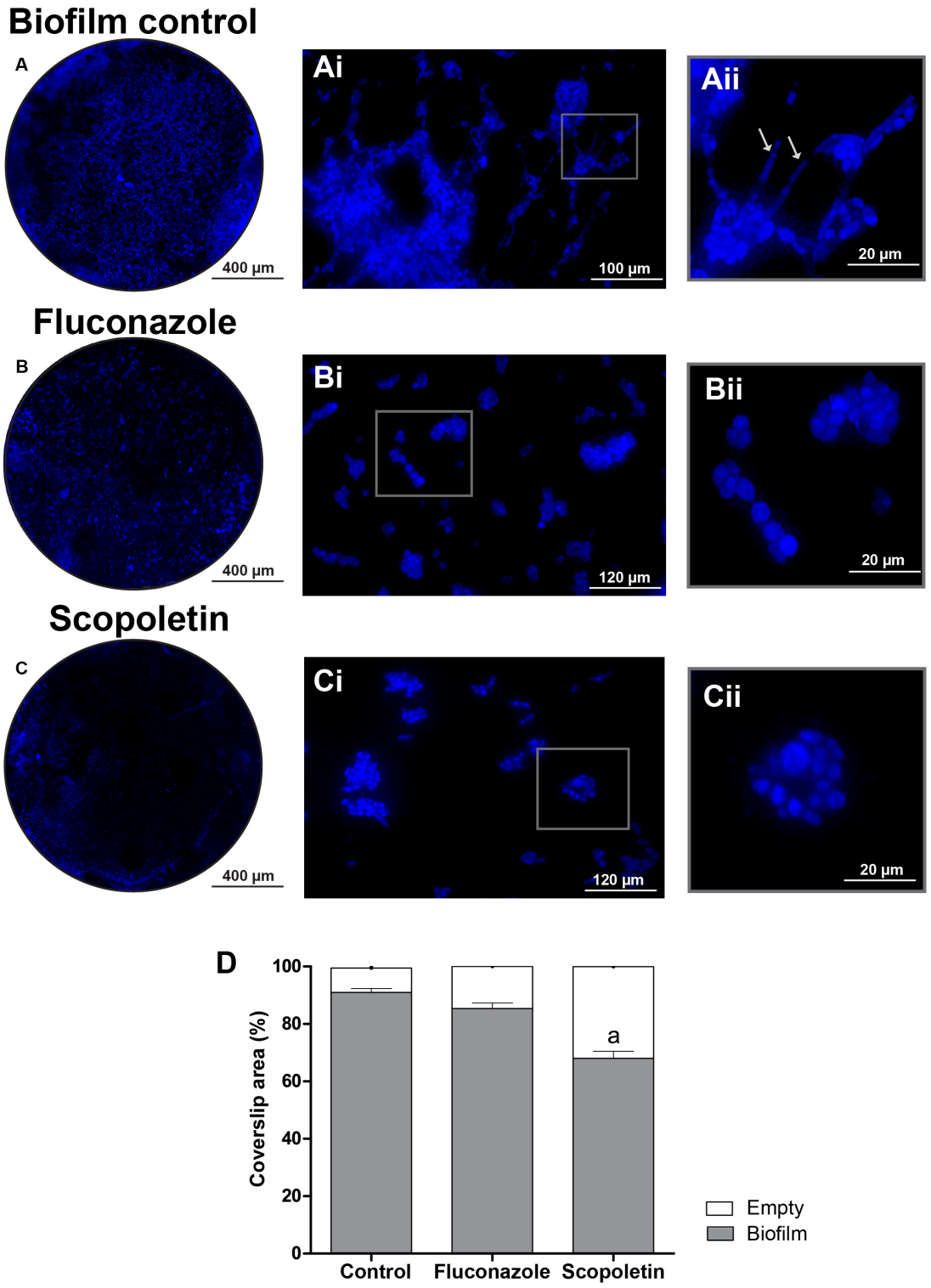

FIGURE 6 | Scopoletin affects *C. tropicalis* ATCC® 28707 biofilm formation. **(A–C)** Representative images of biofilms growing on the surface of coverslips. The whole biofilm area is shown in normal fungal growth conditions **(A)** and after fluconazole **(B)** or scopoletin **(C)** treatments. Observe in panels **(Ai–Cii)** details of fungal cells at higher magnifications. Note in the control **(Ai,Aii)** the formation of hyphae (arrows) while treated-cells **(Bi–Cii)** do not exhibit these fungal forms. Coverslips were stained with DAPI and whole biofilm areas were scanned using a 3D Scan Pannoramic Histech Scanner. After acquisition of whole slide images, areas with biofilm were measured using Image J software. **(D)** Mean percent of biofilm formation was expressed as mean ± SEM and the letter (a) indicate statistical difference (ANOVA followed by Bonferroni, $P < 0.05$).

for novel antifungal drugs, including agents that can enhance the susceptibility of fungi, such as *Candida* spp. to existing drugs (Lu et al., 2017). In the present study, we demonstrated that the natural coumarin scopoletin, isolated here for the first time from *M. frigidus*, has an effective antifungal property against a multidrug-resistant strain of *C. tropicalis* and provided the first insights into its mechanism of action.

The fractioning and liquid chromatography (HPLC) analysis of *M. frigidus* extract enabled optimal performance in terms of recovery and purity of scolopoletin. The chemical structure of scopoletin (**Figure 1**), with three singlets (1H, s and 3H, s, OCH3-6) and two doublets (1H, d), 10 signals of carbons and a methoxy (O-CH3) group is consistent with previous reports (Bhatt Mehul et al., 2011; Darmawan et al., 2012).

M. frigidus-isolated scopoletin showed an antifungal activity against *C. tropicalis* with a suggestive fungistatic effect, as detected by the MIC assay (**Table 1**). We demonstrated that scopoletin induces reduction of fungal growth in *C. tropicalis* similar to fluconazole treatment (**Figures 2**, **3**), which was associated with structural cell damage as demonstrated by ergosterol, sorbitol and efflux pump assays. In fact, by monitoring nucleotide leakage in *C. tropicalis*, we found that scopoletin leads to an increase in nucleotide release similar to fluconazole (**Figure 4**), thus suggesting an increase in fungal cell permeability likely by disturbance of the fungal cell wall and membrane, a property also found in other phytochemicals (Cho et al., 2013).

A feature of all fungal cells is the presence of a plasma membrane surrounded by a complex cell wall, vital structures to protect fungal organisms from the environment and regulate the input/output of essential molecules for fungal growth (Feofilova, 2010). Considering a possible role of scopoletin at the fungal cell wall, this compound was tested with the sorbitol and ergosterol bioassays. Sorbitol has an osmoprotective function (Iwaki et al., 2008). A fungal cell lacking or having an impaired cell wall cannot grow, but if sorbitol is present in the medium, by a supplementation way, fungal growth is still possible. Inhibitors of fungal cell wall can be identified when MIC values obtained with sorbitol are higher than those in their absence (Iwaki et al., 2008). Indeed, scopoletin MIC values increased when tested with medium containing sorbitol, thus indicating a potential property of this compound on the fungal cell wall.

Ergosterol is a fungal lipid responsible for important physical features of the plasma membrane, and its absence/injury causes changes in plasma membrane permeability and growth inhibition (Iwaki et al., 2008). If the activity of an agent is due to binding to ergosterol, the presence of exogenous ergosterol would prevent binding to the membrane ergosterol, resulting in an increase in the MIC of the substance (Leite et al., 2014). Indeed, in these conditions, we found increased MIC values for scopoletin, suggesting the ability of this compound to bind to this fungal sterol.

Overexpression of drug efflux pumps is a key strategy of fungal cells for drug resistance (Hans et al., 2019). Resistance of *Candida* species to antifungal agents can be demonstrated by means of efflux pumps, with the CDR1 and CDR2 (*Candida* Drug Resistance) genes related to the expression of ATP-binding Cassette efflux pumps, and the MDR1 gene to efflux pumps of the major facilitators class (Morschhauser et al., 2007). Increased regulation of CDR1 and CDR2 leads to resistance to almost all antifungal agents, whereas increased regulation of MDR1 leads to resistance to fluconazole (Casalinuovo et al., 2004).

Inhibitors of efflux pumps, even at sub-inhibitory concentrations, interfere with important physiological functions of the yeast cells, such as elimination of metabolites and ion transport (Castelo-Branco et al., 2013). This, in turn, could contribute to a non-specific susceptibility to antifungal agents, since these cells are likely to be weakened by the decrease in efflux activity. The susceptibility of *C. tropicalis* to fluconazole was observed by decreasing the MIC value after a synergistic assay with sub-inhibitory concentrations of scopoletin suggesting that scopoletin might be involved in the regulation of efflux activities that are vital to cell homeostasis. Accordingly, scopoletin, as a phenolic substance with a more lipophilic character, might be able to bind directly to ABC-like transporter proteins, hindering their tertiary structure and inhibiting their functions (Ansari et al., 2013).

Lastly, our findings demonstrated that scopoletin has the ability to affect the growth rate of preformed *C. tropicalis* biofilms (**Figure 5**) as well as the formation of these complex structures (**Figure 6**). As expected, fluconazole did not affect biofilm formation since *Candida* biofilms show high resistance to this antifungal (Cavalheiro and Teixeira, 2018). However, we detected that fluconazole had an effect on the growth rate of preformed biofilms comparable to that of scopoletin (**Figure 5**). In fact, this suppressive effect of fluconazole was previously demonstrated by an elegant study using real-time microscopy (Kaneko et al., 2013). By measuring the change of biofilm thickness every hour, the authors demonstrated that fluconazole reduces biofilm growth rate in a way similar to another antifungal (micafungin), but taking more time to manifest such effect (Kaneko et al., 2013).

Candida biofilms are composed of a community of morphologically distinct microorganisms enclosed in an extracellular matrix (Ramage et al., 2005). Here, the extent of *C. tropicalis* biofilms as well as their structural elements were investigated with high-resolution WSI, which offered an optimal view of the overall morphology of fungal biofilms (**Figure 6**). WSI showed *C. tropicalis* biofilms composed of yeast cells and elongated forms (**Figure 6Aii**) as also observed by scanning electron microscopy (Bizerra et al., 2008). Interestingly, these elongated fungal forms, which characterize a major fungal growth form (Ramage et al., 2005) were detected by WSI only in the control group (**Figure 6Aii**, arrows). This means that scopoletin is likely affecting the vegetative fungal growth.

While different aspects of *C. albicans* biofilms have been addressed, much remain to learn about biofilms of non-*albicans* species, which are emerging as important human pathogens. Because fungal biofilms can display intrinsic levels of resistance against most antifungal agents, our results highlight scopoletin with a potential application to prevent *C. tropicalis* biofilm proliferation. However, considering that scopoletin was tested here just on a strain of *C. tropicalis*, a potential antifungal activity of scopoletin against other *Candida* species remains to be addressed in future studies.

CONCLUSION

Our findings showed, for the first time, that scopoletin isolated here from *Mitracarpus frigidus* is a coumarin with antifungal activity against a clinically relevant fungal species, the multidrug-resistant *C. tropicalis* ATCC® 28707 strain. Our data also provided the first insights to understand the events of microbial growth inhibition and death induced by *M. frigidus*-isolated scopoletin, which acts by interfering with the synthesis of essential fungal cell components and is able to disrupt both cell wall and plasma membrane. Moreover, scopoletin affects the growth rate of preformed *C. tropicalis* biofilms as well as its stages of formation and proliferation. Thus, the present data encourages the development of drugs based on plant isolated-scopoletin to treat candidiasis caused by *C. tropicalis.*

DATA AVAILABILITY STATEMENT

All datasets generated for this study are included in the article/**Supplementary Material**.

AUTHOR CONTRIBUTIONS

RF provided the study design and supervision. AL, JF, NP, LC, RG, PP, GT, and TS performed the experiments. RF and TS prepared the final figures. RF, ES, AA, GT, and RM wrote the manuscript. RF, PP, and RM provided critical editing of the manuscript. All authors approved the final version.

FUNDING

This work was supported by grants from Conselho Nacional de Desenvolvimento Científico e Tecnológico (CNPq, Brazil; grant number 309734/2018-5 to RM) and Fundação de Amparo à Pesquisa do Estado de Minas Gerais (FAPEMIG, Brazil; grant number: APQ-01059-14 to RF and CBB-APQ-03647-16 to RM). Scholarships were provided by Federal University of Juiz de Fora (UFJF/Brazil) and Coordenação de Aperfeiçoamento de Pessoal de Nível Superior (CAPES, Brazil). The funders had no role in study design, data collection and analysis, decision to publish, or preparation of the manuscript.

ACKNOWLEDGMENTS

The authors are grateful to Dr. Vinícius Antônio de Oliveira Dittrich from the Department of Botany, Federal University of Juiz de Fora for their botanical identification of the species.

SUPPLEMENTARY MATERIAL

The Supplementary Material for this article can be found online at: https://www.frontiersin.org/articles/10.3389/fmicb.2020.01525/full#supplementary-material

REFERENCES

Amaral, K. B., Silva, T. P., Dias, F. F., Malta, K. K., Rosa, F. M., Costa-Neto, S. F., et al. (2017). Histological assessment of granulomas in natural and experimental Schistosoma mansoni infections using whole slide imaging. *PLoS One* 12:e0184696. doi: 10.1371/journal.pone.0184696

Ana, L., Perez, A. L., Sousa, J. P., Pinheiro, L. S., Oliveira-Filho, A. A., Siqueira-Junior, J. P., et al. (2017). Antifungal activity of citronellal on *Candida albicans* isolates of pediatric clinical importance. *Latin. Am. J. Pharm.* 36, 2042–2047.

Ansari, M. A., Anurag, A., Fatima, Z., and Hameed, S. (2013). Natural phenolic compounds: a potential antifungal agent. *Microbiology* 15, 189–195.

Bhatt Mehul, K., Dholwani Kishor, K., and Saluja Ajay, K. (2011). Isolation and structure elucidation of scopoletin from *Ipomoea reniformis* (*Convolvulaceae*). *J. Appl. Pharm. Sci.* 1, 138–144.

Bizerra, F. C., Nakamura, C. V., De Poersch, C., Estivalet Svidzinski, T. I., Borsato Quesada, R. M., Goldenberg, S., et al. (2008). Characteristics of biofilm formation by Candida tropicalis and antifungal resistance. *FEMS Yeast Res.* 8, 442–450. doi: 10.1111/j.1567-1364.2007.00347.x

Butts, A., Reitler, P., Nishimoto, A. T., DeJarnette, C., Estredge, L. R., Peters, T. L., et al. (2019). A systematic screen reveals a diverse collection of medications that induce antifungal resistance in *Candida* species. *Antimicrob. Agents Chemother.* 63:e00054-19. doi: 10.1128/AAC.00054-19

Campos, L. M., Melo, L., Lemos, A. S. O., Guedes, M. C. M. R., Silva, T. P., Figueiredo, G. F., et al. (2018). *Mitracarpus frigidus*: a promising antifungal in the treatment of vulvovaginal candidiasis. *Ind. Crops Prod.* 12, 731–739. doi: 10.1016/j.indcrop.2018.07.038

Casalinuovo, I. A., Di Francesco, P., and Garaci, E. (2004). Fluconazole resistance in *Candida albicans*: a review of mechanisms. *Eur. Rev. Med. Pharmacol. Sci.* 8, 69–77.

Castelo-Branco, D. S., Brilhante, R. S., Paiva, M. A., Teixeira, C. E., Caetano, E. P., Ribeiro, J. F., et al. (2013). Azole-resistant *Candida albicans* from a wild Brazilian porcupine (*Coendou prehensilis*): a sign of an environmental imbalance? *Med. Mycol.* 51, 555–560. doi: 10.3109/13693786.2012.752878

Cavalheiro, M., and Teixeira, M. C. (2018). Candida biofilms: threats. challenges, and promising strategies. *Front. Med.* 5:28. doi: 10.3389/fmed.2018.00028

Chai, L. Y., Denning, D. W., and Warn, P. (2010). Candida tropicalis in human disease. *Crit. Rev. Microbiol.* 36, 282–298. doi: 10.3109/1040841X.2010.489506

Chander, J., Singla, N., Sidhu, S. K., and Gombar, S. (2013). Epidemiology of Candida blood stream infections: experience of a tertiary care centre in North India. *J. Infec. Dev. Countr.* 7, 670–675. doi: 10.3855/jidc.2623

Cho, J., Choi, H., Lee, J., Kim, M. S., Sohn, H. Y., and Lee, D. G. (2013). The antifungal activity and membrane-disruptive action of dioscin extracted from *Dioscorea nipponica*. *Biochim. Biophys. Acta* 1828, 1153–1158. doi: 10.1016/j.bbamem.2012.12.010

CSLI (2017). *Clinical and Laboratory Standards Institute. Performance Standards for Antimicrobial. Susceptibility Testing*, 27th Edn. Stanford, CA: CSLI.

Darmawan, A., Kosela, S., Kardono, L. B., and Syah, Y. M. (2012). Scopoletin, a coumarin derivative compound isolated from *Macaranga gigantifolia* Merr. *J. Appl. Pharm. Sci.* 2:175.

Fabri, R., Nogueira, M., Braga, F., Coimbra, E., and Scio, E. (2009). *Mitracarpus frigidus* aerial parts exhibited potent antimicrobial, antileishmanial, and antioxidant effects. *Bioresour. Technol.* 100, 428–433. doi: 10.1016/j.biortech.2008.05.053

Feofilova, E. P. (2010). [The fungal cell wall: modern concepts of its composition and biological function]. *Mikrobiologiia* 79, 723–733.

Fernandes, T., Silva, S., and Henriques, M. (2015). Candida tropicalis biofilm's matrix–involvement on its resistance to amphotericin B. *Diagn. Microbiol. Infect. Dis.* 83, 165–169. doi: 10.1016/j.diagmicrobio.2015.06.015

Frost, D. J., Brandt, K. D., Cugier, D., and Goldman, R. (1995). A whole-cell *Candida albicans* assay for the detection of inhibitors towards fungal cell wall synthesis and assembly. *J. Antibiot.* 48, 306–310. doi: 10.7164/antibiotics.48.306

Gamalier, J. P., Silva, T. P., Zarantonello, V., Dias, F. F., and Melo, R. C. N. (2017). Increased production of outer membrane vesicles by cultured freshwater bacteria in response to ultraviolet radiation. *Microbiol. Res.* 194, 38–46. doi: 10.1016/j.micres.2016.08.002

Godoy, P., Tiraboschi, I. N., Severo, L. C., Bustamante, B., Calvo, B., Almeida, L. P., et al. (2003). Species distribution and antifungal susceptibility profile of *Candida* spp. bloodstream isolates from Latin American hospitals. *Mem. Inst. Oswaldo Cruz.* 98, 401–405. doi: 10.1590/s0074-02762003000300020

Goy, P. A., Signer, H., Reist, R., Aichholz, R., Blum, W., Schmidt, E., et al. (1993). Accumulation of scopoletin is associated with the high disease resistance of the hybrid *Nicotiana glutinosa* x *Nicotiana debneyi*. *Planta* 191, 200–206.

Guinea, J. (2014). Global trends in the distribution of Candida species causing candidemia. *Clin. Microbiol. Infect.* 20(Suppl. 6), 5–10. doi: 10.1111/1469-0691.12539

Gupta, P., Gupta, S., Sharma, M., Kumar, N., Pruthi, V., and Poluri, K. M. (2018). Effectiveness of phytoactive molecules on transcriptional expression, biofilm matrix, and cell wall components of *Candida glabrata* and Its clinical isolates. *ACS Omega* 3, 12201–12214. doi: 10.1021/acsomega.8b01856

Hans, S., Fatima, Z., and Hameed, S. (2019). Retrograde signaling disruption influences ABC superfamily transporter, ergosterol and chitin levels along with biofilm formation in Candida albicans. *J. Mycol. Med.* 29, 210–218. doi: 10.1016/j.mycmed.2019.07.003

Ishida, K., Visbal, G., Rodrigues, J. C., Urbina, J. A., de Souza, W., and Rozental, S. (2011). Two squalene synthase inhibitors, E5700 and ER-119884, interfere with cellular proliferation and induce ultrastructural and lipid profile alterations in a *Candida tropicalis* strain resistant to fluconazole, itraconazole, and amphotericin B. *J. Infect. Chemother.* 17, 563–570. doi: 10.1007/s10156-010-0190-1

Iwaki, T., Iefuji, H., Hiraga, Y., Hosomi, A., Morita, T., Giga-Hama, Y., et al. (2008). Multiple functions of ergosterol in the fission yeast Schizosaccharomyces pombe. *Microbiology* 154, 830–841. doi: 10.1099/mic.0.2007/011155-0

Jamuna, S., Karthika, K., Paulsamy, S., Thenmozhi, K., Kathiravan, S., and Venkatesh, R. (2015). Confertin and scopoletin from leaf and root extracts of *Hypochaeris radicata* have anti-inflammatory and antioxidant activities. *Ind. Crops Prod.* 70, 221–230. doi: 10.1016/j.indcrop.2015.03.039

Kaneko, Y., Miyagawa, S., Takeda, O., Hakariya, M., Matsumoto, S., Ohno, H., et al. (2013). Real-time microscopic observation of Candida biofilm development and effects due to micafungin and fluconazole. *Antimicrob. Agents Chemother.* 57, 2226–2230. doi: 10.1128/AAC.02290-12

Kauffman, C. A. (2015). Complications of candidemia in ICU patients: endophthalmitis, osteomyelitis, endocarditis. *Semin. Respir. Crit. Care Med.* 36, 641–649. doi: 10.1055/s-0035-1562891

Khan, M. S., Ahmad, I., and Cameotra, S. S. (2013). Phenyl aldehyde and propanoids exert multiple sites of action towards cell membrane and cell wall targeting ergosterol in *Candida albicans*. *AMB Expr.* 3:54. doi: 10.1186/2191-0855-3-54

Khan, S., Singhal, S., Mathur, T., Upadhyay, D., and Rattan, A. (2006). Antifungal susceptibility testing method for resource constrained laboratories. *Ind. J. Med. Microbiol.* 24:171.

Kostova, I., Bhatia, S., Grigorov, P., Balkansky, S., Parmar, V. S., Prasad, A. K., et al. (2011). Coumarins as antioxidants. *Curr. Med. Chem.* 18, 3929–3951. doi: 10.2174/092986711803414395

Leema, G., and Tamizhselvi, R. (2018). Protective effect of scopoletin against cerulein-induced acute pancreatitis and associated lung injury in mice. *Pancreas* 47:1. doi: 10.1097/MPA.0000000000001034

Leite, M. C., Bezerra, A. P., de Sousa, J. P., Guerra, F. Q., and Lima Ede, O. (2014). Evaluation of antifungal activity and mechanism of action of citral against *Candida albicans*. *Evid. Based Complement Alternat. Med.* 2014:378280. doi: 10.1155/2014/378280

Lu, M., Li, T., Wan, J., Li, X., Yuan, L., and Sun, S. (2017). Antifungal effects of phytocompounds on *Candida* species alone and in combination with fluconazole. *Int. J. Antimicrob. Agents* 49, 125–136. doi: 10.1016/j.ijantimicag.2016.10.021

McCarthy, M. W., and Walsh, T. J. (2017). Drugs currently under investigation for the treatment of invasive candidiasis. *Expert Opin. Investig. Drugs* 26, 825–831. doi: 10.1080/13543784.2017.1341488

Morschhauser, J., Barker, K. S., Liu, T. T., Bla, B. W. J., Homayouni, R., and Rogers, P. D. (2007). The transcription factor Mrr1p controls expression of the MDR1 efflux pump and mediates multidrug resistance in *Candida albicans*. *PLoS Pathog.* 3:e164. doi: 10.1371/journal.ppat.0030164

Navarro-Garcia, V. M., Rojas, G., Aviles, M., Fuentes, M., and Zepeda, G. (2011). In vitro antifungal activity of coumarin extracted from *Loeselia mexicana* Brand. *Mycoses* 54, e569–e571. doi: 10.1111/j.1439-0507.2010.01993.x

Pereira, Z. V., Carvalho-Okano, R. D., and Garcia, F. C. P. (2006). Rubiaceae Juss. da Reserva Florestal Mata do Paraíso, Viçosa, MG, Brasil. *Acta Bot. Bras.* 20, 207–224. doi: 10.1590/s0102-33062006000100020

Perlin, D., Shor, E., and Zhao, Y. (2015). Update on antifungal drug resistance. *Curr. Clin. Microbiol. Rep.* 2, 84–95. doi: 10.1007/s40588-015-0015-1

Pinto, D., and Silva, A. M. S. (2017). Anticancer natural coumarins as lead compounds for the discovery of new drugs. *Curr. Top. Med. Chem.* 17, 3190–3198. doi: 10.2174/1568026618666171215095750

Prats, E., Bazzalo, M., León, A., and Jorrín, J. (2006). Fungitoxic effect of scopolin and related coumarins on *Sclerotinia sclerotiorum*. A way to overcome sunflower head rot. *Euphytica* 147, 451–460. doi: 10.1007/s10681-005-9045-8

Ramage, G., Saville, S. P., Thomas, D. P., and Lopez-Ribot, J. L. (2005). Candida biofilms: an update. *Eukaryot. Cell* 4, 633–638. doi: 10.1128/EC.4.4.633-638.2005

Ramírez-Pelayo, C., Martínez-Quiñones, J., Gil, J., and Durango, D. (2019). Coumarins from the peel of citrus grown in Colombia: composition, elicitation and antifungal activity. *Heliyon* 5:e01937. doi: 10.1016/j.heliyon.2019.e01937

Rex, J. H. (2008). *Reference Method for Broth Dilution Antifungal Susceptibility Testing of Filamentous Fungi: Approved Standard*. Stanford, CA: Clinical and Laboratory Standards Institute.

Silva, S., Negri, M., Henriques, M., Oliveira, R., Williams, D. W., and Azeredo, J. (2012). *Candida glabrata*, *Candida parapsilosis* and *Candida tropicalis*: biology, epidemiology, pathogenicity and antifungal resistance. *FEMS Microbiol. Rev.* 36, 288–305. doi: 10.1111/j.1574-6976.2011.00278.x

Silva, T. P., Noyma, N. P., Duque, T. L., Gamalier, J. P., Vidal, L. O., Lobao, L. M., et al. (2014). Visualizing aquatic bacteria by light and transmission electron microscopy. *Antonie Van Leeuwenhoek* 105, 1–14. doi: 10.1007/s10482-013-0047-6

Sun, H., Wang, L., Zhang, B., Ma, J., Hettenhausen, C., Cao, G., et al. (2014). Scopoletin is a phytoalexin against *Alternaria alternata* in wild tobacco dependent on jasmonate signalling. *J. Exp. Bot.* 65, 4305–4315. doi: 10.1093/jxb/eru203

Tomasz Kubrak, T., Rafał Podgórski, R., and Monika Sompor, M. (2017). Natural and synthetic coumarins and their pharmacological activity. *Eur. J. Clin. Exp. Med.* 15, 169–175.

Valle, T., López, J. L., Hernández, J. M., and Corchete, P. (1997). Antifungal activity of scopoletin and its differential accumulation in *Ulmus pumila* and *Ulmus campestris* cell suspension cultures infected with *Ophiostoma ulmi* spores. *Plant Sci.* 125, 97–101. doi: 10.1016/s0168-9452(97)00057-5

Woods, R., Bard, M., Jackson, I., and Drutz, D. (1974). Resistance to polyene antibiotics and correlated sterol changes in two isolates of *Candida tropicalis* from a patient with an amphotericin B-resistant funguria. *J. Inf. Dis.* 129, 53–58. doi: 10.1093/infdis/129.1.53

Zhang, X., Xu, M., Zhang, J., Wu, L., Liu, J., and Si, J. (2017). Identification and evaluation of antioxidant components in the flowers of five *Chimonanthus* species. *Ind. Crops Prod.* 102, 164–172. doi: 10.1016/j.indcrop.2017.03.014

Conflict of Interest: The authors declare that the research was conducted in the absence of any commercial or financial relationships that could be construed as a potential conflict of interest.

frontiers in Microbiology

ORIGINAL RESEARCH
published: 15 July 2020
doi: 10.3389/fmicb.2020.01605

Streptococcus mutans Secreted Products Inhibit *Candida albicans* Induced Oral Candidiasis

*Jéssica Diane dos Santos[1†], Luciana Ruano de Oliveira Fugisaki[1†], Rebeca Previate Medina[2], Liliana Scorzoni[1], Mariana de Sá Alves[1], Patrícia Pimentel de Barros[1], Felipe Camargo Ribeiro[1], Beth Burgwyn Fuchs[3], Eleftherios Mylonakis[3], Dulce Helena Siqueira Silva[2] and Juliana Campos Junqueira[1]**

[1] Department of Biosciences and Oral Diagnosis, Institute of Science and Technology, São Paulo State University (UNESP), São José dos Campos, Brazil, [2] Department of Organic Chemistry, Institute of Chemistry, São Paulo State University (UNESP), Araraquara, Brazil, [3] Division of Infectious Diseases, Rhode Island Hospital, Warren Alpert Medical School of Brown University, Providence, RI, United States

In the oral cavity, *Candida* species form mixed biofilms with *Streptococcus mutans,* a pathogenic bacterium that can secrete *quorum sensing* molecules with antifungal activity. In this study, we extracted and fractioned culture filtrate of *S. mutans*, seeking antifungal agents capable of inhibiting the biofilms, filamentation, and candidiasis by *Candida albicans*. Active *S. mutans* UA159 supernatant filtrate components were extracted via liquid-liquid partition and fractionated on a C-18 silica column to resolve *S. mutans* fraction 1 (SM-F1) and fraction 2 (SM-F2). We found anti-biofilm activity for both SM-F1 and SM-F2 in a dose dependent manner and fungal growth was reduced by 2.59 and 5.98 log for SM-F1 and SM-F2, respectively. The SM-F1 and SM-F2 fractions were also capable of reducing *C. albicans* filamentation, however statistically significant differences were only observed for the SM-F2 ($p = 0.004$). SM-F2 efficacy to inhibit *C. albicans* was confirmed by its capacity to downregulate filamentation genes *CPH1*, *EFG1*, *HWP1*, and *UME6*. Using *Galleria mellonella* as an invertebrate infection model, therapeutic treatment with SM-F2 prolonged larvae survival. Examination of the antifungal capacity was extended to a murine model of oral candidiasis that exhibited a reduction in *C. albicans* colonization (CFU/mL) in the oral cavity when treated with SM-F1 (2.46 log) and SM-F2 (2.34 log) compared to the control (3.25 log). Although both SM-F1 and SM-F2 fractions decreased candidiasis in mice, only SM-F2 exhibited significant quantitative differences compared to the non-treated group for macroscopic lesions, hyphae invasion, tissue lesions, and inflammatory infiltrate. Taken together, these results indicate that the SM-F2 fraction contains antifungal components, providing a promising resource in the discovery of new inhibitors for oral candidiasis.

Keywords: *Streptococcus mutans*, *Candida albicans*, biofilm, filamentation, oral candidiasis

OPEN ACCESS

Edited by:
Giovanna Batoni, University of Pisa, Italy

Reviewed by:
Megan L. Falsetta, University of Rochester, United States
Célia F. Rodrigues, University of Porto, Portugal

***Correspondence:**
Juliana Campos Junqueira
juliana.junqueira@unesp.br

† These authors have contributed equally to this work

Specialty section:
This article was submitted to Infectious Diseases, a section of the journal Frontiers in Microbiology

Received: *04 May 2020*
Accepted: *19 June 2020*
Published: *15 July 2020*

Citation:
Santos JD, Fugisaki LRO, Medina RP, Scorzoni L, Alves MS, de Barros PP, Ribeiro FC, Fuchs BB, Mylonakis E, Silva DHS and Junqueira JC (2020) Streptococcus mutans Secreted Products Inhibit Candida albicans Induced Oral Candidiasis. Front. Microbiol. 11:1605. doi: 10.3389/fmicb.2020.01605

INTRODUCTION

Oral candidiasis is the most common opportunistic fungal infection of the oral cavity and represents a significant clinical problem, especially in elderly denture wearers, HIV-infected individuals, and patients undergoing antineoplastic therapy (Coronado-Castellote and Jimenez-Soriano, 2013; Garcia-Cuesta et al., 2014; Seneviratne and Rosa, 2016; Zhang et al., 2016;

Venkatasalu et al., 2020). The manifestations of oral candidiasis can occur in the lips, skin, and mucosa and have different clinical and histopathological variants (Coronado-Castellote and Jimenez-Soriano, 2013; Costa et al., 2013b; Zhang et al., 2016). Among them, the most common lesions are pseudomembranous candidiasis, characterized by white patches on the oral mucosa surface, and erythematous candidiasis, formed by localized erythema mainly on the tongue and the palate (Costa et al., 2013b). Due to damage to the mucosal surface, patients often complain of dysgeusia and burning sensation that can result in significant patient morbidity through dysphagia, dehydration, and malnutrition (Berberi et al., 2015; Salvatori et al., 2016; Zhang et al., 2016).

The pathogenesis of *Candida* species is associated with various virulence factors, including biofilm formation, morphological transition between yeast and hyphae, and secretion of hydrolytic enzymes (Costa et al., 2013b; Shu et al., 2016). Among them, biofilm formation has gained considerable attention in the last years for the ability to augment *Candida albicans* resistance to antifungal drugs (Costa et al., 2013a; Matsubara et al., 2016). *Candida* biofilm formation initiates through adherence of yeast to host cells or abiotic surfaces of dental prostheses and other medical devices. Once attached, yeasts form colonies, produce germ tubes and hyphae, and secret polysaccharides that contribute to the three-dimensional structure of the biofilm (Costa et al., 2013b). Therefore, the pathogenicity of *C. albicans* involves a significant co-regulation between adherence, biofilm formation, and hyphal development (Breger et al., 2007).

Oral candidiasis is generally managed with the use of azoles antifungal, such as nystatin, fluconazole, ketoconazole, and miconazole (Berberi et al., 2015; Moges et al., 2016; Patton, 2016). However, the combination of frequent recurrences and repeated treatment with antifungal agents leads drug resistant *Candida* strains (Vazquez, 2010; Liu et al., 2015), precipitating the necessity of new therapeutic approaches. One of the possible therapeutic alternatives includes the identification of new antifungal agents from natural substances produced by the human microbiome (Vilela et al., 2015; Barbosa et al., 2016; Rossoni et al., 2018). It is known that bacteria-fungi interactions are common in humans and can influence the transition between health and disease in specific environments within the host (Peleg et al., 2010; Barbosa et al., 2016).

In the oral cavity, *C. albicans* can form mixed biofilms with *Streptococcus mutans*, an important oral bacterium present in the majority of the world population (Becker et al., 2002; Mitchell, 2003). One of the main virulence factors of this bacterium is the ability to form biofilm on enamel surface leading to the development of dental caries in the presence of sucrose (Zhang et al., 2009). In mixed biofilms, *C. albicans* and *S. mutans* can influence each other through cell-cell interactions and via secretion of extracellular signaling molecules (*quorum sensing*) (Pereira-Cenci et al., 2008; Barbosa et al., 2016). The physical interactions between *C. albicans* and *S. mutans* in the presence of sucrose have been associated with a mutualism relationship in which the adherence of both species on dental surfaces are stimulated and can increase the severity of dental caries (Falsetta et al., 2014). However, recent studies reported that the secretion of *quorum sensing* molecules by *S. mutans* can inhibit the filamentation and virulence of *C. albicans* (Pereira-Cenci et al., 2008; Joyner et al., 2010; Barbosa et al., 2016). Genetic studies with different *S. mutans* isolates have shown an enormous diversity of genes related to interspecies communication (Bekal-Si Ali et al., 2002; Klein et al., 2006) and production of a antimicrobial peptide called mutacin (Kamiya et al., 2008).

In our previous study, we evaluated the effects of *S. mutans* (UA159) culture filtrate on *C. albicans* and found it exerted inhibitory activity on biofilm formation, morphogenesis, and pathogenicity of *C. albicans* (Barbosa et al., 2016). The present study extracts, fractionates, and identifies *S. mutans* UA159 culture filtrate specific fraction that inhibits *C. albicans*. *In vitro* and *in vivo* assays are undertaken to understand the mechanisms of action to inhibit biofilm, filamentation, and candidiasis development. For the first time, the effects of *S. mutans* extracts were evaluated on murine oral candidiasis to treat this common oral infection.

MATERIALS AND METHODS

Microorganisms and Culture Conditions

The described assays used *C. albicans* ATCC 18804 and *S. mutans* UA 159 strains from the Oral Microbiology and Immunology Laboratory of the Institute of Science and Technology of São José dos Campos/UNESP. *C. albicans* was grown in agar Sabouraud Dextrose (Himedia Laboratories, Mumbai, India) for 24 h at 37°C and *S. mutans* was cultivated in BHI agar (Himedia, Mumbai, India) for 24 h at 37°C with 5% CO_2.

Preparation of *S. mutans* Culture Filtrate

Streptococcus mutans was cultured in BHI broth for 24 h at 37°C with 5% CO_2. After overnight growth, 1 mL of a standardized suspension containing 10^7 cells/mL was inoculated into 6 mL of BHI broth and incubated for 4 h at 37°C (5% CO_2) (Barbosa et al., 2016). The culture was centrifuged at 5000 rpm for 10 min and the supernatant was filtered with a 0.22 μm diameter pore membrane using a vacuum filtration system (Stericup® and Steritop® Filter Unit, Millipore, MA, United States).

Preparation of Crude Extract and Fractions From *S. mutans* Culture Filtrate

The preparations of crude extract and fractions were performed according to National Committee for Clinical Laboratory Standards (2002), Medina et al. (2019) with some modifications. The *S. mutans* culture filtrate was extracted with ethyl acetate (3 × 50% of the supernatant volume) and then the organic solvent was removed under vacuum in a rotary evaporator (Buchi R-114). The obtained crude extract was lyophilized and weighed. Thereafter, the crude extract was fractionated on a C-18 derivatized silica column (150 g, Φ = 3.5 cm) using different MeOH:H_2O solutions (36:64, 49:51, 60:40, 76:24, 100:00) from which the eluent yielded 5 fractions (360 mL each; SM-F1 to SM-F5). The mass efficiency obtained from SM-CE (1,474 g) for

each fraction was: SM-F1 969.3 mg, SM-F2 210.0 mg, SM-F3 22.7 mg, SM-F4 6.0 mg and SM-F5 397.2 mg. Due to the low mass obtained, the fractions SM-F3 and SM-F4 were not included in this study. The fraction SM-F5 was not active on preliminary *in vitro* experiments (data not shown). Therefore, only fractions SM-F1 and SM-F2 were included in this study.

Minimal Inhibitory Concentration

The antifungal activity was determined by broth microdilution method in accordance with the Clinical and Laboratory Standards Institute (CLSI) document M27-A2 (National Committee for Clinical Laboratory Standards, 2002). For this, *C. albicans* was grown in YPD broth (Himedia, Mumbai, India) and incubated at 30°C for 16 h. The SM-F1 and SM-F2 fractions were diluted in RPMI 1640 medium (Merck, Darmstadt, German) and concentrations from 1 to 15 mg/mL were tested. A suspension of *C. albicans* at 1×10^3 cells/mL was added to each well of 96-well microtiter plates (Kasvi, São José dos Pinhais, Brazil) and incubated at 35°C for 48 h. The results were analyzed after 48 h at 595 nm. The minimal inhibitory concentration (MIC) was considered as the concentration in which no turbidly (growth) was observed.

Biofilm Formation Assay

The biofilm formation assay was based on the methodologies described by Thein et al. (2006) and Barbosa et al. (2016). For this, 100 μL of 10^7 cells/mL suspension prepared in Yeast Nitrogen Base broth (YNB, Difco, Detroit, MI, United States) supplemented with 100 mM glucose were added in a 96 well plate and incubated at 37°C at 75 rpm for 90 min. Next, the wells were washed with buffered phosphate saline (PBS, 0.1 M, pH 7.2) two times aiming to remove non-adherent cells. To promote the biofilm formation, YNB supplemented with 100 mM glucose was added and the plates were incubated at 37°C at 75 rpm for 24 h. Then, the media was replaced and fractions SM-F1 and SM-F2 were added. The plates were incubated for 24 h.

After the incubation period, the wells were washed with PBS. A volume of 250 μL of PBS was added to each well and the biofilms were disrupted using an ultrasonic homogenizer (Sonics Vibra Cell) for 30 s at 50 W power setting. Serial dilutions were prepared and 10 μL aliquots of the dilutions were plated on Sabouraud Dextrose agar (Himedia, Mumbai, India). The plates were incubated at 37°C for 48 h and the number of CFU/mL was counted. Two experiments replicates were performed, using five biofilms per group.

C. albicans Filamentation Assay

Candida albicans was grown at 37°C for 24 h in YNB supplemented with 100 mM glucose. In a 24 well plate, 100 μL of 10^7 cells/mL of *C. albicans* were inoculated in 1 mL of sterile distilled water supplemented with 10% fetal bovine serum (Sigma-Aldrich, São Paulo, Brazil) and the fractions SM-F1, SM-F2, or PBS (control group) were added to each well. After incubation at 37°C for 24 h, the pH value was measured and a 50 μL volume was transferred to glass slides, previously demarcated with 10 fields on the back. The slides were then observed under a light microscope (Carl Zeiss, Primo Star, Germany) at 400× magnification (Barbosa et al., 2016). To quantify the hyphae formation, 10 fields were analyzed in each slide, totaling 100 fields for each sample. A score was assigned according to the number of hyphae presence: 0, absence of hyphae; 1, from 1 to 10; 2, from 11 to 20; 3 from 21 to 30; 4, from 31 to 40; 5, more than 40. Three (SM-F1) and five (SM-F2) assays were used per group and the experiment was performed as independent duplicates. Next, the study of *C. albicans* filamentation was complemented with analysis of scanning electron microscopy and gene expression.

Analysis of Filamentation by Scanning Electron Microscopy (SEM)

Acrylic resin disks measuring 5 mm in diameter and 3 mm in thickness were deposited at the bottom of each well in the 24 well plates for filamentation induction. After 24 h of incubation, the disks were removed from the wells and washed with 1 mL of 2.5% glutaraldehyde (Sigma-Aldrich, São Paulo, Brazil) for 1 h at 37°C. The disks were removed from glutaraldehyde and dehydrated with increasing ethanol washes (10, 25, 50, 75, and 90%) for 20 min each, followed by immersion in absolute alcohol for 1 h. They were then transferred to aluminum stubs and analyzed using an Inspect S50 scanning electron microscope (FEI, Czechia). The assay was performed in duplicate with three resin disks per group.

Analysis of Gene Expression Related to Filamentation of *C. albicans*

Five genes associated with *C. albicans* filamentation were evaluated: *CPH1*, *EFG1*, *HWP1*, *UME6,* and *YWP1*. This experiment was performed in 24 well plates using the same conditions and fraction treatments described in section "*C. albicans* Filamentation Assay." After the incubation period, *C. albicans* was collected by centrifugation at 4700 rpm for 5 min and RNA extraction was performed using TRIzol, following the manufacturer's suggested protocol (Ambion, Inc., Carlsbad, CA, United States).

The concentration and purity of the RNA was determined using a NanoDrop 2000 spectrophotometer (Thermo Fisher Scientific Inc., Wilmington, DE, United States) by measuring the absorbance at optical densities (OD): 230, 260, and 280 nm. The OD260/OD280 ranged from 1.80 to 2.00 and OD260/OD230 ranged from 2.00 to 2.10. The integrity of the RNA was further checked in a selected subset of samples by electrophoresis through 1% non-denaturing agarose gels.

The extracted total RNA (720 ng) was treated with DNase I (Turbo DNase Treatment and Removal Reagents - Ambion Inc., Carlsbad, CA, United States) and transcribed into complementary DNA (cDNA) using the SuperScript III First-Strand Synthesis SuperMix for qRT-PCR Kit (Invitrogen, Carlsbad, CA, United States), according to the protocols recommended by the manufacturer. All investigated samples were transcribed with the same reverse transcription reaction conditions. Negative controls, which were run simultaneously and used in all experiments, did not contain either RNA (no template control) or no reverse transcriptase (RT negative

control), that could indicated RNA and genomic DNA contamination, respectively. Primers for the genes analyzed are listed in **Table 1**.

For real-time quantitative PCR (qPCR) reactions, the Platinum SYBR Green qPCR SuperMix-UDG Kit (Invitrogen, Carlsbad, CA, United States) was used as recommended by the manufacturer. The reactions were performed in triplicate in the StepOnePlus Real-Time PCR System (Applied Biosystems, Foster, CA, United States), consisting of 12.5 μL SuperMix Platinum SYBR Green, 1 μL ROX, 0.3 μM each for specific forward and reverse primers (final concentration), and target cDNA, supplemented with RNAse-free ddH_2O to a final volume of 25 μL. Cycling parameters for amplification reactions were 50°C for 2 min; 95°C for 2 min; followed by 40 cycles of 95°C for 15 s and 60°C for 30 s, with dissociation (a melting curve) during the last cycle of 95°C for 15 s, 60°C for 30 s, 95°C for 15 s. All samples showed only a single peak, indicating a single pure product and no primer/dimer formation. Real-time PCR efficiencies were acquired by amplification of standardized serial dilutions of the template cDNA and were determined for each gene as the slope of a linear regression model (**Supplementary Figure S1**). The $2^{-\Delta\Delta CT}$ method was used to analyze the relative changes in gene expression from the quantitative RT-PCR experiment (Livak and Schmittgen, 2001).

The transcribed cDNAs were amplified for relative quantification of the expression of the *CPH1*, *EFG1*, *HWP1*, *UME6,* and *YWP1* genes in relation to the concentration of the reference gene *PMA1*. In this study, three reference genes, *ACT1*, *PMA1*, and *RPP2B*, were tested in all experimental groups. The obtained results were analyzed and the selected reference gene was *PMA1* (**Supplementary Figure S2**).

In vivo Study in *G. mellonella* Model

Galleria mellonella larvae were used in the final larval stage weighting from 250 to 300 mg according to methodologies previously established by our group (Barbosa et al., 2016; Rossoni et al., 2017). Initially, the *S. mutans* extract in various concentrations was injected in healthy larvae to evaluate its toxicity. To study *S. mutans* fractions effects on candidiasis, larvae were infected with 10^8 cells/mL *C. albicans* containing, and after 30 min, treated with an injection of the SM-F1 or SM-F2 fractions. Untouched larvae and PBS injected larvae were used as control groups. After injections, the larvae were stored in petri dishes at 37°C. *G. mellonella* survival were monitored daily for 7 days. Larvae were considered dead when they failed to react to touch. The death of all larvae in the experimental group or the transition to pupa determined the end of the experiment. Sixteen larvae were used in each group.

In vivo Murine Oral Candidiasis Model

Adult male *Swiss* mice, weighing approximately 30 g, from the Central Animal Care Facility of UNESP (Botucatu, SP, Brazil) were used in the study with approval from the Ethics Committee on the Use of Animals of the ICT/UNESP under protocol 005/2016-CEUA- ICT-UNESP. A total of 17 mice were used, divided into the following groups: mice not infected by *C. albicans* and not treated ($n = 2$), mice infected by *C. albicans* and not treated ($n = 5$), mice infected by *C. albicans* and treated with SM-F1 ($n = 5$), and mice infected by *C. albicans* and treated with SM-F2 ($n = 5$).

Oral candidiasis was induced as previously described (Takakura et al., 2003). Animals were immunosuppressed with two intraperitoneal injections of 100 mg/kg prednisolone (Depo-Medrol, Laboratórios Pfizer Ltda., Guarulhos, Brazil) on days alternating with *Candida* inoculations. Tetracycline hydrochloride (Terramycin, Pfizer) was administered at a concentration of 0.83 mg/mL in the drinking water during the experiment period. For *C. albicans* infection, animals were sedated intraperitoneally by injections of ketamine (100 mg/kg) and xylazine (10 mg/kg) and inoculated with a *C. albicans* suspension (10^9 cells/mL) using a sterile swab. After 24 h of the second infection, 200 μL of the SM-F1 or SM-F2 at the concentration of 1 g/Kg were delivered into the oral cavity using a pipette.

Recovery of *C. albicans* From the Oral Cavity After Treatments

After 48 h of treatment, samples were collected from the tongue dorsum with a swab, placed in a tube containing 0.9 mL of PBS, and shaken for 1 min. Considering that the swab absorbed approximately 0.1 mL of saliva from the oral cavity of mice, this solution was estimated to be a 10^{-1} starting dilution of *Candida* from the soaked swab. Serial dilutions were performed and seeded on Sabouraud dextrose agar (Difco, Detroit, United States) supplemented with 0.1 mg/mL of chloramphenicol (Vixmicina, São Paulo, Brazil). The plates were incubated at 37°C for 48 h to determine the number of CFU/mL. Immediately after sample collections, mice were euthanized by administering an overdose of anesthetic and the tongues were removed for macroscopic and microscopic analysis.

Macroscopic Analysis of Oral Candidiasis

Characteristics lesions of candidiasis on the dorsum tongue were analyzed and quantified using a stereomicroscope (Zeiss, Göttingen, Germany). Scores of 0–4 were assigned according to the extension of lesions: 0, absence of lesions (normal aspect of tongue); (1) white plaques in less than 20%; (2) white plaques ranging from 21 to 90%; (3) white plaques in more than 91%; (4) thick white plaque as pseudomembranes in more than 91% (Takakura et al., 2003; Rossoni et al., 2015).

Microscopic Analysis of Oral Candidiasis

For the microscopic analysis, the tongues were fixed in 10% formalin for 24 h and sectioned in two parts in the sagittal direction. After being imbedded in paraffin, serial 5 μm thick sections were obtained, and then Hematoxylin-Eosin (HE) and Schiff's Periodic Acid (PAS) stained (Rossoni et al., 2015). The presence of candidiasis was investigated on the entire surface of the dorsum tongue and the description of the histological sections was carried out according to the presence of yeasts and hyphae, extent of lesions and changes in the tissues involved.

TABLE 1 | Quantitative real-time PCR primers.

Target gene	Oligonucleotide sequence 5′-3′*	Description	Amplicon size (bp)**	References
ACT1	**F**- GAAGCCCAATCCAAAAGA **R**- CTTCTGGAGCAACTCTCAATTC	Structural constituent of cytoskeleton (Normalizing internal standard)	130 bp	Nailis et al., 2006
RPP2B	**F**-TGCTTACTTATTGTTAGTTCAAGGTGGGTA **R**- CAACACCAACGGATTCCAATAAA	Structural constituent of ribosome (Normalizing internal standard)	83 bp	Nailis et al., 2006
PMA1	**F**- TTGCTTATGATAATGCTCCATACGA **R**- TACCCCACAATCTTGGCAAGT	Plasma Membrane H (+) ATPase (Normalizing internal standard)	66 bp	Nailis et al., 2006
CPH1	**F**- ACGCAGCCACAAGCTCTACT **R**- GTTGTGTGTGGAGGTTGCAC	*Candida* pseudohyphal regulator (transcription factor activity)	119 bp	Sherry et al., 2014
EFG1	**F**- CAGTATGGTCAGTATAATGCT **R**- TGTTGTTGCTGTTGGTATGGATATGATGATG	Enhanced filamentous growth (transcription factor activity)	222 bp	Hnisz et al., 2012
HWP1	**F**- GAAACCTCACCAATTGCTCCAG **R**- GTAGAGACGACAGCACTAGATTCC	Hyphal wall protein (cell adhesion molecule binding)	92 bp	Hnisz et al., 2012
UME6	**F**- TCATTCAATCCTACTCGTCCACC **R**- CCAGATCCAGTAGCAGTGCTG	Zn(II)2Cys6 transcription factor (transcription factor activity)	133 bp	Hnisz et al., 2012
YWP1	**F**- ACACCGGAAAATACCGTTGC **R**- ATGGCAGCTTTACCAGAACC	Yeast-form wall protein (adhesion of symbiont to host)	116 bp	Granger, 2012

**F- Forward and R- Reverse; ** bp- base pairs.*

The presence of yeasts and hyphae was quantified according to the methodology described by Junqueira et al. (2005), attributing the following scores to the histological fields: 0, absence of yeasts/hyphae; 1, 1 to 5 yeasts/hyphae; 2, 6 to 15 yeasts/hyphae; 3, 16 to 50 yeasts/hyphae; 4, more than 50 yeasts/hyphae. The intensity of tissue lesions and inflammatory response in connective tissue was made according to Martins Jda et al. (2011). The tissue lesions were evaluated by the presence of epithelial hyperplasia, disorganization of the basal layer, exocytosis, spongiosis, loss filiform papillae, hyperkeratosis, desquamation, acantholysis, loss of stratification and formation of intraepithelial micro abscesses. For the chronic inflammatory infiltrate, the following scores were assigned: 0 (absence of inflammatory cells), 1 (mild inflammatory infiltrate), 2 (moderate inflammatory infiltrate) and 3 (severe inflammatory infiltrate).

Analysis of *S. mutans* Supernatant Fractions by Gas Chromatography

The fractions SM-F1 and SM-F2 were analyzed by gas chromatography coupled to mass spectrometry (GC-MS, Shimadzu, model GC-MS-QP2020, with auto-injector AOC-20i), using a Supelco RTX-5MS column (5% phenyl polymethylsiloxane; 30 m × 0.25 mm × 0.25 μm) (Pellati and Benvenuti, 2007). Chromatographic conditions were: injector temperature −260°C, injection mode - split; detector temperature −260°C; carrier gas flow (He) −1.0 mL min^{-1}; using the following temperature program −80°C with a 3 min hold, ramped to 260°C at 3°C/min and held for 10 min. The mass spectrometer used in the CG-MS analyzes is equipped with an electronic impact ionization (EI) source, set to 70 eV and a mass range of 35–700 *m/z* acquisition. To ensure greater thermal stability and greater volatility of the constituents, as well as better chromatographic resolution (Pellati and Benvenuti, 2007), a derivation step (silylation) was performed during sample preparation. Thus, 5 mg of SM-F1 and SM-F2 fraction were solubilized in 200 μL of pyridine, then 200 μL of N-methyl-N- (trimethylsilyl) - trifluoroacetamide (MSTFA - Sigma) were added.

To compare the GC-MS results obtained from SM-F1 and SM-F2, BHI broth was prepared and extracted with ethyl acetate (3 × 50% of its volume). After the removal of the organic solvent using a rotary evaporator, the obtained material (BHI control) was prepared, including a silylation step as conducted for fractions SM-F1 and SM-F2, to be analyzed by GC-MS in the same conditions described above. The identification of the compounds was carried by the comparison of mass spectra, obtained for each peak during analyses, with data available in Wiley7 and NIST libraries using GCMSsolutions Version 2.5 software. Only compounds that presented similarity higher than 85% were described.

Statistical Analysis

GraphPad Prism 8.4.2 statistical software (San Diego, United States) was used in all tests with a $p \leq 0.05$ considered significant. The results of biofilms (CFU/mL) and gene expression were evaluated by the Student's *t*-test. Kruskal-Wallis and Dunn tests were used to compare the scores obtained in the *in vitro* filamentation assay, macroscopic and microscopic analysis in mice. The number of *C. albicans* CFU/mL recovered from the oral cavity of mice were submitted to ANOVA and Tukey test. For the survival experiments in *G. mellonella*, the survival curve was generated using the Kaplan-Meier method and the level of significance calculated by the Log-rank test (Mantel-Cox).

RESULTS

Antifungal and Anti-biofilm Activities of SM-F1 and SM-F2

Initially, the antifungal activity of SM-F1 and SM-F2 fractions were tested on planktonic growth of *C. albicans*. SM-F2 fraction was active against *C. albicans* with MIC of 15 mg/mL. However,

no antifungal activity on planktonic cells was observed for the SM-F1 fraction. After that, the fractions were tested against *C. albicans* biofilms, using concentrations of 5, 10, and 15 mg/mL for both SM-F1 and SM-F2. We observed reductions in the CFU/mL number of *C. albicans* for the biofilms treated with SM-F1 and SM-F2 in all tested concentrations when compared to the non-treated control group. The biofilms treated with SM-F1 at 5, 10 and 15 mg/mL showed reductions of 1.85, 2.02, and 2.59 logs, respectively. A more substantial reduction was found when biofilms were treated with SM-F2, reaching 2.8 for 5 mg/mL SM-F2, 2.95 for 10 mg/mL SM-F2 and 5.98 logs with 15 mg/mL SM-F2. In the group treated with 15 mg/mL SM-F2 ($n = 5$), three biofilms showed a total inhibition of *C. albicans* cells (**Figure 1**). Therefore, SM-F1 and SM-F2 exhibited anti-biofilm activity against *C. albicans* in a dose dependent manner, with SM-F2 being the most effective inhibitory fraction. Further, SM-F2 had conserved activity against planktonic cell forms.

Activity of SM-F1 and SM-F2 on *Candida* Filamentation

In the microscopic analysis of filamentation, the group treated with SM-F1 faction at 5 mg/mL exhibited numerous hyphae spread along the microscopic fields similar to the profile observed in the non-treated control group (**Supplementary Figure S3**). The SM-F1 fraction of 10 and 15 mg/mL led to a discrete reduction in the quantity of hyphae formation without statistically significant difference in relation to the control group.

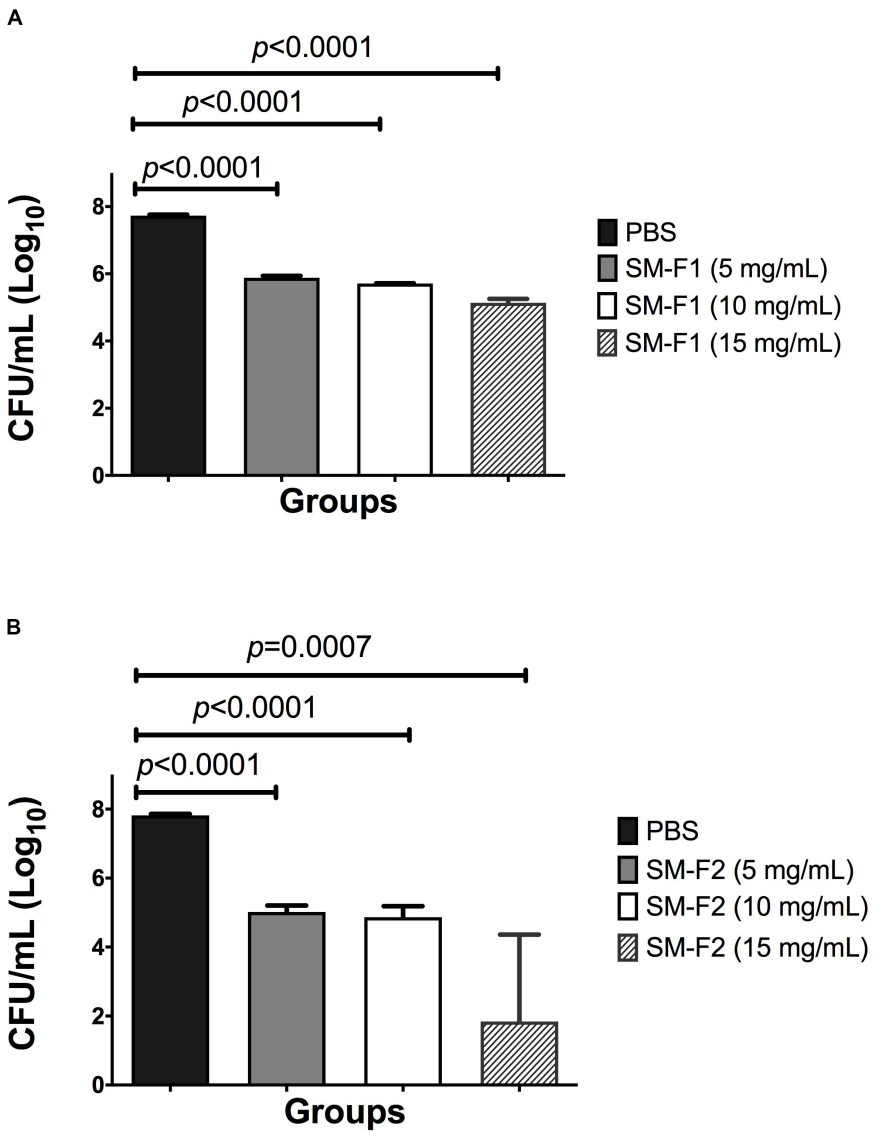

FIGURE 1 | Analysis of *in vitro Candida* biofilms. Mean and SD of CFU/mL (Log_{10}) of *C. albicans* viable cells obtained for the non-treated control group (PBS) and the experimental groups treated with the SM-F1 **(A)** or SM-F2 **(B)** fractions at 5, 10, and 15 mg/mL. Student's *t*-test was used to compare the control group with the experimental groups.

However, when *C. albicans* was cultured with the SM-F2 fraction, a hyphae reduction was found for all tested concentrations (5, 10, and 15 mg/mL). Statistically significant differences in relation to the control group were observed only for the groups treated with 10 mg/mL SM-F2 (**Figure 2**).

Since it is known that the acidic pH may have influence on the *C. albicans* filamentation, the pH value of medium was measured before the microscopic analysis. For all groups, we found pH values from 6.8 to 7.0, indicating that the pH of the medium did not interfere with the hyphae inhibition caused by the treatment with *S. mutans* fractions (**Supplementary Figure S4**).

The results of light microscopy analysis were confirmed by the SEM analysis, in which the non-treated control group showed a large number of yeasts and hyphae that were reduced after the treatments with *S. mutans* fractions. Treatment with SM-F2 was more effective in decreasing the quantity of yeast and hyphae in relation to SM-F1. In addition to reducing the quantity of *C. albicans* cells, the SM-F2 fraction exhibited a strong capacity for inhibiting hyphae formation (**Figure 3**).

Effects of SM-F2 on Gene Expression of *C. albicans*

To investigate the inhibitory mechanisms of SM-F2 on *C. albicans* filamentation, we analyzed the expressions of five virulence genes: *CPH1*, *EFG1*, *UME6, HWP1*, and *YWP1. CPH1*, *EFG1,* and *UME6* are transcriptional regulators involved in morphogenesis (Gulati and Nobile, 2016). *HWP1* encodes a cell wall protein essential for hyphae development (de Barros et al., 2017), while *YWP1* encodes a cell wall glycoprotein present in the yeast

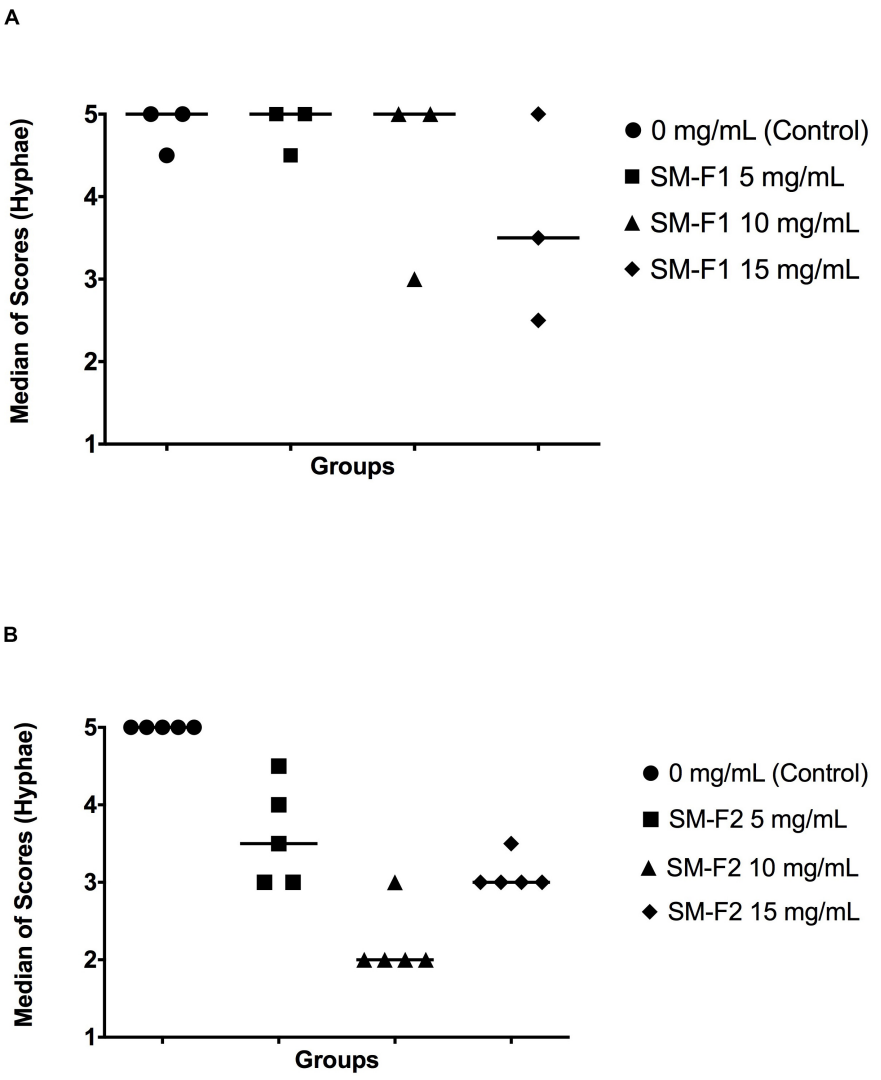

FIGURE 2 | Quantitative analysis of *Candida* filamentation. Median scores obtained by counting hyphae counting. Scores were assigned according to the number of hyphae in each microscopic field. **(A)** *C. albicans* cultured with PBS (control group), SM-F1 5 mg/mL, SM-F1 10 mg/mL, and SM-F1 15 mg/mL. No statistically significant differences were found between groups. **(B)** *C. albicans* cultured with PBS (control group), SM-F2 5 mg/mL, SM-F2 10 mg/mL, and SM-F2 15 mg/mL. Statistically significant difference was observed only between the control group and SM-F2 10 mg/mL ($p = 0.004$). Kruskal-Wallis and Dunn's test.

but absent in the filamentous form (Granger, 2012). Most of the evaluated genes were downregulated when *C. albicans* cells were exposed to SM-F2, with reductions of 10.0-, 4.0-, 23.25-, and 111.1-fold for *CPH1, EFG1*, *HWP1*, and *UME6* genes, respectively ($p < 0.0001$) (**Figure 4A**). Conversely, *YWP1* was upregulated with SM-F2 treatment, increasing expression by 11.22-fold ($p = 0.0092$) (**Figure 4B**). Taken together, these results reinforce the inhibitory activity of SM-F2 observed *in vitro* filamentation assays and suggest repression of the signaling cascade that leads to filamentation of *C. albicans*.

Antifungal Activity of SM-F1 and SM-F2 in *G. mellonella* Model

Streptococcus mutans supernatant fractions ranging between 1 and 15 mg/mL were injected into healthy larvae to evaluate toxicity. None of the tested concentrations interfered with larva survival (data not shown). Based on the results obtained in the *in vitro* assays, 15 mg/mL was selected for larvae therapeutic treatment upon *C. albicans* infection. The treatment with SM-F1 did not prolong larvae survival and resulted in 100% of death after 1 day, similar to the non-treated control group. By contrast, treatment with SM-F2 achieved significant larvae survival, with 70% of the larvae surviving beyond 1 day. Although SM-F2 treatment delayed *G. mellonella* death, only 12.5% of the larvae survived until the end of the experiment (7 days) (**Figure 5**).

Effects of SM-F1 and SM-F2 on Oral Candidiasis in Mice

C. albicans can cause oral infections that are difficult to treat due to biofilm formation. With the encouraging data that SM-F2 reduces biofilm formation and prolongs *G. mellonella* survival, the fractions were evaluated in a murine oral candidiasis model. *C. albicans* cells were recovered from the oral cavity of all infected groups. The CFU/mL counts were 3.25 ± 0.32 (Log_{10}) for the non-treated control group, 2.46 ± 0.83 (Log_{10}) for the group treated with SM-F1 and 2.34 ± 0.41 (Log_{10}) for the group treated with SM-F2. Although both treatments were capable of reducing *C. albicans* colonization, statistically significant difference in relation to the control group was only observed for SM-F2 (**Figure 6**).

Macroscopic analysis of the dorsum tongue revealed extensive candidiasis lesions in the non-treated control group, characterized by whitish regions with the presence of pseudomembrane and areas of papillary atrophy. Promisingly, these lesions were significantly reduced in the groups treated with SM-F1 and SM-F2. Although, the tongues of treated animals showed papillary atrophy, few whitish lesions characteristic of candidiasis were found in these groups (**Figure 7**). These findings were confirmed in the microscopic analysis, in which the non-treated control group presented a large quantity of yeasts and hyphae in the keratin layer. In addition, numerous epithelial lesions (microabscesses, exocytosis, spongiosis, and loss of filiform papillae) and intense inflammatory infiltrate were found (**Figure 8**). Analyzing all the extension of dorsum tongue, we verified that tissue lesions were limited to the areas with the presence of yeast and hyphae. Therefore, the tested concentration exhibited *C. albicans* inhibition without adversely damaging tongue tissue at the tested concentrations.

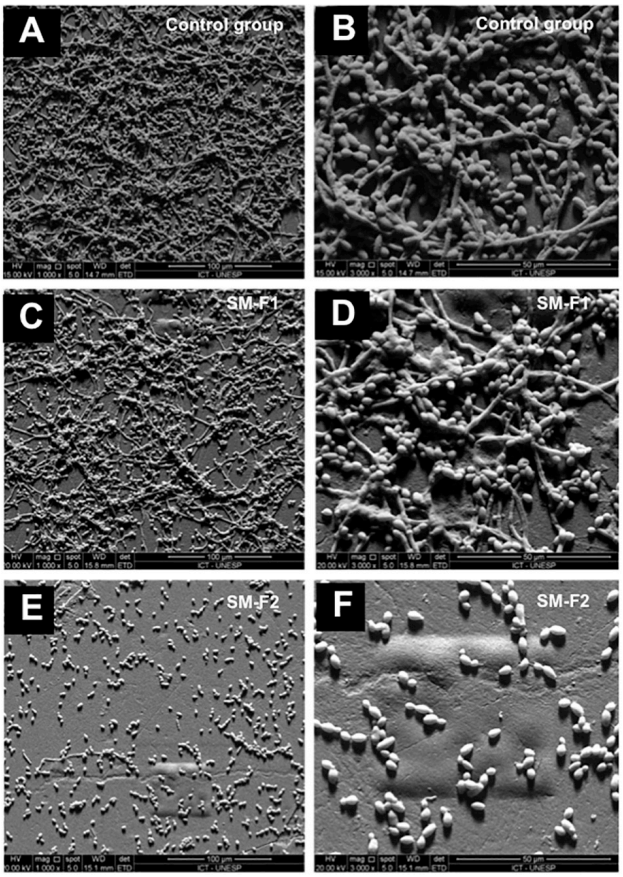

FIGURE 3 | SEM of fungal filamentation. Presence of *C. albicans* yeast and hyphae was assessed within the following groups: non-treated control at 1000× magnification **(A)** and 3000× magnification **(B)**, cells treated with 10 mg/mL SM-F1 at 1000× magnification **(C)** and 3000× magnification **(D)**, and cells treated with 10 mg/mL SM-F2 at 1000× magnifications **(E)** and 3000× magnification **(F)**.

The macroscopic and microscopic lesions were quantified to compare the studied groups. In the macroscopic analysis, we observed a media of 3.6 ± 0.54 for the non-treated control group, 1.60 ± 0.89 for the group treated with SM-F1 and 1.00 ± 0.00 for the group treated with SM-F2. The similar reduction proportions were found in the microscopic analysis. The medians of scores assigned for yeast/hyphae counts were 3 for the non-treated control group, 1 for the group treated with SM-F1 and 0 for the group treated with SM-F2. Interestingly, the SM-F2 showed a median score equal to 0 that corresponded to total absence of yeasts/hyphae. The number of epithelial lesions and intensity of inflammatory filtrate were also lower in the groups treated with SM-F1 and SM-F2 when compared to non-treated control group. In all the analysis, both fractions decreased the oral candidiasis, however only the SM-F2 fraction

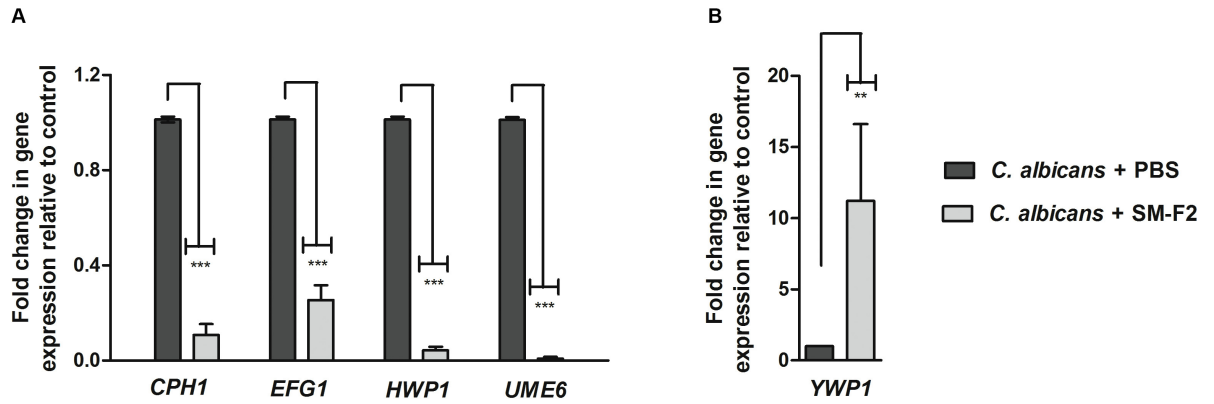

FIGURE 4 | Relative expression of *C. albicans* genes. Relative quantification of *CPH1*, *EFG1*, *HWP1*, and *UME6* genes **(A)** and *YWP1* gene **(B)** for the non-treated control group (PBS) and treated group with SM-F2 (10 mg/mL). Each gene was normalized using the reference gene *PMA1*. Values were expressed as the mean and SD. The Student's *t*-test was used to compare gene expression between the control and treated group (**$p < 0.01$ and *** $p < 0.0001$).

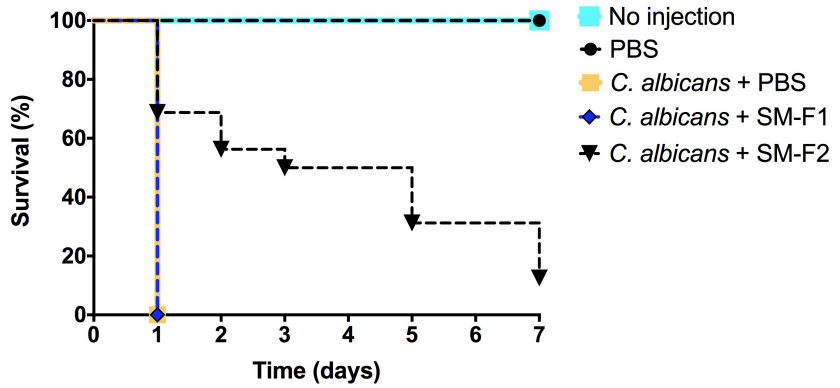

FIGURE 5 | *G. mellonella* survival assays. Antifungal activity of SM-F1 (15 mg/mL) and (SM-F2 15 mg/mL) on larvae infected by *C. albicans*. Statistically significant difference was observed between the group treated with SM-F2 and non-treated control group (PBS) ($p < 0,0001$). Log-rank test (Mantel-Cox).

showed statistically significant difference in relation to the control group (**Figure 9**). Taken together, these results suggest that SM-F2 was the most efficient *S. mutans* fraction to treat the oral candidiasis in mice at the present purification and concentration levels.

Identification of Substances in the SM-F1 and SM-F2 Fractions

The GC-MS analysis of SM-F1 and SM-F2 fractions were performed along with GC-MS analysis of BHI control group in order to identify compounds present in the fractions but absent in the culture medium. Comparison of chromatograms between the SM-F1 fraction and BHI control indicated the presence of peaks in SM-F1 (t_R = 53.12, 55.17, 55.46, 55.84, 56.23, 58.10 min) different from those observed in the BHI control group (**Supplementary Figure S5**). The comparison between the chromatograms of SM-F2 fraction and BHI control (**Supplementary Figure S6**) showed some peaks with different intensities from the peaks in the BHI control, including a peak observed only in SM-F2 chromatogram (t_R = 56.41 min).

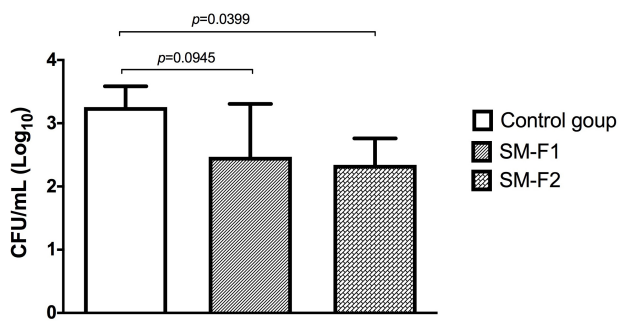

FIGURE 6 | Quantification of *Candida* cells recovered from the oral cavity of mice. Mean and SD of the CFU/mL (Log) of *C. albicans* obtained in the non-treated control group (PBS) and the experimental groups treated with the SM-F1 or SM-F2 fractions (1 g/Kg). ANOVA and Tukey test.

Despite the great number of peaks found in chromatograms, few compounds were identified due to the low similarity with the substances described in the databases. Since a limited numbers of

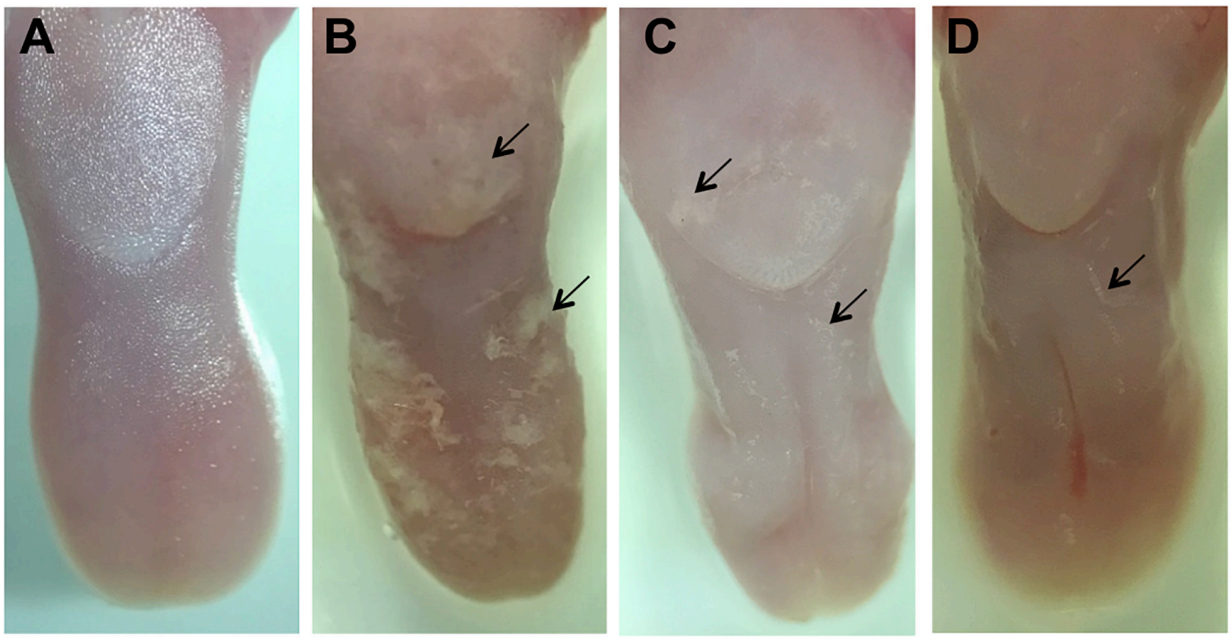

FIGURE 7 | Macroscopic images of the dorsum tongue. Control group not infected by *C. albicans*: normal aspect of tongue **(A)**. Control group infected by *C. albicans* and not treated: presence of numerous white patches of candidiasis lesions (→) and papillary atrophy **(B)**. Groups treated with SM-F1 **(C)** or SM-F2 **(D)** showing few areas of white patches (→) and papillary atrophy.

microbial substances have been identified by GC-MS and inserted in these databases, we could not identify all the compounds presents in the SM-F1 and SM-F2 fractions. Moreover, there is a possibility that some of these substances are not yet known.

The identified substances in the SM-F1 and SM-F2 fractions that showed similarity higher than 85% compared with data from software libraries are described in the **Tables 2**, **3**, respectively. Some of the compounds identified in the SM-F1 fraction were aromatic acids, such as benzoic and benzeneacetic acids (t_R = 13.92 and 16.10 min, respectively), while some of the compounds identified in the SM-F2 fraction were linear carbon chain acids, including hexadecanoic and octadecanoic acids (t_R = 44.30 and 50.33 min, respectively).

DISCUSSION

In an effort to seek new antifungals to treat oral candidiasis, we explored the ecological interactions established by bacteria and fungal in the oral microbiome. Among these interactions, *quorum sensing* molecules play an important role to control the oral microbial population and to manipulate the phenotypes of competing species (Vilchez et al., 2010). Since *C. albicans* are found together with *S. mutans* in dental biofilms, we selected this bacterium to investigate the presence of signaling molecules diffuse into the medium with potential antifungal activities (Vilchez et al., 2010; Barbosa et al., 2016). The presence of competence-stimulating peptides (CSP) (Khan et al., 2016) and universal bacterial signal autoinducer-2 (AI-2) was already confirmed in the cell-free culture filtrate of the *S. mutans* UA159 strain (Vilchez et al., 2010). Based on its well-studied *quorum sensing* system, this strain was employed in our study. Analyzing the free-cell culture filtrate of *S. mutans* UA159 using extraction and fractionation methods, we identified 2 bioactive fractions against *C. albicans* (SM-F1 and SM-F2). Both SM-F1 and SM-F2 were examined for inhibitory activity against planktonic cells, only SM-F2 demonstrating efficacy.

These fractions were then tested on biofilms and filamentation of *C. albicans* that are important virulence factors for the candidiasis development. It is know that antifungal agents with the ability to modulate biofilm formation and suppress dimorphic switching can lead the homeostatic balance of oral microbiome, protecting the host from the pathogenicity of *Candida* species (Chanda et al., 2017). Interestingly, fractions SM-F1, and even more so, SM-F2 were capable of inhibiting both biofilm and filamentation. We found a reduction of 2.59 and 5.98 log (CFU/mL) of mature biofilms treated with SM-F1 and SM-F2, respectively. These results were superior to those found in our previous study when unfractionated *S. mutans* UA159 culture filtrate was tested on *C. albicans* biofilms, resulting in a 1 log (CFU/mL) reduction (Barbosa et al., 2016). The data indicate that the extraction and fractionation methods used in this study were adequate to separate and concentrate active molecules with antifungal activity. The inhibition is encouraging considering inhibition was driven by active elements that were not yet fully purified. Thus, we are working with a diluted product. Further purification and higher concentrations may yet yield more significant reductions.

Although biofilm formation is an important virulence mechanism for *Candida* species, previous *S. mutans* antifungal

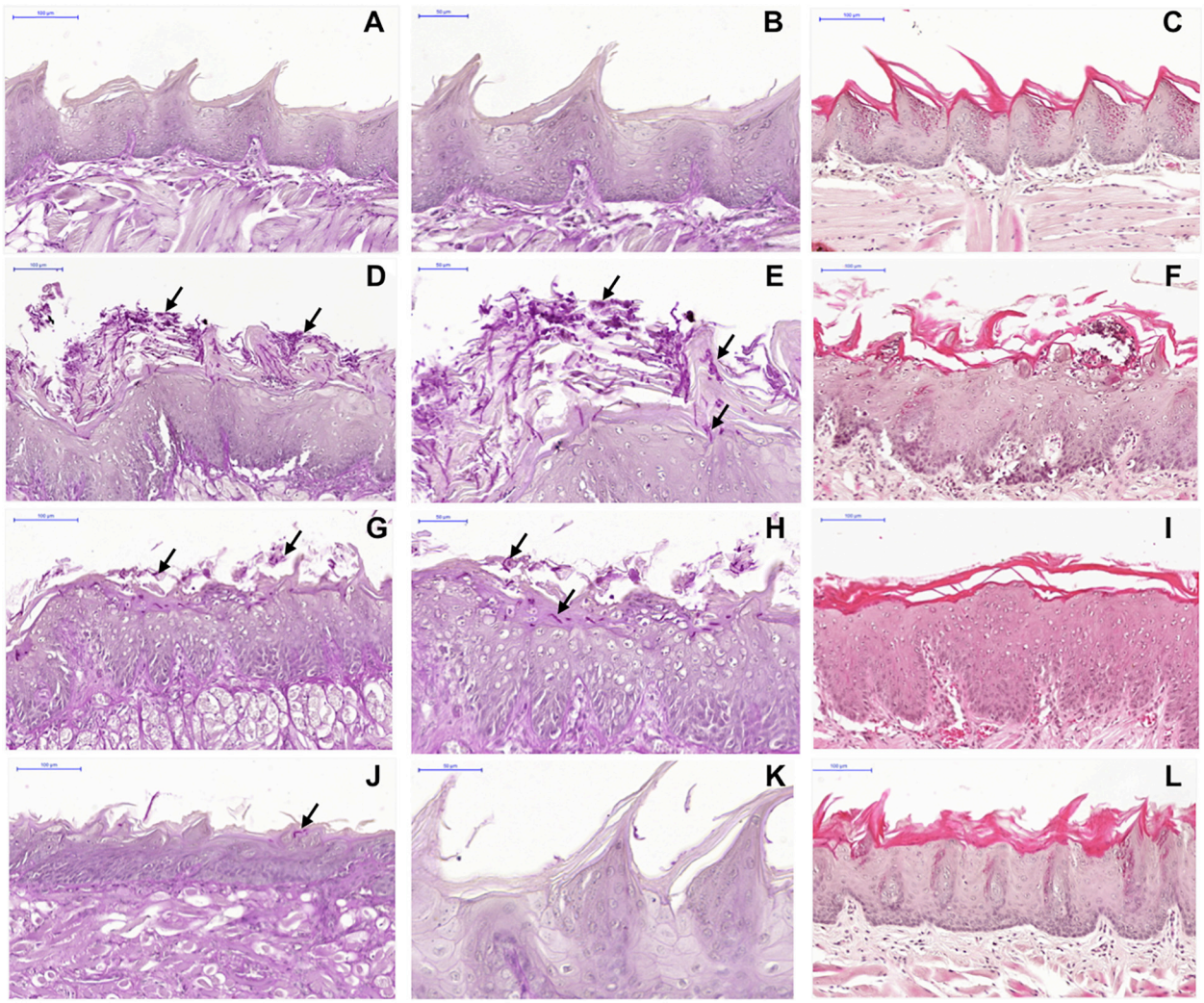

FIGURE 8 | Microscopic images of the dorsum tongue. Control group not infected by *C. albicans* stained by PAS **(A,B)** and H&E **(C)**: normal histological aspect of tongue. Control group infected by *C. albicans* and not treated stained by PAS **(D,E)** and H&E **(F)**: presence of several yeast and hyphae (→) in the keratin layer; epithelial changes with microabscesses, exocytosis, spongiosis and loss of filiform papillae; and formation of inflammatory infiltrate in lamina propria. Groups treated with SM-F1 stained by PAS **(G,H)** and H&E **(I)** or with SM-F2 stained by PAS **(J,K)** and H&E **(L)**: reduction in candidiasis lesions in relation to the not treated control group.

studies were focused on evaluating their effects on germ tubes and hyphae formation. Jarosz et al. (2009) verified that filter sterilized spent medium of *S. mutans* UA159 reduced *C. albicans* germ tube formation from 52 to 17%. These effects were attributed to the *quorum sensing* molecule CSP since a *S. mutans* mutant unable to produce CSP exhibited reduced germ tube inhibition compared to the wild-type strain. Joyner et al. (2010) also found a reduction in the morphological transition of *C. albicans* associated to the mutanobactin peptide produced by *S. mutans*. In co-cultures with mutanobactin-competent *S. mutans* strain, *C. albicans* grew only in the yeast form, whereas the co-culture with a mutanobactin deletion strain permitted *C. albicans* growth in a mycelium pattern. Vilchez et al. (2010) verified inhibitory effects of *S. mutans* extracts on *C. albicans* filamentation that were associated with fatty acid signaling molecule *trans*-2-decenoic acid. These authors observed that extracts from culture filtrates of *Streptococcus mitis*, *Streptococcus oralis,* and *Streptococcus sanguinis* also suppressed hyphae formation, but the strongest inhibition was achieved by the *S. mutans* extract.

In the present study, the *S. mutans* extract was fractionated to identify antifungal containing compounds. We found a significant reduction of hyphae formation when *C. albicans* were grown in contact with the SM-F2 fraction. In this study, *C. albicans* hyphae inhibition was not a condition of pH alteration since it was not a significant variant when the active fraction was added to the culture. The data reinforce that hyphae inhibition resulted from the presence of metabolites within the SM-F2 fraction. In addition, these metabolites seem to have strong inhibitory activity since the hyphae formation was inhibited in the presence of mammalian serum used in

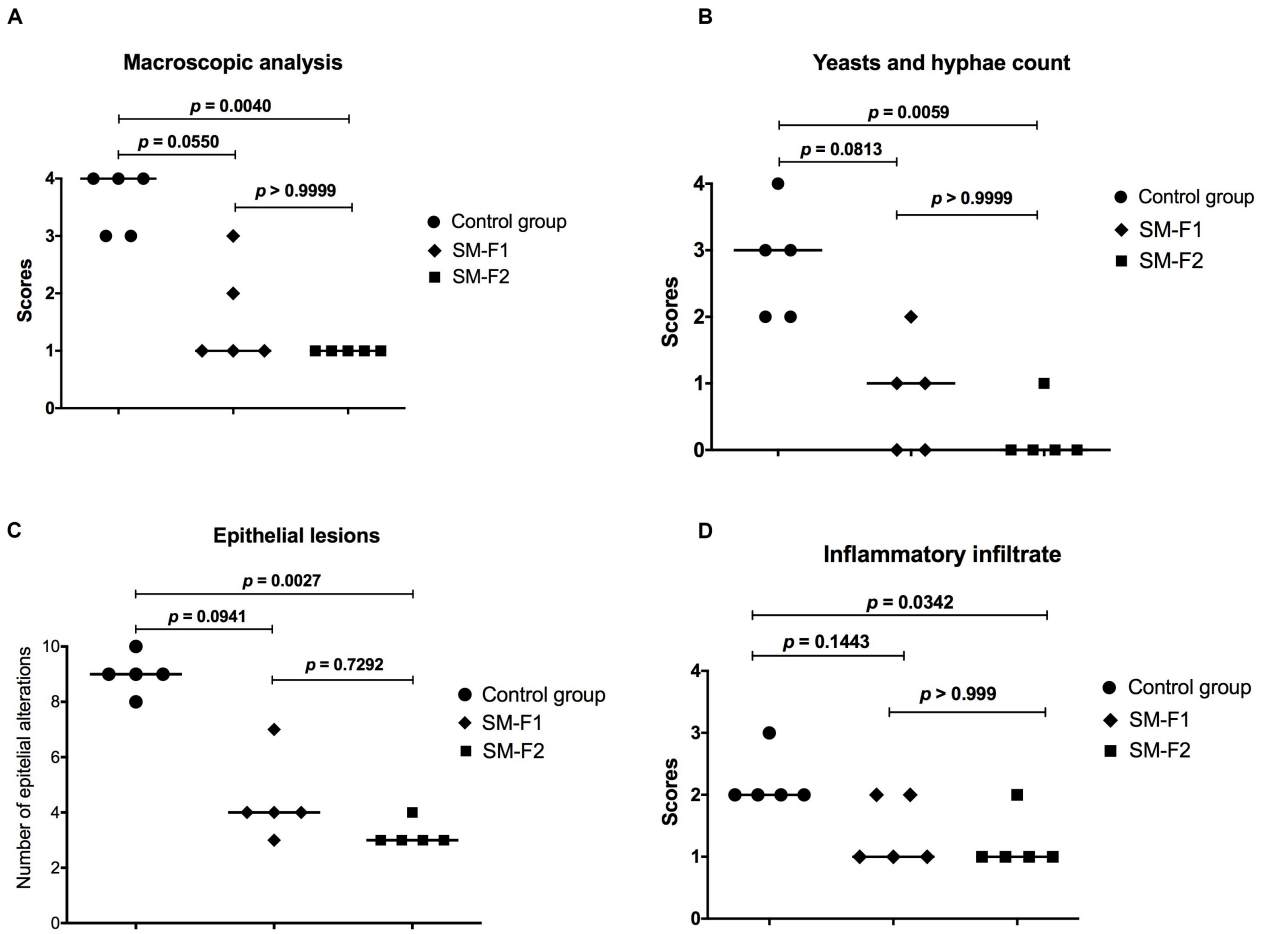

FIGURE 9 | Quantitative analysis of candidiasis lesions formed on the dorsum tongue of mice infected with *C. albicans*. **(A)** Scores and medians obtained in the quantification of macroscopic lesions. **(B)** Scores and medians obtained in yeasts/hyphae counts in the histological cuts stained by PAS. **(C)** Medians of epithelial lesions determined in the histological cuts stained by H&E. **(D)** Scores and medians of infiltrate inflammatory intensity in the histological cuts stained by H&E. Kruskal-Wallis and Dunn's test.

our filamentation assays. Mammalian serum is considered the strongest inducing factor among the conditions that stimulate *C. albicans* filamentation (Graham et al., 2017).

To complement the study about the inhibitory effects of the SM-F2 fraction on filamentation, we analyzed the expression of *C. albicans* genes when cells were cultured in serum bovine at 37°C and 5% CO_2. We analyzed the expression of regulatory genes (*CPH1*, *EFG1*, and *UME6)* that integrate and respond to the environmental signals controlling the morphogenesis of *C. albicans* (Nobile and Mitchell, 2006; Lee et al., 2018). All these transcription factors (TFs) genes that contribute to the activation of the hyphal transcriptional program were downregulated by the SM-F2 fraction. Among them, *UME6* is a common downstream target of regulators promoting hyphal development and plays a role in the expression of *HWP1*, *ECE1*, *ALS3*, and *HGC1* genes (Nobile and Mitchell, 2006; Lee et al., 2018). Interestingly, SM-F2 provoked a 111.1- and 23.25-fold decreased in expression of the *UME6* and *HWP1* genes, respectively, under the same environmental conditions. On the other hand, the *YWP1* gene was upregulated with SM-F2 treatment. *YWP1* (Yeast Wall protein 1) is an anchored glycoprotein of the cell wall present only in the yeast form, absent in filamentous form and chlamydospores (Granger, 2012; McCall et al., 2019). Therefore, these results suggest that the activity of SM-F2 against filamentation observed in the microscopic analysis can be associated with the level of transcription in *C. albicans* cells that leads to retention in the yeast state.

Based on these promising data, we interrogated our *S. mutans* extracts using two different *in vivo* models. The *G. mellonella* model is a prompt and reliable method to evaluate toxicity and efficacy of antifungal agents (Junqueira and Mylonakis, 2019; Lin et al., 2019; Rossoni et al., 2019). The *S. mutans* extract tested concentrations were not toxic to the host. When the efficacy of SM-F1 and SM-F2 fractions were tested on candidiasis, only the SM-F2 fraction was able to prolong larvae survival. Treatment with SM-F2 increased the survival rate by 70% 24 h post-infection. These data were superior to those found in our previous study (Barbosa et al., 2016) in which the larvae were

TABLE 2 | Identified compounds by GC-MS presented in *S. mutans* fraction (SM-F1).

Peak#	t_R (min)	Compounds	Similarity
3	7.15	Propanoic acid, 2-[(trimethylsilyl) oxy]-, trimethylsilyl ester	94%
5	13.92	Benzoic acid, trimethylsilyl ester	93%
6	15.63	Glycerol-tri- trimethylsilyl ether	93%
7	16.10	Benzeneacetic acid, trimethylsilyl ester	98%
9[a]	**18.06**	**Propanoic acid, 2,3-bis[(trimethylsilyl) oxy]-, trimethylsilyl ester**	**94%**
10	18.14	Pyrimidine, 2,4-bis[(trimethylsilyl)oxy]-	92%
12[a]	**20.13**	**(3R)-3-Methyl-1,4-bis(trimethylsilyl)piperazine-2,5-dione**	**93%**
13	20.49	Silanamine, 1,1,1-trimethyl-N-(trimethylsilyl)-N-[2-[(trimethylsilyl)oxy]ethyl]-	89%
14 [a]	**20.85**	**Pyrimidine, 5-methyl-2,4-bis[(trimethylsilyl)oxy]-**	**88%**
15	21.10	Benzenepropanoic acid, trimethylsilyl ester	95%
30	27.60	4-Hydroxyphenylethanol, di-TMS[b]	92%
55	39.97	Pyridine, 2-methyl-3-(trimethylsilyloxy)-4,5-bis-[(trimethylsilyloxy)methyl]-	94%
56	40.42	Pyrrolo[1,2-a]pyrazine-1,4-dione, hexahydro-3-(2-methylpropyl)-	90%
59 [a]	**41.50**	**Gulose, 2,3,4,5,6-pentakis-O-(trimethylsilyl)-**	**89%**
62	44.24	9H-Purine, 9-(trimethylsilyl)-2,6-bis[(trimethylsilyl)oxy]-	90%
83	54.12	Pyrrolo[1,2-a]pyrazine-1,4-dione, hexahydro-3-(phenylmethyl)-	90%

[a]Compound presented only in SM-F1 when compared with BHI control group. [b]TMS - trimethylsilyl group.

TABLE 3 | Identified compounds by GC-MS presented in *S. mutans* fraction (SM-F2).

Peak#	t_R (min)	Compound	Similarity
5	7.12	Propanoic acid, 2-[(trimethylsilyl) oxy]-, trimethylsilyl ester	94%
6	13.08	Silane, trimethyl(2-phenylethoxy)-	93%
7[a]	**14.88**	**Nicotinic acid-TMS[b]**	**92%**
8	15.59	Glycerol-tri-tms ether	93%
41	40.35	Pyrrolo[1,2-a]pyrazine-1,4-dione, hexahydro-3-(2-methylpropyl)-	89%
54	44.30	Hexadecanoic acid, trimethylsilyl ester	88%
66	50.33	Octadecanoic acid, trimethylsilyl ester	86%
71[a]	**52.57**	**Tryptophan, 2TMS[b]**	**86%**
73	53.71	9-Octadecenamide, (Z)-	93%
74	54.30	Pyrrolo[1,2-a]pyrazine-1,4-dione, hexahydro-3-(phenylmethyl)-	91%

[a]Compound presented only in SM-F2 when compared with BHI control. [b]TMS - trimethylsilyl group.

treated only with the culture filtrate of *S. mutans* UA159, resulting in an increase survival rate of 50% at 24 h post infection, suggesting the applied degree of purification increased potency. Therefore, the *G. mellonella* model provided evidences that the bioactivity of antifungal agents within SM-F2 were maintained under *in vivo* conditions.

Next, we used a well-established mouse model (Junqueira et al., 2005; Costa et al., 2013b; de Campos Rasteiro et al., 2014; Rossoni et al., 2015; Ribeiro et al., 2020) to evaluate the effects of the SM-F1 and SM-F2 fractions on oral candidiasis. Treatments with SM-F1 and SM-F2 reduced *C. albicans* cells in 0.79 and 0.91 Log (UFC/mL), respectively, compared to an untreated control group. In additional to affecting fungal oral colonization, the supernatant fractions were capable of inhibiting formation of pseudomembranous lesions on the dorsum tongue. The clinical observations were confirmed in the microscopic analysis, in which the SM-F1 and SM-F2 decreased the hyphae invasion, epithelial lesions and inflammatory infiltrate. Notably, the reductions observed were more pronounced by the treatment with SM-F2 than SM-F1. These data are very promising since the high efficacy of SM-F2 was confirmed in a dynamic infection model that mimics the oral candidiasis in humans. To our knowledge, this is the first report describing the effects of *S. mutans* culture extracts filtrate or mutanobactins on oral candidiasis model. Graham et al. (2017) investigated the development of oral candidiasis in mice treated with the EntV bacteriocin secreted by *Enterococcus faecalis*, a Gram-positive bacterium also presented in the oral microbiome. EntV reduced the fungal burden, hyphae invasion and inflammation in relation to non-treated group. Similarly, to the SM-F2 fraction used in our study, EntV did not eliminate the fungal colonization, but the hyphae invasion in the epithelial tissue was almost entirely eliminated (Graham et al., 2017).

Using GC-MS analysis, we identified compounds in the SM-F1 fraction that differed from the BHI control: Propanoic acid, 2,3-bis[(trimethylsilyl) oxy]-, trimethylsilyl ester; (3R)-3-methyl-1,4-bis(trimethylsilyl)piperazine-2,5-dione; pyrimidine, 5-methyl-2,4-bis[(trimethylsilyl)oxy]; and glucose, 2,3,4,5,6-pentakis-O-(trimethylsilyl). The compounds identified exclusively in the SM-F2 fraction were the nicotinic acid-TMS and Tryptophan,

2TMS. Some of these compounds are previously described in the literature to show antimicrobial activity. The propanoic acid (also called propionic acid) produced by *Propionibacterium acnes*, a commensal bacterium of human skin, was able to inhibit the growth of methicillin-resistant *Staphylococcus aureus*, *Escherichia coli,* and *C. albicans* (Wang et al., 2014). Nicotinic acid, also known as niacin or vitamin B3, is a water-soluble substance that has an important role in the human body, also its activity against *Staphylococcus aureus* was already demonstrated (Daglia et al., 1994). Nicotinamida has demonstrated antimicrobial activity against *C. albicans* (Pfaller et al., 2010), *Aspergillus* spp. (Dagenais and Keller, 2009) and *Botrytis cinerea* (Wang et al., 2019). Tryptophan-rich peptides have potent known antimicrobial activity attributed to the biochemical properties that facilitate crossing the microbial membranes without compromising their integrity, acting internally on nucleic acids and enzymes (Shagaghi et al., 2016; Mishra et al., 2018). Besides these compounds, many others can be present in the SM-F1 and SM-F2 fractions, however we were unable to identify them since a large number of substances from microbial extracts have not yet been described and inserted in the databases. According to Joyner et al. (2010), despite a variety of compounds such as peptides, lipids and acyl-homoserine lactones have emerged as communication agents among microorganisms, important contributions of many other secondary metabolites remains overlooked.

In addition, the compounds produced by microorganisms depend on environmental conditions; therefore, its identification can be limited by the study methods employed. In this study, the SM-F1 and SM-F2 fractions were obtained from pure cultures of *S. mutans*. Indeed, *quorum sensing* molecules have often been studied from pure laboratory cultures (Papenfort and Bassler, 2016; Mukherjee and Bassler, 2019), contributing to our understanding about the molecular mechanisms evolved in different microbial species (Mukherjee and Bassler, 2019). However, the uniform growth and the absence of mixed microbial communities can influence the functions of *quorum sensing* (Papenfort and Bassler, 2016). In this context, co-cultivation became an interesting tool to study *quorum sensing* molecules, in which co-cultures of two or more different microorganisms can mimic the ecological interactions (Marmann et al., 2014). The competition or antagonism experienced during co-cultivation may lead to an enhanced production of diversified compounds that are not detected in pure cultures (Marmann et al., 2014). Another important aspect that should be considered in future studies is the extension of antimicrobial activity of SM-F1 and SM-F2 for other microorganisms. It is probable that the antifungal effects of these fractions can be extended for other *Candida* species. Since *Candida glabrata*, *Candida tropicalis*, and *Candida krusei* also have an important role in the oral candidiasis, SM-F1 and SM-F2 fractions need to be tested on these non-*albicans Candida* species (Junqueira et al., 2011). Furthermore, the effects of extract and fractions of *S. mutans* can be explored against oral bacteria and dental biofilms, seeking mechanisms of action that may contribute for the control of oral bacterial infections, such as dental caries and periodontal diseases.

In conclusion, SM-F2 was the most effective fraction we tested with strong activity against *C. albicans* biofilms and filamentation, resulting in inhibition of candidiasis in an animal model. With further refinement, the extract demonstrates potential to be explored as an antifungal agent to treat oral candidiasis.

DATA AVAILABILITY STATEMENT

The raw data supporting the conclusions of this article will be made available by the authors, without undue reservation.

ETHICS STATEMENT

The animal study was reviewed and approved by Ethics Committee on the Use of Animals of the ICT/UNESP under protocol 005/2016-CEUA- ICT-UNESP.

AUTHOR CONTRIBUTIONS

JJ and DS conceived and designed the experiments. JS, LF, and MA performed the experiments. RM contributed to preparation of *S. mutans* fractions and analysis by gas chromatography coupled to mass spectrometry. PB contributed to the gene expressions analysis. FR contributed to the experiments in oral candidiasis model. BF and EM contributed with reagents, materials or analysis tools in RIH/Brown University. JS, LF, RM, LS, and JJ analyzed the data. JS, LF, LS, BF, EM, and JJ wrote and revised the manuscript. All authors contributed to the article and approved the submitted version.

FUNDING

National Council for Scientific Development (CNPq): Researcher on Productivity PQ-1C for JJ (306330/2018-0). São Paulo Research Foundation (FAPESP): scholarship for JS (2016/03395-4) and MA (2016/05226-5). Coordination for the Improvement of Higher Education Personnel (CAPES): scholarship for LF. Brown-Brazil Initiative (Brown University): international scholarship for JS.

SUPPLEMENTARY MATERIAL

The Supplementary Material for this article can be found online at: https://www.frontiersin.org/articles/10.3389/fmicb.2020.01605/full#supplementary-material

FIGURE S1 | Validation of primers for qPCR. **(A)** Standard curve of the *HWP1* primer for the calculation of efficiency. **(B)** Specificity of the primers demonstrated by melting curve of *HWP1* gene obtained from *C. albicans* group.

FIGURE S2 | Selection of the best reference gene (*ACT1, PMA1*, and *RPP2B*) using BestKeeper, NormFinder, Genorm, and Delta CT.

FIGURE S3 | Light microscopy photomicrographs of *Candida* filamentation. Hyphae formation and presence of yeasts in the microscopic fields for the non-treated control group **(A,E)** and experimental groups treated with SM-F1 5 mg/mL **(B)**, SM-F1 10 mg/mL **(C)**, SM-F1 15 mg/mL **(D)**, SM-F2 5 mg/mL **(F)**, SM-F2 10 mg/mL **(G)**, and SM-F2 15 mg/mL **(H)**.

FIGURE S4 | Measured pH in the *in vitro* filamentation assay. Median and SD of pH values in the medium for each well obtained in the following groups: non-treated control group, SM-F1 5 mg/mL, SM-F1 10 mg/mL, SM-F1 15 mg/mL, SM-F2 5 mg/mL, SM-F2 10 mg/mL, and SM-F2 15 mg/mL (H).

FIGURE S5 | Chromatograms obtained by gas chromatography coupled to mass spectrometry (GC-MS). Comparisons between the SM-F1 fraction (red line) and control group of BHI media (black line). The black arrows indicate the peaks that are different between the SM-F1 and control. The blue arrows show the peaks of SM-F1 that indicate the identified compounds.

FIGURE S6 | Chromatograms obtained by gas chromatography coupled to mass spectrometry (GC-MS). Comparisons between the SM-F2 fraction (pink) and control group of BHI media (black). The black arrows indicate the peaks that are different between the SM-F2 and control. The blue arrows show the peaks of SM-F2 that indicate the identified compounds.

REFERENCES

Barbosa, J. O., Rossoni, R. D., Vilela, S. F., de Alvarenga, J. A., Velloso Mdos, S., Prata, M. C., et al. (2016). *Streptococcus mutans* can modulate biofilm formation and attenuate the virulence of *Candida albicans*. *PLoS One* 11:e0150457. doi: 10.1371/journal.pone.0150457

Becker, M. R., Paster, B. J., Leys, E. J., Moeschberger, M. L., Kenyon, S. G., Galvin, J. L., et al. (2002). Molecular analysis of bacterial species associated with childhood caries. *J. Clin. Microbiol.* 40, 1001–1009. doi: 10.1128/jcm.40.3.1001-1009.2002

Bekal-Si Ali, S., Hurtubise, Y., Lavoie, M. C., and LaPointe, G. (2002). Diversity of *Streptococcus mutans* bacteriocins as confirmed by DNA analysis using specific molecular probes. *Gene* 283, 125–131. doi: 10.1016/s0378-1119(01)00875-7

Berberi, A., Noujeim, Z., and Aoun, G. (2015). Epidemiology of oropharyngeal Candidiasis in human immunodeficiency virus/acquired immune deficiency syndrome patients and CD4+ counts. *J. Int. Oral Health* 7, 20–23.

Breger, J., Fuchs, B. B., Aperis, G., Moy, T. I., Ausubel, F. M., and Mylonakis, E. (2007). Antifungal chemical compounds identified using a *C. elegans* pathogenicity assay. *PLoS Pathog.* 3:e18. doi: 10.1371/journal.ppat.0030018

Chanda, W., Joseph, T. P., Wang, W., Padhiar, A. A., and Zhong, M. (2017). The potential management of oral candidiasis using anti-biofilm therapies. *Med. Hypotheses* 106, 15–18. doi: 10.1016/j.mehy.2017.06.029

Coronado-Castellote, L., and Jimenez-Soriano, Y. (2013). Clinical and microbiological diagnosis of oral candidiasis. *J. Clin. Exp. Dent.* 5, e279–e286. doi: 10.4317/jced.51242

Costa, A. C., Pereira, C. A., Freire, F., Junqueira, J. C., and Jorge, A. O. (2013a). Methods for obtaining reliable and reproducible results in studies of Candida biofilms formed in vitro. *Mycoses* 56, 614–622. doi: 10.1111/myc.12092

Costa, A. C., Pereira, C. A., Junqueira, J. C., and Jorge, A. O. (2013b). Recent mouse and rat methods for the study of experimental oral candidiasis. *Virulence* 4, 391–399. doi: 10.4161/viru.25199

Dagenais, T. R., and Keller, N. P. (2009). Pathogenesis of *Aspergillus fumigatus* in invasive Aspergillosis. *Clin. Microbiol. Rev.* 22, 447–465. doi: 10.1128/CMR.00055-08

Daglia, M., Cuzzoni, M. T., and Dacarro, C. (1994). Antibacterial activity of coffee – relationship between biological-activity and chemical markers. *J. Agr. Food Chem.* 42, 2273–2277. doi: 10.1021/jf00046a036

de Barros, P. P., Freire, F., Rossoni, R. D., Junqueira, J. C., and Jorge, A. O. C. (2017). *Candida krusei* and *Candida glabrata* reduce the filamentation of *Candida albicans* by downregulating expression of HWP1 gene. *Folia Microbiol. (Praha)* 62, 317–323. doi: 10.1007/s12223-017-0500-4

de Campos Rasteiro, V. M., da Costa, A. C., Araujo, C. F., de Barros, P. P., Rossoni, R. D., Anbinder, A. L., et al. (2014). Essential oil of *Melaleuca alternifolia* for the treatment of oral candidiasis induced in an immunosuppressed mouse model. *BMC Complement Altern. Med.* 14:489. doi: 10.1186/1472-6882-14-489

Falsetta, M. L., Klein, M. I., Colonne, P. M., Scott-Anne, K., Gregoire, S., Pai, C. H., et al. (2014). Symbiotic relationship between *Streptococcus mutans* and *Candida albicans* synergizes virulence of plaque biofilms in vivo. *Infect. Immun.* 82, 1968–1981. doi: 10.1128/IAI.00087-14

Garcia-Cuesta, C., Sarrion-Perez, M. G., and Bagan, J. V. (2014). Current treatment of oral candidiasis: a literature review. *J. Clin. Exp. Dent.* 6, e576–e582. doi: 10.4317/jced.51798

Graham, C. E., Cruz, M. R., Garsin, D. A., and Lorenz, M. C. (2017). Enterococcus faecalis bacteriocin EntV inhibits hyphal morphogenesis, biofilm formation, and virulence of *Candida albicans*. *Proc. Natl. Acad. Sci. U.S.A.* 114, 4507–4512. doi: 10.1073/pnas.1620432114

Granger, B. L. (2012). Insight into the antiadhesive effect of yeast wall protein 1 of *Candida albicans*. *Eukaryot. Cell* 11, 795–805. doi: 10.1128/EC.00026-12

Gulati, M., and Nobile, C. J. (2016). *Candida albicans* biofilms: development, regulation, and molecular mechanisms. *Microbes Infect.* 18, 310–321. doi: 10.1016/j.micinf.2016.01.002

Hnisz, D., Bardet, A. F., Nobile, C. J., Petryshyn, A., Glaser, W., Schock, U., et al. (2012). A histone deacetylase adjusts transcription kinetics at coding sequences during *Candida albicans* morphogenesis. *PLoS Genet.* 8:e1003118. doi: 10.1371/journal.pgen.1003118

National Committee for Clinical Laboratory Standards (2002). Reference method for broth dilution antifungal susceptibility testing of yeasts. Approved standard, 2nd Edn, M27-A2. National Committee for Clinical Laboratory Standards, Wayne, Pa.

Jarosz, L. M., Deng, D. M., van der Mei, H. C., Crielaard, W., and Krom, B. P. (2009). *Streptococcus mutans* competence-stimulating peptide inhibits *Candida albicans* hypha formation. *Eukaryot. Cell* 8, 1658–1664. doi: 10.1128/EC.00070-09

Joyner, P. M., Liu, J., Zhang, Z., Merritt, J., Qi, F., and Cichewicz, R. H. (2010). Mutanobactin A from the human oral pathogen *Streptococcus mutans* is a cross-kingdom regulator of the yeast-mycelium transition. *Org. Biomol. Chem.* 8, 5486–5489. doi: 10.1039/c0ob00579g

Junqueira, J. C., Colombo, C. E., Martins Jda, S., Koga Ito, C. Y., Carvalho, Y. R., and Jorge, A. O. (2005). Experimental candidosis and recovery of *Candida albicans* from the oral cavity of ovariectomized rats. *Microbiol. Immunol.* 49, 199–207. doi: 10.1111/j.1348-0421.2005.tb03721.x

Junqueira, J. C., Fuchs, B. B., Muhammed, M., Coleman, J. J., Suleiman, J. M., Vilela, S. F., et al. (2011). Oral *Candida albicans* isolates from HIV-positive individuals have similar in vitro biofilm-forming ability and pathogenicity as invasive Candida isolates. *BMC Microbiol.* 11:247. doi: 10.1186/1471-2180-11-247

Junqueira, J. C., and Mylonakis, E. (2019). Current status and trends in alternative models to study fungal pathogens. *J. Fungi (Basel)* 5:12. doi: 10.3390/jof5010012

Kamiya, R. U., Hofling, J. F., and Goncalves, R. B. (2008). Frequency and expression of mutacin biosynthesis genes in isolates of *Streptococcus mutans* with different mutacin-producing phenotypes. *J. Med. Microbiol.* 57(Pt 5), 626–635. doi: 10.1099/jmm.0.47749-0

Khan, R., Rukke, H. V., Hovik, H., Amdal, H. A., Chen, T., Morrison, D. A., et al. (2016). Comprehensive transcriptome profiles of *Streptococcus mutans* UA159 map core streptococcal competence genes. *mSystems* 1:2. doi: 10.1128/mSystems.00038-15

Klein, M. I., Bang, S., Florio, F. M., Hofling, J. F., Goncalves, R. B., Smith, D. J., et al. (2006). Genetic diversity of competence gene loci in clinical genotypes of *Streptococcus mutans*. *J. Clin. Microbiol.* 44, 3015–3020. doi: 10.1128/JCM.02024-05

Lee, J. H., Kim, Y. G., Choi, P., Ham, J., Park, J. G., and Lee, J. (2018). Antibiofilm and antivirulence activities of 6-Gingerol and 6-Shogaol against *Candida albicans* due to hyphal inhibition. *Front. Cell. Infect. Microbiol.* 8:299. doi: 10.3389/fcimb.2018.00299

Lin, M. Y., Yuan, Z. L., Hu, D. D., Hu, G. H., Zhang, R. L., Zhong, H., et al. (2019). Effect of loureirin A against *Candida albicans* biofilms. *Chin. J. Nat. Med.* 17, 616–623. doi: 10.1016/S1875-5364(19)30064-0

Liu, J. Y., Shi, C., Wang, Y., Li, W. J., Zhao, Y., and Xiang, M. J. (2015). Mechanisms of azole resistance in *Candida albicans* clinical isolates from Shanghai, China. *Res. Microbiol.* 166, 153–161. doi: 10.1016/j.resmic.2015.02.009

Livak, K. J., and Schmittgen, T. D. (2001). Analysis of relative gene expression data using real-time quantitative PCR and the 2(-Delta Delta C(T)) Method. *Methods* 25, 402–408. doi: 10.1006/meth.2001.1262

Marmann, A., Aly, A. H., Lin, W., Wang, B., and Proksch, P. (2014). Co-cultivation–a powerful emerging tool for enhancing the chemical diversity of microorganisms. *Mar. Drugs* 12, 1043–1065. doi: 10.3390/md12021043

Martins Jda, S., Junqueira, J. C., Faria, R. L., Santiago, N. F., Rossoni, R. D., Colombo, C. E., et al. (2011). Antimicrobial photodynamic therapy in rat experimental candidiasis: evaluation of pathogenicity factors of *Candida albicans*. *Oral Surg. Oral Med. Oral Pathol. Oral Radiol. Endod.* 111, 71–77. doi: 10.1016/j.tripleo.2010.08.012

Matsubara, V. H., Wang, Y., Bandara, H. M., Mayer, M. P., and Samaranayake, L. P. (2016). Probiotic lactobacilli inhibit early stages of *Candida albicans* biofilm development by reducing their growth, cell adhesion, and filamentation. *Appl. Microbiol. Biotechnol.* 100, 6415–6426. doi: 10.1007/s00253-016-7527-3

McCall, A. D., Pathirana, R. U., Prabhakar, A., Cullen, P. J., and Edgerton, M. (2019). *Candida albicans* biofilm development is governed by cooperative attachment and adhesion maintenance proteins. *NPJ Biofilms Microb.* 5:21. doi: 10.1038/s41522-019-0094-5

Medina, R. P., Araujo, A. R., Batista, J. M., Cardoso, C. L., Seidl, C., Vilela, A. F. L. et al. (2019). Botryane terpenoids produced by *Nemania bipapillata*, an endophytic fungus isolated from red alga *Asparagopsis taxiformis* – *Falkenbergia* stage. *Sci. Rep.* 9:12318. doi: 10.1038/s41598-019-48655-7

Mishra, A. K., Choi, J., Moon, E., and Baek, K. H. (2018). Tryptophan-rich and proline-rich antimicrobial peptides. *Molecules* 23:815. doi: 10.3390/molecules23040815

Mitchell, T. J. (2003). The pathogenesis of streptococcal infections: from tooth decay to meningitis. *Nat. Rev. Microbiol.* 1, 219–230. doi: 10.1038/nrmicro771

Moges, B., Bitew, A., and Shewaamare, A. (2016). Spectrum and the *in vitro* antifungal susceptibility pattern of yeast isolates in ethiopian HIV patients with oropharyngeal candidiasis. *Int. J. Microbiol.* 2016:3037817. doi: 10.1155/2016/3037817

Mukherjee, S., and Bassler, B. L. (2019). Bacterial quorum sensing in complex and dynamically changing environments. *Nat. Rev. Microbiol.* 17, 371–382. doi: 10.1038/s41579-019-0186-5

Nailis, H., Coenye, T., Van Nieuwerburgh, F., Deforce, D., and Nelis, H. J. (2006). Development and evaluation of different normalization strategies for gene expression studies in *Candida albicans* biofilms by real-time PCR. *BMC Mol. Biol.* 7:25. doi: 10.1186/1471-2199-7-25

Nobile, C. J., and Mitchell, A. P. (2006). Genetics and genomics of *Candida albicans* biofilm formation. *Cell Microbiol.* 8, 1382–1391. doi: 10.1111/j.1462-5822.2006.00761.x

Papenfort, K., and Bassler, B. L. (2016). Quorum sensing signal-response systems in Gram-negative bacteria. *Nat. Rev. Microbiol.* 14, 576–588. doi: 10.1038/nrmicro.2016.89

Patton, L. L. (2016). Current strategies for prevention of oral manifestations of human immunodeficiency virus. *Oral Surg. Oral Med. Oral Pathol. Oral Radiol.* 121, 29–38. doi: 10.1016/j.oooo.2015.09.004

Peleg, A. Y., Hogan, D. A., and Mylonakis, E. (2010). Medically important bacterial-fungal interactions. *Nat. Rev. Microbiol.* 8, 340–349. doi: 10.1038/nrmicro2313

Pellati, F., and Benvenuti, S. (2007). Chromatographic and electrophoretic methods for the analysis of phenethylamine [corrected] alkaloids in *Citrus aurantium*. *J. Chromatogr. A* 1161, 71–88. doi: 10.1016/j.chroma.2007.05.097

Pereira-Cenci, T., Deng, D. M., Kraneveld, E. A., Manders, E. M., Del Bel Cury, A. A., Ten Cate, J. M., et al. (2008). The effect of *Streptococcus mutans* and *Candida glabrata* on *Candida albicans* biofilms formed on different surfaces. *Arch. Oral Biol.* 53, 755–764. doi: 10.1016/j.archoralbio.2008.02.015

Pfaller, M. A., Diekema, D. J., Gibbs, D. L., Newell, V. A., Ellis, D., Tullio, V., et al. (2010). Results from the ARTEMIS DISK global antifungal surveillance study, 1997 to 2007: a 10.5-year analysis of susceptibilities of *Candida* species to fluconazole and voriconazole as determined by CLSI standardized disk diffusion. *J. Clin. Microbiol.* 48, 1366–1367. doi: 10.1128/JCM.02117-09

Ribeiro, F. C., Junqueira, J. C., Dos Santos, J. D., de Barros, P. P., Rossoni, R. D., Shukla, S., et al. (2020). Development of probiotic formulations for oral candidiasis prevention: gellan gum as a carrier to deliver *Lactobacillus paracasei* 28.4. *Antimicrob. Agents Chemother.* 64:e02323-19. doi: 10.1128/AAC.02323-19

Rossoni, R. D., Barbosa, J. O., Vilela, S. F., dos Santos, J. D., de Barros, P. P., Prata, M. C., et al. (2015). Competitive interactions between *C. albicans*, *C. glabrata* and *C. krusei* during biofilm formation and development of experimental candidiasis. *PLoS One* 10:e0131700. doi: 10.1371/journal.pone.0131700

Rossoni, R. D., de Barros, P. P., de Alvarenga, J. A., Ribeiro, F. C., Velloso, M. D. S., Fuchs, B. B., et al. (2018). Antifungal activity of clinical *Lactobacillus* strains against *Candida albicans* biofilms: identification of potential probiotic candidates to prevent oral candidiasis. *Biofouling* 34, 212–225. doi: 10.1080/08927014.2018.1425402

Rossoni, R. D., Fuchs, B. B., de Barros, P. P., Velloso, M. D., Jorge, A. O., Junqueira, J. C., et al. (2017). *Lactobacillus paracasei* modulates the immune system of *Galleria mellonella* and protects against *Candida albicans* infection. *PLoS One* 12:e0173332. doi: 10.1371/journal.pone.0173332

Rossoni, R. D., Ribeiro, F. C., Dos Santos, H. F. S., Dos Santos, J. D., Oliveira, N. S., Dutra, M., et al. (2019). Galleria mellonella as an experimental model to study human oral pathogens. *Arch. Oral Biol.* 101, 13–22. doi: 10.1016/j.archoralbio.2019.03.002

Salvatori, O., Puri, S., Tati, S., and Edgerton, M. (2016). Innate immunity and saliva in *Candida albicans*-mediated oral diseases. *J. Dent. Res.* 95, 365–371. doi: 10.1177/0022034515625222

Seneviratne, C. J., and Rosa, E. A. (2016). Editorial: antifungal drug discovery: new theories and new therapies. *Front. Microbiol.* 7:728. doi: 10.3389/fmicb.2016.00728

Shagaghi, N., Palombo, E. A., Clayton, A. H., and Bhave, M. (2016). Archetypal tryptophan-rich antimicrobial peptides: properties and applications. *World J. Microbiol. Biotechnol.* 32:31. doi: 10.1007/s11274-015-1986-z

Sherry, L., Rajendran, R., Lappin, D. F., Borghi, E., Perdoni, F., Falleni, M., et al. (2014). Biofilms formed by *Candida albicans* bloodstream isolates display phenotypic and transcriptional heterogeneity that are associated with resistance and pathogenicity. *BMC Microbiol.* 14:182. doi: 10.1186/1471-2180-14-182

Shu, C., Sun, L., and Zhang, W. (2016). Thymol has antifungal activity against *Candida albicans* during infection and maintains the innate immune response required for function of the p38 MAPK signaling pathway in *Caenorhabditis elegans*. *Immunol. Res.* 64, 1013–1024. doi: 10.1007/s12026-016-8785-y

Takakura, N., Sato, Y., Ishibashi, H., Oshima, H., Uchida, K., Yamaguchi, H., et al. (2003). A novel murine model of oral candidiasis with local symptoms characteristic of oral thrush. *Microbiol. Immunol.* 47, 321–326. doi: 10.1111/j.1348-0421.2003.tb03403.x

Thein, Z. M., Samaranayake, Y. H., and Samaranayake, L. P. (2006). Effect of oral bacteria on growth and survival of *Candida albicans* biofilms. *Arch. Oral Biol.* 51, 672–680. doi: 10.1016/j.archoralbio.2006.02.005

Vazquez, J. A. (2010). Optimal management of oropharyngeal and esophageal candidiasis in patients living with HIV infection. *HIV AIDS (Auckl)* 2, 89–101.

Venkatasalu, M. R., Murang, Z. R., Ramasamy, D. T. R., and Dhaliwal, J. S. (2020). Oral health problems among palliative and terminally ill patients: an integrated systematic review. *BMC Oral Health* 20:79. doi: 10.1186/s12903-020-01075-w

Vilchez, R., Lemme, A., Ballhausen, B., Thiel, V., Schulz, S., Jansen, R., et al. (2010). *Streptococcus mutans* inhibits *Candida albicans* hyphal formation by the fatty acid signaling molecule trans-2-decenoic acid (SDSF). *Chembiochem* 11, 1552–1562. doi: 10.1002/cbic.201000086

Vilela, S. F., Barbosa, J. O., Rossoni, R. D., Santos, J. D., Prata, M. C., Anbinder, A. L., et al. (2015). *Lactobacillus acidophilus* ATCC 4356 inhibits biofilm

formation by *C. albicans* and attenuates the experimental candidiasis in *Galleria mellonella*. *Virulence* 6, 29–39. doi: 10.4161/21505594.2014.981486

Wang, G., Cui, P., Bai, H., Wei, S., and Li, S. (2019). Late-stage C-H functionalization of nicotinamides for the expedient discovery of novel antifungal leads. *J. Agric. Food Chem.* 67, 11901–11910. doi: 10.1021/acs.jafc.9b05349

Wang, Y., Dai, A., Huang, S., Kuo, S., Shu, M., Tapia, C. P., et al. (2014). Propionic acid and its esterified derivative suppress the growth of methicillin-resistant *Staphylococcus aureus* USA300. *Benef. Microbes* 5, 161–168. doi: 10.3920/BM2013.0031

Zhang, K., Ou, M., Wang, W., and Ling, J. (2009). Effects of quorum sensing on cell viability in *Streptococcus mutans* biofilm formation. *Biochem. Biophys. Res. Commun.* 379, 933–938. doi: 10.1016/j.bbrc.2008.12.175

Zhang, L. W., Fu, J. Y., Hua, H., and Yan, Z. M. (2016). Efficacy and safety of miconazole for oral candidiasis: a systematic review and meta-analysis. *Oral Dis.* 22, 185–195. doi: 10.1111/odi.12380

Conflict of Interest: JJ, DS, JS, LF, and RM have obtained a patent for "Method of obtaining the extract and fractions of the supernatant of *S. mutans* and use of the extract and fractions of the supernatant *S. mutans* as antifungal" [patent number Br 10 2019 019528 2].

The remaining authors declare that the research was conducted in the absence of any commercial or financial relationships that could be construed as a potential conflict of interest.

frontiers in Microbiology

ORIGINAL RESEARCH
published: 28 July 2020
doi: 10.3389/fmicb.2020.01673

Silver Nanoantibiotics Display Strong Antifungal Activity Against the Emergent Multidrug-Resistant Yeast *Candida auris* Under Both Planktonic and Biofilm Growing Conditions

Roberto Vazquez-Munoz[1], Fernando D. Lopez[2] and Jose L. Lopez-Ribot[1]**

[1]South Texas Center for Emerging Infectious Diseases, Department of Biology, The University of Texas at San Antonio, San Antonio, TX, United States, [2]Cockrell School of Engineering, The University of Texas at Austin, Austin, TX, United States

OPEN ACCESS

Edited by:
Juliana Campos Junqueira, São Paulo State University, Brazil

Reviewed by:
Gordon Ramage, University of Glasgow, United Kingdom
Liliana Scorzoni, São Paulo State University, Brazil

***Correspondence:**
Roberto Vazquez-Munoz
roberto.vazquezmunoz@utsa.edu
Jose L. Lopez-Ribot
jose.lopezribot@utsa.edu

Specialty section:
This article was submitted to Fungi and Their Interactions, a section of the journal Frontiers in Microbiology

Received: *09 March 2020*
Accepted: *26 June 2020*
Published: *28 July 2020*

Citation:
Vazquez-Munoz R, Lopez FD and Lopez-Ribot JL (2020) Silver Nanoantibiotics Display Strong Antifungal Activity Against the Emergent Multidrug-Resistant Yeast Candida auris Under Both Planktonic and Biofilm Growing Conditions. Front. Microbiol. 11:1673. doi: 10.3389/fmicb.2020.01673

Candida auris is an emergent multidrug-resistant pathogenic yeast with an unprecedented ability for a fungal organism to easily spread between patients in clinical settings, leading to major outbreaks in healthcare facilities. The formation of biofilms by *C. auris* contributes to infection and its environmental persistence. Most antifungals and sanitizing procedures are not effective against *C. auris*, but antimicrobial nanomaterials could represent a viable alternative to combat the infections caused by this emerging pathogen. We have previously described an easy and inexpensive method to synthesize silver nanoparticles (AgNPs) in non-specialized laboratories. Here, we have assessed the antimicrobial activity of the resulting AgNPs on *C. auris* planktonic and biofilm growth phases. AgNPs displayed a strong antimicrobial activity against all the stages of all *C. auris* strains tested, representative of four different clades. Under planktonic conditions, minimal inhibitory concentration (MIC) values of AgNPs against the different strains were <0.5 μg ml^{-1}; whereas calculated IC_{50} values for inhibition of biofilms formation were <2 μg ml^{-1} for all, but one of the *C. auris* strains tested. AgNPs were also active against preformed biofilms formed by all different *C. auris* strains, with IC_{50} values ranging from 1.2 to 6.2 μg ml^{-1}. Overall, our results indicate potent activity of AgNPs against strains of *C. auris*, both under planktonic and biofilm growing conditions, and indicate that AgNPs may contribute to the control of infections caused by this emerging nosocomial threat.

Keywords: nanoantibiotics, *Candida auris*, biofilms, metallic nanoparticles, silver nanoparticles, antimicrobial nanomaterials

INTRODUCTION

Candida auris is an emergent multidrug-resistant yeast that has been reported worldwide since its detection in Japan in 2009 (Centers for Disease Control and Prevention, 2019). It has been determined that there are four geographic clades of this pathogen, including South Asian (clade I), East Asian (clade II), South African (clade III), and South American (clade IV), which interestingly seemed to have emerged independently in different regions of the world at the same time

(Jeffery-Smith et al., 2017; Rhodes and Fisher, 2019), with a potential fifth clade recently identified in Iran (Chow et al., 2019). *C. auris* is described as an ovoid-shaped non-dimorphic yeast that rarely forms pseudohyphae and exhibits two growing typical phenotypes: aggregative and non-aggregative (Ku et al., 2018; Forsberg et al., 2019). *C. auris* spreads in healthcare settings, posing a risk for hospital patients due to its high mortality rate invasive infections and its healthcare-associated outbreaks (Sears and Schwartz, 2017; Forsberg et al., 2019). It easily contaminates surfaces and medical instrumentation within healthcare facilities for long periods, which poses a risk factor in healthcare facilities worldwide (Sears and Schwartz, 2017). *C. auris* is considered as an urgent threat by the Centers for Disease Control and Prevention (CDC), according to their "Antibiotic Resistance Threats in the United States, 2019" (CDC, 2019a).

Currently, the prevention and treatment of *C. auris* are challenging due to several factors. This yeast is known for its resistance to the main classes of clinically-used antifungal agents, and it is usually found as resistant to multiple drugs; also, its antifungal resistance profile is different in each strain (CDC, 2019b), which negatively impact treatment's effectivity. Additionally, it is commonly misidentified in clinical laboratories, often leading to inappropriate treatments. Furthermore, it is able to form biofilms, *C. auris* biofilms, besides being intrinsically resistant to all antifungal agents (Sherry et al., 2017), can also withstand exposure to harsh setting conditions, such as high temperature and salinity concentration, and can survive in plastic surfaces up to 2 weeks (Welsh et al., 2017). This yeast is highly resistant to current sanitation processes and treatments, such as UV light and quaternary ammonium compounds (Ku et al., 2018), which defy our capacity to control its propagation.

Therefore, new treatments are needed to prevent and control *C. auris* growth and dissemination. Nanotechnology can provide new cost-effective antimicrobial nanomaterials (nanoantibiotics) that work as disinfectants and antimicrobial drugs. In particular, silver nanoparticles (AgNPs) exhibit good antimicrobial properties with a wide range of action against a broad range of microorganisms, including several *Candida* species (Raghunath and Perumal, 2017; Vazquez-Muñoz et al., 2017). Additionally, nanoantibiotics can overcome the microbial drug-resistance to antibiotics (Rudramurthy et al., 2016; Vazquez-Muñoz et al., 2019b). However, to date, only one report from our group has described the effect of AgNPs (synthesized using a different method) against a single isolate of *C. auris* in suspension and on functionalized medical and environmental surfaces (Lara et al., 2020). This study demonstrated that AgNPs effectively inhibit the *C. auris* biofilm formation. Additionally, a non-nanostructured silver commercial formulation [0.01% silver nitrate ($AgNO_3$) with 11% hydrogen peroxide] was shown to be effective against *C. auris* (Biswal et al., 2017).

We have recently reported on a modified facile, inexpensive synthetic method to generate AgNPs in non-specialized laboratories and described their antibacterial and antifungal properties. We hypothesize that AgNPs display strong antifungal activity against multiple strains of *C. auris*, regardless of their clade, antibiotic-resistant profile, or morphological traits. Therefore, the objective of this study was to assess the antimicrobial activity of AgNPs synthesized using our newly described method, on different *C. auris* strains, for which we have evaluated the antimicrobial activity of nanoantibiotics against 10 *C. auris* strains from the CDC panel, representing the four different major clades, both under planktonic and biofilm growing conditions.

Abbreviations: AgNPs, Silver nanoparticles; MIC, Minimal inhibitory concentration; MFC, Minimal fungicidal concentration; IC_{50}, Inhibitory concentration that reduces the microbial activity (XTT reading) by 50%; SEM, Scanning electron microscopy; CDC, Centers for disease control and prevention.

MATERIALS AND METHODS

Reagents

Roswell Park Memorial Institute (RPMI) 1640 culture medium, phosphate saline buffer (PBS), 2,3-bis (2-methoxy-4-nitro-5-sulfophenyl)-2H-tetrazolium-5-carboxanilide salt (XTT) (0.5 g L^{-1}, in PBS), and menadione (for 3 μM final concentration) (Pierce et al., 2008) were acquired from Sigma-Aldrich (MO). Osmium tetroxide (OsO_4; 4% solution) and glutaraldehyde (2.5% solution) were acquired from Ted Pella, Inc. Solutions of the different reagents were prepared in Milli-Q water.

Silver Nanoparticles

AgNPs coated with polyvinylpyrrolidone (PVP) were synthesized by a chemical reduction protocol, reported previously by our group (Vazquez-Muñoz et al., 2019a). The synthesis method uses a simple and fast chemical reduction process that involves the addition of PVP to a warmed $AgNO_3$ solution, followed by sodium borohydride. The AgNPs obtained have an aspect ratio close to 1, an average size of 6.18 ± 5 nm and a zeta potential score of −16.2 mV. The negatively-charged, small, spheroid AgNPs displayed the strong antimicrobial activity against *Staphylococcus aureus* and *Candida albicans* (Vazquez-Muñoz et al., 2019a). This easy-to-replicate-synthesis method was specifically developed so that it can be readily implemented in non-specialized facilities and laboratories.

Strains and Culture Conditions

C. auris strains were acquired from the CDC antimicrobial resistance (AR) Isolate Bank stock (CDC, 2019b).The following AR bank strains were used: clade I (#0382, #0387, #0388, #0389, and #0390), clade II (#0381), clade III (#0383 and #0384), and clade IV (#0385 and #0386). Frozen glycerol stocks of the microbial cells were subcultured onto Yeast extract-Peptone-Dextrose (YPD) (BD Difco, MD, USA) agar plates, for 48 h at 37°C. Then, *C. auris* was cultured into YPD liquid media overnight at 30°C, in an orbital shaker. Cells from these cultures were prepared for the susceptibility tests, as described in the following sections.

Antifungal Susceptibility Testing Under Planktonic Conditions

The antimicrobial activity of the nanoparticles on the *C. auris* planktonic cells was determined by following the guidelines from the CLSI M27 protocol (CLSI, 2017) for *Candida* species,

with minor modifications. Briefly, the yeast cells were washed twice in PBS, counted in a Neubauer chamber, and adjusted for a final concentration of 10^3 cells ml^{-1} in RPMI culture media. Then, 50 µl of the *C. auris* strains was inoculated in 96 multi-well round-bottom plates (Corning Inc., Corning, NY, USA). AgNPs were prepared in a two-fold dilution series in RPMI, and then 50 µl of the dilution series was added to the plates with the yeast, for final AgNPs concentration range from 0.5 to 256 µg ml^{-1}. Plates were incubated at 35°C for 48 h. The minimal inhibitory concentration (MIC) was set as the concentration in the well at which no microbial growth – turbidity or microbial pellet formation – were observed, as suggested by the CLSI guidelines. The minimal fungicidal concentration (MFC) was also established, as follows: after reading the MIC in each plate, 10 µl from each well containing the untreated and treated microbial cells was reinoculated in YPD agar plates and incubated for 24 h at 37°C. The MFC was set as the lowest concentration of nanoparticles for which growth of ≤2 colony-forming units (CFUs) was observed upon plating, corresponding to the killing of 99.9% of the initial inoculum (Cantón et al., 2009). To ensure reproducibility, the experiment was independently performed by two people, on separate days, using different batches of AgNPs and *C. auris* cultures. Experiments were performed using duplicates of the plates, which contained triplicates of each condition.

Antibiofilm Activity Assays

The antibiofilm activity of AgNPs was evaluated in both the biofilm formation phase and on the preformed biofilm, as previously reported by our group (Pierce et al., 2008). For inhibition of biofilm formation, overnight cultures of *C. auris* yeast cells were washed twice in PBS and adjusted to 2×10^6 cells ml^{-1} in RPMI culture media. Fifty microliter of the adjusted cell suspension was transferred to 96 multi-well flat-bottom plates (Corning Inc., Corning, NY, USA). Then, 50 µl of AgNPs prepared in a two-fold dilution series was added into multi-well plates, for a final concentration range from 0.5 to 256 µg ml^{-1}, with appropriate positive and negative controls. The plates were then incubated at 37°C for 24 h to allow for biofilm formation. We also tested the activity against preformed biofilms. Briefly, cells from overnight liquid cultures were washed twice in PBS and adjusted to 1×10^6 cells ml^{-1} in RPMI. Then, 100 µl of the microbial suspension was inoculated into 96-multi-well plates, and then incubated for 24 h at 37°C. After incubation, the preformed biofilms were washed twice in PBS. Then, 100 µl of AgNPs in two-fold dilutions series (prepared in RPMI culture medium and resulting in final concentration ranging from 512 to 1 µl ml^{-1}) was transferred to the wells of the microtiter plates with the preformed biofilms. Finally, the plates were incubated at 37°C for an additional 24 h.

The AgNPs anti-biofilm activity was determined using the XTT colorimetric method (Pierce et al., 2008) for both inhibition of biofilm formation and the preformed biofilm stages. Briefly, at the end of the procedure, biofilms were washed twice with PBS, and then 100 µl XTT/menadione was added to each well containing treated and untreated biofilms and in the empty wells (blank). Plates were protected from light and incubated at 37°C for 2 h. XTT absorbance was measured at λ = 490 nm in a Benchmark microplate reader (Bio-Rad, Inc.). From the collected data, we generated dose-response curves to assess the IC_{50} values – the drug concentration required to reduce the biofilm activity by 50% – , by fitting the normalized results to the variable slope Hill equation (for assessing the nonlinear dose-response relationship) using Prism 8 (GraphPad Software, Inc.). To verify the reproducibility of the antibiofilm activity, the experiment was independently repeated by two different people. AgNPs from different rounds of syntheses were tested using two replicates of multi-well plates, each with three replicates of the treatments.

Ultrastructural Analysis

We assessed the effect of AgNPs on the biofilm structure in all *C. auris* strains from the four clades, using the biofilm inhibition assays. The biofilms were treated with sublethal (yet still inhibitory) concentrations of AgNPs. Treated and untreated (control) biofilms structural analysis was performed using optical and scanning electron microscopy. Biofilms were washed twice with PBS, and then fixed with a 2.5% glutaraldehyde solution for 3 h at 4°C. For the optical microscopy observations, the glutaraldehyde-fixed biofilms were observed under a 400× magnification using the bright field mode, in an inverted optical microscope (Fisher Scientific). For the scanning electron microscopy analysis, the glutaraldehyde-fixed biofilms were postfixed and stained with a 1% OsO_4 solution, for 2.5 h at 4°C. Then, the biofilms were dehydrated in an ascending concentration ethanol series, from 30 to 100%. Finally, the ethanol was completely removed, and the dried samples were coated with gold, with 25 mA current for 3 min, in a sputter coater SC7620 (Quorum Technologies). The gold-coated biofilms were observed in a TM4000Plus scanning electron microscope (SEM) (Hitachi Inc.), with magnifications 500 and 2,500×, at a voltage of 10 KeV in the high vacuum mode. The samples were prepared in duplicates, and different fields of both replicates from each sample were observed.

RESULTS

Silver Nanoparticles Inhibit the Planktonic Growth of *C. auris*

AgNPs exerted the strong antimicrobial activity against all the *C. auris* strains growing under planktonic conditions. Against 9 out of 10 strains, AgNPs MIC values were <0.5 µg ml^{-1}, and the MFC values were only slightly higher, ranging from 1 to 2 µg ml^{-1} for all strains, except for AR #0381 strain, which had an elevated MFC of 32 µg ml^{-1}. AgNPs MIC and MFC values against each strain are summarized in **Table 1**.

Silver Nanoparticles Inhibit *C. auris* Biofilm Formation

AgNPs exhibited a strong activity to prevent biofilm formation in *C. auris*, regardless of the clade. **Figure 1** shows the biofilm-inhibitory effect against representative isolates from each clade, including strains AR #0381 (clade I), #0383 (clade III), #0386 (clade IV), and #0390 (clade II). The AgNPs antibiofilm activity

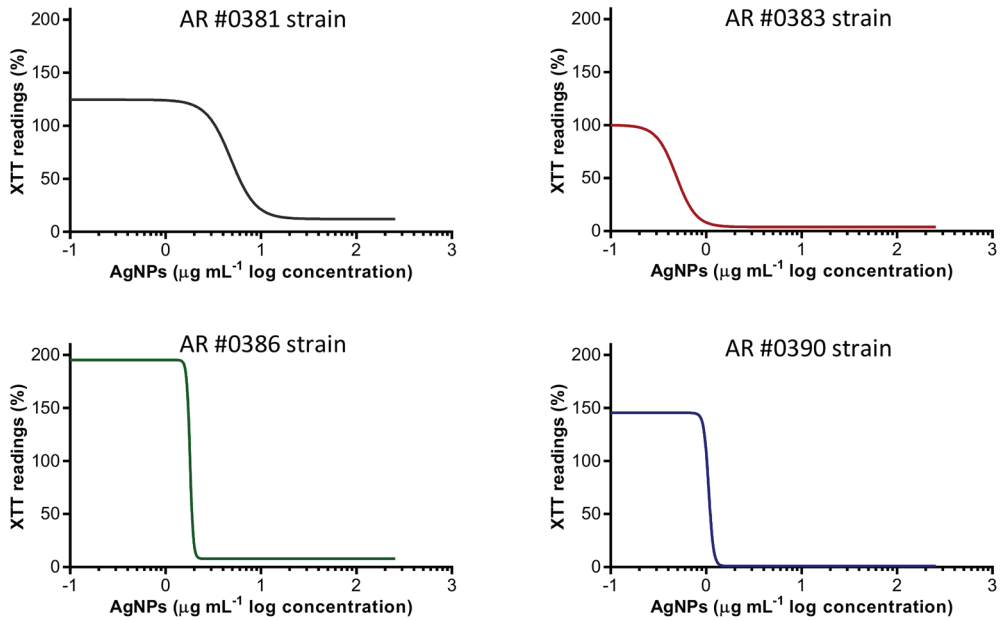

FIGURE 1 | Silver nanoparticles (AgNPs) inhibit the biofilm formation on *C. auris*. The dose-response curves show that AgNPs display potent inhibitory activity (expressed as XTT) readings against the *C. auris* AR #0381 (clade I), #0383 (clade III), #0386 (clade IV), and #0390 (clade II) strains during the biofilm formation phase.

TABLE 1 | Minimal inhibitory concentration (MIC)/minimal fungicidal concentration (MFC) values of silver nanoparticles (AgNPs) against *Candida auris* strains under planktonic growth conditions.

Strains		MIC ($\mu g\ ml^{-1}$)	MFC ($\mu g\ ml^{-1}$)
AR Bank #	Clade		
#0381	II	≤0.5	32
#0382	I	1	1
#0383	III	≤0.5	1
#0384	III	≤0.5	1
#0385	IV	≤0.5	1
#0386	IV	≤0.5	2
#0387	I	≤0.5	2
#0388	I	≤0.5	2
#0389	I	≤0.5	2
#0390	I	≤0.5	1

Clade I (South Asia), clade II (East Asia), clade III (Africa), and clade IV (South America).

TABLE 2 | Calculated IC_{50} values for AgNPs against *C. auris* biofilms by the different strains.

Strains	Clade	Inhibition of biofilm formation ($\mu g\ ml^{-1}$)	Preformed biofilms ($\mu g\ ml^{-1}$)
0381	II	4.9	2.8
0382	I	0.9	6.2
0383	III	0.5	1.8
0384	III	1.0	1.9
0385	IV	1.8	3.9
0386	IV	1.8	3.8
0387	I	1.0	1.9
0388	I	1.5	2.4
0389	I	0.9	1.2
0390	I	1.1	3.9

Clade I (South Asia), clade II (East Asia), clade III (Africa), and clade IV (South America).

against all 10 strains tested is shown in **Supplementary Figure S1A**. The calculated IC_{50} values were ranged from 0.5 to 4.9 $\mu g\ ml^{-1}$ (**Table 2**), and for 9 out of 10 strains, the IC_{50} values were <2 $\mu g\ ml^{-1}$. These results indicate that AgNPs exert a potent activity for the prevention of biofilm formation by the different *C. auris* strains.

Interestingly, we observed that some strains exhibited a significant increase in the biofilm activity (determined by the XTT readings) when grown in the presence of very low concentrations of AgNPs. This effect was consistently observed in all replicates, although with different degrees of intensity. To the extent of our knowledge, this phenomenon has not been observed in yeasts treated with AgNPs, but it has been previously reported in bacteria (Kumar-Krishnan et al., 2015). Nevertheless, this increase in activity is promptly extinguished at just slightly higher concentrations of AgNPs. Additionally, to assess if the augmented activity was specific to the AgNPs, we evaluated the influence of $AgNO_3$ on the *C. auris* AR #0390 strain, under the same culture conditions used for the AgNPs susceptibility assays. We observed an increase in the biofilm activity in subinhibitory concentrations of silver ions (**Supplementary Figure S2**).

Silver Nanoparticles Display Antibiofilm Activity Against Preformed *C. auris* Biofilms

AgNPs displays potent activity against fully mature, preformed biofilms of *C. auris*, irrespective of their clade, as observed for representative isolates AR #0381 (clade I), #0383 (clade III), #0386 (clade IV), and #0390 (clade II) (**Figure 2**). The AgNPs activity on the preformed biofilms from all 10

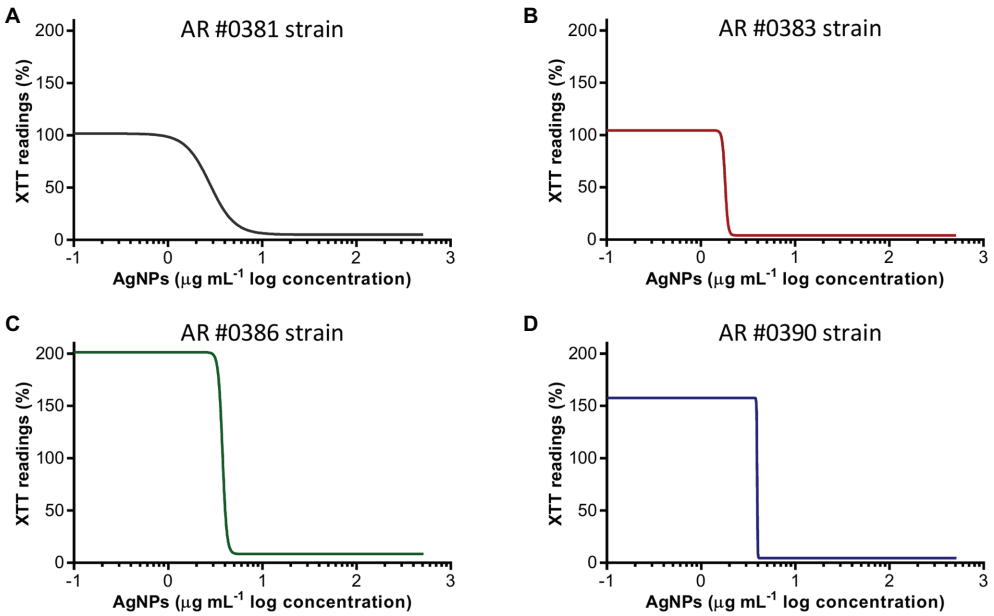

FIGURE 2 | Antibiofilm activity of AgNPs against *C. auris* preformed biofilms. The dose-response curves show that AgNPs display potent inhibitory activity (expressed as the XTT readings) against preformed biofilms of the *C. auris* AR #0381 from clade I **(A)**, #0383 from clade III **(B)**, #0386 from clade IV **(C)**, and #0390 from clade II **(D)** strains.

C. auris strains tested is shown in **Supplementary Figure S1B**. From the dose-response experiments, the resulting calculated IC_{50} values of AgNPs against preformed biofilms of the different *C. auris* strains were ranged from 1.2 to 6.2 μg ml^{-1} (**Table 2**), and were <4 μg ml^{-1} for 9 out of the 10 strains. As with the biofilm-inhibitory assays described before, we also observed an increase in the biofilm activity (determined by the XTT readings) at very low AgNPs concentrations (**Figure 2**; **Supplementary Figure S2**).

Alterations of *C. auris* Biofilm Structure Due to the Inhibitory Activity of AgNPs

Once we had established the activity of AgNPs against *C. auris* biofilms, we were interested in the visualization of the effects of treatment with these nanoantibiotics exerted on the overall biofilm structure, as well as on individual cells within the biofilms. Thus, in another set of experiments, we grew biofilms of the all different *C. auris* strains in the presence of subinhibitory concentrations of the AgNPs, with results for a representative strain from each clade shown in **Figures 2**–**5**, corresponding to strains #0381 (East Asia clade), #0383 (Africa clade), #0386 (South America clade), and #0390 (South Asia clade), respectively. Optical microscopy revealed that AgNPs decrease the ability of *C. auris* to form biofilms. As seen in **Supplementary Figure S3**, in the untreated control samples, biofilms formed by the different strains uniformly covered most of the bottom of the wells in the microtiter plates. In contrast, inhibitory concentrations of AgNPs disrupt the biofilm formation in all *C. auris* strains, as revealed by the noticeable reduction of the coverage area of biofilms on the bottom of the wells. At higher concentrations of AgNPs, biofilm formation was drastically reduced, with only isolated cells scattered on the bottom of the wells being visible under the microscope.

The biofilms were observed using SEM at low (500×) and high (2,500×) magnifications, to further determine the effect of treatment with AgNPs on the biofilm structure and the cell morphology. *C. auris* strains from the distinct clades display differences in the cell morphology and the biofilm organization. SEM images confirmed that exposure to inhibitory concentrations of AgNPs decreases the biofilm forming ability of the different *C. auris* strains (**Figures 3**–**6**; **Supplementary Figure S4**). SEM micrographs showed that untreated biofilms display a uniform distribution with a tight clustering of cells; in contrast, AgNPs-treated biofilms cover a noticeably lesser area, and the cells appear to be less clustered. This finding is similar to that reported recently by Lara et al. (2020), for *C. auris* strain #0390 when exposed to a different type of AgNPs (Lara et al., 2020).

Moreover, when observed at higher magnification, it was revealed that treatment with AgNPs damages the fungal cell structure. In the control (untreated) samples, cells within the biofilms formed by strains #0381 (**Figure 3**), #0383 (**Figure 4**), and #0386 (**Figure 5**) displayed a typical oval yeast shape, whereas those in biofilms formed by strain #0390 (**Figure 6**) mostly exhibited a more elongated (almost pseudohyphal) morphology. For all the strains, inhibitory concentrations of AgNPs caused alterations in the shape and size of individual cells within the biofilms with also less cell clustering observed. In the case of *C. auris* strain #0386, low concentrations of AgNPs induced elongation of the shape in the yeast cells, similar to the pseudohyphae. However, when exposed to a higher concentration of AgNPs, the cell shape becomes spheroid, and no yeast- or pseudohyphae-shaped cells were observed (**Figure 5**).

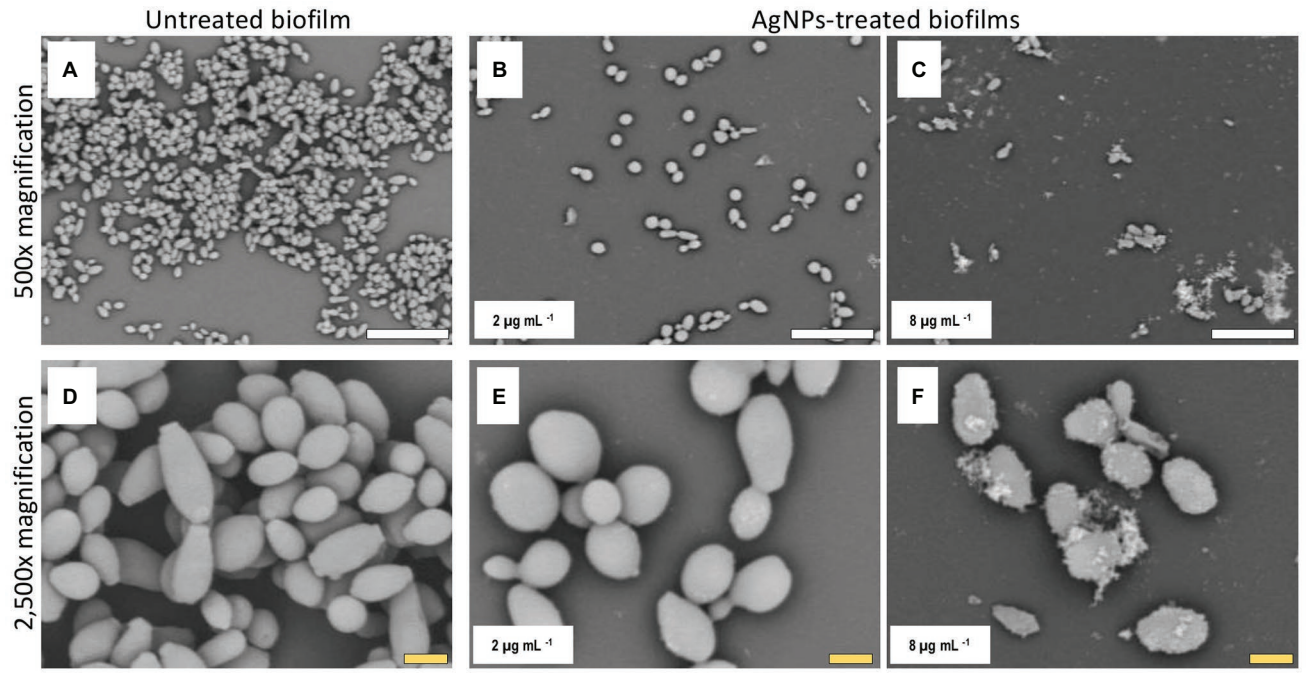

FIGURE 3 | AgNPs affect biofilm structure and cellular morphology of *C. auris* strain #0381. Scanning electron microscope (SEM) micrographs reveal that untreated biofilms have a larger area of distribution **(A)** than the AgNPs-treated biofilms **(B,C)**. Also, the shape and size of the cells are affected by the AgNPs **(E,F)**, whereas the untreated biofilms remain unaltered **(D)**. Scale bar: white = 20 μm, yellow = 2 μm.

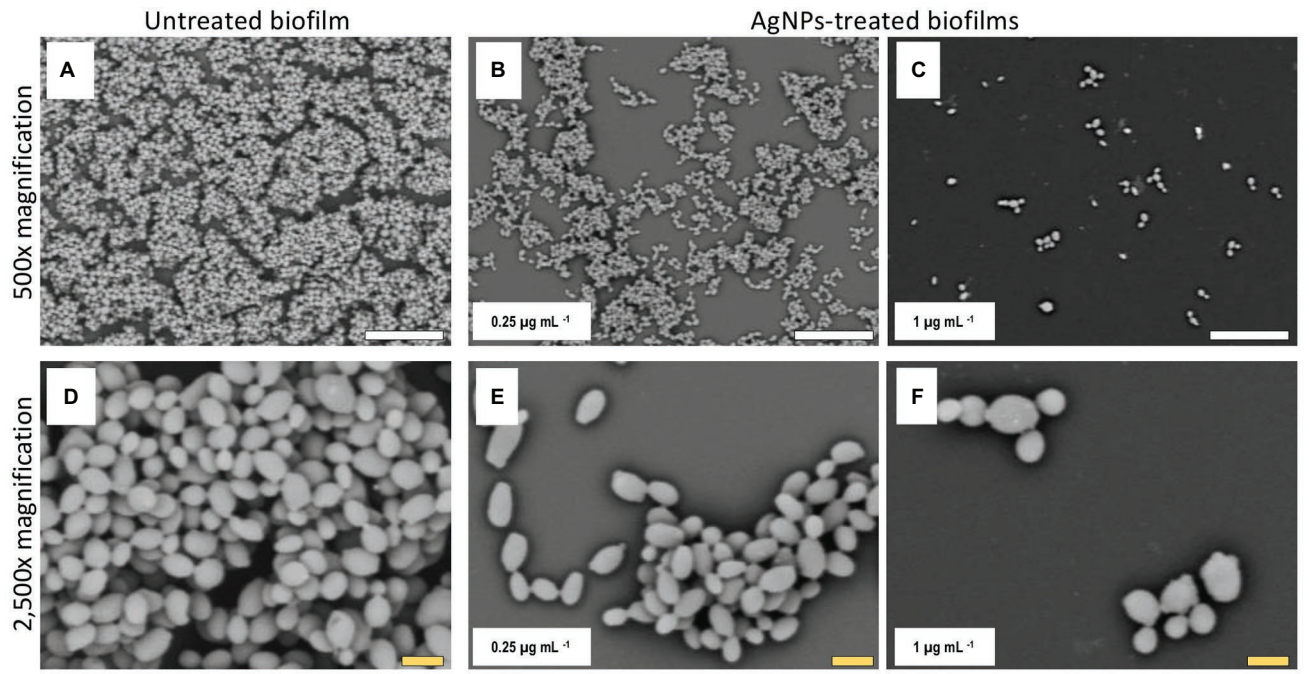

FIGURE 4 | AgNPs reduce biofilm formation of *C. auris* strain #0383. SEM micrographs show a noticeable reduction in the biofilm formation in the AgNPs-treated biofilms **(B,C)** when contrasted with the untreated biofilms **(A)**. However, the impact on cell morphology appears to be minimal **(E,F)**, as the cell shape and size of cells within the treated biofilms are similar to those of the untreated control **(D)**. Scale bar: white = 20 μm, yellow = 2 μm.

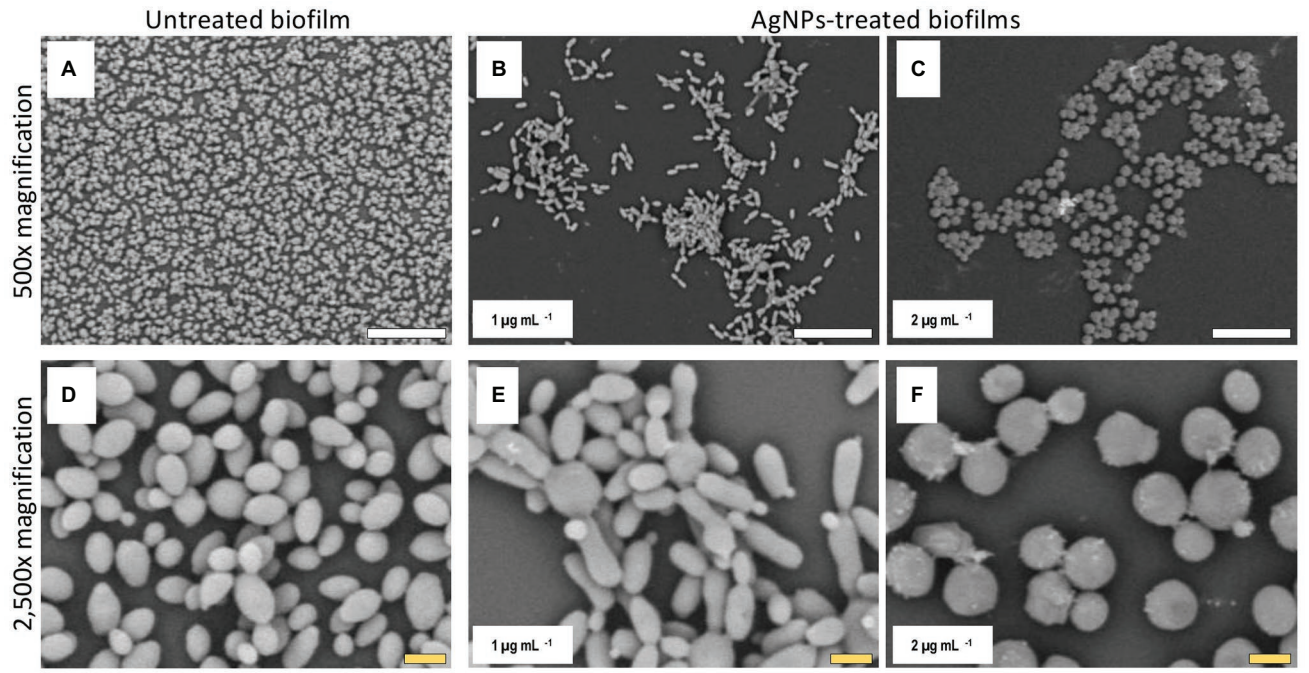

FIGURE 5 | AgNPs affect biofilm structure and cellular morphology of *C. auris* strain #0386. SEM micrographs show that biofilms and individual cell morphology are drastically affected by the AgNPs. Treated biofilms **(B,C)** show an evident decrease in coverage area as compared to untreated biofilms **(A)**, whereas the cell morphology is changed by treatment with AgNPs **(E,F)** as compared to cells in untreated biofilms **(D)**. Scale bar: white = 20 μm, yellow = 2 μm.

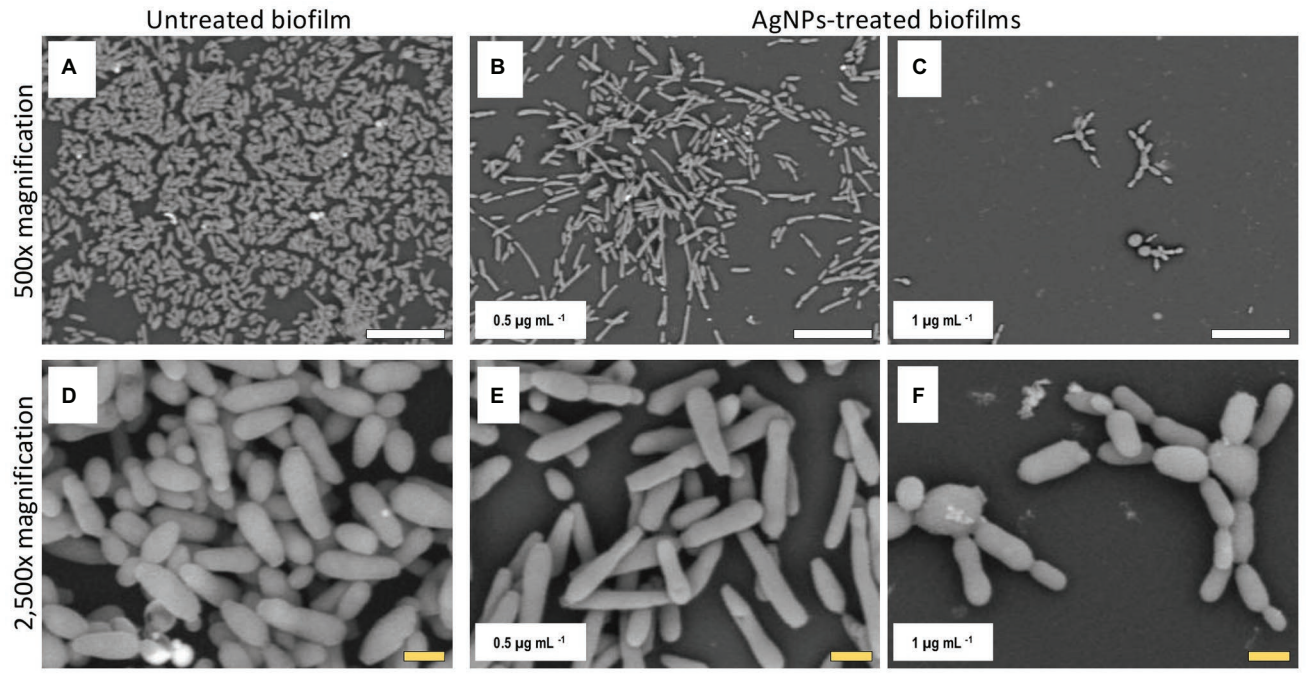

FIGURE 6 | AgNPs affect biofilm structure and cellular morphology of *C. auris* strain #0390. The SEM micrographs of *C. auris* #0390 strain reveal that untreated biofilms **(A)** display a larger area of coverage than the AgNPs-treated biofilms **(B,C)**. Moreover, untreated cells display pseudohyphae-like shape **(D)**, which is also observed at the lowest concentration of AgNPs **(E)**, but higher concentrations of AgNPs induce an aberrant morphology on cells and reduce the cell separation process **(F)** as compared to cells in untreated biofilms **(D)**. Scale bar: white = 20 μm, yellow = 2 μm.

In contrast, in the *C. auris* strain #0390, low concentrations of AgNPs induce enlargement of the pseudohyphae-shaped cells, growing longer than in the control (**Figure 6**), and their presence appears to be relatively higher. However, at higher concentrations of AgNPs, the cells of this strain become yeast-shaped again but with aberrant morphology. Also, in several instances, yeast cells remained attached to each other after cell division, leading to the formation of small multibranched chains of cells, typically in groups of less than 10 cells. **Supplementary Figure S3** includes SEM observations for the reminder of *C. auris* strains, with similar effects on biofilm structure and cellular morphology (**Supplementary Figure S4**).

DISCUSSION

Silver Nanoparticles Inhibit the Planktonic Growth of *C. auris*

Our results show that AgNPs display potent antifungal activity at very low concentrations in virtually all *C. auris* strains tested. However, AgNPs MFC was higher in strain AR #0381 (32 μg ml^{-1}). AR 0381 is the only strain from clade II and might have particular biological mechanisms that allow it to withstand the AgNPs killing effect, even when its growth is still prevented at very low concentrations of AgNPs. In a previous report (Vazquez-Muñoz et al., 2019a), similarly synthesized AgNPs exhibited strong antibacterial and antifungal activities. The MIC for *S. aureus* was 4 μg ml^{-1}, whereas for *C. albicans*, the MIC was 2 μg ml^{-1}, which is similar to the most common antifungals. It is worth noting that all *C. auris* strains are more susceptible to the AgNPs than *C. albicans* tested under similar experimental conditions. Also, the anti-*Candidal* activity of these AgNPs against planktonic cells of *C. auris* parallels other studies using different nanoparticles against different *Candida* species with typical MIC values in the 1–10 μg ml^{-1} range (Monteiro et al., 2011; Wady et al., 2014; Patra and Baek, 2017; Vazquez-Muñoz et al., 2017). Moreover, all *C. auris* strains tested here displayed susceptibility to AgNPs, irrespective of their growth characteristics, susceptibility profiles against conventional antifungal, geographical origin (clade), or their ability to form aggregates in planktonic *in vitro* cultures. Borman's group showed that some clades (South African) form aggregates when grown *in vitro*, whereas other clades (South Asian) do not display that ability. Moreover, the aggregating phenotype may be associated with their drug susceptibility (Szekely et al., 2019). This has been observed in other microorganisms, including other *Candida* species, where the drug-resistant strains and drug-sensitive strains from the same species display a similar susceptibility (MIC value) to AgNPs (Romero-Urbina et al., 2015; Perween et al., 2019). Additionally, our results suggest that AgNPs antimicrobial performance is better than the main antifungals on all the tested *C. auris* CDC AR strains, according to their antifungal susceptibility profile reported by the CDC (CDC, 2020). Although there are not established MIC breakpoints for the main available antifungals against *C. auris*, the tentative MIC breakpoints for some of them are the following: fluconazole >32 μg ml^{-1}, amphotericin B >2 μg ml^{-1}, caspofungin >2 μg ml^{-1}, and micafungin >4 μg ml^{-1} (CDC, 2020). The AgNPs MIC (<0.5 μg ml^{-1}) outperforms even the most potent antifungal drug.

This may be due to the proposed mechanisms of action of AgNPs. The mechanism of action of the antifungal drugs is linked to specific molecular targets that disrupt the cell metabolism or structure, affecting growth. In response to these stresses, specific but relatively small changes at the structural or molecular level may increase their probability to resist the action of antifungals, as previously described for *C. auris* (Krishnasamy et al., 2018; Chaabane et al., 2019). In contrast, AgNPs cause several simultaneous types of structural and metabolic damages in the *Candida* cells, such as membrane depolarization (Zamperini et al., 2013), cell wall/membrane disruption (Lara et al., 2015), increase in ROS production (Radhakrishnan et al., 2018), inhibit enzymatic function (Babele et al., 2019), cell arrest (Zamperini et al., 2013), among many others. This massive disruption of cellular structure and function reduces their ability to withstand the AgNPs effects. Therefore, the metabolic/structural differences among the different strains are not significant when the cells from different *C. auris* strains are exposed to AgNPs.

Silver Nanoparticles Inhibit *C. auris* Biofilm Formation

C. auris is capable of forming biofilms that improve their adherence to surfaces (Forsberg et al., 2019) and increase their resistance to antifungal drugs (Sherry et al., 2017; Ku et al., 2018). The mechanisms that enhance their resistance are mostly unknown, but some factors are known to help *C. auris* withstand harsh conditions include the protection by matrix polysaccharides (Dominguez et al., 2019) and the overexpression of efflux pumps (Kean et al., 2018). Thus, the formation of *C. auris* biofilms represents a current threat to both individual patients and healthcare facilities (Sears and Schwartz, 2017). In previous work, we demonstrated the antimicrobial activity of the AgNPs on the planktonic stage of *C. albicans* (Vazquez-Muñoz et al., 2019a), although their activity was not assessed on the biofilm stages. In this work, we evaluate the anti-biofilm activity of the AgNPs during the biofilm formation phase and against fully mature, preformed biofilms.

Our results show that AgNPs exert a potent activity for the prevention of biofilm formation by the different *C. auris* strains, regardless of the clade. Interestingly, these values are only slightly higher than the MIC values obtained under planktonic growth. These values also compare favorably to those described before for conventional antifungals against biofilm formation for some of the same *C. auris* strains (Dekkerová et al., 2019). We note that the AgNPs IC_{50} value for the *C. auris* AR #0390 strain is higher than the value reported for the same strain as reported by Lara et al. (2015) (1.1 vs. 0.06 μg ml^{-1}, respectively), which is most likely related to the different techniques used for the synthesis of these nanoantibiotics resulting in AgNPs with different characteristics. Also, the antibiofilm activity of our AgNPs is comparable to the activity described for AgNPs synthesized

using different methods against other *Candida* species (Lara et al., 2015; Muthamil et al., 2018; Nadhe et al., 2019).

Regarding the increase in the biofilm activity at very low concentrations of AgNPs, this effect on the biofilm activity must be addressed in further studies, to assess any potential disadvantage of low-silver-content products intended against *C. auris* biofilms. As mentioned above, there are commercially available products containing silver (Biswal et al., 2017), and therefore their viability for combat the biofilms of microbial pathogens must be assessed.

Silver Nanoparticles Display Antibiofilm Activity Against Preformed *C. auris* Biofilms

It is well-known that once a biofilm is established, *Candidal* cells within these biofilms display increased susceptibility to most clinically-used antifungal agents (Ramage et al., 2009; Sherry et al., 2017). This is particularly true in the case of *C. auris* biofilms, which are intrinsically resistant to all the three main classes of antifungals (polyenes, azoles, and echinocandins) as well as to physical and chemical sanitizing methods (Sherry et al., 2017; Ku et al., 2018).

AgNPs displayed potent activity against fully mature, preformed biofilms of all *C. auris* AR strains, irrespective of their clade, with calculated IC_{50} values <4 μg ml^{-1} for 9 out of the 10 strains. Interestingly, these values are similar (typically within one-fold dilution) to those observed for the same strains in the case of biofilm inhibition (compare values in both columns of **Table 2**). Therefore, in stark contrast with conventional antifungal agents, the AgNPs potency does not seem to be particularly reduced after the biofilm has reached maturity. Moreover, the AgNPs antifungal activity against the preformed biofilms is equivalent or even better to that of conventional antifungals. For the *C. auris* AR strains #0383, #0386, and #0390, the AgNPs antibiofilm activity is superior to the activity of fluconazole (range from >64 to >1,024 μg ml^{-1}) and caspofungin (>16 μg ml^{-1}). Furthermore, the AgNPs potency parallels the activity of amphotericin B (1–>8 μg ml^{-1}) (Dekkerová et al., 2019; Nadhe et al., 2019). Overall, although multiple mechanisms confer resistance of cells within biofilms against conventional antifungal agents (Srinivasan et al., 2014), our results suggest that these do not equally affect the anti-biofilm activity of AgNPs.

Alterations of *C. auris* Biofilm Structure Due to the Inhibitory Activity of AgNPs

The observed effects of AgNPs on cellular morphology merit some further discussions. These effects seem to be clade-related, based on our SEM analysis for the 10 strains included in this study. Both strains from clade III (South Africa) were not affected in their cellular morphology. In contrast, in both strains from clade IV (South America), inhibitory concentrations of the AgNPs altered the cell shape, leading to round-shaped cells. Interestingly, in clade I (South Asia), we observed two different effects: in strains AR #0382 and #0387, the cells were altered, from the typical yeast shape to a more elongated, pseudohyphae-like shape and was not uncommon to observe mother-daughter cells attached to each other; whereas cells from strains AR #0388, #0389, and #0390 acquire an aberrant morphology and form small multibranched chains as a result of treatment with AgNPs. In the case of *C. auris* strain AR #0381, the only one from clade II (East Asia), the cells became aberrant but remained separate from each other. Other studies have shown that AgNPs disrupt the biofilm and the cell ultrastructure in other *Candida* species, particularly on *C albicans* (Zamperini et al., 2013; Vazquez-Muñoz et al., 2014; Lara et al., 2015), but the effect on other morphological traits, as the cell wall thickness, extracellular matrix integrity, and intracellular bioaccumulation of cells remained to be further studied.

AgNPs are among the most used nanomaterials for health-related and cosmetic applications worldwide (Vance et al., 2015). AgNPs have been used to control skin infections *in vivo* in wound dressings to treat burn wounds and are used in healthcare and cosmetic applications (Sim et al., 2018). Our results suggest that AgNPs may be used as sanitizers and potentially in future uses to control skin colonization and contribute to control of the nosocomial spread of this emerging pathogen. However, the potential toxicity of these specific nanoantibiotics is still to be addressed before their direct applications in human patients. Research regarding the toxicity and effects *in vivo* of AgNPs is still a challenging topic, due to the complex interactions of silver with the living tissue, although there is a long use of silver in history (Klasen, 2000a,b). Recently, different studies have been aiming to find a balance between potent antimicrobial properties and toxicity, as AgNPs have several properties of clinical interest (Zivic et al., 2018). However, AgNPs may be applied, where no direct contact with humans is needed, particularly for sanitizing surfaces. Overall, our results indicate that AgNps display potent antimicrobial activity against all *C. auris* strains tested, both under planktonic and biofilm growing conditions. Furthermore, the antimicrobial activity is irrespective of their clade or geographical origin and regardless of their susceptibility and resistance patterns against clinically-used antifungals.

DATA AVAILABILITY STATEMENT

The datasets generated for this study are available on request to the corresponding author.

AUTHOR CONTRIBUTIONS

All authors contributed to the study design and execution, data collection and analysis, and the preparation of the manuscript. All authors have approved the final version of the manuscript.

FUNDING

This research was funded by the Mexican Council of Science and Technology of Mexico (CONACYT, RV-M

postdoctoral scholarship). Support in the laboratory was provided by the Margaret Batts Tobin Foundation, San Antonio, TX, USA. The funders had no role in study design, data collection, and analysis, decision to publish, or preparation of the manuscript, and the content is solely the responsibility of the authors.

ACKNOWLEDGMENTS

We thank the South Texas Center for Emerging Infectious Diseases (STCEID) for the purchase of the SEM microscope used in these studies.

SUPPLEMENTARY MATERIAL

The Supplementary Material for this article can be found online at: https://www.frontiersin.org/articles/10.3389/fmicb.2020.01673/full#supplementary-material.

SUPPLEMENTARY FIGURE S1 | Antibiofilm activity of AgNPs against the different *C. auris* strains. The dose-response curve shows that AgNPs display potent inhibitory activity against all the different *C. auris* strains included in this study, including inhibition of biofilm formation **(panel A)** and against preformed biofilms **(panel B)**.

SUPPLEMENTARY FIGURE S2 | Silver compounds exhibit a paradoxical effect on *C. auris* biofilms at low concentrations. Incubation in the presence of low subinhibitory concentrations of AgNO3 and AgNPs lead to an increase in biofilm activity (XTT readings) for biofilms formed by *C. auris* strain #0390 strain. In contrast to silver ions, this effect rapidly disappears in the case of AgNPs, turning into potent inhibitory activity at still relatively low concentrations.

SUPPLEMENTARY FIGURE S3 | AgNPs reduce the biofilm formation in *C. auris*. Optical microscopy images reveal that subinhibitory concentrations AgNPs reduce the ability of *C. auris* to form biofilms – as seen in the reduced area of biofilm surface coverage – when compared with their respective untreated controls.

SUPPLEMENTARY FIGURE S4 | Ultrastructure analysis of the *C. auris* biofilms. SEM images reveal that subinhibitory concentrations of AgNPs reduce the biofilm formation on all *C. auris* strains. Also, AgNPs negatively alter the shape and size in some *C. auris* strains (#0382, #0385, #0387, #0388, and #0389 strains). The effect on morphology is clade-related. Scale bar = 2 μm.

REFERENCES

Babele, P. K., Singh, A. K., and Srivastava, A. (2019). Bio-inspired silver nanoparticles impose metabolic and epigenetic toxicity to *Saccharomyces cerevisiae*. *Front. Pharmacol.* 10:1016. doi: 10.3389/fphar.2019.01016

Biswal, M., Rudramurthy, S. M., Jain, N., Shamanth, A. S., Sharma, D., and Jain, K. (2017). Controlling a possible outbreak of *Candida auris* infection: lessons learnt from multiple interventions. *J. Hosp. Infect.* 97, 363–370. doi: 10.1016/j.jhin.2017.09.009

Cantón, E., Espinel-Ingroff, A., and Pemán, J. (2009). Trends in antifungal susceptibility testing using CLSI reference and commercial methods. *Expert Rev. Anti-infect. Ther.* 7, 107–119. doi: 10.1586/14787210.7.1.107

CDC (2019a). Antibiotic resistance threats in the United States, 2019. Atlanta, GA. Available at: www.cdc.gov/DrugResistance/Biggest-Threats.html. (Accessed February 19, 2020).

CDC (2019b). FDA-CDC antimicrobial resistance isolate bank. CDC website. Available at: https://wwwn.cdc.gov/arisolatebank (Accessed September 3, 2019).

CDC (2020). Antifungal susceptibility testing and interpretation *Candida auris*. Fungal Dis. Available at: https://www.cdc.gov/fungal/candida-auris/c-auris-antifungal.html (Accessed January 15, 2020).

Centers for Disease Control and Prevention (2019). *Candida auris* CDC. CDC Website. Available at: https://www.cdc.gov/fungal/candida-auris/index.html (Accessed August 29, 2019).

Chaabane, F., Graf, A., Jequier, L., and Coste, A. T. (2019). Review on antifungal resistance mechanisms in the emerging pathogen *Candida auris*. *Front. Microbiol.* 10:2788. doi: 10.3389/fmicb.2019.02788

Chow, N. A., De Groot, T., Badali, H., Abastabar, M., Chiller, T. M., and Meis, J. F. (2019). Potential fifth clade of *Candida auris*, Iran, 2018. *Emerg. Infect. Dis.* 25, 1780–1781. doi: 10.3201/eid2509.190686

CLSI (2017). "Chapter 3. Antifungal broth dilutions susceptibility testing process for yeast" in *M27: Reference method for Broth dilution antifungal susceptibility testing of yeasts. 4th Edn.* ed. B. D. Alexander (Wayne, PA: Clinical Laboratory Standards Institute).

Dekkerová, J., Lopez-Ribot, J. L., and Bujdáková, H. (2019). Activity of anti-CR3-RP polyclonal antibody against biofilms formed by *Candida auris*, a multidrug-resistant emerging fungal pathogen. *Eur. J. Clin. Microbiol. Infect. Dis.* 38, 101–108. doi: 10.1007/s10096-018-3400-x

Dominguez, E. G., Zarnowski, R., Choy, H. L., Zhao, M., Sanchez, H., Nett, J. E., et al. (2019). Conserved role for biofilm matrix polysaccharides in *Candida auris* drug resistance. *mSphere* 4, e00680–e00718. doi: 10.1128/mSphereDirect.00680-18

Forsberg, K., Woodworth, K., Walters, M., Berkow, E. L., Jackson, B., Chiller, T., et al. (2019). *Candida auris*: the recent emergence of a multidrug-resistant fungal pathogen. *Med. Mycol.* 57, 1–12. doi: 10.1093/mmy/myy054

Jeffery-Smith, A., Taori, S. K., Schelenz, S., Jeffery, K., Johnson, E. M., Borman, A., et al. (2017). *Candida auris*: a review of the literature. *Clin. Microbiol. Rev.* 31, e00029–e000317. doi: 10.1128/CMR.00029-17

Kean, R., Delaney, C., Sherry, L., Borman, A., Johnson, E. M., Richardson, M. D., et al. (2018). Transcriptome assembly and profiling of *Candida auris* reveals novel insights into biofilm-mediated resistance. *mSphere* 3, 1–12. doi: 10.1128/mSphere.00334-18

Klasen, H. J. (2000a). A historical review of the use of silver in the treatment of burns. II. Renewed interest for silver. *Burns* 26, 131–138. doi: 10.1016/S0305-4179(99)00116-3

Klasen, H. J. (2000b). Historical review of the use of silver in the treatment of burns. I. Early uses. *Burns* 26, 117–130. doi: 10.1016/S0305-4179(99)00108-4

Krishnasamy, L., Krishnakumar, S., Kumaramanickavel, G., and Saikumar, C. (2018). Molecular mechanisms of antifungal drug resistance in *Candida species*. *J. Clin. Diagn. Res.* 12, DE01–DE06. doi: 10.7860/JCDR/2018/36218.11961

Ku, T. S. N., Walraven, C. J., and Lee, S. A. (2018). *Candida auris*: disinfectants and implications for infection control. *Front. Microbiol.* 9:726. doi: 10.3389/fmicb.2018.00726

Kumar-Krishnan, S., Prokhorov, E., Hernández-Iturriaga, M., Mota-Morales, J. D., Vázquez-Lepe, M., Kovalenko, Y., et al. (2015). Chitosan/silver nanocomposites: synergistic antibacterial action of silver nanoparticles and silver ions. *Eur. Polym. J.* 67, 242–251. doi: 10.1016/j.eurpolymj.2015.03.066

Lara, H. H., Ixtepan-Turrent, L., Jose Yacaman, M., and Lopez-Ribot, J. (2020). Inhibition of *Candida auris* biofilm formation on medical and environmental surfaces by silver nanoparticles. *ACS Appl. Mater. Interfaces* 12, 21183–21191. doi: 10.1021/acsami.9b20708

Lara, H. H., Romero-Urbina, D. G., Pierce, C., Lopez-Ribot, J. L., Arellano-Jiménez, M. J., and Jose-Yacaman, M. (2015). Effect of silver nanoparticles on *Candida albicans* biofilms: an ultrastructural study. *J. Nanobiotechnol.* 13:91. doi: 10.1186/s12951-015-0147-8

Monteiro, D. R., Gorup, L. F., Silva, S., Negri, M., de Camargo, E. R., Oliveira, R., et al. (2011). Silver colloidal nanoparticles: antifungal effect against adhered cells and biofilms of *Candida albicans* and *Candida glabrata*. *Biofouling* 27, 711–719. doi: 10.1080/08927014.2011.599101

Muthamil, S., Devi, V. A., Balasubramaniam, B., Balamurugan, K., and Pandian, S. K. (2018). Green synthesized silver nanoparticles demonstrating enhanced *in vitro* and *in vivo* antibiofilm activity against *Candida* spp. *J. Basic Microbiol.* 58, 343–357. doi: 10.1002/jobm.201700529

Nadhe, S. B., Singh, R., Wadhwani, S. A., and Chopade, B. A. (2019). *Acinetobacter* sp. mediated synthesis of AgNPs, its optimization, characterization and synergistic antifungal activity against *C. albicans*. *J. Appl. Microbiol.* 127, 445–458. doi: 10.1111/jam.14305

Patra, J. K., and Baek, K. H. (2017). Antibacterial activity and synergistic antibacterial potential of biosynthesized silver nanoparticles against foodborne pathogenic bacteria along with its anticandidal and antioxidant effects. *Front. Microbiol.* 8:167. doi: 10.3389/fmicb.2017.00167

Perween, N., Khan, H. M., and Fatima, N. (2019). Silver nanoparticles: an upcoming therapeutic agent for the resistant *Candida* infections. *J. Microbiol. Exp.* 7, 49–54. doi: 10.15406/jmen.2019.07.00240

Pierce, C. G., Uppuluri, P., Tristan, A. R., Wormley, F. L., Mowat, E., Ramage, G., et al. (2008). A simple and reproducible 96-well plate-based method for the formation of fungal biofilms and its application to antifungal susceptibility testing. *Nat. Protoc.* 3, 1494–1500. doi: 10.1038/nprot.2008.141

Radhakrishnan, V. S., Mudiam, M. K. R., Kumar, M., Dwivedi, S. P., Singh, S. P., and Prasad, T. (2018). Silver nanoparticles induced alterations in multiple cellular targets, which are critical for drug susceptibilities and pathogenicity in fungal pathogen (*Candida albicans*). *Int. J. Nanomed.* 13, 2647–2663. doi: 10.2147/IJN.S150648

Raghunath, A., and Perumal, E. (2017). Metal oxide nanoparticles as antimicrobial agents: a promise for the future. *Int. J. Antimicrob. Agents* 49, 137–152. doi: 10.1016/j.ijantimicag.2016.11.011

Ramage, G., Mowat, E., Jones, B., Williams, C., and Lopez-Ribot, J. (2009). Our current understanding of fungal biofilms. *Crit. Rev. Microbiol.* 35, 340–355. doi: 10.3109/10408410903241436

Rhodes, J., and Fisher, M. C. (2019). Global epidemiology of emerging *Candida auris*. *Curr. Opin. Microbiol.* 52, 84–89. doi: 10.1016/j.mib.2019.05.008

Romero-Urbina, D. G., Lara, H. H., Velázquez-Salazar, J. J., Arellano-Jiménez, M. J., Larios, E., Srinivasan, A., et al. (2015). Ultrastructural changes in methicillin-resistant *Staphylococcus aureus* induced by positively charged silver nanoparticles. *Beilstein J. Nanotechnol.* 6, 2396–2405. doi: 10.3762/bjnano.6.246

Rudramurthy, G. R., Swamy, M. K., Sinniah, U. R., and Ghasemzadeh, A. (2016). Nanoparticles: alternatives against drug-resistant pathogenic microbes. *Molecules* 21:836. doi: 10.3390/molecules21070836

Sears, D., and Schwartz, B. S. (2017). *Candida auris*: an emerging multidrug-resistant pathogen. *Int. J. Infect. Dis.* 63, 95–98. doi: 10.1016/j.ijid.2017.08.017

Sherry, L., Ramage, G., Kean, R., Borman, A., Johnson, E. M., Richardson, M. D., et al. (2017). Biofilm-forming capability of highly virulent, multidrug-resistant *Candida auris*. *Emerg. Infect. Dis.* 23, 328–331. doi: 10.3201/eid2302.161320

Sim, W., Barnard, R. T., Blaskovich, M. A. T., and Ziora, Z. M. (2018). Antimicrobial silver in medicinal and consumer applications: a patent review of the past decade (2007–2017). *Antibiotics* 7:93. doi: 10.3390/antibiotics7040093

Srinivasan, A., Lopez-Ribot, J. L., and Ramasubramanian, A. K. (2014). Overcoming antifungal resistance. *Drug Discov. Today Technol.* 11, 65–71. doi: 10.1016/j.ddtec.2014.02.005

Szekely, A., Borman, A. M., and Johnsona, E. M. (2019). *Candida auris* isolates of the Southern Asian and South African lineages exhibit different phenotypic and antifungal susceptibility profiles *in vitro*. *J. Clin. Microbiol.* 57, e02055–e02118. doi: 10.1128/JCM.02055-18

Vance, M. E., Kuiken, T., Vejerano, E. P., McGinnis, S. P., Hochella, M. F., and Hull, D. R. (2015). Nanotechnology in the real world: redeveloping the nanomaterial consumer products inventory. *Beilstein J. Nanotechnol.* 6, 1769–1780. doi: 10.3762/bjnano.6.181

Vazquez-Muñoz, R., Arellano-Jimenez, M. J., Lopez, F. D., and Lopez-Ribot, J. L. (2019a). Protocol optimization for a fast, simple and economical chemical reduction synthesis of antimicrobial silver nanoparticles in non-specialized facilities. *BMC. Res. Notes* 12:773. doi: 10.1186/s13104-019-4813-z

Vazquez-Muñoz, R., Avalos-Borja, M., and Castro-Longoria, E. (2014). Ultrastructural analysis of *Candida albicans* when exposed to silver nanoparticles. *PLoS One* 9:e108876. doi: 10.1371/journal.pone.0108876

Vazquez-Muñoz, R., Borrego, B., Juárez-Moreno, K., García-García, M., Mota Morales, J. D., Bogdanchikova, N., et al. (2017). Toxicity of silver nanoparticles in biological systems: does the complexity of biological systems matter? *Toxicol. Lett.* 276, 11–20. doi: 10.1016/j.toxlet.2017.05.007

Vazquez-Muñoz, R., Meza-Villezcas, A., Fournier, P. G. J., Soria-Castro, E., Juarez-Moreno, K., Gallego-Hernández, A. L., et al. (2019b). Enhancement of antibiotics antimicrobial activity due to the silver nanoparticles impact on the cell membrane. *PLoS One* 14:e0224904. doi: 10.1371/journal.pone.0224904

Wady, A. F., Machado, A. L., Foggi, C. C., Zamperini, C. A., Zucolotto, V., Moffa, E. B., et al. (2014). Effect of a silver nanoparticles solution on *Staphylococcus aureus* and *Candida* spp. *J. Nanomater.* 2014, 1–7. doi: 10.1155/2014/545279

Welsh, R. M., Bentz, M. L., Shams, A., Houston, H., Lyons, A., Rose, L. J., et al. (2017). Survival, persistence, and isolation of the emerging multidrug-resistant pathogenic yeast *Candida auris* on a plastic health care surface. *J. Clin. Microbiol.* 55, 2996–3005. doi: 10.1128/JCM.00921-17

Zamperini, C. A., André, R. S., Longo, V. M., Mima, E. G., Vergani, C. E., Machado, A. L., et al. (2013). Antifungal applications of Ag-decorated hydroxyapatite nanoparticles. *J. Nanomater.* 2013, 1–9. doi: 10.1155/2013/174398

Zivic, F., Grujovic, N., Mitrovic, S., Ahad, I. U., and Brabazon, D. (2018). "Characteristics and applications of silver nanoparticles" in *Commercialization of nanotechnologies—A case study approach*. eds. D. Brabazon, E. Pellicer, F. Zivic, J. Sort, M. D. Baró, N. Grujovic et al. (Cham: Springer International Publishing), 227–273. doi: 10.1007/978-3-319-56979-6_10

Conflict of Interest: The authors declare that there the research as performed in the absence of any commercial relationship that may be a potential conflict of interest.

frontiers in Cellular and Infection Microbiology

ORIGINAL RESEARCH
published: 04 August 2020
doi: 10.3389/fcimb.2020.00397

The Postbiotic Activity of *Lactobacillus paracasei* 28.4 Against *Candida auris*

Rodnei Dennis Rossoni[1,2], *Patrícia Pimentel de Barros*[1,2], *Iatã do Carmo Mendonça*[3], *Rebeca Previate Medina*[3], *Dulce Helena Siqueira Silva*[3], *Beth Burgwyn Fuchs*[2], *Juliana Campos Junqueira*[1]* and *Eleftherios Mylonakis*[2]

[1] Department of Biosciences and Oral Diagnosis, Institute of Science and Technology, São Paulo State University/UNESP, São José dos Campos, Brazil, [2] Division of Infectious Diseases, Rhode Island Hospital, Warren Alpert Medical School at Brown University, Providence, RI, United States, [3] Department of Organic Chemistry, Center for Bioassays, Biosynthesis and Ecophysiology of Natural Products, Institute of Chemistry, São Paulo State University, UNESP, Araraquara, Brazil

OPEN ACCESS

Edited by:
Priya Uppuluri, University of California, Los Angeles, United States

Reviewed by:
Taissa Vila, University of Maryland, Baltimore, United States
Vishukumar Aimanianda, Institut Pasteur, France

***Correspondence:**
Juliana Campos Junqueira
juliana.junqueira@unesp.br

Specialty section:
This article was submitted to Fungal Pathogenesis, a section of the journal Frontiers in Cellular and Infection Microbiology

Received: *14 February 2020*
Accepted: *29 June 2020*
Published: *04 August 2020*

Citation:
Rossoni RD, de Barros PP, Mendonça IC, Medina RP, Silva DHS, Fuchs BB, Junqueira JC and Mylonakis E (2020) The Postbiotic Activity of Lactobacillus paracasei 28.4 Against Candida auris. Front. Cell. Infect. Microbiol. 10:397. doi: 10.3389/fcimb.2020.00397

Candida auris has emerged as a medically important pathogen with considerable resistance to antifungal agents. The ability to produce biofilms is an important pathogenicity feature of this species that aids escape of host immune responses and antimicrobial agents. The objective of this study was to verify antifungal action using *in vitro* and *in vivo* models of the *Lactobacillus paracasei* 28.4 probiotic cells and postbiotic activity of crude extract (LPCE) and fraction 1 (LPF1), derived from *L. paracasei* 28.4 supernatant. Both live cells and cells free supernatant of *L. paracasei* 28.4 inhibited *C. auris* suggesting probiotic and postbiotic effects. The minimum inhibitory concentration (MIC) for LPCE was 15 mg/mL and ranges from 3.75 to 7.5 mg/mL for LPF1. Killing kinetics determined that after 24 h treatment with LPCE or LPF1 there was a complete reduction of viable *C. auris* cells compared to fluconazole, which decreased the initial inoculum by 1-logCFU during the same time period. LPCE and LPF1 significantly reduced the biomass ($p = 0.0001$) and the metabolic activity ($p = 0.0001$) of *C. auris* biofilm. There was also a total reduction ($\sim 10^8$ CFU/mL) in viability of persister *C. auris* cells after treatment with postbiotic elements ($p < 0.0001$). In an *in vivo* study, injection of LPCE and LPF1 into *G. mellonella* larvae infected with *C. auris* prolonged survival of these insects compared to a control group ($p < 0.05$) and elicited immune responses by increasing the number of circulating hemocytes and gene expression of antimicrobial peptide galiomicin. We concluded that the *L. paracasei* 28.4 cells and postbiotic elements (LPCE and LPF1) have antifungal activity against planktonic cells, biofilms, and persister cells of *C. auris*. Postbiotic supplementation derived from *L. paracasei* 28.4 protected *G. mellonella* infected with *C. auris* and enhanced its immune status indicating a dual function in modulating a host immune response.

Keywords: probiotic, postbiotic, *Lactobacillus*, *Candida auris*, biofilms

INTRODUCTION

Opportunistic infections are caused by non-pathogenic microorganisms which become pathogenic when the body's defense system is impaired (Riccardi et al., 2019). *Candida* spp. can cause vaginitis, oral candidiasis, cutaneous candidiasis, and candidemia. This genus are responsible the main opportunistic yeast infection in the world (Jacobsen et al., 2012; Wachtler et al., 2012; Martins et al., 2014).

Most of these infections originate from biofilms (Vicariotto et al., 2012; Matsubara et al., 2016a,b), defined as complex and dynamic structures consisting of cells encased in a matrix of extracellular polymeric substances (Serra et al., 2015; Rodrigues M. E. et al., 2019). The adhered cells of the biofilm are protected from the external environment by the extracellular matrix that shields them and contributes to the increased antimicrobial resistance. The development of *Candida* spp. biofilms is one of the main reasons that fungal cells exhibit resistance to antifungals (Davies, 2003; Rodrigues et al., 2016; Cernakova et al., 2019; Rodrigues M. E. et al., 2019). Thus, treatment of infections derived from biofilms represents an important challenge today.

C. auris is a pathogenic yeast associated with invasive infections and it has been reported from 32 countries across six continents within a decade (Chakrabarti and Singh, 2020). Previous studies suggest that this species is highly tolerant to thermal and osmotic stresses, possessing the ability to persistently colonize hospital environments, and thereby causing outbreaks (Rossato and Colombo, 2018; Spivak and Hanson, 2018; Sabino et al., 2020). Recently, the Centers for Disease Control and Prevention (CDC) published a notice to different public health officials informing them of *C. auris* isolation in U.S. patients (Centers for Disease Control and Prevention, 2016; Sekyere and Asante, 2018). The emergence of *C. auris* is concerning because this yeast has or may develop resistance to different antifungal agents (Lockhart et al., 2017; Chaabane et al., 2019), making infections difficult to treat. Lockhart et al. (2017) evaluated the antifungal susceptibility of 41 isolates of *C. auris* from 54 patients during 2012–2015. The authors found that 93 and 35% of *C. auris* isolates were resistant to fluconazole (FLC) and amphotericin B, respectively. In addition, difficulties in its identification in the routine diagnostic laboratory have a significant impact on outbreak detection and appropriate management (Bidaud et al., 2018).

With poor response to standard antimicrobials and the deficiency in developing new antifungal agents into the clinic, it stands that alternate means of treating the fungal diseases are warranted. In this context, the use of probiotics has been considered a promising strategy for prevention and control of several fungal infections (Mailander-Sanchez et al., 2012; Matsubara et al., 2016a; Hu et al., 2017; Rodrigues C. F. et al., 2019). Probiotics are live microorganisms or microbial cell components that beneficially affect host health (Guarner et al., 2012; Janczarek et al., 2016; Matsubara et al., 2016b; Rossoni et al., 2018), but their clinical application in immunocompromised patients is limited due to the possibility of bacteremia caused by bacteria of the genus *Lactobacillus* (Cannon et al., 2005; Salminen et al., 2006).

To address the risk for live cell probiotics potential of bacteremia, postbiotics have emerged based on the concept that bacterial viability is not essential for probiotics to exert beneficial effects on human health (Tsilingiri and Rescigno, 2013; Cicenia et al., 2014). Postbiotics are products of probiotic bacteria that have biological activity in the host (Mosca et al., 2019) and include metabolites, fractions of microbial cells, fatty acids, proteins, polysaccharides, cell lysates, peptidoglycan derived peptides, and structures responsible for adhesion, such as pili (Wegh et al., 2019). In previous studies by our research group, we isolated the *Lactobacillus paracasei* strain 28.4 from the oral cavity and showed its inhibitory activity against the commensal fungus *C. albicans* in both *in vitro* and *in vivo* models (Rossoni et al., 2017, 2018; de Barros et al., 2018; Santos et al., 2019).

In the present study, the supernatant of *L. paracasei* 28.4 was extracted and fractionated to determine if postbiotic elements could be effective at inhibiting the emergent species *C. auris*. Particularly, examining their effects on biofilm state that can plague immunocompromised patients that spur recurrent and invasive infections, also, we examined cell-free postbiotic supernatant inhibitory activity using the invertebrate infection model *Galleria mellonella* to look for host responses.

MATERIALS AND METHODS

Strains

A panel of *C. auris* strains (designated AR-BANK#0381 to AR-BANK#0390) obtained from the antimicrobial resistance bank of the CDC was used in this study. The strains in this panel are listed in **Table 1**. *L. paracasei* 28.4, an isolate from the oral cavity of a caries-free individual, was used to obtain crude extract and supernatant fractions. Our research group isolated, identified, and characterized this probiotic strain demonstrating its antifungal action both *in vitro* and *in vivo* studies (Rossoni et al., 2017, 2018; de Barros et al., 2018; Santos et al., 2019; Ribeiro et al., 2020).

All *C. auris* isolates were cultured in 1% yeast extract, 2% peptone, 2% dextrose (YPD broth, Difco, Detroit, USA) for 24 h at 37°C, and *L. paracasei* 28.4 was grown on Man Rogosa and Sharpe (MRS) agar (Difco, Franklin Lakes, NJ, USA) for 48 h at 37°C (5% CO_2).

In vitro Coinfection Cultures in a Planktonic Environment

Coinfection cultures were performed in 2 mL of BHI broth at 37°C in a rollerdrum according Peleg et al. (2008) with modifications. Standardized inoculants of *C. auris* (1×10^5 cells/mL) and *L. paracasei* 28.4 (1×10^8 cells/mL) were incubated together for 24, 48, and 72 h. At the indicated time points, the CFU were enumerated for each group. YPD plates containing kanamycin (45 μg/mL) and MRS plates containing fluconazole (32 μg/mL) were used to determine *C. auris* and *L.*

Abbreviations: BHI, Brain heart infusion; CDC, Centers for Disease Control and Prevention; CFU, colony-forming unit; CLSI, Clinical and Laboratory Standards Institute; LPCE, *L. paracasei* crude extract; LPF1, *L. paracasei* fraction 1; MIC, minimum inhibitory concentration; MRS, Man, Rogosa and Sharpe; PBS, phosphate buffered saline; YNB, Yeast nitrogen base; YPD, Yeast peptone dextrose.

TABLE 1 | *C. auris* isolates used in this study.

Strain no.	*C. auris* strain designation
CAU-01	AR-BANK#0381
CAU-02	AR-BANK#0382
CAU-03	AR-BANK#0383
CAU-04	AR-BANK#0384
CAU-05	AR-BANK#0385
CAU-06	AR-BANK#0386
CAU-07	AR-BANK#0387
CAU-08	AR-BANK#0388
CAU-09	AR-BANK#0389
CAU-10	AR-BANK#0390

paracasei CFUs, respectively. Results were obtained from three independent experiments.

L. paracasei 28.4 Postbiotic Elements: Supernatant Preparation, Extraction, and Fractionation

First, the *L. paracasei* 28.4 supernatant was produced according to Ribeiro et al. (2017). An inoculum of 1 mL of the standard suspension (10^7 cells/mL) was seeded into 6 mL of MRS broth and incubated at 37°C for 24 h under microaerophilic conditions. After this incubation, the broth was centrifuged (5,000 RPM for 10 min) and filtered with a 0.22 μm pore size membrane (MFS, Dublin, CA, USA).

Next, postbiotic elements were obtained according to Medina et al. (2019). In total, 4 L of supernatant were extracted with EtOAc (3 × 50% of each medium volume) for the extraction of the active compounds. After evaporation of EtOAc using a rotary evaporator (Buchi rotavapor, Buchi, São Paulo, Brazil), *L. paracasei* 28.4 crude extract (LPCE) was obtained (1.18 g). LPCE crude extract was analyzed using HPLC with two LC6AD pumps, CBM-20A communicator, SIL-10AF automatic injector, and SPD-M20A diode array detector (Shimadzu, Columbia, MD, USA), and the column used was a Luna Phenomenex octadecyl silane (C-18) analytical 250 × 4.6 mm, and gradient elution H_2O /MeOH (95:05 → 0:100) for 45 min. LPCE was fractionated using 20 g of C18 silica in an open column in which methanol and water were employed as a stationary phase in a polarity gradient (26:74, 51:49, 75:25, and 90:10). Fraction 1 of the supernatant (LPF1) was used in all subsequent assays as well as the LPCE. An aliquot of LPCE and LPF1 were cultured in brain heart infusion (BHI) broth (Sigma, St. Louis, MO, USA) to ensure that there was no microbial growth in the postbiotic elements.

Minimum Inhibitory Concentration

To determine the minimal inhibitory concentration (MIC) of LPCE and LPF1 against the *C. auris* strains, colonies of each strain were inoculated in 5 mL of yeast peptone dextrose (YPD) media (Sigma, St. Louis, MO, USA) and grown overnight at 37°C. The cells were harvested by centrifugation at 5,000 rpm for 5 min and washed with phosphate-buffered saline (PBS). Subsequently, the cell pellets were suspended in RPMI 1640 medium (Sigma, St. Louis, MO, USA). The cell count was determined using a hemocytometer and adjusted to 1.0×10^3 cells/mL. Susceptibility patterns of the isolates to LPCE and LPF1 were determined by performing the broth microdilution assay. The final concentrations of LPCE and LPF1 ranged from 30 to 0.029 mg/mL. Fluconazole and amphotericin B (Sigma-Aldrich, St. Louis, MO, USA) were used as a positive control and the assay was performed according the Clinical and Laboratory Standards Institute (CLSI) document M27-A2 (National Committee for Clinical Laboratory Standards, 2002). The final concentrations of fluconazole and amphotericin B ranged from 64 to 0.125 μg/mL. The resistance breakpoints were used as described in the Clinical and Laboratory Standards Institute (CLSI) guidelines based on *C. albicans* interpretive breakpoints (Fluconazole: ≤8.0 μg /mL for susceptible, ≥64 μg /mL for resistant; Amphotericin B: >1 μg/ml for resistant) (National Committee for Clinical Laboratory Standards, 2002).

Minimum Fungicidal Concentration

The minimum fungicidal concentration (MFC) was determined as follows. In total, 10 μL of yeast culture from each microwell of the MIC assay was plated on YPD agar and incubated at 35°C overnight. The static/cidal parameter can be roughly estimated by comparing the MFC of a given antifungal to its MIC. If the MFC is ≤4 × MIC the drug is considered cidal (Pfaller et al., 2004).

Time to Kill Assays

After the MIC test of all *C. auris* strains, the CAU-01 strain was selected for the subsequent tests based on its sensitivity to fluconazole and amphotericin B. This strain showed the lowest MIC value for both antifungals, a requirement for inducing persister cells. Therefore, *C. auris* strain CAU-01 was explored to interrogate the killing effects of LPCE and LPF1. The assays were carried out in 10-mL tubes (BD Biosciences, San Diego, CA, USA) in triplicate according to Tharmalingam et al. (2019) with modifications. Briefly, log-phase cultures of CAU-01 were diluted in fresh RPMI medium to a density of 10^6 cells/mL LPCE and LPF1 were added at concentrations 3.75–120 mg/mL (corresponding to 1 × MIC−8 × MIC), and the tubes were incubated at 37°C with agitation (200 rpm). Portions of cell suspensions were withdrawn at predetermined time points (24, 48, and 72 h). Serial dilutions were plated on YPD agar to determine the colony-forming unit/mL (CFU/mL) of the cell suspensions. CFU were determined after incubation for 48 h at 37°C. Three independent experiments were performed. As a positive control, we included the antifungal agent fluconazole at 4, 16 and 32 μg/mL (corresponding to 1 × MIC−8 × MIC).

Biofilm Formation

Evaluation of biofilm formation was performed in 96-well microtiter plates (Corning, New York, NY, USA) following the methodology described by Vilela et al. (2015) and Rossoni et al. (2018), with some modifications. Briefly, 100 μL of *C. auris* standard suspensions (1.0×10^7 cells) were deposited into 96-well microtiter plates, after which the plates were placed on a 75-rpm shaking incubator at 37°C for 90 min. Each well was washed twice with PBS, and 200 μL of yeast nitrogen base (YNB)

broth (Sigma, St. Louis, MO, USA) supplemented with 100 mM glucose with LPCE or LPF1 were added to the wells of each plate at the concentrations of 0.5 × MIC, 1 × MIC, and 2 × MIC. For the control groups, 200 μL of YNB broth supplemented with 100 mM glucose without LPCE or LPF1 was added. The plate was incubated for 48 h at 37°C with shaking at 75 rpm. The liquid medium was replaced after 24 h and the treated groups received fresh LPCE, LPF1, or fluconazole dilutions. After the incubation period, each well was washed twice with PBS for subsequent analysis of total biomass and metabolic activity. As a positive control, we included the antifungal agent fluconazole at 4 and 8 μg/mL (corresponding to 1 × MIC and 2 × MIC).

Analysis of Biofilms by Total Biomass Quantification

After biofilm formation, the biofilm biomass was quantified utilizing an assay previously described by Peeters et al. (2008), with modifications. For biofilm fixation, 100 μL of 99% methanol was added to the wells (Sigma-Aldrich, St. Louis, MO, USA). After 15 min, the supernatants were removed and the plates were air-dried. Then, 100 μL of a 1% crystal violet (CV) solution was added to all wells. After 20 min, the residual CV solution was removed by washing with PBS. Finally, bound CV was released by adding 150 μL of 33% acetic acid (Sigma-Aldrich, St. Louis, MO, USA). The absorbance was measured at 540 nm. All steps were carried out at room temperature. The CV assay was performed as two independent experiments with $n = 6$ biofilms per group.

Analysis of Biofilms by XTT Reduction Assay Colorimetric Assay

The biofilms formed also were evaluated by a metabolic assay based on the reduction of XTT, a tetrazolium salt (Sigma-Aldrich, St. Louis, MO, USA) according Jin et al. (2004) and Rossoni et al. (2019). Briefly, XTT salt was dissolved in PBS at a final concentration of 1 mg/mL. Immediately before each assay, a menadione (Sigma-Aldrich, St. Louis, MO, USA) solution was prepared at a final concentration of 0.4 mM and filter-sterilized. The XTT solution was thawed prior to each assay and mixed with the menadione solution at a ratio of 20:1 (v/v). Each well was washed two times with 200 μL of PBS to remove any non-adherent cells. Next, 158 μL of PBS, 40 μL of XTT, and 2 μL of menadione were added to each of the pre-washed wells. The plates were incubated in the dark at 37°C for 3 h. Afterwards, 100 μL of the solution was transferred to a new well, and any colorimetric change in the solution was measured using a microtiter plate reader (Tp Reader; Thermo Plate, Shenzhen, China) at 490 nm. The XTT assay was performed as two independent experiments with $n = 6$ biofilms per group.

Isolation and Susceptibility of *C. auris* Persisters Cells

For this study, the methodologies described by LaFleur et al. (2006) and Al-Dhaheri and Douglas (2008) were used with some modifications. Briefly, *C. auris* was grown for 72 h at 37°C with shaking in RPMI 1640 with L-glutamine and 0.165 M MOPS growth medium (50 mL in 250-ml flasks) to isolate persister cells in a stationary-phase cultures. After 72 h, cells from the stationary-phase cultures were harvested and washed twice in PBS. All cell suspensions were adjusted to concentrations of ∼5 × 10^8 cells/mL. An aliquot of 1 mL of this suspension, containing 10x, 50x, 100x, 150x, and 200x MICs of indicated antifungals (amphotericin B and fluconazole), was added to the wells of a 2 mL deep well assay block (Corning Costar 3960) and incubated at 37°C, with shaking at 225 rpm for 48 h. In groups containing postbiotic elements, the stationary-phase culture suspension was treated with 10 × MIC of LPCE or LPF1. Control cells were treated similarly with buffered medium without antifungal agent. At designated times, 50 μL samples were removed, serially diluted, and spot-plated on YPD agar plates to enumerate the number of persister cells. This experiment was conducted in triplicate.

G. mellonella Survival

G. mellonella survival was evaluated following the methodologies described by Mylonakis et al. (2005) and Rossoni et al. (2017), with some modifications. *G. mellonella* (Vanderhorst Wholesale, St. Marys, OH, USA) in their final larval stage were stored in the dark and used within 7 days from shipment. Sixteen randomly chosen *G. mellonella* larvae with similar weight and size (250–350 mg) were used per group in all assays. Two control groups were included in the assays—one group was inoculated with phosphate-buffered saline (PBS), while the other group received no injection as a control to evaluate general viability.

In view of the lack of studies in the literature that used postbiotics elements on *G. mellonella* as an experimental model, the toxicity of LPCE and LPF1 was evaluated prior to the study of experimental candidiasis. The postbiotic elements were injected directly into the hemolymph of *G. mellonella* at varying concentrations (10–80 mg/kg), and survival curves were constructed. Larvae were incubated at 37°C and monitored daily for survival.

For the experimental candidiasis, *C. auris* suspension was prepared from cultures in 5 mL of YPD liquid medium and incubated at 37°C for 18 h. Afterwards, cells were centrifuged at 2,000 × *g* for 10 min, and the supernatant was discarded. The cell pellet was washed twice and suspended in PBS. Cell densities were adjusted using a hemocytometer.

To evaluate the effects of LPCE or LPF1 on *C. auris* infection, the larvae were pre-treated by injecting the LPCE (80 mg/kg) or LPF1 (30 mg/kg) through the last left proleg (volume, 10 μL). After 2 h, larvae were infected with 10^6 cells/larvae of *C. auris* suspended in PBS at the last right proleg (10 μL of volume). Larvae were incubated at 37°C and monitored daily for survival. Larvae were considered dead when they displayed no movement in response to touch.

Quantification of *G. mellonella* Hemocytes

In order to investigate the immunological mechanisms associated with the postbiotics elements against infection by *C. auris*, larvae were pre-treated with LPCE (80 mg/kg) or LPF1 (30 mg/kg) and infected with *C. auris* as described above. Hemocytes were collected from the hemocoel at 4 h post-injection with *C. auris*. Larvae were bled into tubes containing cold, sterile

insect physiologic saline (IPS) (150 mM sodium chloride; 5 mM potassium chloride; 100 mM Tris—hydrochloride, pH 6.9 with 10 mM EDTA, and 30 mM sodium citrate). The hemocytes were identified based on cell morphology and quantified using a hemocytometer. The results were averaged from four replicates.

Analysis of Peptide Expression

G. mellonella gene expression was evaluated following the methodologies described by Mowlds et al. (2010) and Rossoni et al. (2017). After pre-treatments and infection, larval RNA was extracted using TRIzol (Ambion, Inc., Carlsbad, CA, USA) at 24 h post-injection of LPCE or LPF1. In brief, a 2 mL volume of TRIzol was added to a 15 mL tube containing the homogenized frozen tissue of larvae and incubated at room temperature (RT) for 10 min. Subsequently, 400 μL of chloroform (Sigma-Aldrich, St. Louis, MO, USA) was added and the tubes were centrifuged at 12,000 × *g* for 15 min at 4°C. The supernatant was then transferred to a new tube, and 1 mL of isopropanol (Sigma-Aldrich, St. Louis, MO, USA) was added. After centrifugation, the obtained pellet was washed with 70% ethanol (Sigma-Aldrich, St. Louis, MO, USA), centrifuged again, and suspended in 50 μL of nuclease-free water (Ambion Inc., Carlsbad, CA, USA). The concentration, purity and quality of the RNA were verified using a NanoVue Plus spectrophotometer (GE Healthcare Bio-Sciences, Pittsburgh, PA, USA).

The extracted total RNA (1 μg) was transcribed into complementary DNA (cDNA) using the Verso cDNA Synthesis Kit (Thermo Fisher Scientific Inc, Waltham, MA, USA), according to the protocols recommended by the manufacturer. The primers for the genes that encode β-actin and galiomicin were designed by Rossoni et al. (2017) and described in **Table 2**. The transcribed cDNAs were amplified for relative quantification of the expression of the gene encoding galiomicin in relation to the concentration of the reference gene (β-actin).

Statistical Analysis

The Student's *t*-test was used to compare the results from the cell-cell interaction, time to kill assay, and *in vitro* biofilm assay. Percent survival and killing curves of *G. mellonella* were plotted and statistical analysis was performed by the Kaplan-Meier test using Stata Statistical Software (Stata Corp LP, College Station, TX, USA). Analysis of variance (ANOVA) and Tukey post-test were used to compare the results obtained in the data of hemocyte count and in the analysis of gene expression. All the tests were performed using GraphPad Prism statistical software (GraphPad Software, Inc., California, CA, USA) and a *P*-value ≤ 0.05 was considered significant.

RESULTS

Probiotic Effect

First, *L. paracasei* 28.4 was screened for antifungal activity against *C. auris* CAU-01 using co-culture. For this purpose, *L. paracasei* 28.4 cells were co-cultured with *C. auris* for 1–3 days. There was a significant reduction in *C. auris* counts for all evaluated times (1 day: 3.6 Log, 2 days: 1.67 Log, and 3 days: 1.8 Log) compared to the control group as demonstrated in **Figure 1**. *L. paracasei* concentration was constant throughout the assay, however *C. auris* experienced growth suppression in the presence of *L. paracasei* 28.4. This probiotic effect can indicate a better ability of *L. paracasei* to utilize nutrients in the media for growth, a direct cell-cell interaction, or possibly inhibition by bacterial metabolites.

Postbiotic Planktonic Inhibition

To explore the possibility of an indirect inhibitory activity posed by bacterial metabolites, we investigated *C. auris* inhibition by cell-free supernatant of *L. paracasei* 28.4. Inhibitory assessment was made using crude extract (LPCE) and a fraction (LPF1) derived from the *L. paracasei* supernatant. The MIC of LPCE and LPF1 was evaluated for 10 strains of *C. auris* (**Table 3**). MICs for LPCE were 15 mg/mL for all strains, and LPF1 MICs ranged from 3.75 to 7.5 mg/mL. For all strains evaluated, the MFC values were ≤4 × MIC, so the postbiotic elements were considered cidal (**Figure 2**). Thus, there does appear to be a postbiotic effect by *L. paracasei* 28.4. The lower MIC of LPCE is reasonable considering that the active component is more diluted in the unfractionated volume.

Since LPCE and LPF1 were active against all of the tested *C. auris* strains, we selected a single strain (CAU-01) for follow-up experiments. The killing kinetics assay determined that the total viable fungal count was about 6-log CFU at 0 h. After 24 h, there was a complete reduction of the total viable count of *C. auris* cells treated with LPCE (4 × MIC: 60 mg/mL) or LPF1 (8 × MIC: 30 mg/mL) (**Figure 3**). As a positive control, we included the antifungal agent fluconazole. Fluconazole decreased the initial inoculum by 1-log CFU during the same time period at all concentrations tested (1 × MIC: 4 μg/mL; 4 × MIC: 16 μg/mL, and 8 × MIC: 32 μg/mL).

Postbiotic Biofilm Inhibition

It is known that antifungal compounds have variable efficacy against biofilms. Therefore, the cell free supernatant extract and fraction were tested for inhibitory activity on biofilms. LPCE and LPF1 at 1 × MIC and 2 × MIC concentrations significantly reduced the biomass ($p = 0.0001$) and the metabolic activity ($p = 0.0001$) of the *C. auris* biofilm as shown in **Figures 4A,B**, respectively. A biomass of *C. auris* showed a reduction of up to 67% for LPF1, 61% for LPCE, and 21% using fluconazole. The metabolic activity of biofilms reduced 89, 85, and 23% for LPF1, LPCE, and fluconazole, respectively. The biofilms treated with the postbiotic elements in the concentration of 0.5 × MIC also caused a reduction in relation to the control groups but there was no statistically significant difference, indicating a dose dependent effect on the biofilms.

We sought to determine the susceptibility of persister cells to the *L. paracasei* 28.4 supernatant derived elements. To generate *C. auris* persisters, *C. auris* CAU-01 was grown to stationary phase and then was treated with different concentrations of amphotericin and fluconazole (10x, 50x, 100x, 150x, and 200x MIC) or postbiotic elements (10 × MIC) for 48 h. The concentration of cells in stationary phase was 5×10^8 CFU/mL (∼8.54 Log) and, after treating with 200 × MIC (25 μg/mL) amphotericin B or 200 × MIC (1,600 μg/mL) fluconazole for

TABLE 2 | List and description of genes and primers sequences used in the qPCR.

Gene name	NCBI genebank	Primer sequence (5′–3′)	Product size (bp*)	Primers source
Galiomicin	AY528421.1	[a]**F**-TCCAGTCCGTTTTGTTGTTG [b]**R**-CAGAGGTGTAATTCGTCGCA	123 bp	Rossoni et al., 2017
β-actin	XM_026909080.1	[a]**F**- ACAGAGCGTGGCTACTCGTT [b]**R**- GCCATCTCCTGCTCAAAGTC	104 bp	Rossoni et al., 2017

[a]*F indicates a forward primer.*
[b]*R indicates a reverse primer.*
**Base pair.*

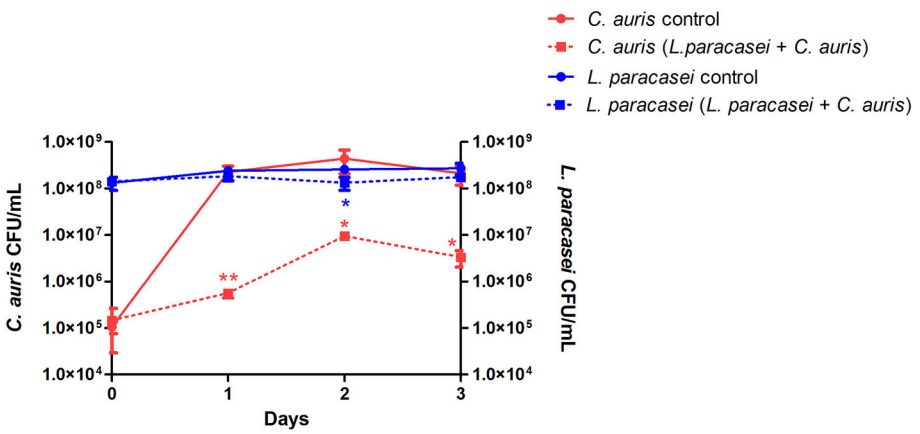

FIGURE 1 | The viability of *C. auris* CAU-01 (solid line) was significantly reduced when co-cultured with *L. paracasei* 28.4 (dashed line). Student *t*-test, $*p \leq 0.01$, $**p \leq 0.001$.

TABLE 3 | MIC for *C. auris* strains.

Specie	Strain	LPCE (mg)	LPF1 (mg)	Fluconazole (μg)	Amphotericin (μg)
C. auris	CAU-01	15	3.75	8	0.125
C. auris	CAU-02	15	3.75	16	0.25
C. auris	CAU-03	15	7.5	>64	0.5
C. auris	CAU-04	15	3.75	>64	0.5
C. auris	CAU-05	15	7.5	>64	0.5
C. auris	CAU-06	15	7.5	>64	0.5
C. auris	CAU-07	15	7.5	8	0.25
C. auris	CAU-08	15	3.75	>64	1
C. auris	CAU-09	15	7.5	>64	1
C. auris	CAU-10	15	7.5	>64	2

48 h, the cell viability was $\sim 10^4$ CFU/mL and $\sim 10^7$ CFU/mL, respectively. Also, we treated the cells in stationary phase with a dose of 10 × MIC LPCE (150 mg/mL) or LPF1 (37.5 mg/mL) for 48 h and there was a complete reduction in the growth of *C. auris* cells. *C. auris* was tolerant of standard of care medications fluconazole and amphotericin at concentrations that are normally detrimental to the fungi, suggesting a persistent state. Under the same conditions, exposure to LPCE, and LPF elicited a cell reduction, suggesting the ability to inhibit persister cells (**Figure 5**).

Postbiotic Treatment in the *G. mellonella* Infection Model

First, *G. mellonella* was used to evaluate acute systemic toxicity of the postbiotic elements. The larvae were injected with varying concentrations of LPCE and LPF1 (80–10 mg/kg), and their survival was monitored for a period of 7 days. LPCE and LPF1 did not exert toxic effects on the larvae when administered at those concentrations (**Figures 6A,B**).

To investigate the antifungal effects of LPF1 and LPCE in a *G. mellonella* model, we tested the efficacy of pretreatment with LPF1 and LPCE in larvae infected with *C. auris*. LPF1 and LPCE were injected into the larvae at 2 h prior to infection with *C. auris* concentrations of 30 and 80 mg/kg, respectively. In the control group, infection with *C. auris* without previous injection of postbiotics elements caused death in 100% of the larvae within 3 days. When the larvae were pretreated with LPF1 or LPCE prior to *C. auris* infection, the survival rate of *G. mellonella* larvae was significantly prolonged ($p < 0.05$) (**Figure 6C**). More specifically, larval survival increased 43% for LPF1 and 37% for LPCE groups.

To investigate the immune mechanisms associated with the effects of LPCE and LPF1 against *C. auris* infection, we determined the number of available hemocytes in the hemolymph of larvae after 4 h of *C. auris* injection. Hemocyte

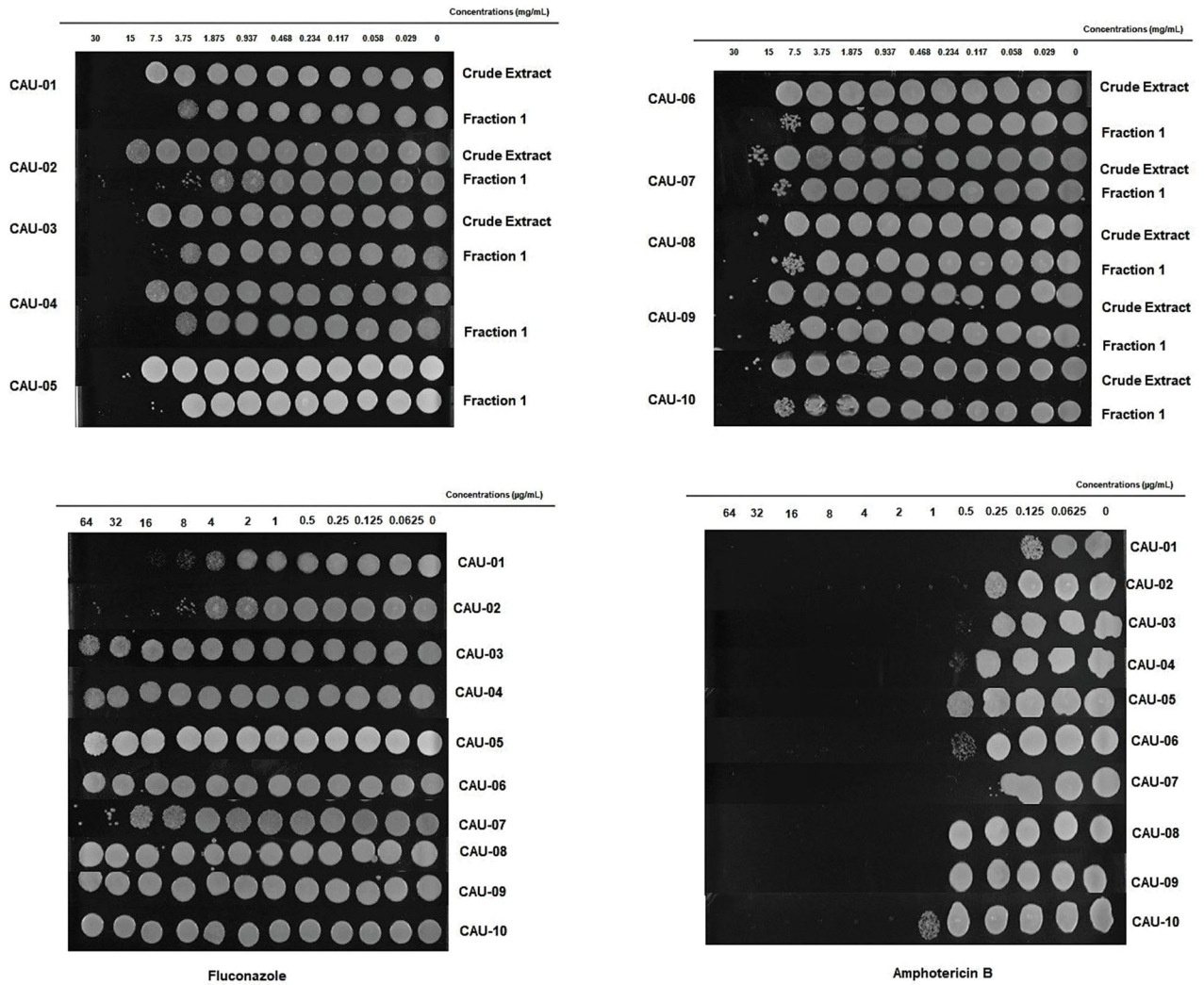

FIGURE 2 | LPCE and LPF1 inhibits *C. auris*. The static vs. cidal nature of the inhibition was examined for the various postbiotics concentrations. Growth at concentration equivalent or higher than the MIC indicated that LPCE and LPF1 were fungistatic and inhibition of growth indicated fungicidal activity.

count was performed after 4 h of infection based on our previous study in which *L. paracasei* 28.4 stimulated hemocyte production in 4 h rather than 24 h (Rossoni et al., 2017). We analyzed only the larvae not infected by *C. auris* and observed an increase in the number of hemocyte in the LPCE (1.43-fold increase) (**Figure 7A**) and LPF1 (1.8-fold increase) (**Figure 7B**) groups compared to the PBS control group, but there was no statistically significant difference. In the larvae infected with *C. auris*, the groups pretreated with LPCE or LPF1 also showed increased hemocyte numbers compared to the *C. auris* control group ($p < 0.05$). The LPCE and LPFI groups reached, respectively, 2.55 (**Figure 7A**) and 2.26-fold increase (**Figure 7B**). Interestingly, we also observed that the *C. auris* group showed a reduction of hemocyte numbers in relation to the PBS control group in agreement with Bergin et al. (2003) that demonstrated an inverse relationship with infectious fungi and hemocyte density, but when the larvae were pretreated with LPCE or LPF1, the hemocyte quantity was very similar to the values found in the PBS control group (**Figures 7A,B**).

The presence of an increased hemocyte count suggests that LPCE and LPF1 could modulate the immune response of *G. mellonella* larvae. Thus, we further explored alterations in the immune response examining the expression of the antifungal peptide galiomicin. For this assay, we evaluated the galiomicin expression after 24 h since the greatest expression of this peptide occurs at a later stage of *Candida* infection (Rossoni et al., 2017). We found that LPCE and LPF1 were able to increase the expression of galiomicin. The groups pretreated with LPCE or LPF1 and then infected with *C. auris* had a statistically significant increase ($p < 0.0001$) in relation to the control group infected by *C. auris* (LPCE group: 1.48-fold increase; LPF1 group: 1.31-fold increase). LPCE and LPF1 induced an increase in gene expression of 4.58 and 3.64-fold compared, respectively, to the control group formed by consecutive PBS injections (**Figures 7C,D**). These

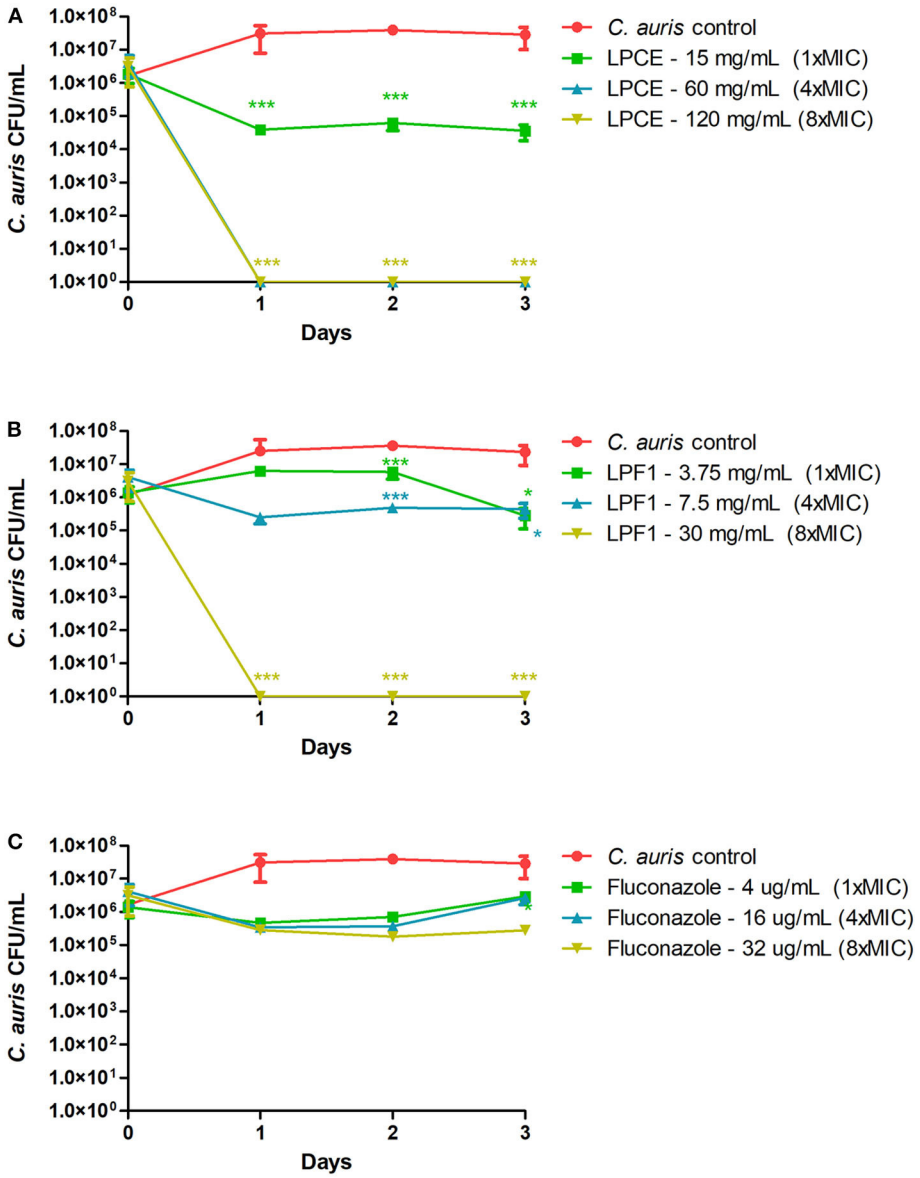

FIGURE 3 | Killing kinetics. **(A)** Growth curves were generated using *C. auris* cells treated with LPCE. **(B)** Growth curves were generated using *C. auris* cells treated with LPF1. **(C)** Growth curves were generated using *C. auris* cells treated with fluconazole. Student *t*-test, $^{*}p \leq 0.01$, $^{***}p \leq 0.0001$.

results indicate that LPCE and LPF1 increased the hemocyte density and levels of galiomicin expression, which may protect *G. mellonella* from *C. auris* infection.

DISCUSSION

Recently, postbiotics have gained more and more attention due to their beneficial actions on the host without the adverse risk of inducing bacteremia in immunocompromised patients from the delivery of live cells (Gao et al., 2019). In this study, we identified LPCE and LPF1 derived from *L. paracasei* 28.4 supernatant as postbiotics and a potentially alternative antifungal treatment against *C. auris*, a globally emerging pathogen. The results obtained in the cell-cell interaction demonstrated that *L. paracasei* strain 28.4 was able to interfere with *C. auris* growth, demonstrating the potential for probiotic activity against *C. auris*. Also, the postbiotic elements reduced *C. auris* in planktonic, biofilm, and persister states, a significant feat. In *in vivo* assays, LPCE and LPF1 protected *G. mellonella* infected with *C. auris*. Our research provides a novel idea for prevention and treatment of *C. auris* infections.

The MIC results of this study demonstrated the antifungal activity of LPCE and LPF1 against all 10 *C. auris* strains, including both fluconazole-sensitive and fluconazole-resistant strains. Although the MIC values found were higher than fluconazole, the postbiotic elements are probably composed of

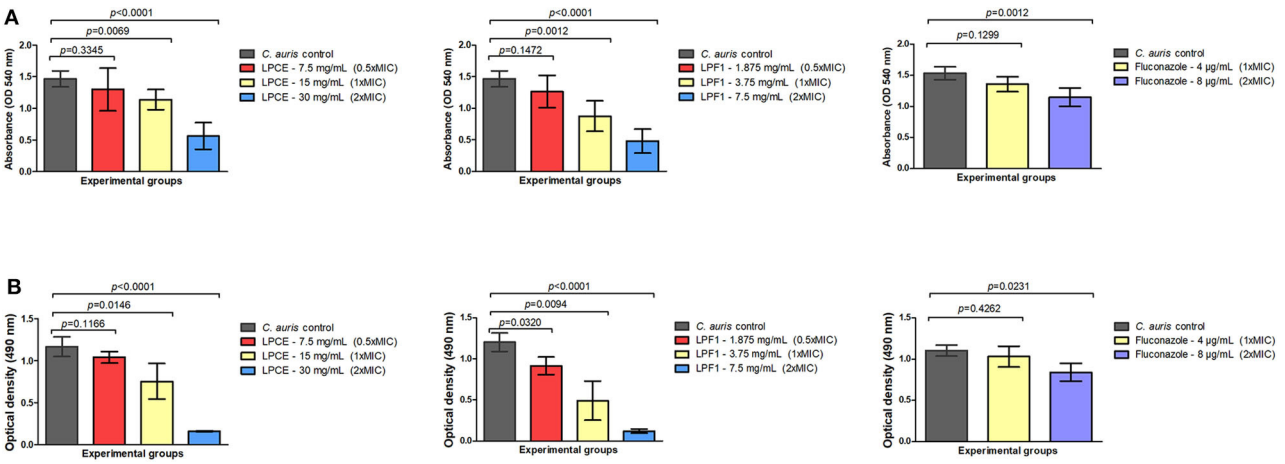

FIGURE 4 | Quantification of cells in biofilms formed at the bottom of 96-well plates. **(A)** Biomass quantification and **(B)** Metabolic activity (XTT analysis) of different treatments (LPCE, LPF1, and Fluconazole). The different concentrations of LPCE and LPF1 used in biofilm formation correspond to 0.5 × MIC, 1 × MIC, and 2 × MIC values. Student's *t*-test, $p \leq 0.05$.

a pool of molecules and are not yet fully purified. In addition, it was observed that the higher its purification and subsequent fractionation, the lower the MIC value obtained (MIC value of LPF1 is four times less than the value of LPCE).

The antibacterial properties of postbiotics have been tested on bacterial diseases; for example, Dunand et al. (2019) determined the protective capacity of postbiotics of fermented milk against *Salmonella enterica* serovar Typhimurium. The authors obtained the postbiotic from five frozen commercial cultures of thermophilic lactobacilli and 11 autochthonous *Lactobacillus* strains. The use of postbiotics for 14 days significantly increased the secretory IgA in feces of mice and a higher survival was also observed compared to controls demonstrating an immunomodulatory and protective capacity against *S. enterica* serovar Typhimurium infection in mice. In addition, studies demonstrate the beneficial role of postbiotics in inflammatory activity (Tsilingiri et al., 2012; Compare et al., 2017; Gao et al., 2019; Johnson et al., 2019). To our knowledge, this is the first study supporting the use of a postbiotic from *Lactobacillus* cells against *C. auris* and its use remains unexplored as a therapeutic option in these fungal infections. Therefore, further studies are needed to evaluate some important aspects such as toxicity, adverse effects, and viability of mass production.

To investigate the antifungal potential of LPCE and LPF1, we evaluated its effects in the growth kinetics of *C. auris*. The use of LPCE and LPF1 completely inhibited *C. auris* growth in contrast to the clinical antifungal agent fluconazole, which did not demonstrate any efficacy more than 1-Log. LPCE and LPF1 also exerted anti-biofilm activity against *C. auris*; significant reductions in biofilm formation were observed in both biomass amount and metabolic activity. In agreement to this result, Rossoni et al. (2018) evaluated the antifungal action of the *L. paracasei* 28.4 supernatant on different *C. albicans* strains. The raw supernatant of *L. paracasei* 28.4 was capable of reducing the growth of *C. albicans* by up to 73% in planktonic cultures, 62% in biofilms and interferes negatively in adhesion (*ALS3*: 66-fold decrease) and hyphae formation genes (*HWP1*: 66-fold decrease; *CPH1*: 1000-fold decrease). Although the postbiotic elements have had effectiveness to reduce *C. auris* biofilms, previous studies have shown that biofilm formation is highly variable between different strains of *C. auris* and this fact merits further exploration (Sherry et al., 2017; Pathirana et al., 2018).

The biofilms of *C. auris* may become increasingly resistant to conventional antifungals according to their formation time. For example, after 4 h of biofilm development, the median MIC increased 16-fold for miconazole and 4-fold for amphotericin B compared to the 0 h time of biofilm formation (Kean et al., 2018). Borman et al. (2016) demonstrated that old cultures of *C. auris* can survive in high concentrations of fluconazole (256 µg/mL), as well as be unresponsive to treatment *in vivo* using *G. mellonella* model. These facts agree with the low sensitivity of biofilms to fluconazole found in this study and reinforce the search for alternative treatments such as postbiotics in *C. auris* infections.

Biofilms harbor drug resistant cells, included among them are persister cells which, in their metabolically dormant state, can be recalcitrant to antifungal agents (LaFleur et al., 2006). One important aspect of postbiotic elements was their ability to eliminate all *C. auris* persister cells that survived high dosages of amphotericin B or fluconazole. Persister cells were reported for the first time as a subpopulation of bacteria tolerant to a particular antibiotic that, after removal of the antimicrobial agent, gave rise to a new population of susceptible microbial cells (Bigger, 1944). In the clinical setting, persisters are usually associated with recurrent infections and the development of chronic infections (Denega et al., 2019). The first report of *Candida* spp. persister cells was described for LaFleur et al. (2006) that showed a biphasic killing curve when *C. albicans* was exposed to amphotericin B, chlorhexidine, or a combination of both. In addition, Al-Dhaheri and Douglas (2008) showed that not all *Candida* spp. and strains are able to form persister cells,

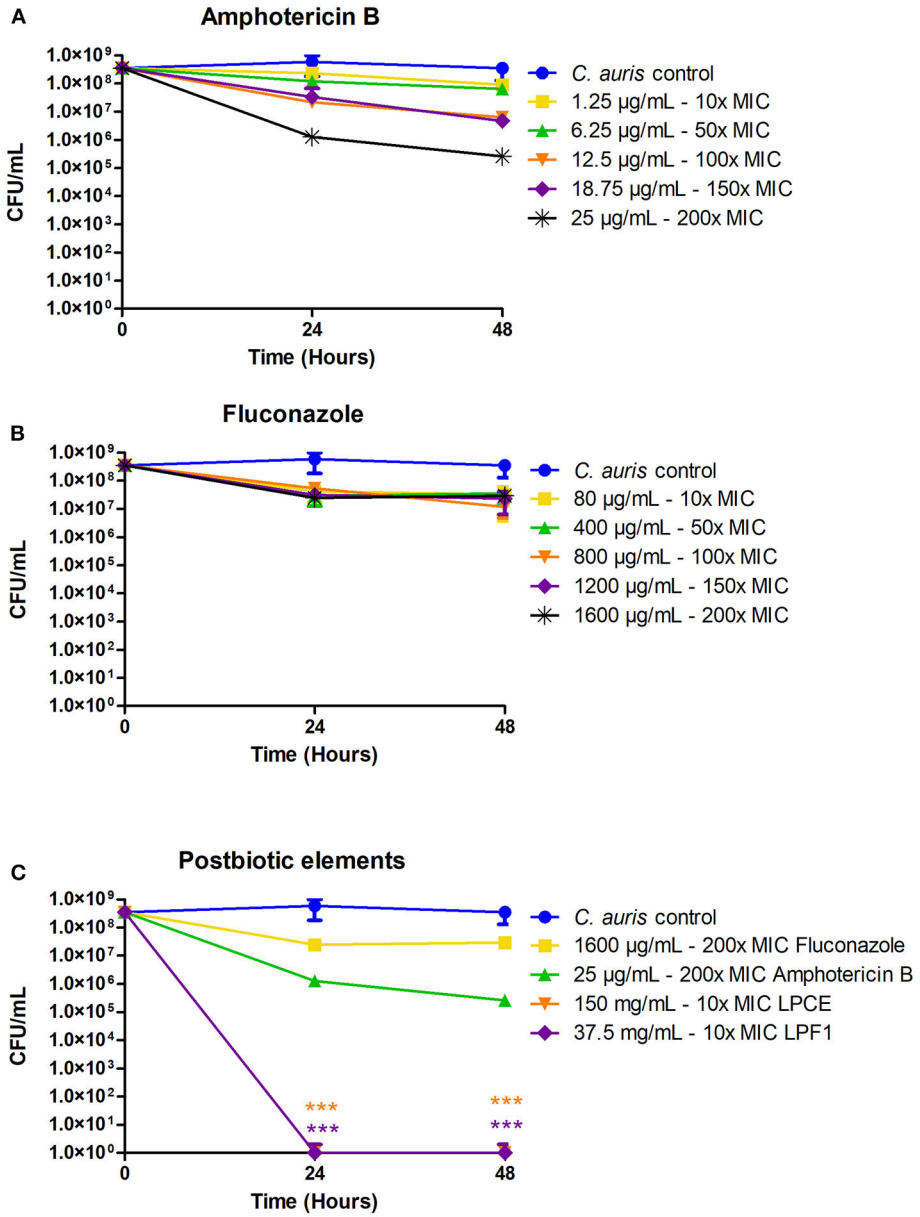

FIGURE 5 | Isolation of *C. auris* persisters. **(A)** *C. auris* persisters cells induced by amphotericin B. **(B)** *C. auris* persisters cells induced by fluconazole. **(C)** LPCE and LPF1 were able to kill all persister cells. Student's *t*-test, ***$p \leq 0.0001$.

for example, *C. albicans* strain SC5314 (Gillum et al., 1984), one of the most commonly used *C. albicans* strains used for molecular genetics studies, is not able to form persister cells *in vitro* (Denega et al., 2019).

The alternative invertebrate model of *G. mellonella* was used to evaluate protective effects of LPCE and LPF1 in experimental candidiasis by *C. auris*. First, in order to evaluate acute systemic toxicity of the postbiotic elements, the larvae were injected with different doses of LPCE and LPF1, and none of the systemic doses (10–80 mg/kg) resulted in death of the larvae. Additionally, we found that the injection of LPCE or LPF1 into *G. mellonella* larvae infected by *C. auris* increased the survival of these insects (43% for LPF1; 37% for LPCE), the number of hemocytes and the gene expression of galiomicin. These data further confirm the excellent performance of LPCE and LPF1, thus providing important insight into combating *C. auris*. To the best of our knowledge, this is the first article in the literature that uses postbiotic elements in *G. mellonella*.

Taken together, these findings indicate that LPCE and LPF1 are capable of stimulating the cellular and humoral immune responses of the larvae and consequently reduce *C. auris*

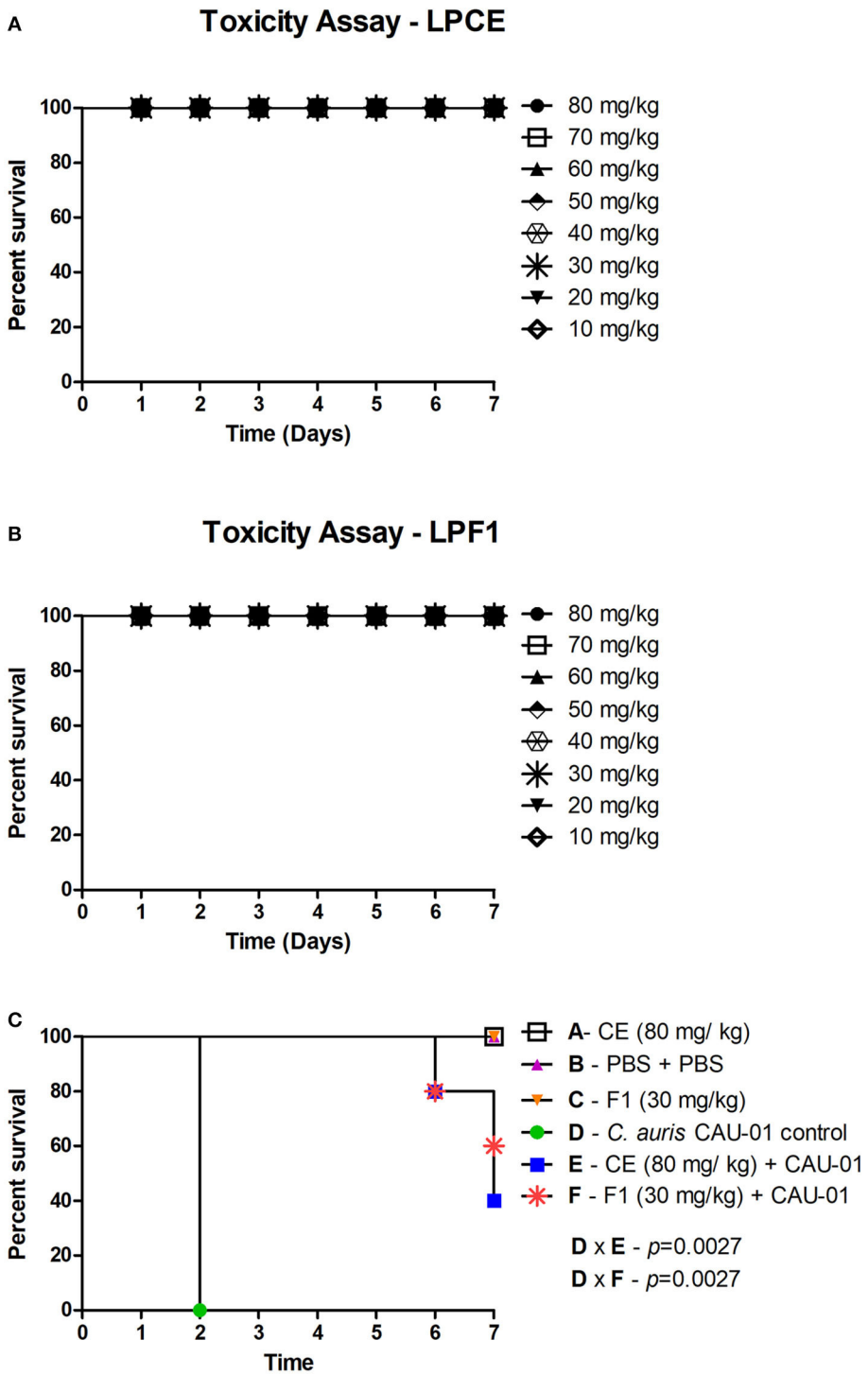

FIGURE 6 | (A) Toxicity evaluation of LPCE in *G. mellonella* model. **(B)** Toxicity evaluation of LPF1 in *G. mellonella* model. *G. mellonella* larvae were injected with serial concentrations of postbiotic elements. No death was observed at the concentrations used. **(C)** LPCE and LPF1 prolong the survival of *G. mellonella* larvae infected with *C. auris*. Significant differences were observed in survival between the "LPCE (80 mg/mL) + CAU-01 group" and "PBS + *C. auris* CAU-01 control group" and between the "LPF1 (30 mg/mL) + CAU-01 group" and "PBS + *C. auris* CAU-01 control group." Kaplan-Meier test, $p \leq 0.05$.

infection. The use of posbiotics elements with antifungal and immunomodulatory properties could be promising in *C. auris* infection, once a recent study questioned the effectiveness of the immune system against this species. It was demonstrated that human neutrophils do not properly recognize *C. auris* as they do with other *Candida* species and this behavior may explain

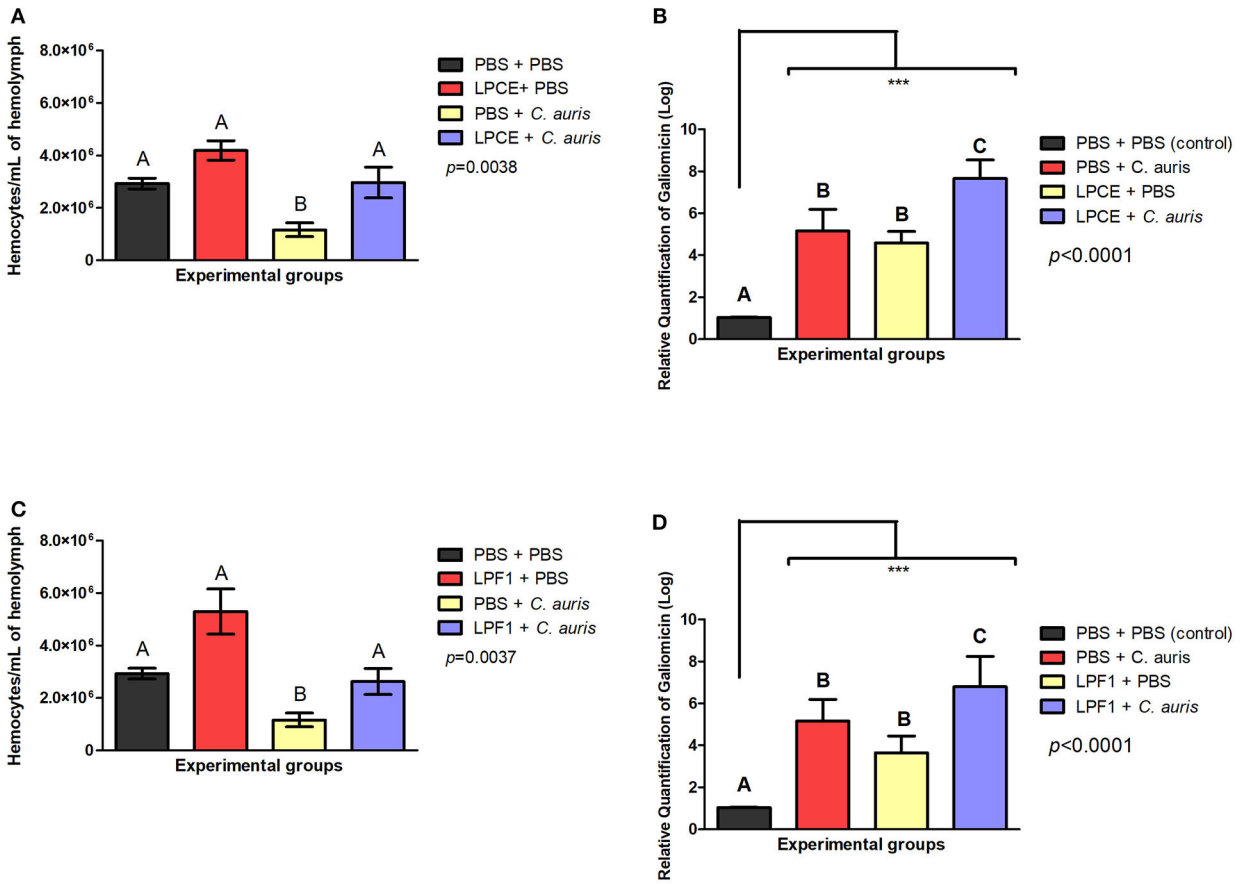

FIGURE 7 | LPCE and LPF1 modulate the immune system of *G. mellonella*. **(A)** LPCE: The group of LPCE + PBS increased the hemocyte number compared to a PBS control (PBS + PBS). The group LPCE + *C. auris* also increased the hemocyte quantity compared to *C. auris* group (PBS + *C. auris*). **(B)** LPF1: The group of LPF1 + PBS increased the hemocyte number compared to a PBS control (PBS + PBS). The group LPF1 + *C. auris* also increased the hemocyte quantity compared to *C. auris* group (PBS + *C. auris*). PBS + *C. auris* group showed a reduction of hemocyte quantity in relation to the PBS control group, but when the larvae were pretreated with LPCE or LPF1, the hemocyte quantity was very similar to the values found in the PBS control group. **(C,D)** LPCE and LPF1 increased the gene expression of galiomicin of *G. mellonella*. Relative quantification (log) of galiomicin for the groups treated with only PBS (Control), pre-treated with PBS and infected with *C. auris*, only treated with LPCE or LPF1, and pre-treated with LPCE or LPF1 and infected with *C. auris*. The units in the Y-axis were calculated based on the $2^{-\Delta\Delta CT}$ method, and they are expressed as the means and standard deviation. Galiomicin expression was normalized and compared with the expression of insects exposed to the control (PBS) using the reference gene β-actin. Different letters (A, B, and C) represent statistically significant differences among the groups. ANOVA and Tukey Tests ($p < 0.05$ was considered significant). $^{***}p \leq 0.001$.

the high mortality rates even for patients treated with antifungals (Nett, 2019).

Modulation of the *G. mellonella* immune response has been reported by different studies using probiotics (Ribeiro et al., 2017; Rossoni et al., 2017; Scalfaro et al., 2017; Geraldo et al., 2019). The main cells involved in the cellular immune response of *G. mellonella* are hemocytes (Bergin et al., 2003; Sheehan and Kavanagh, 2018). These are responsible for important events such as nodulation, encapsulation, and phagocytosis. Phagocytosis is a very important cellular process in which some enzymes are released by hemocytes in order to destroy the invading pathogen (Kavanagh and Reeves, 2004; Pereira et al., 2018; Sheehan and Kavanagh, 2018). The humoral response of these insects is constituted by effector molecules including opsonins, melanin, and antimicrobial peptides (AMPs) (Tsai et al., 2016). Although there are 18 different types of AMPs identified in *G. mellonella* hemolymph, we chose to examine galiomicin because it is a specific *G. mellonella* defense and is one of the most effective AMPs against fungal infection (Wojda, 2017). This AMP shows homology to human cysteine-rich peptides from the ß group of defensins and make up part of the innate immune system. In general, AMPs are the last line of defense and they act on the hemolymph attacking elements of the bacterial or fungal cell wall (Shai, 2002; Mowlds et al., 2010; Rossoni et al., 2017).

Although postbiotic elements of *L. paracasei* 28.4 have shown promising results, the key components of LPCE and LPF1 with antifungal properties are still unknown and need to be further investigated. Future studies should be addressed for the isolation and characterization of the bioactive molecules presents in *L. paracasei* 28.4 supernatant, as well as for the action mechanisms of these postbiotic elements on specific targets in fungal cells.

Within the limitations of the study, it can be concluded that *L. paracasei* 28.4 cells and its postbiotic elements (LPCE and LPF1) have antifungal activity against *C. auris* including activity against planktonic and persister cells, as well as biofilms. Postbiotic derived from *L. paracasei* 28.4 protected *G. mellonella* infected with *C. auris* and enhanced its immune status indicating a dual function in modulating the host immune response. The exact mechanisms related to the action of postbiotic elements against *C. auris* are still unclear and need to be further investigated.

DATA AVAILABILITY STATEMENT

The datasets generated for this study are available on request to the corresponding author.

AUTHOR CONTRIBUTIONS

RR and PB conducted most of the experiments. DS, IM, and RM played a key role in extraction and fractionation of post-biotic elements. RR, BF, JJ, and EM wrote the paper. EM, BF, and JJ conceived and supervised all the work. All authors contributed to the article and approved the submitted version.

FUNDING

JJ was supported by the National Council for Scientific Development/CNPq (306330/2018-0). RR received a scholarship from São Paulo Research Foundation/FAPESP (Grants 2017/19219-3 and 2018/21239-5). BF was supported by NIH grant P20 GM121344.

REFERENCES

Al-Dhaheri, R. S., and Douglas, L. J. (2008). Absence of amphotericin B-tolerant persister cells in biofilms of some *Candida* species. *Antimicrob. Agents Chemother*. 52, 1884–1887. doi: 10.1128/AAC.01473-07

Bergin, D., Brennan, M., and Kavanagh, K. (2003). Fluctuations in haemocyte density and microbial load may be used as indicators of fungal pathogenicity in larvae of *Galleria mellonella*. *Microbes Infect*. 5, 1389–1395. doi: 10.1016/j.micinf.2003.09.019

Bidaud, A. L., Chowdhary, A., and Dannaoui, E. (2018). *Candida auris*: an emerging drug resistant yeast—a mini-review. *J. Mycol. Med*. 28, 568–573. doi: 10.1016/j.mycmed.2018.06.007

Bigger, J. (1944). Treatment of *Staphylococcal* infections with penicillin by intermittent sterilisation. *Lancet* 244, 497–500. doi: 10.1016/S0140-6736(00)74210-3

Borman, A. M., Szekely, A., and Johnson, E. M. (2016). Comparative pathogenicity of United Kingdom isolates of the emerging pathogen *Candida auris* and other key pathogenic candida species. *mSphere* 1, e00189–e00216. doi: 10.1128/mSphere.00189-16

Cannon, J. P., Lee, T. A., Bolanos, J. T., and Danziger, L. H. (2005). Pathogenic relevance of *Lactobacillus*: a retrospective review of over 200 cases. *Eur. J. Clin. Microbiol. Infect. Dis*. 24, 31–40. doi: 10.1007/s10096-004-1253-y

Centers for Disease Control and Prevention (2016). *Global Emergence of Invasive Infections Caused by the Multidrug-Resistant Yeast Candida auris*. Atlanta, GA: Clinical Alert to US Healthcare Facilities.

Cernakova, L., Light, C., Salehi, B., Rogel-Castillo, C., Victoriano, M., Martorell, M., et al. (2019). Novel therapies for biofilm-based *Candida* spp. infections. *Adv. Exp. Med. Biol*. 1214, 93–123. doi: 10.1007/5584_2019_400

Chaabane, F., Graf, A., Jequier, L., and Coste, A. T. (2019). Review on antifungal resistance mechanisms in the emerging pathogen *Candida auris*. *Front. Microbiol*. 10:2788. doi: 10.3389/fmicb.2019.02788

Chakrabarti, A., and Singh, S. (2020). Multidrug-resistant *Candida auris*: an epidemiological review. *Expert Rev. Anti Infect. Ther*. 18, 551–562. doi: 10.1080/14787210.2020.1750368

Cicenia, A., Scirocco, A., Carabotti, M., Pallotta, L., Marignani, M., and Severi, C. (2014). Postbiotic activities of lactobacilli-derived factors. *J. Clin. Gastroenterol*. 48(Suppl.1), S18–S22. doi: 10.1097/MCG.0000000000000231

Compare, D., Rocco, A., Coccoli, P., Angrisani, D., Sgamato, C., Iovine, B., et al. (2017). *Lactobacillus casei* DG and its postbiotic reduce the inflammatory mucosal response: an *ex-vivo* organ culture model of post-infectious irritable bowel syndrome. *BMC Gastroenterol*. 17:53. doi: 10.1186/s12876-017-0605-x

Davies, D. (2003). Understanding biofilm resistance to antibacterial agents. *Nat. Rev. Drug Discov*. 2, 114–122. doi: 10.1038/nrd1008

de Barros, P. P., Scorzoni, L., Ribeiro, F. C., Fugisaki, L. R. O., Fuchs, B. B., Mylonakis, E., et al. (2018). *Lactobacillus paracasei* 28.4 reduces *in vitro* hyphae formation of *Candida albicans* and prevents the filamentation in an experimental model of *Caenorhabditis* elegans. *Microb. Pathog*. 117, 80–87. doi: 10.1016/j.micpath.2018.02.019

Denega, I., d'Enfert, C., and Bachellier-Bassi, S. (2019). *Candida albicans* biofilms are generally devoid of persister cells. *Antimicrob. Agents Chemother*. 63:e01979-18. doi: 10.1128/AAC.01979-18

Dunand, E., Burns, P., Binetti, A., Bergamini, C., Peralta, G. H., Forzani, L., et al. (2019). Postbiotics produced at laboratory and industrial level as potential functional food ingredients with the capacity to protect mice against Salmonella infection. *J. Appl. Microbiol*. 127, 219–229. doi: 10.1111/jam.14276

Gao, J., Li, Y., Wan, Y., Hu, T., Liu, L., Yang, S., et al. (2019). A novel postbiotic from *Lactobacillus rhamnosus* GG with a beneficial effect on intestinal barrier function. *Front. Microbiol*. 10:477. doi: 10.3389/fmicb.2019.00477

Geraldo, B. M. C., Batalha, M. N., Milhan, N. V. M., Rossoni, R. D., Scorzoni, L., and Anbinder, A. L. (2019). Heat-killed *Lactobacillus reuteri* and cell-free culture supernatant have similar effects to viable probiotics during interaction with *Porphyromonas gingivalis*. *J. Periodontal. Res.* 55, 215–220. doi: 10.1111/jre.12704

Gillum, A. M., Tsay, E. Y., and Kirsch, D. R. (1984). Isolation of the *Candida albicans* gene for orotidine-5'-phosphate decarboxylase by complementation of S. cerevisiae ura3 and *E. coli* pyrF mutations. *Mol. Gen. Genet*. 198, 179–182. doi: 10.1007/BF00328721

Guarner, F., Khan, A. G., Garisch, J., Eliakim, R., Gangl, A., Thomson, A., et al. (2012). World gastroenterology organisation global guidelines: probiotics and prebiotics october 2011. *J. Clin. Gastroenterol*. 46, 468–481. doi: 10.1097/MCG.0b013e3182549092

Hu, H. J., Zhang, G. Q., Zhang, Q., Shakya, S., and Li, Z. Y. (2017). Probiotics prevent *Candida* colonization and invasive fungal sepsis in preterm neonates: a systematic review and meta-analysis of randomized controlled trials. *Pediatr. Neonatol*. 58, 103–110. doi: 10.1016/j.pedneo.2016.06.001

Jacobsen, I. D., Wilson, D., Wachtler, B., Brunke, S., Naglik, J. R., and Hube, B. (2012). *Candida albicans* dimorphism as a therapeutic target. *Expert Rev. Anti Infect. Ther*. 10, 85–93. doi: 10.1586/eri.11.152

Janczarek, M., Bachanek, T., Mazur, E., and Chalas, R. (2016). The role of probiotics in prevention of oral diseases. *Postepy Hig. Med. Dosw*. 70, 850–857. doi: 10.5604/17322693.1214381

Jin, Y., Samaranayake, L. P., Samaranayake, Y., and Yip, H. K. (2004). Biofilm formation of *Candida albicans* is variably affected by saliva and dietary sugars. *Arch. Oral Biol*. 49, 789–798. doi: 10.1016/j.archoralbio.2004.04.011

Johnson, C. N., Kogut, M. H., Genovese, K., He, H., Kazemi, S., and Arsenault, R. J. (2019). Administration of a postbiotic causes immunomodulatory responses in broiler gut and reduces disease pathogenesis following challenge. *Microorganisms* 7:268. doi: 10.3390/microorganisms7080268

Kavanagh, K., and Reeves, E. P. (2004). Exploiting the potential of insects for *in vivo* pathogenicity testing of microbial pathogens. *FEMS Microbiol. Rev*. 28, 101–112. doi: 10.1016/j.femsre.2003.09.002

Kean, R., Delaney, C., Sherry, L., Borman, A., Johnson, E. M., Richardson, M. D., et al. (2018). Transcriptome assembly and profiling of *Candida auris* reveals

novel insights into biofilm-mediated resistance. *mSphere* 3, e00334–e00418. doi: 10.1128/mSphere.00334-18

LaFleur, M. D., Kumamoto, C. A., and Lewis, K. (2006). *Candida albicans* biofilms produce antifungal-tolerant persister cells. *Antimicrob. Agents Chemother*. 50, 3839–3846. doi: 10.1128/AAC.00684-06

Lockhart, S. R., Etienne, K. A., Vallabhaneni, S., Farooqi, J., Chowdhary, A., Govender, N. P., et al. (2017). Simultaneous emergence of multidrug-resistant *Candida auris* on 3 continents confirmed by whole-genome sequencing and epidemiological analyses. *Clin. Infect. Dis*. 64, 134–140. doi: 10.1093/cid/ciw691

Mailander-Sanchez, D., Wagener, J., and Schaller, M. (2012). Potential role of probiotic bacteria in the treatment and prevention of localised candidosis. *Mycoses* 55, 17–26. doi: 10.1111/j.1439-0507.2010.01967.x

Martins, N., Ferreira, I. C., Barros, L., Silva, S., and Henriques, M. (2014). Candidiasis: predisposing factors, prevention, diagnosis and alternative treatment. *Mycopathologia* 177, 223–240. doi: 10.1007/s11046-014-9749-1

Matsubara, V. H., Bandara, H. M., Mayer, M. P., and Samaranayake, L. P. (2016a). Probiotics as antifungals in mucosal candidiasis. *Clin. Infect. Dis*. 62, 1143–1153. doi: 10.1093/cid/ciw038

Matsubara, V. H., Wang, Y., Bandara, H. M., Mayer, M. P., and Samaranayake, L. P. (2016b). Probiotic lactobacilli inhibit early stages of *Candida albicans* biofilm development by reducing their growth, cell adhesion, and filamentation. *Appl. Microbiol. Biotechnol*. 100, 6415–6426. doi: 10.1007/s00253-016-7527-3

Medina, R. P., Araujo, A. R., Batista, J. M. Jr., Cardoso, C. L., Seidl, C., Vilela, A. F. L., et al. (2019). Botryane terpenoids produced by *Nemania bipapillata*, an endophytic fungus isolated from red alga *Asparagopsis taxiformis*—Falkenbergia stage. *Sci. Rep*. 9:12318. doi: 10.1038/s41598-019-48655-7

Mosca, F., Gianni, M. L., and Rescigno, M. (2019). Can postbiotics represent a new strategy for NEC? *Adv. Exp. Med. Biol*. 1125, 37–45. doi: 10.1007/5584_2018_314

Mowlds, P., Coates, C., Renwick, J., and Kavanagh, K. (2010). Dose-dependent cellular and humoral responses in *Galleria mellonella* larvae following beta-glucan inoculation. *Microbes Infect*. 12, 146–153. doi: 10.1016/j.micinf.2009.11.004

Mylonakis, E., Moreno, R., El Khoury, J. B., Idnurm, A., Heitman, J., Calderwood, S. B., et al. (2005). *Galleria mellonella* as a model system to study *Cryptococcus neoformans* pathogenesis. *Infect. Immun*. 73, 3842–3850. doi: 10.1128/IAI.73.7.3842-3850.2005

National Committee for Clinical Laboratory Standards (2002). "Reference method for broth dilution antifungal susceptibility testing of yeasts," in *M27-A Wayne* (Pennsylvania, PA: Approved standard M27–A).

Nett, J. E. (2019). *Candida auris*: an emerging pathogen "incognito?" *PLoS Pathog*. 15:e1007638. doi: 10.1371/journal.ppat.1007638

Pathirana, R. U., Friedman, J., Norris, H. L., Salvatori, O., McCall, A. D., Kay, J., et al. (2018). Fluconazole-resistant *Candida auris* is susceptible to salivary histatin 5 killing and to intrinsic host defenses. *Antimicrob. Agents Chemother*. 62, e01872–e01917. doi: 10.1128/AAC.01872-17

Peeters, E., Nelis, H. J., and Coenye, T. (2008). Comparison of multiple methods for quantification of microbial biofilms grown in microtiter plates. *J. Microbiol. Methods* 72, 157–165. doi: 10.1016/j.mimet.2007.11.010

Peleg, A. Y., Tampakakis, E., Fuchs, B. B., Eliopoulos, G. M., Moellering, R. C. Jr., and Mylonakis, E. (2008). Prokaryote-eukaryote interactions identified by using *Caenorhabditis* elegans. *Proc. Natl. Acad. Sci. U. S. A*. 105, 14585–14590. doi: 10.1073/pnas.0805048105

Pereira, T. C., de Barros, P. P., Fugisaki, L. R. O., Rossoni, R. D., Ribeiro, F. C., de Menezes, R. T., et al. (2018). Recent advances in the use of *galleria mellonella* model to study immune responses against human pathogens. *J. Fungi.* 4:128. doi: 10.3390/jof4040128

Pfaller, M. A., Sheehan, D. J., and Rex, J. H. (2004). Determination of fungicidal activities against yeasts and molds: lessons learned from bactericidal testing and the need for standardization. *Clin. Microbiol. Rev*. 17, 268–280. doi: 10.1128/CMR.17.2.268-280.2004

Ribeiro, F. C., de Barros, P. P., Rossoni, R. D., Junqueira, J. C., and Jorge, A. O. (2017). *Lactobacillus rhamnosus* inhibits *Candida albicans* virulence factors *in vitro* and modulates immune system in *Galleria mellonella*. *J. Appl. Microbiol*. 122, 201–211. doi: 10.1111/jam.13324

Ribeiro, F. C., Junqueira, J. C., Dos Santos, J. D., de Barros, P. P., Rossoni, R. D., Shukla, S., et al. (2020). Development of probiotic formulations for oral candidiasis prevention: Gellan gum as a carrier to deliver *Lactobacillus paracasei* 28.4. *Antimicrob. Agents Chemother*. 6, e02323–e02419. doi: 10.1128/AAC.02323-19

Riccardi, N., Rotulo, G. A., and Castagnola, E. (2019). Definition of opportunistic infections in immunocompromised children on the basis of etiologies and clinical features: a summary for practical purposes. *Curr. Pediatr. Rev*. 15, 197–206. doi: 10.2174/1573396315666190617151745

Rodrigues, C. F., Rodrigues, M. E., and Henriques, M. C. R. (2019). Promising alternative therapeutics for oral candidiasis. *Curr. Med. Chem*. 26, 2515–2528. doi: 10.2174/0929867325666180601102333

Rodrigues, M. E., Gomes, F., and Rodrigues, C. F. (2019). *Candida* spp./bacteria mixed biofilms. *J. Fungi.* 6:5. doi: 10.3390/jof6010005

Rodrigues, M. E., Silva, S., Azeredo, J., and Henriques, M. (2016). Novel strategies to fight *Candida* species infection. *Crit. Rev. Microbiol*. 42, 594–606. doi: 10.3109/1040841X.2014.974500

Rossato, L., and Colombo, A. L. (2018). *Candida auris*: what have we learned about its mechanisms of pathogenicity? *Front. Microbiol*. 9:3081. doi: 10.3389/fmicb.2018.03081

Rossoni, R. D., de Barros, P. P., de Alvarenga, J. A., Ribeiro, F. C., Velloso, M. D. S., Fuchs, B. B., et al. (2018). Antifungal activity of clinical *Lactobacillus* strains against *Candida albicans* biofilms: identification of potential probiotic candidates to prevent oral candidiasis. *Biofouling* 34, 212–225. doi: 10.1080/08927014.2018.1425402

Rossoni, R. D., de Barros, P. P., Lopes, L., Ribeiro, F. C., Nakatsuka, T., Kasaba, H., et al. (2019). Effects of surface pre-reacted glass-ionomer (S-PRG) eluate on *Candida* spp: antifungal activity, anti-biofilm properties, and protective effects on *Galleria mellonella* against *C. albicans infection. Biofouling* 35, 997–1006. doi: 10.1080/08927014.2019.1686485

Rossoni, R. D., Fuchs, B. B., Barros, P. P. d., Velloso M. d. S., Jorge, A. O. C., Junqueira, J. C., and Mylonakis, E. (2017). *Lactobacillus paracasei* modulates the immune system of *Galleria mellonella* and protects against *Candida albicans* infection. *PLoS ONE* 12:e0173332. doi: 10.1371/journal.pone.0173332

Sabino, R., Verissimo, C., Pereira, A. A., and Antunes, F. (2020). *Candida auris*, an agent of hospital-associated outbreaks: which challenging issues do we need to have in mind? *Microorganisms* 8:181. doi: 10.3390/microorganisms8020181

Salminen, M. K., Rautelin, H., Tynkkynen, S., Poussa, T., Saxelin, M., Valtonen, V., et al. (2006). *Lactobacillus bacteremia*, species identification, and antimicrobial susceptibility of 85 blood isolates. *Clin. Infect. Dis*. 42, e35–e44. doi: 10.1086/500214

Santos, R. B., Scorzoni, L., Namba, A. M., Rossoni, R. D., Jorge, A. O. C., and Junqueira, J. C. (2019). *Lactobacillus* species increase the survival of *Galleria mellonella* infected with *Candida albicans* and non-albicans *Candida* clinical isolates. *Med. Mycol*. 57, 391–394. doi: 10.1093/mmy/myy032

Scalfaro, C., Iacobino, A., Nardis, C., and Franciosa, G. (2017). *Galleria mellonella* as an *in vivo* model for assessing the protective activity of probiotics against gastrointestinal bacterial pathogens. *FEMS Microbiol. Lett*. 364, 1–6. doi: 10.1093/femsle/fnx064

Sekyere, J. O., and Asante, J. (2018). Emerging mechanisms of antimicrobial resistance in bacteria and fungi: advances in the era of genomics. *Future Microbiol*. 13, 241–262. doi: 10.2217/fmb-2017-0172

Serra, D. O., Klauck, G., and Hengge, R. (2015). Vertical stratification of matrix production is essential for physical integrity and architecture of macrocolony biofilms of *Escherichia coli*. *Environ. Microbiol*. 17, 5073–5088. doi: 10.1111/1462-2920.12991

Shai, Y. (2002). Mode of action of membrane active antimicrobial peptides. *Biopolymers* 66, 236–248. doi: 10.1002/bip.10260

Sheehan, G., and Kavanagh, K. (2018). Analysis of the early cellular and humoral responses of *Galleria mellonella* larvae to infection by *Candida albicans*. *Virulence* 9, 163–172. doi: 10.1080/21505594.2017.1370174

Sherry, L., Ramage, G., Kean, R., Borman, A., Johnson, E. M., Richardson, M. D., et al. (2017). Biofilm-forming capability of highly virulent, multidrug-resistant *Candida auris*. *Emerg. Infect. Dis*. 23, 328–331. doi: 10.3201/eid2302.161320

Spivak, E. S., and Hanson, K. E. (2018). *Candida auris*: an emerging fungal pathogen. *J. Clin. Microbiol*. 56, e01588–e01617. doi: 10.1128/JCM.01588-17

Tharmalingam, N., Khader, R., Fuchs, B. B., and Mylonakis, E. (2019). The anti-virulence efficacy of 4-(1,3-dimethyl-2,3-dihydro-1h-benzimidazol-2-yl)phenol against methicillin-resistant *Staphylococcus aureus*. *Front. Microbiol*. 10:1557. doi: 10.3389/fmicb.2019.01557

Tsai, C. J., Loh, J. M., and Proft, T. (2016). *Galleria mellonella* infection models for the study of bacterial diseases and for antimicrobial drug testing. *Virulence* 7, 214–229. doi: 10.1080/21505594.2015.1135289

Tsilingiri, K., Barbosa, T., Penna, G., Caprioli, F., Sonzogni, A., Viale, G., et al. (2012). Probiotic and postbiotic activity in health and disease: comparison on a novel polarised *ex-vivo* organ culture model. *Gut* 61, 1007–1015. doi: 10.1136/gutjnl-2011-300971

Tsilingiri, K., and Rescigno, M. (2013). Postbiotics: what else? *Benef. Microbes*. 4, 101–107. doi: 10.3920/BM2012.0046

Vicariotto, F., Del Piano, M., Mogna, L., and Mogna, G. (2012). Effectiveness of the association of 2 probiotic strains formulated in a slow release vaginal product, in women affected by vulvovaginal candidiasis: a pilot study. *J. Clin. Gastroenterol*. 46, S73–S80. doi: 10.1097/MCG.0b013e3182684d71

Vilela, S. F., Barbosa, J. O., Rossoni, R. D., Santos, J. D., Prata, M. C., Anbinder, A. L., et al. (2015). *Lactobacillus acidophilus* ATCC 4356 inhibits biofilm formation by *C. albicans* and attenuates the experimental candidiasis in *Galleria mellonella*. *Virulence* 6, 29–39. doi: 10.4161/21505594.2014.981486

Wachtler, B., Citiulo, F., Jablonowski, N., Forster, S., Dalle, F., Schaller, M., et al. (2012). *Candida albicans*-epithelial interactions: dissecting the roles of active penetration, induced endocytosis and host factors on the infection process. *PLoS ONE* 7:e36952. doi: 10.1371/journal.pone.0036952

Wegh, C. A. M., Geerlings, S. Y., Knol, J., Roeselers, G., and Belzer, C. (2019). Postbiotics and their potential applications in early life nutrition and beyond. *Int. J. Mol. Sci*. 20:4673. doi: 10.3390/ijms20194673

Wojda, I. (2017). Immunity of the greater wax moth *Galleria mellonella*. *Insect. Sci*. 24, 342–357. doi: 10.1111/1744-7917.12325

Conflict of Interest: The authors declare that the research was conducted in the absence of any commercial or financial relationships that could be construed as a potential conflict of interest.

frontiers in Microbiology

ORIGINAL RESEARCH
published: 04 September 2020
doi: 10.3389/fmicb.2020.01980

A Two-Way Road: Antagonistic Interaction Between Dual-Species Biofilms Formed by *Candida albicans*/*Candida parapsilosis* and *Trichophyton rubrum*

*Letícia Morais Garcia[1†], Caroline Barcelos Costa-Orlandi[1†], Níura Madalena Bila[1,2], Carolina Orlando Vaso[1], Larissa Naiara Carvalho Gonçalves[1], Ana Marisa Fusco-Almeida[1] and Maria José Soares Mendes-Giannini[1]**

[1] Clinical Mycology Laboratory, Department of Clinical Analysis, School of Pharmaceutical Sciences, São Paulo State University (UNESP), Araraquara, Brazil, [2] School of Veterinary, Eduardo Mondlane University, Maputo, Mozambique

OPEN ACCESS

Edited by:
Juliana Campos Junqueira,
São Paulo State University, Brazil

Reviewed by:
Luis Antonio Pérez-García,
Universidad Autónoma de San Luis Potosí, Mexico
Laura Judith Marcos Zambrano,
IMDEA Alimentación, Spain
Melyssa Negri,
State University of Maringá, Brazil

***Correspondence:**
Maria José Soares Mendes-Giannini
maria.giannini@unesp.br;
gianninimj@gmail.com

[†] These authors have contributed equally to this work

Specialty section:
This article was submitted to Fungi and Their Interactions, a section of the journal Frontiers in Microbiology

Received: 10 February 2020
Accepted: 27 July 2020
Published: 04 September 2020

Citation:
Garcia LM, Costa-Orlandi CB, Bila NM, Vaso CO, Gonçalves LNC, Fusco-Almeida AM and Mendes-Giannini MJS (2020) A Two-Way Road: Antagonistic Interaction Between Dual-Species Biofilms Formed by Candida albicans/Candida parapsilosis and Trichophyton rubrum. Front. Microbiol. 11:1980. doi: 10.3389/fmicb.2020.01980

Dermatomycoses include superficial fungal infections of the skin and its appendages. *Trichophyton rubrum*, *Candida albicans*, and *Candida parapsilosis* are some of the most prevalent species that cause dermatomycoses. Several studies show a variable predominance of *Candida* spp. in relation to dermatophytes, especially in onychomycosis and the possibility of isolating both from the same site. The ability of dermatophytes to form biofilms recently been explored and there is currently no evidence on the involvement of these filamentous fungi in multi-species biofilms. Thus, this study aims to investigate the probable dual-species interaction between *T. rubrum* and *C. albicans* and *T. rubrum* and *C. parapsilosis* biofilms, considering variable formation conditions, as well as the susceptibility of these dual-species biofilms against terbinafine and efinaconazole. Three conditions of formation of dual-species biofilms were tested: (a) the suspensions of *T. rubrum* and *Candida albicans* or *C. parapsilosis* placed together; (b) suspensions of *C. albicans* and *C. parapsilosis* added the pre-adhesion of *T. rubrum* biofilms; (c) after the maturation of *T. rubrum* sessile cells. In the first and second conditions, the quantification of metabolic activities, biomass, and polysaccharide materials of mixed biofilms tended to resemble *Candida* monospecies biofilms. In the third condition, the profiles were modified after the addition of *Candida*, suggesting that *T. rubrum* biofilms served as substrate for the development of *Candida* biofilms. Scanning electron microscopy showed *Candida* predominance, however, numerous blastoconidia were noted, most evident in the conditions under which *Candida* was added after the pre-adhesion and maturation of *T. rubrum* biofilms. Despite the predominance of *Candida*, the presence of *T. rubrum* appears to inhibit *C. albicans* filamentation and *C. parapsilosis* development, confirming an antagonistic interaction. Fungal burden assays performed when the biofilms were formed together confirmed *Candida* predominance, as well as susceptibility to antifungals. Further studies will be needed to identify the components of the *Candida* and *T. rubrum* biofilm supernatants responsible for inhibiting dermatophyte growth and *C. albicans* filamentation.

Keywords: polymicrobial biofilms, *Candida albicans*, *C. parapsilosis*, dermatophytes, antagonistic interaction, dermatomycosis, *Trichophyton rubrum*

INTRODUCTION

Fungal infections of the skin, nails (onychomycosis), and cutaneous-mucous surfaces, known as dermatomycosis, are caused by several etiological agents and are an important cause of morbidity (Rotta et al., 2012). Among dermatomycosis, dermatophytosis, caused by dermatophytes, are the most prevalent worldwide, affecting 20 to 25% of the population (Havlickova et al., 2008; Zhan and Liu, 2017). *Trichophyton rubrum* is the microorganism most frequently associated with superficial mycoses (Costa-Orlandi et al., 2012, 2014; Zhan and Liu, 2017; Celestrino et al., 2019). Previous studies have reported that some strains of *T. rubrum* have a high dissemination power in relation to other dermatophytes, showing the dominance of this microorganism among dermatophytosis (Ghannoum et al., 2013).

Regarding yeasts of the genus *Candida*, *C. albicans* is the pathogen most commonly isolated from superficial mycoses. However, the incidence of infections by non-*C. albicans* species, such as *C. parapsilosis*, *C. tropicalis*, *C. krusei*, *C. glabrata*, and *C. guilliermondii*, has been increasing considerably (Sardi et al., 2013). Among, yeasts of *C. parapsilosis* are considered emerging pathogens and are commensal microorganisms of human skin. This microorganism is able to form biofilms in catheters and is transmitted through physical touch to neonates and in the hemodialysis systems used by chronic renal patients, thereafter evolving into bloodstream infections (Trofa et al., 2008; Pires et al., 2011, 2012).

Clinical practice cases and unpublished studies have demonstrated that it is possible to isolate one or more microorganisms from several infection sites in superficial mycoses, with a marked predominance of dermatophytes in comparison to yeasts of the genus *Candida* (Ghannoum et al., 2000; Aquino et al., 2007; Costa-Orlandi et al., 2012). Other studies indicate a higher prevalence of yeasts, especially *C. parapsilosis* in relation to *C. albicans* and *T. rubrum* in patients with onychomycosis (Pontes et al., 2002; Chadeganipour et al., 2010; Costa-Orlandi et al., 2012).

One of the major virulence factors of *Candida* is its ability to form biofilms (Ramage et al., 2012), which has also been reported recently in dermatophytes (Costa-Orlandi et al., 2014). Biofilms consist of communities of cells embedded in a polymeric extracellular matrix. These communities can be comprised of microorganisms of different species, genera or even kingdoms with a highly complex organization, allowing them to perform various functions, including nutrition, excretion, growth, communication, and protection, with greater efficiency (Ramage et al., 2009, 2012; Costa-Orlandi et al., 2017). Unlike planktonic cells, those found in biofilms have different morphologies depending on their location in the community (Ramage et al., 2012). For example, the morphology of *C. albicans* cells in biofilms vary from that of yeasts, hyphae, pseudohyphae, and germ tube, while *C. parapsilosis* consists mainly of yeasts and few pseudohyphae (Chandra and Mukherjee, 2015). Communities formed by dermatophytes are made up of a dense network of interconnected hyphae covered and embedded by an extracellular matrix that can be dense or thin (Costa-Orlandi et al., 2014). Changes in morphology are often regulated by molecules used for communication between cells, through a mechanism known as *quorum-sensing*, which has been widely studied in *Candida* biofilms but not yet investigated in dermatophytes. In addition to morphology, quorum-sensing is responsible for biofilm development, cell population control, nutrient competition control, dissemination, and the establishment of new communities during infection (Wongsuk et al., 2016).

Compared to the information available on biofilms formed by yeasts of the genus *Candida*, information on biofilms formed by dermatophytes is greatly lacking. Studies have previously found dermatophytes cohabiting with yeasts of the genus *Candida* and other microorganisms in superficial infections (unpublished data). This has also been widely observed in clinical practice. Therefore, the formation of mixed biofilms between these fungi is likely since biofilms provide many advantages for the microorganisms involved and rarely involve only one species (Costa-Orlandi et al., 2017).

There has been an increase in the incidence of mixed infections, namely among dermatophytes with yeasts or even non-dermatophyte filamentous species (Gawaz and Weisel, 2018). This increase has been accompanied by reports of antifungal resistance and, consequently, an increase in therapeutic failures (Gupta and Foley, 2019). Kravvas et al. (2018) found that the majority of routine dermatological infections were in the form of biofilms. Although this has yet to be proven in the case of dermatophytes, biofilm formation has been attributed to the occurrence of onychomycosis, which is often refractory to antifungal treatment and has a high rate of recurrence (Gupta et al., 2016; Gupta and Foley, 2019). The heterogeneity of species within biofilms makes it difficult to characterize the contribution of each microorganism to the pathogenesis and maintenance of infection and disease (dos Santos et al., 2016; Iñigo and Del Pozo, 2018).

Finally, in multi-species biofilms, it is also essential to consider the intercellular communications that occur via quorum-sensing molecules, which allow one species to identify and react to the presence of another. Therefore, these mediators are also able to coordinate the collective behavior of microorganisms in these communities (Demuyser et al., 2014).

There is currently a lack of research demonstrating the involvement of dermatophytes in multi-species biofilms. Thus, this work aims to investigate the probable dual-species interaction between the biofilms of *T. rubrum* and *C. albicans* and *T. rubrum* and *C. parapsilosis*. We will take into account variable conditions of formation to evaluate the susceptibility of these dual-species biofilms against two potent last generation antifungals, both of which have a proven efficacy against these microorganisms alone.

MATERIALS AND METHODS

Microorganisms

In this work, strains of *C. albicans* SC 5314, *C. parapsilosis* ATCC 22019, and *T. rubrum* ATCC MYA-4438 were used. All strains

belonged to the collection of the Clinical Mycology Laboratory of the Department of Clinical Analysis, of the School of Pharmaceutical Sciences at São Paulo State University (UNESP). Strains of *C. albicans* and *C. parapsilosis* were maintained on Sabouraud Dextrose Agar (SDA) (Kasvi) (40 g/L), comprised of a mixture of peptic digestion of animal tissue (10 g/L) and pancreatic digestion of casein (10 g/l) and agar (15 g/L), at 35°C for 48 h. The dermatophytes were then kept on malt extract agar (Kasvi), comprised of 2% peptone from animal tissue (Sigma-Aldrich), 2% glucose (Synth) and 2% agar (Kasvi) at pH 5.7, incubated at 28°C for 7 days or until sporulation (Costa-Orlandi et al., 2014; Jacob et al., 2015; Vila et al., 2015).

In vitro Formation of Monospecies Biofilms

The *Candida* biofilms were formed according to Pierce et al. (2008), with some modifications. Colonies of the stock cultures of *C. albicans* SC5314 and *C. parapsilosis* ATCC 22019 strains were subcultured in Sabouraud Dextrose broth (Kasvi) and incubated at 150 rpm and 35°C for 24 h. A fungal suspension was prepared in RPMI 1640 medium supplemented with L-glutamine without sodium bicarbonate (Gibco) and buffered with MOPS (Sigma-Aldrich) with 2% glucose (Synth) at a final concentration of 1×10^6 cells/mL. Two hundred microliters and one thousand microliters were dispensed in the wells of the 96- and 24-well plates (Kasvi), respectively. The plates were incubated at 37°C for 24 h and 48 h (maturation period) without shaking. A period of 72 h was also added to observe the behavior of biofilms for later standardization in dual-species biofilms, as the maturation period of *T. rubrum* biofilms corresponds to 72 h (Costa-Orlandi et al., 2014).

T. rubrum biofilms were formed as described by Costa-Orlandi et al. (2014). Briefly, *T. rubrum* ATCC MYA-4438 was subcultured in Malt Extract agar and incubated at 28°C for 7 days. The colonies were covered with 5 ml sterile of 0.85% saline, and conidia were gently detached with the aid of a sterile swab. The supernatant was placed in 15-mL conical tubes (Corning) and left to stand for 15–20 min to allow the hyphae to settle, such that only microconidia remained in the supernatant. The microconidia were counted in a hemocytometer and the suspension was adjusted using sterile saline (0.85%) to obtain a final concentration of 1×10^6 cells/mL. Subsequently, 200 μL and 1000 μL of the adjusted inoculum were dispensed in the 96- and 24-well plates, respectively. The plates were incubated at 37°C for 4 h without shaking for pre-adhesion of the biofilms. The supernatant was then removed and 200 μL and 1000 μL of RPMI 1640 medium was added to the wells of the 96- and 24 well plates, respectively. The plates were re-incubated at 37°C for up to 72 h. These biofilms were also formed at 96 h and 120 h for subsequent comparison with one of the conditions proposed for dual-species biofilms.

In vitro Formation of Dual-Species Biofilms

The fungal suspensions of all microorganisms were prepared at a final concentration of 1×10^6 cells/mL when plated. Mixed biofilms were formed under the following conditions: (a) the *T. rubrum*/*C. albicans* and *T. rubrum*/*C. parapsilosis* suspensions were dispensed in 96- and 24-well plates at the same time in a proportion of 1:1. The plates were then incubated at 37°C for up to 72 h; (b) *Candida* suspensions were added after the initial adhesion phase of *T. rubrum* (4 h), followed by incubation at 37°C for up to 72 h; (c) *Candida* suspensions were added after the maturation period of *T. rubrum* biofilms (72 h) before incubating the plates at 37°C for an additional 24 h and 48 h. The culture medium was renewed every 24 h.

Determination of the Metabolic Activity of Biofilms Using XTT Reduction Assay (2,3-Bis (2-Methoxy-4-Nitro-5-Sulfophenyl)-5-[Carbonyl (Phenylamino)]-2H-Tetrazolium Hydroxide)

Biofilms were formed as described above at different time intervals (24 h to 120 h). A solution of XTT (Thermo Fisher Scientific) was prepared at a final concentration of 1 mg/mL in phosphate buffered saline (PBS) and menadione (1 mM) (Sigma-Aldrich). After removing the supernatant and washing the biofilms with PBS, 50 μL of XTT solution + 4 μL of menadione solution were added. The plates were subsequently incubated at 37°C for 3 h and measured using a Biotek Epoch™ 2 spectrophotometer at a wavelength of 490 nm (Martinez and Casadevall, 2007; Costa-Orlandi et al., 2014).

Quantification of Biomass by Crystal Violet (CV) Assay

The biomass quantification test was performed according to Marcos-Zambrano et al. (2014), with some modifications. Briefly, biofilms were formed in 96-well plates (Kasvi) at different incubation times. The resulting supernatants were removed and the remaining biofilms were washed with PBS. Two hundred microliters of methanol (Vetec) were added to each well for 15 min. The methanol was discarded and the plates were dried at room temperature for 45 min. After drying, 200 μL of 0.1% violet crystal solution (Dinamica) was dispensed into the wells for 20 min. The resulting supernatant was carefully aspirated and the wells were washed with distilled water until the complete removal of excess dye. Finally, 200 μL of 33% acetic acid (Synth) was added and plates were read using a spectrophotometer (Biotek Epoch™ 2 Microplate Spectrophotometer) at a wavelength of 570 nm. The resulting absorbance values were directly proportional to the amount of biomass.

Quantification of the Extracellular Matrix and Other Polysaccharides by Safranin Staining

The polysaccharide material and extracellular matrices of mono- and multi-species biofilms were stained with 50 μL of 1% safranin solution for 5 min after removing the supernatant and washing the wells with PBS. The plates were washed with 200 μL of sterile 0.85% saline solution until the supernatant became clear. Lastly,

the absorbance of the plates was measured using a Epoch™ 2 microplate spectrophotometer at 492 nm (Seidler et al., 2008; Costa-Orlandi et al., 2014).

Scanning Electron Microscopy (SEM)

Mono- and dual-species biofilms were formed in 24-well plates and incubated until the maximum time determined in each condition (as described above). The resulting supernatants were removed and the remaining biofilms were fixed with 800 μL of 2.5% glutaraldehyde solution (Sigma-Aldrich) for 1 to 2 h at 4°C. The glutaraldehyde solution was removed from the wells and the biofilms were dehydrated using increasing concentrations of alcohol (50–100%). After drying, the bottom of the plates was cut using a scalpel. The resulting samples were mounted on aluminum cylinders containing carbon strips and evaporated under high vacuum (Denton Vacuum Desk V; Jeol Ltd., Moorestown, NJ, United States) for gold coating. The topographical characteristics of the biofilms were analyzed by electron microscopy (JSM-6610 Series Scanning Electron Microscope; Jeol Ltd., United States) at the School of Dentistry of UNESP at Araraquara, SP, Brazil (Martinez et al., 2010; Costa-Orlandi et al., 2014; Li et al., 2019).

Colony Forming Units Counting Assay (CFU/mL) in Selective Media

For the *C. albicans*/*T. rubrum* and *C. parapsilosis*/*T. rubrum* biofilms (1:1), the colony forming units were counted in selective media. Monospecies biofilms were used as a control. After the formation of biofilms in 96-well plates, the culture media were discarded for the removal of poorly adherent cells. Two hundred microliters of sterile PBS were added, and the biofilms were detached from the wells with the aid of sterile tips. The contents of the wells were transferred to 1.5 ml microtubes (Kasvi) and vortexed until the complete dispersion of the biofilm cells. Serial dilutions were performed in PBS and 10 μL aliquots of the diluted content were plated in 60 × 15 mm Petri dishes containing sterile glass beads and two selective media: CHROMagar™ *Candida* (Difco; BD Biosciences) for the isolation of yeasts and Mycosel agar (Difco; BD Biosciences) for the isolation of *T. rubrum*. The plates were incubated at 28 and 37°C until the formation of colony forming units (dos Santos et al., 2016).

Activity of Terbinafine and Efinaconazole Against Mono- and Dual-Species Biofilms

The activity of terbinafine (Sigma-Aldrich) and efinaconazole (Valeant Pharmaceuticals) was verified against mono- and dual-species biofilms formed using the previously described conditions. Biofilms were formed in 96-well plates. After 72 h, the supernatants were removed and 200 μL of the different concentrations of the terbinafine (0.03 to 32 mg/L) and efinaconazole (0.5 to 256 mg/L) working solutions were prepared in RPMI-1640 medium supplemented with 2% glucose. Two controls were performed: a control for the sterility of the medium (negative control) and a control for growth without treatment (positive control). The plates were incubated without shaking at 37°C for an additional 48 h. Cell viability was evaluated using XTT reduction assay (Pierce et al., 2008). A reduction of at least 50% of metabolic activity was considered an inhibition compared to the metabolic activity of biofilms without treatment.

Statistical Analysis

At least three independent experiments were performed in triplicate for all tests, except for the colony-forming unit count assay. In this test, the assays were conducted with two independent experiments in triplicate. Data were subjected to statistical analysis using analysis of variance (ANOVA) with Bonferroni's *post hoc* test in GraphPad Prism 5.0 software. $P < 0.05$ was considered statistically significant.

RESULTS

Determination of the Metabolic Activity of Biofilms by XTT Reduction Assay

Monospecies Biofilms

The metabolic activities of the *Candida* monospecies biofilms rose significantly until 48 h ($p < 0.0001$) (**Figure 1**). At 72 h, there was a significant decline in the metabolism of both species ($p < 0.0001$). In *T. rubrum* biofilms, there was a significant increase in the metabolic activities for up to 72 h ($p < 0.0001$). After this period, the metabolic activities remained constant until 96 h, followed by a slight decay in 120 h ($p < 0.05$). However, during the periods of decay, there was still a considerable amount of living cells in the biofilm, indicating the beginning of the inhibition of mature biofilm formation.

Dual-Species Biofilms Formed Together (1:1)

The metabolic activities of the dual-species biofilms of *T. rubrum*/*C. albicans* and *T. rubrum*/*C. parapsilosis* were compared to the monospecies biofilms of each strain (**Figure 1**). **Figure 1A** shows the dual-species biofilm formed between *T. rubrum* ATCC MYA-4438 and *C. albicans* SC 5314. Until 48 h, the dual-species biofilm showed a higher metabolism than the monospecies biofilm of *T. rubrum* ($p < 0.0001$), similar to *C. albicans* biofilm. At 72 h, the metabolic activities of the dual-species biofilms were similar to that of the monospecies biofilms of *T. rubrum* and lower compared to that of *C. albicans* ($p < 0.01$).

A similar behavior was observed between the dual-species biofilms formed by *T. rubrum* ATCC MYA-4438 and *C. parapsilosis* ATCC 22019 (**Figure 1B**). At 24 h, the metabolic activity of the dual-species biofilm was equal to that of *C. parapsilosis* and higher than *T. rubrum* ($p < 0.0001$). At 48 h, the dual-species biofilm showed higher metabolic activities than the *T. rubrum* biofilm ($p < 0.0001$) and lower than *C. parapsilosis* ($p < 0.01$). At 72 h, the dual-species biofilms showed a superior metabolic activity compared to *C. parapsilosis* ($p < 0.01$) and similar levels of metabolic activity as *T. rubrum*.

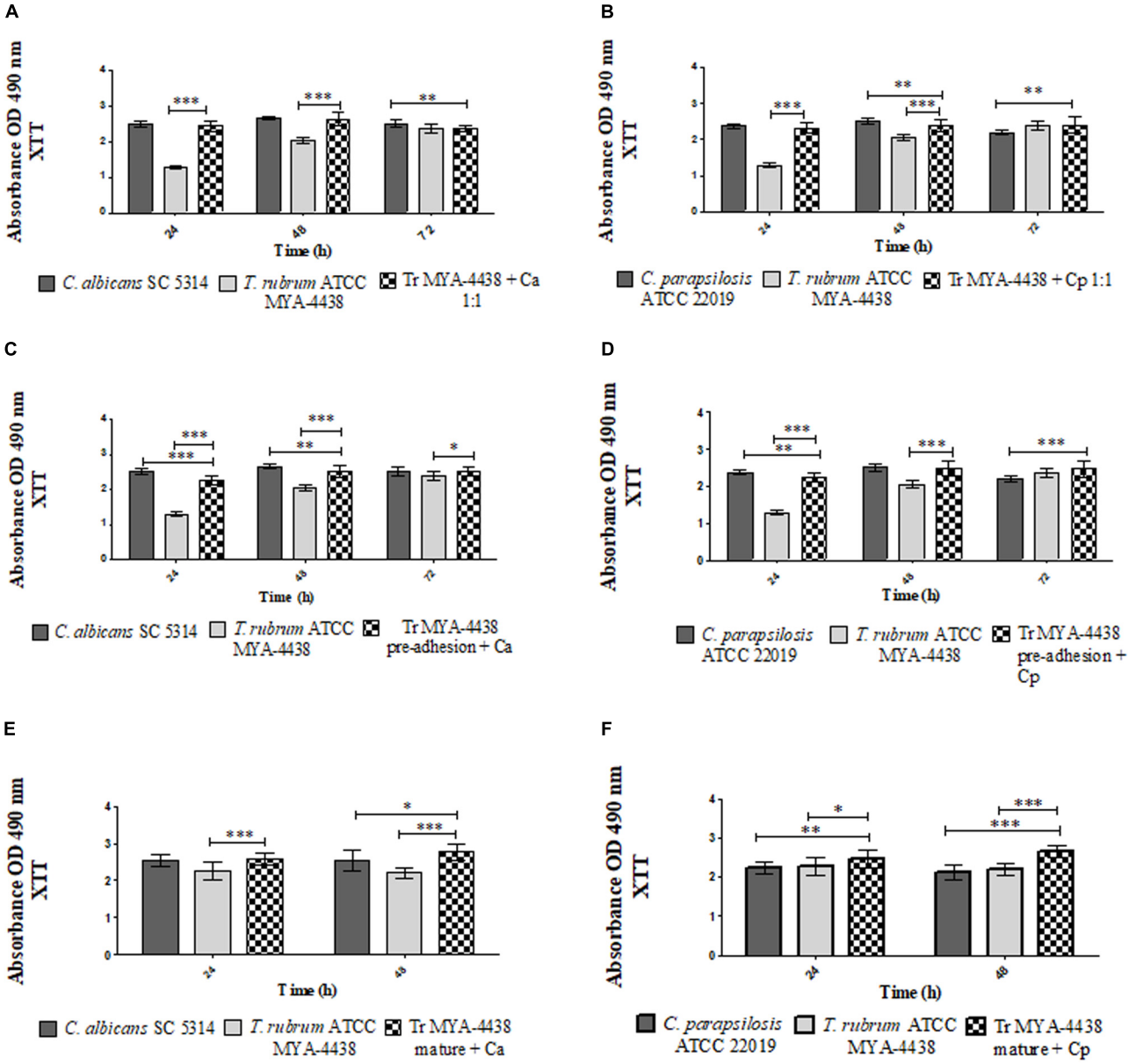

FIGURE 1 | Comparison between the metabolic activities of monospecies biofilms of *T. rubrum* ATCC MYA 4438, *C. albicans* SC 5314, and *C. parapsilosis* ATCC 22019 and the dual-species biofilms formed by *C. albicans*/*T. rubrum* and *C. parapsilosis*/*T. rubrum* under three different conditions: (1) the suspensions of *Candida* and *T. rubrum* were placed together at a proportion of 1:1 **(A,B)**; (2) *Candida* suspensions added after the pre-adhesion of *T. rubrum* biofilm **(C,D)**; (3) *Candida* suspensions added after the maturation of the *T. rubrum* biofilm, followed by an additional incubation of 24 h and 48 h **(E,F)**. Statistical significance: $^{*}p < 0.05$, $^{**}p < 0.01$; $^{***}p < 0.0001$. Tr, *T. rubrum*; Ca, *C. albicans*; Cp, *C. parapsilosis*.

Dual-Species Biofilms Formed After *T. rubrum* Pre-adhesion

The formation of dual-species biofilms in which *Candida* suspensions were added after the pre-adhesion of *T. rubrum* are shown in **Figures 1C,D**. **Figure 1C** shows the dual-species biofilm formed between *T. rubrum* ATCC MYA-4438 and *C. albicans SC 5314*. After 24 h, the mixed biofilm showed a higher metabolic activity than the *T. rubrum* biofilm ($p < 0.0001$) and lower than that of *C. albicans* ($p < 0.0001$). After 48 h of incubation, the dual-species biofilm showed lower metabolic activity than the *C. albicans* biofilm ($p < 0.01$) and higher than the *T. rubrum* biofilm ($p < 0.0001$). In 72 h, the dual-species biofilm exhibited a higher metabolic activity than the *T. rubrum* monospecies biofilm ($p < 0.05$), but similar to *C. albicans*.

When the *C. parapsilosis* suspension was added after *T. rubrum* pre-adhesion (**Figure 1D**), the metabolic activity of the dual-species biofilm was lower to that of *C. parapsilosis* ($p < 0.01$) and superior to that of *T. rubrum* ($p < 0.0001$) until 24 h. At

48 h, the dual-species biofilm showed metabolic activity similar to that of the *C. parapsilosis* monospecies biofilm and superior to that of *T. rubrum* ($p < 0.0001$). At 72 h, the mixed biofilm showed a higher metabolic activity than the *C. parapsilosis* biofilm ($p < 0.0001$), but similar to *T. rubrum*.

Dual-Species Biofilms Formed After Maturation of *T. rubrum* Biofilm

For this condition, *T. rubrum* biofilms were incubated until 72 h, corresponding to the maturation time. During this period, *Candida* suspensions were also added. The plates were then incubated for an additional 24 h and 48 h. Therefore, the plates incubated for 24 h and 48 h shown in **Figures 1E,F** correspond to the same periods after the addition of *Candida* and 96 h and 120 h of *T. rubrum* biofilm incubation. In relation to the additional incubation time of the *T. rubrum* biofilms, it is worth noting that the metabolic activities remained constant until 96 h, with a slight decay at 120 h, which can result in an inhibition phase (data not shown). **Figure 1E** shows that 24 h after the addition of the *C. albicans* suspensions, there was a significant increase in the metabolic activities of the dual-species biofilms compared to those of *T. rubrum* monospecies biofilms ($p < 0.0001$). The same result was observed after 48 h compared to the *C. albicans* ($p < 0.05$) and *T. rubrum* ($p < 0.0001$) monospecies biofilms. When the *C. parapsilosis* suspension was added, the mixed biofilms showed higher values of metabolic activities than the monospecies biofilm of *C. parapsilosis* ($p < 0.01$) and *T. rubrum* ($p < 0.05$) after 24 h (**Figure 1F**). After 48 h, the metabolic activities of mixed biofilms were superior to both monospecies biofilms of *C. parapsilosis* and *T. rubrum* ($p < 0.0001$).

Quantification of Biomass by Crystal Violet (CV) Staining

Monospecies Biofilms

The monospecies biofilms formed by *C. albicans* and *C. parapsilosis* indicated an increase in the development of biomass within the first 48 h ($p < 0.0001$). After this period (at 72 h), there was a significant decrease ($p < 0.0001$) in the absorbance measurements. Regarding *T. rubrum* biofilms, an increase in the biomass was observed until 72 h ($p < 0.0001$). After this period, there was no statistical significance between the absorbances up to 96 h, corresponding to a stationary phase, followed by a significant decay in 120 h ($p < 0.001$) (**Figure 2**). These results are in agreement with the findings of the XTT reduction assay.

Dual-Species Biofilms Formed Together (1:1)

The mass of the dual-species *C. albicans*/*T. rubrum* and *C. parapsilosis*/*T. rubrum* biofilms formed after the addition of fungal suspensions are shown in **Figures 2A,B**, respectively. In the first interaction (**Figure 2A**), the dual-species biofilm at 24 h showed a lower biomass than the monospecies biofilms ($p < 0.0001$). At 48 h, the biomass had significantly increased ($p < 0.001$). Compared to the monospecies biofilms, its development was similar to that of *C. albicans* and superior to the *T. rubrum* biofilm ($p < 0.0001$). The biomass decayed after 72 h of incubation, similar to the *C. albicans* biofilm and in contrast to the *T. rubrum* biofilm, whose biomass increased ($p < 0.0001$).

In the dual-species biofilms formed between *C. parapsilosis* and *T. rubrum* (**Figure 2B**), the biomass was similar to that of the monospecies *C. parapsilosis* biofilm and inferior to the *T. rubrum* biofilms ($p < 0.0001$) at 24 h. After 48 h of incubation, the biomass absorbance measurements were similar to both types of monospecies biofilms. At 72 h, the biomass of the dual-species biofilm was similar to that of *C. parapsilosis* and lower than *T. rubrum* ($p < 0.0001$).

Dual-Species Biofilms Formed After *T. rubrum* Pre-adhesion

When *C. albicans* suspensions were added after *T. rubrum* pre-adhesion (**Figure 2C**), the dual-species biofilms showed higher biomasses compared to both types of monospecies biofilms ($p < 0.0001$) at 24 h of incubation. At 48 h, the biomass of the dual-species biofilm was similar to *C. albicans* and higher than *T. rubrum* ($p < 0.0001$). At 72 h of incubation, the biomass was similar to that of the *T. rubrum* biofilm, which was superior to that of *C. albicans* ($p < 0.0001$).

In the dual-species biofilm formed between *T. rubrum* and *C. parapsilosis* (**Figure 2D**), the biomasses of dual-species biofilms were similar to the *C. parapsilosis* biofilms and inferior to *T. rubrum* ($p < 0.0001$) at 24 h. At 48 h, the biomass of the dual-species biofilms was similar to that of both monospecies biofilms. However, after 72 h, the mass of the biofilm was higher than that of *C. parapsilosis* ($p < 0.0001$) and lower than *T. rubrum* ($p < 0.0001$). These results indicate that *Candida* is predominant in this condition, although less than in the previous condition.

Dual-Species Biofilms Formed After Maturation of *T. rubrum* Biofilm

The biomass of dual-species biofilms formed after the addition of *Candida* suspensions for 24 h and 48 h in mature *T. rubrum* biofilms are shown in **Figures 2E,F**. After the addition of *C. albicans* (**Figure 2E**), the biomasses at 24 h and 48 h was superior to that of the monospecies biofilms of *T. rubrum* and *C. albicans* ($p < 0.05$). After 24 h of incubation with added *C. parapsilosis*, the biomass was similar to that of the *T. rubrum* biofilms and superior to the *C. parapsilosis* biofilms ($p < 0.0001$). After 48 h of incubation, the mass of the mixed biofilms was higher than the *C. parapsilosis* ($p < 0.0001$) and *T. rubrum* ($p < 0.01$) monospecies biofilms.

Quantification of Extracellular Matrix and Other Polysaccharides by Safranin Staining

Monospecies Biofilms

The monospecies biofilms were stained with safranin as a control in order to compare the amount of extracellular matrix and polysaccharide structures produced compared to the dual-species biofilms. In **Figure 3**, the production of polysaccharide material from *C. parapsilosis* ATCC 22019 and *C. albicans* SC 5314 increased until 48 h of incubation ($p < 0.0001$). After 72 h, decays were observed in both types of yeast biofilm ($p < 0.0001$). In *T. rubrum*, the production of polysaccharide material increased

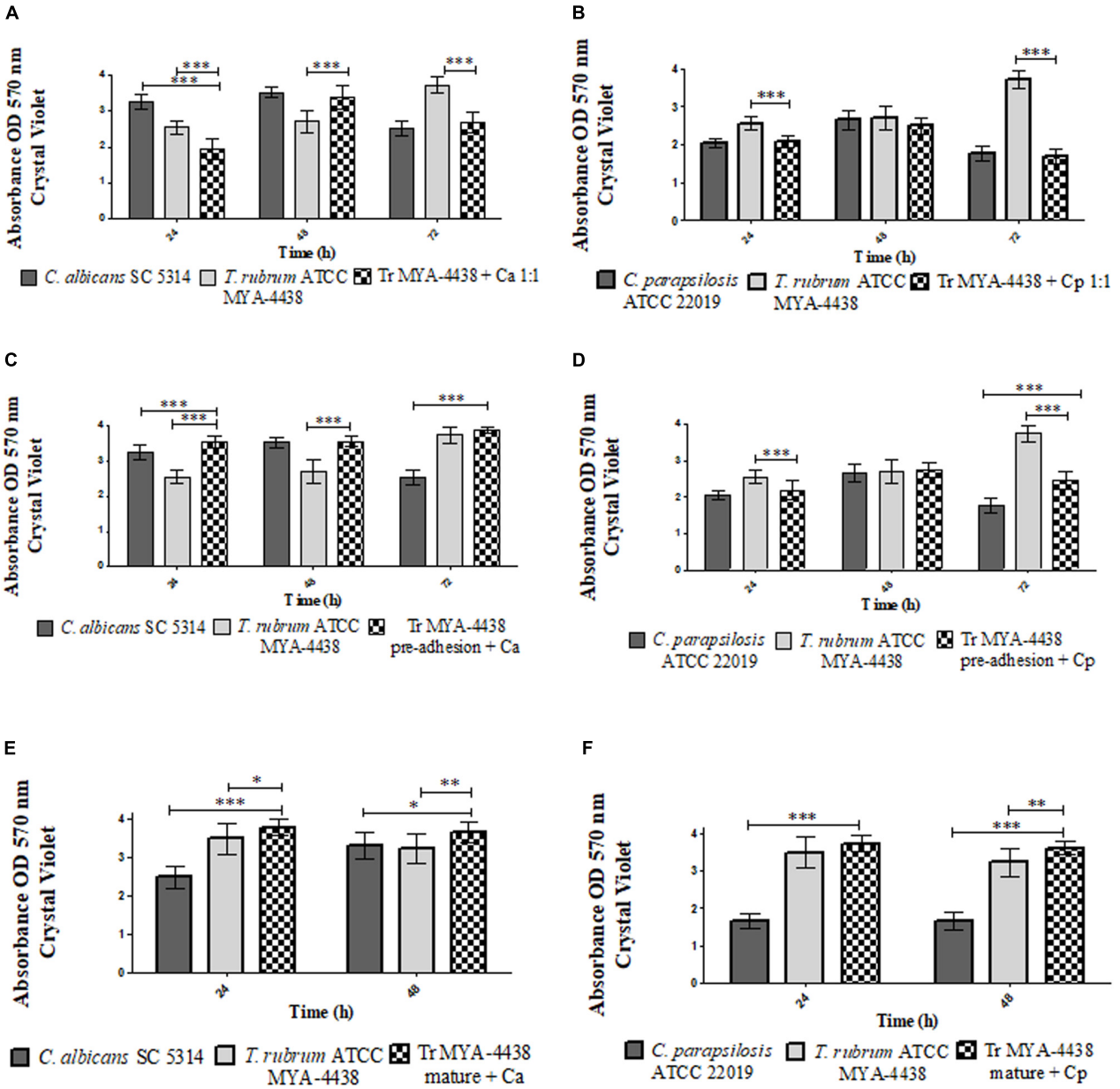

FIGURE 2 | Comparison between the biomasses produced by the monospecies biofilms of *T. rubrum* ATCC MYA 4438, *C. albicans* SC 5314, and *C. parapsilosis* ATCC 22019 and by the dual-species biofilms formed by *C. albicans*/*T. rubrum* and *C. parapsilosis*/*T. rubrum* under three different conditions: (1) suspensions of *Candida* and *T. rubrum* together at a proportion of 1:1 **(A,B)**; (2) *Candida* suspensions added after the pre-adhesion of *T. rubrum* biofilm **(C,D)**; (3) *Candida* suspensions added after the maturation of the *T. rubrum* biofilm, followed by an additional incubation of 24 h and 48 h **(E,F)**. Statistical significance: $^{*}p < 0.05$; $^{**}p < 0.01$; $^{***}p < 0.0001$. Tr, *T. rubrum*; Ca, *C. albicans*; Cp, *C. parapsilosis*.

until 72 h ($p < 0.0001$) and remained stable until 96 h, before declining at 120 h ($p < 0.0001$). These results corroborate with the results obtained in both the XTT and crystal violet assays, suggesting a maturation period for *Candida* biofilms of 48 h and for *T. rubrum* biofilms of 72 h.

Dual-Species Biofilms Formed Together (1:1)

The dual-species biofilm resulting from the *T. rubrum* ATCC MYA-4438 and *C. albicans* SC 5314 suspensions (**Figure 3A**) showed similar amounts of polysaccharide structures as the *C. albicans* biofilm ($p < 0.05$) and superior to the dermatophyte monospecies biofilm ($p < 0.0001$) after 48 h. At 72 h, the amount of polysaccharide material was higher than that of the *C. albicans* biofilm and lower than the *T. rubrum* biofilm ($p < 0.0001$).

For the dual-species biofilm formed using *T. rubrum* ATCC MYA-4438 and *C. parapsilosis* ATCC 22019 (**Figure 3B**), the amount of polysaccharide material formed after 24 h of incubation was greater than that of the *C. parapsilosis*

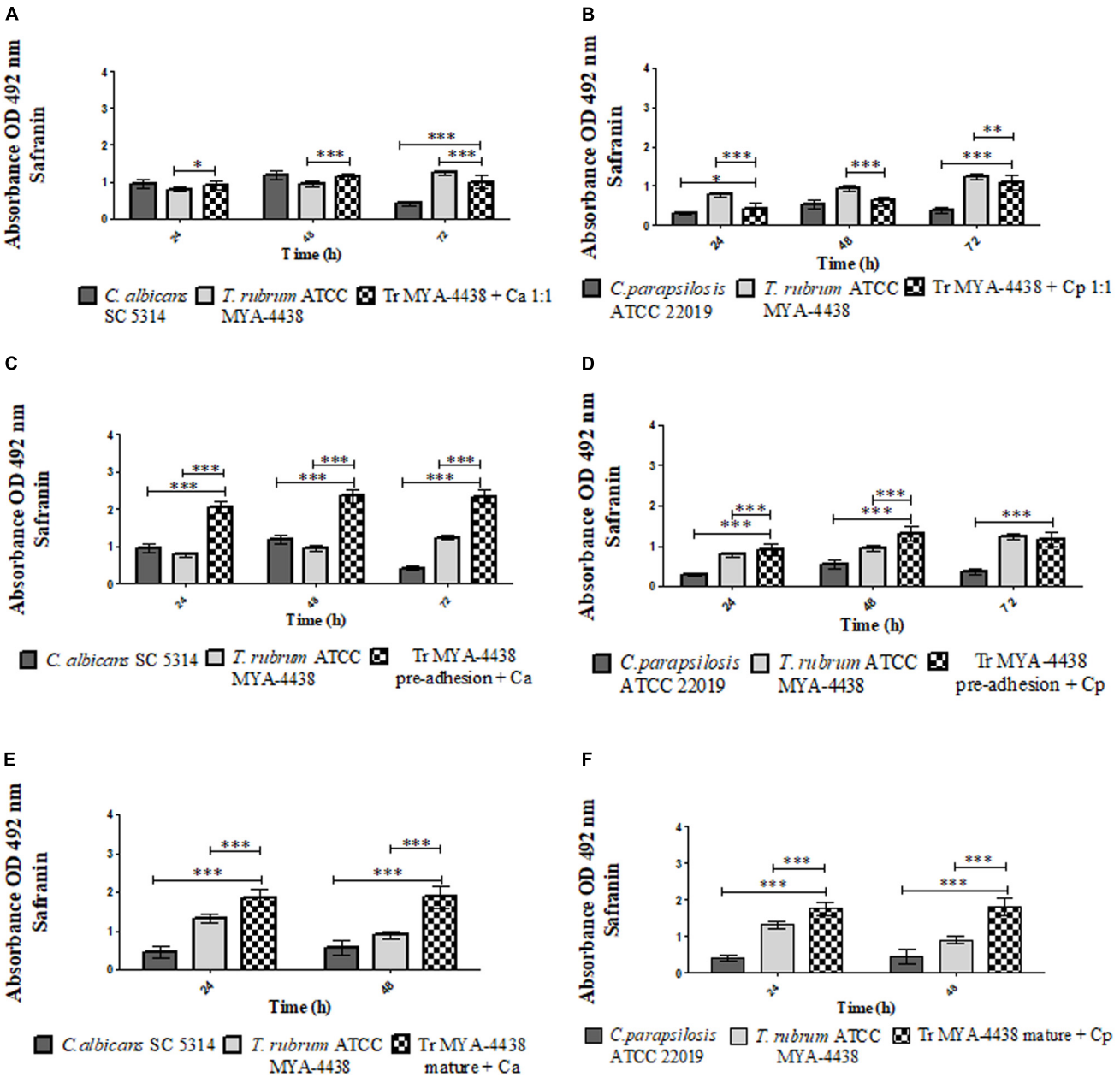

FIGURE 3 | Comparison between the amounts of extracellular matrix and polysaccharide structures produced by the monospecies biofilms of *T. rubrum* ATCC MYA 4438, *C. albicans* SC 5314, and *C. parapsilosis* ATCC 22019 and by the dual-species biofilms formed by *C. albicans*/*T. rubrum* and *C. parapsilosis*/*T. rubrum* under three different conditions: (1) suspensions of *Candida* and *T. rubrum* placed together at a proportion of 1:1 **(A,B)**; (2) *Candida* suspensions added after the pre-adhesion of *T. rubrum* biofilm **(C,D)**; (3) *Candida* suspensions added after the maturation of the *T. rubrum* biofilm, followed by an additional incubation of 24 h and 48 h **(E,F)**. Statistical significance: $^{*}p < 0.05$; $^{**}p < 0.01$; $^{***}p < 0.0001$. Tr, *T. rubrum*; Ca, *C. albicans*; Cp, *C. parapsilosis*.

monospecies biofilms ($p < 0.05$) and lower than that of *T. rubrum* ($p < 0.0001$). After 48 h, the dual-species biofilm showed quantities of polysaccharide structures similar to those of the yeast biofilm and lower than the dermatophyte biofilm ($p < 0.0001$). The dual-species biofilm at 72 h showed extracellular matrix development superior to *C. parapsilosis* ($p < 0.0001$) and lower than *T. rubrum* ($p < 0.01$).

Dual-Species Biofilms Formed After *T. rubrum* Pre-adhesion

Figure 3C shows that the dual-species biofilm of *T. rubrum* ATCC MYA-4438 and *C. albicans* SC 5314 after *T. rubrum* pre-adhesion established a quantity of polysaccharide material superior to both monospecies biofilms ($p < 0.0001$) after 72 h of incubation.

When formed with *C. parapsilosis* (**Figure 3D**), the dual-species biofilm formed after pre-adhesion of the dermatophyte showed an extracellular matrix development superior to both monospecies biofilms ($p < 0.0001$). Lastly, after 72 h of incubation, the dual-species biofilm showed polysaccharide structures similar to that of the dermatophyte and superior to *C. parapsilosis* ($p < 0.0001$).

Dual-Species Biofilms Formed After Maturation of *T. rubrum* Biofilm

When the *C. albicans* suspension was added to the mature *T. rubrum* biofilm, the amounts of polysaccharide material of the dual-species biofilm were higher than those of monospecies biofilms of both *T. rubrum* and *C. albicans* (**Figure 3E**) ($p < 0.0001$) after an additional 24 h and 48 h of incubation. The same behavior was observed in the *C. parapsilosis* and *T. rubrum* dual-species biofilms (**Figure 3F**). These results support the use of dermatophytes as substrates for the development of *Candida* biofilms, and corroborate our quantification of the metabolic activities by XTT assays and of the biomass by crystal violet staining.

Scanning Electron Microscopy (SEM)

The topographies of the dual-species biofilms of *C. albicans*/*T. rubrum* and *C. parapsilosis*/*T. rubrum* established under the three experimental conditions were analyzed by SEM with different magnifications (×1000 and ×3000) and compared to monospecies biofilms (controls) (**Figures 4**–**6**).

Figure 4 shows the topographies of the monospecies biofilms of *C. albicans* SC 5314 (**Figures 4a,b**) and *T. rubrum* ATCC MYA 4438 (**Figures 4c,d**), as well as their dual-species biofilms (1:1) (**Figures 4e,f**) and formation after *T. rubrum* pre-adhesion (**Figures 4g,h**). The biofilm of *C. albicans* SC 5314 (**Figures 4a,b**) was comprised of a dense hyphae network that developed from the yeasts, forming a complex three-dimensional structure. The same structures were observed in the *T. rubrum* ATCC-MYA 4438 biofilms, but appeared less dense than those in the *C. albicans* biofilms. Moreover, the polysaccharide material was at times dense and at other times thin, covering and connecting the hyphae network (**Figures 4c,d**). When the suspensions were placed together to form dual-species biofilms (**Figures 4e,f**), it was not possible to reliably distinguish between the hyphae formed by *C. albicans* and those formed by *T. rubrum* in the images. However, interestingly, a reasonable amount of blastoconidia (represented by the white arrows) was observed, suggesting that the interaction likely affected the mechanisms involved in the filamentation of *C. albicans*. The presence of blastoconidia indicates the probable predominance of *Candida* in relation to *T. rubrum*, more clearly seen in **Figure 4f**. When the *Candida* suspensions were added after 4 h of dermatophyte pre-adhesion (**Figures 4g,h**), similar results to those obtained in the previous condition were observed. However, numerous yeast blastoconidia were also observed, which reinforces our theory of the predominance of *Candida* in relation to *T. rubrum*. In addition, our findings indicate that the interaction with *T. rubrum* may somehow inhibit the filamentation of *C. albicans*. The greater prevalence of *C. albicans* compared to *T. rubrum* can be justified by the fact that yeasts have a faster metabolism than dermatophytes.

The topographies of the *C. parapsilosis* ATCC 22019 and *T. rubrum* MYA-4438 dual-species biofilms (1:1) after *T. rubrum* pre-adhesion are shown in **Figure 5**, along with their controls. **Figures 5a,b** show a predominance of blastoconidia and some rare pseudohyphae in the *C. parapsilosis* monospecies biofilm. The *T. rubrum* ATCC MYA 4438 biofilms are shown in **Figures 5c,d**. The interaction between *T. rubrum* and *C. parapsilosis* (**Figures 5e,f**) shows a predominance of yeast blastoconidia, but more dispersed than the control. We also

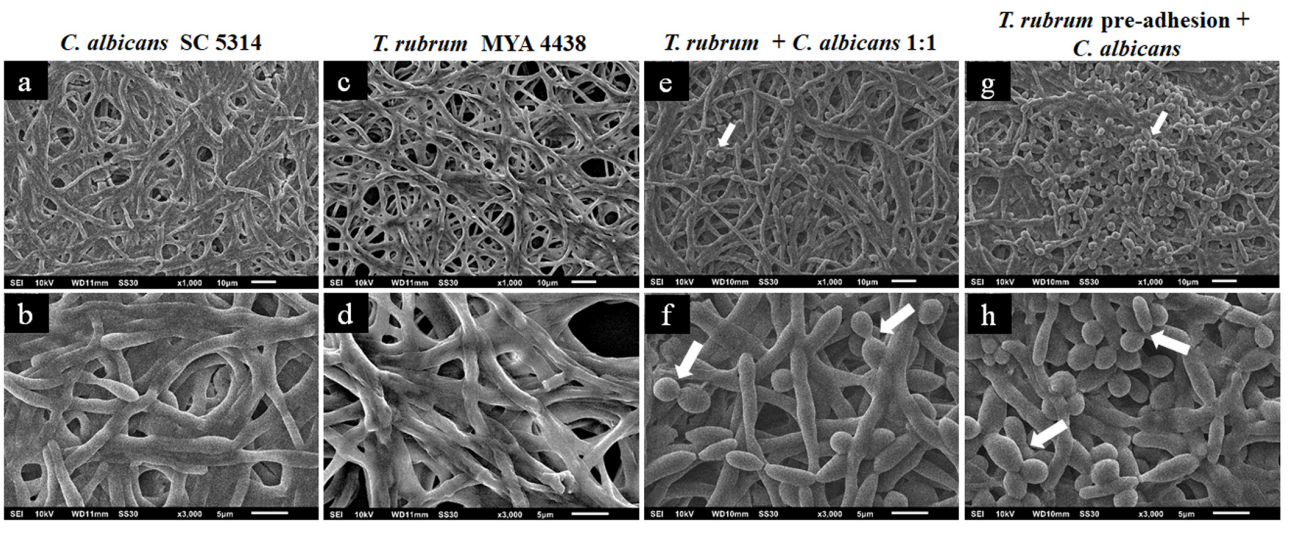

FIGURE 4 | Scanning electron microscopies of *C. albicans* SC 5314 **(a,b)** and *T. rubrum* ATCC MYA 4438 **(c,d)** monospecies biofilms and dual-species biofilms of *C. albicans*/*T. rubrum* formed at a proportion of 1:1 **(e,f)** or formed with the addition of *C. albicans* suspensions after the pre-adhesion of *T. rubrum* biofilm **(g,h)**. White arrows denote the blastoconidia of *C. albicans*.

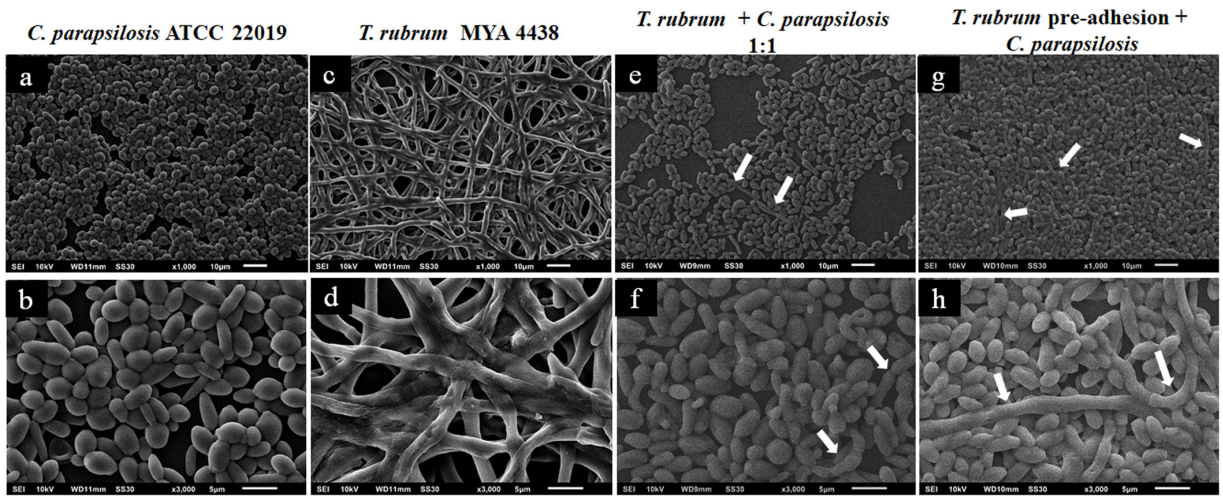

FIGURE 5 | Scanning electron microscopies of monospecies biofilms of *C. parapsilosis* ATCC 22019 **(a,b)** and *T. rubrum* ATCC MYA 4438 **(c,d)** and dual-species biofilms of *C. parapsilosis*/*T. rubrum* formed at a proportion of 1:1 **(e,f)** or formed with the addition of *C. parapsilosis* suspensions after the pre-adhesion of *T. rubrum* biofilm **(g,h)**. White arrows denote the hyphae of *T. rubrum*.

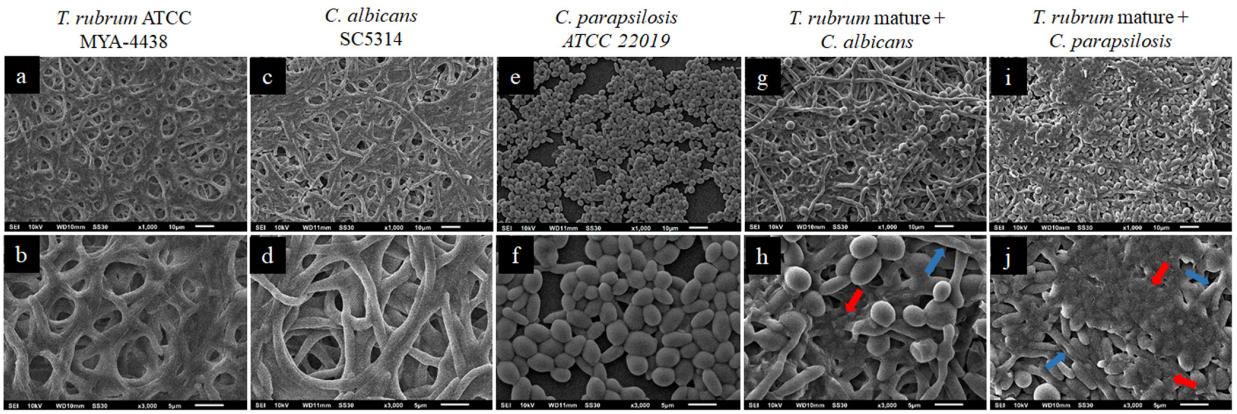

FIGURE 6 | Scanning electron microscopies of *T. rubrum* ATCC MYA 4438 **(a,b)**, *C. albicans* SC 5314 **(c,d)**, and *C. parapsilosis* ATCC 22019 **(e,f)** monospecies biofilms and dual-species biofilms of *C. albicans*/*T. rubrum* **(g,h)** and *C. parapsilosis*/*T. rubrum* **(i,j)**, formed after the maturation of *T. rubrum* biofilm, followed by an additional 48 h incubation. It is possible to observe oval blastoconidia. Red arrows denote the extracellular matrices, while blue arrows denote hyphae.

observed poorly developed hyphae in the early stages, which suggests the inhibition of *C. albicans* filamentation and a low *T. rubrum* development, indicating an antagonistic interaction between the species studied.

A lower inhibition in the formation of mature biofilms, and, consequently, a more robust biomass, was observed when *C. parapsilosis* was added after *T. rubrum* pre-adhesion (**Figures 5g,h**). In addition, the *T. rubrum* hyphae were found to be more developed than in the previous condition (white arrows), although still in small quantities. Therefore, pre-adherence may benefit the development of the hyphae of dermatophytes, the latter of which serves as a substrate for the development of *C. parapsilosis* biofilms.

Figure 6 shows the topographies of the biofilms formed after the addition of the *C. albicans* and *C. parapsilosis* suspensions to the mature *T. rubrum* biofilms. The monospecies biofilms of *T. rubrum*, *C. albicans*, and *C. parapsilosis* are shown in **Figures 6a–f**, respectively. In the mixed biofilms of *C. albicans*/*T. rubrum* (**Figures 6g,h**), we observed numerous blastoconidia and a dense biomass, in addition to a greater amount of polysaccharide matrix (red arrows). The visualization of the mixed biofilms of *C. parapsilosis* and *T. rubrum* was better (**Figures 6i,j**). These findings reinforce our theory and corroborate our results for the quantification of biomass by CV and polysaccharide material by safranin staining.

Colony Forming Units Counting Assay (CFU/mL) in Selective Media

For the colony forming unit count (CFU) assay, only one condition for the formation of dual-species biofilms was chosen: *C. albicans* SC 5314/*C. parapsilosis* ATCC 22019 and

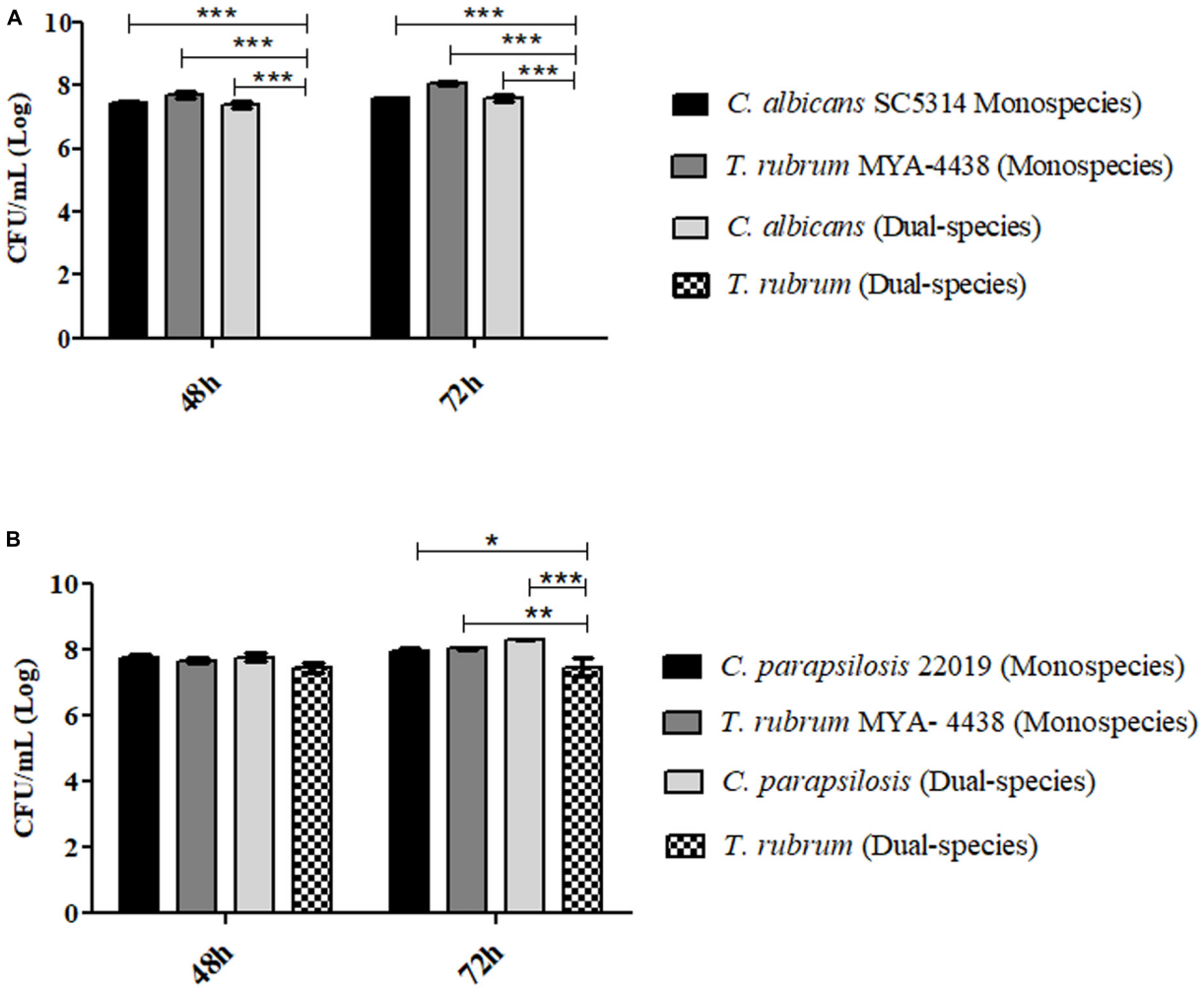

FIGURE 7 | Log of colony forming units per milliliter [CFU/mL] (Log) isolated from mono- and dual-species *C. albicans* SC 5314 and *T. rubrum* ATCC MYA 4438 biofilms (1:1) **(A)** and isolated from mono and dual-species biofilms of *C. parapsilosis* ATCC 22019 and *T. rubrum* ATCC MYA 4438 **(B)** formed under the same conditions after 48 h and 72 h of incubation. Statistical significance: $^{*}p < 0.05$, $^{**}p < 0.01$, and $^{***}p < 0.0001$.

T. rubrum ATCC MYA-4438 (1:1). Petri dishes containing CHROMagar^{TM} *Candida* (Difco; BD Biosciences) were used to isolate *C. albicans* from the mixed biofilm, while Mycosel agar (Difco; BD Biosciences) was used to isolate *T. rubrum* at different temperatures. Monospecies biofilms formed in the same period were used as controls. **Figure 7A** shows the isolation of *C. albicans* from the mixed biofilm with a fungal load after 48 h and 72 h of incubation, similar to that of the monospecies biofilm of the same yeast (no statistical significance). On the other hand, it was not possible to isolate *T. rubrum* from dual-species biofilms, confirming the inhibition of growth by yeast ($p < 0.01$) and reinforcing the results of the quantitative colorimetric tests, especially of CV, and SEM.

In contrast, *T. rubrum* was isolated from dual-species biofilms formed with *C. parapsilosis* (**Figure 7B**). The predominance of yeast in comparison with the dermatophyte was still evident, particularly after 72 h of incubation ($p < 0.0001$), confirming the antagonistic interaction. In terms of the controls, the fungal loads of *C. parapsilosis* and *T. rubrum* were found to be similar to those of dual-species biofilms after 48 h of incubation (no statistical significance). At 72 h, the fungal load of *T. rubrum* isolated from the dual-species biofilm was significantly lower than that of the monospecies biofilm ($p < 0.01$), whereas that of *C. parapsilosis* was similar. Therefore, we concluded that the interaction between *C. parapsilosis* and *T. rubrum* also culminated in the inhibition of *T. rubrum* growth.

Activity of Terbinafine and Efinaconazole Against Mono- and Dual-Species Biofilms

To determine the minimum sessile inhibitory concentration (SMIC), a reduction of at least 50% of cell viability was considered in relation to positive controls. As shown in **Table 1**, both monospecies and dual-species biofilms were resistant to all tested concentrations of efinaconazole and terbinafine.

TABLE 1 | Values of the minimum inhibitory concentration sessile (SMIC) expressed in mg/L for efinaconazole and terbinafine tested against the monospecies biofilms of *T. rubrum*, *C. albicans*, *C. parapsilosis*, and dual-species biofilms formed by *T. rubrum*/*C. albicans* and *T. rubrum*/*C. parapsilosis*.

Antifungals/fungi	*T. rubrum* MYA-4438	*C. albicans* SC 5314	*C. parapsilosis* ATCC 22019	*Tr** MYA + *C. albicans*	*Tr** MYA + *C. parapsilosis*
Efinaconazole	>256	>256	>256	>256	>256
Terbinafine	>32	>32	>32	>32	>32

**Tr: T. rubrum.*

DISCUSSION

In mixed biofilms, interactions between different species can be synergistic, neutral, or antagonistic (dos Santos et al., 2016). Recent studies have shown that *Candida* yeast rarely exists in isolated form (Jack et al., 2015). Synergism is beneficial to all microorganisms involved, whereas antagonistic relationships can cause the death, damage, or inhibition of one microorganism by a product produced by the other. Finally, neutral relationships are indifferent for both species involved in the formation of the biofilm (Thein et al., 2009; Cabezón et al., 2016; Costa-Orlandi et al., 2017).

The development of multi-species biofilms can also be influenced by the sharing of nutrients available in the medium between different species. Therefore, the polymicrobial interactions in a biofilm are significantly modulated by these environmental elements (Thein et al., 2009; Cabezón et al., 2016). On the other hand, it is also essential to consider intercellular communications that occur through quorum-sensing molecules, which allow to coordinate the collective behavior of microorganisms in these communities (Demuyser et al., 2014).

Our results showed an *in vitro* antagonistic interaction between *C. albicans* and *C. parapsilosis* and the dermatophyte *T. rubrum* in RPMI medium. Although it is not known which of the three conditions tested actually occurred in the microbiome and in the pathogenesis of dermatomycoses, this antagonism may be caused by products secreted into the medium by both fungi, or even due to a lack of nutrients. To prevent the latter, the culture medium was changed every 24 h. The predominance of *Candida* was possibly due to its metabolism being more accelerated than that of *T. rubrum*, mainly in the first condition, in which the two microorganisms were added together. This condition can generate competition for adhesion sites. In the other conditions, the absorbance measurements corresponding to metabolic activities, biomasses, and polysaccharide materials were similar or sometimes superior to *T. rubrum* monospecies biofilms, which suggests that pre-adhesion or mature biofilms of *T. rubrum* may served as a substrate for the development of *Candida* biofilms. On the other hand, the *Candida* monospecies biofilms demonstrated differences in the quantity of the same parameters compared to dual-species biofilms. These assumptions were confirmed in the topographies of biofilms observed in SEM, which further evidenced the predominance of yeasts, the inhibition of the development of *T. rubrum* biofilms, and the inhibition of *C. albicans* filamentation, more evident in the conditions where there was a greater amount of the dermatophyte.

Regarding the quantitative tests of the monospecies biofilms, the results corroborated the literature, indicating that the ideal time for the maturation of the biofilms of *Candida* spp. (24 h or 48 h) depended on the species (Pierce et al., 2008). In comparison, the ideal maturation of *T. rubrum* is 72 h (Costa-Orlandi et al., 2014).

According to dos Santos et al. (2016), it is not possible to differentiate between the cellular metabolic activity of a single species in mixed biofilms based only on the XTT reduction assay. Therefore, it is necessary to make comparisons with monospecies biofilms. The same authors stated that the metabolic behavior of biofilms can vary depending on the microorganisms present in the microbial interaction. The presence of *C. krusei* in the mixed biofilm with *C. albicans* stimulated a reduction in cell viability compared to the viability observed in the monospecies biofilm formed by *C. albicans*, suggesting a possible inhibition of *C. albicans*.

Bandara et al. (2010b) used colorimetric assays with XTT to demonstrate that the presence of *Escherichia coli* in dual-species biofilms, after 48 h, decreased the cell viability of *C. parapsilosis*, without significant changes when compared to *C. albicans*.

The metabolic activities of biofilms were quantified through a colorimetric assay with a solution of XTT and menadione acting as an electron coupling agent. XTT is a yellow tetrazolium salt, which converts to orange formazan salts in the presence of metabolic activity. Many authors assume that this assay is an efficient way to indirectly quantify biofilms since the observed colorimetric change is proportional to the number of living cells (Costa-Orlandi et al., 2014; Marcos-Zambrano et al., 2014; Rosato et al., 2016). However, there are also studies indicating that, for *C. albicans* and *C. parapsilosis*, the results obtained with the XTT assay are not directly related to the number of live microorganisms (Kuhn et al., 2003). It is also important to consider that biofilms are surrounded by an extracellular matrix, which can impair the metabolic activity of the microorganisms if it limits the access of cells to nutrients and oxygen. Thus, other methods will be needed in addition to the XTT tests for the characterization of biofilms (Henriques et al., 2006; Costa-Orlandi et al., 2017).

Regarding the quantification of biomass by the crystal violet assay, previous studies have shown that the presence of *C. albicans* biofilms stimulated an increase in the biomass of heterotypic biofilms formed between *C. albicans*, *C. glabrata*, and *C. tropicalis*, indicating that the first species can provide a substrate for non-*C. albicans* species to adhere to acrylic materials (Pathak et al., 2012). The co-cultivation of *Streptococcus mutans* and *C. albicans* in dual-species biofilms resulted in better biomass growth for each species. This may have occurred due

to metabolic interactions that provided additional nutrients for these microorganisms (Sztajer et al., 2014). In contrast, recent studies have shown an inhibitory effect on metabolic activity and biomass formation by *C. tropicalis*, *C. krusei*, and *C. parapsilosis* when co-incubated with probiotic bacteria *Lactobacillus gasseri* and *Lactobacillus rhamnosus* (Tan et al., 2018).

The crystal violet assay is based on the ability of this substance to penetrate the fungal cell wall and remain trapped in the cytoplasm. This quantification technique may have its reproducibility affected by the different growth conditions of the microbial biofilm and the different solvent concentrations used in the assay, among others. In addition, crystal violet is only able to quantify the biomass without distinguishing between dead and living cells, so this analysis must be complementary to other tests (Stepanovic et al., 2007; Pantanella et al., 2013).

In this study, the colony-forming unit counting test was used to complement the previous colorimetric assays, as well as the topographic observation by SEM, since these do not allow to specify the real constitution of the biofilm from a quantitative point of view. This assay confirmed the predominance of *C. albicans* and *C. parapsilosis* over *T. rubrum* in the only tested condition (1:1). Although laborious, many authors use this technique to isolate microorganisms within mixed biofilms and, unlike the XTT reduction assay, this technique is not influenced by the cellular metabolic state, directly enumerating the present cells (Jin et al., 2004; Jabra-Rizk et al., 2006; Bandara et al., 2010a; Fox et al., 2014; dos Santos et al., 2016).

Finally, regarding susceptibility tests, the findings in the present study corroborate the increased resistance that biofilms have against antimicrobial agents. In the dual-species interaction, although there is an antagonistic relationship between the biofilms of *Candida* and the dermatophyte, there is a prevalence of yeasts, making these dual-species biofilms resistant to all tested drug concentrations. The results obtained with the susceptibility tests of *T. rubrum* biofilms against terbinafine and efinaconazole corroborate the results obtained by our group and which are in preparation for publication. Previous studies have demonstrated the ineffectiveness of terbinafine against *C. albicans* biofilms, which agrees with the results presented in this work. However, the same authors demonstrated that terbinafine exerts activity against *C. parapsilosis* biofilms, contrary to what was found in the present study (Lam et al., 2016).

CONCLUSION

This study provides unprecedented data related to the interaction between sessile communities formed by the three microorganisms that are most frequently isolated from dermatomycoses, one of the most prevalent mycoses worldwide. The findings show that *C. albicans*/*T rubrum* and *C. parapsilosis*/*T. rubrum* can grow and form biofilms together, albeit with a degree of antagonism on both sides. If, on the one hand, the growth of the dermatophyte is somewhat inhibited by the presence of yeasts, the presence of the filamentous fungi seems to proportionally inhibit one of the main virulence factors of *C. albicans*, namely filamentation, thereby decreasing the growth of *C. parapsilosis*. Even under condition in which the dermatophyte seems to serve as a substrate for the development of *Candida* biofilms, there is a certain antagonism for the same reasons as mentioned above. Therefore, this work opens several doors to the study of the interaction between *T. rubrum* biofilms and other microorganisms. Further studies are currently being conducted to identify potential substance(s) secreted in the supernatants of these mixed biofilms for use as broad-spectrum compounds. Additional studies should also be conducted using other species with different biofilm formation abilities in order to verify our findings.

DATA AVAILABILITY STATEMENT

All datasets generated for this study are included in the article/supplementary material.

AUTHOR CONTRIBUTIONS

CC-O, LMG, and NB drafted the manuscript. LMG, CC-O, NB, CV, and LNG performed the experiments. CC-O and MM-G designed and supervised the project. All authors participated in data analysis and critical revision of the manuscript and approved the final version.

FUNDING

This work was supported by Fundação de Amparo à Pesquisa do Estado de São Paulo-FAPESP [2017/18388-6 (CC-O), 2018/02785-9 (MM-G), and 2019/22188-8 (NB)], Coordenação de Aperfeiçoamento de Pessoal de Nível Superior (CAPES) (Finance Code 001), Programa de Apoio ao Desenvolvimento Científico (PADC) da Faculdade de Ciências Farmacêuticas da UNESP, Conselho Nacional de Desenvolvimento Científico e Tecnológico [148425/2018-6 (LMG), 142049/2019-0 (NB), 134559/2018-5 (CV), and 142048/2019-4 (LNG)], and Instituto de Bolsas de Estudo (IBE 150/2017).

ACKNOWLEDGMENTS

We thank Dr. Joshua Nosanchuk for kindly providing *T. rubrum* ATCC MYA-4438 strain, Dr. Regina Pires for providing *C. albicans* SC5314 strain, and Dr. Nosanchuk and Adam Friedman for providing efinaconazole.

REFERENCES

Aquino, V. R., Constante, C. C., and Bakos, L. (2007). Frequency of dermatophytosis in mycological examinations at a general hospital in Porto Alegre. *Brazil. An. Bras. Dermatol.* 82, 239–244.

Bandara, H. M., Lam, O. L., Watt, R. M., Jin, L. J., and Samaranayake, L. P. (2010a). Bacterial lipopolysaccharides variably modulate in vitro biofilm formation of *Candida* species. *J. Med. Microbiol.* 59, 1225–1234. doi: 10.1099/jmm.0.021832-0

Bandara, H. M., Yau, J. Y., Watt, R. M., Jin, L. J., and Samaranayake, L. P. (2010b). *Pseudomonas aeruginosa* inhibits in-vitro *Candida* biofilm development. *BMC Microbiol.* 10:125. doi: 10.1186/1471-2180-10-125

Cabezón, V., Vialás, V., Gil-Bona, A., Reales-Calderón, J. A., Martínez-Gomariz, M., Gutiérrez-Blázquez, D., et al. (2016). Apoptosis of *Candida albicans* during the interaction with murine macrophages: proteomics and cell-death marker monitoring. *J. Proteome Res.* 15, 1418–1434. doi: 10.1021/acs.jproteome.5b00913

Celestrino, G. A., Reis, A. P. C., Criado, P. R., Benard, G., and Sousa, M. G. T. (2019). Trichophyton rubrum elicits phagocytic and pro-inflammatory responses in human monocytes through toll-like receptor 2. *Front. Microbiol.* 10:2589. doi: 10.3389/fmicb.2019.02589

Chadeganipour, M., Nilipour, S., and Ahmadi, G. (2010). Study of onychomycosis in Isfahan. *Iran. Mycoses* 53, 153–157. doi: 10.1111/j.1439-0507.2008.01679

Chandra, J., and Mukherjee, P. K. (2015). *Candida* biofilms: development, architecture, and resistance. *Microbiol. Spectr.* 3, 1–14. doi: 10.1128/microbiolspec

Costa-Orlandi, B. C., Sardi, C. J., Pitangui, S. N., de Oliveira, C. H., Scorzoni, L., Galeane, C. M., et al. (2017). Fungal biofilms and polymicrobial diseases. *J. Fungi* 3:22. doi: 10.3390/jof3020022

Costa-Orlandi, C. B., Magalhães, G. M., Oliveira, M. B., Taylor, E. L., Marques, C. R., and de Resende-Stoianoff, M. A. (2012). Prevalence of dermatomycosis in a Brazilian tertiary care hospital. *Mycopathologia* 174, 489–497. doi: 10.1007/s11046-012-9576-1

Costa-Orlandi, C. B., Sardi, J. C., Santos, C. T., Fusco-Almeida, A. M., and Mendes-Giannini, M. J. (2014). In vitro characterization of *Trichophyton rubrum* and *T. mentagrophytes* biofilms. *Biofouling* 30, 719–727.

Demuyser, L., Jabra-Rizk, M. A., and Van Dijck, P. (2014). Microbial cell surface proteins and secreted metabolites involved in multispecies biofilms. *Pathog. Dis.* 70, 219–230. doi: 10.1111/2049-632x.12123

dos Santos, J. D., Piva, E., Vilela, S. F. G., Jorge, A. O. C., and Junqueira, J. C. (2016). Mixed biofilms formed by *C. albicans* and non-albicans species: a study of microbial interactions. *Braz. Oral Res.* 30, S1806–S832.

Fox, E. P., Cowley, E. S., Nobile, C. J., Hartooni, N., Newman, D. K., and Johnson, A. D. (2014). Anaerobic bacteria grow within *Candida albicans* biofilms and induce biofilm formation in suspension cultures. *Curr. Biol.* 24, 2411–2416. doi: 10.1016/j.cub.2014.08.057

Gawaz, A., and Weisel, G. (2018). Mixed infections are a critical factor in the treatment of superficial mycoses. *Mycoses* 61, 731–735. doi: 10.1111/myc.1279

Ghannoum, M. A., Hajjeh, R. A., Scher, R., Konnikov, N., Gupta, A. K., Summerbell, R., et al. (2000). A large-scale North American study of fungal isolates from nails: the frequency of onychomycosis, fungal distribution, and antifungal susceptibility patterns. *J. Am. Acad. Dermatol.* 43, 641–648. doi: 10.1067/mjd.2000.107754

Ghannoum, M. A., Mukherjee, P. K., Warshaw, E. M., Evans, S., Korman, N. J., and Tavakkol, A. (2013). Molecular analysis of dermatophytes suggests spread of infection among household members. *Cutis* 91, 237–245.

Gupta, A. K., Daigle, D., and Carviel, J. L. (2016). The role of biofilms in onychomycosis. *J. Am. Acad. Dermatol.* 74, 1241–1246. doi: 10.1016/j.jaad.2016.01.008

Gupta, A. K., and Foley, K. A. (2019). Evidence for biofilms in onychomycosis. *G. Ital. Dermatol. Venereol.* 154, 50–55.

Havlickova, B., Czaika, V. A., and Friedrich, M. (2008). Epidemiological trends in skin mycoses worldwide. *Mycoses* 51(Suppl. 4), doi: 10.1111/j.1439-0507.2007.01380.x

Henriques, M., Azeredo, J., and Oliveira, R. (2006). *Candida albicans* and *Candida dubliniensis*: comparison of biofilm formation in terms of biomass and activity. *Br. J. Biomed. Sci.* 63, 5–11. doi: 10.1080/09674845.2006.11732712

Iñigo, M., and Del Pozo, J. L. (2018). Fungal biofilms: from bench to bedside. *Revist. Esp. Quimioter.* 31(Suppl. 1), 35–38.

Jabra-Rizk, M. A., Meiller, T. F., James, C. E., and Shirtliff, M. E. (2006). Effect of farnesol on Staphylococcus aureus biofilm formation and antimicrobial susceptibility. *Antimicrob. Agents Chemother.* 50, 1463–1469. doi: 10.1128/aac.50.4.1463-1469.2006

Jack, A. A., Daniels, D. E., Jepson, M. A., Vickerman, M. M., Lamont, R. J., Jenkinson, H. F., et al. (2015). Streptococcus gordonii comCDE (competence) operon modulates biofilm formation with *Candida albicans*. *Microbiology* 161, 411–421. doi: 10.1099/mic.0.000010

Jacob, T. R., Peres, N. T., Martins, M. P., Lang, E. A., Sanches, P. R., Rossi, A., et al. (2015). Heat shock protein 90 (Hsp90) as a molecular target for the development of novel drugs against the dermatophyte *Trichophyton rubrum*. *Front. Microbiol.* 6:1241. doi: 10.3389/fmicb.2015.01241

Jin, Y., Samaranayake, L. P., Samaranayake, Y., and Yip, H. K. (2004). Biofilm formation of *Candida albicans* is variably affected by saliva and dietary sugars. *Arch. Oral Biol.* 49, 789–798. doi: 10.1016/j.archoralbio.2004.04.011

Kravvas, G., Veitch, D., and Al-Niaimi, F. (2018). The increasing relevance of biofilms in common dermatological conditions. *J. Dermatol. Treat.* 29, 202–207. doi: 10.1080/09546634.2017.1360989

Kuhn, D. M., Balkis, M., Chandra, J., Mukherjee, P. K., and Ghannoum, M. A. (2003). Uses and limitations of the XTT assay in studies of *Candida* growth and metabolism. *J. Clin.Microbiol.* 41, 506–508. doi: 10.1128/jcm.41.1.506-508.2003

Lam, P., Kok, S. H., Lee, K. K., Lam, K. H., Hau, D. K., Wong, W. Y., et al. (2016). Sensitization of *Candida albicans* to terbinafine by berberine and berberrubine. *Biomed. Rep.* 4, 449–452. doi: 10.3892/br.2016.608

Li, X., Yin, L., Ramage, G., Li, B., Tao, Y., Zhi, Q., et al. (2019). Assessing the impact of curcumin on dual-species biofilms formed by *Streptococcus mutans* and *Candida albicans*. *Microbiologyopen.* 8:e937.

Marcos-Zambrano, L. J., Escribano, P., Bouza, E., and Guinea, J. (2014). Production of biofilm by *Candida* and non-*Candida* spp. isolates causing fungemia: comparison of biomass production and metabolic activity and development of cut-off points. *Int. J. Med.Microbiol.* 304, 1192–1198. doi: 10.1016/j.ijmm.2014.08.012

Martinez, L. R., and Casadevall, A. (2007). Cryptococcus neoformans biofilm formation depends on surface support and carbon source and reduces fungal cell susceptibility to heat, cold, and UV light. *Appl. Environ. Microbiol.* 73, 4592–4601. doi: 10.1128/aem.02506-06

Martinez, L. R., Mihu, M. R., Tar, M., Cordero, R. J., Han, G., Friedman, A. J., et al. (2010). Demonstration of antibiofilm and antifungal efficacy of chitosan against candidal biofilms, using an in vivo central venous catheter model. *J. Infect. Dis.* 201, 1436–1440. doi: 10.1086/651558

Pantanella, F., Valenti, P., Natalizi, T., Passeri, D., and Berlutti, F. (2013). Analytical techniques to study microbial biofilm on abiotic surfaces: pros and cons of the main techniques currently in use. *Ann. Ig.* 25, 31–42.

Pathak, A. K., Sharma, S., and Shrivastva, P. (2012). Multi-species biofilm of *Candida albicans* and non-*Candida albicans* Candida species on acrylic substrate. *J. Appl. Oral Sci.* 20, 70–75. doi: 10.1590/s1678-77572012000100013

Pierce, C. G., Uppuluri, P., Tristan, A. R., Wormley, F. L., Mowat, E., Ramage, G., et al. (2008). A simple and reproducible 96-well plate-based method for the formation of fungal biofilms and its application to antifungal susceptibility testing. *Nat. Protoc.* 3, 1494–1500. doi: 10.1038/nprot.2008.141

Pires, R. H., Lucarini, R., and Mendes-Giannini, M. J. (2012). Effect of usnic acid on *Candida orthopsilosis* and *C. parapsilosis*. *Antimicrob. Agents Chemother.* 56, 595–597. doi: 10.1128/aac.05348-11

Pires, R. H., Santos, J. M., Zaia, J. E., Martins, C. H., and Mendes-Giannini, M. J. (2011). *Candida parapsilosis* complex water isolates from a haemodialysis unit: biofilm production and in vitro evaluation of the use of clinical antifungals. *Mem. Inst. Oswaldo Cruz.* 106, 646–654. doi: 10.1590/s0074-02762011000600002

Pontes, Z. B., Lima Ede, O., Oliveira, N. M., Dos Santos, J. P., Ramos, A. L., and Carvalho, M. F. (2002). Onychomycosis in Joao Pessoa City. *Brazil. Rev. Argent. Microbiol.* 34, 95–99.

Ramage, G., Mowat, E., Jones, B., Williams, C., and Lopez-Ribot, J. (2009). Ourcurrent understanding of fungal biofilms. *Crit. Rev. Microbiol.* 35, 340–355. doi: 10.3109/10408410903241436

Ramage, G., Rajendran, R., Sherry, L., and Williams, C. (2012). Fungal biofilm resistance. *Int. J. Microbiol.* 2012, 528521.

Rosato, A., Catalano, A., Carocci, A., Carrieri, A., Carone, A., Caggiano, G., et al. (2016). In vitro interactions between anidulafungin and nonsteroidal anti-inflammatory drugs on biofilms of *Candida* spp. *Bioorg. Med. Chem.* 24, 1002–1005. doi: 10.1016/j.bmc.2016.01.026

Rotta, I., Sanchez, A., Goncalves, P. R., Otuki, M. F., and Correr, C. J. (2012). Efficacy and safety of topical antifungals in the treatment of dermatomycosis: a systematic review. *Br. J. Dermatol.* 166, 927–933. doi: 10.1111/j.1365-2133.2012.10815.x

Sardi, J. C., Scorzoni, L., Bernardi, T., Fusco-Almeida, A. M., and Mendes Giannini, M. J. (2013). *Candida* species: current epidemiology, pathogenicity, biofilm formation, natural antifungal products and new therapeutic options. *J. Med. Microbiol.* 62, 10–24. doi: 10.1099/jmm.0.045054-0

Seidler, M. J., Salvenmoser, S., and Muller, F. M. (2008). Aspergillus fumigatus forms biofilms with reduced antifungal drug susceptibility on bronchial epithelial cells. *Antimicrob. Agents Chemother.* 52, 4130–4136. doi: 10.1128/aac.00234-08

Stepanovic, S., Vukovic, D., Hola, V., Di Bonaventura, G., Djukic, S., Cirkovic, I., et al. (2007). Quantification of biofilm in microtiter plates: overview of testing conditions and practical recommendations for assessment of biofilm production by Staphylococci. *APMIS* 115, 891–899. doi: 10.1111/j.1600-0463

Sztajer, H., Szafranski, S. P., Tomasch, J., Reck, M., Nimtz, M., Rohde, M., et al. (2014). Cross-feeding and interkingdom communication in dual-species biofilms of *Streptococcus mutans* and *Candida albicans*. *ISME J.* 8, 2256–2271. doi: 10.1038/ismej.2014.73

Tan, Y., Leonhard, M., Moser, D., Ma, S., and Schneider-Stickler, B. (2018). Inhibitory effect of probiotic lactobacilli supernatants on single and mixed nonalbicans *Candida* species biofilm. *Arch. Oral Biol.* 85, 40–45. doi: 10.1016/j.archoralbio.2017.10.002

Thein, Z. M., Seneviratne, C. J., Samaranayake, Y. H., and Samaranayake, L. P. (2009). Community lifestyle of *Candida* in mixed biofilms: a mini review. *Mycoses* 52, 467–475. doi: 10.1111/j.1439-0507.2009.01719.x

Trofa, D., Gacser, A., and Nosanchuk, J. D. (2008). *Candida parapsilosis*, an emerging fungal pathogen. *Clin. Microbiol. Rev.* 21, 606–625. doi: 10.1128/cmr.00013-08

Vila, T. V., Rozental, S., and de Sa Guimaraes, C. M. (2015). A new model of in vitro fungal biofilms formed on human nail fragments allows reliable testing of laser and light therapies against onychomycosis. *Lasers Med. Sci.* 30, 1031–1039. doi: 10.1007/s10103-014-1689-y

Wongsuk, T., Pumeesat, P., and Luplertlop, N. (2016). Fungal quorum sensing molecules: role in fungal morphogenesis and pathogenicity. *J. Basic Microbiol.* 56, 440–447. doi: 10.1002/jobm.201500759

Zhan, P., and Liu, W. (2017). The changing face of dermatophytic infections worldwide. *Mycopathologia* 182, 77–86. doi: 10.1007/s11046-016-0082-8

Conflict of Interest: The authors declare that the research was conducted in the absence of any commercial or financial relationships that could be construed as a potential conflict of interest.

The handling editor declared a shared affiliation with the authors at the time of review.

frontiers in Microbiology

MINI REVIEW
published: 17 September 2020
doi: 10.3389/fmicb.2020.538602

Advances in Biomaterials for the Prevention and Disruption of *Candida* Biofilms

Noel Vera-González[1] *and Anita Shukla*[1,2]*

[1]Center for Biomedical Engineering, School of Engineering, Brown University, Providence, RI, United States, [2]Institute for Molecular and Nanoscale Innovation, Brown University, Providence, RI, United States

Candida species can readily colonize a multitude of indwelling devices, leading to biofilm formation. These three-dimensional, surface-associated *Candida* communities employ a multitude of sophisticated mechanisms to evade treatment, leading to persistent and recurrent infections with high mortality rates. Further complicating matters, the current arsenal of antifungal therapeutics that are effective against biofilms is extremely limited. Antifungal biomaterials are gaining interest as an effective strategy for combating *Candida* biofilm infections. In this review, we explore biomaterials developed to prevent *Candida* biofilm formation and those that treat existing biofilms. Surface functionalization of devices employing clinically utilized antifungals, other antifungal molecules, and antifungal polymers has been extremely effective at preventing fungi attachment, which is the first step of biofilm formation. Several mechanisms can lead to this attachment inhibition, including contact killing and release-based killing of surrounding planktonic cells. Eliminating mature biofilms is arguably much more difficult than prevention. Nanoparticles have shown the most promise in disrupting existing biofilms, with the potential to penetrate the dense fungal biofilm matrix and locally target fungal cells. We will describe recent advances in both surface functionalization and nanoparticle therapeutics for the treatment of *Candida* biofilms.

Keywords: *Candida*, biofilms, biomaterials, antifungal, surface functionalization, nanoparticles, antifungal polymers

OPEN ACCESS

Edited by:
Sara María Soto, Instituto Salud Global Barcelona (ISGlobal), Spain

Reviewed by:
Renátó Kovács, University of Debrecen, Hungary
Rodnei Dennis Rossoni, São Paulo State University, Brazil
Liliana Scorzoni, São Paulo State University, Brazil

***Correspondence:**
Anita Shukla
anita_shukla@brown.edu

Specialty section:
This article was submitted to Infectious Diseases, a section of the journal Frontiers in Microbiology

Received: *27 February 2020*
Accepted: *24 August 2020*
Published: *17 September 2020*

Citation:
Vera-González N and Shukla A (2020) Advances in Biomaterials for the Prevention and Disruption of Candida Biofilms. Front. Microbiol. 11:538602. doi: 10.3389/fmicb.2020.538602

INTRODUCTION

Candida is one of the most common causes of fungal infections worldwide, responsible for over 400,000 infections per year (Brown et al., 2012; Tsui et al., 2016). A commensal fungus that can readily become pathogenic, *Candida*, is known to form biofilms (Gulati and Nobile, 2016). These surface-attached, three-dimensional communities of tightly packed fungi can serve as infection strongholds, complicating treatment and leading to persistent fungemia (Li et al., 2018). *Candida* biofilm related infections have mortality rates as high as 41% (Rajendran et al., 2016). Biofilms protect fungal cells from the host immune system and often increase drug resistance (Mukherjee and Chandra, 2004; Nett, 2014). Biofilm fungi secrete a dense extracellular polymeric substance (EPS) that acts as a physical barrier for antifungal therapeutics,

most of which are hydrophobic with limited ability to penetrate this matrix (Singh et al., 2018). Persister cells, which are metabolically dormant, can form as quickly as cell attachment occurs, leading to changes in gene expression, with an initial overexpression of drug efflux pumps, followed by a reduction in membrane sterol content in mature *Candida* biofilms (Kumamoto and Vinces, 2005; LaFleur et al., 2006). Although persister cells represent a small subpopulation within the biofilm (~1% of all cells), their tolerance to high doses of antimicrobials allows them to readily repopulate the biofilm once the treatment has stopped, resulting in recurring infections (Galdiero et al., 2020). Quorum sensing can mediate the secretion of signaling factors affecting *Candida* gene expression and behavior, including filamentation (Mallick and Bennett, 2013; Tsui et al., 2016). Changes to the cell wall that enhance drug resistance can also occur; for example, cell walls that are twice as thick as planktonic cells have been observed in biofilm *Candida* (Nett et al., 2007; Lima et al., 2019).

The majority of biofilm-associated *Candida* infections arise from cells that colonize the surfaces of implanted medical devices (Coad et al., 2016). These devices range from plastic cochlear implants and subcutaneous drug delivery devices, silicone or polyurethane catheters, and acrylic dental implants, to titanium hip implants, glass-ceramics used in bone repair, metal pacemakers, and polymeric contact lenses among many others (Vargas-Blanco et al., 2017; Cavalheiro and Teixeira, 2018; Devadas et al., 2019). Treatments for these biofilm-associated infections are extremely limited, with only three primary antifungal drug classes (polyenes, azoles, and echinocandins) and a total of 21 United States Food and Drug Administration (FDA) approved antifungal drugs (Butts and Krysan, 2012; McKeny and Zito, 2020), of which only a subset have demonstrated some level of antibiofilm activity. Innovations in biomaterials have the potential to combat *Candida* biofilms (**Figure 1**). Here, we explore recent promising approaches in this field involving surface modification with antifungal small molecules and polymers aimed at preventing biofilm formation and the design of nanoparticles aimed at both preventing and disrupting *Candida* biofilms.

PREVENTING *CANDIDA* BIOFILMS USING SURFACE MODIFICATION WITH CLINICALLY UTILIZED ANTIFUNGALS

Inhibiting *Candida* attachment to surfaces, the first step of biofilm formation (**Figure 2**: **1A**), is often the most effective way to combat biofilm-associated infections. Various approaches have been investigated to prevent fungi attachment, including surface functionalization with FDA-approved antifungals using covalent and non-covalent interactions (Zelikin, 2010). Caspofungin, the only echinocandin with primary amines, is most commonly used in direct surface tethering (Coad et al., 2015; Michl et al., 2017). Caspofungin tethered titanium disks cultured with *Candida albicans* showed complete inhibition of fungal attachment compared to bare titanium (**Figure 2**: **2A**,**B**). These same caspofungin-tethered disks implanted subcutaneously into the backs of mice and challenged with *C. albicans* showed 89% less *Candida* attached after 2 days compared to bare disks (Kucharíková et al., 2016).

In an example of non-covalent drug tethering, β-cyclodextrins (CD) were grafted to polyethylene and polypropylene surfaces (Nava-Ortiz et al., 2010), commonly used in medical devices. CDs were used to promote host-guest interactions with the hydrophobic antifungal, miconazole, while also regulating interactions with proteins and increasing hemocompatibility. These miconazole loaded CD grafted surfaces exhibited up to

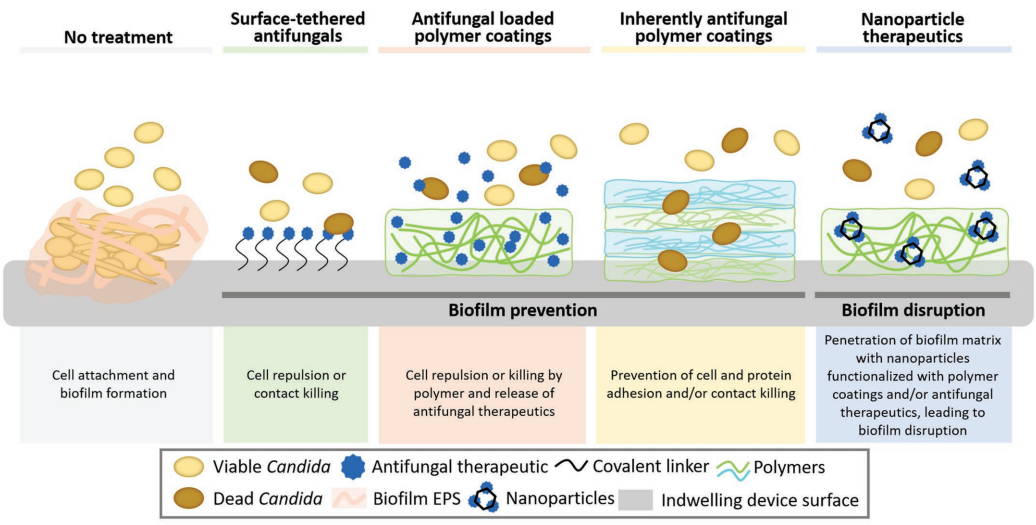

FIGURE 1 | Biomaterials strategies to combat surface-associated *Candida* biofilms. These strategies include direct surface functionalization with antimicrobial small molecules and natural and synthetic polymers and the use of nanoparticles, which may better penetrate the dense biofilm matrix and potentially target fungal cells. Together these strategies can prevent biofilm formation by inhibiting the initial attachment of fungi to surfaces and eradicate existing biofilms.

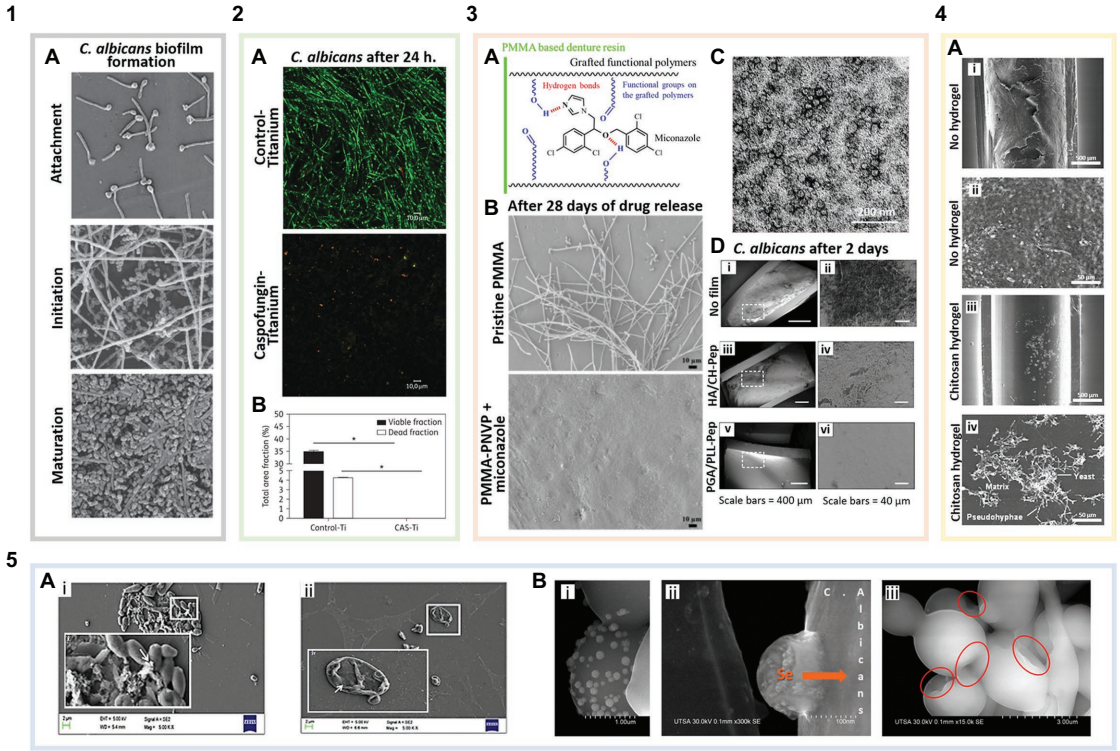

FIGURE 2 | Biomaterials for the prevention and treatment of *Candida* biofilms. **(1)** Biofilm formation of non-functionalized surfaces: **(1A)** *Candida albicans* biofilm formation (adapted with permission from Ramage et al., 2009). **(2)** Surface-tethered antifungals: **(2A)** Live/Dead staining showing caspofungin functionalized titanium disks (with caspofungin surface coverage of ~2,191 pmol/cm^2) inhibiting *C. albicans* attachment and biofilm formation compared to bare titanium (green are live cells, and red indicates membrane compromised cells; adapted with permission from Kucharíková et al., 2016). **(2B)** Quantification of viable cells per area in the images shown in **2A** (adapted with permission from Kucharíková et al., 2016). **(3)** Antifungal loaded polymer coatings: **(3A)** Schematic illustrating miconazole-polymer hydrogen bonding (adapted with permission from Wen et al., 2016a). **(3B)** Miconazole loaded into poly(methyl methacrylate)-poly(1-vinyl-2-pyrrolidinone) (PMMA-PNVP) films inhibits *C. albicans* attachment and biofilm growth for up to 28 days compared to pristine PMMA (adapted with permission from Wen et al., 2016a). **(3C)** Antifungal poly(ethylene glycol) (PEG) + curcumin (CU) nanocomposites in solution after being released from graphene oxide (GO) coatings (adapted with permission from Devadas et al., 2019). **(3D)** Layer-by-layer (LbL) coated catheters prevent *C. albicans* attachment and biofilm formation after 2 days. **(i)** Uncoated catheters showing *C. albicans* attachment and biomass deposition. **(ii)** Magnified region outlined in **3D(i)**. **(iii)** Catheters coated with a hyaluronic acid (HA)/chitosan (CH) LbL film with β-peptide showing no *C. albicans* attachment but some biomass deposition on the surface. **(iv)** Magnified region outlined in **3D(iii)**. **(v)** Poly-L-glutamic acid (PGA)/poly-L-lysine (PLL) LbL film with β-peptide coated catheters showing no cell or biomass attachment. **(vi)** Magnified region outlined in **3D(v)** (adapted with permission from Raman et al., 2016). **(4)** Inherently antifungal polymer coatings: **(4A)** Polyurethane catheter-associated *Candida parapsilosis* biofilms. **(i)** Uncoated catheters exhibiting *Candida* attachment and biofilm formation. **(ii)** Magnified region of image **4A(i)** showing a dense *C. parapsilosis* biofilm. **(iii)** Catheters coated with low molecular weight CH hydrogels significantly reduce *Candida* cell attachment and biofilm formation. **(iv)** Magnified region of image **4A(iii)** showing biofilm disruption (adapted with permission from Silva-Dias et al., 2014). **(5)** Antifungal nanoparticles: **(5A)** Scanning electron microscopy (SEM) images of *C. albicans* biofilms on polystyrene. **(i)** Control biofilm cells [white arrow points to extracellular polymeric substances (EPSs)] and **(ii)** biofilm inhibition in the presence of ferulic acid-chitosan nanoparticles (white arrow indicates the damaged fungal cell wall; adapted with permission from Panwar et al., 2016). **(5B)** SEM images of selenium nanoparticles **(i,ii)** binding to and **(iii)** disrupting *C. albicans* cells in biofilms. The red circles indicate areas of the cell membrane, where the nanoparticles have induced shrinking and folding (adapted with permission from Guisbiers et al., 2017).

a 97% reduction in the amount of recovered *C. albicans* compared to a silicone control incubated with the fungus. Polymers are also commonly used to enable non-covalent functionalization with antifungals, due to their ability to form multivalent interactions promoting loading of antifungal compounds. Wen et al. grafted poly(2-hydroxyethyl methacrylate) (PHEMA) onto poly(methyl methacrylate) (PMMA) denture resins. There is great interest in preventing *Candida* biofilms on dental surfaces, including dentures given the prevalence of *Candida* in the oral microbiota; in fact, *Candida* is responsible for up to 67% of denture-associated stomatitis (Ramage et al., 2006). PHEMA grafting was used to load the antifungal, clotrimazole, mediated *via* hydrogen bonding interactions, leading to a clotrimazole surface coverage of up to 46.0 ± 3.2 µg/cm^2 compared to 5.2 ± 0.4 µg/cm^2 on bare PMMA. A sustained release of clotrimazole was observed from the PHEMA-grafted denture disks over 28 days, yielding approximately a 50 and 36% reduction in *C. albicans* adhesion after 1 and 28 days, respectively, compared with non PHEMA-grafted disks (Wen et al., 2016b). Grafting poly(1-vinyl-2-pyrrolidinone) (PNVP) to PMMA enabled miconazole loading of 127.0 ± 15.1 µg/cm^2, likely mediated *via* hydrophobic interactions and hydrogen bonding (**Figure 2**: **3A**). PNVP-grafted resins with miconazole showed no *Candida* adhesion even after 28 days of drug release (**Figure 2**: **3B**; Wen et al., 2016a).

Along with superior biocompatibility, these functionalized materials can be used for extended biofilm prevention and have the potential to be reloaded with therapeutics.

PREVENTING *CANDIDA* BIOFILMS USING SURFACE MODIFICATION WITH NEW ANTIFUNGAL SMALL MOLECULES AND PEPTIDES

Although promising, surface functionalization with FDA-approved antifungals raises concerns for increased resistance to these therapeutics. Thus, there is an interest in alternative approaches to prevent *Candida* biofilms utilizing non-clinically used small molecules and peptides with inherent antifungal and antibiofilm properties. One example, filastatin, a potent small molecule inhibitor of *Candida* attachment and filamentation was recently identified in a screen of 30,000 compounds (Fazly et al., 2013). Vargas-Blanco et al. (2017) found that incubation of *C. albicans* with various biomaterials in the presence of filastatin can inhibit *Candida* attachment to these materials. Adsorption of filastatin on dental resin and silicone showed that *Candida* cell attachment was reduced on these materials by 62.7 and 79.7%, respectively, compared to uncoated controls. By incorporating filastatin into the silicone matrix during polymerization a 6.5-fold reduction in *C. albicans* adhesion compared to untreated silicone controls was observed (Vargas-Blanco et al., 2017). Other small molecule biofilm inhibitors specifically interrupt *Candida* quorum sensing. These molecules include furanones, which are plant synthesized compounds that prevent microbial fouling on the plant surface. Devadas et al. (2019) coated common catheter materials with a furanone embedded polycaprolactone matrix. These polymer coatings retained 85% or more of the total loaded furanone over at least 30 days in solution. The attachment of clinical isolates of *Candida tropicalis*, *Candida glabrata*, and *Candida krusei* on these coated catheters was completely inhibited as determined by scanning electron microscopy (SEM; Devadas et al., 2019). Other plant derived compounds have also shown activity against *Candida* biofilms when combined with biomaterials. Recently, clove oil and red thyme oil incorporated in polycaprolactone electrospun nanofibers led to a 60 and 80% reduction in *C. tropicalis* attachment, respectively (Sahal et al., 2019). Initial results with these small molecules are promising; future studies will likely examine functionalization *via* covalent tethering or affinity-based interactions with these compounds to enable long-term antibiofilm activity.

Combination approaches to prevent *Candida* biofilms involving the inhibition of fungal cell attachment and simultaneous killing of planktonic fungi have also been investigated. Palmieri et al. (2018) developed a multilayered coating by drop-casting graphene oxide (GO) on polyurethane catheters, followed by curcumin (CU) and poly(ethylene glycol) (PEG). The GO was included to prevent *C. albicans* attachment due to its ability to generate oxidative stress and physically disrupt the cell wall and membrane. CU + PEG self-assembled nanocomposites (75–125 nm in diameter; **Figure 2**: **3C**) were released from these coatings inhibiting planktonic *C. albicans* growth, with a minimum inhibitory concentration of 10.6 μg/ml. The complete catheter coating inhibited *C. albicans* attachment *in vitro* after 24 h with less than 20% biofilm formation compared to uncoated controls (Palmieri et al., 2018).

As an alternative to solvent casting or vapor deposition approaches, many biomedical surfaces have been coated *via* layer-by-layer (LbL) self-assembly to develop antifungal coatings. LbL assembly is a multilayer film fabrication method that involves alternating the adsorption of molecules and macromolecules (e.g., polyelectrolytes, peptides, proteins, small molecules, etc.,) with complementary functionalities most commonly by dip coating (Shukla and Almeida, 2014; Alkekhia and Shukla, 2019; Alkekhia et al., 2020). LbL films have been combined with antifungal peptides to exhibit remarkable antibiofilm properties. Antifungal peptides are considered potent and broad-spectrum antifungals; due to their multiple mechanisms of action, fungi are often unable to develop resistance to these peptides (Oshiro et al., 2019). These peptides are most commonly amphiphilic and cationic allowing them to readily interact with the fungal cell membrane, causing cell death (Karlsson et al., 2010). Raman et al. (2016) assembled an LbL film with hyaluronic acid (HA) and chitosan (CH) on catheter surfaces and used it as a reservoir for a synthetic antifungal β-peptide. The luminal surface of polyurethane catheters coated with these LbL films without any β-peptide was able to reduce viable *C. albicans* by approximately 25-fold after 6 h of exposure when compared to uncoated polyurethane catheters, demonstrating the innate antifungal properties of this polymeric coating. When passively loaded with the antifungal β-peptide, sustained release of the β-peptide was achieved over 50 days with complete eradication of planktonic *C. albicans in vitro*. Catheters coated with the β-peptide-loaded films tested in a rat central venous catheter model exhibited almost no fungal cells following 2 days [**Figure 2**: **3D(i–iv)**]. However, this coated surface was found to contain a network of host proteins, which can yield complications, including fouling with red blood cells, which can stimulate platelet production. Another film architecture examined in the same study utilizing β-peptide-loaded poly-L-lysine (PLL) and poly-L-glutamic acid (PGA) LbL films exhibited both a complete lack of *Candida* cell attachment and host proteins when tested in the same *in vivo* model [**Figure 2**: **3D(v,vi)**], emphasizing the importance of polymer choice in preventing overall fouling (Raman et al., 2016). PMMA denture disks were also recently coated with an LbL film containing the cationic mammalian salivary antifungal peptide, histatin-5 (H-5), and HA with a final H-5 layer. SEM images confirmed over 4 weeks that these LbL coated surfaces were able to completely prevent *Candida* attachment (Wen et al., 2018).

Many other small molecules and peptides not yet incorporated into biomaterials have demonstrated antibiofilm activity. Among these are newly synthesized imidazole derivatives, which have been found to prevent *Candida* biofilm formation and disrupt existing biofilms (Ribeiro et al., 2014; Gabriel et al., 2019). Thiazolylhydrazone derivatives have also recently emerged as effective antifungal compounds with low mammalian cell toxicity (Cruz et al., 2018).

2,6-Bis[(E)-(4-pyridyl)methylidene]cyclohexanone, an antiparasitic compound, was also found to exhibit antifungal properties including the inhibition of *Candida* filamentation, crucial in biofilm formation (de Sá et al., 2018). Antifungal peptide derivatives of H-5 are also being explored (Sultan et al., 2019), and other host defense peptides such as innate defense regulator 1018 and porcine cathelicidins have recently been shown to possess antifungal and antibiofilm properties against *Candida* (Lyu et al., 2016; Freitas et al., 2017). These compounds are potential candidates for incorporation into antifungal biomaterials.

PREVENTING *CANDIDA* BIOFILMS USING POLYMER-ONLY COATINGS

Many polymers themselves possess inherent antifouling, antifungal, and/or antibiofilm properties, while being less susceptible to resistance compared with small molecule antifungals; therefore, the use of polymer-only coatings for combating *Candida* biofilms has gained significant interest. For example, chitosan, a naturally derived polysaccharide, has been widely incorporated into hydrogels and coatings to prevent *Candida* attachment and biofilm formation (Carlson et al., 2008; Ailincai et al., 2016; Tan et al., 2016). It is hypothesized that chitosan interacts electrostatically *via* its positively charged amino groups with anionic moieties on microbial species leading to increased membrane permeability and eventual cell death (Jung et al., 2020). In a recent study, polyurethane intravenous catheters were coated with low molecular weight (50 kDa) chitosan hydrogels, implanted subcutaneously into mice, and subsequently challenged with *Candida parapsilosis*. Following 7 days, the chitosan-coated catheters reduced *Candida* metabolic activity by ~96% when compared to uncoated catheters, showcasing the ability of polymer-only coatings free of small molecule antifungals to achieve excellent antibiofilm activity. Reduced biomass on these chitosan coated catheters was shown using SEM (**Figure 2**: **4A;** Silva-Dias et al., 2014). Chitosan has also been modified to enhance its antibiofilm properties. Jung et al. (2019) examined the use of amphiphilic quaternary ammonium chitosans (AQACs) in LbL coatings. LbL films containing sodium alginate and AQAC, effectively prevented cell attachment on coated PMMA substrates (Jung et al., 2019). AQACs have been shown to disrupt mature *Candida* biofilms by interacting electrostatically with the negatively charged biofilm surface (Jung et al., 2020). Coatings with other polymers including imidazolium salt (IS) conjugated poly(L-lactide) (PLA) have also been used to effectively prevent *Candida* attachment on coated surfaces (Schrekker et al., 2016).

NANOPARTICLES FOR THE PREVENTION OF FUNGAL CELL ATTACHMENT AND BIOFILM ERADICATION

Despite the progress that has been made in antifungal surface functionalization, these approaches are limited in their ability to treat mature biofilms. Nanoparticles are a promising strategy to eradicate existing biofilms, with the potential to carry, stabilize, and protect therapeutic payloads, penetrate the EPS, target fungal cells, and be internalized (Ikuma et al., 2015; Qayyum and Khan, 2016; Stone et al., 2016). Several strategies have been used to develop nanoparticles for the treatment of fungal infections, from using inorganic compounds to antimicrobial polymers (Ahmad et al., 2016; Amaral et al., 2019). In an example of the latter approach, chitosan nanoparticles (20–30 nm diameter) were recently examined for their ability to inhibit *C. albicans* biofilm growth, following initial cell attachment. Incubation with chitosan nanoparticles for 3 h led to a greater than 50% reduction in biofilm mass compared to non-treated controls (Ikono et al., 2019). While these chitosan nanoparticles exhibited some inherent antibiofilm activity, they were unable to entirely inhibit or disrupt *Candida* biofilms. Panwar et al. (2016) instead incorporated ferulic acid, a plant derived small molecule with known antibiofilm properties (Teodoro et al., 2015), into chitosan nanoparticles (~115 nm diameter). On its own, ferulic acid cannot efficiently penetrate fungal biofilms; however, when incorporated into chitosan nanoparticles and incubated with *C. albicans* biofilms, a significant reduction in fungal metabolic activity was observed (22.5% normalized to an untreated biofilm following 24 h). While the mechanism of these nanoparticles is not fully understood, it is believed that their strong cationic surface charge allows them to localize to and disrupt the fungal cell membrane while the surface bound ferulic acid interrupts *Candida* oxidative phosphorylation. This cell damage is evident in SEM images [**Figure 2**: **5A(ii)**] when compared to healthy biofilm cells [**Figure 2**: **5A(i);** Panwar et al., 2016].

Lipid-based self-assembled nanoparticles have also shown promise in penetrating the biofilm matrix and in targeting fungal cells. AmBisome®, a widely utilized liposomal formulation of amphotericin B, is able to disrupt *Candida* biofilms while free amphotericin B is unable to do this (Stone et al., 2016). AmBisome has a strong affinity for *Candida* cells, electrostatically interacting with the cell wall before binding to the cell membrane at sites of high ergosterol content (Soo Hoo, 2017), which may promote their activity against biofilm *Candida* cells, which have been shown to have thicker cell walls (Nett et al., 2007). Liposomal amphotericin B has also been immobilized on biomaterial surfaces for the prevention of biofilm formation (Alves et al., 2019). In our recent work, we have shown that liposomes encapsulating anidulafungin, the latest echinocandin approved by the FDA, are effective against mature *C. albicans* biofilms, reducing metabolic activity to approximately 46% compared to untreated controls over 24 h. Biofilms treated with an equivalent concentration of free anidulafungin did not reduce metabolic activity, further emphasizing the importance of nanoformulations in the treatment of *Candida* biofilms (Vera-González et al., 2020).

In addition to organic nanoparticles, inorganic nanoparticles have also been widely utilized for their antimicrobial properties, most commonly including silver and silica nanoparticles (Cousins et al., 2007; Monteiro et al., 2011; Silva et al., 2013). Silver nanoparticles were recently shown to inhibit biofilm formation

of multi-drug resistant *Candida auris* (Lara et al., 2020), an emerging fungal threat with the unique ability to survive on surfaces for several weeks (Welsh et al., 2017). Selenium nanoparticles, which are less toxic to mammalian cells than silver nanoparticles, have only recently been explored for their antimicrobial properties (Huang et al., 2016). Guisbiers et al. (2017) demonstrated that ~100 nm selenium nanoparticles successfully inhibited the formation of *C. albicans* biofilms by attaching to and penetrating through the cell wall (**Figure 2**: **5B**), replacing sulfur with selenium in important biochemical processes. These particles were able to reduce fungal burden in mature biofilms by over 50% at a nanoparticle concentration of as low as 26 ppm (Guisbiers et al., 2017). Inorganic nanoparticles have also been combined with antimicrobial therapeutics, to enhance antifungal properties. de Alteriis et al. (2018) conjugated the mammalian antimicrobial cathelicidin peptide, indolicidin, to the surface of gold nanoparticles (5 nm diameter) in order to protect it from proteolytic degradation and self-aggregation. These particles were able to penetrate and disrupt mature biofilms, eradicating over 50% of the cells for the most *C. albicans* and *C. tropicalis* strains tested after 24 h of treatment when compared to untreated biofilms, with a hypothesized mechanism involving penetration of the fungal cell membrane and inhibition of intracellular targets, arresting cell metabolism (de Alteriis et al., 2018).

CONCLUSIONS AND PERSPECTIVES

We have discussed several biomaterials strategies from surface functionalization to nanoparticle drug delivery for the prevention and disruption of *Candida* biofilms. Other approaches that can be combined with biomaterials to functionalize surfaces prone to the biofilm formation in the near future include the use of enzymes that target and digest EPS components (Nett, 2014), identification of new drug targets, including inhibition of *Candida* extracellular vesicles (Zarnowski et al., 2018), and incorporation of polymers, such as nylon-3 that have potent and selective activity against *Candida* biofilms (Liu et al., 2014, 2015).

While many advances have been made, development of antifungal biomaterials lags behind the development of antibacterial materials. There is a need for expansion and innovation in antifungal biomaterials, and an emphasis must be placed on advancing technologies beyond preclinical testing. Attention must also be given to polymicrobial biofilms, comprised of multiple fungal and bacterial species, which are currently understudied (Harriott and Noverr, 2009). It is estimated that more than 50% of *C. albicans* infections are polymicrobial in nature (Harriott and Noverr, 2011; Nash et al., 2016). Undoubtedly, it will be critical to use multi-pronged strategies combining effective biomaterials approaches (e.g., surface coatings with nanoparticles) to successfully combat *Candida* and other microbial biofilms.

AUTHOR CONTRIBUTIONS

NV-G and AS organized, prepared, and approved the final version of this manuscript. All authors contributed to the article and approved the submitted version.

FUNDING

AS and NV-G acknowledge support from the Office of Naval Research (grant N000141712651) awarded to AS and from a National Science Foundation Graduate Research Fellowship awarded to NV-G (grant 1644760).

ACKNOWLEDGMENTS

AS and NV-G thank Brown University graduate student, Carly Deusenbery, and postdoctoral researcher, Dr. Akram Abbasi, for useful discussions related to figure preparation.

REFERENCES

Ahmad, A., Wei, Y., Syed, F., Tahir, K., Taj, R., Khan, A. U., et al. (2016). Amphotericin B-conjugated biogenic silver nanoparticles as an innovative strategy for fungal infections. *Microb. Pathog.* 99, 271–281. doi: 10.1016/j.micpath.2016.08.031

Ailincai, D., Marin, L., Morariu, S., Mares, M., Bostanaru, A. -C., Pinteala, M., et al. (2016). Dual crosslinked iminoboronate-chitosan hydrogels with strong antifungal activity against *Candida* planktonic yeasts and biofilms. *Carbohydr. Polym.* 152, 306–316. doi: 10.1016/j.carbpol.2016.07.007

Alkekhia, D., Hammond, P. T., and Shukla, A. (2020). Layer-by-layer biomaterials for drug delivery. *Annu. Rev. Biomed. Eng.* 22, 1–24. doi: 10.1146/annurev-bioeng-060418-052350

Alkekhia, D., and Shukla, A. (2019). Influence of poly-L-lysine molecular weight on antibacterial efficacy in polymer multilayer films. *J. Biomed. Mater. Res. A* 107, 1324–1339. doi: 10.1002/jbm.a.36645

Alves, D., Vaz, A. T., Grainha, T., Rodrigues, C. F., and Pereira, M. O. (2019). Design of an antifungal surface embedding liposomal amphotericin b through a mussel adhesive-inspired coating strategy. *Front. Chem.* 7:431. doi: 10.3389/fchem.2019.00431

Amaral, A. C., Saavedra, P. H. V., Oliveira Souza, A. C., de Melo, M. T., Tedesco, A. C., Morais, P. C., et al. (2019). Miconazole loaded chitosan-based nanoparticles for local treatment of vulvovaginal candidiasis fungal infections. *Colloids Surf. B* 174, 409–415. doi: 10.1016/j.colsurfb.2018.11.048

Brown, G. D., Denning, D. W., Gow, N. A. R., Levitz, S. M., Netea, M. G., and White, T. C. (2012). Hidden killers: human fungal infections. *Sci. Transl. Med.* 4:165rv13. doi: 10.1126/scitranslmed.3004404

Butts, A., and Krysan, D. J. (2012). Antifungal drug discovery: something old and something new. *PLoS Pathog.* 8:e1002870. doi: 10.1371/journal.ppat.1002870

Carlson, R. P., Taffs, R., Davison, W. M., and Stewart, P. S. (2008). Anti-biofilm properties of chitosan-coated surfaces. *J. Biomater. Sci. Polym. Ed.* 19, 1035–1046. doi: 10.1163/156856208784909372

Cavalheiro, M., and Teixeira, M. C. (2018). *Candida* biofilms: threats, challenges, and promising strategies. *Front. Med.* 5:28. doi: 10.3389/fmed.2018.00028

Coad, B. R., Griesser, H. J., Peleg, A. Y., and Traven, A. (2016). Anti-infective surface coatings: design and therapeutic promise against device-associated infections. *PLoS Pathog.* 12:e1005598. doi: 10.1371/journal.ppat.1005598

Coad, B. R., Lamont-Friedrich, S. J., Gwynne, L., Jasieniak, M., Griesser, S. S., Traven, A., et al. (2015). Surface coatings with covalently attached caspofungin are effective in eliminating fungal pathogens. *J. Mater. Chem. B* 3, 8469–8476. doi: 10.1039/C5TB00961H

Cousins, B. G., Allison, H. E., Doherty, P. J., Edwards, C., Garvey, M. J., Martin, D. S., et al. (2007). Effects of a nanoparticulate silica substrate on

cell attachment of *Candida albicans*. *J. Appl. Microbiol.* 102, 757–765. doi: 10.1111/j.1365-2672.2006.03124.x

Cruz, L., Lopes, L., de Camargo Ribeiro, F., de Sá, N., Lino, C., Tharmalingam, N., et al. (2018). Anti-*Candida albicans* activity of thiazolylhydrazone derivatives in invertebrate and murine models. *J. Fungi* 4:134. doi: 10.3390/jof4040134

de Alteriis, E., Maselli, V., Falanga, A., Galdiero, S., Di Lella, F. M., Gesuele, R., et al. (2018). Efficiency of gold nanoparticles coated with the antimicrobial peptide indolicidin against biofilm formation and development of *Candida* spp. clinical isolates. *Infect. Drug Resist.* 11, 915–925. doi: 10.2147/IDR.S164262

de Sá, N. P., de Paula, L. F. J., Lopes, L. F. F., Cruz, L. I. B., Matos, T. T. S., Lino, C. I., et al. (2018). In vivo and in vitro activity of a bis-arylidenecyclo-alkanone against fluconazole-susceptible and -resistant isolates of *Candida albicans*. *J. Glob. Antimicrob. Resist.* 14, 287–293. doi: 10.1016/j.jgar.2018.04.012

Devadas, S. M., Nayak, U. Y., Narayan, R., Hande, M. H., and Ballal, M. (2019). 2,5-Dimethyl-4-hydroxy-3(2H)-furanone as an anti-biofilm agent against non-*Candida albicans Candida* species. *Mycopathologia* 184, 403–411. doi: 10.1007/s11046-019-00341-y

Fazly, A., Jain, C., Dehner, A. C., Issi, L., Lilly, E. A., Ali, A., et al. (2013). Chemical screening identifies filastatin, a small molecule inhibitor of *Candida albicans* adhesion, morphogenesis, and pathogenesis. *Proc. Natl. Acad. Sci. U. S. A.* 110, 13594–13599. doi: 10.1073/pnas.1305982110

Freitas, C. G., Lima, S. M. F., Freire, M. S., Cantuária, A. P. C., Júnior, N. G. O., Santos, T. S., et al. (2017). An immunomodulatory peptide confers protection in an experimental candidemia murine model. *Antimicrob. Agents Chemother.* 61, e02518–e02616. doi: 10.1128/AAC.02518-16

Gabriel, C., Grenho, L., Cerqueira, F., Medeiros, R., Dias, A. M., Ribeiro, A. I., et al. (2019). Inhibitory effect of 5-aminoimidazole-4-carbohydrazonamides derivatives against *Candida* spp. biofilm on nanohydroxyapatite substrate. *Mycopathologia* 184, 775–786. doi: 10.1007/s11046-019-00400-4

Galdiero, E., de Alteriis, E., De Natale, A., D'Alterio, A., Siciliano, A., Guida, M., et al. (2020). Eradication of *Candida albicans* persister cell biofilm by the membranotropic peptide gH625. *Sci. Rep.* 10:5780. doi: 10.1038/s41598-020-62746-w

Guisbiers, G., Lara, H. H., Mendoza-Cruz, R., Naranjo, G., Vincent, B. A., Peralta, X. G., et al. (2017). Inhibition of *Candida albicans* biofilm by pure selenium nanoparticles synthesized by pulsed laser ablation in liquids. *Nanomedicine* 13, 1095–1103. doi: 10.1016/J.NANO.2016.10.011

Gulati, M., and Nobile, C. J. (2016). *Candida albicans* biofilms: development, regulation, and molecular mechanisms. *Microbes Infect.* 18, 310–321. doi: 10.1016/j.micinf.2016.01.002

Harriott, M. M., and Noverr, M. C. (2009). *Candida albicans* and *Staphylococcus aureus* form polymicrobial biofilms: effects on antimicrobial resistance. *Antimicrob. Agents Chemother.* 53, 3914–3922. doi: 10.1128/AAC.00657-09

Harriott, M. M., and Noverr, M. C. (2011). Importance of *Candida*–bacterial polymicrobial biofilms in disease. *Trends Microbiol.* 19, 557–563. doi: 10.1016/j.tim.2011.07.004

Huang, X., Chen, X., Chen, Q., Yu, Q., Sun, D., and Liu, J. (2016). Investigation of functional selenium nanoparticles as potent antimicrobial agents against superbugs. *Acta Biomater.* 30, 397–407. doi: 10.1016/j.actbio.2015.10.041

Ikono, R., Vibriani, A., Wibowo, I., Saputro, K. E., Muliawan, W., Bachtiar, B. M., et al. (2019). Nanochitosan antimicrobial activity against *Streptococcus* mutans and *Candida albicans* dual-species biofilms. *BMC Res. Notes* 12:383. doi: 10.1186/s13104-019-4422-x

Ikuma, K., Decho, A. W., and Lau, B. L. T. (2015). When nanoparticles meet biofilms-interactions guiding the environmental fate and accumulation of nanoparticles. *Front. Microbiol.* 6:591. doi: 10.3389/fmicb.2015.00591

Jung, J., Bae, Y., Kwan Cho, Y., Ren, X., and Sun, Y. (2020). Structural insights into conformation of amphiphilic quaternary ammonium chitosans to control fungicidal and anti-biofilm functions. *Carbohydr. Polym.* 228:115391. doi: 10.1016/j.carbpol.2019.115391

Jung, J., Li, L., Yeh, C. -K., Ren, X., and Sun, Y. (2019). Amphiphilic quaternary ammonium chitosan/sodium alginate multilayer coatings kill fungal cells and inhibit fungal biofilm on dental biomaterials. *Mater. Sci. Eng. C* 104:109961. doi: 10.1016/j.msec.2019.109961

Karlsson, A. J., Flessner, R. M., Gellman, S. H., Lynn, D. M., and Palecek, S. P. (2010). Polyelectrolyte multilayers fabricated from antifungal β-peptides: design of surfaces that exhibit antifungal activity against *Candida albicans*. *Biomacromolecules* 11, 2321–2328. doi: 10.1021/bm100424s

Kucharíková, S., Gerits, E., De Brucker, K., Braem, A., Ceh, K., Majdič, G., et al. (2016). Covalent immobilization of antimicrobial agents on titanium prevents *Staphylococcus aureus* and *Candida albicans* colonization and biofilm formation. *J. Antimicrob. Chemother.* 71, 936–945. doi: 10.1093/jac/dkv437

Kumamoto, C. A., and Vinces, M. D. (2005). Alternative *Candida albicans* lifestyles: growth on surfaces. *Annu. Rev. Microbiol.* 59, 113–133. doi: 10.1146/annurev.micro.59.030804.121034

LaFleur, M. D., Kumamoto, C. A., and Lewis, K. (2006). *Candida albicans* biofilms produce antifungal-tolerant persister cells. *Antimicrob. Agents Chemother.* 50, 3839–3846. doi: 10.1128/AAC.00684-06

Lara, H. H., Ixtepan-Turrent, L., Jose Yacaman, M., and Lopez-Ribot, J. (2020). Inhibition of *Candida* auris biofilm formation on medical and environmental surfaces by silver nanoparticles. *ACS Appl. Mater. Interfaces* 12, 21183–21191. doi: 10.1021/acsami.9b20708

Li, W. -S., Chen, Y. -C., Kuo, S. -F., Chen, F. -J., and Lee, C. -H. (2018). The impact of biofilm formation on the persistence of candidemia. *Front. Microbiol.* 9:1196. doi: 10.3389/fmicb.2018.01196

Lima, S. L., Colombo, A. L., and de Almeida Junior, J. N. (2019). Fungal cell wall: emerging antifungals and drug resistance. *Front. Microbiol.* 10:2573. doi: 10.3389/fmicb.2019.02573

Liu, R., Chen, X., Falk, S. P., Masters, K. S., Weisblum, B., and Gellman, S. H. (2015). Nylon-3 polymers active against drug-resistant *Candida albicans* biofilms. *J. Am. Chem. Soc.* 137, 2183–2186. doi: 10.1021/ja512567y

Liu, R., Chen, X., Falk, S. P., Mowery, B. P., Karlsson, A. J., Weisblum, B., et al. (2014). Structure–activity relationships among antifungal nylon-3 polymers: identification of materials active against drug-resistant strains of *Candida albicans*. *J. Am. Chem. Soc.* 136, 4333–4342. doi: 10.1021/ja500036r

Lyu, Y., Yang, Y., Lyu, X., Dong, N., and Shan, A. (2016). Antimicrobial activity, improved cell selectivity and mode of action of short PMAP-36-derived peptides against bacteria and *Candida*. *Sci. Rep.* 6:27258. doi: 10.1038/srep27258

Mallick, E. M., and Bennett, R. J. (2013). Sensing of the microbial neighborhood by *Candida albicans*. *PLoS Pathog.* 9:e1003661. doi: 10.1371/journal.ppat.1003661

McKeny, P. T., and Zito, P. M. (2020). Antifungal antibiotics. StatPearls publishing. Available at: http://www.ncbi.nlm.nih.gov/pubmed/30844195 (Accessed February 6, 2020).

Michl, T. D., Giles, C., Mocny, P., Futrega, K., Doran, M. R., Klok, H. -A., et al. (2017). Caspofungin on ARGET-ATRP grafted PHEMA polymers: enhancement and selectivity of prevention of attachment of *Candida albicans*. *Biointerphases* 12:05G602. doi: 10.1116/1.4986054

Monteiro, D. R., Gorup, L. F., Silva, S., Negri, M., de Camargo, E. R., Oliveira, R., et al. (2011). Silver colloidal nanoparticles: antifungal effect against adhered cells and biofilms of *Candida albicans* and *Candida glabrata*. *Biofouling* 27, 711–719. doi: 10.1080/08927014.2011.599101

Mukherjee, P., and Chandra, J. (2004). *Candida* biofilm resistance. *Drug Resist. Updat.* 7, 301–309. doi: 10.1016/j.drup.2004.09.002

Nash, E. E., Peters, B. M., Fidel, P. L., and Noverr, M. C. (2016). Morphology-independent virulence of *Candida* species during polymicrobial intra-abdominal infections with *Staphylococcus aureus*. *Infect. Immun.* 84, 90–98. doi: 10.1128/IAI.01059-15

Nava-Ortiz, C. A. B., Burillo, G., Concheiro, A., Bucio, E., Matthijs, N., Nelis, H., et al. (2010). Cyclodextrin-functionalized biomaterials loaded with miconazole prevent *Candida albicans* biofilm formation in vitro. *Acta Biomater.* 6, 1398–1404. doi: 10.1016/j.actbio.2009.10.039

Nett, J. E. (2014). Future directions for anti-biofilm therapeutics targeting *Candida*. *Expert Rev. Anti-Infect. Ther.* 12, 375–382. doi: 10.1586/14787210.2014.885838

Nett, J., Lincoln, L., Marchillo, K., Massey, R., Holoyda, K., Hoff, B., et al. (2007). Putative role of β-1,3 glucans in *Candida albicans* biofilm resistance. *Antimicrob. Agents Chemother.* 51, 510–520. doi: 10.1128/AAC.01056-06

Oshiro, K. G. N., Rodrigues, G., Monges, B. E. D., Cardoso, M. H., and Franco, O. L. (2019). Bioactive peptides against fungal biofilms. *Front. Microbiol.* 10:2169. doi: 10.3389/fmicb.2019.02169

Palmieri, V., Bugli, F., Cacaci, M., Perini, G., De Maio, F., Delogu, G., et al. (2018). Graphene oxide coatings prevent *Candida albicans* biofilm formation with a controlled release of curcumin-loaded nanocomposites. *Nanomedicine* 13, 2867–2879. doi: 10.2217/nnm-2018-0183

Panwar, R., Pemmaraju, S. C., Sharma, A. K., and Pruthi, V. (2016). Efficacy of ferulic acid encapsulated chitosan nanoparticles against *Candida albicans* biofilm. *Microb. Pathog.* 95, 21–31. doi: 10.1016/j.micpath.2016.02.007

Qayyum, S., and Khan, A. U. (2016). Nanoparticles vs. biofilms: a battle against another paradigm of antibiotic resistance. *Med. Chem. Commun.* 7, 1479–1498. doi: 10.1039/C6MD00124F

Rajendran, R., Sherry, L., Nile, C. J., Sherriff, A., Johnson, E. M., Hanson, M. F., et al. (2016). Biofilm formation is a risk factor for mortality in patients with *Candida albicans* bloodstream infection-Scotland, 2012-2013. *Clin. Microbiol. Infect.* 22, 87–93. doi: 10.1016/j.cmi.2015.09.018

Ramage, G., Martínez, J. P., and López-Ribot, J. L. (2006). *Candida* biofilms on implanted biomaterials: a clinically significant problem. *FEMS Yeast Res.* 6, 979–986. doi: 10.1111/j.1567-1364.2006.00117.x

Ramage, G., Mowat, E., Jones, B., Williams, C., and Lopez-Ribot, J. (2009). Our current understanding of fungal biofilms. *Crit. Rev. Microbiol.* 35, 340–355. doi: 10.3109/10408410903241436

Raman, N., Marchillo, K., Lee, M. -R., de L Rodríguez López, A., Andes, D. R., Palecek, S. P., et al. (2016). Intraluminal release of an antifungal β-peptide enhances the antifungal and anti-biofilm activities of multilayer-coated catheters in a rat model of venous catheter infection. *ACS Biomater. Sci. Eng.* 2, 112–121. doi: 10.1021/acsbiomaterials.5b00427

Ribeiro, A. I., Gabriel, C., Cerqueira, F., Maia, M., Pinto, E., Sousa, J. C., et al. (2014). Synthesis and antimicrobial activity of novel 5-aminoimidazole-4-carboxamidrazones. *Bioorg. Med. Chem. Lett.* 24, 4699–4702. doi: 10.1016/j.bmcl.2014.08.025

Sahal, G., Nasseri, B., Ebrahimi, A., and Bilkay, I. S. (2019). Electrospun essential oil-polycaprolactone nanofibers as antibiofilm surfaces against clinical *Candida tropicalis* isolates. *Biotechnol. Lett.* 41, 511–522. doi: 10.1007/s10529-019-02660-y

Schrekker, C. M. L., Sokolovicz, Y. C. A., Raucci, M. G., Selukar, B. S., Klitzke, J. S., Lopes, W., et al. (2016). Multitask imidazolium salt additives for innovative poly(L-lactide) biomaterials: morphology control, *Candida* spp. biofilm inhibition, human mesenchymal stem cell biocompatibility, and skin tolerance. *ACS Appl. Mater. Interfaces* 8, 21163–21176. doi: 10.1021/acsami.6b06005

Shukla, A., and Almeida, B. (2014). Advances in cellular and tissue engineering using layer-by-layer assembly. *Wiley Interdiscip. Rev. Nanomed. Nanobiotechnol.* 6, 411–421. doi: 10.1002/wnan.1269

Silva, S., Pires, P., Monteiro, D. R., Negri, M., Gorup, L. F., Camargo, E. R., et al. (2013). The effect of silver nanoparticles and nystatin on mixed biofilms of *Candida glabrata* and *Candida albicans* on acrylic. *Med. Mycol.* 51, 178–184. doi: 10.3109/13693786.2012.700492

Silva-Dias, A., Palmeira-de-Oliveira, A., Miranda, I. M., Branco, J., Cobrado, L., Monteiro-Soares, M., et al. (2014). Anti-biofilm activity of low-molecular weight chitosan hydrogel against *Candida* species. *Med. Microbiol. Immunol.* 203, 25–33. doi: 10.1007/s00430-013-0311-4

Singh, R., Kumari, A., Kaur, K., Sethi, P., and Chakrabarti, A. (2018). Relevance of antifungal penetration in biofilm-associated resistance of *Candida albicans* and non-albicans *Candida* species. *J. Med. Microbiol.* 67, 922–926. doi: 10.1099/jmm.0.000757

Soo Hoo, L. (2017). Fungal fatal attraction: a mechanistic review on targeting liposomal amphotericin B (AmBisome®) to the fungal membrane. *J. Liposome Res.* 27, 180–185. doi: 10.1080/08982104.2017.1360345

Stone, N. R. H., Bicanic, T., Salim, R., and Hope, W. (2016). Liposomal amphotericin B (AmBisome®): a review of the pharmacokinetics, pharmacodynamics, clinical experience and future directions. *Drugs* 76, 485–500. doi: 10.1007/s40265-016-0538-7

Sultan, A. S., Vila, T., Hefni, E., Karlsson, A. J., and Jabra-Rizk, M. A. (2019). Evaluation of the antifungal and wound-healing properties of a novel peptide-based bioadhesive hydrogel formulation. *Antimicrob. Agents Chemother.* 63, e00888–e00919. doi: 10.1128/AAC.00888-19

Tan, Y., Leonhard, M., Moser, D., Ma, S., and Schneider-Stickler, B. (2016). Inhibition of mixed fungal and bacterial biofilms on silicone by carboxymethyl chitosan. *Colloids Surf. B* 148, 193–199. doi: 10.1016/j.colsurfb.2016.08.061

Teodoro, G. R., Ellepola, K., Seneviratne, C. J., and Koga-Ito, C. Y. (2015). Potential use of phenolic acids as anti-*Candida* agents: a review. *Front. Microbiol.* 6:1420. doi: 10.3389/fmicb.2015.01420

Tsui, C., Kong, E. F., and Jabra-Rizk, M. A. (2016). Pathogenesis of *Candida albicans* biofilm. *Pathog. Dis.* 74:ftw018. doi: 10.1093/femspd/ftw018

Vargas-Blanco, D., Lynn, A., Rosch, J., Noreldin, R., Salerni, A., Lambert, C., et al. (2017). A pre-therapeutic coating for medical devices that prevents the attachment of *Candida albicans*. *Ann. Clin. Microbiol. Antimicrob.* 16:41. doi: 10.1186/s12941-017-0215-z

Vera-González, N., Bailey-Hytholt, C. M., Langlois, L., de Camargo Ribeiro, F., de Souza Santos, E. L., Junqueira, J. C., et al. (2020). Anidulafungin liposome nanoparticles exhibit antifungal activity against planktonic and biofilm *Candida albicans*. *J. Biomed. Mater. Res. A* 108, 2263–2276. doi: 10.1002/jbm.a.36984

Welsh, R. M., Bentz, M. L., Shams, A., Houston, H., Lyons, A., Rose, L. J., et al. (2017). Survival, persistence, and isolation of the emerging multidrug-resistant pathogenic yeast *Candida auris* on a plastic health care surface. *J. Clin. Microbiol.* 55, 2996–3005. doi: 10.1128/JCM.00921-17

Wen, J., Jiang, F., Yeh, C. -K., and Sun, Y. (2016a). Controlling fungal biofilms with functional drug delivery denture biomaterials. *Colloids Surf. B* 140, 19–27. doi: 10.1016/J.COLSURFB.2015.12.028

Wen, J., Yeh, C. -K., and Sun, Y. (2016b). Functionalized denture resins as drug delivery biomaterials to control fungal biofilms. *ACS Biomater. Sci. Eng.* 2, 224–230. doi: 10.1021/acsbiomaterials.5b00416

Wen, J., Yeh, C. -K., and Sun, Y. (2018). Salivary polypeptide/hyaluronic acid multilayer coatings act as "fungal repellents" and prevent biofilm formation on biomaterials. *J. Mater. Chem. B* 6, 1452–1457. doi: 10.1039/C7TB02592K

Zarnowski, R., Sanchez, H., Covelli, A. S., Dominguez, E., Jaromin, A., Bernhardt, J., et al. (2018). *Candida albicans* biofilm–induced vesicles confer drug resistance through matrix biogenesis. *PLoS Biol.* 16:e2006872. doi: 10.1371/journal.pbio.2006872

Zelikin, A. N. (2010). Drug releasing polymer thin films: new era of surface-mediated drug delivery. *ACS Nano* 4, 2494–2509. doi: 10.1021/nn100634r

Conflict of Interest: The authors declare that the research was conducted in the absence of any commercial or financial relationships that could be construed as a potential conflict of interest.

frontiers in Microbiology

ORIGINAL RESEARCH
published: 14 October 2020
doi: 10.3389/fmicb.2020.551256

Dynamics of Mono- and Dual-Species Biofilm Formation and Interactions Between *Paracoccidioides brasiliensis* and *Candida albicans*

*Lariane Teodoro Oliveira[1], Kaila Petronila Medina-Alarcón[1], Junya de Lacorte Singulani[1], Nathália Ferreira Fregonezi[1], Regina Helena Pires[2], Rodrigo Alex Arthur[3], Ana Marisa Fusco-Almeida[1] and Maria José Soares Mendes Giannini[1]**

[1] Department of Clinical Analysis, School of Pharmaceutical Sciences, São Paulo State University-UNESP, Araraquara, Brazil, [2] Laboratory of Mycology and Environmental Diagnosis, University of Franca, Franca, Brazil, [3] Department of Preventive and Community Dentistry, Dental School, Federal University of Rio Grande do Sul, Porto Alegre, Brazil

OPEN ACCESS

Edited by:
Eleftherios Mylonakis, Alpert Medical School of Brown University, United States

Reviewed by:
Renátó Kovács, University of Debrecen, Hungary
Elisa Borghi, University of Milan, Italy
Sónia Silva, University of Minho, Portugal

***Correspondence:**
Maria José Soares Mendes Giannini
maria.giannini@unesp.br

Specialty section:
This article was submitted to Fungi and Their Interactions, a section of the journal Frontiers in Microbiology

Received: *12 April 2020*
Accepted: *15 September 2020*
Published: *14 October 2020*

Citation:
Oliveira LT, Medina-Alarcón KP, Singulani JL, Fregonezi NF, Pires RH, Arthur RA, Fusco-Almeida AM and Mendes Giannini MJS (2020) Dynamics of Mono- and Dual-Species Biofilm Formation and Interactions Between Paracoccidioides brasiliensis and Candida albicans. Front. Microbiol. 11:551256. doi: 10.3389/fmicb.2020.551256

The oral cavity is a highly diverse microbial environment in which microorganisms interact with each other, growing as biofilms on biotic and abiotic surfaces. Understanding the interaction among oral microbiota counterparts is pivotal for clarifying the pathogenesis of oral diseases. *Candida* spp. is one of the most abundant fungi in the oral mycobiome with the ability to cause severe soft tissue lesions under certain conditions. *Paracoccidioides* spp., the causative agent of paracoccidioidomycosis, may also colonize the oral cavity leading to soft tissue damage. It was hypothesized that both fungi can interact with each other, increasing the growth of the biofilm and its virulence, which in turn can lead to a more aggressive infectivity. Therefore, this study aimed to evaluate the dynamics of mono- and dual-species biofilm growth of *Paracoccidioides brasiliensis* and *Candida albicans* and their infectivity using the *Galleria mellonella* model. Biomass and fungi metabolic activity were determined by the crystal violet and the tetrazolium salt reduction tests (XTT), respectively, and the colony-forming unit (CFU) was obtained by plating. Biofilm structure was characterized by both scanning electronic- and confocal laser scanning- microscopy techniques. Survival analysis of *G. mellonella* was evaluated to assess infectivity. Our results showed that dual-species biofilm with *P. brasiliensis* plus *C. albicans* presented a higher biomass, higher metabolic activity and CFU than their mono-species biofilms. Furthermore, *G. mellonella* larvae infected with *P. brasiliensis* plus *C. albicans* presented a decrease in the survival rate compared to those infected with *P. brasiliensis* or *C. albicans*, mainly in the form of biofilms. Our data indicate that *P. brasiliensis* and *C. albicans* co-existence is likely to occur on oral mucosal biofilms, as per *in vitro* and *in vivo* analysis. These data further widen the knowledge associated with the dynamics of fungal biofilm growth that can potentially lead to the discovery of new therapeutic strategies for these infections.

Keywords: *Candida albicans*, *Paracoccidioides brasiliensis*, dual-species biofilm, oral cavity, *Galleria mellonella*

INTRODUCTION

An important step in the development of infectious diseases involves the ability of microorganisms to adhere to host surfaces. Adherence is a widely distributed biological phenomenon and is also the first step in the process of biofilm formation (Verstrepen and Klis, 2006; Pitangui et al., 2012; Martinez and Casadevall, 2015). Biofilm arrangement can protect fungal pathogens from host defenses and reduce the diffusion of antifungal drugs (Martinez and Casadevall, 2006; Kernien et al., 2017; Tulasidas et al., 2018; Thomaz et al., 2020). Clinically, fungal biofilms can adhere to both abiotic surfaces, comprised of medical and dental devices, as well as to mucous membranes (Kernien et al., 2017). Many clinically relevant fungi can grow as biofilms, including *Candida* spp. (Hawser and Douglas, 1994) and *Paracoccidioides* spp. (Sardi Jde et al., 2015; Cattana et al., 2017).

Paracoccidioidomycosis (PCM) is a human systemic mycosis which assumes increasing clinical importance due to the increase in their frequency and mortality rates in South and Central America (Coutinho et al., 2002). *Paracoccidioides* spp. are dimorphic fungi that change their morphology according to the environmental temperature, with a transition from mold at 25°C to yeast at 37°C in human lungs (San-Blas and Vernet, 1977; Gauthier, 2017). Although the primary route of PCM infection is pulmonary, the disease is frequently diagnosed by extensive, ulcerative and painful buccal manifestations corresponding to the clinical form of the multifocal type (Franco et al., 1987; Mendes et al., 2017; de Arruda et al., 2018).

Candida spp. is a commensal fungus found in the gastrointestinal tract, on oropharyngeal and vaginal mucosa of humans, with the ability to cause mucosal infections under certain conditions, such as immunosuppression, radiotherapy, antibiotics, and corticosteroids (Fotos et al., 1992; Akpan and Morgan, 2002; Epstein et al., 2002; Fangtham et al., 2014). *Candida albicans* is one of the most abundant fungi in the oral mycobiome (Ramage et al., 2004; Dongari-Bagtzoglou et al., 2009; Millsop and Fazel, 2016). Increasing evidence indicate that the coexistence of *C. albicans* and oral bacteria as well as other interactions with different kingdoms affect both the dynamics of biofilm growth and the course and severity of mucosal lesions, as reviewed by Negrini et al. (2019).

Considering that both *Candida* and *Paracoccidioides* may co-exist in the oral cavity, the impact of such fungal-fungal interaction on biofilm formation and its pathogenic potential are still unknown. Therefore, this study aimed to evaluate the dynamics of mono- and dual-species biofilm formed by *P. brasiliensis* plus *C. albicans* and their infectivity using the *Galleria mellonella* model. Our hypothesis is that both fungi interact with each other boosting the biofilm growth, that in turn could lead to a more aggressive infectivity.

MATERIALS AND METHODS

Fungal Strains and Growth Conditions

Paracoccidioides strains are currently classified as a complex of five cryptic species (*P. brasiliensis, P. americana, P. restrepiensis, P. venezuelensis*, and *P. lutzii*) distinguished by the phylogeny findings and studies using molecular techniques (Matute et al., 2006; Carrero et al., 2008; Turissini et al., 2017; De Macedo et al., 2019). We used the *P. brasiliensis* strain (former S1 phylogenetic group, Pb 18 strain, De Macedo et al., 2019), originally isolated from a case of pulmonary paracoccidioidomycosis in São Paulo, SP, Brazil. This strain belongs to the collection of the Clinical Mycology Laboratory, Department of Clinical Analysis, School of Pharmaceutical Sciences, UNESP. *C. albicans* ATCC 90028 was also used and it was cultured on Sabouraud dextrose agar (Difco—BD Biosciences, Sparks, MD, United States) and incubated at 37°C for 48 h. *P. brasiliensis* (Pb18) was cultured in Fava-Netto standard medium (Fava Netto et al., 1969) and incubated at 37°C for 5 days.

In vitro Biofilm Growth

The inocula were prepared as previously published, as per the *C. albicans* biofilm formation protocol (Jin et al., 2004). Briefly, a suspension of each fungus was standardized in Brain Heart Infusion (BHI) broth at 1×10^6 cells/mL using a hemocytometer. In all experiments, the fungal cell viability was evaluated using trypan blue (do Carmo Silva et al., 2015). Monospecies biofilms were developed on a polystyrene 96-well microtiter plate by adding 200 μL of *C. albicans* or *P. brasiliensis* standard inoculum to six wells. The plates were incubated at 37°C for 168 h with both fungi. The medium was changed during the total incubation time every 24 h. To compare the growth rates, both the biofilms were incubated for 168 h according to the kinetics for the biofilm of *P. brasiliensis* previously determined by our group (Sardi Jde et al., 2015).

Dual-species biofilms were developed on a 96-well microtiter plate by adding 100 μL of *P. brasiliensis* and 100 μL of *C. albicans* standard inoculum to six wells and by incubating them for 168 h at 37°C. Based on the assumption that *C. albicans* already exists in the oral microenvironment, we developed a second group of dual-species biofilms. In this group, we inoculated 100 μL of *P. brasiliensis* standard inoculum to a preformed 12 h *C. albicans* biofilm at 37°C. This was followed by incubation for a total period of 168 h at 37°C. In both dual-species biofilm groups, the medium was changed every 24 h of incubation.

Quantitative Biofilm Analysis

Biomass Quantification

Biofilm biomass was quantified based on the crystal violet (CV) assay (Peeters et al., 2008) with modifications. One microplate containing mono-species and dual-species biofilms was subjected to the CV methodology every 24 h until a 168 h total period. After each 24 h of incubation, the plates were washed with PBS to remove non-adherent cells. The biofilms were fixed with 100 μL of 99% methanol (Sigma-Aldrich, São Paulo, Brazil). After 15 min, the supernatants were removed, and the plates were air-dried. Then, 100 μL of 0.1% CV solution was added to all wells. After 20 min, the excess CV was removed by washing with PBS. Finally, the bound CV was released by adding 150 μL of 33% acetic acid (Sigma-Aldrich, São Paulo, Brazil). The absorbance was measured at 570 nm using a microplate reader (Epoch, Biotek).

All steps were carried out at room temperature. Three independent experiments were performed with six replicates each.

Biofilm Metabolic Activity Assessment

The biofilm metabolic activity was assessed through the XTT (2.3-bis (2-methoxy-4-nitro-5-sulfophenyl)-5-[carbonyl (phenylamino)]-2H-tetrazolium hydroxide) reduction assay. About 50 μL of XTT salt solution (1 mg/mL in PBS) and 4 μL of menadione solution (1 mM in ethanol; Sigma-Aldrich, São Paulo, SP., Brazil) were added to each well of the 96-well plate and incubated at 37°C for 3 h. The test was carried out every 24 h until a total period of 168 h for both mono-species and dual-species biofilms. The absorbance was measured using a microplate reader (Epoch, Biotek) at 490 nm (Martinez and Casadevall, 2006; Silva et al., 2010). In all assays, the culture media were included as negative control. Three independent experiments were performed with six replicates each.

Counts of Fungal Viable Cells

After biofilm formation, at different point times (0, 24, 48, 72, 96, 120, 144, and 168 h), the wells were washed thrice with PBS to remove loosely adhered cells. The biofilms were then mechanically disrupted, filling the wells with 100 μL of BHI broth and then vigorously mixed. Each individual well content was transferred to microtubes containing 900 μL of BHI broth. The suspensions were serially diluted and plated onto BHI agar supplemented with 1% glucose, 5% of *P. brasiliensis* 339 culture filtrate and 4% fetal bovine serum and caspofungin 0.25 μg/mL (for *P. brasiliensis* counts) and on Sabouraud dextrose agar (for *C. albicans* counts) that were incubated at 37°C for 10 days and 48 h, respectively. The number of viable fungal colony-forming units (CFU) was determined under a stereomicroscope and the results were expressed as $\log_{10}$ CFU/mL. Three independent experiments were performed with six replicates each.

Structural Biofilm Analysis

Confocal Laser Scanning Microscopy (CLSM)

The standardized *P. brasiliensis* inoculum was treated with carboxyfluorescein diacetate succinimidyl ester dye (CFSE, 100 μM/mL, BioChemika), kindly provided by Dr Paula Aboud Barbugli from Araraquara School of Dentistry (São Paulo State University - UNESP) for 30 min at 37°C. The fungi cells were washed with PBS and resuspended in BHI medium by restoring the initial volume. This inoculum was then incubated with 12 h preformed *C. albicans* biofilms in 24-well plates. Mono-species biofilms of *P. brasiliensis* or *C. albicans* grown for a time that allowed their maturation (144 and 48 h, respectively) were used as controls (Sardi Jde et al., 2015). For the formation of dual-species biofilms of *P. brasiliensis* and *C. albicans*, equitable volumes of the standardized inoculum of the two organisms were co-cultivated and grown for 120 h, the time of greatest metabolic activity determined by the XTT test (section "Biofilm Metabolic Activity Assessment"). Next, the biofilms were washed carefully with sterile PBS to remove non-adherent cells. The biofilms were stained with calcofluor white (1 g/L; Sigma-Aldrich St. Louis, MO, United States) for 30 min at room temperature and washed again with PBS. The biofilms were photographed under a 20× dry immersion objective (numerical aperture 1.0) using a Zeiss LSM 800 confocal microscope. Each field of view was photographed using a 405 nm laser to capture calcofluor with an emission range up to 450 and 488 nm for CFSE detection with an emission range up to 540 nm.

Scanning Electron Microscopy (SEM)

To access the morphology, the biofilms were formed in 24-well plates according to previously published protocols (Morris et al., 1997; Ells and Truelstrup Hansen, 2006) with modifications. Mono-species biofilms of *P. brasiliensis* or *C. albicans* grown at 37 C for 144 and 48 h, respectively, were used as controls. Dual-species biofilms were formed over a period of 120 h. Next, the plates were washed with PBS to remove non-adherent cells. The biofilms were fixed with 1,000 μL of 2.5% glutaraldehyde solution (Sigma-Aldrich, St Louis, MO, United States) in sterile distilled water overnight (for both *P. brasiliensis* mono-species and dual-species biofilms) or for 3 h (*C. albicans* mono-species biofilms), washed thrice with PBS and sequentially dehydrated with ethanol (50–100%) at room temperature. All samples were dried in a 780A Samdri desiccator (Rockville, MD, United States). Subsequently, the samples were mounted on aluminum and silver cylinders and disposed in a high vacuum evaporator (Denton Vacuum Desk V, Jeol, Moorestown, NJ, United States) for gold coating. The topographic images of biofilms were captured under a scanning electron microscope (Jeol JSM- 6610LV, Peabody, MA, United States).

Survival Assay Using *G. mellonella* Model

Survival assay was performed according to the previous protocol (Scorzoni et al., 2015), with some modifications. *G. mellonella* larvae (School of Pharmaceutical Sciences, São Paulo State University–UNESP) with a body weight ranging from 150 to 200 mg were randomly chosen for the experiments. The larvae were separated into six infection groups, each group consisting of 9–10 larvae which were kept in Petri plates at 37°C overnight, prior to use. To obtain planktonic cells, *C. albicans* was grown in Sabouraud agar at 25°C for 48 h and *P. brasiliensis* was grown in BHI broth supplemented with 1% glucose at 37°C and 150 rpm for 72 h. Pre-formed biofilms of *C. albicans* for 12 h and *P. brasiliensis* for 120 h in a 24-well plate were scrapped using a sterile tip and utilized for inoculum preparation. The inoculum of fungi for planktonic cells or cells from biofilms were prepared in PBS and counted using a hemocytometer. For each group, the larvae were injected at a concentration of 1×10^6 cells/larvae of *C. albicans* or *P. brasiliensis* (2×10^6 cells/larvae total for co-infection) into the last pro-leg using a 10 μL Hamilton syringe (Chibebe Junior et al., 2013; Scorzoni et al., 2015; de Barros et al., 2018). Survival larvae were monitored daily for up to 7 days of infection. Larvae were considered dead when they displayed no movement in response to touch. Larvae inoculated once or twice with sterile PBS were used as controls. Three independent experiments were performed, resulting in an $n = 27–30$ larvae/group.

Statistical Analysis

The statistical analysis was conducted using the GraphPad Prism 5.0 software (GraphPad Software, Inc., San Diego, CA). The results were presented as mean ± standard deviation and compared by analysis of variance (ANOVA) followed by Bonferroni test. The data from the survival of *G. mellonella* larvae were plotted as Kaplan–Meier survival curves and compared using log-rank tests. Statistical significance was considered when $p < 0.05$.

RESULTS

Biomass Quantification

Overall, a biomass increase of all tested biofilms was observed in the period from 24 to 96 h growth, and this increase extended to up to 144 h in the case of *P. brasiliensis* mono-species biofilm (**Figure 1**). Comparison of mono-species with dual-species biofilms was performed using the analysis of variance (ANOVA) followed by Bonferroni test. Two different approaches have been done in relation to the dual-species genera interaction: (1) *P. brasiliensis* and *C. albicans* incubated simultaneously; (2) *P. brasiliensis* incubated after *C. albicans* pre-formed biofilm. The biomass of dual-species biofilms formed after *P. brasiliensis* was added to pre-formed 12 h *C. albicans* biofilms was statistically higher than the biomass of simultaneously formed dual-species biofilms at 48 h growth ($p < 0.05$). The biomass of *P. brasiliensis* mono-species biofilms was statistically lower than the biomass of simultaneously formed dual-species biofilms at 48 h ($p < 0.01$), 72 h ($p < 0.05$), and 96 h ($p < 0.001$) of growth and lower than the biomass of dual-species biofilms grown from *P. brasiliensis* added to 12 h pre-formed *C. albicans* biofilms at 48, 72, and 96 h ($p < 0.001$) and at 120 and 168 h ($p < 0.01$) of growth. No difference was found in the biomass of *C. albicans* as a mono-species biofilm compared to simultaneously formed dual-species biofilms in all periods analyzed, except the biomass at 48 h that was statistically lower than the biomass of dual-species biofilms grown from *P. brasiliensis* added to 12 h preformed *C. albicans* biofilms ($p < 0.01$).

Biofilm Metabolic Activity

P. brasiliensis biofilm presents an increase in the metabolic activity from 24 h to up to 120 h of growth, whereas the *C. albicans* biofilm exhibits an increase in metabolic activity up to 48 h. Dual-species biofilms showed higher metabolic activity, mainly when *P. brasiliensis* was added to preformed 12 h *C. albicans* biofilms and there was a slight reduction after 72 h. Comparison of mono-species biofilms with dual-species was performed using analysis of variance (ANOVA) followed by Bonferroni test. The metabolic activity of *P. brasiliensis* biofilms was statistically lower than simultaneously formed dual-species biofilms at all time points ($p < 0.001$ for 24, 48, 72, 96, and 168 h and $p < 0.05$ for 120 and 144 h) and statistically lower than dual-species biofilms grown from *P. brasiliensis* added to preformed 12 h *C. albicans* biofilms at all time points ($p < 0.001$) except at 120 h of growth. Metabolic activities of *P. brasiliensis* and *C. albicans* biofilms were statistically lower than simultaneously formed dual-species biofilms only at 120 h of growth ($p < 0.01$) and at 24 h ($p < 0.05$), 48 and 72 h ($p < 0.001$) in comparison to dual-species biofilms when *P. brasiliensis* was added to preformed 12 h *C. albicans* biofilms. The metabolic activity of simultaneously formed dual-species biofilms was statistically lower than those in other conditions at 48 and 72 h of growth ($p < 0.01$) (**Figure 2**).

Determination of Viable Cells as CFU/mL

Comparison between the *C. albicans* CFU values were similar in mono or dual-species biofilms (ANOVA followed by Bonferroni test). However, the values of dual-species biofilms when *P. brasiliensis* was added to 12 h preformed *C. albicans* biofilms were statistically significant and higher than *C. albicans* biofilm at 144 h ($p < 0.001$) (**Figure 3A**). Similarly, the comparison between the CFU values of *P. brasiliensis* was similar in mono or dual-species biofilms (**Figure 3B**). There was no significant difference in the evaluated times, suggesting that both fungi are able to co-exist in dual-species biofilms resembling those formed on oral mucosal surfaces.

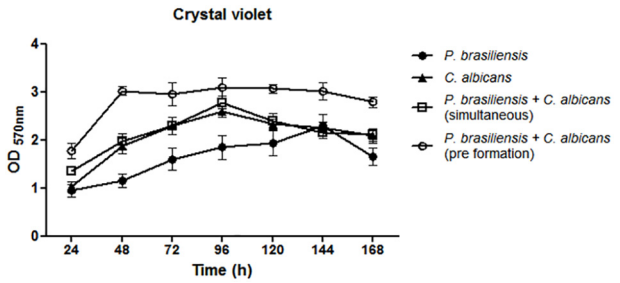

FIGURE 1 | Quantification of mono and dual-species biofilm biomass by crystal violet methodology. Co-cultivated dual-species biofilms and dual-species biofilms formed by the addition of *P. brasiliensis* inoculum to preformed 12 h *C. albicans* biofilms. Three independent experiments with six replicates each were performed. Error bars indicate the standard error. Statistical significances were calculated by using analysis of variance (ANOVA) followed by Bonferroni test.

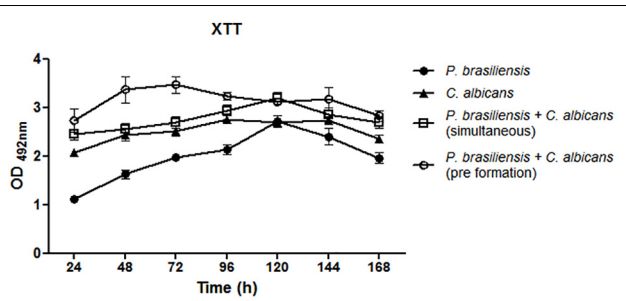

FIGURE 2 | Metabolic activity of mono- and dual-species biofilms. Three independent experiments with six replicates each were performed. Co-cultivated dual-species biofilms and dual-species biofilms formed by the addition of *P. brasiliensis* inoculum to preformed 12 h *C. albicans* biofilms. Error bars indicate the standard error. Statistical significances were calculated by using analysis of variance (ANOVA) followed by Bonferroni test.

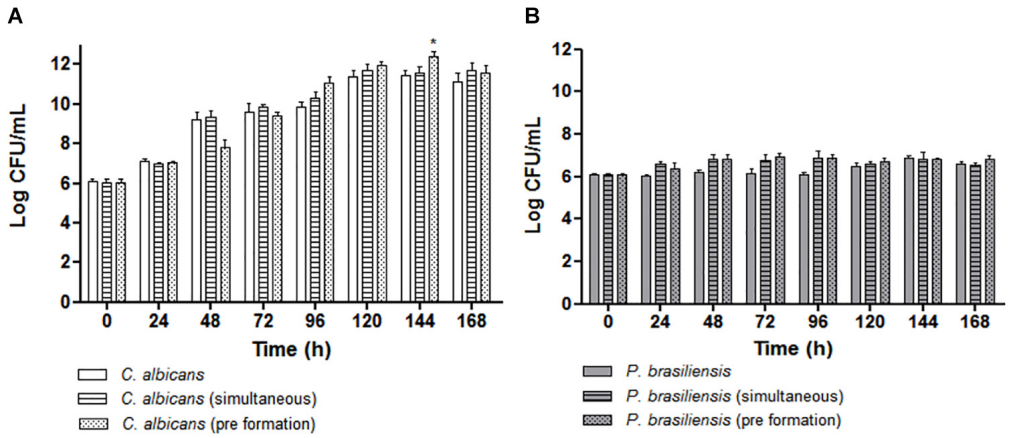

FIGURE 3 | Quantitative analysis of biofilm formation *in vitro* by CFU/mL (Log10) count for the following groups: **(A)** Mono-species biofilms formed by *C. albicans*, co-cultivated *C. albicans* plus *P. brasiliensis* biofilms or dual-species biofilms formed by the addition of *P. brasiliensis* inoculum to preformed 12 h *C. albicans* biofilms (*$p < 0.001$). **(B)** Mono-species biofilms formed by *P. brasiliensis*, co-cultivated *C. albicans* plus *P. brasiliensis* biofilms or dual-species biofilms formed by the addition of *P. brasiliensis* inoculum to preformed 12 h *C. albicans* biofilms. Statistical significances were calculated by using analysis of variance (ANOVA) followed by Bonferroni test.

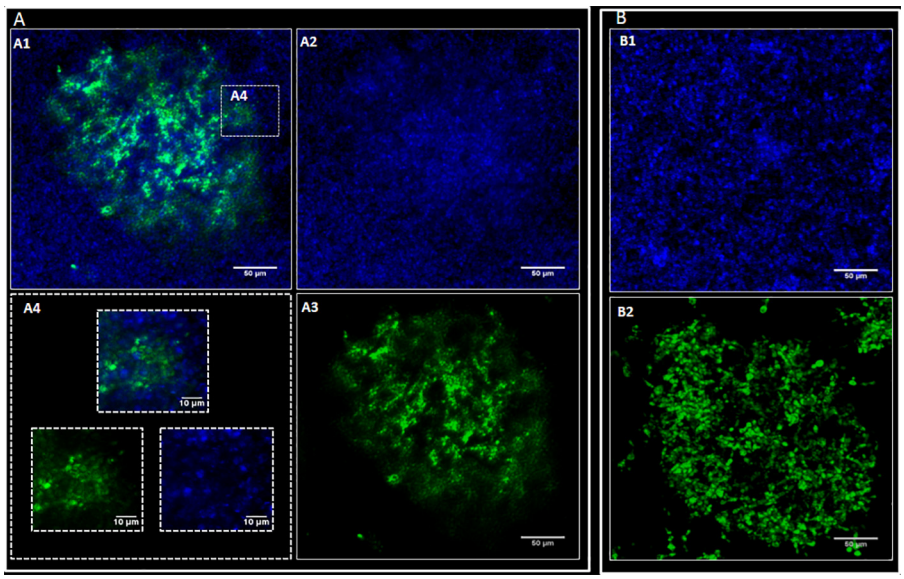

FIGURE 4 | Representative confocal microscopy images. *P. brasiliensis* was marked with CFSE (green) and *C. albicans* with Calcofluor white (blue). *C. albicans* (CA) and *P. brasiliensis* (PB) mono-species biofilms formed for 48 and 144 h, respectively. For dual-species biofilms, *P. brasiliensis* previously treated with CFSE was added to 12 h preformed *C. albicans* biofilm, and incubated for 120 h. **(A)** Dual-species biofilms: overlay of CA and PB (A1), CA (A2), PB (A3) and zoom in image showing dual-species interaction (A4); **(B)** Mono-species biofilms: CA biofilm (B1) and PB biofilm (B2).

Biofilm Structure

Confocal images showed *C. albicans* as a carpet-like biofilm (either as mono or as dual-species biofilms) whereas in dual-species biofilms, *P. brasiliensis* presented as organized clusters surrounded by *C. albicans* cells (**Figure 4**). The SEM images showed homogeneous and organized biofilms which were interspaced by an extracellular polysaccharide matrix (**Figure 5**). *C. albicans* and *P. brasiliensis* mono-species biofilms presented mainly yeasts forms (A) whilst (C) dual-species biofilms grown from *P. brasiliensis* added to preformed 12 h *C. albicans* biofilms presented a dense colonization by *C. albicans* (E). It appears that the interaction between *C. albicans* and *P. brasiliensis,* in addition to the direct physical contact, is also mediated by extracellular polysaccharides (F).

Microbial Interaction in the *G. mellonella* Model

The pathogenicity of cells released from the disrupted biofilms of *P. brasiliensis* and *C. albicans* and its co-infection were tested in the *G. mellonella* model (**Figure 6**). The data from larvae survival

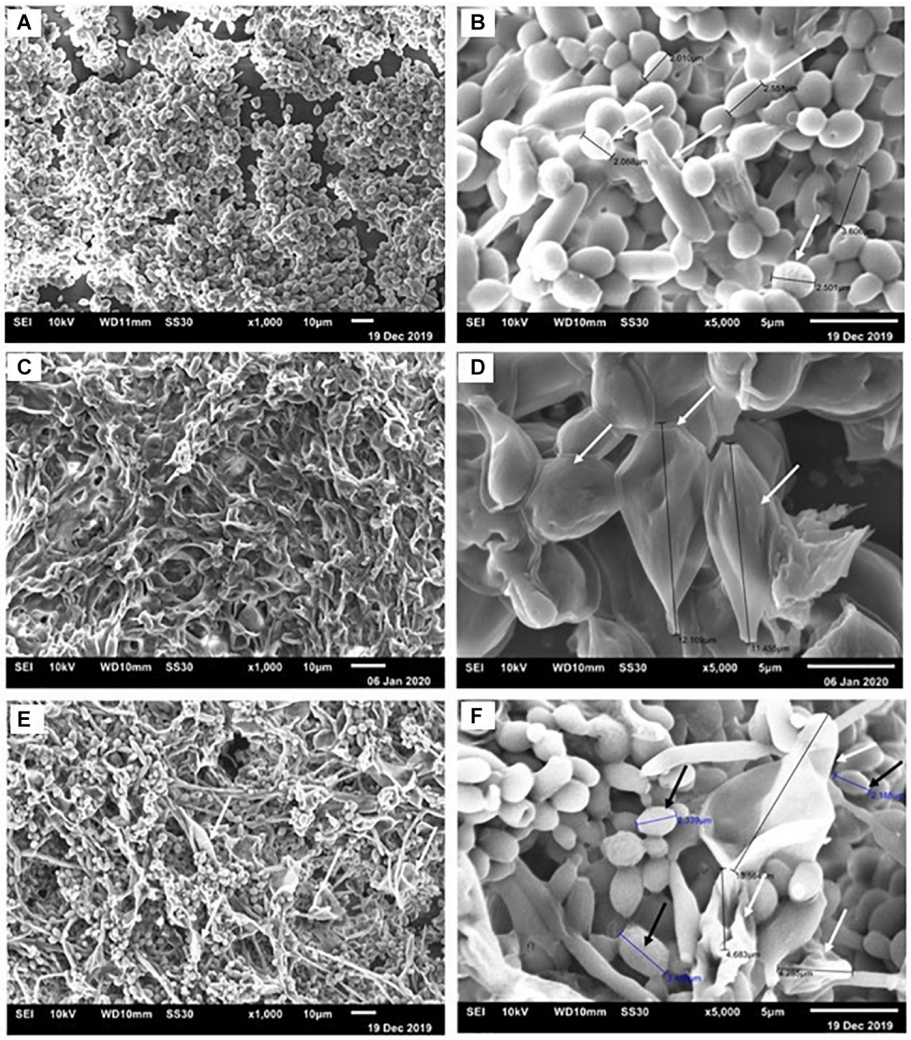

FIGURE 5 | Representative scanning electron micrographs of *C. albicans* and *P. brasiliensis* mono-species biofilms formed for 48 and 144 h, respectively. For dual-species biofilms, *P. brasiliensis* was added to 12 h preformed *C. albicans* biofilm for 120 h. Biofilms formed by *C. albicans* **(A)** 1,000× and **(B)** 5,000× magnification. The white arrows indicate the yeast size **(B)**. Biofilms formed by *P. brasiliensis* **(C)** 1,000× and **(D)** 5,000×. The black arrows denote the measure of yeast **(D)**. Dual-species biofilms grown from *P. brasiliensis* added to 12 h preformed *C. albicans* biofilms **(E)** 1,000× and **(F)** 5,000×.

were plotted as Kaplan–Meier survival curves and compared using log-rank tests. Firstly, we observed a decrease in the survival rate of the larvae when infected with the mono- and dual-species biofilm cells compared to their planktonic cells. About 55% of the larvae were alive on the 7th day when infected with *P. brasiliensis* planktonic cells, but up to 38% were alive for its biofilm form. Likewise, infections by the two fungi in planktonic form led to the death of the larvae in the first 24 h, while larvae death was observed after 12 h of infection by the biofillm form. No larvae died with the single or double injection of PBS.

Secondly, when we compared the profile curve of larvae infected with mono- and dual-species biofilms with planktonic cells, there was a significant difference between *P. brasiliensis* and *P. brasiliensis* plus *C. albicans* ($p < 0.05$). On the other hand, the profile curve between *C. albicans* and *P. brasiliensis* plus *C. albicans* did not show a statistical difference, although the dual-species infection led to faster larvae mortality compared to *C. albicans* (1 vs. 2 days).

Thirdly, the comparison of larvae infected with mono- and dual-species biofilms cells showed a significant difference between *P. brasiliensis* or *C. albicans* and *P. brasiliensis* + *C. albicans* ($p < 0.05$).

DISCUSSION

Candida species, the most representative oral mycobiome microorganism (Bertolini and Dongari-Bagtzoglou, 2019), is normally found in the oral cavity at levels compatible to health. However, under certain conditions, especially those related to immune suppression or even in neonates or elderly, there is an increase in *Candida* carriage in the oral cavity that ultimately

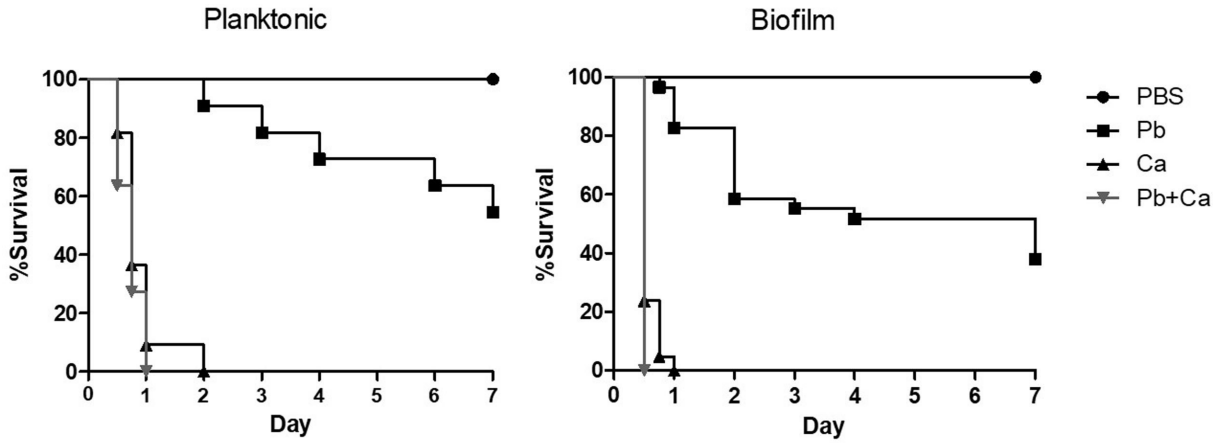

FIGURE 6 | Survival curve of *Galleria mellonella* larvae infected with 1×10^6 cells/larvae of planktonic cells, mono-, and dual-species biofilms grown after *P. brasiliensis* (Pb) was added to preformed *C. albicans* (Ca) biofilms. Larvae inoculated with PBS was used as control. The values are plotted as Kaplan–Meier survival curves and compared using log-rank tests.

leads to the development of opportunistic mucosal infections (Nicolatou-Galitis et al., 2001; Bertolini and Dongari-Bagtzoglou, 2019). In this context, many studies have reported inter-kingdom *Candida*-bacterial interactions in the oral cavity, as well as *Candida-Candida* interactions and their role in oral diseases, especially at the mucosal sites (Baena-Monroy et al., 2005; Thein et al., 2009; Martins et al., 2016; Negrini et al., 2019; Pathirana et al., 2019; Rodrigues et al., 2019). Moreover, *Paracoccidioides* spp. can also be found in the oral mucosal lesions as loose or dense granulomas (de Carli et al., 2015). Thus, both fungi can be found in a suitable niche in the oral cavity to exert their pathogenicity.

Both fungi may grow as *in vitro* or *in vivo* mono-species biofilms (Hawser and Douglas, 1994; Douglas, 2003; Sardi Jde et al., 2015; Cattana et al., 2017). Therefore, evaluating the dynamics of mono- and dual-species biofilm formed by *P. brasiliensis* and *C. albicans* can widen the knowledge about the PCM infection mechanism, the most important mycotic disease in Latin America. To our knowledge, this is the first time that such dual-species biofilm has been developed and reported.

Despite the disadvantages of reproducing some biological conditions (Diaz-Garcia et al., 2019), polystyrene microtiter plates are commonly used as the standard system to study adhesion and biofilm formation by bacteria and fungi (Simoes et al., 2010; Pemmaraju et al., 2013; Sardi Jde et al., 2015).

Both biomass and biofilm metabolic activity were used in this study to characterize the dynamics of biofilm growth. Based on the quantification of biomass, we found that *C. albicans* mono-species biofilms reached a mature stage from 72 to 96 h in agreement with previous data (Pierce et al., 2010; Cavalheiro and Teixeira, 2018). *P. brasiliensis* needed 144 h to reach its highest biomass, which corroborates with the previous studies carried out by Sardi Jde et al. (2015). In addition, the *C. albicans* mono-species biofilm showed higher values of biomass, metabolic activity and CFU than that found in the *P. brasiliensis* mono-species biofilm in most of the evaluated times.

Interestingly, the growth dynamics of dual-species biofilms was different. The mature stage (in terms of biomass) of co-cultivated dual-species biofilms was reached after 96 h of growth, while the dual-species biofilm formed after *P. brasiliensis* was added to 12 h preformed *C. albicans* biofilm reached its highest biomass in 48 h. In line with the fast growth of dual-species biofilms, their metabolic activity was also higher than the mono-species biofilms, almost at all time points, mainly in 72 h. In agreement with the biomass and metabolic activity results, the *C. albicans* CFU values in dual-species biofilms were higher compared to the CFU values of mono-species biofilms, specially from 96 h. The increase in metabolic activity, biomass and CFU, primarily in the dual-species biofilms grown after *P. brasiliensis* was added to preformed 12 h *C. albicans* biofilms, compared to *P. brasiliensis* mono-species biofilms, indicate that there were no loss to *P. brasiliensis* and that can coexist in the same environment as *C. albicans*.

There are common functional organization principles that occur at sites of polymicrobial infection, including exploration of metabolites, immunological modulation, niche optimization and induction of virulence. Thus, the presence of a microorganism can generate a niche for other pathogenic microorganisms or predispose the host to colonization by other microorganisms, or two or more non-pathogenic microorganisms together can cause disease (Brogden et al., 2005; Peters et al., 2012). Clinically, we could hypothesize that oral cavity lesions caused by *P. brasiliensis* would be more aggressive when both fungi (*C. albicans* and *P. brasiliensis*) are present at both the same time and site, once we observe an improvement in the biofilm features. The surface first settled by *C. albicans* cells has already been related to increased adhesion, accompanied by a significant increase in cell viability with bacterial biofilms (Bartnicka et al., 2019). Interactions in mixed biofilms are essential to produce a rich exopolysaccharide matrix. In a previous study, the synergism between *C. albicans* and *Streptococcus mutans* increased the virulence of mixed biofilms formed on the surfaces of teeth,

thus contributing to the severity of caries (Falsetta et al., 2014; Sztajer et al., 2014). Here, the enhanced growth through intergeneric cooperation may be taking place and the damage to oral mucosa tissues caused by *Candida* may be influence the PCM pathogenesis.

The SEM images of mono-species biofilms showed *C. albicans* and *P. brasiliensis* yeasts embedded in extracellular polysaccharide matrix and presenting an average size from 2 to 4 μm and from 11 to 12 μm, respectively. Dual-species biofilms also showed similar features of mono species biofilms, however, presenting a higher proportion of *C. albicans* yeast cells. This higher proportion of *C. albicans* may be due to the slower growth of *P. brasiliensis*. Interestingly, the interaction between *C. albicans* and *P. brasilensis* in dual-species biofilms seem to happen both by direct physical contact and mediated by the extracellular polysaccharide matrix. It is known that some *Candida* surface adhesins, such as Als3, exert an important role on *Candida* biofilm formation as well as mediating the co-aggregation between *Candida* and other microorganisms (Verstrepen and Klis, 2006; Cavalheiro and Teixeira, 2018; Negrini et al., 2019). Moreover, *Candida* cell-wall mannan-residues might also act as an adhesion element for extracellular polysaccharides (Negrini et al., 2019). In addition, several *Paracoccidioides* adhesin proteins have been shown to be extracellular matrix ligands, such as 43 kDa glycoprotein (gp43), enolase and glyceraldehyde-3-phosphate dehydrogenase (GAPDH) (Vicentini et al., 1994; Mendes-Giannini et al., 2004; Barbosa et al., 2006; Donofrio et al., 2009). These adhesins may be used in the adhesion process, the initial phase of biofilm formation. In recent studies, GP43, GAPDH, and proteinase genes were considered to be overexpressed in the biofilm (Sardi Jde et al., 2015). Then, we hypothesize that agglutinin-like sequence (Als) surface proteins optimize the physical interaction and co-aggregation between *C. albicans* and *P. brasiliensis* and the cell-wall mannan-residues might act as a receptor to extracellular polysaccharides, which in turn act as a bridge, facilitating the adhesion between both microorganisms. It is unclear though, at this moment, which of those adhesion mechanisms are the most predominant and whether other adhesion mechanisms might be involved in such interactions. These interactions between two organisms can induce additional responses among themselves and modify the immediate environment to influence pathogenesis. Although we have begun to investigate the consequences of these interactions, much is still unknown. This highlights the need for future mechanistic studies to be properly designed to address those questions.

Galleria mellonella has been presented as a useful invertebrate model to assess the fungi virulence, innate immune response and antifungal efficacy due to the ease of breeding it in the laboratory as well as in carrying out experiments with the larvae (Fuchs and Mylonakis, 2006). The model is especially advantageous in the study of dimorphic fungi due to the possibility that the larvae are kept at 37°C during survival assays, which represents the conditions of human physiology and contributes to maintaining the yeast phase of fungi such as *Paracoccidioides* spp. (Singulani et al., 2018). More recently, *G. mellonella* has been used to evaluate co-infection between fungi (Alcazar-Fuoli et al., 2015) or fungus and bacteria (Kean et al., 2017; Rossoni et al., 2017; Reece et al., 2018; Sheehan et al., 2020). Furthermore, some results are similar to those found in mammal models (Sheehan et al., 2020). Here, we used the *G. mellonella* model to evaluate the virulence of mono-species and dual-species *P. brasiliensis* and *C. albicans* biofilm formation. Cells from biofilms usually exhibit different phenotypes compared to planktonic cells and are associated with a higher pathogenicity of the microorganisms, including resistance to host immune mechanisms (Martinez and Fries, 2010). In this aspect, our results showed that cells released from the disrupted biofilms increased the virulence of both fungi compared to their planktonic cells and consequently, it decreased the survival rate of the larvae. Similar results were presented for *Cryptococcus neorfomans* in a previous study (Benaducci et al., 2016). Furthermore, the comparison of larvae infected with mono-species and dual-species biofilms presented the difference between *P. brasiliensis* or *C. albicans* and *P. brasiliensis* plus *C. albicans,* especially for biofilm formation. This means that the larvae survival on dual-species biofilms was lower when compared to survival with mono-species biofilms. Thus, our results from *G. mellonella* are based on *in vitro* assays since dual-species biofilms showed greater biomass and metabolic activity, and therefore were more virulent than mono-species biofilms. Finally, our data may indicate that *P. brasiliensis* and *C. albicans* co-existence is likely to occur on oral mucosal as biofilms, using an *in vivo* model. In the same way, when G. *mellonella* larvae were infected with *C. albicans* and *Staphylococcus aureus*, there was an increase in the virulence of these microorganisms and the antifungal resistance, which indicated a synergic interaction (Kean et al., 2017).

One may argue that the dynamics of dual-species biofilm growth could be affected by the different growth kinetics of *P. brasiliensis* and *C. albicans* and that both strains should ideally present similar growth curves. We acknowledge that the maturity of *P. brasiliensis* mono-species biofilms was reached later compared with *C. albicans* biofilms. This way, we might consider the contribution of *C. albicans* to dual-species biofilms (in terms of biofilm dry weight, biofilm metabolic activity and infectivity on the *G. mellonella* model) to be greater than *P. brasiliensis*. *Paracoccidioides* and *Candida* are often co-isolated in the oral mucosa. This presence may represent a polymicrobial association with mutual collaboration or advantage for one of the agents, that can lead to more exacerbated clinical and pathological manifestations. Moreover, the comparison of larvae infected with mono- and dual-species biofilms cells showed a significant difference between *C. albicans* and *P. brasiliensis* plus *C. albicans* ($p < 0.05$), which can be a consequence of virulence factors and *quorum sensing* mechanisms of biofilms.

Irrespective of any difference in growth kinetics, both the strains were able to co-exist on the studied dual-species biofilms, suggesting that a fungal-fungal interaction is likely to occur on oral mucosal sites. In fact, an *in vivo* rodent model should be adopted in further studies to assess both the infectivity of this dual-species biofilms on oral mucosal surfaces and the elicited immune-response against those fungal biofilms. Thus, a deeper understanding of the adhesion and signaling mechanisms

involved in the interactions between both fungi will provide a new perspective on the role of known virulence determinants and the relevant factors for both diseases.

CONCLUSION

This study suggested that the *C. albicans* and *P. brasiliensis* can coexist in the same environment and that a fungal-fungal interaction is likely to occur on oral mucosal sites. These data widen the knowledge associated with the dynamics of fungal biofilm growth that can potentially lead to the discovery of new therapeutic strategies for fungal infections.

DATA AVAILABILITY STATEMENT

All datasets generated for this study are included in the article/supplementary material.

AUTHOR CONTRIBUTIONS

LO and MMG contributed to the research idea and experimental design. LO, KM-A, and NF performed the experiments. LO, KM-A, JS, NF, and RA analyzed the data, prepared, and wrote the manuscript. RA, AF-A, RP, and MMG revised the final draft of the manuscript. All authors contributed to the article and approved the submitted version.

FUNDING

This study was supported by the Fundação de Amparo à Pesquisa do Estado de São Paulo (FAPESP Grants Nos. 2017/06658-9; 2018/15877-9), the Coordenação de Aperfeiçoamento de Pessoal de Nível Superior–Brasil (PROEX-CAPES), the Conselho Nacional de Desenvolvimento Científico e Tecnológico (CNPq Grants Nos. 431455/2018-0; 310524/2018-2; 134009/2018-5), and the PADC-FCF.

REFERENCES

Akpan, A., and Morgan, R. (2002). Oral candidiasis. *Postgrad. Med. J.* 78, 455–459.

Alcazar-Fuoli, L., Buitrago, M., Gomez-Lopez, A., and Mellado, E. (2015). An alternative host model of a mixed fungal infection by azole susceptible and resistant *Aspergillus* spp strains. *Virulence* 6, 376–384. doi: 10.1080/21505594.2015.1025192

Baena-Monroy, T., Moreno-Maldonado, V., Franco-Martinez, F., Aldape-Barrios, B., Quindos, G., and Sanchez-Vargas, L. O. (2005). *Candida albicans*, *Staphylococcus aureus* and *Streptococcus mutans* colonization in patients wearing dental prosthesis. *Med. Oral Patol. Oral Cir. Bucal.* 10(Suppl. 1), E27–E39.

Barbosa, M. S., Báo, S. N., Andreotti, P. F., Faria, F. P., Felipe, M. S. S., Feitosa, L. S., et al. (2006). Glyceraldehyde-3-phosphate dehydrogenase of *Paracoccidioides brasiliensis* is a cell surface protein involved in fungal adhesion to extracellular matrix proteins and interaction with cells. *Infect. Immun.* 74, 382–389. doi: 10.1128/IAI.74.1.382-389.2006.

Bartnicka, D., Karkowska-Kuleta, J., Zawrotniak, M., Satala, D., Michalik, K., Zielinska, G., et al. (2019). Adhesive protein-mediated cross-talk between *Candida albicans* and *Porphyromonas gingivalis* in dual species biofilm protects the anaerobic bacterium in unfavorable oxic environment. *Sci. Rep.* 9:4376.

Benaducci, T., Sardi Jde, C., Lourencetti, N. M., Scorzoni, L., Gullo, F. P., Rossi, S. A., et al. (2016). Virulence of *Cryptococcus* spp. biofilms in vitro and in vivo using *Galleria mellonella* as an alternative model. *Front. Microbiol.* 7:290. doi: 10.3389/fmicb.2016.00290

Bertolini, M., and Dongari-Bagtzoglou, A. (2019). The relationship of *Candida albicans* with the oral bacterial microbiome in health and disease. *Adv. Exp. Med. Biol.* 1197, 69–78. doi: 10.1007/978-3-030-28524-1_6

Brogden, K. A., Guthmiller, J. M., and Taylor, C. E. (2005). Human polymicrobial infections. *Lancet* 365, 253–255. doi: 10.1016/s0140-6736(05)70155-0

Carrero, L. L., Niño-Vega, J., Teixeira, M. M., Carvalho, M. J. A., Soares, C. M. A., Pereira, M., et al. (2008). New *Paracoccidioides brasiliensis* isolate reveals unexpected genomic variability in this human pathogen. *Fungal Genet. Biol.* 45, 605–612. doi: 10.1016/j.fgb.2008.02.002

Cattana, M. E., Tracogna, M. F., Marques, I., Rojas, F., Fernandez, M., De Los Angeles Sosa, M., et al. (2017). In Vivo *Paracoccidioides* spp. biofilm on vascular prosthesis. *Mycopathologia* 182, 747–749. doi: 10.1007/s11046-017-0126-8

Cavalheiro, M., and Teixeira, M. C. (2018). *Candida* biofilms: threats, challenges, and promising strategies. *Front. Med.* 5:28. doi: 10.3389/fmed.2018.00028

Chibebe Junior, J., Sabino, C. P., Tan, X., Junqueira, J. C., Wang, Y., Fuchs, B. B., et al. (2013). Selective photoinactivation of *Candida albicans* in the non-vertebrate host infection model *Galleria mellonella*. *BMC Microbiol.* 13:217. doi: 10.1186/1471-2180-13-217

Coutinho, Z. F., Silva, D., Lazera, M., Petri, V., Oliveira, R. M., Sabroza, P. C., et al. (2002). Paracoccidioidomycosis mortality in Brazil (1980-1995). *Cad. Saude. Publica* 18, 1441–1454. doi: 10.1590/s0102-311x2002000500037

de Arruda, J. A. A., Schuch, L. F., Abreu, L. G., Silva, L. V. O., Mosconi, C., Monteiro, J., et al. (2018). A multicentre study of oral paracoccidioidomycosis: Analysis of 320 cases and literature review. *Oral Dis.* 24, 1492–1502. doi: 10.1111/odi.12925

de Barros, P. P., Rossoni, R. D., Freire, F., de Camargo Ribeiro, F., Lopes, L. A. D. C., Junqueira, J. C., et al. (2018). *Candida tropicalis* affects the virulence profile of *Candida albicans*: an in vitro and in vivo study. *Pathog. Dis.* 76:10.

de Carli, M. L., Cardoso, B. C., Malaquias, L. C., Nonogaki, S., Pereira, A. A., Sperandio, F. F., et al. (2015). Serum antibody levels correlate with oral fungal cell numbers and influence the patients' response to chronic paracoccidioidomycosis. *Mycoses* 58, 356–361. doi: 10.1111/myc.12325

De Macedo, P. M., Teixeira, M. M., Barker, B. M., Zancopé-Oliveira, R. M., Almeida-Paes, R., and Francesconi do Valle, A. C. (2019). Clinical features and genetic background of the sympatric species *Paracoccidioides brasiliensis* and *Paracoccidioides americana*. *PLoS Negl. Trop. Dis.* 13:4. doi: 10.1371/journal.pntd.0007309

Diaz-Garcia, J., Marcos-Zambrano, L. J., Munoz, P., Guinea, J., and Escribano, P. (2019). Does the composition of polystyrene trays affect *Candida* spp. biofilm formation?. *Med. Mycol.* 57, 504–509. doi: 10.1093/mmy/myy064

do Carmo Silva, L., Tamayo Ossa, D. P., Castro, S. V., Bringel Pires, L., Alves De Oliveira, C. M., Conceição Da Silva, C., et al. (2015). Transcriptome profile of the response of *Paracoccidioides* spp. to a camphene thiosemicarbazide derivative. *PLoS One* 10:e0130703. doi: 10.1371/journal.pone.0130703

Dongari-Bagtzoglou, A., Kashleva, H., Dwivedi, P., Diaz, P., and Vasilakos, J. (2009). Characterization of mucosal *Candida albicans* biofilms. *PLoS One* 4:e7967. doi: 10.1371/journal.pone.0007967

Donofrio, F. C., Calil, A. C. A., Miranda, E. T., Almeida, A. M. F., Benard, G., Soares, C. P., et al. (2009). Enolase from *Paracoccidioides brasiliensis*: isolation and identification as a fibronectin-binding protein. *J. Med. Microbiol.* 58, 706–713. doi: 10.1099/jmm.0.003830-0

Douglas, L. J. (2003). *Candida* biofilms and their role in infection. *Trends Microbiol.* 11, 30–36. doi: 10.1016/s0966-842x(02)00002-1

Ells, T. C., and Truelstrup Hansen, L. (2006). Strain and growth temperature influence *Listeria* spp. attachment to intact and cut cabbage. *Int. J. Food Microbiol.* 111, 34–42. doi: 10.1016/j.ijfoodmicro.2006.04.033

Epstein, J. B., Gorsky, M., and Caldwell, J. (2002). Fluconazole mouthrinses for oral candidiasis in postirradiation, transplant, and other patients. *Oral Surg. Oral Med. Oral Pathol. Oral Radiol. Endod.* 93, 671–675. doi: 10.1067/moe.2002.122728

Falsetta, M. L., Klein, M. I., Colonne, P. M., Scott-Anne, K., Gregoire, S., Pai, C. H., et al. (2014). Symbiotic relationship between *Streptococcus mutans* and

Candida albicans synergizes virulence of plaque biofilms in vivo. *Infect. Immun.* 82, 1968–1981. doi: 10.1128/iai.00087-14

Fangtham, M., Magder, L. S., and Petri, M. A. (2014). Oral candidiasis in systemic lupus erythematosus. *Lupus* 23, 684–690. doi: 10.1177/0961203314525247

Fava Netto, C., Vegas, V. S., Sciannamea, I. M., and Guarnieri, D. B. (1969). Antígeno polissacarídico do *Paracoccidioides brasiliensis*. Estudo do tempo de cultivo do P. brasiliensis necessário ao preparo do antígeno. *Rev. Inst. Med. Trop. Sao Paulo* 11, 177–181.

Fotos, P. G., Vincent, S. D., and Hellstein, J. W. (1992). Oral candidosis. Clinical, historical, and therapeutic features of 100 cases. *Oral Surg. Oral Med. Oral Pathol.* 74, 41–49.

Franco, M., Montenegro, M. R., Mendes, R. P., Marques, S. A., Dillon, N. L., and Mota, N. G. (1987). *Paracoccidioidomycosis*: a recently proposed classification of its clinical forms. *Rev. Soc. Bras. Med. Trop.* 20, 129–132. doi: 10.1590/s0037-86821987000200012

Fuchs, B. B., and Mylonakis, E. (2006). Using non-mammalian hosts to study fungal virulence and host defense. *Curr. Opin. Microbiol.* 9, 346–351. doi: 10.1016/j.mib.2006.06.004

Gauthier, G. M. (2017). Fungal dimorphism and virulence: molecular mechanisms for temperature adaptation, immune evasion, and in vivo survival. *Mediat. Inflamm.* 2017:8491383.

Hawser, S. P., and Douglas, L. J. (1994). Biofilm formation by *Candida* species on the surface of catheter materials in vitro. *Infect. Immun.* 62, 915–921. doi: 10.1128/iai.62.3.915-921.1994

Jin, Y., Samaranayake, L. P., Samaranayake, Y., and Yip, H. K. (2004). Biofilm formation of *Candida albicans* is variably affected by saliva and dietary sugars. *Arch. Oral. Biol.* 49, 789–798. doi: 10.1016/j.archoralbio.2004.04.011

Kean, R., Rajendran, R., Haggarty, J., Townsend, E. M., Short, B., Burgess, K. E., et al. (2017). *Candida albicans* mycofilms support *Staphylococcus aureus* colonization and enhances miconazole resistance in dual-species interactions. *Front. Microbiol.* 8:258. doi: 10.3389/fmicb.2017.00258

Kernien, J. F., Snarr, B. D., Sheppard, D. C., and Nett, J. E. (2017). The interface between fungal biofilms and innate immunity. *Front. Immunol.* 8:1968. doi: 10.3389/fimmu.2017.01968

Martinez, L. R., and Casadevall, A. (2006). Susceptibility of *Cryptococcus neoformans* biofilms to antifungal agents in vitro. *Antimicrob. Agents Chemother.* 50, 1021–1033. doi: 10.1128/aac.50.3.1021-1033.2006

Martinez, L. R., and Casadevall, A. (2015). Biofilm formation by *Cryptococcus neoformans*. *Microbiol. Spectr.* 3:6.

Martinez, L. R., and Fries, B. C. (2010). Fungal biofilms: relevance in the setting of human disease. *Curr. Fungal Infect. Rep.* 4, 266–275. doi: 10.1007/s12281-010-0035-5

Martins, C. H., Pires, R., Cunha, A., Pereira, C., Lacorte Singulani, J., Abrão, F., et al. (2016). *Candida*/*Candida biofilms*. First description of dual-species *Candida albicans*/*C. rugosa* biofilm. *Fungal Biol.* 120, 530–537. doi: 10.1016/j.funbio.2016.01.013

Matute, D. R., Sepúlveda, V. E., Quesada, L. M., Goldman, G. H., Taylor, J. W., Restrepo, A., et al. (2006). Microsatellite analysis of three phylogenetic species of *Paracoccidioides brasiliensis*. *J. Clin. Microbiol.* 44, 2153–2157. doi: 10.1128/jcm.02540-05

Mendes, R. P., Cavalcante, R. S., Marques, S. A., Marques, M. E. A., Venturini, J., Sylvestre, T. F., et al. (2017). *Paracoccidioidomycosis*: current perspectives from Brazil. *Open Microbiol J* 11, 224–282. doi: 10.2174/1874285801711010224

Mendes-Giannini, M. J., Hanna, S. A., Da Silva, J. L., Andreotti, P. F., Vincenzi, L. R., Benard, G., et al. (2004). Invasion of epithelial mammalian cells by *Paracoccidioides brasiliensis* leads to cytoskeletal rearrangement and apoptosis of the host cell. *Microbes Infect.* 6, 882–891. doi: 10.1016/j.micinf.2004.05.005

Millsop, J. W., and Fazel, N. (2016). Oral candidiasis. *Clin. Dermatol.* 34, 487–494.

Morris, C. E., Monier, J., and Jacques, M. (1997). Methods for observing microbial biofilms directly on leaf surfaces and recovering them for isolation of culturable microorganisms. *Appl. Environ. Microbiol.* 63, 1570–1576. doi: 10.1128/aem.63.4.1570-1576.1997

Negrini, T. C., Koo, H., and Arthur, R. A. (2019). *Candida*-bacterial biofilms and host-microbe interactions in oral diseases. *Adv. Exp. Med. Biol.* 1197, 119–141. doi: 10.1007/978-3-030-28524-1_10

Nicolatou-Galitis, O., Dardoufas, K., Markoulatos, P., Sotiropoulou-Lontou, A., Kyprianou, K., Kolitsi, G., et al. (2001). Oral pseudomembranous candidiasis, herpes simplex virus-1 infection, and oral mucositis in head and neck cancer patients receiving radiotherapy and granulocyte-macrophage colony-stimulating factor (GM-CSF) mouthwash. *J. Oral Pathol. Med.* 30, 471–480. doi: 10.1034/j.1600-0714.2001.030008471.x

Pathirana, R. U., McCall, A., Norris, R., and Edgerton, M. (2019). Filamentous non-albicans *Candida* species adhere to *Candida albicans* and benefit from dual biofilm growth. *Front. Microbiol.* 10:1188. doi: 10.3389/fmicb.2019.01188

Peeters, E., Nelis, H. J., and Coenye, T. (2008). Comparison of multiple methods for quantification of microbial biofilms grown in microtiter plates. *J. Microbiol. Methods* 72, 157–165. doi: 10.1016/j.mimet.2007.11.010

Pemmaraju, S. C., Pruthi, P. A., Prasad, R., and Pruthi, V. (2013). *Candida albicans* biofilm inhibition by synergistic action of terpenes and fluconazole. *Indian J. Exp. Biol.* 51, 1032–1037.

Peters, B. M., Jabra-Rizk, M. A., O'May, G. A., Costerton, W., and Shirtliff, M. (2012). Polymicrobial interactions: impact on pathogenesis and human disease. *Clin. Microbiol. Rev.* 25, 193–213. doi: 10.1128/cmr.00013-11

Pierce, C. G., Uppuluri, P., Tummala, S., and Lopez-Ribot, J. L. (2010). A 96 well microtiter plate-based method for monitoring formation and antifungal susceptibility testing of *Candida albicans* biofilms. *J. Vis. Exp.* 21:2287.

Pitangui, N. S., Sardi, J. C., Silva, J. F., Benaducci, T., Moraes Da Silva, R. A., Rodríguez-Arellanes, G., et al. (2012). Adhesion of Histoplasma capsulatum to pneumocytes and biofilm formation on an abiotic surface. *Biofouling* 28, 711–718. doi: 10.1080/08927014.2012.703659

Ramage, G., Tomsett, K., Wickes, B. L., Lopez-Ribot, J. L., and Redding, S. W. (2004). Denture stomatitis: a role for *Candida biofilms*. *Oral Surg. Oral Med. Oral Pathol. Oral Radiol. Endod.* 98, 53–59. doi: 10.1016/j.tripleo.2003.04.002

Reece, E., Doyle, S., Greally, P., Renwick, J., and Mcclean, S. (2018). *Aspergillus fumigatus* inhibits *Pseudomonas aeruginosa* in co-culture: implications of a mutually antagonistic relationship on virulence and inflammation in the CF airway. *Front. Microbiol.* 9:1205. doi: 10.3389/fmicb.2018.01205

Rodrigues, M. E., Gomes, F., and Rodrigues, C. F. (2019). *Candida* spp./bacteria mixed biofilms. *J. Fungi* 6:5. doi: 10.3390/jof6010005

Rossoni, R. D., Fuchs, B. B., De Barros, P. P., Velloso, M. D., Jorge, A. O., Junqueira, J. C., et al. (2017). *Lactobacillus paracasei* modulates the immune system of *Galleria mellonella* and protects against *Candida albicans* infection. *PLoS One* 12:e0173332. doi: 10.1371/journal.pone.0173332

San-Blas, G., and Vernet, D. (1977). Induction of the synthesis of cell wall alpha-1,3-glucan in the yeastlike form of *Paracoccidioides brasiliensis* strain IVIC Pb9 by fetal calf serum. *Infect. Immun.* 15, 897–902. doi: 10.1128/iai.15.3.897-902.1977

Sardi Jde, C., Pitangui Nde, S., Voltan, A. R., Braz, J. D., Machado, M. P., Fusco Almeida, A. M., et al. (2015). In vitro *Paracoccidioides brasiliensis* biofilm and gene expression of adhesins and hydrolytic enzymes. *Virulence* 6, 642–651. doi: 10.1080/21505594.2015.1031437

Scorzoni, L., De Paula, E., Silva, A. C., Singulani Jde, L., Leite, F. S., De Oliveira, H. C., et al. (2015). Comparison of virulence between *Paracoccidioides brasiliensis* and *Paracoccidioides lutzii* using *Galleria mellonella* as a host model. *Virulence* 6, 766–776.

Sheehan, G., Tully, L., and Kavanagh, K. A. (2020). *Candida albicans* increases the pathogenicity of Staphylococcus aureus during polymicrobial infection of *Galleria mellonella* larvae. *Microbiology* 166, 375–385. doi: 10.1099/mic.0.000892

Silva, S., Henriques, M., Oliveira, R., Williams, D., and Azeredo, J. (2010). In vitro biofilm activity of non-*Candida albicans Candida* species. *Curr. Microbiol.* 61, 534–540. doi: 10.1007/s00284-010-9649-7

Simoes, L. C., Simoes, M., and Vieira, M. J. (2010). Adhesion and biofilm formation on polystyrene by drinking water-isolated bacteria. *Antonie Van Leeuwenhoek* 98, 317–329. doi: 10.1007/s10482-010-9444-2

Singulani, J. L., Scorzoni, L., De Oliveira, H. C., Marcos, C. M., Assato, P. A., Fusco-Almeida, A. M., et al. (2018). Applications of invertebrate animal models to dimorphic fungal infections. *J. Fungi* 4:118. doi: 10.3390/jof4040118

Sztajer, H., Szafranski, S. P., Tomasch, J., Reck, M., Nimtz, M., Rohde, M., et al. (2014). Cross-feeding and interkingdom communication in dual-species biofilms of *Streptococcus mutans* and *Candida albicans*. *ISME J.* 8, 2256–2271. doi: 10.1038/ismej.2014.73

Thein, Z. M., Seneviratne, C. J., Samaranayake, Y. H., and Samaranayake, L. P. (2009). Community lifestyle of *Candida* in mixed biofilms: a mini review. *Mycoses* 52, 467–475. doi: 10.1111/j.1439-0507.2009.01719.x

Thomaz, D. Y., Melhem, M. S. C., De Almeida Junior, J. N., Benard, G., and Del Negro, G. M. B. (2020). Lack of efficacy of echinocandins against high metabolic activity biofilms of *Candida parapsilosis* clinical isolates. *Braz. J. Microbiol.* 51, 1129–1133. doi: 10.1007/s42770-019-00219-7

Tulasidas, S., Rao, P., Bhat, S., and Manipura, R. (2018). A study on biofilm production and antifungal drug resistance among *Candida* species from vulvovaginal and bloodstream infections. *Infect. Drug Resist.* 11, 2443–2448. doi: 10.2147/idr.s179462

Turissini, D. A., Gomez, O. M., Teixeira, M. M., Mcewen, J. G., and Matute, D. R. (2017). Species boundaries in the human pathogen *Paracoccidioides*. *Fungal Genet. Biol.* 106, 9–25. doi: 10.1016/j.fgb.2017.05.007

Verstrepen, K. J., and Klis, F. M. (2006). Flocculation, adhesion and biofilm formation in yeasts. *Mol. Microbiol.* 60, 5–15. doi: 10.1111/j.1365-2958.2006.05072.x

Vicentini, A. P., Gesztesi, J. L., Franco, M. F., De Souza, W., De Moraes, J. Z., Travassos, L. R., et al. (1994). Binding of *Paracoccidioides brasiliensis* to laminin through surface glycoprotein gp43 leads to enhancement of fungal pathogenesis. *Infect. Immun.* 62, 1465–1469. doi: 10.1128/iai.62.4.1465-1469.1994

Conflict of Interest: The authors declare that the research was conducted in the absence of any commercial or financial relationships that could be construed as a potential conflict of interest.

frontiers in Microbiology

REVIEW
published: 11 November 2020
doi: 10.3389/fmicb.2020.544480

Pathogenesis and Clinical Relevance of *Candida* Biofilms in Vulvovaginal Candidiasis

Carmen Rodríguez-Cerdeira[1,2,3,4], Erick Martínez-Herrera[4,5], Miguel Carnero-Gregorio[1,6], Adriana López-Barcenas[3,4,7], Gabriella Fabbrocini[3,8], Monika Fida[3,9], May El-Samahy[3,10] and José Luís González-Cespón[1]*

[1] *Efficiency, Quality, and Costs in Health Services Research Group (EFISALUD), Health Research Institute, SERGAS-UVIGO, Vigo, Spain,* [2] *Department of Dermatology, Hospital do Meixoeiro and University of Vigo, Vigo, Spain,* [3] *European Women's Dermatologic and Venereologic Society, Tui, Spain,* [4] *Psychodermatology Task Force of the Ibero-Latin American College of Dermatology (CILAD), Buenos Aires, Argentina,* [5] *Unidad de Investigación, Hospital Regional de Alta Especialidad de Ixtapaluca, Ixtapaluca, Mexico,* [6] *Department of Molecular Diagnosis (Array & NGS Division), Institute of Cellular and Molecular Studies, Lugo, Spain,* [7] *Section of Mycology, Department of Dermatology, Manuel Gea González hospital, Mexico City, Mexico,* [8] *Department of Dermatology, University of Naples Federico II, Naples, Italy,* [9] *Department of Dermatology, University of Medicine, Tirana, Tirana, Albania,* [10] *Department of Dermatology, Faculty of Medicine, Ain Shams University, Cairo, Egypt*

OPEN ACCESS

Edited by:
Juliana Campos Junqueira, São Paulo State University, Brazil

Reviewed by:
Rohitashw Kumar, University at Buffalo, United States
Noelly Queiroz Ribeiro, Federal University of Minas Gerais, Brazil

***Correspondence:**
Carmen Rodríguez-Cerdeira
crodcer@uvigo.es;
carmen.rodriguez.cerdeira@sergas.es;
carmencerdeira33@gmail.com

Specialty section:
This article was submitted to Fungi and Their Interactions, a section of the journal Frontiers in Microbiology

Received: *20 March 2020*
Accepted: *23 October 2020*
Published: *11 November 2020*

Citation:
Rodríguez-Cerdeira C, Martínez-Herrera E, Carnero-Gregorio M, López-Barcenas A, Fabbrocini G, Fida M, El-Samahy M and González-Cespón JL (2020) Pathogenesis and Clinical Relevance of Candida Biofilms in Vulvovaginal Candidiasis. Front. Microbiol. 11:544480. doi: 10.3389/fmicb.2020.544480

The ability of *Candida* spp. to form biofilms is crucial for its pathogenicity, and thus, it should be considered an important virulence factor in vulvovaginal candidiasis (VVC) and recurrent VVC (RVVC). Its ability to generate biofilms is multifactorial and is generally believed to depend on the site of infection, species and strain involved, and the microenvironment in which the infection develops. Therefore, both cell surface proteins, such as Hwp1, Als1, and Als2, and the cell wall-related protein, Sun41, play a critical role in the adhesion and virulence of the biofilm. Immunological and pharmacological approaches have identified the NLRP3 inflammasome as a crucial molecular factor contributing to host immunopathology. In this context, we have earlier shown that *Candida albicans* associated with hyphae-secreted aspartyl proteinases (specifically SAP4-6) contribute to the immunopathology of the disease. Transcriptome profiling has revealed that non-coding transcripts regulate protein synthesis post-transcriptionally, which is important for the growth of *Candida* spp. Other studies have employed RNA sequencing to identify differences in the 1,245 *Candida* genes involved in surface and invasive cellular metabolism regulation. *In vitro* systems allow the simultaneous processing of a large number of samples, making them an ideal screening technique for estimating various physicochemical parameters, testing the activity of antimicrobial agents, and analyzing genes involved in biofilm formation and regulation (*in situ*) in specific strains. Murine VVC models are used to study *C. albicans* infection, especially in trials of novel treatments and to understand the cause(s) for resistance to conventional therapeutics. This review on the clinical relevance of *Candida* biofilms in

VVC focuses on important advances in its genomics, transcriptomics, and proteomics. Moreover, recent experiments on the influence of biofilm formation on VVC or RVVC pathogenesis in laboratory animals have been discussed. A clear elucidation of one of the pathogenesis mechanisms employed by *Candida* biofilms in vulvovaginal candidiasis and its applications in clinical practice represents the most significant contribution of this manuscript.

Keywords: vulvovaginal candidiasis, *Candida* spp., biofilm models, proteomic, genomic, new anti-*Candida* targets

INTRODUCTION

Vulvovaginal candidiasis (VVC) is a usual fungal infection caused by *Candida* species, mainly *Candida albicans*. It is characterized by inflammatory signs and symptoms detected in the vulva and vaginal mucosa that are caused and linked by an overgrowth of *Candida* species, which are generally present as quiescent vaginal commensals (Sobel, 2007).

The genus *Candida* belongs to the *Saccharomycetaceae* family. The organisms reproduce asexually or anamorphically through blastoconidia, do not produce melanin pigments, have diverse morphologies (globose, oval, cylindrical, and elliptical), and are sized between 3 and 10 μm. In humans, different species of this genus are identified as commensals of the gastrointestinal tract, upper respiratory tract, skin, oral, vulvar, and vaginal mucosa (Neppelenbroek et al., 2014).

Comparative *Candida* species genomics will enhance our understanding of the genetic and phenotypic variations that occur inside the vulva and vagina and will further facilitate better understanding of the pathogenesis of these commensals in VVC (Bradford et al., 2017).

Despite the fact that *C. albicans* is the most common VVC-causing pathogen, the identification of non-*C. albicans Candida* (NCAC) species, mainly *C. glabrata*, as the originator of this infection appears to be continuously increasing. It is difficult to determine its prevalence because the diagnosis and treatment are often based on the symptoms and not dependent on the confirmation by microscopic examination or using culture techniques (Mahmoudi Rad et al., 2011).

Other NCAC species that must be taken into account are *C. tropicalis*, *C. parapsilosis*, *C. kefyr*, *C. krusei*, *C. guilliermondii*, *C. famata*, and *C. lusitaniae*. The production of virulence factors by these strains depends on the site and degree of invasion, as well as the nature of host response. Early identification of the involved strain is, therefore, essential for rapid diagnosis (Bitew and Abebaw, 2018). The techniques used most frequently for their identification are shown in **Figure 1**.

Yeasts that are present in the vagina become pathogenic when the host vagina allows it (Miró et al., 2017). Host-related factors involve pregnancy (Brown et al., 2019), hormonal imbalance, ill-treated diabetes, immunosuppression (either through immunosuppressive drugs or infection with the human immunodeficiency virus), which can act as a predisposing factor (Yano et al., 2019), use of broad-spectrum antibiotics (Shukla and Sobel, 2019) and glucocorticoids, and genetic predispositions (Gonçalves et al., 2016).

Other less recognized or more debatable factors are oral contraceptive administration (especially when the estrogen dose is high), estrogen therapy, use of intrauterine devices, spermicides, and condoms, and certain hygiene, clothing, and sexual practice-related routines (Corsello et al., 2003; Maraki et al., 2019). In general, the most common clinical characteristic related to vaginal inflammation is itching, which is followed by burning.

Recurrent vulvovaginal candidiasis (RVVC) is featured by four or more episodes of symptomatic infection in the same year, and clearly affects the quality of life in women (Blostein et al., 2017). Djohan et al. (2019) have reported a prevalence of RVVC in 23.5% (CI95: 19.49–28.02%) of women of reproductive age and identified five *Candida* species in a group of 94 patients with RVVC: *C. albicans* (59.6%), *C. glabrata* (19.1%), *C. tropicalis* (16%), *C. krusei* (4.2%), and *C. inconspicua* (1.1%). However, other authors have provided lower figures, but there is a consensus that the frequency of RVVC is increasing (Gonçalves et al., 2016; Denning et al., 2018).

Among other species, *C. kefyr* is frequently found to be present in the polyfungal population (Ozcan et al., 2010; Guzel et al., 2011).

However, a new pathogen, *C. auris*, has emerged recently (Kumar et al., 2015). Another emerging pathogen that has been identified is *C. nivariensis*, which is genetically related to *C. glabrata*. *C. nivariensis* was reported for the first time in Canary Islands, Spain, and at present, it seems to widely distributed worldwide. Inhibition of quorum sensing molecules with natamycin against *C. tropicalis* haven been used successfully by researchers (Agustín et al., 2019). However, the number of cases is low possibly due to the impossible phenotypic identification of *C. glabrata* (Aznar-Marin et al., 2016).

New compounds have been developed, with more candidates in the pipeline, for the treatment of biofilms associated with *Candida* spp. infections. Some of these are naturally occurring, while others have been developed by synthetic routes optimized in the laboratory. New antifungals such as acridone (de Oliveira et al., 2019) or nanotechnology-based techniques, such as the encapsulation of citric acid into Mg-Al-layered double hydroxides, have shown optimistic trends.

Prebiotics, probiotics, and symbiotics also offer promising results, as these are related to the stimulation of host immunity

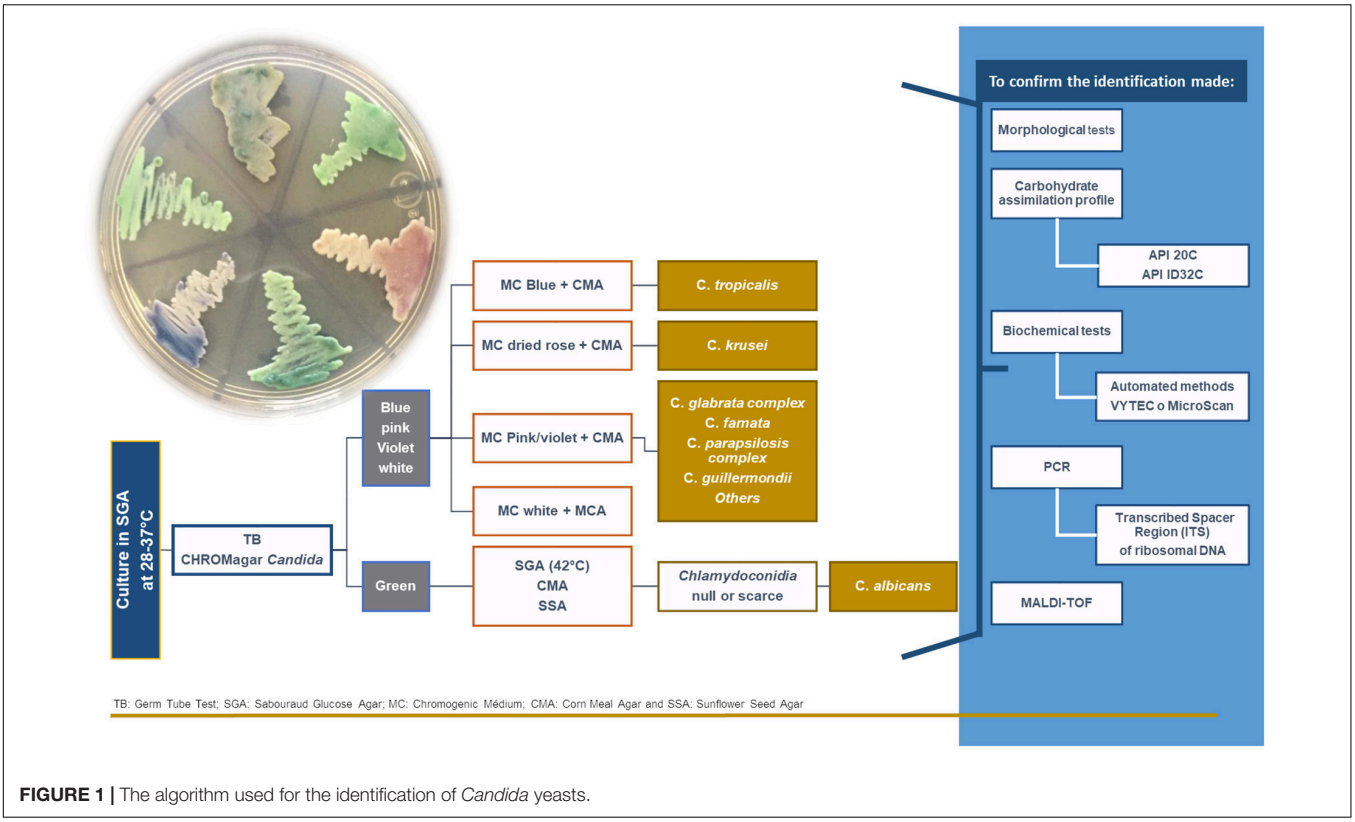

FIGURE 1 | The algorithm used for the identification of *Candida* yeasts.

and their presence is known to decrease the prevalence of *Candida* spp. (Davani-Davari et al., 2019).

Plant extracts and essential oils derived from the leaves of plants of Brazilian origin described by Costa et al. (2017), such as *Hymenaea courbaril* var. *courbaril*, *Myroxylon peruiferum*, and *Vismia guianensis*, have shown therapeutic potential in this regard. The derivatives of flavonoids, such as methylated isoflavones (i.e., formononetin 7-*O*-apiosyl glucoside) (Martins et al., 2016), or the polyphenol, licochalcone-A, found in the roots of *Glycyrrhiza* spp. (Seleem et al., 2016) or honey (Fernandes et al., 2020), have also been demonstrated to be useful.

Photodynamic therapy (Ghasemi et al., 2019), quorum sensing molecules and antibodies/peptides (Carrano et al., 2019) have emerged as viable treatment modalities in recent years. More sophisticated techniques, such as lock therapy (Visek et al., 2019), represent an important potential breakthrough in the treatment of biofilms produced due to infection by *Candida* spp.

In this review, we aimed to discuss the main characteristics of the female vulvovaginal mucosa, and the mechanisms employed by *Candida* spp. to colonize the host. Furthermore, the different kinds of biofilms formed by *Candida* spp., their impact on clinical practices, and the development of new agents against them will also be reviewed in depth.

MATERIALS AND METHODS

The databases MEDLINE (PubMed), and Embase were searched extensively for articles published from January 2003 to January 2020, using the following search terms: vulvovaginal candidiasis, *Candida* spp., *C. albicans, C. glabrata, C. parapsilosis, C. tropicalis, C. kefyr, C. auris*, *C. nivariensis*, biofilm, and antifungal agents. PRISMA Flow Diagram (**Figure 2**) depicted the flow of reports through the different stages of this systematic review. It mapped the number of records that were identified, included or excluded, and the reasons for exclusions.

CHARACTERISTICS OF THE VULVOVAGINAL MUCOSA AND MECHANISMS THAT *Candida* spp. DEPLOYS COLONIZE IT

Vaginal Ecosystem

The vaginal microbiota, which mainly constitutes of *Lactobacillus* spp., forms the most important defensive barrier against candidal infections (Smith and Ravel, 2017). The vaginal ecosystem balance is maintained at the expense of articulated interactions of different mechanisms, which keeps the female genital tract (FGT) healthy. Both epithelial cells of the vaginal mucosa and FGT immune system are under the control of the female sex hormones, estradiol, and progesterone. On the vaginal epithelium, estrogens regulate trophism, vascularity, and tissue vitality; in addition, it influences conditions such as humidity, pH, and vaginal discharge as well as vaginal microbiota composition (Achilles et al., 2018).

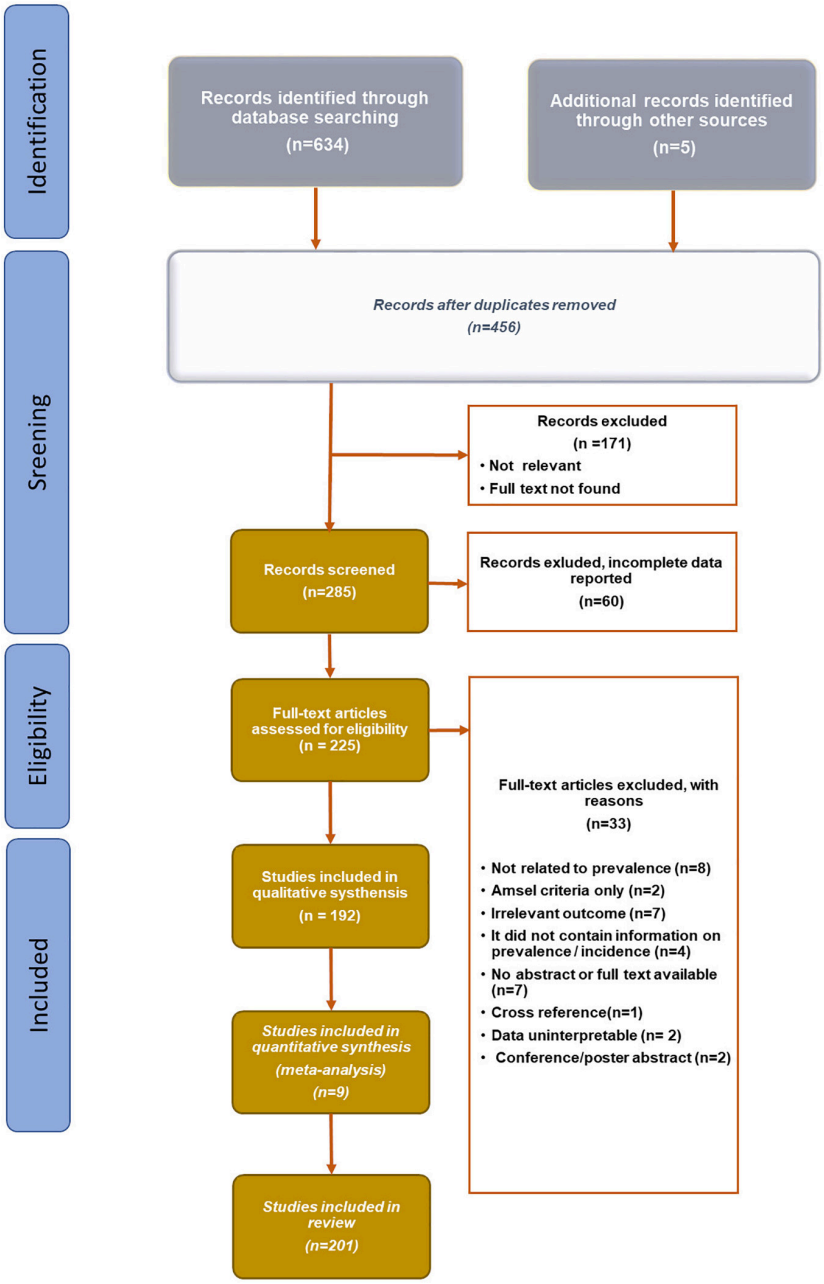

FIGURE 2 | PRISMA Flow diagram (Moher et al., 2015).

Candida spp. is considered as opportunistic pathogens. Although initially it was thought that yeast participates passively in the pathogenesis process and fungal infection establishment, but recently this concept has been modified, proposing an active participation of these microorganisms via the action of virulence factors (El-Houssaini et al., 2019).

Factors contributing to *C. albicans* pathogenesis include morphogenesis (transition between single-celled yeast cells to filamentous growth forms), secretion of enzymes like aspartyl proteases (SAP) and phospholipases, and host recognition biomolecules (adhesins), which lead to the biofilm formation process. Likewise, the phenotypic change is accompanied by alterations in antigen expression, colonial morphology, and affinity of *C. albicans* to tissues (El-Houssaini et al., 2019; Monika, 2019).

The experimental information on the contribution of these virulence factors has revealed that their individual participation is not sufficient to explain the mechanisms of damage in the

host; moreover, there is a combined regulation mechanism operating between them. This was further demonstrated with polymorphism and gene expression analyses of SAPs. The studies currently being carried out on the genetic expression of virulence factors, which depends on different environmental conditions, will allow us to better understand how the biological activity of *Candida* spp. modifies to favor adhesion or penetration processes and, consequently, modifies its role to become a pathogenic microorganism (Silva et al., 2012; Kalaiarasan et al., 2018; Willems et al., 2018).

Araújo Paulo, de Medeiros et al. (2017) reported that the virulence characteristics of *C. albicans* contributing to its pathogenicity include the skill to adhere to human epithelial and endothelial cells, yeast to hyphae transition, extracellular hydrolytic enzyme (proteinases and phospholipases) secretion, phenotypic adaptability, and biofilm formation. Further, there is a relationship between virulence factor expression and VVC signs and symptoms identified in the patients, but it does not seem to be essential for the transition from colonization to infection.

Adherence

Adhesion is initiated by non-specific binding, which is based on attractive and repulsive forces that bring the pathogen close to the host surface. Adhesins are biomolecules that promote the binding of specific ligands to host cells. The investigations by Zhao et al. (2003) stake the adhesion about the family of adhesins called ALS (Agglutinin-Like Sequence), which belongs to a group of eight genetically related glycosylated proteins with great allelic variability (ALS1–ALS7 and ALS9). ALS1 and ALS3 are particularly found to be important in the adhesion process. Other molecules that also promote the adhesion and penetration of *C. albicans* into the tissues are the polysaccharides, proteins, and lipids present on cell surface. Data supplied by the *C. albicans* genome sequencing project provided the main indication that the strain SC5314 encodes two different ALS9-like sequences and three ALS genes (ALS5, ALS1, and ALS9) next to chromosome 6 (Araújo et al., 2017).

Wilkins et al. (2018) showed that the eukaryotic proteome contains certain components that are encoded by open reading frame (ORF)s possessing protein-coding tandem repeat (TRs) (TR-ORFs, pcTRs), but their biological consequences are not clearly known. Ichikawa et al. (2019) analyzed the adherence and cytotoxicity of *C. glabrata* that selectively adhered to the epithelial cells. On the contrary, *C. parapsilosis* showed poor adherence to the HaCaT keratinocytes. *C. glabrata* caused more damage to the A549 cells than to the HaCaT cells, suggesting that *Candida* spp. exhibits different effects depending on the tissue on which they can adhere.

Modrzewska and Kurnatowski (2015) demonstrated that the adherence of *Candida* spp. on the tissue or cell wall of a host is based on the relationship that might exist between the two. A variety of genes that are responsible for the adhesion capacity of fungal cell wall, like HWP1, which encodes protein 1 of the hyphal wall and germ tubes and is responsible for biofilm formation. It is also responsible for the fungal virulence capacity and therefore, provides resistance to antifungal agents. This gene is identified in both oral cavity and vaginal yeast infections (Fan et al., 2013).

Ardehali et al. (2019) identified that the frequency of HWP1 gene among *C. albicans* was 95%, with HWP1 being the most detected virulence factor, and SAP4 being the least detected one in the clinical specimens collected from patients hospitalized in the Intensive Care Unit (ICU) of Milad hospital, Tehran, Iran.

According to Cota and Hoyer (2015), the ALS genes encode fungal glycoproteins on the cell surface. A total of eight ALS genes have been reported so far (ASL1–7 and ALS9). According to Liu and Filler (2011), the ALS3 gene exhibits a dual function of adhesin and invasion. ALS3 is used for the preparation of vaccines because of its level of *in vivo* dispersion. According to Zajac et al. (2016), other genes that have been involved in cell adhesion are EPA (epithelial adhesin) genes that are specifically identified in *C. glabrata*, as in this *Candida* sp., ALS genes have not been identified to date.

According to Modrzewska and Kurnatowski (2015), the most important adhesins present on the fungal cell wall in *Candida* spp. are: ALS, EPA, HWP1, but also EAP1, SUN41, CSH1 and probably HYR1; for significant adhesion, they also possess Sap (secreted aspartyl proteases). Various other genes reported to positively affect adhesion and hyphal formation are CZF1, EFG1, TUP1, TPK1, TPK2, HGC1, RAS1, RIM101, VPS11, ECM1, CKA2, BCR1, BUD2, RSR1, IRS4, CHS2, SCS7, UBI4, UME6, TEC1, and GAT2.

Morphogenesis

Morphogenesis refers to the conversion of a particular yeast form (unicellular) to the filamentous form of the fungus (hypha or pseudohypha), making it possible to adapt to different biological niches, which favors the fungal spread.

According to Min et al. (2019), *N*-acetylglucosamine (GlcNAc) potently induces the transition of *C. albicans* from budding to filamentous hypha growth. It also stimulates an epigenetic change that converts the white cells to opaque cells, which vary in morphology, metabolism, and virulence properties.

According to Min et al. (2018), the presence of TF (transcription factor) Ndt80 is necessary for the growth of hyphae in *C. albicans* and its presence is significant since it is conserved in most of the fungal species; however, it must be taken into account that its quantity is variable among the different fungal species. It regulates a variety of processes, such as sexual development, resistance to antifungals, fibrillation, virulence, and nutritional stress response, among others.

The human fungal pathogen *C. albicans* contains three virulence genes, namely NDT80, REP1, and RON1. RON1 deletion leads to growth defects when grown in GlcNAc media and hypha induction. To avoid this, a new short cross-linked palindromic/CRISPR repeat associated with Cas9 has been used for gene deletions (Min et al., 2019).

Phenotypic Switch

Tang et al. (2019) demonstrated that the majority of *C. albicans* strains are capable of undergoing the phenomenon of phenotypic switch, which is associated with the manifestation of phenotypic changes at high frequency and a consequence of the action

of numerous environmental factors. This phenomenon induces an epigenetic change in colonial morphology. Hu et al. (2016) collected and subsequently employed 231 clinical isolates for genotyping as well as phenotypic switch analysis. A total of 65 different genotypes were recognized by microsatellite locus (CAI) genotyping assay, and some prominent genotypes were identified from certain human niches. The authors established that there is an association between the phenotypic switching and genotypes of the CAI microsatellite locus in these *C. albicans* clinical isolates.

During this process, enzymes able to break down the structural polymers that provide accessible nutrients for fungal growth, capability to evade the immune system, and suppress the host pro-inflammatory response are released. They are also responsible for inactivating certain molecules that are directly linked to the host defense mechanisms (Hu et al., 2016). The main extracellular enzymes (Basmaciyan et al., 2019) that are related to the pathogenesis of *Candida* spp. are described below:

Secreted aspartic proteinases (Sap) (Kadry et al., 2018) are regarded as one of the most critical virulence factors as they are related to adhesion, invasion, tissue damage, and evasion of the host immune system, due to its ability to hydrolyze various host proteins, including albumin, keratin, collagen, fibronectin, interleukin 1β (IL-1β), and Immunoglobulin A.

Phospholipases

Studies by Richmond and Smith (2011) and Dabiri et al. (2018) demonstrated the existence of glycoproteins with hydrolase activity (glyphospholipid esters are hydrolyzed) and lysophospholipase transacylase (release fatty acids from lysophospholipids and transfer free fatty acid to another phospholipid), which play key roles in the infection process.

BIOFILMS

For a long time, investigations in the area of microbial biofilms have received increasing momentum and scientific evidence has led to a change in the way we consider microbial life (de Barros et al., 2020). Biofilms are defined as heterogeneous and dynamic microbial communities undergoing continuous transformation. They can be comprised by a single bacterial/fungal species, or can be polymicrobial. Since there are differences between biofilms formed on mucosal and abiotic cells, it is precise to have *in vitro* and *in vivo* models that can mimic these processes (Tournu and Van Dijck, 2012).

In this context, new tools to analyze *Candida* biofilms have been implemented, including genomic, transcriptomic, proteomic, and metabolomics approaches, using a wide variety of animal models.

According to Cavalheiro and Teixeira (2018), biofilm formation is a complicated process, which starts with adhesion on an abiotic surface, a tissue, or the air–liquid interface. It is a continuous process, which undergoes different stages of development: (a) conditioning, (b) adhesion, (c) quorum sensing-induced extracellular matrix synthesis, (d) maturation, and (e) dispersion.

These phases lead to the formation of a uniform structure in the form of homogeneous deposits and cellular viscous accumulations surrounded by a matrix of polymers with open channels for water movement (Chandra and Mukherjee, 2015).

Cells in the biofilms have different properties than those of isolated cells, which is because they have low growth rates and great resistance to antimicrobial treatment, and it makes their behavior different from those of planktonic cells (Muzny and Schwebke, 2015). Biofilms are biological systems that interact and evolve together. Hence, they need a wide network of genetic regulation to carry out both intra- and inter-cellular communication and specialization and originate biofilms made up of the same species or multi-species (Rodríguez-Cerdeira et al., 2019). *C. albicans* biofilm formation is a complex process that begins when the yeast cells adhere to host tissue surface, and the biofilm starts to form at an early stage (8–11 h), undergoes an intermediate stage (12–30 h), and finally reaches the mature stage (38–72 h) (Mathé and Van Dijck, 2013).

The mature biofilm comprises a dense network of yeasts, hyphae, and pseudohyphae, which is covered by an extracellular matrix and frequently associated with bacteria, as also described by Silva et al. (2012, 2014). Each *Candida* species (*C. albicans*, *C. glabrata*, *C. parapsilosis*, *C. tropicalis*, *C. nivariensis*, *C. kefyr*, and *C. auris*) shows significant peculiarities in terms of biofilm formation, which results in different morphologies, extracellular matrix composition, and resilience to antifungal agents (Cavalheiro and Teixeira, 2018) (**Figure 3**).

The importance of certain virulence factors was found to be closely related to Sap, which is related to biofilm production as described by Kadry et al. (2018). Isolates that were found to be resistant to three different anti-fungal drugs were reported as strong biofilm producers and shown to possess proteolytic activity as they contained either Sap9 or Sap10, or both (Ćernáková et al., 2019).

El-Houssaini et al. (2019) identified the virulence factors related to hydrolases, which are involved in cell surface hydrophobicity and biofilm production in vaginal samples. *C. albicans* resistance and virulence patterns observed in the samples were variable. The samples were highly resistant to physical and chemical treatments, making it difficult to treat them (Marak and Dhanashree, 2018).

Genomics of the Biofilm

Numerous genes involved in biofilm formation have been identified in the *C. albicans* genome, including 50 transcriptional regulatory genes, and 101 transcriptional non-regulatory genes (Shukla and Sobel, 2019). Nobile et al. (2012) described the six main transcriptional regulatory genes known as "master" transcriptional regulators, including Efg1 (enhanced filamentous growth), Tec1 (transposon enhancement control), Bcr1 (biofilm and cell wall regulator), Ntd80 (meiosis-specific transcription factor), Brg1 (biofilm regulator), and Rob1 (biofilm regulator). Each of these genes are mandatory for normal biofilm development and have been identified both *in vitro*, under standard laboratory conditions and *in vivo*, in laboratory animals (rats).

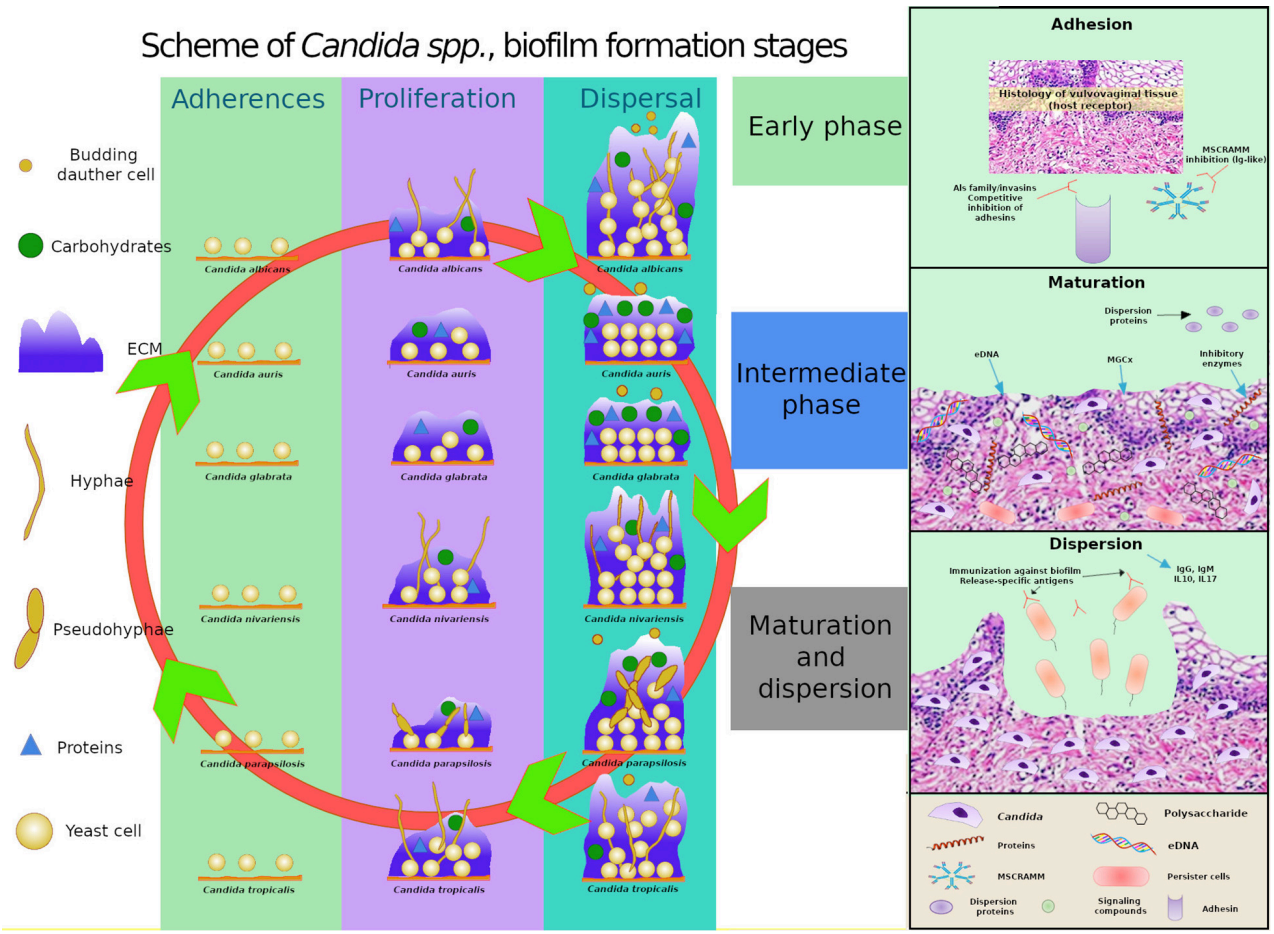

FIGURE 3 | Comparative schematics of three stages of biofilm formation in *C. albicans, C. glabrata, C. tropicalis, and C. parapsilosis, C. auris and C. nivariensis* highlighting the different capacities of the species in producing extracellular matrix (ECM), the varying components present in the ECM, and the ability of the species to exhibit different cell morphologies, and highlights of the transcriptional factors involved in adhesion, extracellular polymeric substances, filamentation, and biofilm formation. MSCRAMM, microbial surface components recognizing adhesive matrix molecules; MGCx, extracellular matrix mannan-glucan complex; eDNA, external DNA.

Apart from these 6 genes, 44 other transcriptional regulatory genes have also been identified, and the deletion of these genes has been associated with erroneous biofilm formation (Ni et al., 2009). Chatterjee et al. (2015) identified eight OPT genes encoding the oligopeptide transporters that help *C. auris* to adapt to different host tissues. They also found orthologs for these genes that were believed to carry hexose, maltose, and permeases (amino acid permeases, sulfur permeases, allantoic permeases, glycerol permeases, and iron permeases), which also help the fungi to adapt and live in their host. Other transcriptional regulators have also been recently found to be involved in adherence (Finkel et al., 2012).

The first step in biofilm formation process is surface adhesion, in which the *Candida* cell wall interacts with the host cell surfaces. This process involves a series of genes that encode several proteins, such as ALS adhesins, of which ALS1, ALS3, and ALS5 are implicated in the adhesion process; Eap1, regulated by the factor EFG1; HWP1, which promotes the fixation of *Candida* cells to the host surface and is a potential pathogenicity factor (it is absent in *C. glabrata*); PGA10 and PBR1—it has been shown that when the PBR1 gene is deleted, the adhesion of *C. albicans* to blood cells decreases; EPA family of genes, of which EPA1, EPA6, and EPA7 are the main epithelial adhesins, and their deletion hinders or decreases adhesion to surfaces; AWP adhesins, whose expression is higher in biofilms than in plant cells (Orsi et al., 2014; Valotteau et al., 2019).

Inglis and Sherlock (2013) showed that the expression of these wall proteins is regulated by two main genes: BCR1 and TEC1. TEC1 regulates BCR1 via cell signaling cascades and is involved in yeast differentiation into hypha. EPAs (epithelial adhesin) are specific for *C. glabrata* and the genes encoding ALS proteins have not been observed in mucosa yet.

CKA2, BCR1, BUD2, RSR1, and HWP1 are the genes that modify adhesion and tissue damage, but not invasion, in the host. Other genes that positively affect adhesion and hyphal formation have been reported, including CHS2 (synthesizes

chitin), SCS7 (involved in cell membrane sphingolipid formation), UBI4 (contributes to ubiquitination), and genes that participate in adhesion and filamentation. UME6, TEC1, and GAT2 are involved in subsequent biofilm formation (Modrzewska and Kurnatowski, 2015).

The importance of the adherence regulatory genes (Bcr1, Ace2, and Snf5) lies in the fact that they are necessary for biofilm formation *in vitro* (Guan et al., 2013; van Wijlick et al., 2016; Burgain et al.; 2019).

After the initial adhesion of round yeast cells to the host surface to form a basal layer, the next phase of biofilm establishment is the growth and proliferation of hyphal cells. During the *C. albicans* proliferation phase, it multiplies and forms a monolayer adhesion zone where filamentation occurs, with the hyphae leading to general stability and acting as a support for the different cell morphologies: yeast, pseudohypha, hypha, and other cells of microorganisms that might be a part of the biofilm (Chandra and Mukherjee, 2015). According to McCall et al. (2018) and Min et al. (2018), hyphal growth in *C. albicans* is dependent on the presence of TF (transcription factor) Ndt80, which is responsible for regulating a variety of processes, including sexual development, resistance to antifungals, fibrillation, virulence, and nutritional stress response, among others. Hence, *C. albicans* possesses three paralogs (genes of different species, which descends to a single gene by genetic duplication in evolution) of NDT80 (NDT80, RON1, and REP1), and each of them provides *C. albicans* with specific characteristics. NDT80 is involved in resistance under different stress conditions, as well as in hyphal growth, and RON1 deletion has *shown to cause growth defects when C. albicans* is grown in GlcNAc media.

Glazier et al. (2017) highlighted that biofilm maturation is regulated by several transcription factors in *C. albicans*, including BCR1, EFG1, TEC1, NDT80, ROB1, and BRG1. When any one of them is deleted, biofilms are not formed correctly. Other transcription factors, such as CZF1, GZF3, UME6, CPH2, and ACE2, are also shown to be involved in *C. parapsilosis* biofilm formation. Biofilm formation decreases dramatically if ACE2 is deleted, and it also regulates biofilm development in *C. albicans*; however, in *C. glabrata*, the ability to cause disease is increased when ACE2 is inactive.

Ng and Dean (2017) reported that the increased expression and maturation of sgRNA facilitates and improves the CRISPR/Cas9 mutagenesis in *C. albicans* by about 10 times. This may help us edit the *C. albicans* genome. Finally, REP1 has been shown to be negatively involved in the expression of the MDR1 drug flow pump, which provides resistance against several microorganisms (Chen et al., 2009).

In the maturation phase, biofilm development continues via morphological modifications, an increase in the number of cells, and extracellular polysaccharide matrix production. This extracellular matrix mediates adhesive and cohesive interactions, grants mechanical stability and integrity, allows cell dispersion, limits the diffusion of toxic substances and nutrients, and even acts as an enzyme system. However, the main function of the extracellular matrix is to protect the biofilm from the important clinical repercussions, acting as a physical barrier to protect the biofilm cells from environmental factors (Chandra and Mukherjee, 2015; Rodríguez-Cerdeira et al., 2019).

Apart from the composition of the matrix, several recent studies have focused on its genetic regulation. *C. albicans* biofilm matrix *in vivo* and *in vitro* models were biochemically analyzed by Flemming and Wingender (2010) to identify the macromolecular components. The composition was as follows: 55% proteins and their glycosylated counterparts, 25% carbohydrates, 15% lipids, and 5% non-coding DNA. α-1,2-branched α-1,6-mannans were the most frequent polysaccharides related to unbranched α-1,6-glucans, forming a mannan–glucan complex on the matrix. However, they were a smaller proportion of extracellular matrix (ECM) components in *C. albicans* than β-1,3-glucan and β-1,6-glucan (Zarnowski et al., 2014).

Mitchell et al. (2015) and Dominguez et al. (2018) highlighted the importance of mannan and β-1,6-glucan in ECM formation. The elimination of proteins involved in ECM formation by deleting any one of the seven genes that governs the level of matrix mannan and β-1,6-glucan (ALG11, MNN9, MNN11, VAN1, MNN4-4, PMR1, and VRG4 for mannan production; BIG1 and KRE5 for β-1,6-glucan production) resulted in complete disappearance of the biofilm. In *C. parapsilosis*, the main function of Efg1 is to behave as a regulatory switch and participate in biofilm formation. Its absence leads to the production of an incomplete biofilm (Connolly et al., 2013).

In *C. albicans*, Cph1 acts as the terminal transcription factor of the MAP kinase pathway (Freire et al., 2018). This protein belongs to the family of the STE type transcription factor*, which is also present in other Candida* spp. (Bandara et al., 2013).

Brg1 controls the growth of hyphae in *C albicans*. When it is overexpressed, there is an increase in the expression of hyphae-specific genes, along with ALS3, HWP1, and ECE1 (Su et al., 2018). In *C. parapsilosis*, a homolog of Brg1 has been identified (Holland et al., 2014). According to Mendelsohn et al. (2017), the transcription factor Ume6, together with Nrg1 and Rfg1 decreases the expression of hypha specific genes ALS3, ECE1, and HWP1 in both *C. albicans* and *C. tropicalis*.

The cell surface proteins encoded by HYR1, ECE1, RBT5, ECM331, HWP1, ALS3, ALS1, and ALS9 genes are all regulated by Bcr1 gene. Upon overexpression of ALS3 in a bcr1/bcr1 cell, the biofilm formation phenotype was shown to be completely restored (Freire et al., 2018).

Vandeputte et al. (2012) identified that Rca1/Cst6 in *C. albicans* regulates hypha formation by facilitating the expression of GWP1, ECE1, HGC1, and ALS3 genes and the transcription factor Efg1. Cst6 is also a transcriptional controller of biofilm growth. It is a bZIP transcription factor, which belongs to the ATF/CREB family that inhibits the expression of the EPA6 gene and encodes an adhesion protein in the *C. glabrata* biofilm (Pohlers et al., 2017).

In *C. glabrata,* Leiva-Peláez et al. (2018) demonstrated that the expression of several related genes is subjected to subtelomeric silencing. HYR1, EPA1, EPA2, EPA3, EPA4, EPA5, EPA6, *and EPA7 genes of C. glabrata* undergo subtelomeric silencing due to their loci proximity to a telomere. The Sir complex (Sir2–Sir4),

Rap1, Rif1, yKu70, and yKu80, as well as the Swi/Snf complex are shown to be involved in regulating biofilm formation.

Deletion of the PMR1, KRE5, and FKS1 genes was associated with the increased susceptibility to fluconazole (Navarro-Arias et al., 2016; Tanaka et al., 2016; Jiang et al., 2018). Chowdhary et al. (2018) demonstrated that persistent cells cultured from the biofilm exhibit higher expression of CDR genes (Khosravi Rad et al., 2016). According to Feng et al. (2016), a set of isogenic *C. albicans* strains carrying single or double deletions in genes encoding efflux pumps (Δcdr1, Δcdr2, Δmdr1/drc2, and Δmdr1/cdr1) show antifungal resistance with paired strains. Tan et al. (2018) demonstrated that β-1,3-glucan has a crucial role in *Candida* biofilm formation and stress response in biofilm-forming *Candida*. They also showed that β-1,3-glucanase might be useful as an anti-biofilm agent.

In contrast, there are two major regulators of ECM production: Rml1 and Zap1. It has been shown that Rm11 deletion leads to the reduction in matrix levels (Nett et al., 2011; Pierce et al., 2017). However, Zap1 deletion leads to an increase in matrix levels, which is due to the overexpression of the glucoamylases, Gca1 and Gca2, as these enzymes, together with other hydrolyzing enzymes, are important for biopolymer degradation (Gulati and Nobile, 2016). Previous studies revealed that Δzap1 mutant, which is defective in the expression of zinc regulator Zap1, enhances the accumulation of yeast cells in biofilms (Ganguly et al., 2011).

In the late or dispersal phase, unbound *Candida* cells scatter from the biofilm and attempt to colonize other surfaces. Thus, it is possible for the cells to initiate the formation of new biofilms or spread in the host tissues, which ultimately leads to the development of candidemia and disseminated invasive diseases. Dispersed cells exhibit strong adherence, capacity to form new biofilms, and virulence. This process depends on three identified transcriptional regulators: Pes1, Nrg1, and Ume6. The transcriptional regulators, Nrg1 and Ume6, are of significant importance as their overexpression is shown to increase the number of sprawling cells actively released from the biofilm (Araújo et al., 2017).

In the biofilm maturation phase, ECM production is also extremely important. The gene responsible for glucan synthesis is FKS1, which is involved in resistance to fluconazole in *C. albicans* and promotes biofilm maturation in the presence of high glucose levels in *C. parapsilosis*. RLM1 and ZAP1 are the other two regulatory genes involved in matrix formation in *C. albicans*. Some ZAP1 target genes are CSH1 and IFD6 (negative regulators), and GCA1, GCA2, and ADH5 (positive regulators) that are associated with β-1,3-glucan production from the biofilm matrix. RML1 is a positive regulator, and its deletion reduces the matrix levels significantly. Other glucan regulatory genes associated with matrix formation are BGL2, PHR1, XOG1, CCR4, GAS1, GAS2, and GAS5 (Araújo et al., 2017).

The last step in biofilm formation is the detachment and dispersion of cells or parts of the biofilm, which further get displaced and colonize other parts of the host. The lack of nutrients or changes in the environment can favor this phase, which then leads to the development of infection in other organs. For this step, there are three genes involved: PES1, UME6 and NRG1. NRG1 is a negative regulator of filamentation and UME6 is necessary for the extension of hyphae (Beitelshees et al., 2018).

The main genes implicated in the genetic control of biofilm formation in *Candida* spp. are collated in **Table 1**.

Proteomics of the Biofilms

Biofilm associated proteins (55% of the biofilm dry weight) are mainly glycoproteins, glycolytic enzymes, and heat shock proteins. Around 565 different proteins have been identified, representing a total of 458 different biochemical activities (Thomas et al., 2006). Many of them are categorized as secretion signals, but most of these proteins do not have any such signal, indicating a non-canonical secretion pathway and/or protein increment occurring after cell death. In addition, host proteins including proteins related to the heme group and inflammatory and leukocyte-associated proteins, like hemoglobin, myeloperoxidase, C-reactive protein, and alarmin S100-A9 *have also been found in vivo* (Nett et al., 2015).

According to Hirota et al. (2017), the extracellular matrix of *C. albicans* is composed of extracellular DNA (eDNA), which has a crucial role in *Candida* biofilm formation and its structural integrity, and promotes the morphological transition from yeast to hyphal growth form during *C. albicans* biofilm development. The eDNA is mostly made up of random non-coding sequences and might also have an important role in antifungal resistance.

The adhesins of the fungal wall are modular proteins, and their precursors possess signal peptides to enter in the ER and GPI anchors. The mature proteins possess an N-terminal domain, which generally determines the ligand binding specificity of adhesins and is followed by a low complexity domain that in most cases contains internal tandem repeats. These internal tandem repeats have an important role in the adhesion of the fungal cells and exposure of the ligand-binding domains, which is modulated by the number of repeated copies, and consequently by the size variations of the adhesin-encoding genes identified in the clinical isolates (Willaert, 2018). According to Wagener et al. (2012), there are numerous phenotypic variations between the clinical isolates of *C. glabrata* in their ability to adhere to the abiotic surfaces for medical importance.

As high expression of heat shock proteins encourages *Candida* yeast–hyphae switch, which is an essential step in biofilm development, the expression of Hsp genes during *C. albicans* biofilm formation has been investigated previously (Becherelli et al., 2013). In contrast, heat shock protein 90 (Hsp 90) has also been shown to be involved in the dispersion process. The overexpression of the same leads to a decrease in the number of dispersed cells that are released and induction of the filamentation process. The authors recognized 226 *C. albicans* Hsp90 genetic interactors under planktonic conditions, of which 56 were identified to be implicated in transcriptional regulation. Six of these transcriptional regulators have previously been involved in biofilm development, proposing that the genetic interactors of Hsp90 found in planktonic conditions might have functional significance in biofilm formation. They further studied the relationship between Hsp90 and five of these transcription factor genetic interactors: BCR1, MIG1, TEC1, TUP1, and UPC2 (Diezmann et al., 2015).

TABLE 1 | The main genes involved in biofilm formation in *Candida* spp.

Type	Gene	References
Adhesion	ALS1	Finkel et al., 2012; Holland et al., 2014
	ALS3	Finkel et al., 2012; Holland et al., 2014; Mendelsohn et al., 2017; Freire et al., 2018; Su et al., 2018
	ALS5	Finkel et al., 2012
	ASL9	Holland et al., 2014
	AWP	Finkel et al., 2012
	BCR1	Guan et al., 2013; Inglis and Sherlock, 2013; Holland et al., 2014; Orsi et al., 2014; Modrzewska and Kurnatowski, 2015; Marak and Dhanashree, 2018; Burgain et al., 2019; Valotteau et al., 2019
	BUD2	Valotteau et al., 2019
	CHS2	Valotteau et al., 2019
	CKA2	Valotteau et al., 2019
	CSH1	Gulati and Nobile, 2016
	CZF1	Burgain et al., 2019
	EAP1	Finkel et al., 2012
	ECE1	Holland et al., 2014; Mendelsohn et al., 2017; Freire et al., 2018; Su et al., 2018
	ECM1	Orsi et al., 2014
	ECM331	Holland et al., 2014
	EFG1	Orsi et al., 2014; Mitchell et al., 2015; Mendelsohn et al., 2017; Dominguez et al., 2018; Marak and Dhanashree, 2018; Burgain et al., 2019
	EPA1	Finkel et al., 2012; Vandeputte et al., 2012
	EPA2	Vandeputte et al., 2012
	EPA3	Vandeputte et al., 2012
	EPA4	Vandeputte et al., 2012
	EPA5	Vandeputte et al., 2012
	EPA6	Finkel et al., 2012; Freire et al., 2018
	EPA7	Finkel et al., 2012; Vandeputte et al., 2012
	GAT2	Valotteau et al., 2019
	HGC1	Mendelsohn et al., 2017
	HWP1	Finkel et al., 2012; Holland et al., 2014; Freire et al., 2018; Su et al., 2018; Valotteau et al., 2019
	HYR1	Vandeputte et al., 2012; Holland et al., 2014
	PBR1	Finkel et al., 2012
	PGA10	Finkel et al., 2012
	RBT5	Holland et al., 2014
	RSR1	Valotteau et al., 2019
	SCS7	Valotteau et al., 2019
	SNF5	Inglis and Sherlock, 2013; Modrzewska and Kurnatowski, 2015; van Wijlick et al., 2016
	TEC1	Valotteau et al., 2019
	UBI4	Valotteau et al., 2019
	UME6	Ganguly et al., 2011; Gulati and Nobile, 2016; Su et al., 2018; Burgain et al., 2019; Valotteau et al., 2019
Biofilm formation	ADH5	Gulati and Nobile, 2016
	ALG11	Mitchell et al., 2015
	BIG1	Mitchell et al., 2015
	FKS1	Gulati and Nobile, 2016; Navarro-Arias et al., 2016; Jiang et al., 2018; Leiva-Peláez et al., 2018
	GCA1	Nett et al., 2011; Gulati and Nobile, 2016
	GCA2	Nett et al., 2011; Gulati and Nobile, 2016
	IFD6	Gulati and Nobile, 2016
	KRE5	Mitchell et al., 2015; Navarro-Arias et al., 2016; Jiang et al., 2018; Leiva-Peláez et al., 2018
	MNN11	Mitchell et al., 2015
	MNN4-4	Mitchell et al., 2015
	MNN9	Mitchell et al., 2015
	PMR1	Mitchell et al., 2015; Navarro-Arias et al., 2016; Jiang et al., 2018; Leiva-Peláez et al., 2018
	RAP1	Vandeputte et al., 2012
	RIF1	Vandeputte et al., 2012
	RM11	Feng et al., 2016; Tan et al., 2017
	SIR Complex	Vandeputte et al., 2012
	SWI/SNF	Vandeputte et al., 2012
	VAN1	Mitchell et al., 2015
	VRG4	Mitchell et al., 2015
	YKU70	Vandeputte et al., 2012
	YKU80	Vandeputte et al., 2012
Morphogenesis	NTD80	van Wijlick et al., 2016; Marak and Dhanashree, 2018; Min et al., 2018; Burgain et al., 2019
	REP1	Glazier et al., 2017; Min et al., 2018
	RON1	Min et al., 2018
Oligopeptide transporter genes	OPT	Ni et al., 2009
Resistance	CDR1	Pohlers et al., 2017; Chowdhary et al., 2018
	CDR2	Pohlers et al., 2017; Chowdhary et al., 2018
	MDR1	Glazier et al., 2017
	TPO1_2	Pohlers et al., 2017
Transcriptional regulatory genes	ACE2	Guan et al., 2013; Inglis and Sherlock, 2013; Modrzewska and Kurnatowski, 2015; Burgain et al., 2019
	BGL2	Gulati and Nobile, 2016

(Continued)

TABLE 1 | Continued

Type	Gene	References
	BRG1	Bandara et al., 2013; Freire et al., 2018; Marak and Dhanashree, 2018; Burgain et al., 2019
	CCR4	Gulati and Nobile, 2016
	CPH1	Connolly et al., 2013; Yano et al., 2019
	CPH2	Burgain et al., 2019
	CST6	Mendelsohn et al., 2017; Freire et al., 2018
	GAS1	Gulati and Nobile, 2016
	GAS2	Gulati and Nobile, 2016
	GAS5	Gulati and Nobile, 2016
	GWP1	Mendelsohn et al., 2017
	GZF3	Burgain et al., 2019
	NRG1	Ganguly et al., 2011; Gulati and Nobile, 2016; Su et al., 2018
	PES1	Ganguly et al., 2011; Gulati and Nobile, 2016
	PHR1	Gulati and Nobile, 2016
	RCA1	Mendelsohn et al., 2017
	RFG1	Su et al., 2018
	RLM1	Gulati and Nobile, 2016
	ROB1	Marak and Dhanashree, 2018; Burgain et al., 2019
	TEC1	Orsi et al., 2014; Marak and Dhanashree, 2018; Burgain et al., 2019
	XOG1	Gulati and Nobile, 2016
	ZAP1	Feng et al., 2016; Gulati and Nobile, 2016; Pierce et al., 2017; Tan et al., 2017

The overexpression of Ywp1 protein in the cell wall makes the biofilm more adherent, as it negatively regulates the dispersion process. It has previously been shown that Ywp1 can collaborate biofilm detachment in early stages. On the contrary, it can contribute to biofilm maintenance during the late phases of biofilm growth. It has been proposed that Ywp1 interacts with other C. albicans adhesin proteins expressed in early, but not late phases of biofilm growth (Karkowska-Kuleta et al., 2019).

The process of cell dispersion begins early and occurs during the development phase of the biofilm. These dispersed cells have differences in their transcriptome that confer improved virulence characteristics and drug resistance, as well as a superior expression of transporters necessary for the achievement of nutrients. However, initial adhesion and maintenance are keys to biofilm biomass development. The filamentation process is important for the expression of proteins that maintain adhesion, and thus the deletion of individual proteins in *C. albicans*, such as Efg1 and Bcr1, resulted in an almost complete loss of initial adhesion and a collapse of biofilm development. However, the suppression of the expression of the ALS1 and ALS3 adhesins and Hyr1 lead to a shortage of adhesion and biofilm biomass. The hyperfilamentous strains generated by the suppression of Hog1 and Sfl1, formed a more robust biofilm. In addition, in a previous study, it was found that *C. albicans* that lacks Ywp1 protein had a weak adhesion maintenance force, but its effect on initial binding was minimal. This finding indicates that Ywp1 protein interferes with other *C. albicans* adhesive proteins (McCall et al., 2019).

The proteins expressed in *Candida* spp. biofilm formation are summarized in **Table 2**.

Quorum Sensing (QS)

Quorum sensing or "quorum perception" designates a complex intercellular communication system, wherein the microorganisms coordinate to generate a uniform response for their survival and ensure the colonization of their habitats. It is the so-called "language of microorganisms" (Saxena et al., 2019).

Due to the environment, the metabolic pathways of *C. albicans* that are involved in the yeast–hypha transition, as well as its virulence, depend on a large number of molecules generated during QS (Padder et al., 2018). This process includes the production and deliverance of a signal molecule (autoinducer) that, according to cell density, will increase its concentration and favor the collective and synchronized expression of specific genes in all the species associated with biofilm formation.

According to Riekhof and Nickerson (2017), it has been demonstrated that *C. albicans* is a dimorphic fungus in the presence of farnesoic acid (FA) and farnesol (F), the two sensor molecules of related sesquiterpene quorums, and when accumulated, they do not allow the change from yeast to mycelium. Studies were conducted with three different ATCC strains of *C. albicans*, 10231, A72, and SC5314. The first strain excretes a high concentration of FA, while the remaining two secretes only F, although it is important to note that the *Candida*

TABLE 2 | Differential expression of the proteins involved in biofilm formation in *Candida* spp.

Type	Protein	References
Adhesion	Adhesins	Nett et al., 2015; Hirota et al., 2017
	Als1	Diezmann et al., 2015
	Als3	Diezmann et al., 2015
	Bcr1	Diezmann et al., 2015
	Efg1	Diezmann et al., 2015
	Hog1	Diezmann et al., 2015
	Hyr1	Diezmann et al., 2015
	Sfl1	Diezmann et al., 2015
	Ywp1	Becherelli et al., 2013; Diezmann et al., 2015
Biofilm associated	Alarmin S100-A9	Beitelshees et al., 2018
	C-reactive protein	Beitelshees et al., 2018
	eDNA	Thomas et al., 2006
	Hemoglobin	Beitelshees et al., 2018
	Myeloperoxidase	Beitelshees et al., 2018
Heat shock	Hsp 90	Wagener et al., 2012; Willaert, 2018

spp. that produce FA do produce F in undetectable amounts. In conclusion, although F and FA possess close chemical similarity, they use separate pathways to block hyphal development.

Previously, CaPHO81, a key component of the phosphate starvation response signal transduction pathway, has been shown to be implicated in inhibition of hyphal development via FA. First, it must be taken into account that the Δhot1 mutant cells used in this study, lost their sensitivity to FA but were still sensitive to F. Second, *HOT1* and *PHO81* mRNA abundance increased dramatically between 40 and 240 min after FA treatment, but these expression levels remained unchanged after F treatment as well. However, the genetic and biochemical factors that contribute to the selection for FA production versus F production are currently unexplored. Moreover, further studies will likely provide more details on the differences in virulence and immune responses between the ATCC 10231 strain used in various studies and other clinical isolates of C. albicans (Dižová and Bujdáková, 2017; Paluch et al., 2020).

Farnesol synthesized by *C. albicans* acts as a negative regulator of morphogenesis, as it inhibits the yeast–hyphae transformation. Thus, the aforesaid effect on morphological transformation via cyclic AMP (cAMP)/protein kinase A (cAMP-PKA) pathway also affects other biochemical pathways of yeasts, such as the ones for sterol biosynthesis or triggering of apoptosis via accumulation of ROS (reactive oxygen species) that damages essential cellular compartments. ROS activate intracellular caspases that indicate apoptotic response in *C. albicans* (Lindsay et al., 2012; Polke et al., 2018).

Regarding QS, we would like to highlight that Paluch et al. (2020) investigated the quorum quenching (QQ) technique and highlighted its importance because it interrupts the microbial communication and ultimately, the biofilm formation. QQ-driving molecules can decrease or even completely inhibit virulence factor production, and consequently, biofilm formation. One of the strategies is to use structural analogs of the QS receptor autoinducers. Most QQ molecules are enzymes with the ability to degrade the signaling molecules or cascades. The techniques that are being used to measure QS/QQ are mass chromatography-spectroscopy, bioluminescence, chemiluminescence, fluorescence, electrochemistry, and colorimetry. The importance of these research methods lies in their medical and biotechnological application.

Candida BIOFILM MODELS

To determine whether *Candida* spp. can form biofilms on vaginal mucosa, the use of *in vivo*, *ex vivo*, and *in vitro* models are essential. Studying the implications of *Candida* spp. in clinical practice may help in the discovery of new therapeutic targets in *Candida* spp.

In vitro Models

To facilitate the detection of compounds that are active against biofilms, high-performance biofilm models are needed. Tsui et al. (2016) used a microtiter plate model to evaluate the variability between *C. albicans* biofilms formed in independent wells of the same microtiter plate. The biofilms that constituted over a 24 h period showed consistent metabolic activity.

Nweze et al. (2012) and Almshawit et al. (2014) used the Calgary Biofilm Device (CBD) for the understanding of *Candida* spp. biofilms. The CBD was also used to study the susceptibility of *Candida* spp. biofilms to metal ions and chelating agents (Harrison et al., 2007a) and identify persistent cells in such biofilms (Harrison et al., 2007b).

Samaranayake et al. (2005) used a perfusion model involving three commonly used antifungal agents, amphotericin B, fluconazole, and flucytosine, and biofilms established on microporous filters by *C. albicans*, *C. parapsilosis*, and *C. krusei*. The authors found that biofilm growth is dependent both on the antimycotic agent used and *Candida* spp. Shao et al. (2015) described a free-flow incubator that allowed biofilm organization under continuous flow conditions. The system displayed stability and continuity during the 96 h experiment. *C. albicans* and *C. glabrata* might co-exist in the dual-species biofilms under the flow regime.

Catheter-associated infections can be caused by biofilms formed on catheter surfaces. Within the biofilm, cells are protected from the host immune system. Authors studied the formation of *C. albicans* biofilms on catheters, including latex urinary catheters, and with artificial urine and antimicrobial therapies (Negri et al., 2011).

Recently, Srinivasan et al. (2012) have developed a *C. albicans* biofilm chip microarray system (CaBChip). The system is composed of more than 700 uniform and independent nano-biofilms encapsulated in a collagen matrix and is the first miniature biofilm model for *C. albicans*. In spite of multiple miniaturizations, the biofilms formed on the chip had phenotypic features that were similar to those of biofilms organized *in vitro*, containing a combination of yeast, pseudohyphae, and hyphal cells, and high concentrations of antifungal compounds. The models will allow the identification of possible anti-biofilm drugs.

The use of SkinEthic^{TM} reconstituted human epithelia models is based on the fact that the epithelial cells are placing in inert filter substrates that rise to the air–liquid interface in a humidified air incubator. Nutrient medium is added to feed the basal cells through the filter substrate. After the first 5 days, a stratified epithelium similar to human tissue is formed. The oral and vaginal epithelial tissues formed express all the major natural markers of epithelial basement membrane and epithelial differentiation, behave like human epithelium, and reflect natural wound resolution processes *in vivo*. Damage can be visualized by histopathological examination and precisely analyzed using available techniques. Confocal laser microscopy is being used (Schaller et al., 2003, 2005), although no conclusive data have yet been published.

Samaranayake et al. (2005) and other authors have verified that *Candida* spp. biofilms on mucosal surfaces exhibit characteristics similar to those of cells growing on abiotic surfaces. Murine models with vaginal yeast infections established on mucosal surfaces have demonstrated that *Candida* biofilms harbor many yeast, hyphae, and extracellular material.

Table 3 shows the main studies on *Candida* biofilm models conducted *in vitro*.

In vivo Models

Experimental animal models are crucial to completely understand the candidate factors of pathogenesis and develop new therapeutic approaches, mainly in light of the increased incidence of fungal infections.

Rodents are one of the most useful animals to study candidiasis, since the disease process and host immune responses are similar to those of humans. A well-established estrogen-dependent mouse model has been developed for the study of vaginitis (Yano and Fidel, 2011). Even though, unlike humans, laboratory rodents do not naturally have *C. albicans* as a commensal, the experimentally induced infection resembles human infection. Therefore, the investigations of the animal model are translatable to the human host (Peters et al., 2014).

Wang and Fries (2011) made a murine model to investigate catheter-associated urogenital tract infections and candiduria. In this model, a guidewire is inserted through the urethra of a female mouse and a catheter segment is inserted over the guidewire into the bladder. While mucosal biofilms share many characteristics with the device-associated biofilms, whether they exhibit the same degree of resistance to antifungal compounds is unclear. Clinically, mucosal biofilms respond more frequently to antifungal therapies, including azoles (Wang and Fries, 2011).

After 5–7 days, the animal is infected intravascularly with *C. albicans*. The infection persists for approximately 28 days. During this time period, a dense biofilm of adherent yeast and hyphae forms on the luminal and extraluminal surfaces. The difficulty is that, since there is only one catheter segment, the flow will probably be less. This system can also be used in other mammalian animals, including wild or immunocompromised animals.

Since there is only one catheter segment in place in the model, the flow conditions are probably less than what would be seen for a catheter installed in a patient, which functions to drain the bladder. The model includes the mammalian immune system. In addition, the model may use wild type or immunocompromised animals. To the best of our knowledge, this model has not been used to investigate the activity of anti-biofilm therapies yet.

Naglik et al. (2008) administered 0.1 mg 17-β-oestradiol in 0.1 ml sesame seed oil subcutaneously for 3 days to female mice prior to intravaginal inoculation with 20 μl *C. albicans* 3153A (2.5×10^6 cells/ml), *C. albicans* DAY185 (2.5×10^8 cells/ml), or biofilm mutant (2.5×10^8 cells/ml) suspension. After a period of time, the mice were euthanized. The vagina was removed from each mouse and examined through confocal or scanning electron microscopy.

Harriott et al. (2010) performed an *ex vivo* investigation that involved female mice treated with estrogen. After euthanizing, the vagina was removed from each mouse. *C. albicans* isolates (1×10^6 blastoconidia) in 0.1 ml PBS was incubated at 37°C in an atmosphere of CO_2 and instilled on the vaginal surface. The fungal load was determined and microscopy examination was performed.

TABLE 3 | Schema for *in vitro Candida* spp. related to biofilm models.

In vitro models	Components	Characteristics
Plastic/microtiter plates (Tsui et al., 2016)	Polystyrene surfaces at different temperatures (10, 20, and 37°C), flat-bottomed 96-well microtiter plates, and plastic slides	Useful for biofilm formation for different *Candida* spp. strongly associated with the type and phenotypic behavior of the isolates
Calgary Biofilm Device (CBD) (Harrison et al., 2007a; Nweze et al., 2012; Almshawit et al., 2014)	CBD was developed from polypropylene microcentrifuge tubes and pipette type boxes, as well as 96-well polystyrene pegs/plates	A useful, simple, low cost miniature device for parallel study of *Candida* biofilms and factors modulating this phenomenon.
Microporous membrane filters (Gu et al., 2015)	Microporous polycarbonate (25-mm diameter)	Quantitative evaluation of the antifungals that diffused into the disk through the biofilm
Flow system biofilm models (Shao et al., 2015)	Automated microfluidic device under laminar flow conditions	Used to study biofilm formation in real-time. The flow of liquids can influence nutrient exchange and the structural integrity of biofilms.
Catheters (Negri et al., 2011)	Silicone, polyurethane, and latex urinary catheters, with artificial urine	Used under flow conditions to study *Candida* spp. adhesion and biofilm formation
Robotic microarrayer is used to dispense yeast cells of *C. albicans* onto a solid substrate. (CaBChip) (Srinivasan et al., 2012, 2013)	CaBChip composed of ∼750 equivalent and spatially distinct biofilms with cell-based microarray platform allows for miniaturization of microbial cell culture and is fully compatible with other high-throughput screening technologies	The main advantages of the fungal biofilm chip are automation, miniaturization, savings in amount and cost of reagents and analyses time, as well as the elimination of labor intensive steps. This chip significantly speeds up the antifungal drug discovery process.
Reconstituted human epithelia (RHE) models (Schaller et al., 2003, 2005)	Epithelial cells are seeded on inert filter substrates that are raised to the air-liquid interface in a humidified air incubator	Epithelial damage can be visualized by histological analysis of the embedded and quantified based on the extracellular activity of lactate dehydrogenase (LDH) in the culture medium released by the damaged epithelial cells. Additionally, microscopy. fluorescence-activated cell sorting. ELISA can be used to measure and detect protein expression, and real-time *immune*-PCR (used to show them)

Another recently used model for the *in vivo* study of *Candida* spp. biofilms is the nematode *Caenorhabditis elegans*. The model is relevant for aspects of human infections, including resistance to antifungal agents (Madende et al., 2020).

The most relevant studies on *Candida in vivo*/*ex vivo* biofilms are summarized in **Table 4**

Biofilm Inhibition

It should be noted that despite the existence of numerous investigations, no specific drugs are available for treating biofilm-produced VVC/RVVC yet.

Posaconazole shows *in vitro* and *in vivo* synergy with caspofungin against *C. albicans*, including echinocandin-resistant isolates. Furthermore, an *in vitro* study of *C. albicans*, *C. glabrata*, and *C. parapsilosis* showed that azole-resistant *Candida* spp. are not resistant to the combination of both compounds (Cui et al., 2015). Similar results were obtained by Ning et al. (2015) with epigallocatechin gallate bound to azoles.

In a study of the various biological properties of the thiazolidinone scaffold, 100 compounds were synthesized and characterized by a 1,3-thiazolidin-4-one nucleus derivatized at the C2 with a hydrazine bridge, linked to (cyclo) aliphatic or hetero (aryl) moieties. The *N*-benzylated derivatives of these compounds were found to be highly effective against *Candida* spp. (Carradori et al., 2017).

Mannich base-type eugenol derivatives have also been synthesized and shown to be particularly effective against *C. glabrata* (Abrão et al., 2015).

Piperazine derivatives 1c–34e have been synthesized from phenol, 2,4-dichlorophenol and 4-hydroxybiphenyl. Their inhibitory activity during hyphae formation was verified and it correlated with the inhibition of biofilm formation by *C. albicans*, thus possibly indicating the vital role of hyphae development in the *C. albicans* biofilm formation process (Zhao et al., 2018).

A new series of glycosides modified in their saccharide units has been analyzed against *Candida* sp. The newly synthesized glycoside is called eugenol glucosiso 5 and can be considered a new structural pattern in anti-*Candida* drugs, fundamentally against *C. glabrata* (de Souza et al., 2016).

When a cationic peptide antibiotic was used in combination with antifungal agents, such as polymyxin B with azoles, a synergist effect was seen (Pankey et al., 2014; Raman et al., 2015). Aminoglycosides, like tobramycin, have been shown to possess antifungal potential (Fosso et al., 2018). Silva et al. (2014) showed that cerium nitrate has fungicidal activity against planktonic *Candida* cells. Similarly, the ability of cerium nitrate to pare and disarticulate biofilms has been demonstrated, which represents an important advance in clinical practice. Thamban Chandrika et al. (2018) identified fluconzaol analogs and found that the antifungal activity of alkyl-amino fluconazole derivatives depends on the alkyl chain length. Recently, compounds 6–9 were identified as promising antifungal agents, with low cytotoxicity and hemolytic activity. These compounds have higher activity levels and lower toxicity than fluconazole.

Antifungal lock therapy is used to inhibit biofilm formation. Micafungin (5 and 15 mg/L), especially combined with ethanol; capsofungin (5 and 25 mg/L); and posaconazole (10 mg/L) have been used in this form of therapy (Walraven and Lee, 2013). Liposomal amphotericin B (5 mg/mL) or anidulafungin (3.33 mg/mL) has also been successfully used (Basas et al., 2019).

Nikkomycin Z has been shown to act synergistically in association with caspofungin or micafungin against biofilms (Kovács et al., 2019).

Given the resistance of fungi to fluconazole, new compounds derived from this antifungal compound have been investigated. A total of 27 new fluconazole derivatives have been tested for their antifungal activity against a panel of 13 clinically relevant fungal strains (Shrestha et al., 2017).

Classically, the combination of antifungals and antibiotics, such as rifampicin, have been shown to have a general role in regulating signal transduction or modulating gene expression by other mechanisms in *C. albicans* (Vogel et al., 2008). Similarly, synergistic interactions between fluoroquinolones and antifungal agents (amphotericin B or caspofungin) have been demonstrated, potentially improving the outcome in immunosuppressed patients with concurrent bacterial and fungal infections (Stergiopoulou et al., 2009). Recently,

TABLE 4 | Schema for *in vivo/ex vivo Candida*-associated urogenital biofilm models.

***In vivo* models**	**Device**	**Animal species**	**Characteristics**	**References**
Catheter-associated models	Candiduria model: a subcutaneous foreign body system featuring a catheter through the urethra of a female mouse	Rat, mouse, and rabbit	Rat and mouse models have advantages over rabbit models that include relatively low cost, ease of use, and ability to mimic the clinical conditions of rabbit models	Wang and Fries, 2011; Yano and Fidel, 2011; Peters et al., 2014
Models in which the vagina of each animal is excised and cut longitudinally to expose the mucosal surface.	17-β-Estradiol subcutaneous + intravaginally administered *C. albicans*	Female mice	Tissue is used to determine fungal load through confocalor scanning electron microscopy	Naglik et al., 2008
Models using biotic surfaces, such as vaginal mucosa	*Ex vivo* models	Mouse (treated with estradiol prior to infection)	Low cost and mimics clinical conditions	Harriott et al., 2010
Animal is infected with fungi by consuming the yeast cells as a food source	*In vivo* models	Nematode *Caenorhabditis elegans*	Identification of antifungal chemical compounds	Madende et al., 2020

chloramphenicol has been shown to have activity, mainly against *C. albicans* and C. *glabrata* (Joseph et al., 2015). The combination of antifungals and QS molecules is also of interest. Farnesol, a QS molecule, inhibits the formation of hyphae and biofilms, and tyrosol and farnesol are excellent antifungal candidates (Monteiro et al., 2017; Mehmood et al., 2019).

Using nanotechnology, amphotericin B-loaded silver nanoparticles have been developed and shown promise in improving the antifungal capacity of amphotericin B against *Candida* spp. (Leonhard et al., 2018).

Some success has also been obtained with 0.43–1.736 mM acetylsalicylic acid use. It is especially effective due to its synergistic effects with amphotericin B (Zhou et al., 2012). Ibuprofen (Sharma et al., 2015) and ambroxol (Li et al., 2017) have also been successfully used as antifungal agents.

Synthetic compounds, such as the peptides, KSL-W and SM21, which inhibit the transition from yeast to hypha, also inhibit biofilm formation (Theberge et al., 2013; Cavalheiro and Teixeira, 2018).

Photodynamic therapies using light of a certain wavelength and a photosensitizing dye are also being investigated. These therapies produce reactive oxygen species (ROS), and after treatment, substances such as hydrogen peroxide can be used. The absence of dye toxicity and low cost of the technique suggest that this alternative approach has great potential (Bujdáková, 2016).

Polymers incorporated in medical devices can also be modified to prevent fungal contamination. Lumbrical organ water-insoluble polyethylamine derivatives are capable of inhibiting *C. albicans* growth, by altering the membrane integrity. Furthermore, the natural polymer, chitosan, is also effective against *C. albicans* biofilms (Hoque et al., 2015).

Table 5 shows the main advances in new compounds involving new therapeutic options directed toward fungal biofilms.

Immune Response Intervention

Peptide-derived antibody therapies against *Candida* spp. are currently being developed. These therapies increase the oxidative stress of the yeast and membrane permeability to significantly decrease the expression levels of biofilm generation-related genes (Paulone et al., 2017).

New targets are also being investigated to develop vaccines for RVVC. An effective RVVC vaccine is a possible option to treat this chronic condition. An ideal vaccine should be able to induce an efficient immune response that promotes fungus elimination and virulence factor neutralization, without causing harmful changes in the vaginal microenvironment (Cassone, 2015). Vaccines that target the adhesin, Als3, and the enzyme, Sap2, have been developed. Although no vaccine has been approved for use in humans currently, important advances in this area are expected in the near future (Sui et al., 2017; Tso et al., 2018). In a recent study, 70 women of fertile age were recruited and divided into two groups. One group was treated by intravaginal autolymphocyte therapy, in conjunction with traditional treatment, and a control group only received conventional treatment. The group of patients treated by autolymphocyte therapy recovered fully in half the time than that required by the control group (Alyautdina and Esina, 2019).

Probiotics

The term probiotics refers to microorganisms with beneficial actions on the human body. To be classified as a probiotic, a microorganism must be correctly identified at the genus, species, and strain levels using phenotypic and genotypic methods, since the demonstrated beneficial effects of a specific strain cannot be extrapolated and attributable to another strain of the same species. The strain is also required to be deposited in an internationally recognized collection. Probiotics should lack virulence factors and/or the ability to produce metabolites that are undesirable for the host. The main objective of probiotic therapy is not to re-establish the vaginal canal bacterial microbiome; and there is no consensus for its use in vaginal infection treatment or their sequelae (Hewadmal and Jangra, 2019). However, Rodríguez-Cerdeira et al. (2019) have extensively reported the importance of probiotics in VVC/RVVC treatment. Ongoing research on this topic and recently performed studies are discussed below.

Tsimaris et al. (2019) studied a group of 70 women treated with *Lactobacillus* during the pre-diagnosis period. Administration of intravaginal *B. coagulans*, alone and in combination with standard antibiotic therapy, provided significant benefits in the treatment of vaginal symptoms in VVC patients in this clinical trial.

Previous studies support the notion that vaginal microbiota restoration and/or local mucosal immune response modulation can be achieved via supplementation with probiotics, which can be administered orally as a probiotic food supplement, intravaginally as vaginal suppositories, or applied topically as a gel (Köhler et al., 2012; Gille et al., 2016).

Gabrielli et al. (2018) have verified the probiotic capacity of *Saccharomyces cerevisiae* CNCM I-3856 to modulate the expression of *C. albicans* pathogenicity in mice with vaginal candidiasis. Daily intravaginal administration of *S. cerevisiae* CNCM I-3856 was shown to eliminate various components of the fungus necessary for its virulence in the vagina and modulate the expression of aspartyl proteinase and genes associated with hyphal growth, *Hwpl* and *Ecel*, in the epithelium. The decreased inflammatory response observed in this study was likely due to the decrease in IL-8 production and aspartyl proteinase expression inhibition. Despite the assumption that *S. cerevisiae* administration would produce undesirable effects, it did not alter the architecture of vaginal epithelial cells or organs, either *in vitro* or in the human vaginal epithelium *in vivo* (Handalishy et al., 2014; van de Wijgert and Verwijs, 2020).

In general, the studies reported contradictory results and probiotics were generally not effective in preventing or curing VVC. None of the studies showed safety issues with the tested probiotics. There was no evidence of vaginal colonization by the probiotic strains and thus, vaginal detection is restricted to the dosing period. It should be noted that the different probiotic products used in these studies differ in their components, such as the active ingredients and excipients, and the application methods and dosages differ between the different studies. There

TABLE 5 | New anti-*Candida* spp. biofilm compounds.

Compound	Action	References
Posaconazole plus caspofungin (*in vitro* and in animals) or Concomitant use of epigallocatechin gallate and miconazole, fluconazole, or amphotericin B	*C. albicans*, *C. glabrata*, and *C. parapsilosis* Highly effective against *C. albicans, C. glabrata* and *C. parapsilosis in vitro* and in animal experiments	Cui et al., 2015 Ning et al., 2015
1,3-thiazolidin-4-one nucleus and its N-benzylated derivatives at the C2 with a hydrazine bridge linked to (cyclo)aliphatic or hetero(aryl)	Strong activity against *Candida* spp. Lack of cytotoxic effects	Carradori et al., 2017
Mannich base-type eugenol derivatives: : 4-allyl-2-methoxy-6- (morpholin-4-ylmethyl) phenyl benzoate (7) and 4- {5-allyl-2 - [(4-chlorobenzoyl) oxy] -3-methoxybenzyl}. Morpholin-4-io (8) chloride was found	Highly effective against *C. albicans, C. glabrata,* and *C. krusei*	Abrão et al., 2015 Yano et al., 2012
1-(4-ethoxyphenyl)-4-(1-biphenylol-2-hydroxypropyl)-piperazine	Acts primarily on *C. albicans* Low cytotoxic effects	Zhao et al., 2018
Glucosides with modified saccharides	Fungistatic activity against *C. glabrata*	de Souza et al., 2016
Amphiphilic, helical β-peptide structural mimetics of natural antimicrobial α-peptides	Specific planktonic antifungal and anti-biofilm activity against *C. albicans, C. glabrata, C. parapsilosis*, and *C. tropicalis*	Pankey et al., 2014 Raman et al., 2015
Aminoglocosides derived from tobramycin	The triazole is most effective against *Candida* spp.	Fosso et al., 2018
Cerium nitrate, a member of the lanthanide family	Active against planktonic and sessile *Candida* spp. cells It is able to prevent biofilm formation by *C. albicans* and *C. parapsilosis* both *in vitro* and *in vivo* Application in medical devices	Silva-Dias et al., 2015
Fluconazole analogs with alkyl-, aryl-, cycloalkyl-, and dialkyl-amino substituents	These compounds are active against some of the *C. albicans* and non-*albicans Candida* strains and are highly effective against clinical strains of *C. glabrata* and *C. parapsilosis*	Thamban Chandrika et al., 2018
Micafungin + ethanol Capsofungin/posaconazole, or amphotericin B, or anidulafungin, or Caspofungin/micafungin in combination with nikkomycin Z	Antifungal lock therapy is used to inhibit the formation of the biofilm	Walraven and Lee, 2013 Basas et al., 2019 Kovács et al., 2019
27 new FLC derivatives	Broad-spectrum antifungal activity. All compounds inhibit the sterol 14α-demethylase enzyme involved in ergosterol biosynthesis	Shrestha et al., 2017
Fluoroquinolones and antifungal agents (from amphotericin B or caspofungin) or rifampicin Chloramphenicol	Very useful in immunosuppressed patients	Stergiopoulou et al., 2009 Vogel et al., 2008
	Not valid for use against *C. albicans* or *C. glabrata* Antifungal activity comparable to caspofungin and ketoconazole	Joseph et al., 2015
Tyrosol and farnesol	Strong biofilm inhibition Inhibit the formation of hyphae	Monteiro et al., 2017 Mehmood et al., 2019
Amphotericin B plus silver hybrid nanoparticles	Powerful antifungal activity although the toxicity of the nanoparticles depends on the size, concentration, and pH of the medium and the exposure time to pathogens	Leonhard et al., 2018
Amphotericin B plus acetylsalicylic/ibuprofen/ambroxol	They are inexpensive, but they increase the risk of bleeding and hyperkalaemia	Zhou et al., 2012 Sharma et al., 2015 Li et al., 2017
KSL-W and SM21 peptides	Inhibit biofilm formation by *Candida* spp.	Theberge et al., 2013 Cavalheiro and Teixeira, 2018

is also no consensus on which specific strains of *Lactobacillus* may be most beneficial for dysbiosis. However, the efficacy of the different probiotics analyzed in the studies was highly similar.

DISCUSSION

The importance of the present review lies in the fact that it raises awareness regarding the impact of biofilms on practical clinical management and treatment of VVC/RVVC and highlights the need for additional research toward the development of novel therapeutics targeting pathogenic vulvovaginal biofilms.

As discussed in the present review, numerous transcriptional events related to morphogenesis, key molecule expression, and virulence factor manifestation occur during the invasion and infection processes. Experimental evidence indicates that *C. albicans* can differentially regulate its genes during adaptation to and subsequent colonization of a biological niche, and it exhibits a specific profile of virulence factors depending on the type of mucosa in which the infection occurs. In this

review, we focussed on the mucosa of the lower genital tract (TGI) with a special emphasis on the vulvovaginal mucosa (El-Houssaini et al., 2019).

Candida spp. that form biofilms exhibit high resistance to antifungal drugs and are known to successfully evade host defense mechanisms. This resistance is responsible for the perpetuation and reappearance of this type of infection, causing collateral damage to the surrounding tissues.

Present interventions for preventing biofilm formation are based on attempts to modulate surface chemistries to ensure prevention of attachment (Li et al., 2018) or blocking molecules involved in signal transduction, such as c-di-GMP, from regulating attachment and matrix production (Hall and Lee, 2018).

Other substances used are proteases immobilized on a polypropylene surface, which decreases the adhesion of *C. albicans* required for biofilm formation, although the toxicity of these enzymes remains an issue (Andreani et al., 2017).

Disruption of the maturation of *Candida* biofilms with the alkaloid berberine has been successfully demonstrated in both planktonic and biofilm conditions, as described by Xie et al. (2020). The authors observed significant alterations in the architecture of biofilms formed by *C. albicans* (ATCC 10231 and ATCC 90028), *C. krusei* (ATCC 6258), *C. glabrata* (ATCC 90030), and *C. dubliniensis* (MYA 646).

The role of epithelial cell-mediated immunity of the vulvovaginal mucosa is crucial in the context of protection against vaginal *Candida* infections. The FGT is equipped with various mechanisms responsible for innate immunity that are important in maintaining immunological surveillance against microorganisms, upholding the basic tenets of commensalism, and ensuring protection against invasion (Cassone, 2018). These include neutrophil polymorphonuclear cells (PMNs), macrophages, dendritic cells, natural killer (NK) cells, T lymphocytes, and innate lymphocytes, which actively contribute to the localized antifungal response (Richardson et al., 2018; Yano et al., 2018). Most of these cells reside in the mucous membranes of the TGI, although additional molecules are recruited in response to infection. In addition to the transforming growth factor (TGF) involved in immunoregulation, epithelial cells express innate immunity receptors, such as pattern recognition receptors (PRRs) and a broad spectrum of antimicrobial peptides including alarmins, chemokines, and cytokines [such as IL-1, IL-6, IL-8, and tumor necrosis factor (TNF)]. All these factors initiate the first phase of the response and contribute to the recruitment of other cell populations (Doerflinger et al., 2014; Pericolini et al., 2015).

Epithelial cells can discern between the saprophytic and hyphal forms of *C. albicans*, leading to activation of the inflammatory response if necessary. Yeast to hypha transition and virulence factor production causes epithelial disruption and results in PMN recruitment, which, in turn, exacerbates the inflammation (Yano et al., 2018). Previous studies have identified the alarmins, S100A8 and S100A9, as key chemotactic mediators of the acute PMN response toward Candida infection (Yano et al., 2012).

According to Jaeger et al. (2013), epithelial cells express PRRs, which are capable of detecting the presence of microorganisms and sending activation signals to induce immune mediator secretion. There are 3 PRR families involved in the recognition of *Candida* pathogen-associated molecular patterns (PAMPs). The different PAMPs of *Candida* spp. recognized by these PRRs are well-characterized. Toll-like receptors (TLR)2, TLR4, TLR7, and TLR9 recognize phospholipomannans, *O*-mannoside-rich structures, *Candida* RNA, and *Candida* DNA, respectively. NOD-like receptors (NLRs) are found in the cytosol of cells. NLRP3 constitutes a part of the inflammasome, which is a cytoplasmic multiprotein complex with enzymatic activity. Other receptors, such as mannose receptor, dectin-2, DC-SIGN, and mincle recognize other glucidic structures, such as mannose and fucose, located in the *Candida* cell wall (Stoddart et al., 2011; Yano et al., 2018).

As described by Yu and Gaffen (2008), Th17 cells within the $CD4^+$ T lymphocyte population secrete IL-17A, IL-17F, IL-22, and IL-263, but differ in their production of cytokines such as IL-1, IL-6, and TGF3. IL-23 is an absolute requirement for the expansion, maintenance, and effector functions of this cell population. NKT cells, T lymphocytes, and group 3 innate lymphoid cells (ILC3s) produce abundant IL-17 and play important roles in defending the mucosa (Conti et al., 2009).

Identification of the key role of morphogenic changes in fungus and production of Sap as a virulence factor that activates the local inflammatory response have been associated with the discovery of mutations and genetic polymorphisms in the PRRs (Kalia et al., 2019) and their activation pathways. These observations collectively highlight the mechanism of VVC pathogenesis.

Biofilm formation in RVVC is usually related to the host immune system, when evasion of the defense system occurs at both humoural and acquired levels. Complement activation is known to be decreased in biofilms compared to that in plankton cells, and altered phagocytosis occurs due to the surrounding extracellular matrix of polymeric substances (Duggan et al., 2015).

It is important to highlight that persister cells that remain latent inside the biofilm evade elimination by macrophages (Mina and Marques, 2016; Wuyts et al., 2018). Therefore, understanding the contributions of these biofilms in fungal burden and in shaping subsequent strategies that influence and modulate the local immunopathogenic response is imperative for the development of efficient therapeutic modalities.

Emerging therapeutic approaches have centered on harnessing the complex interaction between commensal and pathogenic organisms in the vaginal environment. This is implemented mainly by diets rich in probiotics or vaginally administered probiotics, and this has been shown to restore the vaginal microbiota and decrease the incidence of VVC/RVVC. The work of Miyazima et al. (2017) provides support to these claims.

Combinations of prebiotics and probiotics, also called symbiotics, not only have therapeutic applications in infections in the intestinal tract but also for the urogenital area (Olveira and González-Molero, 2016).

Special care is taken with infections associated with mucosal devices (Nett, 2016). In these cases, inhibition of yeast adhesion to surfaces or devices (coating surfaces) constitute an important

therapeutic aspect for patients with a catheter or similar device inserted in the urogenial tract (Palmieri et al., 2018).

Novel associations, emerging drugs, and new activities are being studied in response to yeasts in *Candida* spp. biofilms, as described in the previous section (Fosso et al., 2018; Thamban Chandrika et al., 2018; Černáková et al., 2019).

The resolution of these challenges would enable important advances in understanding and therapeutic management of this mycosis. Here, we summarize the potential therapeutic targets in three parts: (a) those aimed at inhibiting or eliminating biofilms, (b) those intervening in the immune response, and (c) those mediated by probiotics.

CONCLUSION

Mycological diagnosis requires a comprehensive knowledge of the complex mechanisms underlying the interaction between a fungus and its host, and the identification of fungi is not solely limited to complete and fine technical handling in the laboratory. Fungi are eukaryotic entities with a markedly more intricate physiology and pathophysiology than viruses or bacteria, and they are an increasingly frequent cause of morbidity and mortality.

Rapid and accurate identification of pathogenic yeasts is an objective in proper patient management, especially for fungal infection control. Incorporation of modern methodologies based on molecular, genomic, proteomic, and genetic engineering techniques has facilitated the identification of different strains of *Candida* spp. These methodologies have contributed toward preventing the irrational use of antifungals and selecting appropriate empirical therapy.

Candida spp. biofilms have considerable clinical repercussions in VVC/RVVC owing to the increasing frequency in resistance to antifungals presented by these patients. The capacity of *Candida* spp. strains to acquire resistance confers various advantages, such as the colonization of host tissues, expression of virulent characteristics, metabolic cooperation, efficient capture of nutrients, cell–cell communication, and exchange of genetic material, which provide a considerable ecological advantage, as it protects against antifungals.

Thus, the genes involved in biofilm formation and development as well as the quorum-sensing systems are considered new targets in the development of specific inhibitors as an alternative to currently available treatments.

The ability of yeasts of the genus *Candida* to generate a biofilm is multifactorial and generally considered to be dependent on the site of infection, species and strain involved, and microenvironment in which it develops. Thus, as presented in this manuscript, the virulence attribute is not exclusive to a particular *Candida* species and new strains with greater formative capacity may emerge any time.

Although the *in vitro* systems studied in the present study had certain limitations, they allowed simultaneous processing of a large number of samples, which is ideal for screening. The systems also enabled easy testing of various physicochemical and biochemical parameters as well as studying the activity of antimicrobial agents. From a genomic point of view, the systems allowed us to analyze the genes involved in biofilm regulation and formation in the strains capable of forming biofilms *(in situ)*.

In vivo studies in murine VVC/RVVC models are commonly used to study *C. albicans* infection. Using these models, we will first investigate the virulence factors associated with *Candida* spp., including adhesins, aspartyl proteases, and hydrophobic properties. Second, we will analyze the factors favoring such infections, such as alterations in the bacterial flora. Third, we will examine the immune response to this infection in mice with genetic alterations. Finally, we can evaluate antifungal molecules through pharmacokinetic studies; prophylactic, therapeutic, and new molecule models; synergism studies; and *in vitro, in vivo,* and *ex vivo* correlation analyses.

The future of *Candida* spp. infection biology should simultaneously integrate the study of pathogenic factor analysis and host immunological characteristics to generate a comprehensive and detailed assessment of host-pathogen interactions. Therefore, the new VVC/RVVC approach aims to not only control fungal load, but also develop strategies targeted for modulating the local immunopathogenic response.

Finally, we must be particularly careful with immunocompromised patients with VVC/RVVC, as the release of new fungal cells from the biofilm may spread the infection throughout the body, which can lead to systemic candidiasis.

AUTHOR CONTRIBUTIONS

CR-C conceived, designed, and wrote the review. EM-H, MC-G, and AL-B provided the ideas and contributed to writing the manuscript. GF, MF, ME-S, and JG-C addressed the questions related to bibliography and summaries. All the authors have read and approved the final version of the manuscript.

REFERENCES

Abrão, P. H., Pizi, R. B., de Souza, T. B., Silva, N. C., Fregnan, A. M., Silva, F. N., et al. (2015). Synthesis and biological evaluation of new eugenol mannich bases as promising antifungal agents. *Chem. Biol. Drug Des.* 86, 459–465. doi: 10.1111/cbdd.12504

Achilles, S. L., Austin, M. N., Meyn, L. A., Mhlanga, F., Chirenje, Z. M., and Hillier, S. L. (2018). Impact of contraceptive initiation on vaginal microbiota. *Am. J. Obstet. Gynecol.* 218, 622.e1–622.e10. doi: 10.1016/j.ajog.2018.02.017

Agustín, M., Viceconte, F. R., Vela Gurovic, M. S., Costantino, A., and Brugnoni, L. I. (2019). Effect of quorum sensing molecules and natamycin on biofilms of *Candida tropicalis* and other yeasts isolated from industrial juice filtration membranes. *J. Appl. Microbiol.* 126, 1808–1820. doi: 10.1111/jam.1424

Almshawit, H., Macreadie, I., and Grando, D. (2014). A simple and inexpensive device for biofilm analysis. *J. Microbiol. Methods* 98, 59–63. doi: 10.1016/j.mimet.2013.12.020

Alyautdina, O. S., and Esina, E. V. (2019). Immunological methods for treatment of vulvovaginal infections in the preconception period. *J. Med. Life* 12, 368–373. doi: 10.25122/jml-2019-0068

Andreani, E. S., Villa, F., Cappitelli, F., Krasowska, A., Biniarz, P., Łukaszewicz, M., et al. (2017). Coating polypropylene surfaces with protease weakens the adhesion and increases the dispersion of Candida albicans cells. *Biotechnol. Lett.* 39, 423–428. doi: 10.1007/s10529-016-2262-5

Araújo, D., Henriques, M., and Silva, S. (2017). Portrait of *Candida* species biofilm regulatory network genes. *Trends Microbiol.* 25, 62–75. doi: 10.1016/j.tim.2016.09.004

Araújo Paulo, de Medeiros, M., Vieira, de Melo, A. P., Maia, de Sousa, A. M., et al. (2017). Characterization of virulence factors of vaginal and anal isolates of *Candida albicans* sequentially obtained from patients with vulvovaginal candidiasis in north-east Brazil. *J. Mycol. Med.* 27, 567–572. doi: 10.1016/j.mycmed.2017.06.002

Ardehali, S. H., Azimi, T., Fallah, F., Aghamohammadi, N., Alimehr, S., Karimi, A. M., et al. (2019). Molecular detection of ALS1, ALS3, HWP1 and SAP4 genes in *Candida* genus isolated from hospitalized patients in Intensive Care Unit, Tehran, Iran. *Cell. Mol. Biol.* 65, 15–22.

Aznar-Marin, P., Galan-Sanchez, F., Marin-Casanova, P., García-Martos, P., and Rodríguez-Iglesias, M. (2016). Candida nivariensis as a new emergent agent of vulvovaginal candidiasis: description of cases and review of published studies. *Mycopathologia* 181, 445–449. doi: 10.1007/s11046-015-9978-y

Bandara, H. M., Cheung, B. P., Watt, R. M., Jin, L. J., and Samaranayake, L. P. (2013). Secretory products of *Escherichia coli* biofilm modulate *Candida* biofilm formation and hyphal development. *J. Investig. Clin. Dent.* 4, 186–199. doi: 10.1111/jicd.12048

Basas, J., Palau, M., Gomis, X., Almirante, B., and Gavaldà, J. (2019). Efficacy of liposomal amphotericin B and anidulafungin using an antifungal lock technique (ALT) for catheter-related *Candida albicans* and *Candida glabrata* infections in an experimental model. *PLoS One* 14:e0212426. doi: 10.1371/journal.pone.0212426

Basmaciyan, L., Bon, F., Paradis, T., Lapaquette, P., and Dalle, F. (2019). Candida albicans interactions with the host: crossing the intestinal epithelial barrier. *Tissue Barr.* 7:1612661. doi: 10.1080/21688370.2019.1612661

Becherelli, M., Tao, J., and Ryder, N. S. (2013). Involvement of heat shock proteins in *Candida albicans* biofilm formation. *J. Mol. Microbiol. Biotechnol.* 23, 396–400. doi: 10.1159/000351619

Beitelshees, M., Hill, A., Jones, C. H., and Pfeifer, B. A. (2018). Phenotypic variation during biofilm formation: implications for anti-biofilm therapeutic design. *Materials* 11:1086. doi: 10.3390/ma11071086

Bitew, A., and Abebaw, Y. (2018). Vulvovaginal candidiasis: species distribution of Candida and their antifungal susceptibility pattern. *BMC Womens Health* 18:94. doi: 10.1186/s12905-018-0607-z

Blostein, F., Levin-Sparenberg, E., Wagner, J., and Foxman, B. (2017). Recurrent vulvovaginal candidiasis. *Ann. Epidemiol.* 27, 575.e3–582.e3. doi: 10.1016/j.annepidem.2017.08.010

Bradford, L. L., Chibucos, M. C., Ma, B., Bruno, V., and Ravel, J. (2017). Vaginal *Candida* spp. genomes from women with vulvovaginal candidiasis. *Pathog. Dis.* 75:ftx061. doi: 10.1093/femspd/ftx061

Brown, S. E., Schwartz, J. A., Robinson, C. K., O'Hanlon, D. E., Bradford, L. L., He, X., et al. (2019). The vaginal microbiota and behavioral factors associated with genital *Candida albicans* detection in reproductive-age women. *Sex. Transm. Dis.* 46, 753–758. doi: 10.1097/OLQ.0000000000001066

Bujdáková, H. (2016). Management of Candida biofilms: state of knowledge and new options for prevention and eradication. *Fut. Microbiol.* 11, 235–251. doi: 10.2217/fmb.15.139

Burgain, A., Pic, É, Markey, L., Tebbji, F., Kumamoto, C. A., and Sellam, A. (2019). A novel genetic circuitry governing hypoxic metabolic flexibility, commensalism and virulence in the fungal pathogen *Candida albicans*. *PLoS Pathog.* 15:e1007823. doi: 10.1371/journal.ppat.1007823

Carradori, S., Bizzarri, B., D'Ascenzio, M., De Monte, C., Grande, R., Rivanera, D., et al. (2017). Synthesis, biological evaluation and quantitative structure-active relationships of 1,3-thiazolidin-4-one derivatives. A promising chemical scaffold endowed with high antifungal potency and low cytotoxicity. *Eur. J. Med. Chem.* 140, 274–292. doi: 10.1016/j.ejmech.2017.09.026

Carrano, G., Paulone, S., Lainz, L., Sevilla, M. J., Blasi, E., and Moragues, M. D. (2019). Anti-*Candida albicans* germ tube antibodies reduce in vitro growth and biofilm formation of *C. albicans*. *Rev. Iberoam. Micol.* 36, 9–16. doi: 10.1016/j.riam.2018.07.005

Cassone, A. (2015). Vulvovaginal *Candida albicans* infections: pathogenesis, immunity and vaccine prospects. *BJOG* 122, 785–794. doi: 10.1111/1471-0528.12994

Cassone, A. (2018). The case for an expanded concept of trained immunity. *mBio* 9:e00570-18. doi: 10.1128/mBio.00570-18

Cavalheiro, M., and Teixeira, M. C. (2018). Candida biofilms: threats, challenges, and promising strategies. *Front. Med.* 5:28. doi: 10.3389/fmed.2018.00028

Černáková, L., Light, C., Salehi, B., Rogel-Castillo, C., Victoriano, M., Martorell, M., et al. (2019). Novel therapies for biofilm-based *Candida* spp. infections. *Adv. Exp. Med. Biol.* 1214, 93–123. doi: 10.1007/5584_2019_400

Chandra, J., and Mukherjee, P. K. (2015). Candida biofilms: development, architecture, and resistance. *Microbiol. Spectr.* 3:10.1128/microbiolsec.MB–0020–2015. doi: 10.1128/microbiolspec.MB-0020-2015

Chatterjee, S., Alampalli, S. V., Nageshan, R. K., Chettiar, S. T., Joshi, S., and Tatu, U. S. (2015). Draft genome of a commonly misdiagnosed multidrug resistant pathogen *Candida auris*. *BMC Genomics* 16:686. doi: 10.1186/s12864-015-1863-z

Chen, C. G., Yang, Y. L., Tseng, K. Y., Shih, H. I., Liou, C. H., Lin, C. C., et al. (2009). Rep1p negatively regulating MDR1 efflux pump involved in drug resistance in *Candida albicans*. *Fungal Genet. Biol.* 46, 714–720. doi: 10.1016/j.fgb.2009.06.003

Chowdhary, A., Prakash, A., Sharma, C., Kordalewska, M., Kumar, A., Sarma, S., et al. (2018). A multicentre study of antifungal susceptibility patterns among 350 Candida auris isolates (2009-17) in India: role of the ERG11 and FKS1 genes in azole and echinocandin resistance. *J. Antimicrob. Chemother.* 73, 891–899. doi: 10.1093/jac/dkx480

Connolly, L. A., Riccombeni, A., Grózer, Z., Holland, L. M., Lynch, D. B., Andes, D. R., et al. (2013). The APSES transcription factor Efg1 is a global regulator that controls morphogenesis and biofilm formation in *Candida parapsilosis*. *Mol. Microbiol.* 90, 36–53. doi: 10.1111/mmi.12345

Conti, H. R., Shen, F., Nayyar, N., Stocum, E., Sun, J. N., Lindemann, M. J., et al. (2009). Th17 cells and IL-17 receptor signaling are essential for mucosal host defense against oral candidiasis. *J. Exp. Med.* 206, 299–311. doi: 10.1084/jem.20081463

Corsello, S., Spinillo, A., Osnengo, G., Penna, C., Guaschino, S., Beltrame, A., et al. (2003). An epidemiological survey of vulvovaginal candidiasis in Italy. *Eur J Obstet. Gynecol. Reprod. Biol.* 110, 66–72. doi: 10.1016/s0301-2115(03)00096-4

Costa, M., Silva, A., Silva, A., Lima, V., Bezerra-Silva, P. C., Rocha, S., et al. (2017). Essential oils from leaves of medicinal plants of Brazilian flora: chemical composition and activity against *Candida* species. *Medicines* 4:27. doi: 10.3390/medicines4020027

Cota, E., and Hoyer, L. L. (2015). The Candida albicans agglutinin-like sequence family of adhesins: functional insights gained from structural analysis. *Fut. Microbiol.* 10, 1635–1548. doi: 10.2217/fmb.15.79

Cui, J., Ren, B., Tong, Y., Dai, H., and Zhang, L. (2015). Synergistic combinations of antifungals and anti-virulence agents to fight against *Candida albicans*. *Virulence* 6, 362–371. doi: 10.1080/21505594.2015.1039885

Dabiri, S., Shams-Ghahfarokhi, M., and Razzaghi-Abyaneh, M. (2018). Comparative analysis of proteinase, phospholipase, hydrophobicity and biofilm forming ability in *Candida* species isolated from clinical specimens. *J. Mycol. Med.* 28, 437–442. doi: 10.1016/j.mycmed.2018.04.009

Davani-Davari, D., Negahdaripour, M., Karimzadeh, I., Seifan, M., Mohkam, M., Masoumi, S. J., et al. (2019). Prebiotics: definition, types, sources, mechanisms, and clinical applications. *Foods* 8:92. doi: 10.3390/foods8030092

Denning, D. W., Kneale, M., Sobel, J. D., and Rautemaa-Richardson, R. (2018). Global burden of recurrent vulvovaginal candidiasis: a systematic review. *Lancet. Infect. Dis.* 18, e339–e347. doi: 10.1016/S1473-3099(18)30103-8

de Barros, P. P., Rossoni, R. D., de Souza, C. M., Scorzoni, L., Fenley, J. C., and Junqueira, J. C. (2020). Candida biofilms: an update on developmental mechanisms and therapeutic challenges. *Mycopathologia* 185, 415–424. doi: 10.1007/s11046-020-00445-w

de Oliveira, D., Silva, L. B., da Silva, B. V., Borges, T. C., Marques, B. C., Dos Santos, M. B., et al. (2019). A new acridone with antifungal properties against *Candida* spp. and dermatophytes, and antibiofilm activity against *C. albicans*. *J. Appl. Microbiol.* 127, 1362–1372. doi: 10.1111/jam.14381

de Souza, T. B., Brito, K. M., Silva, N. C., Rocha, R. P., de Sousa, G. F., Duarte, L. P., et al. (2016). New eugenol glucoside-based derivative shows fungistatic and fungicidal activity against opportunistic *Candida glabrata*. *Chem. Biol. Drug Des.* 87, 83–90. doi: 10.1111/cbdd.12625

Diezmann, S., Leach, M. D., and Cowen, L. E. (2015). Functional divergence of Hsp90 genetic interactions in biofilm and planktonic cellular states. *PLoS One* 10:e0137947. doi: 10.1371/journal.pone.0137947

Dižová, S., and Bujdáková, H. (2017). Properties and role of the quorum sensing molecule farnesol in relation to the yeast *Candida albicans*. *Die Pharm.* 72, 307–312. doi: 10.1691/ph.2017.6174

Djohan, V., Angora, K. E., Vanga-Bosson, A. H., Konaté, A., Kassi, K. F., Kiki-Barro, P., et al. (2019). Recurrent vulvo-vaginal candidiasis in Abidjan (Côte d'Ivoire): aetiology and associated factors. *J. Mycol. Med.* 29, 127–131. doi: 10.1016/j.mycmed.2019.04.002

Doerflinger, S. Y., Throop, A. L., and Herbst-Kralovetz, M. M. (2014). Bacteria in the vaginal microbiome alter the innate immune response and barrier properties of the human vaginal epithelia in a species-specific manner. *J. Infect. Dis.* 209, 1989–1999. doi: 10.1093/infdis/jiu004

Dominguez, E., Zarnowski, R., Sanchez, H., Covelli, A. S., Westler, W. M., Azadi, P., et al. (2018). Conservation and divergence in the *Candida* species biofilm matrix mannan-glucan complex structure, function, and genetic control. *mBio* 9:e00451-18. doi: 10.1128/mBio.00451-18

Duggan, S., Leonhardt, I., Hünniger, K., and Kurzai, O. (2015). Host response to *Candida albicans* bloodstream infection and sepsis. *Virulence* 6, 316–326. doi: 10.4161/21505594.2014.988096

El-Houssaini, H. H., Elnabawy, O. M., Nasser, H. A., and Elkhatib, W. F. (2019). Correlation between antifungal resistance and virulence factors in *Candida albicans* recovered from vaginal specimens. *Microb. Pathog.* 128, 13–19. doi: 10.1016/j.micpath.2018.12.028

Fan, Y., He, H., Dong, Y., and Pan, H. (2013). Hyphae-specific genes HGC1, ALS3, HWP1, and ECE1 and relevant signaling pathways in *Candida albicans*. *Mycopathologia* 176, 329–335. doi: 10.1007/s11046-013-9684-6

Feng, W., Yang, J., Pan, Y., Xi, Z., Qiao, Z., and Ma, Y. (2016). The correlation of virulence, pathogenicity, and itraconazole resistance with SAP activity in *Candida albicans* strains. *Can. J. Microbiol.* 62, 173–178. doi: 10.1139/cjm-2015-0457

Fernandes, L., Oliveira, A., Henriques, M., and Rodrigues, M. E. (2020). Honey as a strategy to fight *Candida tropicalis* in mixed-biofilms with *Pseudomonas aeruginosa*. *Antibiotics* 9:43. doi: 10.3390/antibiotics9020043

Finkel, J. S., Xu, W., Huang, D., Hill, E. M., Desai, J. V., Woolford, C. A., et al. (2012). Portrait of *Candida albicans* adherence regulators. *PLoS Pathog.* 8:e1002525. doi: 10.1371/journal.ppat.1002525

Flemming, H. C., and Wingender, J. (2010). The biofilm matrix. *Nat. Rev. Microbiol.* 8, 623–633. doi: 10.1038/nrmicro2415

Fosso, M. Y., Shrestha, S. K., Thamban Chandrika, N., Dennis, E. K., Green, K. D., and Garneau-Tsodikova, S. (2018). Differential effects of linkers on the activity of amphiphilic tobramycin antifungals. *Molecules* 23:899. doi: 10.3390/molecules23040899

Freire, F., de Barros, P. P., Pereira, C. A., Junqueira, J. C., and Jorge, A. (2018). Photodynamic inactivation in the expression of the *Candida albicans* genes ALS3, HWP1, BCR1, TEC1, CPH1, and EFG1 in biofilms. *Lasers Med. Sci.* 33, 1447–1454. doi: 10.1007/s10103-018-2487-8

Gabrielli, E., Pericolini, E., Ballet, N., Roselletti, E., Sabbatini, S., Mosci, P., et al. (2018). *Saccharomyces cerevisiae*-based probiotic as novel anti-fungal and anti-inflammatory agent for therapy of vaginal candidiasis. *Benef. Microbes* 9, 219–230. doi: 10.3920/BM2017.0099

Ganguly, S., Bishop, A. C., Xu, W., Ghosh, S., Nickerson, K. W., Lanni, F., et al. (2011). Zap1 control of cell-cell signaling in *Candida albicans* biofilms. *Eukaryot. Cell* 10, 1448–1454. doi: 10.1128/EC.05196-11

Ghasemi, M., Etemadi, A., Nedaei, M., Chiniforush, N., and Pourhajibagher, M. (2019). Antimicrobial efficacy of photodynamic therapy using two different light sources on the titanium-adherent biofilms of *Aggregatibacter actinomycetemcomitans*: an in vitro study. *Photodiagn. Photodyn. Ther.* 26, 85–89. doi: 10.1016/j.pdpdt.2019.03.004

Gille, C., Böer, B., Marschal, M., Urschitz, M. S., Heinecke, V., Hund, V., et al. (2016). Effect of probiotics on vaginal health in pregnancy. EFFPRO, a randomized controlled trial. *Am. J. Obstet. Gynecol.* 215, 608.e1–608.e7. doi: 10.1016/j.ajog.2016.06.021

Glazier, V. E., Murante, T., Murante, D., Koselny, K., Liu, Y., Kim, D., et al. (2017). Genetic analysis of the *Candida albicans* biofilm transcription factor network using simple and complex haploinsufficiency. *PLoS Genet.* 13:e1006948. doi: 10.1371/journal.pgen.1006948

Gonçalves, B., Ferreira, C., Alves, C. T., Henriques, M., Azeredo, J., and Silva, S. (2016). Vulvovaginal candidiasis: epidemiology, microbiology and risk factors. *Crit. Rev. Microbiol.* 42, 905–927. doi: 10.3109/1040841X.2015.1091805

Gu, W., Xu, D., and Sun, S. (2015). In vitro models to study *Candida albicans* biofilms. *J. Pharm. Drug Dev.* 3:301. doi: 10.15744/2348-9782.3.301

Guan, G., Xie, J., Tao, L., Nobile, C. J., Sun, Y., Cao, C., et al. (2013). Bcr1 plays a central role in the regulation of opaque cell filamentation in *Candida albicans*. *Mol. Microbiol.* 89, 732–750. doi: 10.1111/mmi.12310

Gulati, M., and Nobile, C. J. (2016). Candida albicans biofilms: development, regulation, and molecular mechanisms. *Microbes Infect.* 18, 310–321. doi: 10.1016/j.micinf.2016.01.002

Guzel, A. B., Ilkit, M., Akar, T., Burgut, R., and Demir, S. C. (2011). Evaluation of risk factors in patients with vulvovaginal candidiasis and the value of chromID Candida agar versus CHROMagar Candida for recovery and presumptive identification of vaginal yeast species. *Med. Mycol.* 49, 16–25. doi: 10.3109/13693786.2010.497972

Hall, C. L., and Lee, V. T. (2018). Cyclic-di-GMP regulation of virulence in bacterial pathogens. *Wiley Interdiscip. Rev. RNA* 9:10.1002/wrna.1454. doi: 10.1002/wrna.1454

Handalishy, I. I., Behery, M. A., Elkhouly, M., Farag, E. A., and Elsheikh, W. A. (2014). Comparative study between probiotic vaginal tampons and oral metronidazole in treatmentof bacterial vaginosis. *Al_Azhar. Assiut. Med. J.* 12(Suppl. 2), 185–203.

Harriott, M. M., Lilly, E. A., Rodriguez, T. E., Fidel, P. L., and Noverr, M. C. (2010). *Candida albicans* forms biofilms on the vaginal mucosa. *Microbiology* 156(Pt 12), 3635–3644. doi: 10.1099/mic.0.039354-0

Harrison, J. J., Ceri, H., Yerly, J., Rabiei, M., Hu, Y., Martinuzzi, R., et al. (2007a). Metal ions may suppress or enhance cellular differentiation in *Candida albicans* and *Candida tropicalis* biofilms. *Appl. Environ. Microbiol.* 73, 4940–4949. doi: 10.1128/AEM.02711-06

Harrison, J. J., Turner, R. J., and Ceri, H. (2007b). A subpopulation of *Candida albicans* and *Candida tropicalis* biofilm cells are highly tolerant to chelating agents. *FEMS Microbiol. Lett.* 272, 172–181. doi: 10.1111/j.1574-6968.2007.00745.x

Hewadmal, N., and Jangra, S. (2019). A review on probiotic and health benefits of probiotics. *Int. J. Curr. Microbiol. Appl. Sci.* 8, 1863–1880. doi: 10.20546/ijcmas.2019.805.218

Hirota, K., Yumoto, H., Sapaar, B., Matsuo, T., Ichikawa, T., and Miyake, Y. (2017). Pathogenic factors in Candida biofilm-related infectious diseases. *J. Appl. Microbiol.* 122, 321–330. doi: 10.1111/jam.13330

Holland, L. M., Schröder, M. S., Turner, S. A., Taff, H., Andes, D., Grózer, Z., et al. (2014). Comparative phenotypic analysis of the major fungal pathogens *Candida parapsilosis* and *Candida albicans*. *PLoS Pathog.* 10:e1004365. doi: 10.1371/journal.ppat.1004365

Hoque, J., Akkapeddi, P., Yadav, V., Manjunath, G. B., Uppu, D. S., Konai, M. M., et al. (2015). Broad spectrum antibacterial and antifungal polymeric paint materials: synthesis, structure-activity relationship, and membrane-active mode of action. *ACS Appl. Mater. Interfaces* 7, 1804–1815. doi: 10.1021/am507482y

Hu, J., Guan, G., Dai, Y., Tao, L., Zhang, J., Li, H., et al. (2016). Phenotypic diversity and correlation between white-opaque switching and the CAI microsatellite locus in *Candida albicans*. *Curr. Genet.* 62, 585–593. doi: 10.1007/s00294-016-0564-8

Ichikawa, T., Kutsumi, Y., Sadanaga, J., Ishikawa, M., Sugita, D., and Ikeda, R. (2019). Adherence and cytotoxicity of *Candida* spp. to HaCaT and A549 cells. *Med. Mycol. J.* 60, 5–10. doi: 10.3314/mmj.18-00011

Inglis, D. O., and Sherlock, G. (2013). Ras signaling gets fine-tuned: regulation of multiple pathogenic traits of *Candida albicans*. *Eukaryot. Cell* 12, 1316–1325. doi: 10.1128/EC.00094-13

Jaeger, M., Plantinga, T. S., Joosten, L. A., Kullberg, B. J., and Netea, M. G. (2013). Genetic basis for recurrent vulvo-vaginal candidiasis. *Curr. Infect. Dis. Rep.* 15, 136–142. doi: 10.1007/s11908-013-0319-3

Jiang, L., Wang, J., Asghar, F., Snyder, N., and Cunningham, K. W. (2018). CaGdt1 plays a compensatory role for the calcium pump CaPmr1 in the regulation of calcium signaling and cell wall integrity signaling in *Candida albicans*. *Cell Commun. Signal.* 16:33. doi: 10.1186/s12964-018-0246-x

Joseph, M. R., Al-Hakami, A. M., Assiry, M. M., Jamil, A. S., Assiry, A. M., Shaker, M. A., et al. (2015). In vitro anti-yeast activity of chloramphenicol: a preliminary report. *J. Mycol. Med.* 25, 17–22. doi: 10.1016/j.mycmed.2014.10.019

Kadry, A. A., El-Ganiny, A. M., and El-Baz, A. M. (2018). Relationship between Sap prevalence and biofilm formation among resistant clinical isolates of *Candida albicans*. *Afr. Health Sci.* 18, 1166–1174. doi: 10.4314/ahs.v18i4.37

Kalaiarasan, K., Singh, R., and Chaturvedula, L. (2018). Changing virulence factors among vaginal non-albicans *Candida* species. *Indian J. Med. Microbiol.* 36, 364–368. doi: 10.4103/ijmm.IJMM_18_94

Kalia, N., Singh, J., and Kaur, M. (2019). Immunopathology of recurrent vulvovaginal infections: new aspects and research directions. *Front. Immunol.* 10:2034. doi: 10.3389/fimmu.2019.02034

Karkowska-Kuleta, J., Satala, D., Bochenska, O., Rapala-Kozik, M., and Kozik, A. (2019). Moonlighting proteins are variably exposed at the cell surfaces of *Candida glabrata*, *Candida parapsilosis* and *Candida tropicalis* under certain growth conditions. *BMC Microbiol.* 19:149. doi: 10.1186/s12866-019-1524-5

Khosravi Rad, K., Falahati, M., Roudbary, M., Farahyar, S., and Nami, S. (2016). Overexpression of MDR-1 and CDR-2 genes in fluconazole resistance of *Candida albicans* isolated from patients with vulvovaginal candidiasis. *Curr. Med. Mycol.* 2, 24–29. doi: 10.18869/acadpub.cmm.2.4.24

Köhler, G. A., Assefa, S., and Reid, G. (2012). Probiotic interference of *Lactobacillus rhamnosus* GR-1 and Lactobacillus reuteri RC-14 with the opportunistic fungal pathogen *Candida albicans*. *Infect. Dis. Obstet. Gynecol.* 2012, 636474. doi: 10.1155/2012/636474

Kovács, R., Nagy, F., Tóth, Z., Bozó, A., Balázs, B., and Majoros, L. (2019). Synergistic effect of nikkomycin Z with caspofungin and micafungin against *Candida albicans* and *Candida parapsilosis* biofilms. *Lett. Appl. Microbiol.* 69, 271–278. doi: 10.1111/lam.13204

Kumar, D., Banerjee, T., Pratap, C. B., and Tilak, R. (2015). Itraconazole-resistant *Candida auris* with phospholipase, proteinase and hemolysin activity from a case of vulvovaginitis. *J. Infect. Dev. Ctries* 9, 435–437. doi: 10.3855/jidc.4582

Leiva-Peláez, O., Gutiérrez-Escobedo, G., López-Fuentes, E., Cruz-Mora, J., De Las Peñas, A., and Castaño, I. (2018). Molecular characterization of the silencing complex SIR in *Candida glabrata* hyperadherent clinical isolates. *Fungal Genet. Biol.* 118, 21–31. doi: 10.1016/j.fgb.2018.05.005

Leonhard, V., Alasino, R. V., Munoz, A., and Beltramo, D. M. (2018). Silver nanoparticles with high loading capacity of amphotericin B: characterization, bactericidal and antifungal effects. *Curr. Drug Deliv.* 15, 850–859. doi: 10.2174/1567201814666170918162337

Li, X., Wu, B., Chen, H., Nan, K., Jin, Y., Sun, L., et al. (2018). Recent developments in smart antibacterial surfaces to inhibit biofilm formation and bacterial infections. *J. Mater. Chem. B* 6, 4274–4292. doi: 10.1039/c8tb01245h

Li, X., Zhao, Y., Huang, X., Yu, C., Yang, Y., and Sun, S. (2017). Ambroxol hydrochloride combined with fluconazole reverses the resistance of *Candida albicans* to fluconazole. *Front. Cell Infect Microbiol.* 7:124. doi: 10.3389/fcimb.2017.00124

Lindsay, A. K., Deveau, A., Piispanen, A. E., and Hogan, D. A. (2012). Farnesol and cyclic AMP signaling effects on the hypha-to-yeast transition in *Candida albicans*. *Eukaryot. Cell* 11, 1219–1225. doi: 10.1128/EC.00144-12

Liu, Y., and Filler, S. G. (2011). Candida albicans Als3, a multifunctional adhesin and invasin. *Eukaryot. Cell* 10, 168–173. doi: 10.1128/EC.00279-10

Madende, M., Albertyn, J., Sebolai, O., and Pohl, C. H. (2020). Caenorhabditis elegans as a model animal for investigating fungal pathogenesis. *Med. Microbiol. Immunol.* 209, 1–13. doi: 10.1007/s00430-019-00635-4

Mahmoudi Rad, M., Zafarghandi, S., Abbasabadi, B., and Tavallaee, M. (2011). The epidemiology of *Candida* species associated with vulvovaginal candidiasis in an Iranian patient population. *Eur. J. Obstet. Gynecol. Reprod. Biol.* 155, 199–203. doi: 10.1016/j.ejogrb.2010.11.022

Marak, M. B., and Dhanashree, B. (2018). Antifungal susceptibility and biofilm production of *Candida* spp. isolated from clinical samples. *Int. J. Microbiol.* 2018:7495218. doi: 10.1155/2018/7495218

Maraki, S., Mavromanolaki, V. E., Stafylaki, D., Nioti, E., Hamilos, G., and Kasimati, A. (2019). Epidemiology and antifungal susceptibility patterns of Candida isolates from Greek women with vulvovaginal candidiasis. *Mycoses* 62, 692–697. doi: 10.1111/myc.12946

Martins, N., Ferreira, I. C. F. R., Henriques, M., and Silva, S. (2016). In vitro anti-Candida activity of *Glycyrrhiza glabra* L. *Ind. Crop. Prod.* 83, 81–85. doi: 10.1016/j.indcrop.2015.12.029

Mathé, L., and Van Dijck, P. (2013). Recent insights into *Candida albicans* biofilm resistance mechanisms. *Curr. Genet.* 59, 251–264. doi: 10.1007/s00294-013-0400-3

McCall, A. D., Kumar, R., and Edgerton, M. (2018). *Candida albicans* Sfl1/Sfl2 regulatory network drives the formation of pathogenic microcolonies. *PLoS Pathog.* 14:e1007316. doi: 10.1371/journal.ppat.1007316

McCall, A. D., Pathirana, R. U., Prabhakar, A., Cullen, P. J., and Edgerton, M. (2019). *Candida albicans* biofilm development is governed by cooperative attachment and adhesion maintenance proteins. *NPJ Biofilms Microbiomes* 5:21. doi: 10.1038/s41522-019-0094-5

Mehmood, A., Liu, G., Wang, X., Meng, G., Wang, C., and Liu, Y. (2019). Fungal quorum-sensing molecules and inhibitors with potential antifungal activity: a review. *Molecules* 24:1950. doi: 10.3390/molecules24101950

Mendelsohn, S., Pinsky, M., Weissman, Z., and Kornitzer, D. (2017). Regulation of the *Candida albicans* hypha-inducing transcription factor Ume6 by the CDK1 cyclins Cln3 and Hgc1. *mSphere* 2:e00248-16. doi: 10.1128/mSphere.00248-16

Min, K., Biermann, A., Hogan, D. A., and Konopka, J. B. (2018). Genetic analysis of NDT80 family transcription factors in *Candida albicans* using new CRISPR-Cas9 approaches. *mSphere* 3:e00545-18. doi: 10.1128/mSphere.00545-18

Min, K., Naseem, S., and Konopka, J. B. (2019). N-acetylglucosamine regulates morphogenesis and virulence pathways in fungi. *J. Fungi* 6:E8. doi: 10.3390/jof6010008

Mina, E. G., and Marques, C. N. (2016). Interaction of *Staphylococcus aureus* persister cells with the host when in a persister state and following awakening. *Sci. Rep.* 6:31342. doi: 10.1038/srep31342

Miró, M. S., Rodríguez, E., Vigezzi, C., Icely, P. A., Gonzaga de Freitas-Araújo, M., Riera, F. O., et al. (2017). Vulvovaginal candidiasis: an old disease with new challenges. *Rev. Iberoam. Micol.* 34, 65–71. doi: 10.1016/j.riam.2016.11.006

Mitchell, K. F., Zarnowski, R., Sanchez, H., Edward, J. A., Reinicke, E. L., Nett, J. E., et al. (2015). Community participation in biofilm matrix assembly and function. *Proc. Natl. Acad. Sci. U.S.A.* 112, 4092–4097. doi: 10.1073/pnas.1421437112

Miyazima, T. Y., Ishikawa, K. H., Mayer, M., Saad, S., and Nakamae, A. (2017). Cheese supplemented with probiotics reduced the Candida levels in denture wearers-RCT. *Oral Dis.* 23, 919–925. doi: 10.1111/odi.12669

Modrzewska, B., and Kurnatowski, P. (2015). Adherence of *Candida* sp. to host tissues and cells as one of its pathogenicity features. *Ann. Parasitol.* 61, 3–9.

Moher, D., Shamseer, L., Clarke, M., Ghersi, D., Liberati, A., Petticrew, M., et al. (2015). Preferred reporting items for systematic review and meta-analysis protocols (PRISMA-P) 2015 statement. *Syst. Rev.* 4:1. doi: 10.1186/2046-4053-4-1

Monika, S. (2019). Virulence factors in *Candida* species. *Curr. Protein Pept. Sci.* 21, 313–323. doi: 10.2174/1389203720666190722152415

Monteiro, D. R., Arias, L. S., Fernandes, R. A., Deszo da Silva, L. F., de Castilho, M., da Rosa, T. O., et al. (2017). Antifungal activity of tyrosol and farnesol used in combination against *Candida* species in the planktonic state or forming biofilms. *J. Appl. Microbiol.* 123, 392–400. doi: 10.1111/jam.13513

Muzny, C. A., and Schwebke, J. R. (2015). Biofilms: an underappreciated mechanism of treatment failure and recurrence in vaginal infections. *Clin. Infect. Dis.* 61, 601–606. doi: 10.1093/cid/civ353

Naglik, J. R., Fidel, P. L. Jr., and Odds, F. C. (2008). Animal models of mucosal Candida infection. *FEMS Microbiol Lett.* 283, 129–139. doi: 10.1111/j.1574-6968.2008.01160.x

Navarro-Arias, M. J., Defosse, T. A., Dementhon, K., Csonka, K., Mellado-Mojica, E., Dias Valério, A., et al. (2016). Disruption of protein mannosylation affects *Candida guilliermondii* cell wall, immune sensing, and virulence. *Front. Microbiol.* 7:1951. doi: 10.3389/fmicb.2016.01951

Negri, M., Silva, S., Henriques, M., Azeredo, J., Svidzinski, T., and Oliveira, R. (2011). Candida tropicalis biofilms: artificial urine, urinary catheters and flow model. *Med. Mycol.* 49, 739–747. doi: 10.3109/13693786.2011.560619

Neppelenbroek, K. H., Seó, R. S., Urban, V. M., Silva, S., Dovigo, L. N., Jorge, J. H., et al. (2014). Identification of *Candida* species in the clinical laboratory: a review of conventional, commercial, and molecular techniques. *Oral dis.* 20, 329–344. doi: 10.1111/odi.12123

Nett, J. E. (2016). The host's reply to Candida biofilm. *Pathogens* 5:33. doi: 10.3390/pathogens5010033

Nett, J. E., Sanchez, H., Cain, M. T., Ross, K. M., and Andes, D. R. (2011). Interface of *Candida albicans* biofilm matrix-associated drug resistance and cell wall integrity regulation. *Eukaryot. Cell* 10, 1660–1669. doi: 10.1128/EC.05126-11

Nett, J. E., Zarnowski, R., Cabezas-Olcoz, J., Brooks, E. G., Bernhardt, J., Marchillo, K., et al. (2015). Host contributions to construction of three device-associated *Candida albicans* biofilms. *Infect. Immun.* 83, 4630–4638. doi: 10.1128/IAI.00931-15

Ng, H., and Dean, N. (2017). Dramatic improvement of CRISPR/Cas9 editing in *Candida albicans* by increased single guide RNA expression. *mSphere* 2:e00385-16. doi: 10.1128/mSphere.00385-16

Ni, L., Bruce, C., Hart, C., Leigh-Bell, J., Gelperin, D., Umansky, L., et al. (2009). Dynamic and complex transcription factor binding during an inducible response in yeast. *Genes Dev.* 23, 1351–1363. doi: 10.1101/gad.1781909

Ning, Y., Ling, J., and Wu, C. D. (2015). Synergistic effects of tea catechin epigallocatechin gallate and antimycotics against oral *Candida* species. *Arch. Oral Biol.* 60, 1565–1570. doi: 10.1016/j.archoralbio.2015.07.001

Nobile, C. J., Fox, E. P., Nett, J. E., Sorrells, T. R., Mitrovich, Q. M., Hernday, A. D., et al. (2012). A recently evolved transcriptional network controls biofilm development in *Candida albicans*. *Cell* 148, 126–138. doi: 10.1016/j.cell.2011.10.048

Nweze, E. I., Ghannoum, A., Chandra, J., Ghannoum, M. A., and Mukherjee, P. K. (2012). Development of a 96-well catheter-based microdilution method to test antifungal susceptibility of Candida biofilms. *J. Antimicrob. Chemother.* 67, 149–153. doi: 10.1093/jac/dkr429

Olveira, G., and González-Molero, I. (2016). An update on probiotics, prebiotics and symbiotics in clinical nutrition. *Endocrinol. Nutr.* 63, 482–494. doi: 10.1016/j.endonu.2016.07.006

Orsi, C. F., Borghi, E., Colombari, B., Neglia, R. G., Quaglino, D., Ardizzoni, A., et al. (2014). Impact of *Candida albicans* hyphal wall protein 1 (HWP1) genotype on biofilm production and fungal susceptibility to microglial cells. *Microb. Pathog.* 6, 20–27. doi: 10.1016/j.micpath.2014.03.003

Ozcan, K., Ilkit, M., Ates, A., Turac-Bicer, A., and Demirhindi, H. (2010). Performance of chromogenic *Candida agar* and CHROMagar Candida in recovery and presumptive identification of monofungal and polyfungal vaginal isolates. *Med. Mycol.* 48, 29–34. doi: 10.3109/13693780802713224

Padder, S. A., Prasad, R., and Shah, A. H. (2018). Quorum sensing: a less known mode of communication among fungi. *Microbiol. Res.* 210, 51–58. doi: 10.1016/j.micres.2018.03.007

Palmieri, V., Bugli, F., Cacaci, M., Perini, G., Maio, F., Delogu, G., et al. (2018). Graphene oxide coatings prevent *Candida albicans* biofilm formation with a controlled release of curcumin-loaded nanocomposites. *Nanomedicine* 13, 2867–2879. doi: 10.2217/nnm-2018-0183

Paluch, E., Rewak-Soroczyńska, J., Jędrusik, I., Mazurkiewicz, E., and Jermakow, K. (2020). Prevention of biofilm formation by quorum quenching. *Appl. Microbiol. Biotechnol.* 104, 1871–1881. doi: 10.1007/s00253-020-10349-w

Pankey, G., Ashcraft, D., Kahn, H., and Ismail, A. (2014). Time-kill assay and etest evaluation for synergy with polymyxin B and fluconazole against *Candida glabrata*. *Antimicrob. Agents Chemother.* 58, 5795–5800. doi: 10.1128/AAC.03035-14

Paulone, S., Ardizzoni, A., Tavanti, A., Piccinelli, S., Rizzato, C., Lupetti, A., et al. (2017). The synthetic killer peptide KP impairs *Candida albicans* biofilm in vitro. *PLoS One* 12:e0181278. doi: 10.1371/journal.pone.0181278

Pericolini, E., Gabrielli, E., Amacker, M., Kasper, L., Roselletti, E., Luciano, E., et al. (2015). Secretory aspartyl proteinases cause vaginitis and can mediate vaginitis caused by *Candida albicans* in mice. *mBio* 6:e00724. doi: 10.1128/mBio.00724-15

Peters, B. M., Yano, J., Noverr, M. C., and Fidel, P. L. Jr. (2014). Candida vaginitis: when opportunism knocks, the host responds. *PLoS Pathog.* 10:e1003965. doi: 10.1371/journal.ppat.1003965

Pierce, C. G., Vila, T., Romo, J. A., Montelongo-Jauregui, D., Wall, G., Ramasubramanian, A., et al. (2017). The *Candida albicans* biofilm matrix: composition, structure and function. *J. Fungi* 3:14. doi: 10.3390/jof3010014

Pohlers, S., Martin, R., Krüger, T., Hellwig, D., Hänel, F., Kniemeyer, O., et al. (2017). Lipid signaling via Pkh1/2 regulates fungal CO2 sensing through the kinase Sch9. *mBio* 8:e02211-16. doi: 10.1128/mBio.02211-16

Polke, M., Leonhardt, I., Kurzai, O., and Jacobsen, I. D. (2018). Farnesol signalling in *Candida albicans* - more than just communication. *Crit. Rev. Microbiol.* 44, 230–243. doi: 10.1080/1040841X.2017.1337711

Raman, N., Lee, M. R., Lynn, D. M., and Palecek, S. P. (2015). Antifungal activity of 14-Helical β-peptides against planktonic cells and biofilms of *Candida* Species. *Pharmaceuticals* 8, 483–503. doi: 10.3390/ph8030483

Richardson, J. P., Willems, H., Moyes, D. L., Shoaie, S., Barker, K. S., Tan, S. L., et al. (2018). Candidalysin drives epithelial signaling, neutrophil recruitment, and immunopathology at the vaginal mucosa. *Infect. Immun.* 86:e00645-17. doi: 10.1128/IAI.00645-17

Richmond, G. S., and Smith, T. K. (2011). Phospholipases A_1. *Int. J. Mol. Sci.* 12, 588–612. doi: 10.3390/ijms12010588

Riekhof, W. R., and Nickerson, K. W. (2017). Quorum sensing in *Candida albicans*: farnesol versus farnesoic acid. *FEBS Lett.* 591, 1637–1640. doi: 10.1002/1873-3468.12694

Rodríguez-Cerdeira, C., Gregorio, M. C., Molares-Vila, A., López-Barcenas, A., Fabbrocini, G., Bardhi, B., et al. (2019). Biofilms and vulvovaginal candidiasis. *Coll. Surf. B Biointerfaces* 174, 110–125. doi: 10.1016/j.colsurfb.2018.11.011

Samaranayake, Y. H., Ye, J., Yau, J. Y., Cheung, B. P., and Samaranayake, L. P. (2005). In vitro method to study antifungal perfusion in Candida biofilms. *J. Clin. Microbiol.* 43, 818–825. doi: 10.1128/JCM.43.2.818-825.2005

Saxena, P., Joshi, Y., Rawat, K., and Bisht, R. (2019). Biofilms: architecture, resistance, quorum sensing and control mechanisms. *Indian J. Microbiol.* 59, 3–12. doi: 10.1007/s12088-018-0757-6

Schaller, M., Bein, M., Korting, H. C., Baur, S., Hamm, G., Monod, M., et al. (2003). The secreted aspartyl proteinases Sap1 and Sap2 cause tissue damage in an in vitro model of vaginal candidiasis based on reconstituted human vaginal epithelium. *Infect. Immun.* 71, 3227–3234. doi: 10.1128/iai.71.6.3227-3234.2003

Schaller, M., Korting, H. C., Borelli, C., Hamm, G., and Hube, B. (2005). *Candida albicans*-secreted aspartic proteinases modify the epithelial cytokine response in an in vitro model of vaginal candidiasis. *Infect. Immun.* 73, 2758–2765. doi: 10.1128/IAI.73.5.2758-2765.2005

Seleem, D., Benso, B., Noguti, J., Pardi, V., and Murata, R. M. (2016). In vitro and in vivo antifungal activity of lichochalcone-A against *Candida albicans* biofilms. *PLoS One* 11:e0157188. doi: 10.1371/journal.pone.0157188

Shao, J., Lu, K., Tian, G., Cui, Y., Yan, Y., Wang, T., et al. (2015). Lab-scale preparations of *Candida albicans* and dual *Candida albicans-Candida glabrata* biofilms on the surface of medical-grade polyvinyl chloride (PVC) perfusion tube using a modified gravity-supported free-flow biofilm incubator (GS-FFBI). *J. Microbiol. Methods* 109, 41–48. doi: 10.1016/j.mimet.2014.12.006

Sharma, M., Biswas, D., Kotwal, A., Thakuria, B., Kakati, B., Chauhan, B. S., et al. (2015). Ibuprofen-mediated reversal of fluconazole resistance in clinical isolates of Candida. *J. Clin. Diagn. Res.* 9, DC20–DC22. doi: 10.7860/JCDR/2015/10094.5494

Shrestha, S. K., Garzan, A., and Garneau-Tsodikova, S. (2017). Novel alkylated azoles as potent antifungals. *Eur. J. Med. Chem.* 133, 309–318. doi: 10.1016/j.ejmech.2017.03.075

Shukla, A., and Sobel, J. D. (2019). Vulvovaginitis caused by *Candida* species following antibiotic exposure. *Curr. Infect. Dis. Rep.* 21:44. doi: 10.1007/s11908-019-0700-y

Silva, N. C., Nery, J. M., and Dias, A. L. (2014). Aspartic proteinases of *Candida* spp.: role in pathogenicity and antifungal resistance. *Mycoses* 57, 1–11. doi: 10.1111/myc.12095

Silva, S., Negri, M., Henriques, M., Oliveira, R., Williams, D. W., and Azeredo, J. (2012). *Candida glabrata*, *Candida parapsilosis* and *Candida tropicalis*: biology, epidemiology, pathogenicity and antifungal resistance. *FEMS Microbiol. Rev.* 36, 288–305. doi: 10.1111/j.1574-6976.2011.00278.x

Silva-Dias, A., Miranda, I. M., Branco, J., Cobrado, L., Monteiro-Soares, M., Pina-Vaz, C., et al. (2015). In vitro antifungal activity and in vivo antibiofilm activity of cerium nitrate against *Candida* species. *J. Antimicrob. Chemother.* 70, 1083–1093. doi: 10.1093/jac/dku511

Smith, S. B., and Ravel, J. (2017). The vaginal microbiota, host defence and reproductive physiology. *J. Physiol.* 595, 451–463. doi: 10.1113/JP271694

Sobel, J. D. (2007). Vulvovaginal candidosis. *Lancet* 369, 1961–1971. doi: 10.1016/S0140-6736(07)60917-9

Srinivasan, A., Leung, K. P., Lopez-Ribot, J. L., and Ramasubramanian, A. K. (2013). High-throughput nano-biofilm microarray for antifungal drug discovery. *mBio* 4:e00331-13. doi: 10.1128/mBio.00331-13

Srinivasan, A., Lopez-Ribot, J. L., and Ramasubramanian, A. K. (2012). *Candida albicans* biofilm chip (CaBChip) for high-throughput antifungal drug screening. *J. Vis. Exp.* e3845. doi: 10.3791/3845

Stergiopoulou, T., Meletiadis, J., Sein, T., Papaioannidou, P., Tsiouris, I., Roilides, E., et al. (2009). Comparative pharmacodynamic interaction analysis between ciprofloxacin, moxifloxacin and levofloxacin and antifungal agents against *Candida albicans* and *Aspergillus fumigatus*. *J. Antimicrob. Chemother.* 63, 343–348. doi: 10.1093/jac/dkn473

Stoddart, C. A., Maidji, E., Galkina, S. A., Kosikova, G., Rivera, J. M., Moreno, B. R., et al. (2011). Superior human leukocyte reconstitution and susceptibility to vaginal HIV transmission in humanized NOD-scid IL-2Rγ(-/-) (NSG) BLT mice. *Virology* 417, 154–160. doi: 10.1016/j.virol.2011.05.013

Su, C., Yu, J., and Lu, Y. (2018). Hyphal development in *Candida albicans* from different cell states. *Curr. Genet.* 64, 1239–1243. doi: 10.1007/s00294-018-0845-5

Sui, X., Yan, L., and Jiang, Y. Y. (2017). The vaccines and antibodies associated with Als3p for treatment of *Candida albicans* infections. *Vaccine* 35, 5786–5793. doi: 10.1016/j.vaccine.2017.08.082

Tan, Y., Leonhard, M., Ma, S., Moser, D., and Schneider-Stickler, B. (2017). Dispersal of single and mixed non-albicans *Candida* species biofilms by β-1,3-glucanase in vitro. *Microb. Pathog.* 113, 342–347. doi: 10.1016/j.micpath.2017.10.057

Tan, Y., Ma, S., Leonhard, M., Moser, D., and Schneider-Stickler, B. (2018). β-1,3-glucanase disrupts biofilm formation and increases antifungal susceptibility of Candida albicans DAY185.ăInt. J. Biol.ă108, 942–946. doi: 10.1016/j.ijbiomac.2017.11.003

Tanaka, Y., Sasaki, M., Ito, F., Aoyama, T., Sato-Okamoto, M., Takahashi-Nakaguchi, A., et al. (2016). KRE5 suppression induces cell wall stress and alternative ER stress response required for maintaining cell wall integrity in *Candida glabrata*. *PLoS One* 11:e0161371. doi: 10.1371/journal.pone.0161371

Tang, Y., Yu, F., Huang, L., and Hu, Z. (2019). The changes of antifungal susceptibilities caused by the phenotypic switching of *Candida* species in 229 patients with vulvovaginal candidiasis. *J. Clin. Lab. Anal.* 33:e22644. doi: 10.1002/jcla.22644

Thamban Chandrika, N., Shrestha, S. K., Ngo, H. X., and Howard, K. C. (2018). Novel fluconazole derivatives with promising antifungal activity. *Bioorg. Med. Chem.* 26, 573–580. doi: 10.1016/j.bmc.2017.12.018

Theberge, S., Semlali, A., Alamri, A., Leung, K. P., and Rouabhia, M. (2013). C. albicans growth, transition, biofilm formation, and gene expression modulation by antimicrobial decapeptide KSL-W. *BMC Microbiol.* 13:246. doi: 10.1186/1471-2180-13-246

Thomas, D. P., Bachmann, S. P., and Lopez-Ribot, J. L. (2006). Proteomics for the analysis of the *Candida albicans* biofilm lifestyle. *Proteomics* 6, 5795–5804. doi: 10.1002/pmic.200600332

Tournu, H., and Van Dijck, P. (2012). Candida biofilms and the host: models and new concepts for eradication. *Int. J. Microbiol.* 2012:845352. doi: 10.1155/2012/845352

Tsimaris, P., Giannouli, A., Tzouma, C., Athanasopoulos, N., Creatsas, G., and Deligeoroglou, E. (2019). Alleviation of vulvovaginitis symptoms: can probiotics lead the treatment plan? *Benef. Microbes* 10, 867–872. doi: 10.3920/BM2019.0048

Tso, G., Reales-Calderon, J. A., and Pavelka, N. (2018). The elusive anti-Candida vaccine: lessons from the past and opportunities for the future. *Front. Immunol.* 9:897. doi: 10.3389/fimmu.2018.00897

Tsui, C., Kong, E. F., and Jabra-Rizk, M. A. (2016). Pathogenesis of *Candida albicans* biofilm. *Pathog. Dis.* 74:ftw018. doi: 10.1093/femspd/ftw018

Valotteau, C., Prystopiuk, V., Cormack, B. P., Dufrêne, Y. F., and Mitchell, A. P. (2019). Atomic force microscopy demonstrates that *Candida glabrata* uses three Epa proteins to mediate adhesion to abiotic surfaces. *mSphere* 4, e00277-19. doi: 10.1128/mSphere.00277-19

van de Wijgert, J., and Verwijs, M. C. (2020). Lactobacilli-containing vaginal probiotics to cure or prevent bacterial or fungal vaginal dysbiosis: a systematic review and recommendations for future trial designs. *BJOG* 127, 287–299. doi: 10.1111/1471-0528.15870

van Wijlick, L., Swidergall, M., Brandt, P., and Ernst, J. F. (2016). *Candida albicans* responds to glycostructure damage by Ace2-mediated feedback regulation of Cek1 signaling. *Mol. Microbiol.* 102, 827–849. doi: 10.1111/mmi.13494

Vandeputte, P., Pradervand, S., Ischer, F., Coste, A. T., Ferrari, S., Harshman, K., et al. (2012). Identification and functional characterization of Rca1, a transcription factor involved in both antifungal susceptibility and host response in *Candida albicans*. *Eukaryot. Cell* 11, 916–931. doi: 10.1128/EC.00134-12

Visek, J., Ryskova, L., Safranek, R., Lasticova, M., and Blaha, V. (2019). In vitro comparison of efficacy of catheter locks in the treatment of catheter related blood stream infection. *Clin. Nutr. ESPEN* 30, 107–112. doi: 10.1016/j.clnesp.2019.01.010

Vogel, M., Hartmann, T., Köberle, M., Treiber, M., Autenrieth, I. B., and Schumacher, U. K. (2008). Rifampicin induces MDR1 expression in *Candida albicans*. *J. Antimicrob. Chemother.* 61, 541–547. doi: 10.1093/jac/dkm513

Wagener, J., Weindl, G., de Groot, P. W., de Boer, A. D., Kaesler, S., Thavaraj, S., et al. (2012). Glycosylation of *Candida albicans* cell wall proteins is critical for induction of innate immune responses and apoptosis of epithelial cells. *PLoS One* 7:e50518. doi: 10.1371/journal.pone.0050518

Walraven, C. J., and Lee, S. A. (2013). Antifungal lock therapy. *Antimicrob. Agents Chemother.* 57, 1–8. doi: 10.1128/AAC.01351-12

Wang, X., and Fries, B. C. (2011). A murine model for catheter-associated candiduria. *J. Med. Microbiol.* 60(Pt 10), 1523–1529. doi: 10.1099/jmm.0.026294-0

Wilkins, M., Zhang, N., and Schmid, J. (2018). Biological roles of protein-coding tandem repeats in the yeast *Candida albicans*. *J. Fungi* 4:78. doi: 10.3390/jof4030078

Willaert, R. G. (2018). Adhesins of yeasts: protein structure and interactions. *J. Fungi* 4:119. doi: 10.3390/jof4040119

Willems, H., Lowes, D. J., Barker, K. S., Palmer, G. E., and Peters, B. M. (2018). Comparative analysis of the capacity of the Candida species to elicit vaginal immunopathology. *Infect. Immun.* 86:e00527-18. doi: 10.1128/IAI.00527-18

Wuyts, J., Van Dijck, P., and Holtappels, M. (2018). Fungal persister cells: the basis for recalcitrant infections? *PLoS Pathog.* 14:e1007301. doi: 10.1371/journal.ppat.1007301

Xie, Y., Liu, X., and Zhou, P. (2020). In vitro antifungal effects of berberine against *Candida* spp. in planktonic and biofilm conditions. *Drug. Des. Devel. Ther.* 14, 87–101. doi: 10.2147/DDDT.S230857

Yano, J., and Fidel, P. L. Jr. (2011). Protocols for vaginal inoculation and sample collection in the experimental mouse model of *Candida vaginitis*. *J. Vis. Exp.* 8:3382. doi: 10.3791/3382

Yano, J., Noverr, M. C., and Fidel, P. L. Jr. (2012). Cytokines in the host response to *Candida vaginitis*: identifying a role for non-classical immune mediators, S100 alarmins. *Cytokine* 58, 118–128. doi: 10.1016/j.cyto.2011.11.021

Yano, J., Peters, B. M., Noverr, M. C., and Fidel, P. L. Jr. (2018). Novel mechanism behind the immunopathogenesis of vulvovaginal candidiasis: "neutrophil anergy". *Infect. Immun.* 86, e684–e617. doi: 10.1128/IAI.00684-17

Yano, J., Sobel, J. D., Nyirjesy, P., Sobel, R., Williams, V. L., Yu, Q., et al. (2019). Current patient perspectives of vulvovaginal candidiasis: incidence, symptoms, management and post-treatment outcomes. *BMC Womens Health* 19:48. doi: 10.1186/s12905-019-0748-8

Yu, J. J., and Gaffen, S. L. (2008). Interleukin-17: a novel inflammatory cytokine that bridges innate and adaptive immunity. *Front. Biosci.* 13:170–177. doi: 10.2741/2667

Zajac, D., Karkowska-Kuleta, J., Bochenska, O., Rapala-Kozik, M., and Kozik, A. (2016). Interaction of human fibronectin with *Candida glabrata* epithelial adhesin 6 (Epa6). *Acta Biochim. Pol.* 63, 417–426. doi: 10.18388/abp.2016_1328

Zarnowski, R., Westler, W. M., Lacmbouh, G. A., Marita, J. M., Bothe, J. R., Bernhardt, J., et al. (2014). Novel entries in a fungal biofilm matrix encyclopedia. *mBio* 5:e01333-14. doi: 10.1128/mBio.01333-14

Zhao, S., Huang, J. J., Sun, X., Huang, X., Fu, S., Yang, L., et al. (2018). (1-aryloxy-2-hydroxypropyl)-phenylpiperazine derivatives suppress *Candida albicans* virulence by interfering with morphological transition. *Microb. Biotechnol.* 11, 1080–1089. doi: 10.1111/1751-7915.13307

Zhao, X., Pujol, C., Soll, D. R., and Hoyer, L. L. (2003). Allelic variation in the contiguous loci encoding *Candida albicans* ALS5, ALS1 and ALS9. *Microbiology* 149(Pt 10), 2947–2960. doi: 10.1099/mic.0.26495-0

Zhou, Y., Wang, G., Li, Y., Liu, Y., Song, Y., Zheng, W., et al. (2012). In vitro interactions between aspirin and amphotericin B against planktonic cells and biofilm cells of *Candida albicans* and *C. parapsilosis*. *Antimicrob. Agents Chemother.* 56, 3250–3260. doi: 10.1128/AAC.06082-11

Conflict of Interest: The authors declare that the research was conducted in the absence of any commercial or financial relationships that could be construed as a potential conflict of interest.

Frontiers in Microbiology

Explores the habitable world and the potential of microbial life

The largest and most cited microbiology journal which advances our understanding of the role microbes play in addressing global challenges such as healthcare, food security, and climate change.

Discover the latest Research Topics

See more →

Frontiers

Avenue du Tribunal-Fédéral 34
1005 Lausanne, Switzerland
frontiersin.org

Contact us

+41 (0)21 510 17 00
frontiersin.org/about/contact